Journal of Advanced Transportation

Safety, Behavior, and Sustainability under the Mixed Traffic Flow Environment

Lead Guest Editor: Feng Chen
Guest Editors: Jaeyoung Lee, Young-Ji Byon, and Qiang Zeng

Safety, Behavior, and Sustainability under the Mixed Traffic Flow Environment

Journal of Advanced Transportation

Safety, Behavior, and Sustainability under the Mixed Traffic Flow Environment

Lead Guest Editor: Feng Chen
Guest Editors: Jaeyoung Lee, Young-Ji Byon, and Qiang Zeng

Contents

Contents

Hindawi
Journal of Advanced Transportation
Volume 2020, Article ID 1269415, 16 pages
https://doi.org/10.1155/2020/1269415

WILEY | Hindawi

Research Article

A Proportional-Switch Adjustment Model towards Mixed Equilibrium with Multiroute Choice Behaviour Criterion

Zhongxiang Huang, Xiangjun Jiang, and Wei Hao

School of Traffic & Transportation Engineering, Changsha University of Science & Technology, Changsha 410076, Hunan, China

Correspondence should be addressed to Xiangjun Jiang; 18874033439@163.com

Received 17 December 2019; Revised 5 February 2020; Accepted 6 July 2020; Published 7 August 2020

Academic Editor: Young-Ji Byon

Based on the price-quantity adjustment behaviour principle of the non-Walrasian equilibrium theory, this paper adopted a new QUE (quantity adjustment user equilibrium) criterion to formulate the route comfort choice behaviour. The purpose of the present paper is to establish a proportional-switch adjustment model which aims to reflect the route adjustment behaviour interaction between the traditional UE (user equilibrium) travellers and the QUE travellers and converge to a mixed equilibrium state. It is assumed that a group of road network travellers follow the UE criteria by choosing the travel route with the purpose of minimizing their route travel time (travel cost). In addition, the other group of travellers follow the QUE criteria by selecting the route with the largest residual capacity to achieve a more comfortable travel experience. The travel route adjustment behaviour of the two group travellers generates the dynamic traffic flow evolution towards the mixed equilibrium, and the route adjusting flow is proportional to the difference of traveller decision-making variable among the alternative routes. Simple illustrative examples are used to evaluate the performance of the proposed model, and the uniqueness and stability of the solution are demonstrated by applying the variational inequality and Lyapunov stability theorem.

1. Introduction

DTA (dynamic traffic assignment) model has been a focus research area for a long time with a growing influence on the traffic control and guidance promoted by the development of ITS (intelligence transportation system) emerging, leading to a greater interest in understanding the travel choice decision behaviour and the adjustment behavioural mechanisms [1–4]. Route choice behaviour is the basis of the traffic flow, and researchers have carried out a number of studies for dynamic traffic flow evolution problems to deepen the understanding of travellers' route choice behaviour decision-making mechanism [5–8]. The dynamic models are classified into five categories in the early researches: the simplex gravity flow dynamics, proportional-switch adjustment process, network tatonnement process, projected dynamical system, and evolutionary traffic flow dynamics. The difference between the five types of methods lies in the convergence speed of the established evolutionary model and the stability in equilibrium state [9–12]. Guo et al. [13] established a link-based discrete dynamic system model and depicted the rational adjustment process of network traffic flow from disequilibrium to an equilibrium state, which formulated more general behaviour compared with the five categories of dynamical system models.

Traditional dynamic traffic assignment problem assumes that travellers' route adjustment behaviour is aimed to reduce their travel cost; therefore, dynamic traffic flow evolution models converged to the equilibrium solution with minimizing the travel cost. There are three well-known network equilibrium states in the network traffic flow analysed studies. In detail, both of them capture travellers' cost-minimization behaviour with a difference in the form of the travel cost. Furthermore, travellers choose the actual shortest route in the route decision process to form a UE (user equilibrium), and travellers shift to the route to decrease the system aggregate travel time to form an SO (system optimum). At last, travellers adjust their routes

according to the perceived route travel time to form an SUE (stochastic user equilibrium). Although these classical traffic flow equilibrium conditions differ in the form of travel time, they share the same route rapidity choice criterion, which can embody the travellers' preference of route rapidity and reflect the price signal affection. It is apparent that all existing models in the literature were formulated based on a single route rapidity choice preference, where the route travel time is the core indicator. This approach has been widely applied in various network traffic flow models [14–18]. However, with the rapid economic growth and social development, people-oriented considerations, such as traffic safety and travel satisfaction, have been the dominant research direction [19–22].

Basically, the existing dynamic traffic flow evolution models are mainly classified according to the modelling approaches as daily and intraday, deterministic and stochastic, continuous time and discrete time, and route-based and link-based. Huang and Lam [23] established a route-based day-to-day dynamic system to depict the traffic flow adjustment process considering the network queuing, studied travellers' equilibrium path and travel time decision-making behaviour, and demonstrated the existence of discrete time dynamic UE solution with the iterative stability of the proposed algorithm. Secondly, Peeta and Yang [24] established route guidance control strategies and analysed the stability of dynamic traffic assignment with the example of UE objective model and SO objective model, which develops a general procedure for the stability analysis of dynamic traffic assignment problems. In addition, He et al. [25] showed that the route-based traffic flow evolution model had the path-overlapping problem and the route-flow-non-uniqueness problem caused by different initial route flow patterns. A link-based dynamic traffic flow assignment model is established, which has the classic UE solution, to depict the traveller's daily route adjustment behaviour and the evolution process of traffic flow. In order to depict the joint evolution trajectory of travellers' departure time and mode choices, Liu et al. [26] established a traffic flow dynamic model considering the impact of traveller inertia in a bimodal transportation system and analysed the dynamic interactions between transport users and traffic information provider.

With the purpose to deepen the understanding of travellers' route choice decision behaviour mechanisms, Watling and Hazelton [27] established a mathematical model to simulate the day-to-day dynamic adjustment system through the deterministic process and stochastic process models for both continuous and discrete time and described the route selection behaviour made by network travellers based on their travel experiences. Interestingly, Ehrgott et al. [28] considered several alternative principles of traveller's route decision-making behaviour and established an SUE model based on random utility theory to study this multiobjective problem, which extends the conventional SUE model with single route choice quality. In addition, Long et al. [29] proposed an SO-DTA (system optimum dynamic traffic assignment) model that accommodated the environmental objectives, which are more accurate than existing models and can capture the trade-off between emissions and travel time. Meanwhile, Hoang et al. [30] proposed a novel mathematical programming framework for the information-based SUE-DTA (stochastic user equilibrium dynamic traffic assignment) problem, which can underpin the linkage between UE and SO solutions by the FIFO (first in first out) principle. An ISM (incremental solution methods) is developed with the improvement of finding global optimal information-based SUE solution in terms of both accuracy and computation.

With the continuous improvement of science and technology, road network travellers can obtain the network information reflecting the travel environment and conditions through various methods, which are the real basis of travellers' different travel route decision-making criteria [31, 32]. In the reality, travellers make their route decision based on their preference, such as travel safety degree, travel service degree, travel outlay, or travel time, which have been the hot issue for the travellers' behaviour research [33–40]. Traffic flows based on these route choice preferences evolve into different equilibrium trajectories and converged to different equilibrium states [41, 42]. Therefore, all kinds of traffic flows formed by travellers exist simultaneously under different criteria.

Aiming to find a link or route flow patterns in a traffic network with various route choice behaviour criteria and to describe the interaction evolution process of mixed traffic flow, extensive studies have focused on the mixed traffic flow of multiple classes of travellers in recent years. Huang and Li [43] grouped the travellers according to their own value of time (VOT) and further divided them into two categories with different travel disutility perception variations according to whether the ATIS device is equipped. A multiclass, multicriteria (cost versus time) logit-based traffic equilibrium assignment problem is established, which was solved by combining logit assignment with a successive average method, providing an insight into the different responses of heterogeneous travellers to the information service. Furthermore, Zhang et al. [44] considered travellers' perceived utility differences by combining the travel time disutility and the time-irrelevant travel disutility and assumed that travellers follow either UE or CN (Cournot–Nash equilibrium) routing criteria. And a multiclass multicriteria mixed equilibrium model is proposed to study this evolution behaviour. Meanwhile, a uniform road toll strategy is developed by utilising the dual theory to promote the UE-CN mixed equilibrium to the SO. Moreover, Han et al. [45] established a daily dynamic adjustment system of the traffic flow under ATIS (advanced travel information system) and analysed the influence of ATIS on the stability of the traffic network. They concluded that the route flows associated with travellers equipped with ATIS satisfied the UE conditions and the travellers without ATIS will choose their routes in accordance with the logit-based route choice probability.

To flexibly reveal the various traffic flow dynamic adjusting processes induced by different criteria of route choice behaviour, several dynamic traffic flow models have been studied recently. Zhou et al. [46, 47] established a

discrete dynamic evolution model of traffic flow mixed equilibrium, which described traveller's multiple route adjustment behaviour with and without ATIS and simulated the evolution trajectory of traffic flow converging to UE-SUE mixed equilibrium state under given ATIS market penetration. Their research revealed the effect of the adoption of ATIS on the day-to-day flow dynamics. Bagloee et al. [48] divided travellers into two categories: perfect cooperation and perfect competition, where travellers with perfect cooperation followed the SO criterion and travellers with perfect competition were subject to the UE criterion. A UE-SO mixed equilibrium model is formulated by applying the nonlinear complementarity problem, which can accommodate a more general type of functions, namely, asymmetric delay functions. Moreover, Delle Site [49] separated travellers into three categories: (a) travellers equipped with predictive ATIS, (b) travellers equipped with static ATIS and subject to it, and (c) travellers not equipped with ATIS or not subject to it. They proposed an MUE (mixed user equilibrium) model to form the dynamic day-to-day processes and investigated the impacts of the inertia and the availability of ATIS with differentiated functionalities (predictive and static) on equilibrium travel times. Furthermore, the dynamic evolution models can be categorised by travellers' route choice behaviour criterion and the corresponding stable equilibrium state. Prominent examples include the single equilibrium models and the mixed equilibrium models, in which travellers follow the UE, SO, SUE, CN, or their hybrid behaviour criterion, respectively. We summarize the typical day-to-day flow dynamic models in Table 1.

Previous studies assumed that the equilibrium state of the road network is generated by the decision-making process of traveller's route rapid choice behaviour criterion, which means that travellers always shift to a less costly alternative route if such a route is available. In the dynamic evolution model of mixed equilibrium traffic flow that does not consider the route comfort choice behaviour criterion, all travellers' route adjustment behaviours conform to the cost-minimization principle, and the corresponding mixed equilibrium state is generally manifested as UE-SUE, UE-SO, UE-CN-SO, etc. This kind of mixed equilibrium only differs in the expression form of travel time, and in fact, it still takes route travel time as the travellers' only decision variable, which is inconsistent with the real transportation system. In actuality, travellers have independent characteristics, and their route choice decision behaviour is influenced by many internal factors as well as external conditions. Even under the same traffic condition and provided with the same road network information, some travellers may choose the fastest route, while others pay more attention to the overall travel comfort, such as road scenery, service level, and safety degree. In order to effectively describe the evolution process of traffic flow in road network under multiple traveller classes and multiple equilibrium criteria more effectively, Huang et al. [50] established a daily traffic flow dynamic regulation model based on the economic price-quantity regulation principle utilising the network tatonnement process method and proposed a new route residual capacity index to reflect road network travellers' comfort pursuit behaviour.

Unlike the existing studies with a single route rapidity adjustment behaviour criterion in which all the travellers were assumed to follow the same route cost-minimum behaviour mechanism, route comfort adjustment principles are considered in this study. We apply the route rapidity and comfort adjustment criteria stimulatingly to individual travel route selection behaviour, which means that individuals will comprehensively consider the route cost and the route surplus capacity to make a route decision. When applied to the traveller group, the aggregated effect is performed the way that some travellers choose the shortest route and some travellers choose the most comfortable route, as discussed in this study [51]. Specifically, travellers with route rapidity requirement are likely to choose the shortest route with the minimum route cost under the current traffic condition for their trips in the next day, and their traffic flow evolution process converges to the traditional UE state, while travellers with route comfort requirement are supposed to follow the route comfort behaviour criterion based on the current traffic condition, and their traffic flow evolves to a stable state, which is defined as QUE (quantity adjusting user equilibrium). Taking the route cost and the route surplus capacity as the decision variables for two group travellers, respectively, this paper established a dynamic proportional-switch adjustment model to depict the day-to-day evolution process and visualise the UE-QUE mixed equilibrium state formed by the interaction between the mixed traffic flows. In addition, the properties of the proposed dynamic switch model and its mixed equilibrium solution are analysed and discussed. Reasonable interpretations of these assumptions are presented to demonstrate that the route adjustment principle and the dynamic model proposed in this study have rich behavioural implications other than being a mathematical expression.

The proposed mixed traffic flow proportion-switch adjustment model with multiroute choice behaviour criterion not only reflected the heterogeneity of travellers within the different route adjustment principles but also described the different travel route adjusting process of travellers related to their different decision variables. Meanwhile, it also considered the influence of the road network traffic flow and travel costs generated by the two groups of travellers on each other's route decisions and effectively depicted the interaction relationship between the road network travellers. The research results of this paper can not only enrich the existing research on mixed equilibrium evolution by reflecting the adjustment mechanism of road network traffic flow and its equilibrium state more comprehensively but also describe the evolution process of traffic flow in line with the actual road network conditions more effectively. Hence, it improves the perception of the automatic adjustment mechanism and the changing pattern of road network traffic flow after the disturbance, which lays a foundation for the rational formulation of urban traffic congestion evacuation policy and the acquisition of reliable traffic flow prediction results. In

Table 1: Typical day-to-day flow dynamic models.

Authors	Behaviour criterion	Stable state	Remarks
Guo et al. [13]	UE	Single equilibrium	A link-based discrete dynamic system model was proposed to depict the rational adjustment process of traffic flow to an equilibrium state
Huang and Lam [23]	UE	Single equilibrium	A route-based day-to-day dynamic system considering the network queuing was formulated to study travellers' equilibrium path and travel time decision-making behaviour
Peeta and Yang [24]	UE/SO	Single equilibrium	Route guidance control strategies and a general procedure for the stability analysis of dynamic traffic assignment problems were developed
He et al. [25]	UE	Single equilibrium	A link-based dynamic traffic flow assignment model was established to depict the traveller's daily route adjustment behaviour and the evolution process of traffic flow
Liu et al. [26]	UE	Single equilibrium	A traffic flow dynamic model considering the impact of traveller inertia in a bimodal transportation system was investigated
Watling and Hazelton [27]	SUE	Single equilibrium	A mathematical model to simulate the day-to-day dynamic adjustment system and the route selection behaviour made by network travellers based on their travel experiences was described
Ehrgott et al. [28]	SUE	Single equilibrium	An SUE model based on random utility theory was performed to study the multiobjective problem
Long et al. [29]	SO	Single equilibrium	A system optimum dynamic traffic assignment model that accommodated the environment objectives was introduced
Hoang et al. [30]	SUE	Single equilibrium	A novel mathematical programming framework was investigated for the information-based stochastic user equilibrium dynamic traffic assignment problem
Huang and Li [43]	SUE-SUE	Mixed equilibrium	A multiclass, multicriteria (cost versus time) logit-based traffic equilibrium assignment problem was analysed, which grouped travellers according to their own value of time and further divided travellers with different travel disutility perception variations
Zhang et al. [44]	UE-CN-SO	Mixed equilibrium	A multiclass multicriteria mixed equilibrium model that considered travellers' perceived utility differences was proposed to study the evolution behaviour, and a uniform road toll strategy by utilising the dual theory was developed
Han et al. [45]	UE-SUE	Mixed equilibrium	A daily traffic flow dynamic adjustment system was presented under ATIS environment
Zhou et al. [46]	UE-SUE	Mixed equilibrium	A discrete dynamic evolution model of traffic flow mixed equilibrium was shown to describe traveller's multiple route adjustment behaviour with and without ATIS
Delle Site [49]	SUE-SUE-SUE	Mixed equilibrium	A mixed user equilibrium model was proposed to form the dynamic day-to-day processes and investigate the impacts of the inertia and the availability of ATIS with differentiated functionalities (predictive and static) on equilibrium travel times

Note: UE: user equilibrium; SO: system optimum; SUE: stochastic user equilibrium; CN: Cournot–Nash equilibrium.

addition, this study expands the decision influencing factors of travellers' route choice, which reflects travellers' individual characteristics more flexible, and significantly deepens the understanding of network traffic flow and improves the level of urban traffic management.

2. Mixed Equilibrium State

2.1. Quantity Adjustment User Equilibrium. Existing studies on the equilibrium state of traffic flow assumed that the network travellers behave in a way to minimize their travel time, which is defined as the route rapidity choice behaviour criterion in this paper. According to the different manifestation of travel time, they can be divided into three categories: the traffic flow generated by the route decisions based on actual travel time decision convergences to the traditional UE (user equilibrium) state, the traffic flow formed by the route decision according to perceived path travel time leads to an SUE (stochastic user equilibrium) state, and the traffic flow produced by the system marginal time minimization oriented decision forms an SO (system optimal) state. Such equilibrium states take route travel time-travel price as the only decision variable of travellers' route choice behaviour.

Based on the price-quantity adjustment behaviour principle of the non-Walrasian equilibrium theory in economics, this paper assumes that the travellers' route choice behaviour is not only affected by the travel price signal-travel time but also influenced by the quantity signal, which is considered through the route surplus capacity indicator to reflect the travellers' preference to travel comfort degree. The route surplus capacity is the difference between the route maximum capacity and the route flow, which concerns the physical capacity of the network route and indicates the travel comfort degree. In addition, the route with a larger surplus capacity indicates a higher degree of the route service level, including road infrastructure facilities, environmental satisfaction, and travel fluency.

When the current network flow is zero, the traveller chooses the route with the largest capacity to experience the most comfortable travel. With the gradual increase of road network flow, the residual capacity on all alternative paths will decrease, and the route travel comfort degree will decrease. Therefore, travellers will adjust their route selection according to the route travel comfort, and the route flow will shift to the alternative path with larger residual capacity. This route adjustment behaviour will lead the traffic flow to a stable state, which is defined as QUE (quantity adjustment user equilibrium) state in this research.

2.2. Mixed Equilibrium. When applying the dual constraint of price and quantity to the route selection behaviour of road network travellers, it means that a group of network travellers take the minimum travel price as the goal, and the traffic flow formed by such travellers' route decision-making behaviour finally stabilises in the price adjustment user equilibrium, that is, Wardrop UE state, while the other group of travellers expect the maximum comfort travel experience, and the traffic flow formed by such travellers' route decision-making behaviour finally stabilises in the QUE state. These two groups of travellers coexist in the road network, so that different decision-making behaviours of route selection interact and influence each other and finally form a UE-QUE mixed equilibrium state. The corresponding dynamic adjustment behaviour of traffic flow is the evolution process of mixed regulation traffic flow.

Given a network $G = (T, A)$, assuming that the travel demand of travellers in the first group following the UE principle is expressed as d_w, the travel demand of travellers in the second group following the QUE principle is denoted by $\widehat{d}_w$. The flows of travellers on route $r \in R_w$ in these two groups are represented by f_w^r and $\widehat{f}_w^r$, respectively. These route flows are grouped into two vectors and can be expressed by

$$\begin{cases} \mathbf{f} = \left(f_w^r \colon w \in W, r \in R_w\right), \\ \widehat{\mathbf{f}} = \left(\widehat{f}_w^r \colon w \in W, r \in R_w\right). \end{cases} \tag{1}$$

The flow conservation condition is given by

$$\begin{aligned} \sum_{r \in R_w} f_w^r &= d_w, \\ \sum_{r \in R_w} \widehat{f}_w^r &= \widehat{d}_w. \end{aligned} \tag{2}$$

The traffic flow on the link $a \in A$ is the aggregated link flow from two groups, which is

$$x_a = \sum_{w \in W} \sum_{r \in R_w} \delta_w^{ra} \left(f_w^r + \widehat{f}_w^r\right), \quad a \in A. \tag{3}$$

Travellers in the first group take the minimum travel price as the goal, following the UE route rapidity choice behaviour assumption, in which all travellers are supposed to shift to the alternative shorter route to reduce their actual travel time given the current information. The corresponding traffic flow evolution process finally stabilises in the price adjustment user equilibrium, that is, Wardrop UE state. When the traffic network travel demand is low, the route travel time is relatively low, so travellers in the first group select the shortest route with the most rapid time. With an increase in the network travel demand, the route travel time is increased since the traffic demand is gradually assigned to the traffic route network, which evolves to a congested state. Under this circumstance, travellers in the first group are supposed to shift to an alternative route where travel time is less compared with the current route. In addition, the traffic flow will be stable in the equilibrium state where all routes have the same travel time which is equal to the minimum route travel time for the OD pair. This route shift behaviour is predefined as route rapidity choice behaviour, and the formed network equilibrium state is the Wardrop UE state.

In the UE state, the route cost of all used routes between each OD pair is equal to the minimum route cost and less than (or equal to) the other routes with no flows. The equilibrium condition of travellers in the first group following the UE principle is

$$\begin{cases} f_w^r > 0, \ \sum\limits_{a \in A} \delta_w^{ra} \left[t_a\left(x_a\right)\right] = u_w, \\ f_w^r = 0, \ \sum\limits_{a \in A} \delta_w^{ra} \left[t_a\left(x_a\right)\right] \geq u_w, \\ a \in A, \ r \in R_w, \ w \in W, \end{cases} \tag{4}$$

where u_w denotes the minimal travel time between OD pair w.

Whereas travellers in the second group expect the maximum comfort travel experience, they follow the QUE route comfort choice behaviour assumption, in which all travellers are supposed to shift to the alternative path with a larger residual capacity to increase their travel comfort degree given the current information. The corresponding traffic flow evolution process finally stabilises in the quantity adjustment user equilibrium, QUE state. When the traffic network travel demand is low, the capacities of all routes are relatively high, and travellers in the second group will select the maximum-surplus-capacity route with the most comfortable travel route. With the increase of travel demand, the surplus capacities of all routes are reduced since the network gradually evolves to a congested state. Under this circumstance, travellers in the second group are supposed to shift to an alternative route where the surplus capacity is greater compared with the current route. In addition, the traffic flow will be stable in the equilibrium state where all route surplus capacities are the same and equal to the maximum surplus capacity of the OD pair. This route shift behaviour is predefined as the route comfort choice behaviour, and the formed network equilibrium state is called the quantity adjustment user equilibrium.

The maximum traffic capacity of the route $r \in R_w$ is expressed as

$$K_r = \min\left(\delta_w^{ra} K_a\right). \tag{5}$$

The surplus capacity of the route $r \in R_w$ is given by

$$s_w^r\left(\widehat{f}_w^r\right) = \max\left\{K_r - \widehat{f}_w^r, 0\right\}. \tag{6}$$

The maximum surplus capacity in the OD pair w is defined as

$$v_w = \max_{r \in R_w} \left\{ s_w^r \left(\widehat{f}_w^r \right) \right\}. \tag{7}$$

In the QUE state, the route surplus capacities of all used routes between each OD pair are equal to the maximum surplus capacity and greater than (or equal to) the other routes with no flows [51]. The equilibrium condition of travellers in the second group followed the QUE principle is

$$\begin{cases} \widehat{f}_w^r > 0, \; s_w^r \left(\widehat{f}_w^r \right) = v_w, \\ \widehat{f}_w^r = 0, \; s_w^r \left(\widehat{f}_w^r \right) \le v_w, \\ r \in R_w, \; w \in W. \end{cases} \tag{8}$$

3. Mixed Equilibrium Switch Model

The adjustment route flow of route l in OD pair w on day n, selected by travellers in the first group, is denoted by $\dot{f}_w^l(n) = y_w^l(n)$. Assume that the adjustment route flow of the first group travellers between two alternative routes is proportional to the route cost difference in the dynamical system [24]. When the route cost of the route k is larger than the route cost of route l on time n: $c_w^k > c_w^l$, the adjustment flow from route k to l is positive: $y_w^{k \longrightarrow l}(n) > 0$; conversely, if the route k has lesser cost than the route l: $c_w^k < c_w^l$, the corresponding adjustment flow is negative: $y_w^{k \longrightarrow l}(n) < 0$; and the travellers do not switch if the route costs are equal. Mathematically, the adjustment route flow can be expressed as

$$y_w^{k \longrightarrow l}(n) = \alpha \cdot \varphi_w^{k \longrightarrow l}(c, f(n)), \quad k, l \in R_w; \; w \in W, \tag{9}$$

$$\varphi_w^{k \longrightarrow l}(c, f(n)) = \begin{cases} \dfrac{(c_k - c_l)}{c_k} \cdot f_w^k(n), & \text{if } c_k - c_l \ge 0, \\ \dfrac{(c_k - c_l)}{c_l} \cdot f_w^l(n), & \text{if } c_k - c_l < 0, \end{cases} \tag{10}$$

$$y_w^l(n) = \sum_{k \ne l} y_w^{k \longrightarrow l}(n) = \sum_{k \ne l} \alpha \cdot \varphi_w^{k \longrightarrow l}(c, f(n)), \quad k, l \in R_w; \; w \in W, \tag{11}$$

where $\alpha (0 < \alpha < 1)$ is the route flow adjustment ratio. Since the right-hand side of equation (9) is continuous, there exists a solution $f_w^l(n)$ to equation (9) as a well-defined dynamical system. Equation (9) describes the magnitude and direction of the flow switching between two paths. $y_w^l(n)$ is continuous because it is a summation of $y_w^{k \longrightarrow l}(n)$.

Likewise, the adjustment route flow of route l in OD pair w on day n, chosen by travellers in the second group, is denoted by $\widehat{f}_w(n) = \widehat{y}_w^l(n)$. Assume that the adjustment route flows of the second group travellers are inverse rate with the route surplus capacity difference. When the route surplus capacity of route k is larger than route l on time n: $s_w^k > s_w^l$, the adjustment flow from route k to l is negative: $\widehat{y}_w^{k \longrightarrow l}(n) < 0$; if the route surplus capacity of route k is less than route l: $s_w^k < s_w^l$, the corresponding adjustment flow is positive: $\widehat{y}_w^{k \longrightarrow l}(n) > 0$; and the travellers do not switch if the route surplus capacity is equal. Mathematically, the adjustment route flow can be stated as

$$\widehat{y}_w^{k \longrightarrow l}(n) = \alpha \cdot \phi_w^{k \longrightarrow l}(s, \widehat{f}(n)), \quad k, l \in R_w; \; w \in W, \tag{12}$$

$$\phi_w^{k \longrightarrow l}(s, \widehat{f}(n)) = \begin{cases} \dfrac{(s_l - s_k)}{s_l} \cdot \widehat{f}_w^l(n), & \text{if } s_k - s_l \ge 0, \\ \dfrac{(s_l - s_k)}{s_k} \cdot \widehat{f}_w^k(n), & \text{if } s_k - s_l < 0, \end{cases} \tag{13}$$

$$\widehat{y}_w^l(n) = \sum_{k \ne l} \widehat{y}_w^{k \longrightarrow l}(n) = \sum_{k \ne l} \alpha \cdot \phi_w^{k \longrightarrow l}(s, \widehat{f}(n)), \quad \alpha > 0; \; k, l \in R_w; \; w \in W. \tag{14}$$

Since the right-hand side of equation (12) is continuous, there exists a solution $\widehat{f}_w^l(n)$ to equation (12) as a well-defined dynamical system. Equation (12) describes the magnitude and direction of the flow switching between two paths. $\widehat{y}_w^l(n)$ is continuous because it is a summation of $\widehat{y}_w^{k \longrightarrow l}(n)$.

Combining equations (11) and (14), we obtain

$$\begin{cases} y_w^l(n) = \sum_{k \neq l} \alpha \varphi_w^{k \longrightarrow l}(c, f(n)), \\ \widehat{y}_w^l(n) = \sum_{k \neq l} \alpha \phi_w^{k \longrightarrow l}(s, \widehat{f}(n)), \\ \alpha > 0;\ k, l \in R_w;\ w \in W. \end{cases} \tag{15}$$

Based on equations (9)–(11), the aggregate route adjustment flow of travellers in the first group on day n can be formulated as

$$\begin{aligned} y_w(n) &= \sum_{r \in R_w} y_w^r(n) \\ &= \sum_{k,l \in R_w \cap k \neq l} \left(y_w^k(n) + y_w^l(n) \right) \\ &= \sum_{k,l \in R_w \cap k \neq l} \left(\alpha \varphi_w^{k \longrightarrow l}(c, f(n)) + \alpha \varphi_w^{k \longrightarrow l}(c, f(n)) \right) \\ &= \begin{cases} \sum_{k,l \in R_w \cap k \neq l} \left(\alpha \dfrac{(c_l - c_k)}{c_k} \cdot f_w^k(n) + \alpha \dfrac{(c_k - c_l)}{c_k} \cdot f_w^k(n) \right) = 0, & \text{if } c_k - c_l \geq 0, \\ \sum_{k,l \in R_w \cap k \neq l} \left(\alpha \dfrac{(c_l - c_k)}{c_l} \cdot f_w^l(n) + \alpha \dfrac{(c_k - c_l)}{c_l} \cdot f_w^l(n) \right) = 0, & \text{if } c_k - c_l < 0. \end{cases} \end{aligned} \tag{16}$$

Since $\sum_{r \in R_w} y_w^r(n) = 0$, it follows that $\sum_{r \in R_w} f_w^r(n)$ is a constant; hence from $\sum_{r \in R_w} f_w^r(0) = d_w$, then $\sum_{r \in R_w} f_w^r(n) = d_w$.

According to equations (12)–(14), the summation of the route adjustment flow of travellers in the second group on day n can be expressed by

$$\begin{aligned} \widehat{y}_w(n) &= \sum_{r \in R_w} \widehat{y}_w^r(n) \\ &= \sum_{k,l \in R_w \cap k \neq l} \left(\widehat{y}_w^k(n) + \widehat{y}_w^l(n) \right) \\ &= \sum_{k,l \in R_w \cap k \neq l} \left(\alpha \phi_w^{l \longrightarrow k}(s, \widehat{f}(n)) + \alpha \phi_w^{k \longrightarrow l}(s, \widehat{f}(n)) \right) \\ &= \begin{cases} \sum_{k,l \in R_w \cap k \neq l} \left(\alpha \dfrac{(s_k - s_l)}{s_l} \cdot \widehat{f}_w^l(n) + \alpha \dfrac{(s_l - s_k)}{s_l} \cdot \widehat{f}_w^l(n) \right) = 0, & \text{if } s_k - s_l \geq 0, \\ \sum_{k,l \in R_w \cap k \neq l} \left(\alpha \dfrac{(s_k - s_l)}{s_k} \cdot \widehat{f}_w^k(n) + \alpha \dfrac{(s_l - s_k)}{s_k} \cdot \widehat{f}_w^k(n) \right) = 0, & \text{if } s_k - s_l < 0, \end{cases} \end{aligned} \tag{17}$$

where $\sum_{r \in R_w} \widehat{f}_w^r(n) = \sum_{r \in R_w} \widehat{f}_w^r(0) = \widehat{d}_w$; the flow conservation constraint is satisfied.

Furthermore, the route adjustment flow switching model for a general network with multiple O-D pairs can be expressed as

$$\begin{cases} \mathbf{y}(n) = \sum \alpha \cdot \Psi((\mathbf{c}, \mathbf{f}(n)), \\ \widehat{y}(n) = \sum \alpha \cdot \Phi((\mathbf{s}, \widehat{\mathbf{f}}(n)), \end{cases} \tag{18}$$

where

$$\Psi(\mathbf{c},\mathbf{f}(n)) = \begin{bmatrix} \Psi_1(\mathbf{c},\mathbf{f}(n)) & 0 & \cdot & 0 \\ 0 & \Psi_2(\mathbf{c},\mathbf{f}(n)) & 0 & \cdot \\ \cdot & 0 & \cdot & 0 \\ 0 & \cdot & 0 & \Psi_w(\mathbf{c},\mathbf{f}(n)) \end{bmatrix},$$

$$\Phi(\mathbf{s},\widehat{\mathbf{f}}(n)) = \begin{bmatrix} \Phi_1(\mathbf{s},\widehat{\mathbf{f}}(n)) & 0 & \cdot & 0 \\ 0 & \Phi_2(\mathbf{s},\widehat{\mathbf{f}}(n)) & 0 & \cdot \\ \cdot & 0 & \cdot & 0 \\ 0 & \cdot & 0 & \Phi_w(\mathbf{s},\widehat{\mathbf{f}}(n)) \end{bmatrix},$$

$$\Psi_w(\mathbf{c},\mathbf{f}(n)) = \begin{bmatrix} 0 & \varphi_w^{k\longrightarrow l}(c,k\longrightarrow l(n)) & \cdot & \cdot & \cdot \\ \varphi_w^{k\longrightarrow l}(c,k\longrightarrow l(n)) & 0 & \cdot & \cdot & \cdot \\ \cdot & \cdot & 0 & \varphi_w^{k\longrightarrow l}(c,\mathbf{f}(n)) & \cdot \\ \cdot & \cdot & \varphi_w^{k\longrightarrow l}(c,\mathbf{f}(n)) & 0 & \cdot \\ \cdot & \cdot & \cdot & \cdot & 0 \end{bmatrix}, \tag{19}$$

$$\Phi_w(\mathbf{s},\widehat{\mathbf{f}}(n)) = \begin{bmatrix} 0 & \phi_w^{k\longrightarrow l}(s,\widehat{\mathbf{f}}(n)) & \cdot & \cdot & \cdot \\ \phi_w^{k\longrightarrow l}(s,\widehat{\mathbf{f}}(n)) & 0 & \cdot & \cdot & \cdot \\ \cdot & \cdot & 0 & \phi_w^{k\longrightarrow l}(s,\widehat{f}(n)) & \cdot \\ \cdot & \cdot & \phi_w^{k\longrightarrow l}(s,\widehat{\mathbf{f}}(n)) & 0 & \cdot \\ \cdot & \cdot & \cdot & \cdot & 0 \end{bmatrix}.$$

Each element ($y_w^l(n)$ and $\widehat{y}_w^l(n)$) in system (18) is continuous. Consequently, the solution existence for system (18) is guaranteed.

Therefore, the route flow of the first group in route l on day $n+1$ is

$$f_w^l(n+1) = f_w^l(n) + \sum_{k\longrightarrow l} \alpha\varphi_w^{k\longrightarrow l}(c,f(n)). \tag{20a}$$

And the route flow of the second group in route l on day $n+1$ can be stated as

$$\widehat{f}_w^l(n+1) = \widehat{f}_w^l(n) + \sum_{k\neq l} \alpha\phi_w^{k\longrightarrow l}(s,\widehat{f}(n)). \tag{20b}$$

Then, the adjustment route flow switching model can be restated as

$$f_w^l(n+1) = f_w^l(n) + \sum_{k\neq l} \alpha\varphi_w^{k\longrightarrow l}(c,f(n)), \tag{21a}$$

$$\widehat{f}_w^l(n+1) = \widehat{f}_w^l(n) + \sum_{k\neq l} \alpha\phi_w^{k\longrightarrow l}(s,\widehat{f}(n)). \tag{21b}$$

Combining equations (18), (21a), and (21b), given the initial conditions: ($n\in[0,N]$), $\mathbf{f}(n=0)=\mathbf{f}^0$ and $\widehat{\mathbf{f}}(n=0)=\widehat{\mathbf{f}}^0$, the mixed equilibrium switch model is given by

$$\begin{cases} \mathbf{f}(n+1) = \mathbf{f}(n) + \mathbf{y}(n), \\ \widehat{\mathbf{f}}(n+1) = \widehat{\mathbf{f}}(n) + \widehat{y}(n), \\ \mathbf{f}(0) = \mathbf{f}^{(0)}, \\ \widehat{\mathbf{f}}(0) = \widehat{\mathbf{f}}^{(0)}. \end{cases} \tag{22}$$

4. Property Analyse

4.1. Equivalence between Stable State and Mixed Equilibrium Condition. In the present section, we establish a mixed equilibrium switch model, and if it reaches a stable point $(\mathbf{f}^*,\widehat{\mathbf{f}}^*)$, which means

$$\begin{cases} \mathbf{f}^*(n+1) = \mathbf{f}^*(n), \\ \widehat{\mathbf{f}}^*(n+1) = \widehat{\mathbf{f}}^*(n), \end{cases} \tag{23}$$

then, it follows that all the adjustment route flow is zero:

$$\begin{cases} \mathbf{y}^*(n) = \sum \alpha\Psi\left(\mathbf{c},\mathbf{f}^*(n)\right) = 0, \\ \widehat{y}^*(n) = \sum \alpha\Phi\left(\mathbf{s},\widehat{f}^*(n)\right) = 0. \end{cases} \tag{24}$$

Assume that the route l is the shortest route with the minimum route travel cost in OD pair w, stated as

$$c_w^k \geq c_w^l = u_w > 0, \quad k\neq l\in R_w. \tag{25}$$

Substituting equations (10) into (24), we have

$$y_w^{l*} = \sum_{k \neq l} \alpha \varphi_w^{k \longrightarrow l}(c, f(n)) = \sum_{k \neq l} \alpha \frac{(c_k - c_l)}{c_k} \cdot f_w^k(n) = 0. \tag{26}$$

The route flow is nonnegative, and so, there is $f_w^k(n) \geq 0$, $k \in R_w$, $w \in W$; combining it with equations (25) and (26) we get

$$\begin{cases} f_w^k > 0, c_w^k = c_w^l = u_w, \\ f_w^k = 0, c_w^k > c_w^l = u_w, \\ k, l \in R_w, w \in W. \end{cases} \tag{27}$$

Likewise, assuming that the route l is the most comfortable route with the maximum surplus capacity in the OD pair w, then

$$s_w^l = v_w \geq s_w^k \geq 0, \quad k \neq l \in R_w. \tag{28}$$

Substituting equations (13) into (24), we have

$$\hat{y}_w^{l*} = \sum_{k \neq l} \alpha \phi_w^{k \longrightarrow l}(s, \hat{f}(n)) = \sum_{k \neq l} \alpha \frac{(s_l - s_k)}{s_k} \cdot \hat{f}_w^k(n) = 0. \tag{29}$$

With the nonnegative property of route flow, which is $\hat{f}_w^k \geq 0$, $k \in R_w$, $w \in W$, and combining it with equations (28) and (29), it then follows that

$$\begin{cases} \hat{f}_w^k > 0, \quad s_w^k = s_w^l = v_w, \\ \hat{f}_w^k = 0, \quad s_w^k \leq s_w^l = v_w, \\ k, l \in R_w, \quad w \in W. \end{cases} \tag{30}$$

It can be seen that equations (27) and (30) are actually the equilibrium conditions of the travellers in two groups, which shows that the stable point $(\mathbf{f}^*, \hat{\mathbf{f}}^*)$ of the proposed switch model is equivalent to the mixed equilibrium condition.

4.2. Uniqueness of Solution. Based on the variational inequality (VI) theory, it is clear that the mixed equilibrium switch model (22) can be rewritten as the following VI problem:

$$\begin{aligned} F(\mathbf{f}^*, \hat{\mathbf{f}}^*)^{\mathrm{T}} \cdot \begin{pmatrix} \mathbf{f} - \mathbf{f}^* \\ \hat{\mathbf{f}} - \hat{\mathbf{f}}^* \end{pmatrix} &= \sum \sum \alpha \cdot \Psi(\mathbf{c}, \mathbf{f}^*) \cdot (\mathbf{f} - \mathbf{f}^*) \\ &\quad + \sum \sum \alpha \cdot \Phi(\mathbf{s}, \hat{\mathbf{f}}^*) \cdot (\hat{\mathbf{f}} - \hat{\mathbf{f}}^*) \\ &\geq 0. \end{aligned} \tag{31}$$

We note that it is known that if the function $F(\mathbf{f}, \hat{\mathbf{f}})$ is strictly monotone with $(\mathbf{f}, \hat{\mathbf{f}})$, then there exists a unique model solution.

Proof. Assume that $(\mathbf{f}\prime, \hat{\mathbf{f}}')$ and $(\mathbf{f}^*, \hat{\mathbf{f}}^*)$ are solutions to the VI problem (31), and $(\mathbf{f}\prime, \hat{\mathbf{f}}') \neq ((\mathbf{f}^*, \hat{\mathbf{f}}^*)$, so that

$$\sum \left(\sum \alpha \cdot \Psi(\mathbf{c}, \mathbf{f}\prime) \right) \cdot (\mathbf{f} - \mathbf{f}\prime) + \sum \sum \alpha \cdot \Phi(\mathbf{s}, \hat{\mathbf{f}}') \cdot (\hat{\mathbf{f}} - \hat{\mathbf{f}}') \geq 0, \tag{32}$$

$$\sum \left(\sum \alpha \cdot \Psi(\mathbf{c}, \mathbf{f}^*) \right) \cdot (\mathbf{f} - \mathbf{f}^*) + \sum \left(\sum \alpha \cdot \Phi(\mathbf{s}, \hat{\mathbf{f}}^*) \right) \cdot (\hat{\mathbf{f}} - \hat{\mathbf{f}}^*) \geq 0. \tag{33}$$

Let $(\mathbf{f}, \hat{\mathbf{f}}) = (\mathbf{f}^*, \hat{\mathbf{f}}^*)$ in equation (32) and $(\mathbf{f}, \hat{\mathbf{f}}) = (\mathbf{f}\prime, \hat{\mathbf{f}}')$ in equation (33), and adding the resulting inequalities, one obtains

$$\begin{pmatrix} \sum \left[\left(\sum \alpha \cdot \Psi(\mathbf{c}, \mathbf{f}\prime) \right) - \left(\sum \alpha \cdot \Psi(\mathbf{c}, \mathbf{f}^*) \right) \right]^{\mathrm{T}} \\ \sum \left[\left(\sum \alpha \cdot \Phi(\mathbf{s}, \mathbf{f}\prime) \right) - \left(\sum \alpha \cdot \Phi(\mathbf{s}, \hat{\mathbf{f}}^*) \right) \right]^{\mathrm{T}} \end{pmatrix}^{\mathrm{T}} \cdot \begin{pmatrix} \mathbf{f}^* - \mathbf{f}\prime \\ \hat{\mathbf{f}}^* - \hat{\mathbf{f}}' \end{pmatrix} \geq 0. \tag{34}$$

Apparently, the inequality (34) is in contradiction to the definition of strict monotonicity. Hence $(\mathbf{f}\prime, \hat{\mathbf{f}}') = (\mathbf{f}^*, \hat{\mathbf{f}}^*)$; the uniqueness of the solution holds. □

4.3. Stability of Solution. LaSalle's theorem is used to address the stability properties of the mixed equilibrium switch model. The candidate Lyapunov function [11] that we applied for the travellers of the first group is

$$V(f(n)) = \int_0^{x(n)} t(\eta) \mathrm{d}\eta. \tag{35}$$

It represents the objective function of the UE assignment. Since $x(n)$ is a linear transformation of $f(n)$ from equation (3), $\|f(n)\| \longrightarrow \infty$, $\|x(n)\| \longrightarrow \infty$, and $t(x(n))$ is a monotonically increasing function of $x(n)$. Hence, $f(n) \longrightarrow \infty$, $\int_0^{x(n)} t(\eta)\, \mathrm{d}\eta \longrightarrow \infty$ and $\lim_{\|f(n)\| \longrightarrow \infty} V(f(n)) = \infty$, which means that $V(f(n))$ is a continuously differentiable, positive definite radially unbounded function. Equation (35) can be expanded as

$$\begin{aligned} V(f(n)) &= \int_0^{x(n)} t(\eta) \mathrm{d}\eta = \int_{n^0}^{n\prime} t(\eta) \frac{\mathrm{d}\eta}{\mathrm{d}n} \mathrm{d}n \\ &= \int_{n^0}^{n\prime} t(\eta) \frac{\mathrm{d}\eta}{\mathrm{d}f} \frac{\mathrm{d}f}{\mathrm{d}n} \mathrm{d}n. \end{aligned} \tag{36}$$

Here, n^0 is the initial time in the dynamical switch system corresponding to the initial state $f(0)$, $n\prime$ is the time in the dynamical switch system when the system reaches the state $f(n)$. Equation (36) converts equation (35) to an integral along a route in the plane parameterized by n. The conversion is to avoid dealing with the complex interactions among $x(n)$, which is caused by the different classes of route choice behaviour principle in this research. And so the derivative of the Lyapunov function along the trajectories of the switch process is

$$\dot{V}(f(n)) = \frac{\mathrm{d}V}{\mathrm{d}n}(f(n)) = \frac{d\left(\int_{n^0}^{n\prime} t(\eta)(\mathrm{d}\eta/\mathrm{d}f)(\mathrm{d}f/\mathrm{d}n)\mathrm{d}n \right)}{\mathrm{d}t}, \tag{37}$$

where $(\mathrm{d}\eta/\mathrm{d}f) = (\mathrm{d}x/\mathrm{d}f) = (\mathrm{d}(\delta f)/\mathrm{d}f) = \delta$, $t(\eta)(\mathrm{d}\eta/\mathrm{d}f) = t(\eta)\delta = c$, and $(\mathrm{d}f/\mathrm{d}n) = \dot{f} = y$. Therefore,

$$\dot{V}(f(n)) = \frac{d\left(\int_{n^0}^{n} t(\eta)(\mathrm{d}\eta/\mathrm{d}f)(\mathrm{d}f/\mathrm{d}n)\mathrm{d}n\right)}{\mathrm{d}t} = \mathbf{c}\cdot\mathbf{y}(n) = \mathbf{c}\cdot\sum\alpha\Psi(\mathbf{c},\mathbf{f}(n)). \tag{38}$$

Now, from our earlier remark in Section 4.1, if and only if the dynamic switch process reaches the mixed equilibrium state, condition $\begin{cases} c_k > c^*, f_w^k = 0 \\ c_k = c^*, f_w^k > 0 \end{cases}$ holds and $\dot{V}(f^*(n)) = \mathbf{c}^*\cdot\sum\alpha\Psi^*(\mathbf{c},\mathbf{f}(n)) = 0$. Then, $c>0$, $\alpha>0$, $f(n)\geq 0$, and $\Psi(\mathbf{c},\mathbf{f}(n))$ is not positively invariant, so $\dot{V}(f(n))$ is nonpositive definite.

The candidate Lyapunov function [25] that we applied for the travellers of the second group is

$$W(\widehat{f}(n)) = \sum\widehat{f}(n)\cdot(v-s). \tag{39}$$

Apparently, the surplus capacity decreases with the increase of network route flow, that is, $\widehat{f}(n)\uparrow, s\downarrow, (v-s)\uparrow$. Hence $\widehat{f}(n)\longrightarrow\infty, \sum\widehat{f}(n)\cdot(v-s)\longrightarrow\infty$ and $\lim_{\|\widehat{f}(n)\|\longrightarrow\infty} W(\widehat{f}(n)) = \infty$, which means that $W(\widehat{f}(n))$ is a continuously differentiable, positive definite radially unbounded function. Equation (39) can be rewritten as

$$\dot{W}(\widehat{f}(n)) = \frac{\mathrm{d}W}{\mathrm{d}n}(\widehat{f}(n)) = \frac{\mathrm{d}W}{\mathrm{d}(\widehat{f}(n))}(\widehat{f}(n))\cdot\frac{\mathrm{d}(\widehat{f}(n))}{\mathrm{d}n} = \frac{\mathrm{d}W}{\mathrm{d}(\widehat{f}(n))}(\widehat{f}(n))\cdot\widehat{y}(n), \tag{40}$$

where

$$\frac{\mathrm{d}W(\widehat{f}(n))}{\mathrm{d}(\widehat{f}(n))} = \left[\frac{\partial W(\widehat{f}(n))}{\partial(\widehat{f}_1(n))}\ \frac{\partial W(\widehat{f}(n))}{\partial(\widehat{f}_2(n))}\ \cdots\ \frac{\partial W(\widehat{f}(n))}{\partial(\widehat{f}_r(n))}\right] = [-s_1\ \ -s_2\ \ \cdots\ \ -s_r] = -\mathbf{s}, \tag{41}$$

and so,

$$\dot{W}(\widehat{f}(n)) = -\mathbf{s}\cdot\mathbf{y}(n) = -\mathbf{s}\cdot\sum\alpha\Phi(\mathbf{s},\widehat{f}(n)). \tag{42}$$

If and only if the dynamic switch process reaches the mixed equilibrium state, condition $\begin{cases} s_k < s^*, \widehat{f}_w^k = 0 \\ s_k = s^*, \widehat{f}_w^k > 0 \end{cases}$ holds, and $\dot{W}(\widehat{f}^*(n)) = -\mathbf{s}^*\cdot\sum\alpha\Phi^*(\mathbf{s},\widehat{f}(n)) = 0$. Then, $s\geq 0$, $\alpha>0$, $\widehat{f}(n)\geq 0$, and $\Phi(\mathbf{s},\widehat{f}(n))$ is not positively invariant, so $\dot{W}(\widehat{f}(n))$ is nonpositive definite too.

Above all, the dynamic switch model (22) is stable and the solution of the dynamic switch model (22) converges to the mixed equilibrium state.

5. Numerical Example

In this subsection, we study the performance of the proposed dynamic traffic flow adjustment model, which synthetically considers the travellers with a different route choice behaviour principle. The tested network is shown in Figure 1 [25]. The traffic demand pattern between the OD pairs is assumed to be $D = 240$; assuming that 50% of the travellers follow the quantity adjustment principle, $\beta = 50\%$, then the traffic demand of the first group and the second group is $d = 120$ and $\widehat{d} = 120$. The route adjustment flow ratio is assumed as $\alpha = 0.6$.

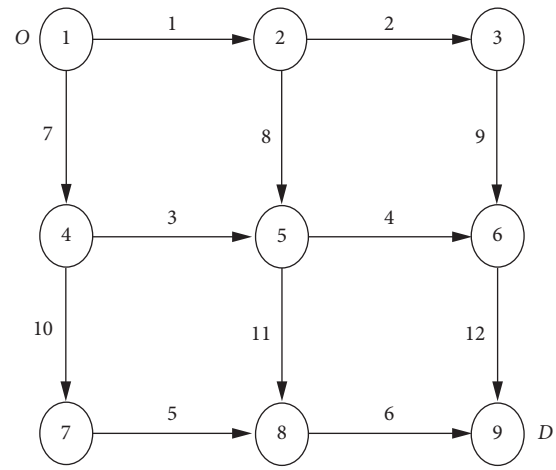

Figure 1: Test traffic network.

Table 2: The parameters in the link travel time functions.

Link	t_a^0	c_a
1	8	63
2	16	60
3	6	74
4	12	65
5	10	60
6	10	68
7	12	68
8	14	71
9	8	60
10	6	66
11	7	64
12	8	67

The incidence matrix of routes and links for the network is given in equation (43), and a simplified link travel time function that is often used in practice developed by the U.S. BPR (Bureau of Public Roads) is listed as follows, with free-flow travel time and link capacity given in Table 2:

$$\Delta^{\mathrm{T}} = \begin{bmatrix} 1&1&0&0&0&0&0&0&1&0&0&1 \\ 1&0&0&1&0&0&0&1&0&0&0&1 \\ 1&0&0&0&0&1&0&1&0&0&1&0 \\ 0&0&1&1&0&0&1&0&0&0&0&1 \\ 0&0&1&0&0&1&1&0&0&0&1&0 \\ 0&0&0&0&1&1&1&0&0&1&0&0 \end{bmatrix}, \tag{43}$$

$$t_a(x_a) = t_a^0\left[1 + 0.15\left(\frac{x_a}{c_a}\right)^4\right], \quad \forall a\in A. \tag{44}$$

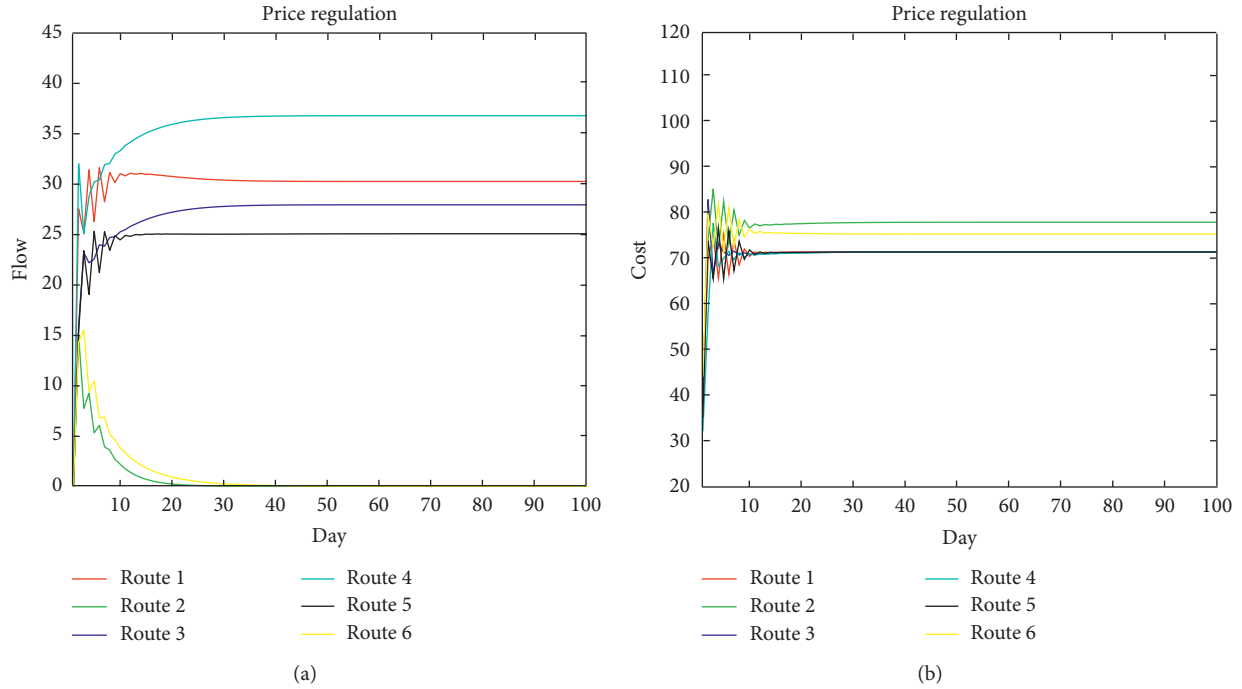

Figure 2: Evolutionary trajectories of route flows (a) and route travel costs (b) for travellers in the first group.

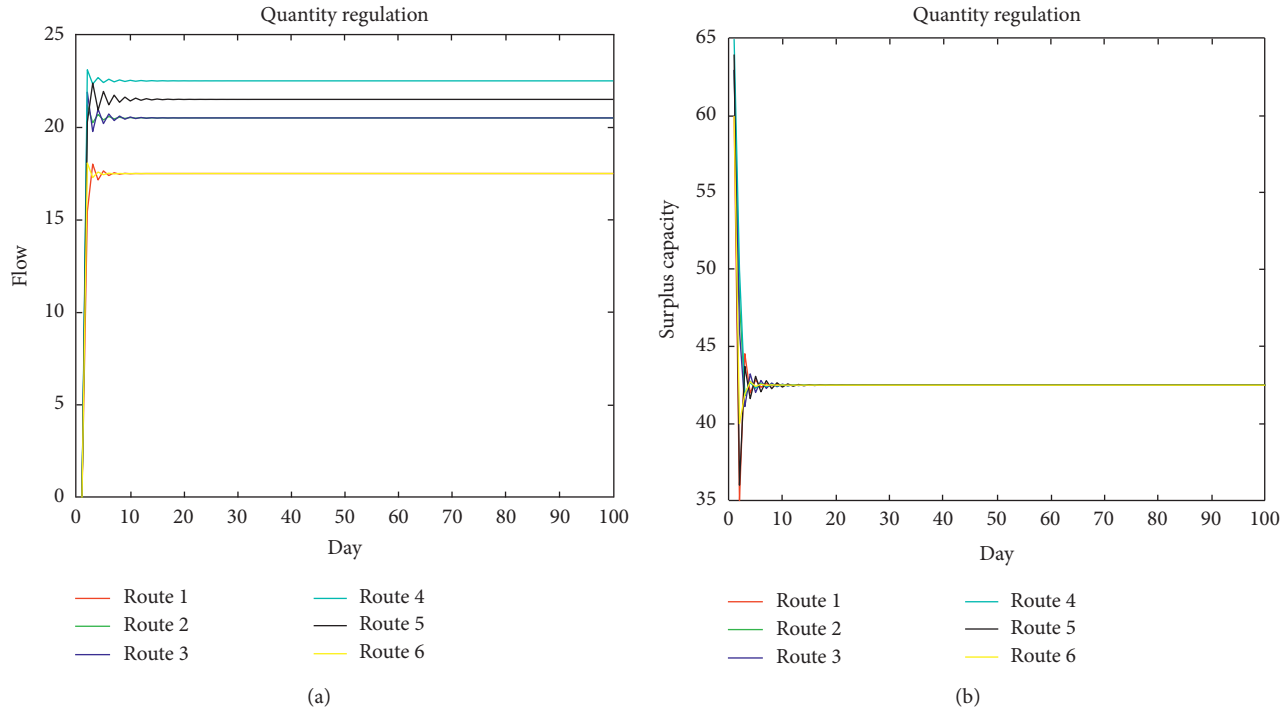

Figure 3: Evolutionary trajectories of route flows (a) and route surplus capacity (b) for travellers in the second group.

Figure 2 shows the evolution process of route flows and correspondent route travel time for travellers in the first group, while Figure 3 depicts the evolution process of route flows and correspondent route surplus capacity for travellers in the second group. Meanwhile, the route flow pattern and the corresponding route travel time in the mixed equilibrium state for travellers in the first group are tabulated in Table 3 as f and c, and the route flow pattern and the corresponding route surplus capacity in the mixed equilibrium state for travellers in the second group are tabulated in Table 3 as $\widehat{f}$ and s.

By combining Figures 2 and 3 with Table 3, it shows that the specific evolution process wherein the traffic flows

Table 3: Route flow, route travel cost, and surplus capacity in mixed equilibrium for travellers.

Route	Link	f	c	$\widehat{f}$	s
1	1, 2, 9, 12	30.25	71.30	17.50	42.50
2	1, 4, 8, 12	0.00	77.81	20.50	42.50
3	1, 6, 8, 11	27.93	71.30	20.50	42.50
4	3, 4, 7, 12	36.77	71.30	22.50	42.50
5	3, 6, 7, 11	25.06	71.30	21.50	42.50
6	5, 6, 7, 10	0.00	75.23	17.50	42.50

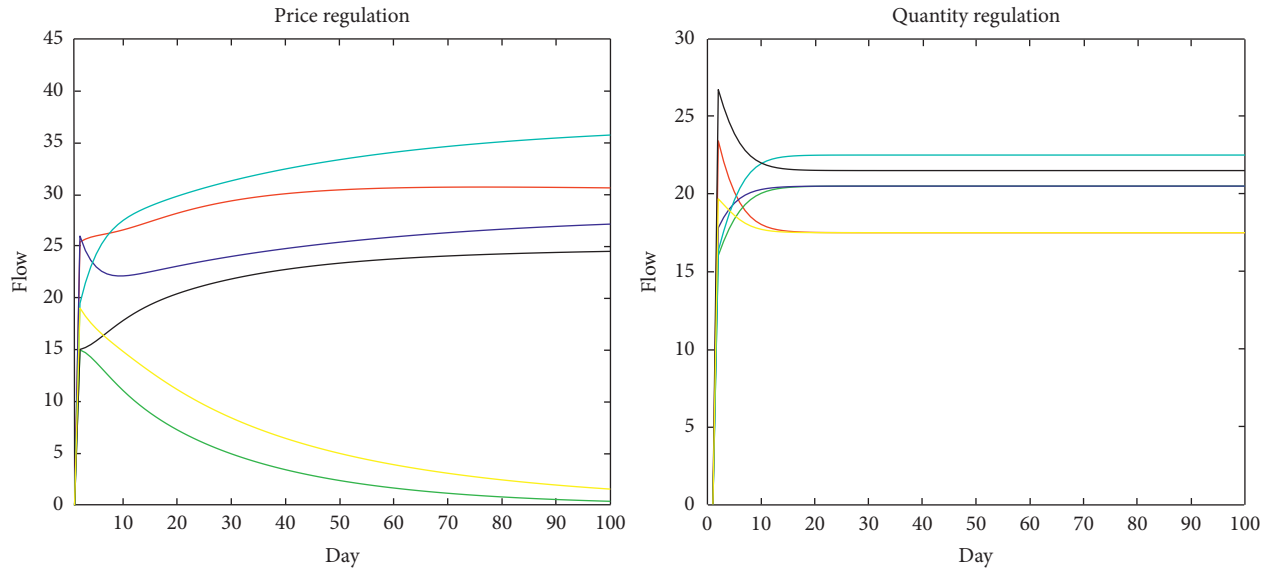

(a)

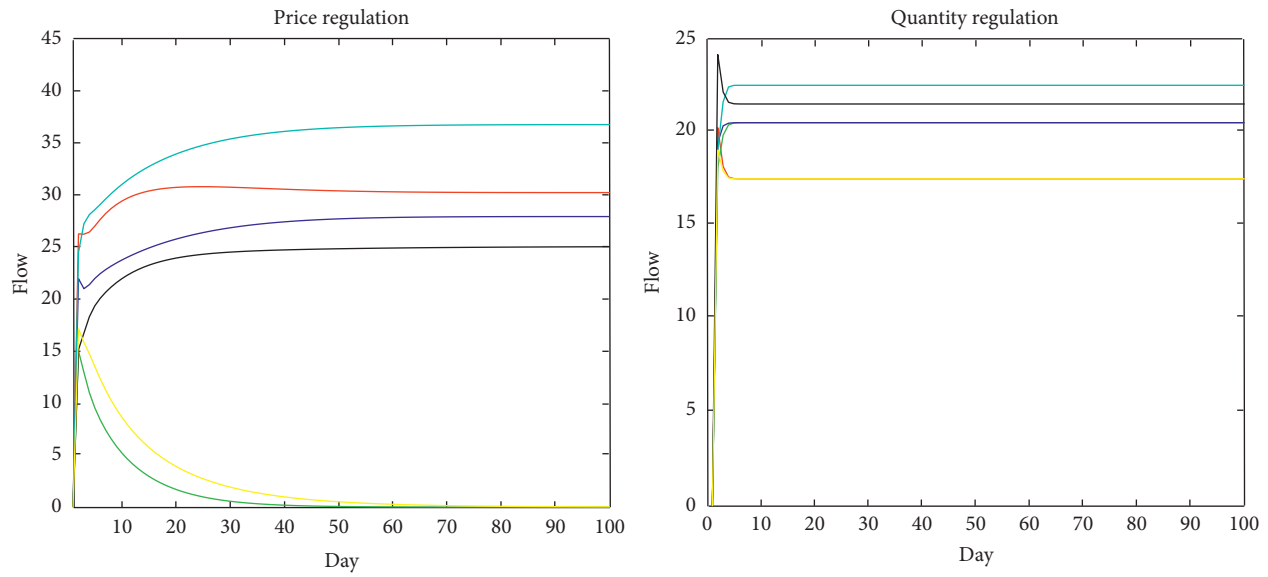

(b)

Figure 4: Continued.

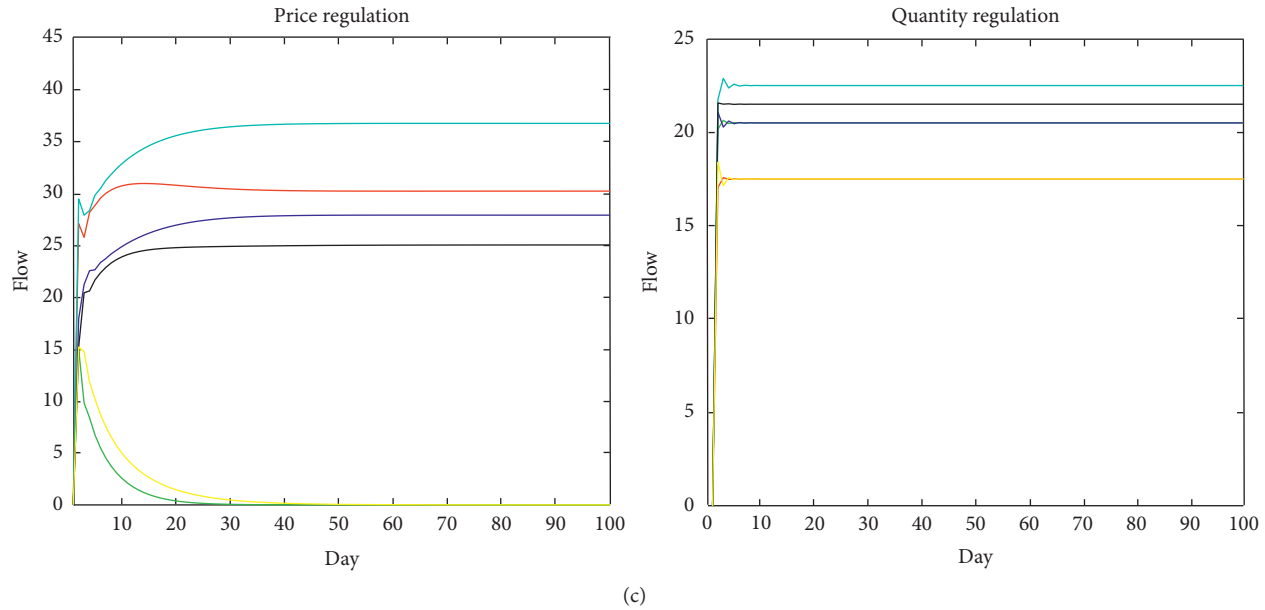

(c)

Figure 4: Flow evolution of test traffic network with different traffic flow proportional adjustment ratios. (a) $\alpha = 0.1$. (b) $\alpha = 0.3$. (c) $\alpha = 0.5$.

gradually converges to the equilibrium state after a fluctuant period. The above observation indicates that travellers in the first group, following UE principle, will evolve to a UE state, in which the travel costs of all used routes between the same OD pairs are equal and minimal, and travellers in the second group, following QUE principle, will evolve to a quantity-adjusted user equilibrium state in which the route surplus capacities of all used routes between the same OD pairs are equal and maximum.

Next, we test the performance of our mixed equilibrium switch model under different small constant flow adjustment ratios. Figures 4(a)–4(c) depict the evolution processes of flows in the mixed equilibrium state for travellers in the first group and the second group when the adjustment ratio is set to be 0.1, 0.3, and 0.5, respectively. It shows that, with different initial traffic flow patterns and route adjustment ratios, the dynamic system shares the same final equilibrium traffic flow pattern, which further testifies the uniqueness and stability of solution for the proposed mixed equilibrium switch model.

Parameter α represents the proportion of travellers who reconsider their routes in the next day according to the current network information, where the travellers in the first group shift to the route with lesser route travel time and the travellers in the second group switch to the route with higher route surplus capacity to experience more comfortable travel. Figure 4 shows that, with the increased value of α, the number of travellers who adjust their route choice is increased. This shows that a larger α will make the corresponding trajectory smoother and steadier and the fluctuation smaller. This means that, with an increase in the number of travellers who adjust their current route choice in accordance with the network information during the evolution process, the total benefit achieved by the route adjustment decision increases, which encourages travellers to shift to the equilibrium state. Therefore, the convergent speed is accelerated, and the evolution process from disequilibrium to equilibrium is shortened.

Clearly, from the above results, we can observe that traffic flows all converge to the stable state after a fluctuant period and that the proposed route adjustment switch model simulates the ideal traffic flow evolution of the two groups of travellers' route choice behaviour. Table 3 shows that, for travellers in the first group, the demand is entirely loading in the routes with the minimum travel times in the stable state, and the flows in the second group are stable when all of the surplus capacities of the routes are equal. Hence, the stable state is exactly the mixed equilibrium state formed by the different behaviours of these two groups of travellers. From Figure 4, we find that a smaller flow adjustment ratio will make the corresponding trajectory converge to the equilibrium slower, which is caused by the inactive route adjustment behaviour of travellers. And the evolution process under the quantity regulation is always smoother compared with the one under the price regulation with the same other condition, which is mainly caused by the different perception degree of price signal and quantity signal in the traffic network. In general, the travel surplus capacity is more visualised than the travel cost, so that the quantity adjustment behaviour is a universal phenomenon that should not be neglected in the areas of travel behaviour analysis.

6. Conclusions

With the rapid development of science and technology and the urbanisation process, new traffic patterns have emerged from large-scale urban infrastructure construction, road network expansion, and so on. To rationally characterise the traffic flow dynamic evolution process from disequilibrium to equilibrium, we studied the new quantity adjustment user

equilibrium criterion and the classic user equilibrium criterion based on the price-quantity adjustment behaviour principle of the non-Walrasian equilibrium theory. This paper categorises all travellers into two groups according to their route choice behaviour and simulates the dynamic evolution process of the interacted traffic flow. Thus, a proportional-switch adjustment model is established to reflect the route adjustment behaviour interaction between the traditional UE travellers and the QUE travellers, which converged to a mixed equilibrium state. This mixed equilibrium not only considers the diversity of the route selection criteria of the travellers but also elaborates on the interaction between the different travellers' groups. This deepens the understanding of network traffic flows and improves the level of urban traffic planning and management.

This work opens up several opportunities for further research, including (1) the possibility of ascertaining the proportional relationship of different traveller groups in mixed equilibrium, (2) possibilities to devise the appropriate forms defining the different route comfort and the corresponding traffic flow equilibrium conditions, and (3) the extension of the decision factors in route choice process, such as the inherent preference, previous experience, and social interaction of transportation information.

Notations

T: Set of nodes
A: Set of links, where $a \in A$
W: Set of origin-destination pairs, where $w \in W$
R_w: Set of routes in OD pair w, where $r, k, l \in R_w$
x_a: Traffic flow on the link $a \in A$
$t_a = t_a(x_a)$: Travel time function on link $a \in A$
δ_w^{ra}: Element of link-route incidence matrix, where $\delta_w^{ra} = 1$ if the route $r \in R_w$ contains link a, and 0 otherwise
d_w: Travel demand of travellers in the first group
$\widehat{d}_w$: Travel demand of travellers in the second group
f_w^r: Traffic flows of travellers in the first group on route $r \in R_w$
$\widehat{f}_w^r$: Traffic flows of travellers in the second group on route $r \in R_w$
$\mathbf{f} = (f_w^r : w \in W, r \in R_w)$: Set of route flows of travellers in the first group
$\widehat{\mathbf{f}} = (\widehat{f}_w^r : w \in W, r \in R_w)$: Set of route flows of travellers in the second group
c_w^r: Travel time of route $r \in R_w$
u_w: Minimal travel time between OD pair w
K_r: Maximum traffic capacity of the route $r \in R_w$
s_w^r: Surplus capacity of the route $r \in R_w$
v_w: Maximum surplus capacity in OD pair
$y_w^l(n)$: Adjustment route flow of travellers in the first group on the route l in OD pair w at day n
$\widehat{y}_w^l(n)$: Adjustment route flow of travellers in the second group on the route l in OD pair w at day n
$\mathbf{y} = (y_w^l : w \in W, l \in R_w)$: Set of adjustment route flows of travellers in the first group
$\widehat{y} = (\widehat{y}_w^l : w \in W, l \in R_w)$: Set of adjustment route flows of travellers in the second group
$\alpha (0 < \alpha < 1)$: Route flow adjustment ratio
β: Proportion of the travellers in the second group follows the quantity adjustment principle
$\varphi_w^{k \longrightarrow l}$: Adjustment flow function of travellers in the first group from route k to l in OD pair w
$\phi_w^{k \longrightarrow l}$: Adjustment flow function of travellers in the second group from route k to l in OD pair w
n: The dynamical system time unit that relates only to the solution procedure and has no mapping to the real system, which is defined as a day in this paper.

Data Availability

The data used to support the findings of this study are available from the corresponding author upon request.

Conflicts of Interest

The authors declare that there are no conflicts of interest regarding the publication of this paper.

Acknowledgments

This work was supported by the National Natural Science Foundation of China under Grant nos. 51338002, 51978082, and 51808057. This work was in part supported by Hunan Provincial Natural Science Foundation of China (no. 2019JJ30026), the Young Elite Scientists Sponsorship Program by Hunan Province of China (2018RS3074), Changsha Science and Technology Bureau Project (kq1801056), Open Fund of Hunan Key Laboratory of Smart Roadway and Cooperative Vehicle-Infrastructure Systems (kfj180702 and kfj190702), Innovation Team Project for Transportation Engineering in CSUST, and Ministry of Science Project with Montenegro (3-2).

References

[1] J. Y. Hao and Z. B. He, "A day-to-day invariant macroscopic fundamental diagrams for probe vehicles," *IOP Conference Series: Earth and Environmental Science*, vol. 189, no. 6, Article ID 062017, 2018.

[2] Z. He, L. Yang, and W. Guan, "A day-to-day route choice model based on travellers' behavioural characteristics," *Procedia—Social and Behavioral Sciences*, vol. 138, pp. 738–747, 2014.

[3] W. Zhang, Z. He, W. Guan, and G. Qi, "Day-to-day rerouting modeling and analysis with absolute and relative bounded rationalities," *Transportmetrica A: Transport Science*, vol. 14, no. 3, pp. 256–273, 2018.

[4] Z. He, W. Guan, and S. Ma, "A traffic-condition-based route guidance strategy for a single destination road network," *Transportation Research Part C: Emerging Technologies*, vol. 32, pp. 89–102, 2013.

[5] D. F. Xie, X. M. Zhao, and Z. B. He, "Heterogeneous traffic mixing regular and connected vehicles: modeling and stabilization," *IEEE Transactions on Intelligent Transportation Systems*, vol. 20, no. 6, pp. 2060–2071, 2019.

[6] Z. B. He, W. Zhang, and N. Jia, "Estimating carbon dioxide emissions of freeway traffic: a spatiotemporal cell-based model," *IEEE Transactions on Intelligent Transportation Systems*, vol. 21, no. 5, pp. 1976–1986, 2020.

[7] Z. B. He, B. K. Chen, N. Jia, W. Guan, B. C. Lin, and B. H. Wang, "Route guidance strategies revisited: comparison and evaluation in an asymmetric two-route traffic network," *International Journal of Modern Physics C*, vol. 25, no. 4, Article ID 1450005, 2014.

[8] Z. He, S. Ma, and X. Tang, "Empirical study on the influence of learning ability to individual travel behavior," *Journal of Transportation Systems Engineering and Information Technology*, vol. 9, no. 2, pp. 75–80, 2009.

[9] F. Yang, *An Evolutionary Game Theory Approach to the Day-to-Day Traffic Dynamics Dissertation*, University of Wisconsin-Madison, Madison, WI, USA, 2005.

[10] F. Yang and D. Zhang, "Day-to-day stationary link flow pattern," *Transportation Research Part B: Methodological*, vol. 43, no. 1, pp. 119–126, 2009.

[11] X. Z. He and H. X. Liu, "Modeling the day-to-day traffic evolution process after an unexpected network disruption," *Transportation Research Part B: Methodological*, vol. 46, no. 1, pp. 50–71, 2012.

[12] J. Bie and H. K. Lo, "Stability and attraction domains of traffic equilibria in a day-to-day dynamical system formulation," *Transportation Research Part B: Methodological*, vol. 44, no. 1, pp. 90–107, 2010.

[13] R.-Y. Guo, H. Yang, and H.-J. Huang, "A discrete rational adjustment process of link flows in traffic networks," *Transportation Research Part C: Emerging Technologies*, vol. 34, pp. 121–137, 2013.

[14] Z. Huang, J. Wu, A. Kuang, S. Zhang, and Y. Xu, "Modeling and simulation of travelers' route choice behavior based on disequilibrium theory," *Journal of System Simulation*, vol. 30, no. 11, pp. 4067–4078, 2018.

[15] Z. Huang, J. Wu, R. Huang, and Y. Xu, "Network traffic flow evolution model based on disequilibrium theory," *Mathematical Problems in Engineering*, vol. 2018, Article ID 8478910, 10 pages, 2018.

[16] L. Wu, Z. Huang, and Y. Wang, "A dynamic evolution model of disequilibrium network traffic flow with quantity regulation of congestion," *Journal of Traffic Transportation Engineering*, vol. 18, no. 3, pp. 167–178, 2018.

[17] Z. Huang, D. Qin, and A. Kuang, "Capacity model of road network considering the impact of the autonomous vehicles," *Journal of Changsha University of Science and Technology (Natural Science)*, vol. 15, no. 4, pp. 45–51, 2018.

[18] L. Wu, Z. Huang, J. Wu, Z. Gao, and D. Qin, "A day-to-day stochastic traffic flow assignment model based on mixed regulation," *IEEE Access*, vol. 8, pp. 12815–12823, 2020.

[19] L. Hu, X. Hu, J. Wan, M. Lin, and J. Huang, "The injury epidemiology of adult riders in vehicle-two-wheeler crashes in China, Ningbo, 2011–2015," *Journal of Safety Research*, vol. 72, pp. 21–28, 2020.

[20] L. Hu, J. Ou, J. Huang, Y. Chen, and D. Cao, "A review of research on traffic conflicts based on intelligent vehicles," *IEEE Access*, vol. 8, pp. 24471–24483, 2020.

[21] H. Zhao, Y. Li, W. Hao, S. Peeta, and Y. Wang, "Evaluating the effects of switching period of communication topologies and delays on electric connected vehicles stream with car-following theory," *IEEE Transactions on Intelligent Transportation Systems*, vol. 2020, no. 99, pp. 1–11, 2020.

[22] Y. Li, W. Chen, S. Peeta, and Y. Wang, "Platoon control of connected multi-vehicle systems under V2X communications: design and experiments," *IEEE Transactions on Intelligent Transportation Systems*, vol. 21, no. 5, pp. 1891–1902, 2020.

[23] H.-J. Huang and W. H. K. Lam, "Modeling and solving the dynamic user equilibrium route and departure time choice problem in network with queues," *Transportation Research Part B: Methodological*, vol. 36, no. 3, pp. 253–273, 2002.

[24] S. Peeta and T.-H. Yang, "Stability issues for dynamic traffic assignment," *Automatica*, vol. 39, no. 1, pp. 21–34, 2003.

[25] X. He, X. Guo, and H. X. Liu, "A link-based day-to-day traffic assignment model," *Transportation Research Part B: Methodological*, vol. 44, no. 4, pp. 597–608, 2010.

[26] W. Liu, X. Li, F. Zhang, and H. Yang, "Interactive travel choices and traffic forecast in a doubly dynamical system with user inertia and information provision," *Transportation Research Part C: Emerging Technologies*, vol. 85, pp. 711–731, 2017.

[27] D. Watling and M. L. Hazelton, "The dynamics and equilibria of day-to-day assignment models," *Networks and Spatial Economics*, vol. 3, no. 3, pp. 349–370, 2003.

[28] M. Ehrgott, J. Y. T. Wang, and D. P. Watling, "On multi-objective stochastic user equilibrium," *Transportation Research Procedia*, vol. 7, pp. 96–109, 2015.

[29] J. Long, J. Chen, W. Y. Szeto, and Q. Shi, "Link-based system optimum dynamic traffic assignment problems with environmental objectives," *Transportation Research Part D: Transport and Environment*, vol. 60, pp. 56–75, 2018.

[30] N. H. Hoang, H. L. Vu, and H. K. Lo, "An informed user equilibrium dynamic traffic assignment problem in a multiple origin-destination stochastic network," *Transportation Research Part B: Methodological*, vol. 115, pp. 207–230, 2018.

[31] L. Y. Xiang, G. Q. Guo, J. M. Yu, V. S. Sheng, and P. Yang, "A convolutional neural network-based linguistic steganalysis for synonym substitution steganography," *Mathematical Biosciences and Engineering*, vol. 17, no. 2, pp. 1041–1058, 2020.

[32] L. Xiang, X. Shen, J. Qin, and W. Hao, "Discrete multi-graph hashing for large-scale visual search," *Neural Processing Letters*, vol. 49, no. 3, pp. 1055–1069, 2019.

[33] C. X. Ma, W. Hao, F. Q. Pan et al., "Road screening and distribution route multi-objective robust optimization for hazardous materials based on neural network and genetic algorithm," *PLoS One*, vol. 13, no. 6, Article ID e0198931, 2018.

[34] M. S. Rahman, M. Abdel-Aty, J. Lee, and M. H. Rahman, "Safety benefits of arterials' crash risk under connected and automated vehicles," *Transportation Research Part C: Emerging Technologies*, vol. 100, pp. 354–371, 2019.

[35] F. Chen, H. R. Peng, X. X. Ma, J. Y. Liang, W. Hao, and X. D. Pan, "Examining the safety of trucks under crosswind at bridge-tunnel section: a driving simulator study," *Tunnelling and Underground Space Technology*, vol. 92, Article ID 103034, 2019.

[36] W. Hao, C. Kamga, X. Yang et al., "Driver injury severity study for truck involved accidents at highway-rail grade crossings in the United States," *Transportation Research Part F: Traffic Psychology and Behaviour*, vol. 43, pp. 379–386, 2016.

[37] Q. Zeng, W. Gu, X. Zhang, H. Wen, J. Lee, and W. Hao, "Analyzing freeway crash severity using a Bayesian spatial generalized ordered logit model with conditional autoregressive priors," *Accident Analysis & Prevention*, vol. 127, pp. 87–95, 2019.

[38] W. Hao, C. Kamga, and J. Daniel, "Driver's injury severity at U.S. highway-rail grade crossings by driver's age and gender," *Journal of Safety Research*, vol. 55, pp. 105–113, 2015.

[39] W. Hao and J. Daniel, "Driver's injury severity at U.S. highway-rail grade crossings by varied control devices," *Journal of Safety Research*, vol. 51, pp. 41–48, 2014.

[40] Z. Wang, J. Yu, W. Hao et al., "Two-step coordinated optimization model of mixed demand responsive feeder transit," *Journal of Transportation Engineering, Part A: Systems*, vol. 146, no. 3, Article ID 04019082, 2020.

[41] J. J. Tang, Y. W. Wang, W. Hao, F. Liu, H. L. Huang, and Y. H. Wang, "A mixed path size logit-based taxi customer-search model considering spatio-temporal factors in route choice," *IEEE Transactions on Intelligent Transportation Systems*, vol. 21, no. 4, pp. 1347–1358, 2020.

[42] W. Hao, Y. J. Lin, Y. Cheng, and X. F. Yang, "Signal progression model for long arterial: intersection grouping and coordination," *IEEE Access*, vol. 6, pp. 30128–30136, 2018.

[43] H.-J. Huang and Z.-C. Li, "Discrete optimization: a multiclass, multicriteria logit-based traffic equilibrium assignment model under ATIS," *European Journal of Operational Research*, vol. 176, no. 3, pp. 1464–1477, 2007.

[44] X. Zhang, H. Yang, and H.-J. Huang, "Multiclass multicriteria mixed equilibrium on networks and uniform link tolls for system optimum," *European Journal of Operational Research*, vol. 189, no. 1, pp. 146–158, 2008.

[45] L. Han, H. Sun, J. Wu, and C. Zhu, "Day-to-day evolution of the traffic network with advanced traveler information system," *Chaos, Solitons & Fractals*, vol. 44, no. 10, pp. 914–919, 2011.

[46] B. Zhou, M. Xu, Q. Meng, and Z. Huang, "A day-to-day route flow evolution process towards the mixed equilibria," *Transportation Research Part C: Emerging Technologies*, vol. 82, pp. 210–228, 2017.

[47] M. Xu, Q. Meng, and Z. Huang, "Global convergence of the trial-and-error method for the traffic-restraint congestion-pricing scheme with day-to-day flow dynamics," *Transportation Research Part C: Emerging Technologies*, vol. 69, pp. 276–290, 2016.

[48] S. A. Bagloee, M. Sarvi, M. Patriksson, and A. Rajabifard, "A mixed user-equilibrium and system-optimal traffic flow for connected vehicles stated as a complementarity problem," *Computer-Aided Civil and Infrastructure Engineering*, vol. 32, no. 7, pp. 562–580, 2017.

[49] P. Delle Site, "A mixed-behaviour equilibrium model under predictive and static advanced traveller information systems (ATIS) and state-dependent route choice," *Transportation Research Part C: Emerging Technologies*, vol. 86, pp. 549–562, 2018.

[50] Z. X. Huang, X. J. Jiang, and J. H. Wu, "An evolution model for network traffic flow based on price-quantity regulation," *Journal of Management Sciences in China*, vol. 20, no. 8, pp. 102–111, 2017.

[51] X. J. Jiang, Z. X. Huang, and Z. Y. Zhao, "A traffic flow evolution process toward mixed equilibrium with multi-criteria of route choice behaviour," *Journal of Advanced Transportation*, vol. 2020, Article ID 1720949, 17 pages, 2020.

Hindawi
Journal of Advanced Transportation
Volume 2020, Article ID 4795830, 15 pages
https://doi.org/10.1155/2020/4795830

Research Article

Discovering the Graph-Based Flow Patterns of Car Tourists Using License Plate Data: A Case Study in Shenzhen, China

He Bing,[1] Kong Bo,[2] Yin Ling,[1] Wu Qin,[3] Hu Jinxing,[1] Huang Dian,[4] and Ma Zhanwu[1]

[1]*Shenzhen Institutes of Advanced Technology, Chinese Academy of Sciences, Shenzhen 518055, China*
[2]*Institute of Mountain Hazards and Environment, Chinese Academy of Sciences, Chengdu 610041, China*
[3]*Chengdu University of Information Technology, School of Computer Science, Chengdu 610225, China*
[4]*National Supercomputing Center in Shenzhen, Shenzhen 518055, China*

Correspondence should be addressed to Kong Bo; kongbo827@imde.ac.cn

Received 2 January 2020; Revised 16 March 2020; Accepted 18 July 2020; Published 6 August 2020

Academic Editor: Young-Ji Byon

Identifying flow patterns from massive trajectories of car tourists is considered a promising way to improve the management of tourism traffic. Previous researches have mainly focused on tourist movements at the macro-scale, such as inbound, domestic, and urban tourism using flow maps. Compared with modeling the flow patterns of tourists at the macro-scale, modeling tourist flow at the microscale is more complicated. This paper takes Dapeng Island located in Shenzhen as the study area and uses the car recognition devices to collect traffic flow. Firstly, car tourists are separated from the mixed traffic flow after analyzing the spatial-temporal characteristics of tourists and residents. Next, daily graphs of tourist movements between road segments and tourist attractions are constructed. Finally, a frequent subgraph mining algorithm is used to extract the flow patterns of car tourists. The experimental results show that (1) car tourists have obvious preferences in the selection of trip time and tourist attractions; (2) the intercity tourists tend to take multidestination trips rather than a single destination trip in the same type of attractions; (3) car tourists are inclined to park their cars in an easy-to-access place, even if the attractions visited are changed. The main contribution of this paper is to present a new method for discovering the flow patterns of car tourists hidden in massive amounts of license plate data.

1. Introduction

Due to the flexibility and convenience of road transportation, car-based tourism (travel in owned or rented cars, also named driving tours [1], car tourism [2], and self-driving tours [3]; for simplicity, this paper uses the term car tourism) has been one of the popular forms for leisure and recreation. Recently, car tourism has been growing rapidly in China, and its scale is continuing to expand with the improvement of road infrastructure and the growth of car ownership. A statistical report indicated that by 2015, there were 2.34 billion car tourists in China, accounting for more than 58.5% of the total domestic tourists [4]. It can be foreseen that the percentage of car tourists will increase over time. However, car tourists need to share roads in urban areas or tourist attractions with residents, and they depend on the road network to achieve circulation between the places of origin and multiple tourist attractions. Currently, urban roads are heavily crowded. When a large number of tourist cars enter the road network during peak tourist season, the pressure on road traffic management may be increased. It is worth noting that this phenomenon is severe for coastal tourist attractions.

Coastal islands are one of the favorite tourist destinations. The development of road network on the islands often precedes the development of tourist attractions, and new infrastructures and facilities are being built to handle the increase in tourist traffic. Thus, tourism activities tend to be superimposed on a spatial system and infrastructure network that was not explicitly designed to cater to them and tourism activities can be unevenly distributed [5]. Additionally, some islands are connected to the mainland. The roads entering and leaving these islands have become bottlenecks for tourism transportation, which poses challenges

to the coordination of traffic on and off islands. Moreover, in contrast to commuting transportation, tourism transportation has different characteristics in time and space, and it requires more comfort and convenience. The problems mentioned above show that if tourism transportation is not taken seriously in traffic management, it is likely to increase travel difficulties for residents, and it will affect the travel willingness of tourists and the sustainable development of tourism transportation.

The recording and analysis of trajectories are essential for understanding the movement of tourists and the management of tourist traffic, such as the optimal location and development of transportation facilities and the redistribution of tourists. However, the lack of practical approaches for the collection of relevant data limits the detailed exploration of tourist mobility. The traditional method involves paper-and-pencil or computer interviews, which are expensive and time-consuming. The collected data are also typically limited in terms of personal information such as family composition, age structure, and favorite tourist attractions [6]. Recently, with the development of sensors such as GPS tracker, video recognition device, and RFID, which can capture movement data in real-time and with spatial and temporal details, the trajectory-based data analysis methods have been widely used in transportation research. The analysis results provide real-time and future traffic information for road traffic managers and travelers, as well as technical support for the relief of traffic jams. However, current observations of road traffic are limited to statistical information such as traffic volume, occupancy, and speed. Movement patterns are depicted in a flow graph or reported by visual descriptions rather than exploring flow patterns. Additionally, road traffic has the characteristics of variability and correlation in time and space. Previous researches have demonstrated that sectional traffic flow is interrelated to the distances and locations of monitoring points and the topology of road network. Therefore, it is necessary to consider the structure of road network and the correlation between time and space in the analysis of tourist traffic. This consideration is more useful in explaining the deeper behavior of tourist traffic.

This study is an attempt to investigate the flow patterns of car tourists by applying a frequent subgraph mining algorithm. This algorithm can take into account the correlation of traffic flows captured by video sensors. From the graph and flow perspective, a coastal island is used as an experimental area to explore the dynamic relationship between multiple tourist attractions and key road segments. This paper is organized as follows. The next section reviews related work on movement pattern mining and the methods for analyzing trajectory-based data on tourists and traffic flows. Section 3 introduces the study area (Dapeng Island, Shenzhen, China). Section 4 describes the distribution of the monitoring points in detail. Section 5 introduces the data and methods used in this paper. Section 6 presents the results of flow patterns generated by car tourists. Finally, we finish with a discussion and conclusion.

2. Related Work

In recent years, movement patterns have been analyzed frequently from transportation to tourism, such as the research of movement patterns hidden in taxis [7–11], buses [12, 13], railways [14], tourist movements [15–20], and even in geo-tagged media datasets [21, 22]. In terms of tourism transportation research, the efficient management of tourist traffic requires a sound understanding of car tourists' spatial movement patterns because these patterns provide critical information, e.g., the flow volume and spatial transfer direction, for the planning of new transportation facilities and the redistribution of tourist flow. As is well known, movement is an intrinsic attribute of traffic flow that changes over time with respect to the spatial location of people, goods, and cars. The patterns implied in moving datasets are not repeatedly produced by a single car tourist, but rather by a huge number of cars that appear in the same area. In most cases, the collected moving datasets of traffic entities are relatively large in volume and complex in structure. Therefore, it is necessary to use data mining algorithms and visual analytics techniques to extract useful and relevant information, regularities, and structures from massive movement datasets. The data mining algorithms used in transportation are varied. These algorithms focus on clustering [8], density, and sequential characteristics [9, 10] in time and space. The leisure activities of car tourists are carried out in a road network. The activity sequences can be modeled in a graph that consists of different nodes (for example, parking lots and cultural sites) and edges with direction that are the order of locations visited. For this kind of dataset, graph mining is a widely used method that finds interesting patterns in graph representation data [23]. The detected patterns are typically expressed as graphs, which may be subgraphs of graphical data or more abstract expressions of the trends reflected in data [24]. One form of graph mining is frequent subgraph mining, which is used to identify frequently occurring patterns (subgraphs) across a collection of "small" graphs or in a "large" graph [25]. Various subgraph mining algorithms have been proposed. These algorithms can be further classified based on the search strategies, i.e., either breadth-first or depth-first searches. The depth-first search strategy is more computationally efficient, such as in gSpan (graph-based Substructure pattern mining) [26], MoFa (Molecule Fragment Miner) [27], FFSM (Fast Frequent Subgraph Mining) [28], and Gaston (GrAph/Sequence/Tree extractiON) [29], SPIN (Spanning tree based maximal graph mining) [30]. However, FFSM and Gaston cannot be used for directed graphs without major changes. Only MoFa is suitable for finding directed frequent subgraphs, and for gSpan, only minor changes are necessary [31]. Other related works include significant pattern mining Leap [32], maximal frequent subgraph mining Margin [33], and frequent subgraphs in multigraphs [34].

During the past few years, trajectory-based methods have been used to analyze transportation systems

[10, 11, 13, 14]. In many applications, moving entities are considered moving points whose trajectories (i.e., paths through space and time) can be visualized and analyzed. In transportation, the collected trajectory data can be presented in origin-destination (OD) data with aggregation methods [35]. Such OD data can be visualized with a set of techniques, including flow maps [36, 37] and OD maps [38]. Nevertheless, the study of the spatial dimensions of tourism remains a mostly underexplored area of research, although this research area is expanding due to the advances of new information and communication technologies (ICT). Traditional approaches in tourism can be divided into two categories, which are direct observation techniques (e.g., interviews, trip diaries, and recall diaries) and non-observation techniques (e.g., GPS tracking and video tracking), but the use of nonparticipant observation only is the best technique for privacy reasons [5]. Even with ICT support, this technique has difficulties in data collection, and the large-scale sampling of passenger data is costly. Most published studies related to movement patterns are still descriptive, and they employ small sample sizes that are highly controlled. Moreover, this kind of research is focused on the human movement in tourist intradestination. There have been a few studies that have explored car-related spatial movement patterns in tourist destinations. Even so, the research was aimed at large-scale car tourists' activities [39] or used the questionnaire method, which is prone to biases and errors [40]. Therefore, given the requirements of protecting privacy, increasing data volume, and avoiding investigator biases, it is necessary to conduct flow pattern research based on continuous time-series data acquired from sensors.

3. Study Area

Dapeng Island, located in the east of Shenzhen (as shown in Figure 1), is an essential node in the "Guangdong-Hong Kong-Macao Greater Bay Area," and it is the only pioneer zone of national tourism reform and innovation in Guangdong province. Dapeng has abundant tourism resources, such as Dapeng Ancient City, National Geological Park, and Folk Village. The "Shenzhen Tourism Statistics Bulletin" showed that a total of 139 million tourists visited this city in 2018. The increase was 5.97 percent each year, of which only one-tenth was group tourists. This indicates that most tourism activities are carried out by individual visitors. Because of topographical constraints, tourism transportation on the island has not been fully developed. Owned and rented car tours are the main modes of visiting the island for individual tourists. The Dapeng Transportation Bureau has analyzed the trend of motorized travel demand on the island and predicted that the total annual traffic flow would be 504000 cars/year. At the peak time of "Golden Week," about 35000 cars/day entered into the island, of which 79% were car tourists.

4. Distribution of Monitoring Points

Urban transportation systems usually employ GPS technology to capture taxi and bus tracks. Different from this kind of public transportation research, this paper aims to analyze the flow patterns of car tourists at multiple attractions. It is difficult to install GPS device on each personal car. Therefore, we chose roadside monitoring devices to collect traffic flow. In addition, urban road network includes expressways, ordinary roads, and community roads. It has a large number of nodes and complex structure. In order to monitor each road segment, many devices will need to be deployed on roads. So, the key road segments and tourist attractions were selected as the locations of monitoring points. Five video devices were deployed at key roads, and two video devices were deployed in parking lots. The labels of monitoring devices are $A1$, $A2$, $A5$, $A7$, $A10$, $P1$, and $P2$ (as shown in Figure 2).

The detected tourist flow at each monitoring point is shown in Table 1.

5. Methods

In this study, a cloud-based database system was established to store traffic data after they were uploaded via 4G communication technologies. The collected data includes license plate numbers, time of passage, and labels for monitoring points. In order to protect tourists' private information, license plate numbers were changed into car IDs and only the registration places of cars were extracted. After data collection period, the license plate numbers will be deleted from the database.

The proposed approach is outlined in Figure 3. This section introduces the detailed steps for the mining of frequent flow patterns of car tourists at the microscale in a tourist intradestination. First, car tourists were separated from mixed traffic flow after analyzing the temporal characteristics of collected data. Second, spatial movement graphs of traffic flow were reconstructed for each day. Each movement graph is a connected and directed graph where vertices are monitoring points and directed edges are tourist flow between two monitoring points. Then, a frequent subgraph mining algorithm (gSpan) was used to detect the flow patterns between road segments and tourist attractions. Next, in order to reduce the number of frequent flow patterns, small overlapping subgraphs were removed from the results. Finally, we analyzed the spatial-temporal characteristics of flow patterns intradestination.

5.1. Preprocessing Source Data. When collecting data, it is inevitable that problem data will be collected. This can be caused by a problem with the device, such as an aging or damaged camera. Additionally, a license plate may be blurred, blocked, or damaged, especially in bad weather, which can affect the efficiency of car recognition. Furthermore, it is challenging to identify some special characters and confusing numbers on license plates. The above issues can lead to data distortion. To ensure the accuracy and reliability of the analyzed results, the collected data need to be processed at first. The rules of processing are as follows:

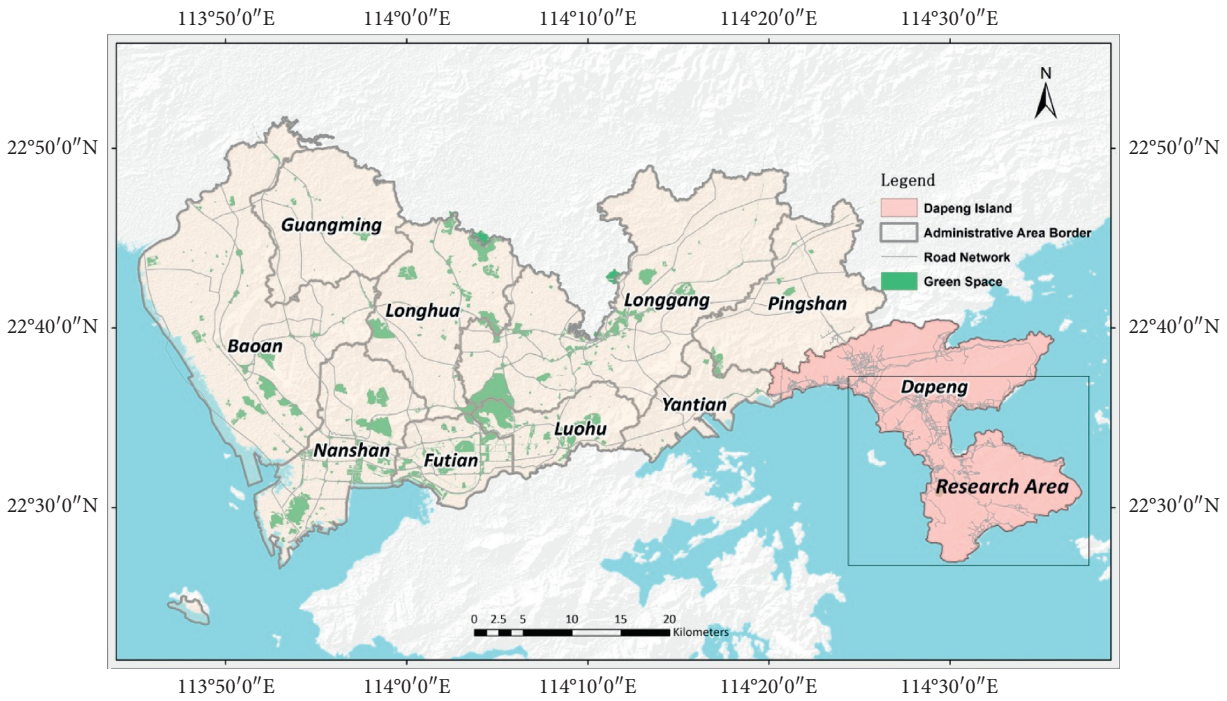

Figure 1: The location of dapeng island, Shenzhen.

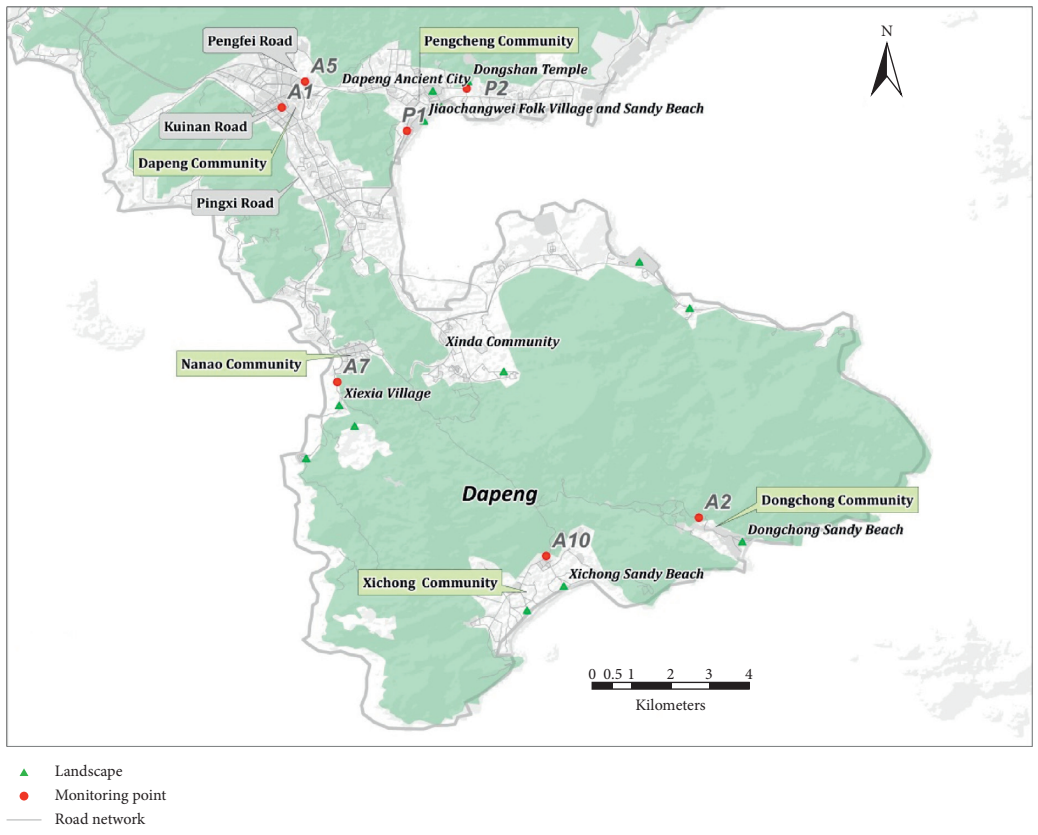

Figure 2: Distribution of monitoring points for tourist traffic flow.

Table 1: Car tourists detected at monitoring points.

Label	Location	Detected car tourists
*A*1	Kuinan Road	Dapeng Community and Xinda Community
*A*2	Dongchong Road	Dongchong Community
*A*5	Pengfei Road	Dapeng community and Dapeng Ancient City, Jiaochangwei Folk Village, Dongshan Temple
*A*7	Fumin Road	Nan'ao Community
*A*10	Nanxi Road	Xichong Community
*P*1	Jiaochangwei Park Lots	Jiaochangwei Folk Village
*P*2	Ancient City Park Lots	Dapeng Ancient City, Dongshan Temple

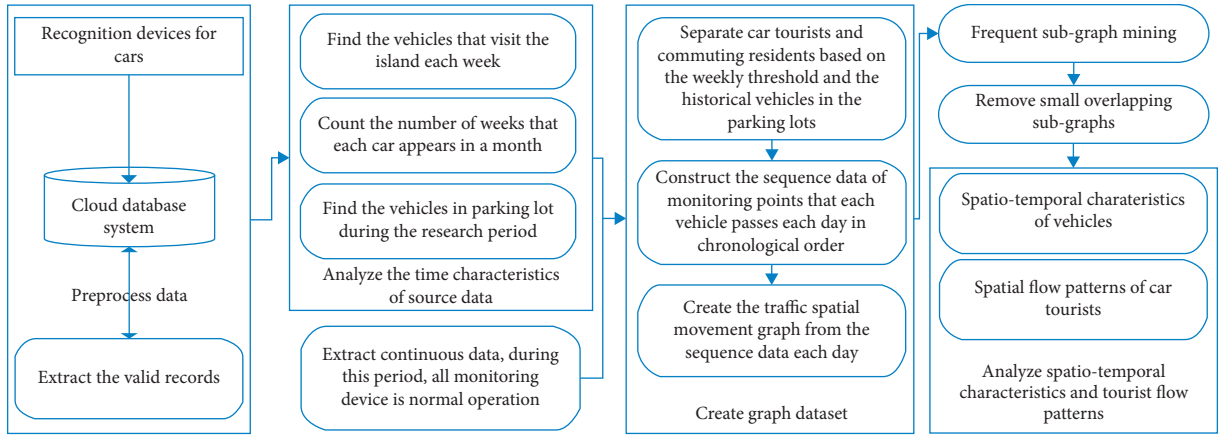

Figure 3: The detailed steps for mining frequent patterns in tourist flow.

(1) Deleted irrelevant fields: The primary information such as car license plate number, label of monitoring device, and collection time is retained.

(2) Removed null values and corrected license plate attributions.

(3) Eliminated invalid data, such as special car license plates and duplicate data.

(4) Corrected confusing letters and numbers in car license plates.

5.2. Identifying Car Tourists. In this study, tourist flow was divided into three types. One type consisted of commuters on the island, the next consisted of intracity tourists (local weekend tourists in Shenzhen), and the last type consisted of intercity tourists (leisure tourists from outside of Shenzhen). The collected data came from the cameras on the roads and in parking lots. These three types of flows were mixed together in the collected data. It is necessary to separate the different types of traffic flows. The detailed steps are shown in Figure 4.

The data collected from the parking lots were classified into intracity tourists and intercity tourists according to the registration location of car license plates.

As we know, the number of trips made by tourists and local commuters is different. Tourists only visit the island occasionally on weekends or holidays. Local residents on the island might drive more times per week. Therefore, we took a week as a unit and determined if a car had visited the island during that week. If so, this car would be tagged once. Then, we counted the number of weeks a car appeared in each month. If the number of weeks visited exceeded a predefined threshold, this car was considered to be a commuter. Otherwise, this car was considered to be a tourist.

Therefore, for the data collected from roads, we first set a threshold manually based on the statistics of the number of weeks visited in one month to distinguish island commuters and tourists. Next, we categorized visitors into intracity car tourists and intercity car tourists based on where their license plates are registered. Finally, different types of traffic flows were separated and aggregated.

In order to verify the usability and reliability of the proposed method, the visiting characteristics of all cars were analyzed. The result is shown in Figure 5. As can be seen, the proportion of weeks in one month in which the car appears is the highest, reaching 88.86%. The percentage of cars appearing on the island for less than two weeks is 95%. In addition, we counted the percentage of cars in the parking lots relative to the total number of cars. The ratio is 78.6%, which is close to the ratio of 79% counted by Dapeng Transportation Bureau during peak tourist periods. The ratio of the number of weeks visited in one month (88.86%) is greater than the statistical result of Transportation Bureau (79%). We think that the Transportation Bureau only considered the tourists in parking lots. Therefore, the threshold in this study is one week for extracting car tourists.

5.3. Reconstructing the Spatial Movement Graphs. In order to model the flow patterns of car tourists, labeled direct graphs are used to construct movement relationships between monitoring points. In particular, each vertex of the direct

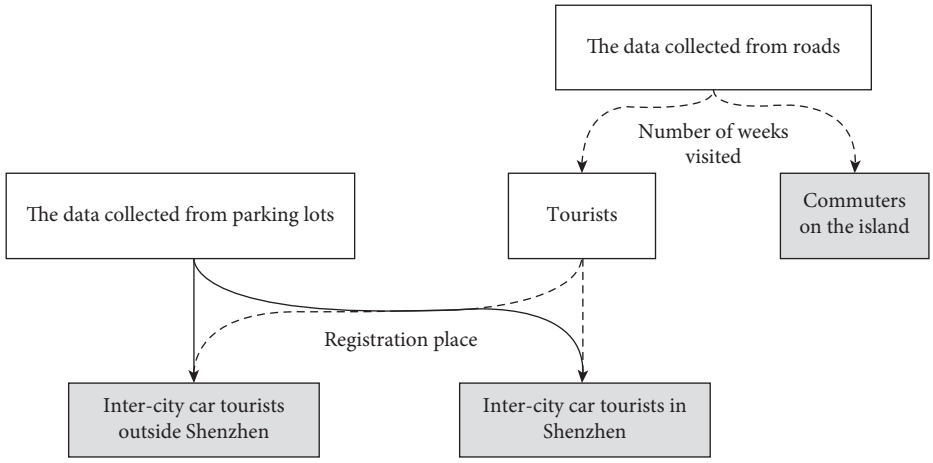

Figure 4: The workflow of traffic flow separation.

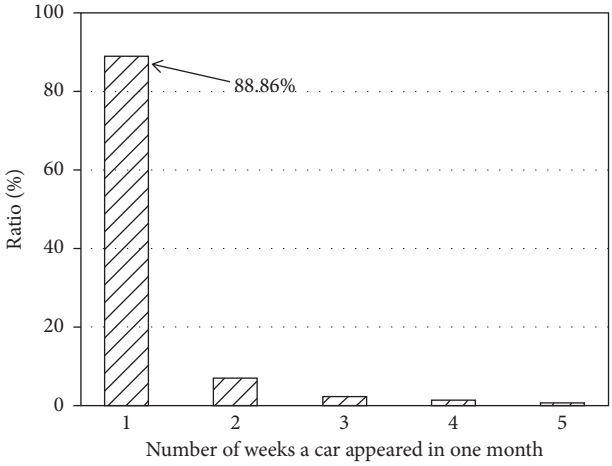

Figure 5: Number of weeks visited by tourists in one month.

graph corresponds to a monitoring point, and each edge corresponds to a directed connection between two monitoring points passed by car tourists. The related definitions are as follows:

Definition 1. Label Graph. Given a set of vertices $V = \{v_1, v_2, \ldots, v_k\}$, a set of edges connecting two vertex in V, $E = \{e_h = (v_i, v_j) | v_i, v_j \in V\}$, a set of vertex labels $L(V) = \{lb(v_i) | \forall v_i \in V\}$, and a set of edge labels $L(E) = \{lb(e_h) \mid \forall e_h \in E\}$, e_h is a direct edge that has the start vertex v_i and end vertex v_j, then a label graph G is represented as

$$G = (V, E, L(V), L(E)). \quad (1)$$

In the graph dataset, the label of an edge is represented by a label pair of two monitoring points in the tourist visiting order. A graph consists of edges connecting the monitoring points visited by each tourist in one day. The advantage of using the vertex label pair as an edge label is that it maintains the temporal and spatial order of the two monitoring points that tourists pass through. When mining a labeled graph, the spatial-temporal order of monitoring points in results could be preserved. Using this representation, the problem of finding frequent flow patterns of car tourists becomes a problem of mining frequent subgraphs in all movement graphs.

5.4. Mining Frequent Subgraphs. Some definitions related to frequent subgraph mining are given below.

Definition 2. Subgraph. A subgraph $g_2 = (V_2, E_2)$ of graph g_1 is a graph in which $V_2 \subseteq V_1$, $E_2 = E_1 \cap (V_2 \times V_1)$

Definition 3. Support of a subgraph g. Given a labeled graph dataset $G_D = \{g_1, g_2, \ldots, g_n\}$, the support or frequency of a subgraph g is the percentage (or number) of graphs in G_D.

Definition 4. Frequent subgraph. A frequent subgraph is a graph whose support is not less than a minimum support threshold. The minimum support threshold represents the minimum number of occurrences of a subgraph. To obtain the frequent patterns, we chose to manually set the value of minimum threshold.

Definition 5. Mini Code. First, a depth-first search is performed on the graph to form a DFS (depth-first search) tree, and then this tree is scanned. The order of the scanned edges constitutes a sequence called the DFS Code. The DFS Codes are sorted in a lexicographic order to find the smallest DFS code that uniquely identifies the graph. This minimum DFS Code is called the mini Code.

After constructing the movement graphs of tourist flow, the subgraph mining method was used to explore the frequent patterns. As demonstrated in related works, there are many kinds of subgraph mining algorithms. The AGM (Apriori-based Graph Mining) [41] can discover all frequent subgraphs (both connected and disconnected) in a graph database that satisfy a specific minimum support constraint. This algorithm uses an approach similar to Apriori, and it requires 40 minutes to 8 days to find the result subgraphs in a dataset containing 300 chemical compounds. The algorithm FSG (finding frequently occurring subgraphs in large graph) [42] adopts an adjacent representation of a graph and an edge-

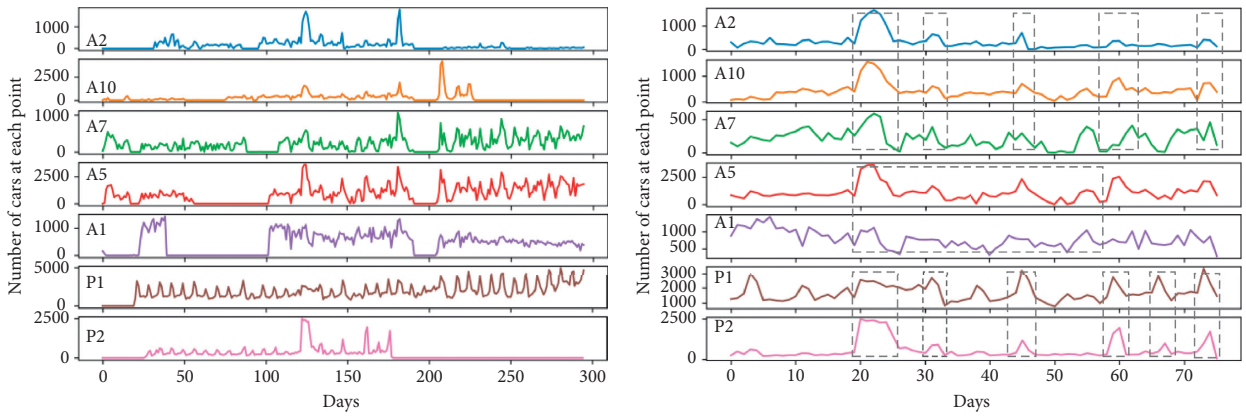

Figure 6: Daily traffic flow at each monitoring point.

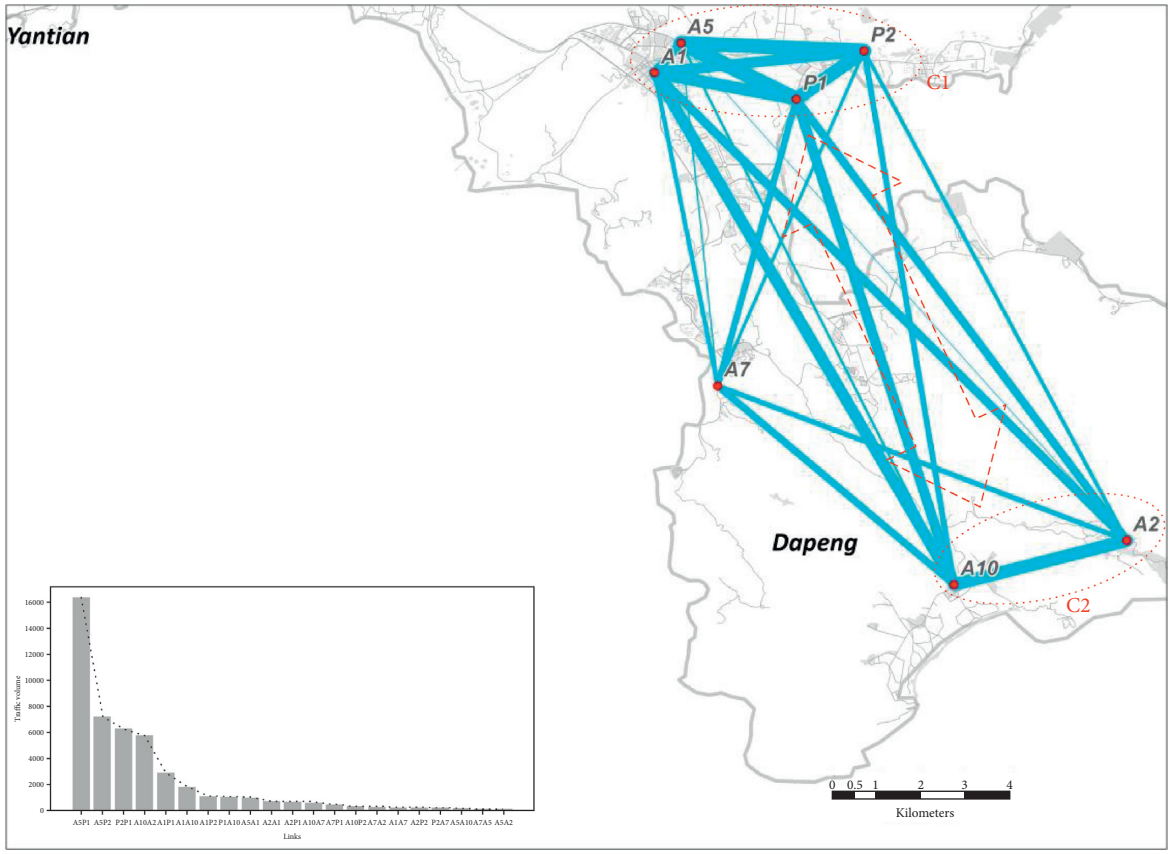

Figure 7: Flow map of tourism traffic.

Table 2: Types of car tourist visiting the island.

Types	Number of records	Number of graphs
All car tourists	361693	76
Intracity car tourists in Shenzhen	240452	76
Intercity car tourists outside Shenzhen	121241	75

growing strategy to find all of the connected subgraphs that frequently appear in a graph database. The results have shown that FSG can be finished in 600 seconds. gSpan [26] is designed to reduce or avoid the candidate generation and pruning false positives used in AGM and FSG. gSpan can complete the same task in 10 seconds. Considering the efficiency, in this study, gSpan was used to mine frequent subgraphs in a directed graph dataset and then find the

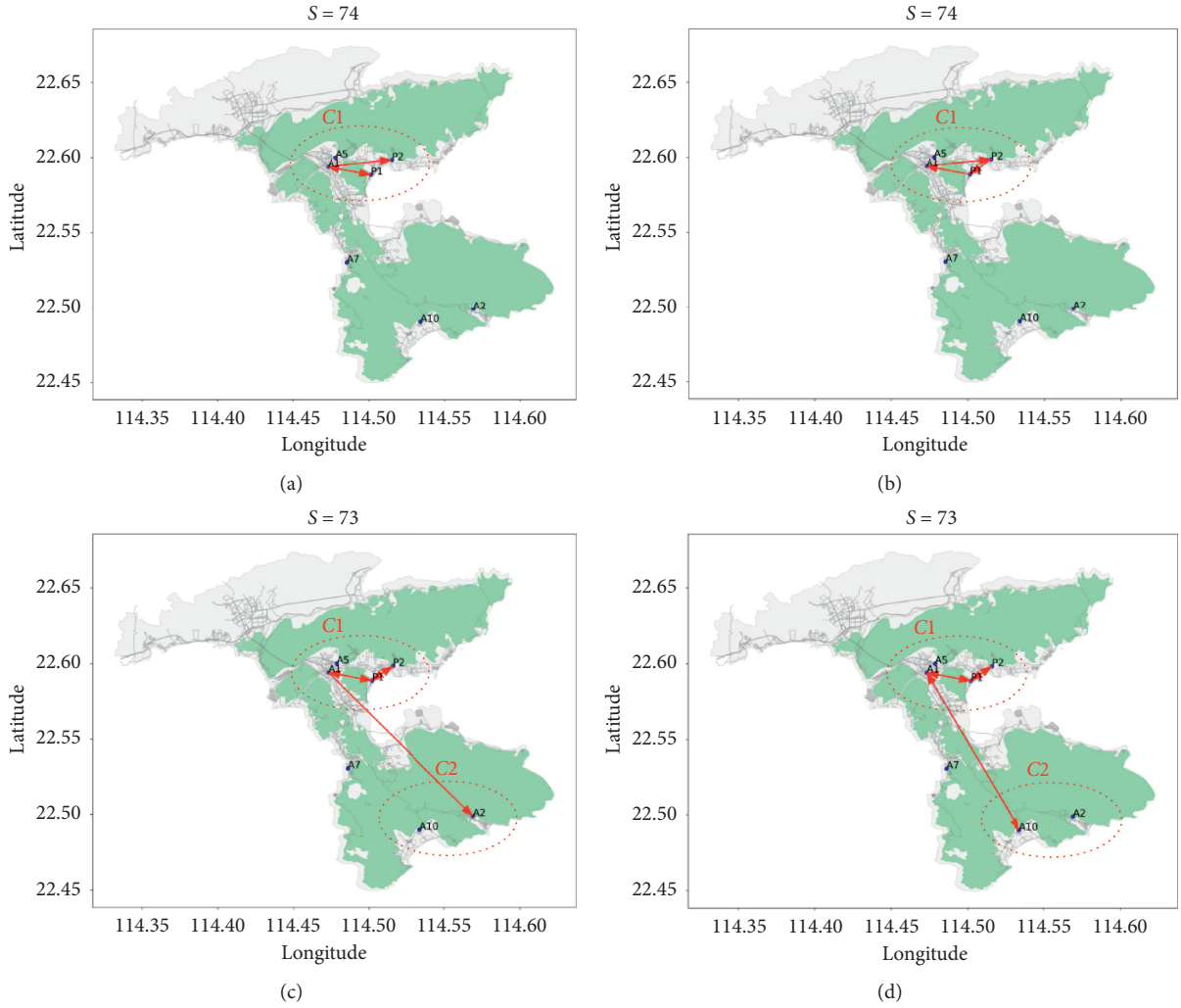

Figure 8: Flow patterns inferred from intracity tourists.

Table 3: The list of flow patterns inferred from intracity tourists.

Figures	Patterns
Figure 8(a)	$(A1 \longrightarrow P2$ and $A1 \Leftrightarrow P1)$
Figure 8(b)	$A1 \longrightarrow P2 \longrightarrow P1 \longrightarrow A1$
Figure 8(c)	$A1 \longrightarrow A2$ and $A1 \Leftrightarrow P1 \Leftrightarrow P2$
Figure 8(d)	$A1 \longrightarrow A10$ and $A1 \Leftrightarrow P1 \Leftrightarrow P2$

frequent subgraphs with maximum length in the results as the flow patterns of car tourists. The algorithmic details of gSpan are available in reference [26]. An extended instruction is given below. The method consisted of two steps: (1) Finding the frequent subgraphs using gSpan: First, the frequencies of edges and nodes of all graphs was calculated. Second, the frequencies were compared with the minimum support threshold and the infrequent edges and nodes were removed. Then, the remaining nodes and edges were reordered according to the frequency. And, the frequency of each edge was calculated again. Finally, the subgraphs of the restored graph were mined according to mini Code and it was determined whether the current DFS encoding is the minimum code or not. If so, current edges were added to the results, and further attempts were made to add possible edges. If not, the mining process was finished. (2) Finding frequent subgraphs with maximum length: There are a large number of subgraphs in the obtained results, and some subgraphs are partial graphs of the others. Therefore, this kind of subgraph was deleted by comparing the labels of nodes and edges, and the final results were the maximum frequent subgraphs.

6. Results

In this section, we first analyzed the spatial and temporal distribution of tourist flows by statistical methods and maps. Then, we divided the tourist flows into intracity car tourists and intercity car tourists and used a frequent subgraph mining algorithm for pattern recognition. Finally, we summarized the movement patterns of all tourists.

6.1. Spatial-Temporal Characteristics of the Tourist Traffic Flow

6.1.1. Temporal Characteristics. Figure 6(a) depicts 295 days of data before any preprocessing was applied. Due to

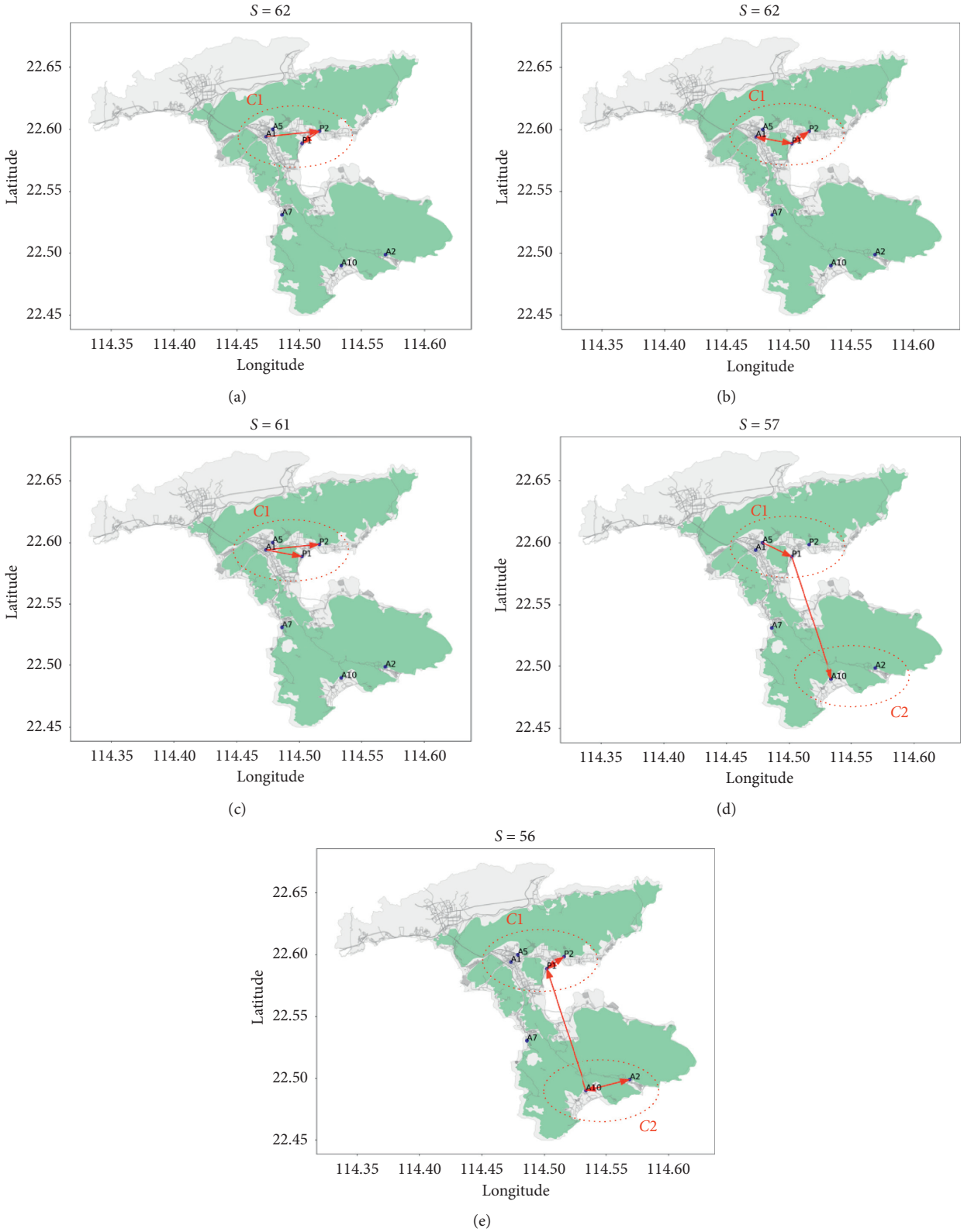

Figure 9: Flow patterns inferred from intercity tourists.

Table 4: The list of the flow patterns inferred from intercity tourists.

Figures	Patterns
Figure 9(a)	$A1 \longrightarrow P2 \longrightarrow P1$
Figure 9(b)	$A1 \Leftrightarrow P1 \Leftrightarrow P2$
Figure 9(c)	$A1 \longrightarrow P1$ and $A1 \longrightarrow P2$
Figure 9(d)	$A5 \longrightarrow P1 \longrightarrow A10$
Figure 9(e)	$A10 \longrightarrow P1 \Leftrightarrow P2$ and $A10 \Leftrightarrow A2$

the failure of device communication or power, the constructed movements graphs may be incomplete, which would lead to the loss of frequent subgraphs. Therefore, we selected 76 days of valid data as the dataset for frequent pattern mining. Figure 6(b) shows that (1) the tourist flows at $A2$ and $A10$ near the sandy beaches has similar temporal characteristics. Their peak hours of tourist volume occur both on holidays and weekends, while on weekdays, the flow curves are relatively stable. (2) $P1$ and $P2$ are located in two parking lots. Although there are differences in the tourist volumes, the trends are similar. (3) For the two entrances to the tourist attractions, the average daily volume of tourist traffic at $A1$ is 0.7 times that of $A5$. After sorting the volume of tourist traffic, Pengcheng Community has the most car tourists, followed by two tourist attractions with a sandy beach (i.e., Dongchong and Xichong Community), and the least visited attraction is Nanao Community.

6.1.2. Spatial Characteristics. Figure 7 shows the flow map of the aggregated tourists transferring in multiple monitoring point pairs. The tourist volumes are depicted and sorted in the left bar chart in the figure, and the link thickness represents the traffic volume. As can be seen, the links with the largest traffic volume are $A5\,P1$, $A5\,P2$, $P2\,P1$, $A10\,A2$, $A1\,P1$, and $A1\,P2$ ($A5\,P1$ is a simplified form for $A5 \leftrightarrow P1$, which represents the forth and back tourist flow between $A5$ and $P1$). These links could be divided into two areas, $C1\,(A1, A5, P1, P2)$ and $C2\,(A2, A10)$. Further inspection reveals that the number of tourists transferring between $P1$ and $P2$ in area $C1$ is close to the value between $A2$ and $A10$ in area $C2$, but the number of tourists visiting $P1$ and $P2$ is 3.12 times that of $A2$ and $A10$.

6.2. Analyses of the Detected Flow Patterns. The flow map is intuitive, but it suffers from serious visual clutter, and it is difficult to read because of overlapping flows. It can also be seen in Figure 7 that the flow map only shows the traffic volumes between the monitoring points in the tourist destination. But, it could not express the spatial transfer directions of car tourists. Therefore, these facts motivate us to find a new approach to solve these problems. This section describes the use of frequent subgraph mining algorithm to explore the spatial flow patterns with directions in tourist traffic and to obtain the maximum frequent patterns from the daily tourist movement graphs according to a predefined minimum support threshold. By using the identification method of car tourists introduced in Section 5, two types of data were extracted and used for the subsequent flow pattern mining (listed in Table 2).

6.2.1. Flow Patterns of Intracity Tourists in Shenzhen. The experiments were conducted with the dataset of intracity car tourists in Shenzhen (as shown in Table 2). The minimum support threshold for gSpan was set to 73. The spatial flow patterns are represented in Figure 8 and listed in Table 3. The inferred patterns could be divided into two groups. One group consists of the patterns shown in Figures 8(a) and 8(b), which show the tourist spatial transfer process in area $C1$. The other group contains the patterns shown Figures 8(c) and 8(d), which represent the tourists transferring between area $C1$ and area $C2$. The two groups demonstrate that the intracity car tourists who arrived at $P1$ and $P2$ preferred to choose Kuinan Road at $A1$ instead of Pengfei Road at $A5$. The difference between Figures 8(a) and 8(b) is the existence of the circle tourist flow. The difference between Figures 8(c) and 8(d) is the presence of tourists flow back and forth. The tourist flow from $A1$ to $A2$ have only one direction. One of the reasons may be that this study failed to find a suitable monitoring point on Pingxi Road, resulting in the loss of directionality for this part of tourist flow.

6.2.2. Flow Patterns of Intercity Car Tourists. Figure 9 shows flow patterns of intercity car tourists. The dataset used in this section is composed of intercity tourists (as shown in Table 2). The minimum support threshold for gSpan was set to 56. The result flow patterns are sorted by the support threshold, as listed in Table 4.

From these patterns, the following could be concluded. (1) The most frequent patterns are shown in Figures 9(a)–9(c). The frequencies of the discovered flow patterns are 62, 62, and 61, respectively. These three patterns describe the preference of intercity tourists for area $C1$. This kind of tourists first visited one of attractions near a parking lot $P1$ or $P2$ and then visited another attraction, or just visited one tourist attraction near $P1$ or $P2$. (2) The above three patterns are different from those of the intracity tourists in Shenzhen. There is no circle tour between $P1$, $P2$, and $A1$. The reason for this is that some tourists chose to continue drive to area $C2$. (3) The minimum support threshold of these two patterns, as shown in Figures 9(d) and 9(e), is significantly smaller than that shown in Figures 9(a)–9(e), but it reflects the spatial transfer preferences of tourists from neighboring cities in areas $C1$ and $C2$. In Figure 9(d), the car tourists tended to drive directly from $A5$ to $A10$ after visiting

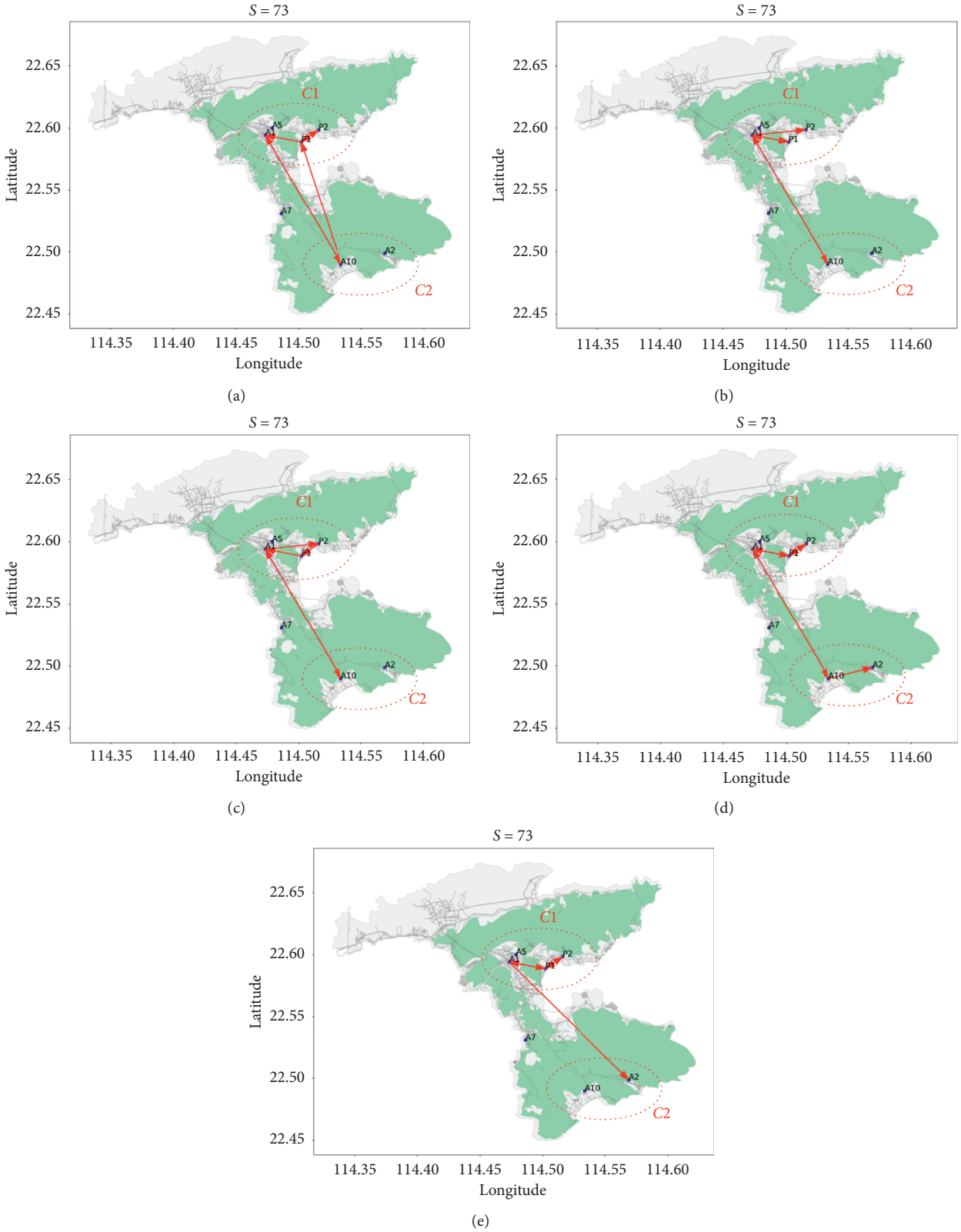

Figure 10: Flow patterns of all tourists.

attractions near $P1$. As shown in Figure 9(e), the car tourists that flowed between $A10$ and $A2$ went back to $P1$ and changed car parking lots between $P1$ and $P2$. However, there is no tourist flow to $A1$ and $A5$. The reason for this may be that the traffic flow of Pingxi Road (the expressway in and out of the peninsula) was not

Table 5: The list of flow patterns inferred from all tourists.

Figures	Patterns
Figure 10(a)	$(A1 \longrightarrow A10 \longrightarrow A1)$ and $(A10 \longrightarrow P1 \Leftrightarrow P2)$ and $(P1 \longrightarrow A1)$
Figure 10(b)	$(A1 \Leftrightarrow A10$ and $A1 \longrightarrow P1$ and $A1 \longrightarrow P2)$
Figure 10(c)	$(A1 \Leftrightarrow P10$ and $A1 \longrightarrow P2 \longrightarrow P1 \longrightarrow A1)$
Figure 10(d)	$(A1 \Leftrightarrow P1 \Leftrightarrow P2$ and $A1 \Leftrightarrow A10 \Leftrightarrow A2)$
Figure 10(e)	$(A1 \Leftrightarrow P1 \Leftrightarrow P2$ and $A1 \longrightarrow A2)$

monitored. This part of traffic flow could directly arrive and then leave from $A10$.

6.2.3. Flow Patterns of All Tourists. This section presents an exploration of the spatial flow patterns of all car tourists. The results are shown in Figure 10. The minimum support threshold for gSpan was set to 73, which means that 73 of the 76 graphs contained the discovered flow pattern. The result patterns are listed in Table 5.

All of the patterns shown in Figure 10 have tourist flow between area $C1$ and area $C2$. This is consistent with the trend in the flow map (shown in Figure 7). As the picture shows, $A1$ is the main entrance for tourists to enter and exit Dapeng Island. Some of the car tourists drove to $P1$ or $P2$, and the rest flowed to $A10$ or $A2$. Figures 10(a)–10(c) show the directions of tourist flows between the Dapeng Community, Pengcheng Community, and Xichong Community. Figure 10(d) shows the directions of tourist flows between Dapeng Community, Pengcheng Community, and Dongchong Community. Figure 10(e) represents only the directions of tourist flows between Dapeng Community and Dongchong Community. Furthermore, the directions of tourist flows in area $C1$ and area $C2$ or between area $C1$ and area $C2$ are different. Taking Figures 10(a)–10(c) as examples, although the orders of $P1$ and $P2$ that are accessed from $A1$ have a lack of regularity, they have their own characteristics when considering the accompanying paths to $A10$. These examples indicate that if there is a tourist flow between $A1$ and $A10$, it could be divided into two cases. In one case, some of the tourists returned directly, and in the other case, some of the tourists flowed to $P1$. In the first case, either the tourist flow passing by $A1$ first accessed $P2$ and then visited $P1$, or both $P1$ and $P2$ had tourists at the same time. In the second case, some of the tourists returned from $A10$, visited $P1$ and $P2$, and then left the island.

7. Conclusions and Discussions

7.1. Conclusions. In order to facilitate the management of tourist traffic flow, the car tourists in Dapeng Island were taken as a research case. The experimental analysis used real data captured by video devices in the research area. Due to the lack of suitable device installation locations, the captured picture from the video device had a certain distance from the road. The catch rate of the tourists' cars was low. However, the detailed time-series data in one day could be collected. Compared with the manual survey, the collected data was improved in terms of reliability and richness. A day was chosen as the time unit for frequent pattern mining. After selecting the available data, we divided the data of cars into intracity and intercity tourists. Next, the license plate data were transformed into movement graphs according to the visited location sequence between multiple monitoring points. The intricate flow patterns of the car tourists were discovered by gSpan algorithm, which had the best performance in terms of the quality of the results and the execution time and which had already proven to be efficient for frequent subgraph mining. The conclusions are as follows:

(1) The car tourists had obvious preferences in the selection of trip time and tourist attractions (shown in Figures 6 and 7). In terms of time, the curves of tourist flow at each monitoring point were similar. There were a large number of car tourists at various attractions on holidays, but the volume of car tourists was relatively lower on weekdays. The same types of attractions had the similar trends in tourist flow, such as the two attractions with a sandy beach (Dongchong Community and Xichong Community) and the ancient city and cultural attractions (Dapeng Ancient City and Dongshan Temple). In terms of space, the attractions that are close to the entrance of a scenic area and rich in tourist resources were more popular with tourists. However, due to the terrain barrier in the scenic area, the traffic conditions affected the movements of tourists between multiple attractions.

(2) Different types of car tourists had similar spatial choices in scenic area (shown in Figures 8–10). For example, different types of tourists had flow patterns that described the movements in one area (as shown in Figures 8(a), 8(b) and 9(a)–9(c)) and the movements between different areas (as shown in Figures 8(c), 8(d), 9(d), and 9(e)). The intercity tourists and intracity tourists had different choices in scenic spots. The intercity tourists would take multidestination trips instead of single destination trips in the same type of attractions. As can be seen in Figures 8 and 9, there are the two sandy beach attractions in area $C2$, the intracity tourists tend to visit one of them, while the intercity tourists would visit both attractions. Specifically, to save time and money, intercity tourists would visit multiple attractions in one trip instead of making multiple trips. Additionally, another difference was that there was no circlet in area $C1$ for intercity tourists and no traffic flow between $A2$ and $A10$ for intracity tourists.

(3) Although the patterns depicted on the map look complicated and messy, after the patterns are converted to rules, they become clear. In pattern maps, only Figures 8(b), 9(a), and 9(d) show a clear unidirectionality. The rest is complex and is difficult to compare. As we can see from Figure 8(a), the intracity tourists passing point $A1$ could be divided into two groups, one group flowed to parking lot $P1$, and then leaved the scenic area from $P1$. The other group flowed to parking lot $P2$. Two groups have simultaneity in tourist routes. So, we could convert the flow patterns to rules and use "and" to illustrate the simultaneity of different routes in the same pattern (as shown in Tables 3–5). By this way, all patterns can be applied to traffic control system for regional tourism.

(4) Large primary attractions are more attractive than smaller secondary attractions. Looking from the arrow on the pattern maps, tourists always visit area $C1$ first and then select area $C2$. The main reason is that area $C1$ has abundant tourism resources and diverse tourism activities. For example, there are cultural attractions (e.g., Dapeng Ancient City and Dongshan Temple), sandy beach entertainments, and large parking lots for tourists in area $C1$. These factors are also often considered in the evaluation of the importance of attractions in tourism network.

(5) The tourists tended to park their cars in an easy-to-access place, even if the visited attractions are changed, as shown in Figures 8(a)–8(d), 9(b), and 9(e). Again, here we take area $C1$ as an example. The distance between the Dapeng Ancient City and Dongshan Temple is about 1 km. On the pattern maps, we can see that there are two-way arrows pointing to the two parking lots $P1$ and $P2$. This indicates that the car tourists tended to park their cars to the nearest parking lot, so that they could pick them up when the tour destination is changed.

7.2. Discussions. Tourist flow is the key to traffic management in tourism destinations, and it affects the development of tourism on an island and the experience of tourists. The recent development of transport technologies has shown that traffic flow data will be increasingly collected and it will be available for data analysis. Therefore, advanced data analytics should be used to interpret and depict the complex movements of car tourists. The proposed approach in this study was intended to find (i) the statistical summaries of the spatial-temporal characteristics of car tourists in the research area, helping to discover patterns from the mass car license plate data; (ii) the flow patterns of intercity and intracity tourists, helping to illustrate the different preferences of the two types of car tourists; and (iii) the most frequent patterns of all tourists, helping to identify the law of tourist movement and make efficient policy for the management of tourist traffic flow. The presented approach enriched the analytical methodology of tourist traffic flow and suggested a shift from the conventional and complicated paper or computer interview-based method to a dynamic flow graph-based method. Furthermore, we have shown how transportation data provides hard-to-obtain insights and quantitative results for tourists.

In order to illustrate the law of spatial movement of tourists, related studies have proposed a variety of macro flow patterns [43–45]. For example, in 2008, McKercher [46] proposed 11 prominent route styles in urban destinations. The macropatterns retain only the main components and simplify the details and are often used in tourism management to guide destination development. Compared with modeling the flow patterns of tourists at the macrolevel, modeling tourist flow at the microscale is more complicated. Lew and McKercher [17] noted that it is a challenge to balance model effectiveness and usability. The reason is that simple patterns may not provide enough details for use and complex patterns may be difficult to interpret and apply. In this study, we used the video devices installed at key nodes of road network to collect tourist traffic flows and used the frequent subgraph mining algorithm to discover flow patterns at the microscale. The extracted patterns can be converted into rules and applied to the traffic control system for the management of regional tourists. The difficulty of finding and applying patterns at microscale could be overcome by this way.

During the peak period of tourism, the number of car tourists in the scenic area increases sharply. It is easy to result in road congestion and uneven distribution of tourists between attractions. With the use of traffic flow data, the daily, monthly, and seasonal characteristics of tourists can be analyzed, the future tourist flow can be predicted, and the flow patterns can be obtained by data mining methods. Thus, the traffic management department can effectively control the tourist traffic flow, and the tourism department can develop attractive tourism products to achieve a spatial balance of the distribution of tourists, reduce traffic congestion and harmful gas emissions and weaken the impact of tourism environment and human body.

Inside a scenic area, attractions form a complex network of tourist flow due to the frequent spatial interaction. Each attraction is both the origin and destination of car tourists. Due to the differences in attractiveness, degree of development, and convenience of transportation, tourists have shown special preferences when choosing attractions and trip routes. Accordingly, effective identification of these preferences will be beneficial to the development of tourist market and will also helpful for tour planners to understand how tourists see the spatial connection of multiple attractions. However, traditional manual surveys are time-consuming and laborious, and the amount of data obtained is small. It is difficult to reveal tourist preferences by this way. Frequent subgraph mining algorithms provide a desirable method for identifying the spatial preferences of tourists. This kind of method could perform well under the support of a large amount of movement data between attractions.

This study has several limitations. Firstly, due to lack of power supply facilities, it was unable to collect the traffic data for each day. When applying the model to the actual control of tourist traffic flow, it is necessary to further co-operate with the traffic management department to obtain comprehensive traffic flow data. Secondly, this study focused on the mining of flow patterns, the influencing factors behind the identified patterns were not further analyzed. As mentioned by Lew and McKercher [17], factors related to tourists and destinations can affect how tourists move or travel in a destination. These factors include family composition, income, and valid information obtained before travelling. It is difficult to obtain these factors by relying only on the traffic flow data collected in the traffic monitoring system. Therefore, in future work, field investigation will be necessary.

Data Availability

As the data also form part of an ongoing study, the raw data needed to reproduce these findings cannot be shared at this time.

Conflicts of Interest

The authors declare no conflicts of interest.

Acknowledgments

The authors gratefully acknowledge the support of this research from the National Science Foundation of China (41701167) and the Basic Research Project of Shenzhen City (JCYJ20170307164104491 and JCYJ20190812171419161).

References

[1] D. W. Eby and L. J. Molnar, "Importance of scenic byways in route choice: a survey of driving tourists in the United States," *Transportation Research, Part A (Policy and Practice)*, vol. 36, no. 2, pp. 95–106, 2003.

[2] B. Wang, Z. Yang, F. Han, and H. Shi, "Car tourism in xinjiang: the mediation effect of perceived value and tourist satisfaction on the relationship between destination image and loyalty," *Sustainability*, vol. 9, no. 1, pp. 1–16, 2016.

[3] X. M. Zhang and Q. Y. Pen, "A study on tourism information and self-driving tour traffic," in *Proceedings of the First International Conference on Transportation Engineering*, Southwest Jiaotong University, Chengdu, China, July 2007.

[4] China National Tourism Administration, *The Yearbook of China Tourism Statistics 2016*, China Travel & Tourism Press, Beijing, China, 2017.

[5] M. A. Mohamad Toha and H. N. Ismail, "A heritage tourism and tourist flow pattern: a perspective on traditional versus modern technologies in tracking the tourists," *International Journal of Built Environment and Sustainability*, vol. 2, no. 2, pp. 85–92, 2015.

[6] K. Siła-Nowicka and A. S. Fotheringham, "Calibrating spatial interaction models from gps tracking data: an example of retail behaviour," *Computers, Environment and Urban Systems*, vol. 74, pp. 136–150, 2019.

[7] F. Mao, M. Ji, and T. Liu, "Mining spatiotemporal patterns of urban dwellers from taxi trajectory data," *Frontiers of Earth Science*, vol. 10, no. 2, pp. 205–221, 2016.

[8] L. J. Zheng, D. Xia, X. Zhao, and W. L. Liu, "Mining trip attractive areas using large-scale taxi trajectory data," in *Proceedings of the 2017 IEEE International Symposium on Parallel and Distributed Processing with Applications and 2017 IEEE International Conference on Ubiquitous Computing and Communications*, pp. 1217–1222, ISPA/IUCC, Guangzhou, China, December 2017.

[9] I. Rami and M. O. Shafiq, "Detecting taxi movements using random swap clustering and sequential pattern mining," *Journal of Big Data*, vol. 6, no. 39, pp. 1–26, 2019.

[10] G. Kautsar and S. Akbar, "Trajectory pattern mining using sequential pattern mining and k-means for predicting future location," *Journal of Physics: Conference Series*, vol. 801, no. 1, 2017.

[11] D. Guo, X. Zhu, H. Jin, P. Gao, and C. Andris, "Discovering spatial patterns in origin-destination mobility data," *Transactions in GIS*, vol. 16, no. 3, pp. 411–429, 2012.

[12] J. D. Mazimpaka and S. Timpf, "A visual and computational analysis approach for exploring significant locations and time periods along a bus route," in *Proceedings of the 9th ACM SIGSPATIAL International Workshop on Computational Transportation Science*, pp. 43–48, San Francisco, CA, USA, October 2016.

[13] H. Faroqi, M. Mesbah, and J. Kim, "Spatial-temporal similarity correlation between public transit passengers using smart card data," *Journal of Advanced Transportation*, vol. 2017, Article ID 1318945, 14 pages, 2017.

[14] Z. Wang, Y. Hu, P. Zhu, Y. Qin, and L. Jia, "Ring aggregation pattern of metro passenger trips: a study using smart card data," *Physica A: Statistical Mechanics and Its Applications*, vol. 491, pp. 471–479, 2018.

[15] X. Zhao, X. Lu, Y. Liu, J. Lin, and J. An, "Tourist movement patterns understanding from the perspective of travel party size using mobile tracking data: a case study of Xi'an, China," *Tourism Management*, vol. 69, pp. 368–383, 2018.

[16] M. Versichele, L. De Groote, M. Claeys Bouuaert, T. Neutens, I. Moerman, and N. Van De Weghe, "Pattern mining in tourist attraction visits through association rule learning on bluetooth tracking data: a case study of ghent, Belgium," *Tourism Management*, vol. 44, pp. 67–81, 2014.

[17] A. Lew and B. Mckercher, "Modeling tourist movements," *Annals of Tourism Research*, vol. 33, no. 2, pp. 403–423, 2006.

[18] A. Birenboim, S. Anton-Clavé, A. P. Russo, and N. Shoval, "Temporal activity patterns of theme park visitors," *Tourism Geographies*, vol. 15, no. 4, pp. 601–619, 2013.

[19] H. J. Yun and M. H. Park, "Time-space movement of festival visitors in rural areas using a smart phone application," *Asia Pacific Journal of Tourism Research*, vol. 20, no. 11, pp. 1246–1265, 2015.

[20] S. Kang, "Associations between space-time constraints and spatial patterns of travels," *Annals of Tourism Research*, vol. 61, pp. 127–141, 2016.

[21] C. Comito, D. Falcone, and D. Talia, "Mining human mobility patterns from social geo-tagged data," *Pervasive and Mobile Computing*, vol. 33, pp. 91–107, 2016.

[22] Y. T. Zheng, Y. Li, Z. J. Zha, and T. S. Chua, "Mining travel patterns from GPS-tagged photos," in *Lecture Notes in Computer Science*, K. T. Lee, W. H. Tsai, H. Y. M. Liao, T. Chen, J. W. Hsieh, and C. C. Tseng, Eds., Springer, Berlin, Germany, 2011.

[23] K. M. Borgwardt, H. P. Kriegel, and P. Wackersreuther, "Pattern mining in frequent dynamic subgraphs," in *Proceedings of the 6th IEEE International Conference on Data*

Mining (ICDM 2006), Hong Kong, China. IEEE, December 2006.

[24] D. J. Cook and L. B. Holder, *Mining Graph Data*, Wiley Press, Hoboken, NJ, USA, 2015.

[25] C. Jiang, F. Coenen, and M. Zito, "Frequent sub-graph mining on edge weighted graphs," in *Lecture Notes in Computer Science*, T. Bach Pedersen, M. K. Mohania, and A. M. Tjoa, Eds., Springer, Berlin, Germany, pp. 77–88, 2010.

[26] X. Yan and J. Han, "gSpan: graph-based substructure pattern mining," in *Proceedings of the 2002 IEEE International Conference on Data Mining, ICDM'02*, pp. 721–724, IEEE Computer Society, Maebashi City, Japan, December 2002.

[27] C. Borgelt and M. R. Berthold, "Mining molecular fragments: finding relevant substructures of molecules," in *Proceedings of the 2002 IEEE International Conference on Data Mining, ICDM'02*, pp. 51–58, IEEE Computer Society, Maebashi City, Japan, December 2002.

[28] J. Huan, W. Wang, and J. Prins, "Efficient mining of frequent subgraphs in the presence of isomorphism," in *Proceedings of the Third IEEE International Conference on Data Mining, ICDM'03*, pp. 549–552, IEEE Computer Society, Melbourne, FL, USA, November 2003.

[29] S. Nijssen, "A quickstart in frequent structure mining can make a difference," in *Proceedings of the Tenth ACM SIGKDD International Conference on Knowledge Discovery and Data Mining, KDD'04*, pp. 647–652, ACM, Seattle, WA, USA, August 2004.

[30] J. Huan, W. Wang, J. Prins, and J. Yang, "SPIN: mining maximal frequent subgraphs from graph databases," in *Proceedings of the Tenth ACM SIGKDD International Conference on Knowledge Discovery and Data Mining*, Seattle, WA, USA, ACM, August 2004.

[31] M. Wörlein, T. Meinl, I. Fischer, and M. &Philippsen, "A quantitative comparison of the subgraph miners MoFa, gSpan, FFSM, and gaston," in *Proceedings of the 9th European Conference on Principles and Practice of Knowledge Discovery in Databases PKDD'05*, Springer, Porto, Portugal, pp. 392–403, 2005.

[32] X. Yan, H. Cheng, J. Han, and P. &Yu, "Mining significant graph patterns by leap search," in *Proceedings of the 2008 ACM SIGMOD*, pp. 433–444, Vancouver Canada, June 2008.

[33] L. T. Thomas, S. R. Valluri, and K. Karlapalem, "Margin: maximal frequent subgraph mining," in *Proceedings of the Sixth International Conference on Data Mining (ICDM'06)*, Hong Kong, China, December 2006.

[34] V. Ingalalli, D. Ienco, and P. Poncelet, "Mining frequent subgraphs in multigraphs," *Information Sciences*, vol. 451-452, pp. 50–66, 2018.

[35] L. Min, Z. C. Wang, J. Liang, and X. R. Yuan, "OD-wheel: visual design to explore OD patterns of a central region," in *Proceedings of the Visualization Symposium 2015*, Hangzhou, China, April 2015.

[36] B. Jenny, D. M. Stephen, I. Muehlenhaus, and B. E. Marston, "Design principles for origin-destination flowmaps," *Cartography and Geographic Information Science*, vol. 45, no. 1, pp. 1–15, 2016.

[37] S. Kim, S. Jeong, I. Woo, Y. Jang, R. Maciejewski, and D. S. Ebert, "Data flow analysis and visualization for spatiotemporal statistical data without trajectory information," *IEEE Transactions on Visualization and Computer Graphics*, vol. 24, no. 3, pp. 1287–1300, 2018.

[38] J. Wood, J. Dykes, and A. Slingsby, "Visualisation of origins, destinations and flows with OD maps," *The Cartographic Journal*, vol. 47, no. 2, pp. 117–129, 2010.

[39] M. Zillinger, "Tourist routes: a time-geographical approach on German car-tourists in Sweden," *Tourism Geographies*, vol. 9, no. 1, pp. 64–83, 2007.

[40] S. Page and J. Connell, "Exploring the spatial patterns of car-based tourist travel in loch lomond and trossachs national park, Scotland," *Tourism Management*, vol. 29, no. 3, pp. 561–580, 2008.

[41] A. Inokuchi, T. Washio, and H. &Motoda, "An apriori-based algorithm for mining frequent substructures from graph data," in *Proceedings of the 4th European Conference on Principles of Data Mining and Knowledge Discovery, PKDD'00*, pp. 13–23, Lyon, France, September 2000.

[42] M. Kuramochi and G. Karypis, "Frequent subgraph discovery," in *Proceedings of the 2001 IEEE International Conference on Data Mining, ICDM'01*, pp. 313–320, IEEE Computer Society, San Jose, CA, USA, August 2001.

[43] M. Oppermann, "A model of travel itineraries," *Journal of Travel Research*, vol. 33, no. 4, pp. 57–61, 1995.

[44] N. Shoval and A. Raveh, "Categorization of tourist attractions and the modeling of tourist cities: based on the co-plot method of multivariate analysis," *Tourism Management*, vol. 25, no. 6, pp. 741–750, 2004.

[45] G. Lau and B. McKercher, "Understanding tourist movement patterns in a destination: a gis approach," *Tourism and Hospitality Research*, vol. 9, no. 1, pp. 39–49, 2007.

[46] B. McKercher and G. Lau, "Movement patterns of tourists within a destination," *Tourism Geographies*, vol. 10, no. 3, pp. 355–374, 2008.

Hindawi
Journal of Advanced Transportation
Volume 2020, Article ID 9401062, 9 pages
https://doi.org/10.1155/2020/9401062

Research Article

Deployment Optimization of Connected and Automated Vehicle Lanes with the Safety Benefits on Roadway Networks

Zhibo Gao,[1] Zhizhou Wu ,[1] Wei Hao ,[2,3] and Kejun Long[2,3]

[1]*The Key Laboratory of Road and Traffic Engineering, Ministry of Education, Tongji University, 4800 Cao'an Road, Shanghai 201804, China*
[2]*School of Traffic & Transportation Engineering, Changsha University of Science &Technology, Changsha 410076, China*
[3]*Hunan Key Laboratory of Smart Roadway and Cooperative Vehicle-Infrastructure Systems, Changsha University of Science & Technology, Changsha 410205, China*

Correspondence should be addressed to Zhizhou Wu; wuzhizhou@tongji.edu.cn and Wei Hao; haowei@csust.edu.cn

Received 3 January 2020; Revised 17 March 2020; Accepted 10 July 2020; Published 1 August 2020

Academic Editor: Jaeyoung Lee

Reasonable deployment of connected and automated vehicle (CAV) lanes which separating the heterogeneous traffic flow consisting of both CAVs and human-driven vehicles (HVs) can not only improve traffic safety but also greatly improve the overall roadway efficiency. This paper simplified CAV lane deployment plan into the problem of traffic network design and proposed a comprehensive decision-making method for CAV lane deployment plan. Based on the traffic equilibrium theory, this method aims to reduce the travel cost of the traffic network and the management cost of CAV lanes using a bilevel primary-secondary programming model. In addition, the upper level is the decision-making scheme of the lane deployment, while the lower level is the traffic assignment model including CAV and HV modes based on the decision-making scheme of the upper level. After that, a genetic algorithm was designed to solve the model. Finally, a medium-scaled traffic network was selected to verify the effectiveness of the proposed model and algorithm. The case study shows that the proposed method obtained a feasible scheme for lane deployment considering from both the system travel cost and management cost of CAV lanes. In addition, a sensitivity analysis of the market penetration rate of CAVs, traffic demand, and the capacity of CAVLs further proves the applicability of this model, which can achieve better allocation of system resources and also improve the traffic efficiency.

1. Introduction

Recently, connected and automated driving technology has attracted the attention of automobile enterprises, universities, and scientific research institutions due to the great function of intelligent networking technology in improving traffic safety [1, 2], road capacity [3, 4], energy consumption [5–7], driving experience [8], etc. In addition, the development of connected and automated driving technology has prompted the rapid progress of a new generation of intelligent transportation systems [9]. It can be predicted for a considerable time to come with the scenario for a traffic development mode coexisting with CAVs and HVs.

As a new generation of the automobile, CAVs have natural differences in driving behavior compared with HVs. They need more accurate environmental perception, less headway, and shorter reaction times with following and changing lanes [10]. Currently, the main control strategies for CAV technology focus on adaptive cruise control (ACC) and cooperative adaptive cruise control (CACC). First of all, ACC strategy is to obtain the acceleration and speed of the front vehicle through on-board detection equipment (via vehicle-to-vehicle (V2V) communication) and realize acceleration optimization control through the ACC control system. Secondly, CACC is based on ACC and realizes vehicle formation via V2V technology to maintain a smaller headway, thus can greatly improving traffic efficiency [11–13]. Due to truck drivers experience significantly higher risk of suffering serious injury and fatality than passenger vehicle drivers [14, 15], a number of machine learning

models were established to examine crash severity on roadway segments [16, 17]. Until now, truck CACC is believed as one of the potentially effective solutions to these challenges. However, CACC will be affected by HVs or other emergencies, when the CACC market penetration rate (MPR) is low. In addition, the formation of CACC vehicles will deactivate and switch to ACC or human-driven mode, which results in a drop for the road's vehicle capacity. Zeng et al. [18] studied the impairment of capacity caused by the failure of a CACC formation in the freeway merging area. The simulation results showed that the reduction of capacity in the merging area is 15.4%–17.2% under the same MPR compared with the pipeline capacity. In addition, Qin et al. [19] established the fundamental diagram model for the heterogeneous traffic flow of CACC vehicles mixed with ACC vehicles and found that the capacity of the heterogeneous traffic flow is lower than an HV traffic flow situation when the CACC MPR is less than 40%.

In order to better accommodate CAVs, some scholars considered providing special roadway rights for CAVs so that they make a separation of CAVs from the mixed traffic, such as the Connected and Automated Vehicle Lanes (CAVLs) which are studied in this paper. In this strategy, CAVs are supposed to use the dedicated lane on which homogeneous traffic flow of CAVs is created [20]. On the contrary, setting CAVL will reduce the number of lanes for accommodating other HVs. If the CAVL deployment is not set properly, it will lead to a great waste of road system resource and cause drastic congestion in the traffic flow and decreases the overall performance of the road. For system planning, policymakers are interested in understanding possible sets of system enhancement options to meet their performance goals and obtain the most cost-effective deployment strategies for the future. Therefore, to improve the capacity and safety characteristics of existing traffic facilities, how to design and deploy CAVLs become an urgent problem for policymakers.

In traffic flow research, one important problem has aroused much attention: how the impact in roadway capacity will evolve as the connected and automated driving technologies mature and the penetration rate gradually increases? Some existing studies provide effective methods to solve this issue. During the theoretical research, Ghiasi et al. [21] developed an analytical capacity model to calculate the impact of different CAV technology scenarios and determine the optimal number of dedicated CAV lanes using the Markov chain method. Chen et al. [22] presented a mathematical framework to optimize a time-dependent deployment plan of autonomous vehicle lanes on a transportation network with heterogeneous traffic stream. In their work, the per-lane capacity can become tripled when it is converted from a regular lane to an AV lane. In order to shed light on how traffic operational capacity will change with the introduction of AVs, Chen et al. [23] developed a general theoretical framework to determine the valid domains of different lane policies and, more generally, AV distributions across lanes with respect to demand, as well as optimal solutions to accommodate AVs. Simulation is another significant method which can be utilized to investigate this problem. Liu et al. [24] analyzed the influence of the CAVL strategy on multilane freeway facilities under the mixed traffic flow. The analysis results showed that the strategy of CAVs lanes can improve pipeline capacity by 22% compared with conventional strategy with the CACC MPR approaching 60%. Talebpour et al. [25] examined the impacts of reserving one lane of a four-lane highway for AVs on traffic flow dynamics and travel time reliability. It was found that throughput can be improved significantly if the AV penetration rate is greater than 30%. Ye and Yamamoto [20] investigated the performance of traffic flow under different numbers of CAV dedicated lanes, compared it with mixed flow situation, and found that the benefit of setting CAVLs can only be obtained within a medium density range.

However, it is well known from "Braess" paradox [26, 27] that unilaterally improving the capacity of an existing link or adding a new link in the network instead of reducing the unit travel cost within the network. Therefore, some scholars turned to study the CAVL deployment problem for the transport network level. For example, Chen et al. [28] developed a mathematical framework to optimally design AV zones and developed a mixed-integer bilevel programming model to optimize the deployment plan. However, there is limited systematic research talking about the optimization of CAVLs deployment considering the total travel expense and the management cost of CAVLs.

As a result, this paper proposes an optimization method for CAVL deployment plan considering from the viewpoints of the whole traffic network. The objective of this method is to reduce the travel cost of the traffic network as well as the management cost of CAVLs. A primary-secondary method with a bilevel programming model is established. The upper level is the decision-making scheme of lane deployment, while the lower level assigns traffic flow including CAV mode and HV mode using the upper-level scheme. Based on the characteristics of the model, a genetic algorithm is creatively designed to solve the abovementioned models, and a medium-sized network is listed as an example to be analyzed in this research.

The remainder of this paper is structured as follows. Section 2 presents the mathematical formulation to optimize the CAVLs deployment plan and to describe the flow distributions of both CAVs and HVs. Section 3 designs a genetic algorithm to solve the proposed bilevel programming optimization model. Section 4 conducts numerical studies and sensitivity analysis. Finally, conclusions and recommendations are delivered in Section 5.

2. Mathematical Formulation

2.1. Problem Description. "Connected and automated vehicle lanes" refer to a lane management method that provides the exclusive right for CAVs to travel on some links of the traffic network according to the traffic demand. The following conditions need to be considered when setting CAVLs: the first condition is lane conditions, which exists at least two or more lanes going on the same direction and there is no interference from other traffic modes besides HVs; the second condition is the traffic conditions, which

the basic capacity of HV lanes will not be affected by the CAVLs; and the third one is the link conditions, which the link has the construction conditions needed for CAVLs, such as the requirements for the layout of communication equipment and the construction cost.

One of the key points for CAVL deployment is that the decision-making scheme for every kind of lane should be coordinated in order to achieve the best combination effect. The best combination effect will be achieved only after setting a reasonable scale on the network. The second key point is that travellers will choose the most advantageous route for themselves according to the well-established CAVL schemes, and the traffic flow can be balanced under the current network conditions. The third consideration is that the traffic organizer will optimize the scheme of the CAVLs based on the equilibrium state caused by the travellers route choice behavior. Finally, a master-slave game (also known as a Stackelberg game) is formed between the traffic organizers and the travellers.

In summary, CAVL deployment is a systematic problem that is really necessary to consider the deployment, considering from the level of the traffic network. In addition, the master-slave game relationship exists between traffic planning organizers and travellers. Finally, a comprehensive decision will be achieved based on the traffic equilibrium theory.

2.2. Assumptions and Definitions. The analyzed model established in this section is based on the following assumptions:

(i) There are only two kinds of managed lanes in this research: CAVLs and HV lanes

(ii) The topology of the traffic network is predefined known

(iii) The traffic demand among the origin-destination (OD) pairs is predefined known and unsaturated

(iv) The scope of CAVs cooperation could not affected by V2V communication distance in CAVLs, that is, CAVs are all fully communicated in each CAVLs

2.3. Primary-Secondary Method with Bilevel Programming Model. For the optimization problem of CAVL deployment, the traveller aims to minimize the travel cost or travel time, while the government planning department enhances how to design or improve the traffic network under a limited investment to maximize the performance of a certain system. With the need of comprehensive decision-making for two different lanes, this paper establishes a primary-secondary bilevel programming model. The upper level establishes the decision-making scheme for lane deployment, and the objective function is the system cost including the travel cost and the management cost of CAVLs. In addition, the lower level utilizes the User-Equilibrium (UE) model to describe the traffic flow assignment of the CAV mode and HV mode, respectively, according to the decision-making scheme of the upper level. The assignment results obtained from the route choice of two travel modes are used to evaluate the performance of the decision-making scheme.

Considering the constraints of the number of lanes and link capacity, a decision-making scheme to minimize the system cost is established in the upper-level planning. The formulation of the model is listed as follows:

$$\min F\left(n_a^{\mathrm{Cv}}\right) = \sum_{a\in D}\left(x_a^{\mathrm{Cv}} t_a^{\mathrm{Cv}} + x_a^{\mathrm{Hv}} t_a^{\mathrm{Hv}}\right) + \sum_{a\in \overline{D}}\left[\left(x_a^{\mathrm{Cv}} + x_a^{\mathrm{Hv}}\right) t_a^{\mathrm{Hv}}\right] + \sum_{a\in A} w_C n_a^{\mathrm{Cv}}, \tag{1}$$

$$1 \le n_a^{\mathrm{Hv}} \le n_a, \quad \forall a \in A, \tag{2}$$

$$0 \le n_a^{\mathrm{Cv}} \le n_a - 1, \quad \forall a \in A, \tag{3}$$

$$n_a = n_a^{\mathrm{Cv}} + n_a^{\mathrm{Hv}}, \quad \forall a \in A, \tag{4}$$

$$x_a = x_a^{\mathrm{Cv}} + x_a^{\mathrm{Hv}}, \quad \forall a \in A, \tag{5}$$

where equation (1) is the objective function; equations (2) and (3) are the constraints of the number of CAVLs and HV lanes, which ensure that the number of HV lanes is not less than one; equation (4) is the conservation of lane number; and equation (5) is the conservation of link flow. In equation (1), the first term is the sum travel cost of links with CAVLs, the second term is the sum travel cost of links without CAVLs, and the third term is the sum management cost of CAVLs.

In the lower-level planning, the flows should be differentiated in the route selection for the HV mode and CAV mode. In order to promote the CAV mode, CAV traffic flow is first loaded, initial cost of the unmodified links is updated when the network is balanced, and then HV traffic flow is loaded. Therefore, there is a primary-secondary relationship for the two traffic flow assignment models.

The assignment model of CAV traffic flow is listed as follows:

$$\min \quad \sum_{a\in A}\int_0^{x_a^{\mathrm{Cv}}} t_a^{\mathrm{Cv}}\left(x_a^{\mathrm{Cv}}, n_a^{\mathrm{Cv}}\right)\mathrm{d}\omega, \tag{6}$$

$$s.t. \quad \sum_{k\in P_{\mathrm{rs}}} f_{\mathrm{rs}}^{\mathrm{Cv},k} = q_{\mathrm{rs}}^{\mathrm{Cv}}, \ (r,s) \in \mathrm{RS}, \tag{7}$$

$$f_{\mathrm{rs}}^{\mathrm{Cv},k} \ge 0, \quad k \in P_{\mathrm{rs}}, \ (r,s) \in \mathrm{RS}, \tag{8}$$

$$x_a^{\mathrm{Cv}} = \sum_{(r,s)\in \mathrm{RS}} \sum_{k\in P_{\mathrm{rs}}} f_{\mathrm{rs}}^{\mathrm{Cv},k} \delta_{\mathrm{rs}}^{\mathrm{Cv},k}, \quad a \in A, \tag{9}$$

$$t_a^{\mathrm{Cv}} = t_a^0\left\{1 + \alpha\left[\frac{x_a^{\mathrm{Cv}}}{n_a^{\mathrm{Cv}} C_l^{\mathrm{Cv}} + (1-\eta_a) n_a C_l^{\mathrm{Hv}}}\right]^{\beta}\right\}, \quad a \in A. \tag{10}$$

The assignment model of HV traffic flow is listed as follows:

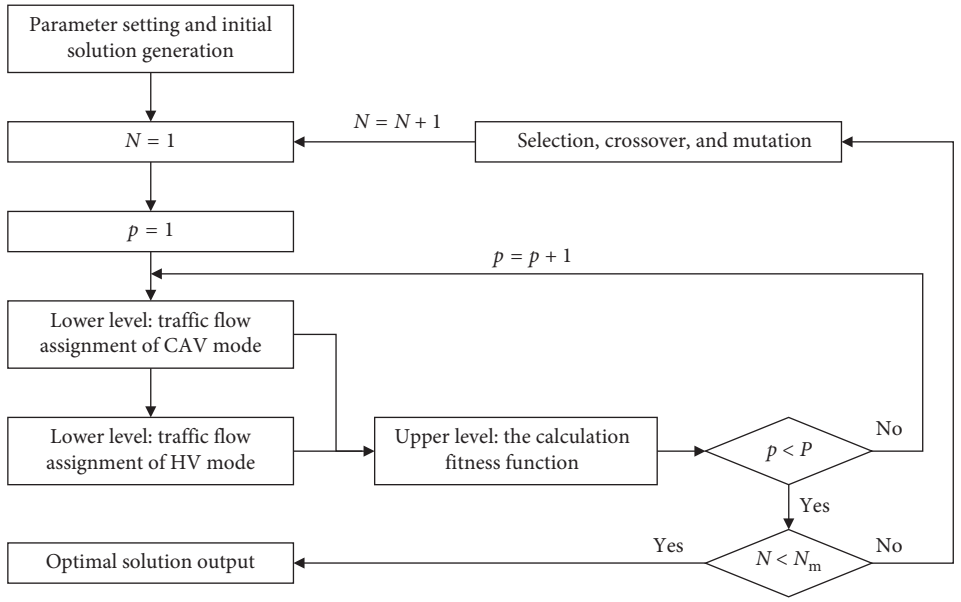

Figure 1: Flow chart of algorithm.

$$\min \sum_{a\in A}\int_0^{x_a^{\mathrm{Hv}}} t_a^{\mathrm{Hv}}\left(x_a^{\mathrm{Cv}}, x_a^{\mathrm{Hv}}, n_a^{\mathrm{Cv}}\right)\mathrm{d}\omega, \tag{11}$$

$$s.t. \quad \sum_{k\in P_{\mathrm{rs}}} f_{\mathrm{rs}}^{\mathrm{Hk}} = q_{\mathrm{rs}}^{\mathrm{Hv}}, \quad (r,s)\in \mathrm{RS}, \tag{12}$$

$$f_{\mathrm{rs}}^{\mathrm{Hk}} \geq 0, k\in P_{\mathrm{rs}}, \quad (r,s)\in \mathrm{RS}, \tag{13}$$

$$x_a^{Hv} = \sum_{(r,s)\in \mathrm{RS}}\sum_{k\in P_{\mathrm{rs}}} f_{\mathrm{rs}}^{\mathrm{Hk}}\delta_{\mathrm{rs}}^{\mathrm{Hk}}, \quad a\in A, \tag{14}$$

$$t_a^{\mathrm{Hv}} = t_a^0\left\{1+\alpha\left[\frac{x_a^{\mathrm{Hv}}+(1-\eta_a)x_a^{\mathrm{Cv}}}{(n_a-n_a^{\mathrm{Cv}})C_l^{\mathrm{Hv}}}\right]^{\beta}\right\}, \quad a\in A, \tag{15}$$

where equations (7) and (12) are flow conservation constraints; equations (8) and (13) are nonnegative constraints on the route flow; equations (9) and (14) describe the relationship between the link flow and route flow; and equations (10) and (15) are Bureau of Public Road (BPR) functions which are undetermined coefficients.

3. Solution Algorithm

In view of the complexity of the bilevel programming model, this paper creatively utilizes the genetic algorithm to search the optimal scheme. The specific steps of the algorithm are listed and shown in Figure 1.

Step 1 (initialization): relevant parameters of the genetic algorithm are defined, including population size P, generation gap, crossover probability, mutation probability, and maximum evolution number N_m. This algorithm uses integer coding: the specific form of coding is $\{n_1^{\mathrm{Cv}}, n_1^{\mathrm{Cv}}, \ldots, n_a^{\mathrm{Cv}}\}$, whose values range among $\{0, 1, \ldots, (n_a - 1)\}$. Let generation $N = 1$ and population $p = 1$, and randomly generate the CAVLs deployment scheme.

Step 2 (traffic assignment model of lower level): the Frank–Wolfe (F-W) algorithm [29] is used to solve the traffic flow assignment model of the CAV mode. The link cost is updated according to the equilibrium result, and choose it as the initial cost of the HV mode. After that, our research team continues to solve the traffic flow assignment model of the HV mode with the F-W

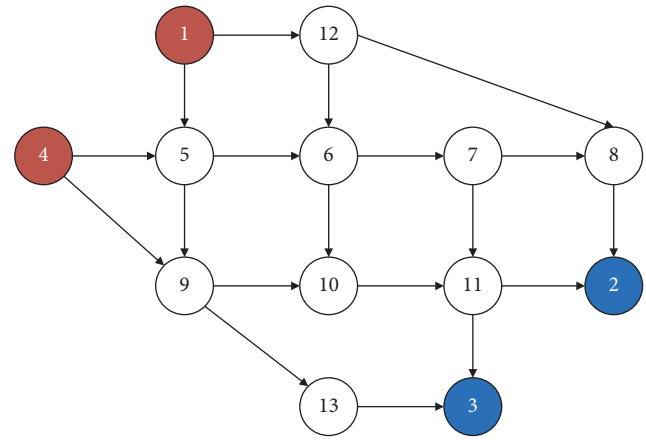

Figure 2: Nguyen–Dupuis network schematic diagram.

Table 1: Basic traffic demand of each OD pair.

OD	Origin	Destination	Demand
1	1	2	600
2	1	3	900
3	4	2	750
4	4	3	750

Table 2: Parameters of the Nguyen–Dupuis network.

Link	Origin	Destination	Number of lanes	Free flow time	Current lane capacity
1	1	5	2	4	150
2	1	12	3	6	150
3	4	5	2	5	150
4	4	9	2	8	150
5	5	6	4	4	150
6	5	9	3	10	150
7	6	7	4	4	150
8	6	10	3	8	150
9	7	8	4	4	150
10	7	11	3	10	150
11	8	2	2	6	150
12	9	10	4	4	150
13	9	13	2	8	150
14	10	11	4	4	150
15	11	2	3	5	150
16	11	3	2	7	150
17	12	6	2	4	150
18	12	8	2	12	150
19	13	3	2	6	150

Table 3: Optimal scheme of CAVLs.

Link	1	2	3	4	5	6	7	8	9	10	11	12	13	14	15	16	17	18	19	11
Number of CAVLs	0	0	0	0	0	1	0	0	1	0	0	1	0	0	0	0	0	0	0	0

algorithm, and the results of the two assignment results are transmitted back to the upper level.

Step 3 (calculate the fitness function of upper level): The objective function of bilevel programming established in this paper is the system cost with the value greater than zero, and this is a minimization problem. Hence, the reciprocal of the objective function is chosen as the fitness function, and the fitness of each individual is calculated according to x_a^{Cv}, t_a^{Cv}, x_a^{Hv}, and t_a^{Hv} which can be solved from the lower level.

Step 4: let $p = p + 1$. Repeat Steps 2 and 3 until $p \geq P$.

Step 5 (iteration): evolutionary operations such as selection, crossover, and mutation [30] are carried out according to the fitness of individuals, and then the population is updated.

Step 6: let $N = N + 1$. Repeat Steps 2 to 5 until $N = N_m$; then, we get the optimal solution.

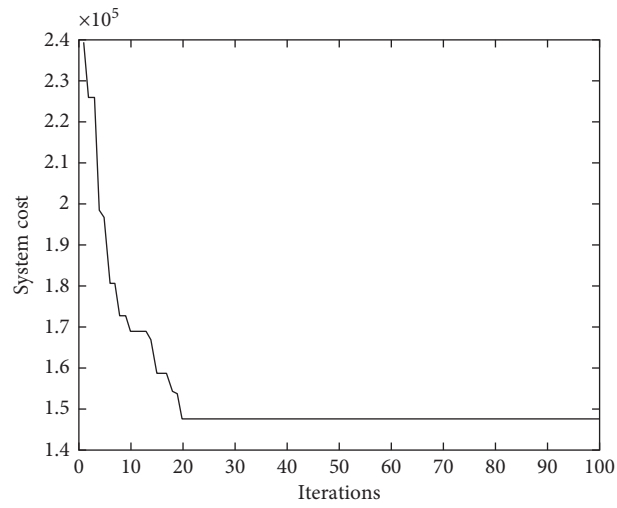

Figure 3: Evolutionary process diagram of algorithm.

4. Numerical Examples

4.1. Basic Settings and Results. This paper uses the Nguyen and Dupuis test network as a case study. The network has 13 nodes, 19 links, and 4 OD pairs [31]. The basic topology of the network is shown in Figure 2, where the red node represents the traffic demand generation point and the blue node represents the traffic demand attraction point. Table 1 shows the OD traffic demand. Table 2 is the basic attribute information of the network including the number of lanes, free-flow time, and current lane capacity.

According to the existing literature [25], the basic traffic capacity of a CAV lane is about twice of an HV lane, and

Table 4: Lane deployment schemes for different MPR.

MPR (%)	Link 6	Link 9	Link 12	Link 14	Link 18	Other links
10	1	0	2	0	0	0
20	1	2	0	0	0	0
30	1	1	1	0	0	0
40	1	1	1	1	0	0
50	0	2	1	2	0	0
60	2	0	2	0	1	0
70	1	1	3	0	0	0
80	2	2	2	0	0	0
90	2	2	2	0	0	0

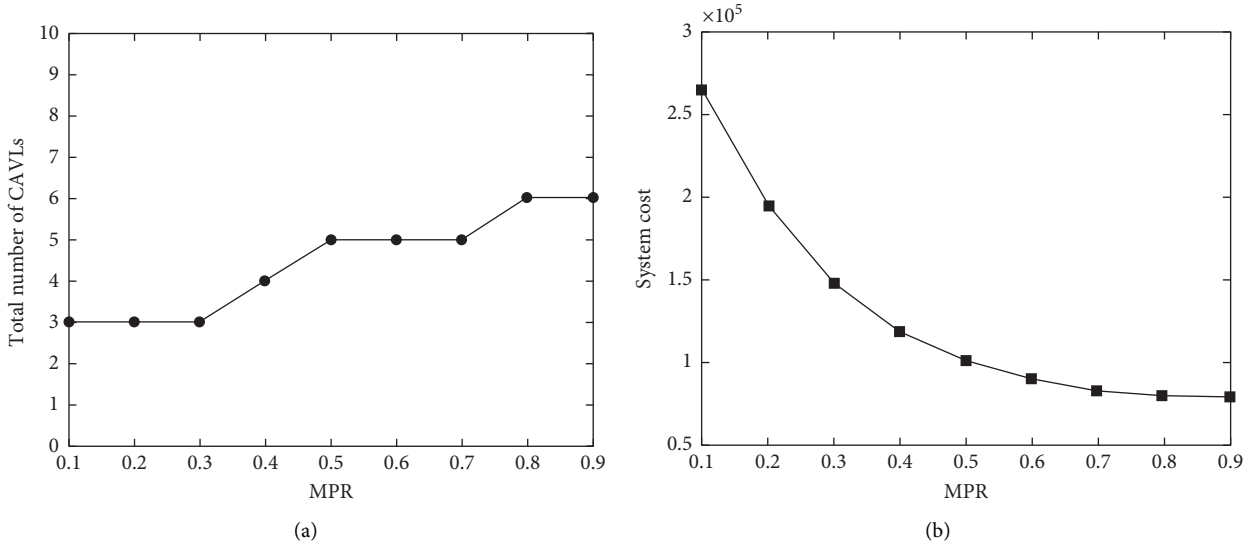

Figure 4: Sensitivity analysis of the CAV MPR. (a) The total number of CAVLs. (b) System cost.

CACC strategy is effective only when CACC MPR is more than 30%. The management cost of CAVLs includes construction cost and maintenance cost with the management cost of a single CAVL is 500. Let α be 0.15 and β be 4.0 in the BPR function. The basic parameters of the genetic algorithm, respectively, are the population size is 50, generation gap is 0.9, crossover probability is 0.75, mutation probability is 0.05, and maximum evolution times is 100. When CAV MPR reaches 30%, the lane deployment scheme is shown in Table 3, and the running process of the algorithm is shown in Figure 3. As can be seen from Figure 3, the algorithm converges when iterations reach the 20th generation. The total number of CAVLs is 3 with the management cost is 1500. In addition, the system cost is 147416.8 and the system travel cost is 145916.8.

4.2. Sensitivity Analysis. In this section, the authors mainly analyze the impact of market penetration rate of CAVs, traffic demands, and the capacity of the CAVLs in the proposed method.

4.2.1. Market Penetration Rate of CAVs. In the future, the market will inevitably experience a long transition phase of CAVs coexisting with HVs as connected and automated driving technology. Therefore, it is greatly necessary to analyze the influence of this method when CAV MPR changes.

Fixing the traffic demand of each OD pair and the capacity of the CAVLs, the CAV MPR is adjusted between 10% and 90%. Then, the genetic algorithm designed in this paper was used to solve the bilevel programming model. Considering the local convergence of the genetic algorithm, ten experiments were carried out on each group of parameters, and the minimum target was chosen as the final result, which is shown in Table 4 and Figure 4.

As can be seen from Table 4 and Figure 4(a), the total number of CAVLs can be the same with the increase of CAV MPR, but the deployment location of the lanes is different. This analysis shows that MPR in the planning year needs to be accurately estimated when lanes are set up, and it also shows the necessity of CAVLs deployment considering from the network level. The traffic volume of CAV increases with the increase of MPR. Only when the traffic volume of CAV reaches a certain scale and the cost of adding CAVLs is lower than the increase of the travel cost, the strategy of adding CAVLs is beneficial. According to the statistics of CAV lanes under all the MPRs, it is found that the probability of CAV lanes set in links 6, 9, 12, and 14 is the greatest, which also verifies the feasibility of the calculation results shown in this paper.

Likewise, the system cost shows a downward trend with the increasing of CAV MPR, which declines rapidly in the early stage and slowly in the later stage as seen in Figure 4(b). This is because the MPR is gradually approaching its critical value with the increasing of CAV MPR accompanied with the utilization rate of CAVLs and the actual capacity of the link increasing. However, when the CAV MPR exceeds its critical value, the utilization rate of HV lanes decreases together with the actual capacity of the link. In the latter stage, the increase of CAV MPR has little effect on the decreasing of the travel time due to the traffic demand constraints. If the number of CAVLs continue to increase, it will add to the cost of lane management together with increasing the system cost of the system at the same time.

4.2.2. Traffic Demand. During the design of CAVLs, the impact of traffic demand on the decision-making scheme is also needed to be analyzed except considering the change of CAV MPR. In addition, the intrinsic mechanism of the model is complex with many factors involved in traffic demand forecasting. Additionally, it is necessary to

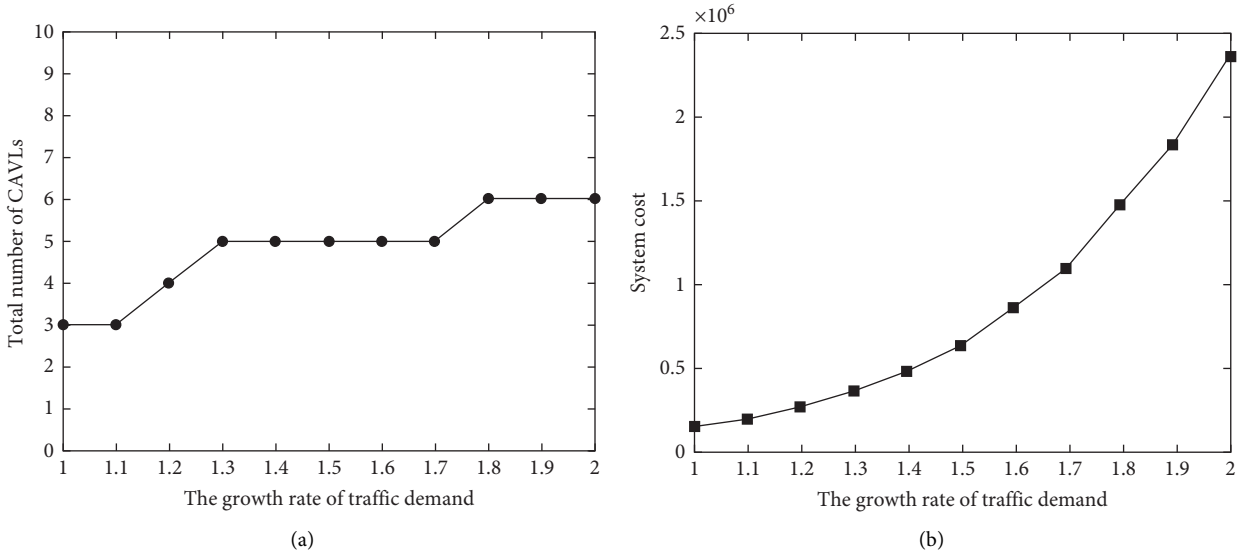

Figure 5: Sensitivity analysis of traffic demand. (a) The total number of CAVLs. (b) System cost.

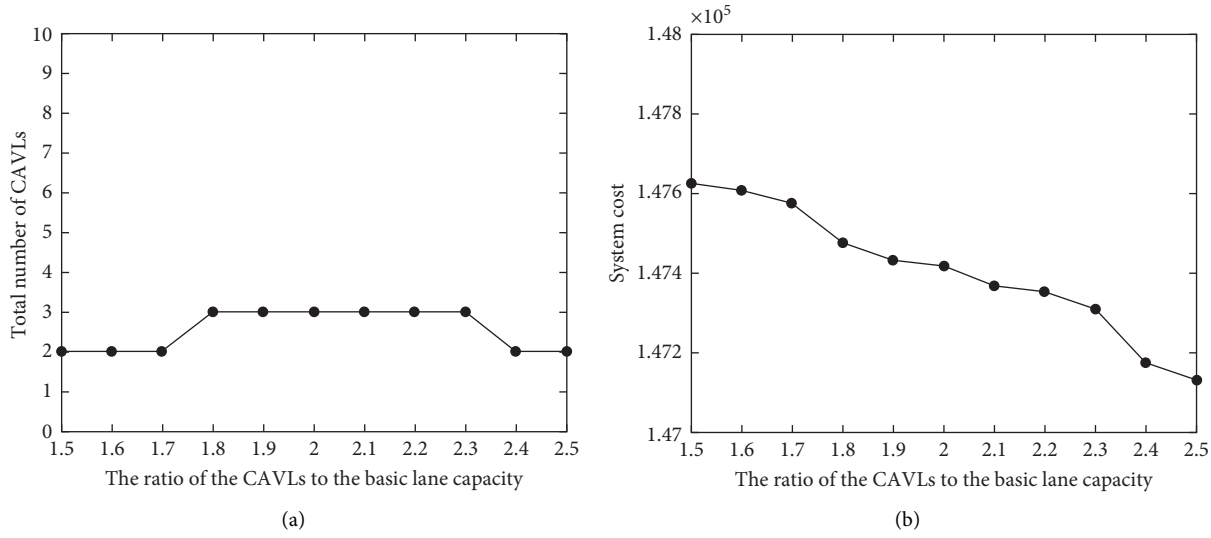

Figure 6: Sensitivity analysis of the capacity of CAVLs. (a) The total number of CAVLs. (b) System cost.

consider the variations of system performance under different traffic demands with many uncertainties in the actual situation. Therefore, CAV MPR is fixed and located at 30%. The total traffic demand is multiplied by the growth factor of 100%–200% compared with the original basis, while the proportion of OD traffic demand remains unchanged.

In addition, the total number of CAVLs is the same (Figure 5(a)) when the growth rate of traffic demand varies between 1.3 and 1.7, which results from the optimal utilization of lane function by the route selection behavior of CAVs. The total number of CAVLs also doubles when traffic demand doubles. In addition, Figure 5(b) shows that the system cost increases exponentially with the increase of traffic demand.

4.2.3. Capacity of the CAVLs. Since the capacity of the CAVLs is highly sensitive to the performance of CAV in terms of its average headway, sensitivity analysis on the capacity of the CAV lane would be necessary. Therefore, fixing the CAV MPR and the traffic demand, the capacity of CAVLs is multiplied by the factor of 150%–300% compared with the basic lane capacity. The results of the total number of CAVLs and the system cost are shown in Figure 6(a) and Figure 6(b), respectively.

As can be seen from Figure 6(a), the total number of CAVLs shows a trend of increasing first and decreasing later, and its values are the same when the ratio of CAVLs to the basic lane capacity varies between 1.8 and 2.3. When the capacity of CAVLs is low, the cost of adding CAVLs is greater than the reduction of system travel cost, so CAVLs

are deployed in a small number. When the capacity of CAVLs is high, fewer CAVLs can meet the traffic demand. In addition, Figure 6(b) shows that the system cost decreases with the increase of CAVLs capacity.

5. Conclusions

To sum up, this paper proposes an optimization method for CAVL deployment plan, which aims to solve the problem with capacity drops when HVs are mixed into CACC systems. This method creatively simplified the CAVL deployment into a traffic network design problem and established a bilevel primary-secondary programming model. The upper level generated the decision-making scheme of the lane deployment scheme, and the lower level assigned the traffic flow including the CAV mode and HV mode according to the decision-making scheme of the upper level. The equilibrium results of the lower level were used to evaluate the performance of the upper level. Due to the characteristics of the model, a genetic algorithm was designed to solve this model. The numerical results show that the proposed method can obtain a feasible scheme with the consideration of both the system cost and the management cost for CAVLs. The sensitivity analysis results of CAV MPR, traffic demands, and the capacity of CAVLs further validate the feasibility and flexibility of the proposed method.

However, there are also some limitations where HVs give preferences to CAVs when assigning flow in the lower-level model, which is different from the general situation with two-mode flow assigned simultaneously. Regarding to the value of lane management cost, it needs to be quantified more accurately by considering from much more aspects. Due to the large number of variables when applying the proposed model in large-size network, the genetic algorithm may not converge. A combination algorithm combining the advantages of genetic algorithm and active set algorithm will be proposed in future studies.

Abbreviations

$G(V, A)$: Traffic network, where V is the node of the traffic network and A is the link set
D: Set of links with CAVLs
$\overline{D}$: Set of links without CAVLs
RS: Set of demand of OD pair
x_a: Flow of link a
x_a^{Hv}: Flow of HVs on link a
x_a^{Cv}: Flow of CAVs on link a
$f_{\mathrm{rs}}^{\mathrm{Cv},k}$: Route flow of CAVs
$f_{\mathrm{rs}}^{\mathrm{Hv},k}$: Route flow of HVs
t_a^0: Link cost of link a under free flow
$t_a(\bullet)$: Cost function of link a
t_a^{Cv}: Cost function of link $a \in D$
t_a^{Hv}: Cost function of link $a \in \overline{D}$
w_C: Management cost of single CAVL
η_a: 0-1 variables; if $a \in D$, then $\eta_a = 1$; otherwise, $\eta_a = 0$
t_a^0: Link cost of link a under free flow
C_l^{Hv}: Basic capacity of HV lane
C_l^{Cv}: Basic capacity of CAVLs
n_a: Total number of lanes of link a
n_a^{Hv}: Number of HV lanes on link a
n_a^{Cv}: Number of CAVLs on link a.

Data Availability

The data used to support the findings of this study are available from the corresponding author upon request.

Conflicts of Interest

The authors declare that there are no conflicts of interest regarding the publication of this paper.

Acknowledgments

This study was supported by the National Natural Science Foundation of China under Grant nos. 61773288, 51808057, and 51678076. This study was in part supported by National Key Research and Development Program of China (no. 2018YFB1600805).

References

[1] T. X. Li and K. M. Kockelman, "Valuing the safety benefits of connected and automated vehicle technologies," in *Proceedings of the 95st Transportation Research Board Annual Meeting*, San Francisco, CA, USA, September 2016.

[2] J. Liu and A. J. Khattak, "Delivering improved alerts, warnings, and control assistance using basic safety messages transmitted between connected vehicles," *Transportation Research Part C: Emerging Technologies*, vol. 68, pp. 83–100, 2016.

[3] C. Letter and L. Elefteriadou, "Efficient control of fully automated connected vehicles at freeway merge segments," *Transportation Research Part C: Emerging Technologies*, vol. 80, pp. 190–205, 2017.

[4] P. Tientrakool, Y. C. Ho, and N. F. Maxemchuk, "Highway capacity benefits from using vehicle-to-vehicle communication and sensors for collision avoidance," in *Proceedings of the 2011 IEEE Vehicular Technology Conference (VTC Fall)*, San Francisco, CA, USA, September 2011.

[5] H. Jiang, J. Hu, S. An, M. Wang, and B. B. Park, "Eco approaching at an isolated signalized intersection under partially connected and automated vehicles environment," *Transportation Research Part C: Emerging Technologies*, vol. 79, pp. 290–307, 2017.

[6] H. Yang, H. Rakha, and M. V. Ala, "Eco-cooperative adaptive cruise control at signalized intersections considering queue effects," *IEEE Transactions on Intelligent Transportation Systems*, vol. 18, no. 6, pp. 1575–1585, 2011.

[7] Z. Wang, G. Y. Wu, and M. J. Barth, "Cooperative eco-driving at signalized intersections in a partially connected and automated vehicle environment," *IEEE Transactions on Intelligent Transportation Systems*, vol. 21, pp. 1–10, 2019.

[8] A. Talebpou and H. S. Mahmassani, "Influence of connected and autonomous vehicles on traffic flow stability and throughput," *Transportation Research Part C: Emerging Technologies*, vol. 71, pp. 143–163, 2016.

[9] F.-Y. Wang, "Parallel control and management for intelligent transportation systems: concepts, architectures, and applications," *IEEE Transactions on Intelligent Transportation Systems*, vol. 11, no. 3, pp. 630–638, 2010.

[10] L. Li, W.-L. Huang, Y. Liu, N.-N. Zheng, and F.-Y. Wang, "Intelligence testing for autonomous vehicles: a new approach," *IEEE Transactions On Intelligent Vehicles*, vol. 1, no. 2, pp. 158–166, 2016.

[11] G. Marsden, M. McDonald, and M. Brackstone, "Towards an understanding of adaptive cruise control," *Transportation Research Part C: Emerging Technologies*, vol. 9, no. 1, pp. 33–51, 2001.

[12] L. Xiao and F. Gao, "A comprehensive review of the development of adaptive cruise control systems," *Vehicle System Dynamics*, vol. 48, no. 10, pp. 1167–1192, 2010.

[13] L. Li and X. Li, "Parsimonious trajectory design of connected automated traffic," *Transportation Research Part B: Methodological*, vol. 119, pp. 1–21, 2019.

[14] L. Xiao, M. Wang, W. Schakel, and B. van Arem, "Unravelling effects of cooperative adaptive cruise control deactivation on traffic flow characteristics at merging bottlenecks," *Transportation Research Part C: Emerging Technologies*, vol. 96, pp. 380–397, 2018.

[15] F. Chen and S. Chen, "Injury severities of truck drivers in single- and multi-vehicle accidents on rural highways," *Accident Analysis & Prevention*, vol. 43, no. 5, pp. 1677–1688, 2011.

[16] F. Chen, H. R. Peng, X. X. Ma, J. Y. Liang, W. Hao, and X. D. Pan, "Examining the safety of trucks under crosswind at bridge-tunnel section: a driving simulator study," *Tunnelling and Underground Space Technology*, vol. 92, p. 103034, 2019.

[17] Q. Zeng, W. Gu, X. Zhang, H. Wen, J. Lee, and W. Hao, "Analyzing freeway crash severity using a Bayesian spatial generalized ordered logit model with conditional autoregressive priors," *Accident Analysis & Prevention*, vol. 127, pp. 87–95, 2019.

[18] Q. Zeng, H. Wen, H. Huang, and M. Abdel-Aty, "A Bayesian spatial random parameters Tobit model for analyzing crash rates on roadway segments," *Accident Analysis & Prevention*, vol. 100, pp. 37–43, 2017.

[19] Y. Y. Qin, H. Wang, W. Wang, and Q. Wan, "Fundamental diagram model of heterogeneous traffic flow mixed with cooperative adaptive cruise control vehicles and adaptive cruise control vehicles," *China Journal of Highway and Transport*, vol. 30, no. 10, pp. 127–136, 2017.

[20] L. Ye and T. Yamamoto, "Impact of dedicated lanes for connected and autonomous vehicle on traffic flow throughput," *Physica A: Statistical Mechanics and Its Applications*, vol. 512, pp. 588–597, 2018.

[21] A. Ghiasi, O. Hussain, Z. Qian, and X. Li, "A mixed traffic capacity analysis and lane management model for connected automated vehicles: a Markov chain method," *Transportation Research Part B: Methodological*, vol. 106, pp. 266–292, 2017.

[22] Z. Chen, F. He, L. Zhang, and Y. Yin, "Optimal deployment of autonomous vehicle lanes with endogenous market penetration," *Transportation Research Part C: Emerging Technologies*, vol. 72, pp. 143–156, 2016.

[23] D. Chen, S. Ahn, M. Chitturi, and D. A. Noyce, "Towards vehicle automation: roadway capacity formulation for traffic mixed with regular and automated vehicles," *Transportation Research Part B: Methodological*, vol. 100, pp. 196–221, 2017.

[24] H. Liu, X. Kan, S. E. Shladover, X.-Y. Lu, and R. E. Ferlis, "Modeling impacts of cooperative adaptive cruise control on mixed traffic flow in multi-lane freeway facilities," *Transportation Research Part C: Emerging Technologies*, vol. 95, pp. 261–279, 2018.

[25] A. Talebpour, H. S. Mahmassani, and A. Elfar, "Investigating the effects of reserved lanes for autonomous vehicles on congestion and travel time reliability," *Transportation Research Record: Journal of the Transportation Research Board*, vol. 2622, no. 1, pp. 1–12, 2017.

[26] H. Yang and M. G. H. Bell, "A capacity paradox in network design and how to avoid it," *Transportation Research Part A: Policy and Practice*, vol. 32, no. 7, pp. 539–545, 1998.

[27] D. Braess, A. Nagurney, and T. Wakolbinger, "On a paradox of traffic planning," *Transportation Science*, vol. 39, no. 4, pp. 446–450, 2005.

[28] Z. Chen, F. He, Y. Yin, and Y. Du, "Optimal design of autonomous vehicle zones in transportation networks," *Transportation Research Part B: Methodological*, vol. 99, pp. 44–61, 2017.

[29] Y. B. Wang, M. Papageorgiou, and G. Sarros, "Real-time route guidance for large-scale express ring-roads," in *Proceedings of IEEE Intelligent Transportation Systems Conference*, Toronto, Ont., Canada, September 2007.

[30] F. Shi, H. Y. Su, and X. Wang, "Design of reversible lanes with tidal flow on road network," *Journal of Transportation Systems Engineering and Information Technology*, vol. 15, no. 4, pp. 57–62, 2015.

[31] S. Nguyen and C. Dupuis, "An efficient method for computing traffic equilibria in networks with asymmetric transportation costs," *Transportation Science*, vol. 18, no. 2, pp. 185–202, 1984.

Hindawi
Journal of Advanced Transportation
Volume 2020, Article ID 3754062, 9 pages
https://doi.org/10.1155/2020/3754062

Research Article

Research on Mandatory Lane-Changing Behavior in Highway Weaving Sections

Wei Hao,[1] **Zhaolei Zhang**,[1] **Zhibo Gao**,[2] **Kefu Yi**,[3] **Li Liu**,[3] **and Jie Wang**[1]

[1]*Hunan Key Laboratory of Smart Roadway and Cooperative Vehicle-Infrastructure Systems, Changsha University of Science &Technology, Changsha 410205, China*
[2]*The Key Laboratory of Road and Traffic Engineering, Ministry of Education, Tongji University, 4800 Cao'an Road, Shanghai 201804, China*
[3]*School of Automotive and Mechanical Engineering, Changsha University of Science &Technology, Changsha 410076, China*

Correspondence should be addressed to Wei Hao; haowei@csust.edu.cn, Zhibo Gao; gaozhibo@tongji.edu.cn, and Kefu Yi; corfyi@csust.edu.cn

Received 2 January 2020; Revised 25 June 2020; Accepted 29 June 2020; Published 23 July 2020

Academic Editor: Young-Ji Byon

As the accident-prone sections and bottlenecks, highway weaving sections will become more complicated when it comes to the mixed-traffic environments with connected and automated vehicles (CAVs) and human-driven vehicles (HVs). In order to make CAVs accurately identify the driving behavior of manual-human vehicles to avoid traffic accidents caused by lane changing, it is necessary to analyze the characteristics of the mandatory lane-changing (MCL) process in the weaving area. An analytical MCL method based on the driver's psychological characteristics is proposed in this study. Firstly, the driver's MLC pressure concept was proposed by leading in the distance of the off-ramp. Then, the lane-changing intention was quantified by considering the driver's MLC pressure and tendentiousness. Finally, based on the lane-changing intention and the headway distribution of the target lane, an MLC positions probability density model was proposed to describe the distribution characteristics of the lane-changing position. Through the NGSIM data verification, the lane-changing analysis models can objectively describe the vehicle lane-changing characteristics in the actual scenarios. Compared with the traditional lane-changing model, the proposed models are more interpretable and in line with the driving intention. The results show significant improvements in the lane-changing safe recognition of CAVs in heterogeneous traffic flow (both CAVs and HVs) in the future.

1. Introduction

As one of the basic driving behaviors, lane-changing manoeuver directly affects the fluency and safety of traffic flow. Compared with car-following, the lane-changing process is more complicated and dangerous. Previous studies have shown that lane changing is a key factor causing highway accidents [1–7]. As CAVs enter the road, highway weaving areas will become more chaotic and dangerous. CAV, as a passive party, needs to change its operating state in real time according to the operating state of manual-human vehicles to avoid collisions. Therefore, it is crucial to study the lane-changing characteristics of manual-human vehicles to avoid vehicle collisions. However, most researches mainly use statistical models and probability models to analyze various factors influencing traffic accidents in a fixed scenario, lacking the analysis of traffic flow theory, which is of low extensibility [8]. Based on the above research foundation, this paper will use the traffic flow theory and driver characteristics to analyze the vehicles' lane-changing behavior in expressway weaving area.

The lane-changing manoeuver is divided into discretionary lane change (DLC) and mandatory lane change (MLC) according to its motivation [9, 10]. MLC is the necessary lane-changing behavior to achieve certain demands; DLC is an unnecessary lane change behavior. It can be seen that the MLC is an aggressive and necessary manoeuver, which has a great influence on the traffic flow. As an important part of the highway, the weaving section undertakes the merging and the diverging of the traffic flow.

In weaving section, all lane-changing manoeuvers belong to MLC (driving into the highway; leaving the highway), which are the manoeuver that must be completed in time; otherwise, it will affect the operation of the highway segment. So the weaving section becomes the bottleneck of the highway [3–5, 11, 12].

In the past research, in order to simplify and facilitate the modeling, it is considered that the lane-changing process is only affected by the traffic conditions (the gap of the target lane, the traffic capacity, and the speed, etc.). Sun and Elefteriadou [13] found that the MLC process is also closely related to the driver's psychological characteristics (such as aggressiveness, vigilance, and lane-changing pressure) through data investigation. However, the existing models have not fully analyzed the influence of the driver's psychological characteristics on the lane-changing process [13].

To address this challenge, the concept of lane-changing pressure is introduced to describing the drivers' pressure fluctuation in MLC. The MLC pressure is quantified by the distance between the vehicle and the off-ramp. Then, using the lane-changing pressure as an indicator, this paper proposed an MLC intention model and a gap acceptance model to analyze the driver's intention to change lanes. The proposed model is based on the driver's intention and inclination, which overcomes the defect of traditional models only using traffic conditions as a fixed indicator. Finally, combining the target lane headway distribution and MLC intention, a lane change probability density model is proposed to describe the lane-changing characteristics in the weaving area.

The rest of the paper is structured as follows: Section 2 reviews previous literature on mandatory lane-changing models. Section 3 analyzes the characteristics of MLC and proposes that the MLC is a continuous behavior. Section 4 constructs an MLC positions probability density function. Section 5 uses NGSIM data to verify the proposed theory and models. Finally, the conclusions and future work are presented in Section 6.

2. Literature Review

At present, the lane-changing decision-making models mainly include rule-based models [14–19], discrete models based on utility theory [9, 10, 20, 21], and artificial intelligence models [22–28].

The main idea of the rule-based model is to formulate different driving rules according to different driving environments. The advantages of rule-based models are traceability and simple implementation for specific scenarios. The drivers choose whether to change lanes by some simple rules. However, for complicated traffic conditions, a rule-based model can require a substantial work in order to be extended into more general scenarios. The most representative rule-based model is Gipps' lane-changing model [14]. Gipps believes that a driver's lane-changing decision is the result of three problems: (1) Is it possible to change lanes? (2) Is it necessary to change lanes? (3) And is it desirable to change lanes? After Gipps' pioneering work, many people have expanded the lane-changing decision-making model, such as CORSIM Model [29], ARTEMiS Model [12], Cellular Automata Model [30], and Game Theory Model [31]. By extending Gipps' model to the highway, Yang and Koutsopoulos [19] invented a microscopic traffic simulator (MITSIM) that includes a car-following model and a lane-changing model. They classify lane changing as mandatory or discretionary and model the lane-changing decision-making as a continuous four-step process: (1) decide to consider the LC, (2) select the target lane, (3) find acceptable gaps, (4) and implement the changes. The gap acceptance algorithm receives and checks for gaps in the target lane to perform the required lane change. Although the rule-based modeling framework in Yang et al. is similar to the Gipps' model (1986), one of the distinguishing features of their model is that, instead of considering the lane-changing decision-making as a deterministic process, it introduces the lane-changing probability to build the model.

The main idea of the discrete model is to use the utility function to evaluate the driving gain of each lane. Discrete models based on utility functions have the advantage of allowing evaluation of multiple decision criteria by combined weighting and can thus more easily be extended to complex scenarios. However, a large number of different weighting parameters can result in time-consuming parameter tuning and tractability difficulties, and vehicle lane change is a continuous process. The first discrete-choice model based on the utility function was proposed by Ahmed et al. [10, 11] and further refined by Toledo et al. [20, 32]. Ahmed et al. [9, 10] used the gap between the vehicles as the main influencing factor of the utility function, using the utility function to simulate the impact of the gap on the driver. Then, through the field data, the binomial logit model is used to calibrate the weighting parameters of the utility function. Ahmed's model divides the lane change type into MLC and DLC but does not explain the driver's choice of both sides. For a clearer understanding of the type of vehicle lane change, based on the basis of the Ahmed model, Toledo et al. [20, 32] proposed a probabilistic lane-changing decision model to describe the relationship between MLC and DLC. The relationship is captured by considering two types of lane changes in a single utility function, and a discrete-choice framework is chosen to simulate the strategy and operation of the driver's lane change decision. Most of the above studies are modeled on vehicle trajectory data, even though driver characteristics have a significant impact on all aspects of the lane process. But driver characteristics are not considered because driver's feature data extraction is difficult and the workload is huge, so most lane change decision models lack them. To explicitly incorporate the impact of driver characteristics, Sun and Elefteriadou [13] conducted a survey to determine and understand the driver's driving behavior in various lane change scenarios. The study reveals the types, causes, and main factors of each driver type in the lane-changing decision process and the links between them.

The artificial intelligence lane-changing decision methods use a computer to simulate the driver's thinking

and actions during the driving process and judge the environment to determine whether it is necessary to change lanes, whether it is necessary to change lanes, and the choice of target lanes. The artificial intelligence models impose some artificial intelligence algorithms, such as fuzzy logic [22], artificial neural networks [23], and Bayesian classification [24, 25], to explore the potential determinants of driver lane change behavior. The artificial intelligence models are completely data-driven and do not have any physical meaning parameters; it is inconvenient to analyze the performance of the method and the scenario expansion and does not consider the driver's psychological factors.

Through a review of the lane-changing models, it is found that the existing lane-changing models have not fully considered the driver's influence on the lane changing. However, these features are important for accurately describing the lane-changing behavior, and the relevant explanatory variables should be included in the future lane-changing model. In this paper, a new research idea based on lane-changing pressure is proposed to express the characteristics of the MCL in highway weaving section, and an MCL model is established based on the driver's driving characteristics. The traditional methods only consider the influence of the traffic flow characteristics of the target lane on the lane change. Considering the driver's psychology of being forced to change lanes, this paper introduces the driver's pressure to lane change (which is reflected by the distance between the vehicle and the off-ramp) into the MCL model, which is supposed to better describe the actual traffic situation.

3. Mandatory Lane Change Behavior

MLC is a necessary lane-changing behavior to achieve a certain demand, such as merging and diverging. DCL is an unessential lane-changing behavior, usually to achieve expectations speed or keep a certain distance from the car in front [9, 10]. Therefore, compared with the DCL, the drivers who have MLC demand will improve aggressiveness, and it is easy to cause traffic accidents. For this issue, this paper studies the MLC scenarios of vehicles leaving the highway, as shown in Figure 1. When the vehicle has the demand leaving the highway, it will choose whether to change lanes to the right lane according to the current driving environment, then enter the weaving section, and finally enter the off-ramp. The MLC process is a continuous process and is divided into four phases: (1) determining the target lane, (2) generating the intention to change lanes, (3) finding acceptable gaps, and (4) executing lane changing. The lane-changing decision process is shown in Figure 2. The MLC is a complicated process involving road conditions (total traffic capacity, vehicle arrival rate of on-ramp and off-ramp, and auxiliary lane layout), driver characteristics, and so on. Therefore, it is difficult to quantify various factors. After introducing the concept of driver's lane-changing pressure, this paper will systematically study the various stages of the MLC process.

4. MLC Models

4.1. MLC Pressure. MLC pressure refers to the pressure generated by the drivers who havse lane-changing demand before the last lane-changing node (LLCN). It is easy to know that the closer the driver is to the off-ramp, the stronger the desire to change lanes is generated. So, assume that the driver's MLC pressure is quantified by the available parameter of distance in this paper. The quantitative models were proposed as follows:

$$f = \begin{cases} \left[\omega\left(\dfrac{x_n - d_i}{S}\right)\right]^{-\alpha}, & d_i \le x_n \le S, \\ 0, & x_n > S, \end{cases} \tag{1}$$

where f denotes the lane-changing pressure value; x_n denotes the distance of the vehicle n from the off-ramp; d_i denotes the distance of the LLCN of the lane i from the off-ramp; S denotes the length of the weaving. While the vehicle does not enter the weaving $(x_n > S)$, the drivers do not have MLC pressure; that is, $f = 0$. While $x_n < S$, the pressure that the driver starts to generate, the closer the distance to the off-ramp, the greater the lane change pressure. While the vehicle reaches the LLCN $(x_n = d_i)$, the MLC pressure is ∞, and the vehicle must change lanes. $\alpha \in N^*$.

The formula for calculating ω is as follows:

$$\omega = \beta_0 + \beta_1 N + \beta_2 \lambda_1 + \beta_3 \lambda_2, \tag{2}$$

where $\beta_0, \beta_1, \beta_2$, and β_3 denote coefficient of each parameter, respectively; N denotes the number of lanes that need to be crossed; λ_1 denotes the average arrival rate of vehicles on the segment at time unit; λ_2 denotes the average arrival rate of the on-ramp vehicles at time unit.

The MLC pressure model is helpful to analyze the influence of the driver's psychological factors on the lane-changing behavior. Secondly, quantifying the driver's pressure is helpful to promote the identification and behavior prediction of the MHV characteristics on the heterogeneous traffic flow in the future and reduce the conflict between the CAVs and the MHV. Some characteristic parameters of drivers (gender, age, occupation, etc.) can also be added into the model.

4.2. MLC Intention. Yang and Koutsopoulos [19] proposed that mandatory lane changing occurs when drivers have to change lanes in order to

(a) connect the link on their path

(b) bypass a lane blockage downstream

(c) avoid entering a restricted use lane

(d) respond to lane use sign or speed limit sign

The MCL studied by Yang et al. are limited to (b) and (c). In addition, the intention to change lanes in the weaving area belongs to (a); drivers tend to change lanes early to avoid the lane-changing pressure. That is, the lower the pressure, the stronger the driver's intention to change lanes. Based on the MLC model, a new MLC intention model is proposed:

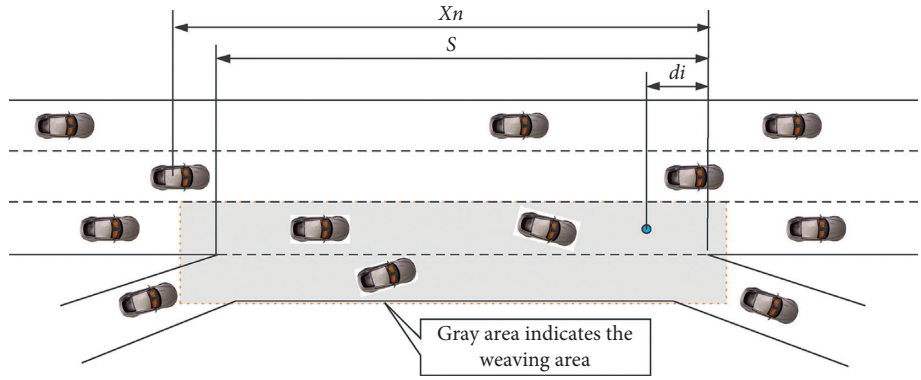

Figure 1: Highway weaving area.

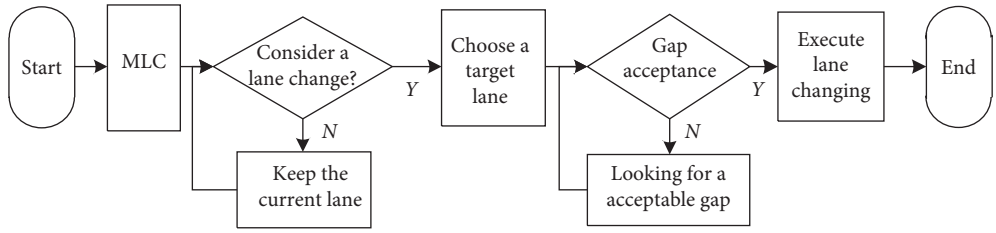

Figure 2: Lane-changing process.

$$\varphi\left(x_n/t_{x_n} \geq t_{x_n\_\min}\right) = \exp\left(-f\left(x_n\right)^{-1}\right) = \exp\left[-\frac{\left[\left(\beta_0 + \beta_1 N + \beta_2\lambda_1 + \beta_3\lambda_2\right)\left(x_n - d_i\right)\right]^{\alpha}}{S^{\alpha}}\right], \quad d_i \leq x_n \leq S, \tag{3}$$

where $\varphi(x_n/t_{x_n} \geq t_{x_n\_\min})$ denotes the intention generated of the vehicle n at a distance of x meters from off-ramp. $t_{x_n} \geq T_{x_n\_\min}$ denotes that there is a traversable gap in the target lane, which will analyze the determination of the traversable gap in the next section. The MLC intention model describes the intensity of the MLC intention at different location. The model is helpful to analyze the driving behavior characteristics in the weaving section and also obtains some driving potential preferences of the driver.

4.3. Gap Acceptance. The lane-changing decision is not only determined by the driver's personal driving-preference but also closely related to the driving environment. Only when there is an acceptable gap in the target lane, the vehicles can enter into the target lane. Therefore, the headway of the target lane is the key factor for the successful implementation of lane changing. Erlang distribution is a more general distribution model of traffic characteristics such as headway and speed. According to the change of parameter "k" in the distribution function, there are different distribution functions. The Erlang probability density function is as follows (as shown in Figure 3):

$$g(t) = \lambda e^{-\lambda t}\frac{(\lambda t)^{k-1}}{(k-1)!}, \quad k = 1, 2, 3, \ldots. \tag{4}$$

When $k = 1$, the Erlang distribution is equal to the negative exponential distribution; when $k = \infty$, a steady headway distance is produced. This shows that the parameter k in the Erlang distribution can reflect the conditions of various traffic flows between the free traffic flow and the crowded traffic flow. As the value of k increases, the more crowded the traffic is, the more crowded the traffic flow becomes. So that, it is difficult for drivers to drive freely. Therefore, the value of k is a rough representation of the degree of nonrandomness, and the degree of nonrandomness increases as the value of k increases.

The value of k is calculated as follows:

$$k = \frac{m^2}{S^2}, \tag{5}$$

$$m = \lambda_1 t = \frac{\sum_{j=1}^{g} k_j f_j}{\sum_{j=1}^{g} f_i} = \frac{\sum_{j=1}^{g} k_j f_j}{N}, \tag{6}$$

$$S^2 = \frac{1}{N-1}\sum_{i=1}^{N}\left(k_i - m\right)^2 = \frac{1}{N-1}\sum_{i=1}^{g}\left(k_i - m\right)^2 f_i, \tag{7}$$

where m denotes the vehicle arrival rate during time t; S^2 denotes the variance; t denotes the duration (s) or distance (m) of each count interval; g denotes the number of the groups; f_i denotes the frequency of the number of vehicles arriving is k_i in t; k_i denotes the number of vehicles arriving in t; N denotes the total number of observation intervals; K is an integer.

Previous studies [12, 32] assumed that the safe crossing gap was a fixed value or followed a normal distribution. However, due to the fact that lane changing is mandatory in the weaving area, the closer the vehicle was to the LLCN, the

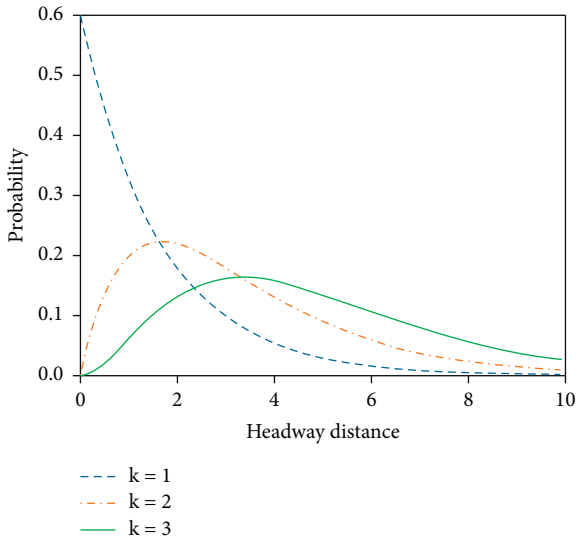

Figure 3: Erlang distribution.

greater the driver's desire to enter the target lane was. As a result, it is assumed that the minimum acceptable gap is proportional to the distance and proposes a minimum acceptable gap model:

$$t_{x_n\_\min} = \frac{t_d}{S}(S - x_n), \tag{8}$$

where $t_{x_n\_\min}$ is minimum acceptable merging headway chosen by the vehicle n. t_d is minimum acceptable merging headway expected by drivers in general driving environment.

So, the probability of acceptable gap in the target lane is as follows:

$$\begin{aligned} G\left(h \geq t_{x_n\_\min}\right) &= \int_{t_{x_n}}^{\infty} \lambda e^{-\lambda t_x} \frac{\left(\lambda t_{x_n}\right)^{k-1}}{(k-1)!} \\ &= \sum_{i=0}^{i} \left(\lambda k t_{x_n\_\min}\right)^{i} \frac{e^{-\lambda k t_{x_n}}}{i!}. \end{aligned} \tag{9}$$

The selection of manual-human vehicles' lane-changing gap is dynamic, which has great interference to CAVs trajectory planning. If CAVs are blindly conservative or aggressive, it is easy to cause vehicle collisions. Therefore, the acceptable gap acceptance model proposed in this paper can provide an important technical means for MCL identification of CAVs, which provides a guarantee for traffic safety in mixed-traffic flows.

4.4. MLC Execution. Two conditions should be met for the successful implementation of MLC: the driver has the MLC intention and the target lane has an acceptable gap. When both conditions are met, the vehicle can successfully change lanes to the target lane. Suppose the driver has the intention to change lanes which is event A, and there is the acceptable gap in the target lane which is event B. According to the lane change intention model and headway distribution model proposed previously, the MLC probability density function can be obtained:

$$\begin{aligned} P(x_n) &= P(AB) = P(A)P(B), \\ P(x_n) &= \exp\left[\frac{-(x_n - d_i)^{\alpha}}{S^{\alpha}\left(\beta_0 + \beta_1 N + \beta_2 \lambda_1 + \beta_3 \lambda_2\right)^{-\alpha}}\right] \\ &\cdot \int_{(t_d/S)x_n}^{\infty} \lambda e^{-\lambda t_x} \frac{\left(\lambda (t_d/S) x_n\right)^{k-1}}{(k-1)!}, \end{aligned} \tag{10}$$

where $P(x_n)$ is the probability density function of MLC in the weaving area. This model can predict the lane-changing behavior for advanced driver assistance system (ADAS) to avoid crash and trajectory planning [27, 28].

5. Case Study and Models Verification

5.1. Scenarios and Data Description. The NGSIM trajectory data is obtained by the US Federal Highway Administration (FHWA) for the purpose of conducting the "Next Generation Simulation" program [33]. The data is collected by the high-altitude camera to capture the vehicle's driving process, and then the video processing software is used to restore the precise position of each vehicle in the study section at 10 frames per frame or 15 frames per second. This paper uses the data of the US-101 highway section in NGSIM. The length of the detected section is 640 meters and there are five lanes. In addition, it also includes a couple of ramps and an auxiliary lane. The effective data is obtained by processing the trajectory data, as shown in Table 1. The road segment diagram is shown in Figure 4.

It can be seen from the figure that the segment has a weaving section and the collected trajectory data is complete. 157 cars which have finished MLC were extracted from the data.

5.2. MLC Analysis and Models Verification

5.2.1. MLC Intention Model. In order to accurately capture the driver's intention to change lanes and to verify the reliability of the MLC intention model proposed in this paper, we extracted some trajectory in free flow. That is, there are no vehicles in auxiliary lane (lane 6) during this period. As shown in Figure 5, in the absence of other vehicle interferences, lane-changing positions are mainly concentrated at 140–200 meters from the downstream. There are few vehicles that choose to change lanes at the end of lane 5. The reason for this phenomenon is that drivers with MLC demand tend to enter lane 6 as early as possible to relieve pressure. While $\lambda_2 = 0$, the MLC intention model is as follows:

$$\varphi\left(x_n \mid \lambda_2 = 0,\ i = 1\right) = \exp\left[\frac{-(x_n - d_i)^{\alpha}}{S^{\alpha}\left(\beta_0 + \beta_1 N + \beta_2 \lambda_1\right)^{-\alpha}}\right]. \tag{11}$$

As shown in Figure 6, the curve represents the relationship between φ and x_n, and the histogram represents the

Table 1: Detecting road parameters.

Number of lanes	Road type	Traffic state	Segment length (m)	Auxiliary lane (m)
5	Highway	Free	640	232

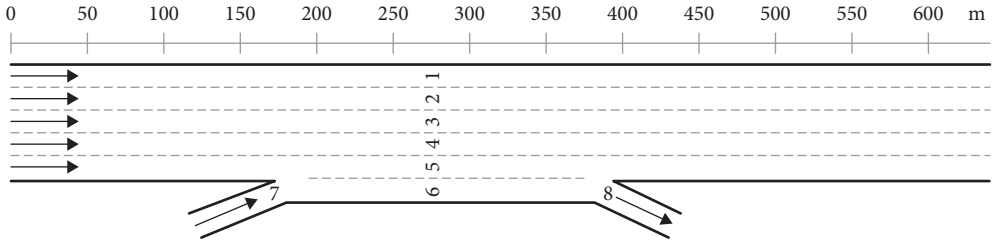

Figure 4: Detecting road geometry.

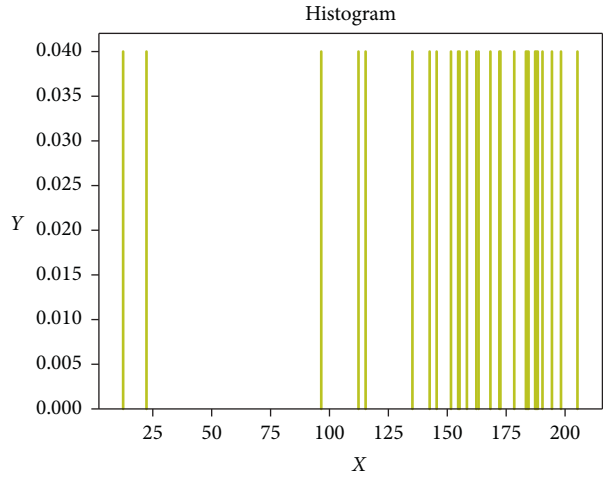

Figure 5: Lane-changing points distribution.

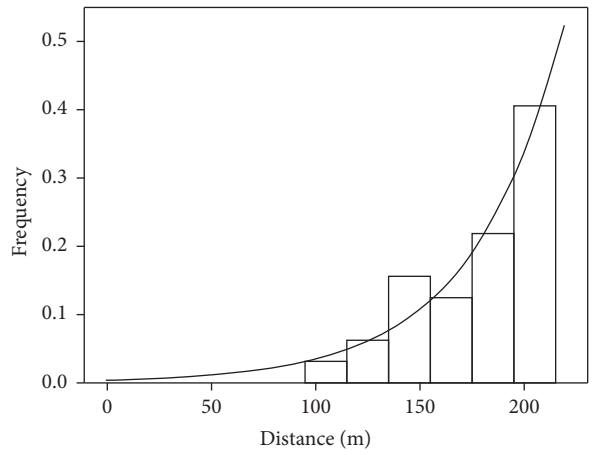

Figure 6: Lane-changing willingness fitting.

frequency at which all vehicles change lanes at x_n during the detection period. The fit of the model proposed is 92.3%, which can more accurately describe the intention of the driver to change lanes.

5.2.2. Gap Acceptance Model. When there is no vehicle in front of the subject vehicle within the detection section, the default ID of the vehicle in front is "0," and the headway is also "0." Although the headway is zero in data, but the actual

headway is large. To this end, we divide the headway into two parts. The first part is that there is a certain headway, and the other part is "0." Therefore, the driver's acceptable headway is divided into two parts $t = 0$ or $t \geq t_a$:

$$t = \begin{cases} \text{Refuse changing lanes}, & 0 < t < t_{x_n\_\min}, \\ \text{Accept changing lanes}, & t = 0 \text{ or } t \geq t_{x_n\_\min}, \end{cases} \tag{12}$$

where t denotes headway.

This paper uses the Erlang distribution to fit the lane headway of lane 6, as shown in Figure 7. It is found that the frequency of the headway is zero, accounting for 43%, which indicates that the weaving zone is in good operating condition. When $k = 2$, the Erlang distribution function fits better to the headway of lane 6 (Figure 8).

The driver's acceptable gap is related to the driver's own driving style and is also related to the distance from on-ramp. The vehicle headway ($t_{x\_\max}$)-distance (x_n) scatter plot is drawn by collecting the headway data at the time of the vehicles change lanes. Vehicles mainly change lanes within 150–200 meters. As the distance decreases, the range of the headway is also reduced. They conform to the following relationship:

$$t_{\min} < t_a \leq t_{x\_\max} = S \cdot e^{(-2/x_n)}. \tag{13}$$

5.2.3. MLC Positions Distribution. In this paper, the local coordinates of the MLC lane-changing positions are collected in weaving section of US-101 highway. The trajectory scatter plot (Figure 9) and heat map (Figure 10) of the lane change position are drawn according to the local coordinates. Lane 6 starts at 636.7 feet and ends at 1333.8 feet, respectively. As can be seen from the two figures, lane change points are mainly concentrated in the range of 650–750 feet in the horizontal coordinate. Drivers tend to change lanes at the front of weaving area to lane 6 which can eliminate the pressure of lane change, instead of choosing lanes after measuring lane utility. This indicates that there is a trace to follow when the vehicle chooses to change lanes. And the rule of driver changing lanes can provide important guidance for CAVs lane-changing recognition to avoid collision.

According to the MCL probability density function proposed in this paper, the following formula can be obtained:

$$\begin{aligned} P(x_n) &= \varphi\left(x_n / t_{x_n} \geq T_{x\_\min}\right) \cdot G\left(h \geq t_x\right), \\ &= \left(1 + \lambda_2 \frac{t_d}{S} x_n\right) \exp\left[\frac{-(x_n - d)}{\beta_0 + \beta_1 N + \beta_2 \lambda_1 + \beta_3 \lambda_2} - \frac{2\lambda_2 t_d}{S} x_n\right] \\ &\quad + 0.43 \cdot \exp\left[\frac{(x_n - d)}{\beta_0 + \beta_1 N + \beta_2 \lambda_1}\right], \end{aligned} \tag{14}$$

where $P(x_n)$ represents MLC probability density function and 0.43 in the model represents the proportion when the headway is zero, as shown in Figure 7. It can be seen from Figure 11 that the model proposed in this paper can

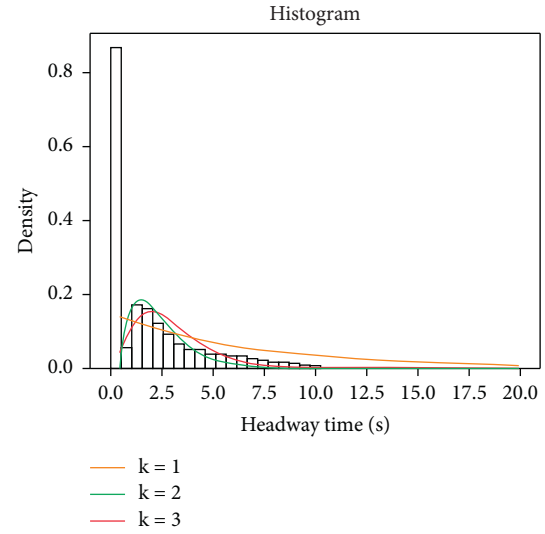

Figure 7: Headway distribution.

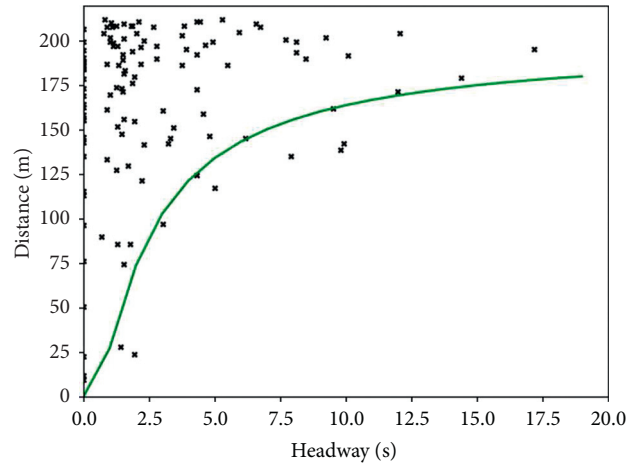

Figure 8: Headway of lane changing.

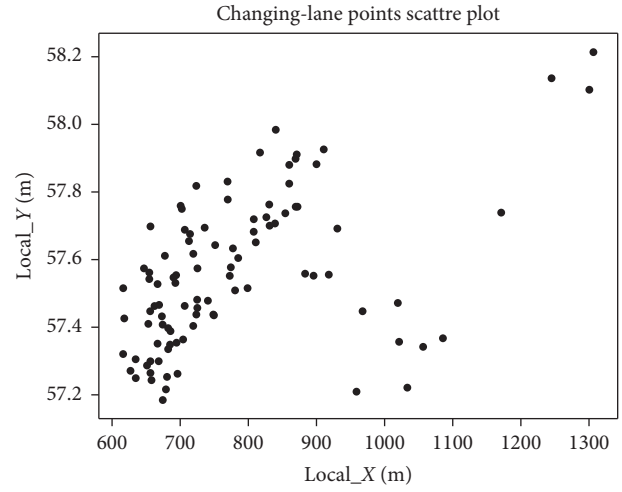

Figure 9: Lane-changing positions.

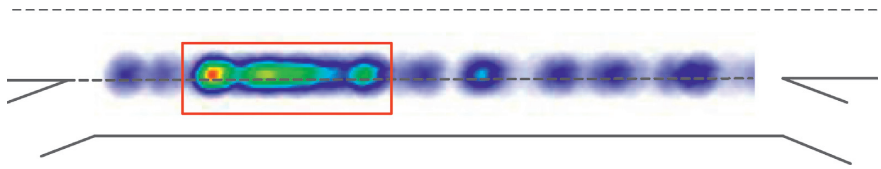

Figure 10: Lane-changing location heat map.

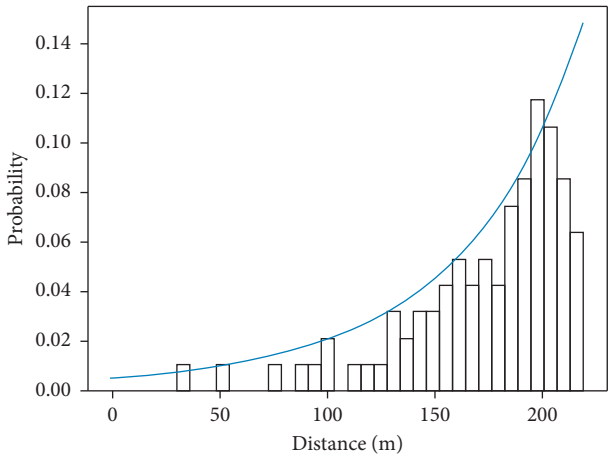

Figure 11: Histogram of lane-changing position.

accurately describe the drivers' selection trend of the lane-changing timing in the weaving section. But there is a difference in a part at $x_n > 200$ meters for the reason that when establishing the MLC pressure model, this paper assumes that the pressure of the lane change is inversely proportional to the intention which makes the default optimal position of changing lanes be at front position of the auxiliary lane. However, when the pressure accumulates to a certain value, the MCL intention reaches the maximum value. How much pressure the driver generates is needed to be studied; the MCL intention will reach the peak.

6. Conclusion

Inspired by the principle of discretionary lane change models, this paper proposes a method based on driver's psychological pressure to analysis MLC. The main factor for driving the driver to DLC is the lanes' utility, and the main factor for driving the driver to MLC is the lane-changing pressure. Therefore, this paper proposes a new concept named lane-changing pressure to analyze the MLC stages. And obtaining the following research results, (1) the MLC pressure model is proposed by leading in the lane-changing pressure from the distance of the off-ramp. (2) Based on the MLC pressure, an MLC intention model is proposed, which describes the driver's preference for lane-changing positions in the weaving section. (3) By researching the driver's MLC intention and the probability of acceptable gaps, an MLC positions probability density function is proposed.

It is verified that the proposed models can objectively describe the characteristics of the lane-changing process in the weaving section by the NGSIM data. Compared with the traditional model, the proposed models explore the vehicle lane-changing process from the driver's level, which is more explanatory and expandable. It can provide the basis for CAVs vehicle to change lane recognition in heterogeneous traffic flow in the future.

Data Availability

The data used to support the findings of this study are available from the corresponding author upon request.

Conflicts of Interest

The authors declare that there are no conflicts of interest regarding the publication of this paper.

Acknowledgments

This work was supported by the Natural Science Foundation of China (nos.51808057, 71861023, and 61403047) and in a part supported by Hunan Provincial Natural Science Foundation of China (no. 2019JJ30026), the Young Elite Scientists Sponsorship Program by Hunan province of China (2018RS3074), Hunan Provincial Natural Science Foundation of China (2018JJ3553), Changsha Science and Technology Bureau Project (kq1801056), Open Fund of Hunan Key Laboratory of Smart Roadway and Cooperative Vehicle-Infrastructure Systems (kfj180702 and kfj190702), Innovation Team Project for Transportation Engineering in CSUST, and Ministry of Science Project with Montenegro (3-2).

References

[1] Y. Ali, M. M. Haque, Z. Zheng, S. Washington, and M. Yildirimoglu, "A hazard-based duration model to quantify the impact of connected driving environment on safety during mandatory lane-changing," *Transportation Research Part C: Emerging Technologies*, vol. 106, pp. 113–131, 2019.

[2] H. Adeli and A. Karim, "Fuzzy-wavelet RBFNN model for freeway incident detection," *Journal of Transportation Engineering*, vol. 126, no. 6, pp. 464–471, 2000.

[3] H. Adeli and A. Samant, "An adaptive conjugate gradient neural network-wavelet model for traffic incident detection," *Computer-Aided Civil and Infrastructure Engineering*, vol. 15, no. 4, pp. 251–260, 2000.

[4] S. Ahn and M. J. Cassidy, "Freeway traffic oscillations and vehicle lane-change maneuvers," in *Proceedings of the 17th International Symposium of Transportation and Traffic Theory*, R. E. Allsop, M. G. H. Bell, and B. G. Heydecker, Eds., pp. 691–710pp. 691–, London, UK, July 2007.

[5] A. Duret, S. Ahn, and C. Buisson, "Passing rates to measure relaxation and impact of lane-changing in congestion," *Computer-Aided Civil and Infrastructure Engineering*, vol. 26, no. 4, pp. 285–297, 2011.

[6] S. Ghosh-Dastidar and H. Adeli, "Wavelet-clustering-neural network model for freeway incident detection," *Computer-Aided Civil and Infrastructure Engineering*, vol. 18, no. 5, pp. 325–338, 2003.

[7] Q. Zeng, W. Gu, X. Zhang, H. Wen, J. Lee, and W. Hao, "Analyzing freeway crash severity using a Bayesian spatial generalized ordered logit model with conditional autoregressive priors," *Accident Analysis & Prevention*, vol. 127, pp. 87–95, 2019.

[8] M. Rahman, M. Chowdhury, Y. Xie, and Y. He, "Review of microscopic lane-changing models and future research opportunities," *IEEE Transactions on Intelligent Transportation Systems*, vol. 14, no. 4, pp. 1942–1956, 2013.

[9] K. I. Ahmed, *Modeling Drivers' Acceleration and Lane Changing behavior*, Massachusetts Institute of Technology, Cambridge, CA, USA, 1999.

[10] K. L. Ahmed, M. Ben-Akiva, H. Koutsopoulos, and R. G. Mishalani, "Models of freeway lane changing and gap acceptance behavior," in *Transportation and traffic theory. Proceedings of the 13th International Symposium on Transportation and Traffic Theory*, vol. 13, pp. 501–515, Lyon, France, July 1996.

[11] Q. Zeng, H. Wen, H. Huang, and M. Abdel-Aty, "A Bayesian spatial random parameters Tobit model for analyzing crash rates on roadway segments," *Accident Analysis & Prevention*, vol. 100, pp. 37–43, 2017.

[12] F. Chen, M. Song, and X. Ma, "Investigation on the injury severity of drivers in rear-end collisions between cars using a random parameters bivariate ordered Probit model," *International Journal of Environmental Research and Public Health*, vol. 16, no. 14, p. 2632, 2019.

[13] D. J. Sun and L. Elefteriadou, "Lane-changing behavior on urban streets: an "In-Vehicle" field experiment-based study," *Computer-Aided Civil and Infrastructure Engineering*, vol. 27, no. 7, pp. 525–542, 2012.

[14] P. G. Gipps, "A model for the structure of lane-changing decisions," *Transportation Research Part B: Methodological*, vol. 20, no. 5, pp. 403–414, 1986.

[15] K. Nagel and M. Schreckenberg, "A cellular automaton model for freeway traffic," *Journal de Physique I*, vol. 2, no. 12, pp. 2221–2229, 1992.

[16] K. Nagel, D. E. Wolf, P. Wagner, and P. Simon, "Two-lane traffic rules for cellular automata: a systematic approach," *Physical Review E*, vol. 58, no. 2, pp. 1425–1437, 1998.

[17] P. Hidas, "Modelling vehicle interactions in microscopic simulation of merging and weaving," *Transportation Research Part C: Emerging Technologies*, vol. 13, no. 1, pp. 37–62, 2005.

[18] H. Yu, H. E. Tseng, and R. Langari, "A human-like game theory-based controller for automatic lane changing," *Transportation Research Part C: Emerging Technologies*, vol. 88, pp. 140–158, 2018.

[19] Q. Yang and H. N. Koutsopoulos, "A Microscopic Traffic Simulator for evaluation of dynamic traffic management systems," *Transportation Research Part C: Emerging Technologies*, vol. 4, no. 3, pp. 113–129, 1996.

[20] T. Toledo, H. N. Koutsopoulos, and M. Ben-Akiva, "Integrated driving behavior modeling," *Transportation Research Part C: Emerging Technologies*, vol. 15, no. 2, pp. 96–112, 2007.

[21] J. Nilsson, J. Silvlin, M. Brannstrom, E. Coelingh, and J. Fredriksson, "If, when, and how to perform lane change maneuvers on highways," *IEEE Intelligent Transportation Systems Magazine*, vol. 8, no. 4, pp. 68–78, 2016.

[22] S. Das and B. Ba, "Simulations of highway chaos using fuzzy logic," in *18th International Conference of the North American Fuzzy Information Processing Society - NAFIPS (Cat. No.99TH8397)*, June 1999.

[23] J. Peng, Y. Guo, R. Fu, W. Yuan, and C. Wang, "Multi-parameter prediction of drivers' lane-changing behaviour with neural network model," *Applied Ergonomics*, vol. 50, pp. 207–217, 2015.

[24] Yi Hou, E. Praveen, and C. Sun, "Modeling mandatory lane changing using Bayes classifier and decision trees," *IEEE Transactions on Intelligent Transportation Systems*, vol. 15, no. 2, pp. 647–655, 2014.

[25] J. C. McCall, D. P. Wipf, M. M. Trivedi, and B. D. Rao, "Lane change intent analysis using robust operators and sparse bayesian learning," *IEEE Transactions on Intelligent Transportation Systems*, vol. 8, no. 3, pp. 431–440, 2007.

[26] D. C. K. Ngai and N. H. C. Yung, "A multiple-goal reinforcement learning method for complex vehicle overtaking maneuvers," *IEEE Transactions on Intelligent Transportation Systems*, vol. 12, no. 2, pp. 509–522, 2011.

[27] V. Butakov and P. Ioannou, "Personalized driver/vehicle lane change models for ADAS," *IEEE Transactions on Vehicular Technology*, vol. 64, no. 10, pp. 4422–4431, 2015.

[28] M. McNaughton, C. Urmson, J. M. Dolan, and J.-W. Lee in *Proceedings of IEEE International Conference on Robotics and Automation*, pp. 4889–4895, IEEE, Shanghai, China, May 2011.

[29] A. Halati, H. Lieu, and S. Walker, "CORSIM—corridor traffic simulation model," in *Proceedings of Traffic Congestion and Traffic Safety in the 21st Century: Challenges, Innovations, and Opportunities*, pp. 570–576, Chicago, IL, USA, June 1997.

[30] M. Rickert, K. Nagel, M. Schreckenberg, and A. Latour, "Two lane traffic simulations using cellular automata," *Physica A: Statistical Mechanics and Its Applications*, vol. 231, no. 4, pp. 534–550, 1996.

[31] H. Kita, "A merging-giveway interaction model of cars in a merging section: a game theoretic analysis," *Transportation Research Part A: Policy and Practice*, vol. 33, no. 3-4, pp. 305–312, 1999.

[32] T. Toledo, H. N. Koutsopoulos, and M. Ben-Akiva, "Estimation of an integrated driving behavior model," *Transportation Research Part C: Emerging Technologies*, vol. 17, no. 4, pp. 365–380, 2009.

[33] https://www.fhwa.dot.gov/publications/research/operations/07030/index.cfm.

Hindawi
Journal of Advanced Transportation
Volume 2020, Article ID 1528028, 12 pages
https://doi.org/10.1155/2020/1528028

Research Article

Sectional Information-Based Collision Warning System Using Roadside Unit Aggregated Connected-Vehicle Information for a Cooperative Intelligent Transport System

Sehyun Tak,[1] **Jinsu Yoon**,[1] **Soomin Woo**,[2] **and Hwasoo Yeo**[3]

[1]*The Korea Transport Institute, 370 Sicheong-daero, Sejong-si, Republic of Korea*
[2]*University of California, Berkeley, CA, USA*
[3]*Korea Advanced Institute of Science and Technology, 291 Daehak-ro, Yuseong-gu, Daejeon, Republic of Korea*

Correspondence should be addressed to Sehyun Tak; sehyun.tak@koti.re.kr

Received 3 January 2020; Revised 12 May 2020; Accepted 23 June 2020; Published 21 July 2020

Academic Editor: Jaeyoung Lee

Vehicular collision and hazard warning is an active field of research that seeks to improve road safety by providing an earlier warning to drivers to help them avoid potential collision danger. In this study, we propose a new type of a collision warning system based on aggregated sectional information, describing vehicle movement processed by a roadside unit (RSU). The proposed sectional information-based collision warning system (SCWS) overcomes the limitations of existing collision warning systems such as the high installation costs, the need for high market penetration rates, and the lack of consideration of traffic dynamics. The proposed SCWS gathers vehicle operation data through on-board units (OBUs) and shares this aggregated information through an RSU. All the data for each road section are locally processed by the RSU using edge computing, allowing the SCWS to effectively estimate the information describing the vehicles surrounding the subject vehicle in each road section. The performance of the SCWS was evaluated through comparison with other collision warning systems such as the vehicle-to-vehicle communication-based collision warning system (VCWS), which solely uses in-vehicle sensors; the hybrid collision warning system (HCWS), which uses information from both infrastructure and in-vehicle sensors; and the infrastructure-based collision warning system (ICWS), which only uses data from infrastructure. In this study, the VCWS with a 100% market penetration rate was considered to provide the most theoretically similar result to the actual collision risk. The comparison results show that in both aggregation and disaggregation level analyses, the proposed SCWS exhibits a similar collision risk trend to the VCWS. Furthermore, the SCWS shows a high potential for practical application because it provides acceptable performance even with a low market penetration rate (30%) at the relatively low cost of OBU installation, compared to the VCWS requirement of a high market penetration rate at a high installation cost.

1. Introduction

Roadway safety is one of the most critical issues that researchers have studied to improve safety and reduce fatalities. Previous research has demonstrated a causal relationship between driver inattention, close distance between vehicles, and car accidents [1, 2]. In addition to the effects of driver inattention, the limits of human cognitive abilities, especially near curves or intersections, have also been found to be a causal factor in many accidents. Many studies have accordingly developed systems to prevent accidents and mitigate their consequences by adopting advanced technology, such as the advanced driver assistance system (ADAS) [3] and cooperative intelligent transportation service (C-ITS), based on sensor technologies, vehicle-to-vehicle (V2V) communication, and vehicle-to-infrastructure (V2I) communication [4].

An ADAS is designed to mitigate the severity of an accident and prevent it if possible by supporting the driver's abilities to avoid it. The forward collision warning system or forward collision avoidance system is the most extensively studied type of ADAS and is mainly based on in-vehicle

sensors [3, 5–9]. An ADAS contributes to improving vehicle safety by providing a warning signal to the driver and automatically activating the braking system in an emergency situation [10]. However, many current implementations of ADAS have a limited ability to completely prevent an accident. First, due to the limited field of view of distance sensors, the detection ability of an ADAS is degraded in some situations such as near curves, hills, or intersections [11]. Second, an ADAS requires a high installation cost to provide sufficient accuracy with a large field of view [5, 12, 13]. In other words, sensors that can detect the activity of other vehicles at a sufficient distance to prevent an accident considering driver reaction times and Vehicle speed can be too costly to widely penetrate the market. Many ADAS implementations therefore use in-vehicle sensors to produce warning signals based on information from a limited range of up to 100 or 150 meters from the vehicle [14]. However, this range may not be sufficient to anticipate a possible collision risk arising from traffic further downstream from the subject vehicle in time for the driver to safely conduct necessary actions to prevent a dangerous situation, especially in a free flow traffic state. By the time the limited range of these in-vehicle sensors finally detect danger downstream, an abrupt and potentially late warning may be issued as the necessary information cannot be updated in the system in time.

The C-ITS is designed to improve vehicle safety using a combination of V2V communication and V2I communication. In a C-ITS, connected vehicles (CVs) equipped with on-board units (OBUs) communicate safety-related information such as vehicle speed, vehicle acceleration, traffic signals, weather conditions, and steering status to each other and obtain road condition information from a roadside unit (RSU). This system can use these data to provide a warning signal to the driver when a hazardous event occurs downstream, such as an accident, road work, or a slow-moving or stopped vehicle. By allowing the driver to react to an upcoming hazardous situation in advance, a C-ITS can reduce the frequency and severity of accidents.

Due to the tremendous potential of the C-ITS approach for improving vehicle safety, various types of collision and hazard warning systems have been proposed and tested in the United States, Europe, Japan, and South Korea, including curve warning, right turn warning, and slow vehicle warning systems [15, 16]. The collision and hazard warning systems applied by a C-ITS can be classified as V2V communication-based or V2I communication-based according to the communication method. A V2V communication-based system is based on safety messages generated from the OBUs contained in vehicles. Representative V2V applications include forward collision warnings in the United States [17] and in South Korea [16], as well as emergency electronic braking lights [18] and precrash/postcrash warnings [19] in Europe. A V2I communication-based system provides a warning signal to the driver based on information generated by and transmitted from an RSU. In this system, accidents and hazardous events are detected by roadside sensors using technology such as lidar, radar, and cameras [20, 21]. Representative V2I applications include queue warnings [22] in the United States, hazardous location notifications [16] in South Korea, and traffic jam ahead and stationary vehicle notifications [19] in Europe.

In previous research and predeployment projects, C-ITS applications have shown good safety performance and considerable potential in terms of accident reduction and improvement of user comfort [16, 18, 23]. However, a C-ITS requires a high market penetration rate of OBUs to realize a high quality of service or justify the high RSU installation cost. Additionally, the performance of a C-ITS may be considerably hindered by the communication latency of the connected sensors.

Collision warning systems based solely on data collected by infrastructure without OBUs, known as infrastructure-based collision warning systems (ICWS), have also been studied [24, 25]. These systems determine collision risk using only information from road infrastructure to provide a warning signal to drivers. This system has advantages such as easy implementation and fully utilization of legacy transportation systems. However, this system is of limited use as a practical warning service to drivers because it cannot produce a personalized collision risk for each driver. Specifically, the utility of the data acquired by road infrastructure may be hindered by an averaging effect that only produces an aggregate value for a vehicle population in a given link when this data is created by, for instance, a wide distribution of speeds and acceleration. Even if the vehicle population within a given link is smoothly distributed with speeds similar to that of the subject driver, a small number of aggressive drivers that constitute a minority of the entire population in the link may disrupt the stability of the vehicle population and pose a serious danger to the subject driver. Accordingly, the hybrid collision warning system (HCWS) has been proposed to overcome such limitations of the ICWS [26, 27]. These hybrid systems use information that represents each road section together with information from individual vehicles. However, they also possess a limited ability to produce highly accurate collision risks for each vehicle in a link. Collision warning systems solely based on V2V communication may offer a solution to this weakness; however, the success of such V2V-based collision warning systems (VCWS) is contingent upon a high market penetration rate in order to provide reliable communications, as mentioned above.

Previously proposed collision warning systems must overcome several limitations before they can be widely used. Collision warning systems based on in-vehicle sensors such as ADAS have a limited field of view, resulting in a weakness in detecting danger arising from downstream areas. Additionally, the application of ADAS is limited due to its high installation cost. Collision warning systems based on infrastructure only acquire averaged data from their target road links; thus, they lack detailed information describing individual drivers in a calculation that may be critical in disturbing the link stability. Communications-based collision warning systems, also known as CV technology, can overcome the limitations of the in-vehicle sensor-based collision warning systems by transmitting microscopic information such as vehicle speed, location, and angle to

surrounding vehicles. This system can quickly and cost-effectively determine the collision risk arising in a downstream area by utilizing information from neighboring vehicles and infrastructure. However, this system requires a high market penetration rate of OBUs and highly reliable information obtained from roadside infrastructure. Failure to meet these requirements leads to a low performance of communication-based collision warning systems. Indeed, collision warning information generated from roadside detection systems is yet not reliable as they are still being developed for commercial use.

To provide a satisfactory and reliable warning service under a lower market penetration rate, in this study we propose the sectional information-based collision warning system (SCWS). The proposed SCWS estimates the movement of surrounding vehicles using sectional traffic information gathered from OBUs in each vehicle. This information is then gathered and distributed using edge computing technology installed in RSUs. This system was designed to meet three objectives. First, the proposed collision warning system must achieve high warning signal accuracy under a relatively low market penetration rate. Second, by actively utilizing information from the OBUs in CVs, the system should be implemented at a lower installation cost compared to sensor-based collision warning systems. Third, the system must have the ability to consider the dynamic changes in surrounding traffic status and collision risk of the subject vehicle. The following sections describe and evaluate the proposed SCWS according to these objectives.

2. Sectional Information-Based Collision Warning System

n this paper, we propose the SCWS, which estimates the collision risk of a subject vehicle based on data gathered from the OBUs of the CVs in each road section. This system provides a warning signal to the driver when the vehicle is in a dangerous situation, such as a high collision risk. Unlike the VCWS, in which vehicles directly communicate and transfer in-vehicle information such as the exact location, speed, and acceleration of the leading vehicle to each other, the SCWS calculates the collision risk on its own by combining the data from the subject vehicle such as speed and acceleration with data acquired from RSUs. This system only shares the representative information for each road segment from the RSU, which describes the surrounding traffic state that the subject vehicle will experience in the immediate future.

The proposed SCWS calculates the collision risk of the subject vehicle using the surrogate safety measure [28]. This measure is a safety performance indicator that represents the accident risk based on microscopic traffic parameters such as speed, space headway, and acceleration. In the following sections, we describe the surrogate safety measure used to calculate collision risk in the proposed SCWS.

2.1. Measurement for Collision Risk Calculation. The surrogate safety measure is a widely used method for calculating the collision risk of a subject vehicle, and many safety surrogate measures have been proposed by researchers such as the time-to-collision and stopping distance index [29–31]. Among these various safety surrogate measures, the deceleration-based safety surrogate measure (DSSM) was applied in this study [28]. This measure reflects the mechanical performance of individual vehicles, such as braking performance and maximum acceleration rate, as well as personal driving behavior, such as jerk and transition time, with higher hazard detection accuracy than other surrogate safety measures [32, 33]. The equations governing the DSSM are as follows:

$$b_n(t) = b_{\max,n-1} \cdot \frac{\left[v_n(t) + a_n(t) \cdot \tau\right]^2}{\left[2 \cdot K \cdot b_{\max,n-1} + v_{n-1}(t)^2\right]} < 0, \tag{1}$$

$$\begin{aligned} K = {} & \left[x_n(t) - x_{n-1}(t) + s_{n-1}\right] + \left[2v_n(t) + a_n(t) \cdot \tau\right] \cdot \frac{\tau}{2} \\ & - \left[\frac{v_{n-1}(t)}{2} + \left(a_{n-1}(t) + b_{\max,n-1}\right) \cdot \frac{a_{n-1}(t) - b_{\max,n-1}}{4L_{n-1}}\right] \\ & \cdot \frac{\left(a_{n-1}(t) - b_{\max,n-1}\right)}{L_{n-1}} \\ & + \left[\frac{v_n(t)}{2} + a_n(t) \cdot \frac{\tau}{2} + \left(a_n(t) + b_{\max,n}\right) \cdot \frac{a_n(t) - b_{\max,n}}{4L_n}\right] \\ & \cdot \frac{a_n(t) - b_{\max,n}}{L_n}, \end{aligned} \tag{2}$$

$$\mathrm{DSSM}(t) = \frac{b_n(t)}{b_{\max,n}}, \tag{3}$$

where $a_n(t)$ and $a_{n-1}(t)$ are the respective acceleration rates of the subject vehicle and leading vehicle at time t, $b_{\max,n}$ and $b_{\max,n-1}$ are the respective maximum braking performances of the subject vehicle and leading vehicle, $v_n(t)$ and $v_{n-1}(t)$ are the respective speeds of the subject vehicle and leading vehicle at time t, $v_n(t+\tau)$ is the expected speed of the subject vehicle after τ, $x_n(t)$ and $x_{n-1}(t)$ are the respective locations of the subject vehicle and leading vehicle at time t, L_n and L_{n-1} are the respective maximum variations of acceleration of the subject vehicle and leading vehicle, s_{n-1} is the length of the leading vehicle, and $b_n(t)$ is the required deceleration rate of the subject vehicle to avoid an accident at time t.

In equation (3), DSSM estimates the collision risk using the ratio of the required deceleration rate to the maximum braking performance of the subject vehicle. The required deceleration is determined as the minimum deceleration rate required to avoid an accident when the leading vehicle reduces its speed at its maximum deceleration rate. The maximum braking performance of the subject vehicle depends on its braking capabilities. By dividing the required deceleration rate by the maximum braking performance, the DSSM can estimate a customized collision risk for any subject vehicle.

2.2. SCWS Architecture. This study constructed the SCWS based on equations (1)–(3). Figures 1 and 2 show the configuration and data flow of the proposed SCWS. As seen

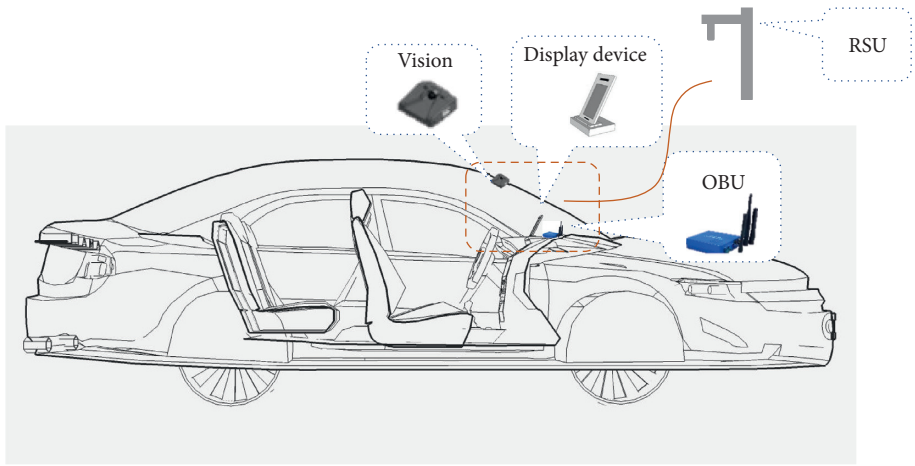

Figure 1: Configuration of the proposed SCWS.

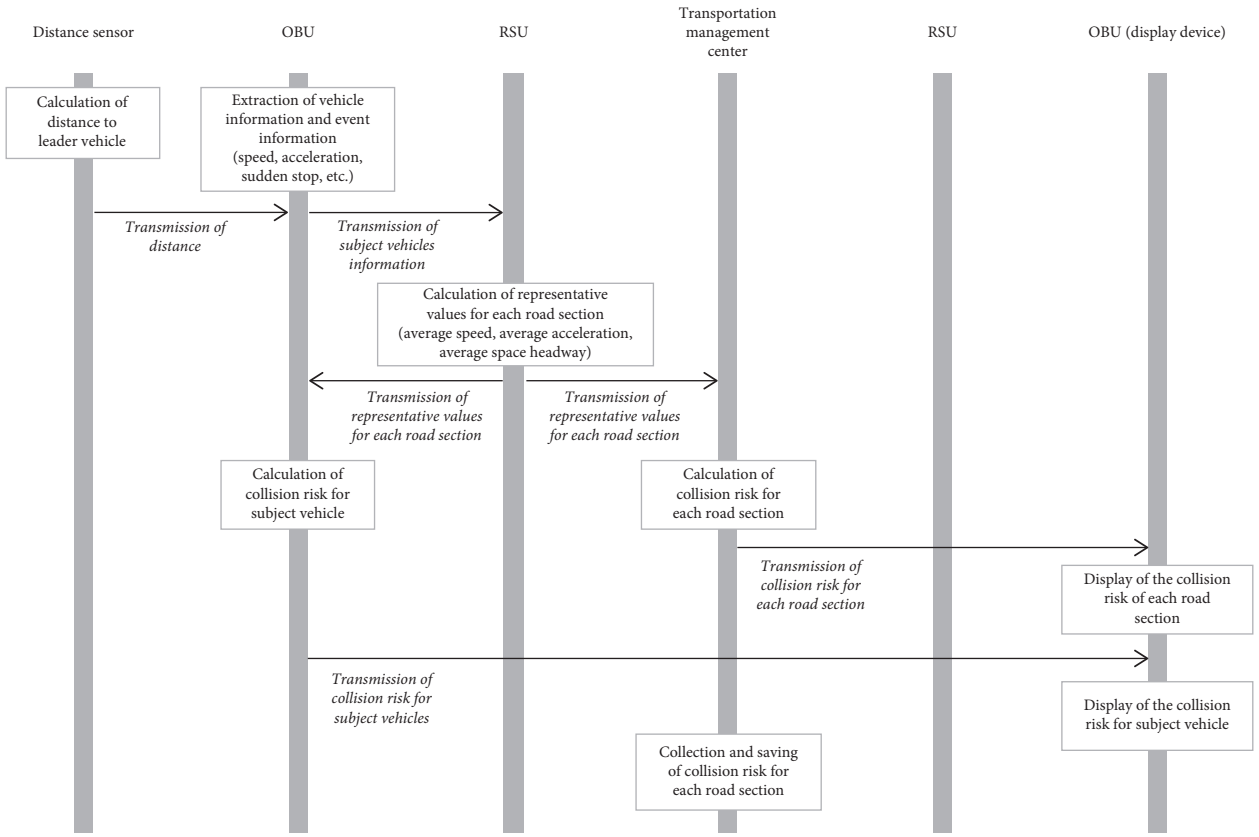

Figure 2: Data flow of the proposed SCWS.

in Figure 1, the SCWS consists of three parts: (1) a distance sensor such as a radar sensor or vision sensor, (2) an RSU, and (3) an OBU. Using the distance sensor, the distance between the subject vehicle and the leading vehicle is estimated every 0.1 seconds and transmitted to the OBU. Four functions are implemented within the OBU. First, it gathers the sensor data from the subject vehicle, such as speed, acceleration, jerk, and preferred braking performance, in real-time. Second, it uploads these data to the RSU, which calculates the representative values for each road segment using edging computing. Third, the OBU downloads the representative traffic-related values for the road segment from the RSU, which is regarded as describing the leading vehicle, to calculate the collision risk using the driving data from the subject vehicle. Fourth, the estimated collision risk is displayed on the screen of the OBU, which provides appropriate warning signals to the driver through audio and visual indicators.

The data from individual drivers on the subject road segment is processed by the RSU as shown in Figure 3, which

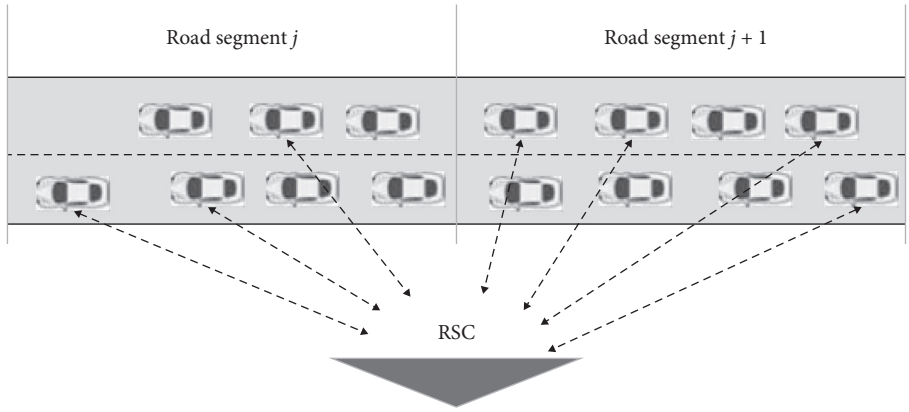

Road segment	ID	Space headway (m)	Speed (m/s)	Acceleration (m/s^2)	Jerk (m/s^3)	Braking Performance (m/s^2)
j	0001	150	20	−5	−2	10
j	0002	200	27	−6.1	−4	10
j	0003	80	15	−4.8	−3	12
⋮	⋮	⋮	⋮	⋮	⋮	⋮
$j + 1$	001	70	12	5	3	11
$j + 1$	002	50	20	4	2	10

Figure 3: Concept of data gathering method applied in the proposed SCWS.

demonstrates the major point of differentiation between the SCWS and previously proposed collision warning systems [13, 34–36]. In previously proposed collision warning systems, especially the VCWS, the exact location of the leading vehicle and detailed information describing its operation (e.g., acceleration and speed) are required. These requirements necessitate a highly reliable communication system and high market penetration rate of various in-vehicle sensors and communication devices [13, 34–36]. However, in the proposed SCWS, the information describing the surrounding vehicles is gathered in a representative form as shown in Figure 3. The data collected from each road segment is regarded as the leading vehicle information used in equations (1)–(3) for each subject vehicle and is calculated as follows:

$$v_{n-1}^{j}(t) = \frac{\sum_{i=1}^{N^j(t)} v_i^j(t)}{N^j(t)}, \tag{4}$$

$$a_{n-1}^{j}(t) = \frac{\sum_{i=1}^{N^j(t)} a_i^j(t)}{N^j(t)}, \tag{5}$$

$$h_{n-1}^{j}(t) = \frac{\sum_{i=1}^{N^j(t)} h_i^j(t)}{N^j(t)}, \tag{6}$$

where $v_{n-1}^{j}(t)$ is the speed of the leading vehicle in road segment j containing a total of $N^j(t)$ sample vehicles at time t, v_i^j is the speed of the ith vehicle in road segment j at time t, $a_{n-1}^{j}(t)$ is the acceleration of the leading vehicle in road segment j containing a total of $N^j(t)$ sample vehicles at time t, a_i^j is the acceleration of the ith vehicle in road segment j at time t, $h_{n-1}^{j}(t)$ is the space headway of leading vehicle in road segment j containing a total of $N^j(t)$ sample vehicles at time t, and h_i^j is the space headway of the ith vehicle in road segment j at time t.

As shown in equations (4)–(6), the SCWS does not require any individual driving information from the surrounding vehicles or a high market penetration rate to provide road condition information, as is required by the VCWS. Instead, the proposed SCWS calculates the collision risk based on average data and the estimated traffic situation in each road segment. This method is intimately linked with previous research that claims that traffic state and changes are closely related to collision risk and accident frequency [37, 38]. Compared to other collision warning systems such as the VCWS and ADAS, which respectively require a high market penetration rate and a high installation cost, the SCWS can be efficiently applied in practice because the cost of an OBU is much lower than the installation cost of an ADAS.

3. Case Study

3.1. Benchmark Models. To evaluate the proposed SCWS, its performance was compared with that of three other collision warning systems, the VCWS, HCWS, and ICWS. The VCWS uses information from the in-vehicle sensors of both the subject vehicle and the surrounding vehicles through V2V communication. The HCWS uses information from both

infrastructure and in-vehicle sensors. The ICWS uses only data from road infrastructure.

The VCWS is the most advanced collision warning method and as such is able to calculate the most accurate collision risk between the subject and leading vehicles under the assumption that all information describing the leading vehicle can be shared with adjacent vehicles through a novel V2V communication technology [27]. Thus, it is regarded as the ideal system in this paper. The collision risk using VCWS was calculated with equations (1)–(3).

The HCWS has been proposed as an improved collision warning system by providing higher stability than a collision warning system based solely on in-vehicle sensors when implemented before VCWS technologies have a sufficient market penetration rate. The HCWS estimates the surrounding traffic situation of the subject vehicle and hybridizes this estimated data with in-vehicle sensor data to calculate the collision risk [27]. The HCWS extracts representative values describing the traffic situation on the road segment using macroscopic traffic variables such as density, flow, and speed collected from loop detectors, as opposed to the use of microscopic driving data to do so in the SCWS. The representative values for each road segment and the associated collision risk are calculated in the HCWS using the following equations:

$$b_{\text{Subject}}(t) = \frac{b_{\max,\text{Subject}} \cdot \left[v_{\text{Subject}}(t) + A_{\text{Subject}}(t) \cdot \tau\right]^2}{\left[2 \cdot K \cdot b_{\max,\text{Subject}} + V_{\text{Leader}}^{\text{Hybrid}}(t)^2\right]}, \tag{7}$$

$$\begin{aligned} K = & -H_i^{\text{Infra}} + \left[2 \cdot v_{\text{Subject}}(t) + A_{\text{Subject}}(t) \cdot \tau\right] \cdot \frac{\tau}{2} \\ & - \left[\frac{V_{\text{Leader}}^{\text{Hybrid}}(t)}{2} + \left(A_{\text{Leader}}^{\text{Hybrid}}(t) + b_{\max,\text{Subject}}\right) \right. \\ & \left. \cdot \frac{\left(A_{\text{Leader}}^{\text{Hybrid}}(t) - b_{\max,\text{Subject}}\right)}{4J}\right] \cdot \frac{\left(A_{\text{Leader}}^{\text{Hybrid}}(t) - b_{\max,\text{Subject}}\right)}{J} \\ & + \left[\frac{v_{\text{Subject}}(t)}{2} + \frac{A_{\text{Subject}}(t) \cdot \tau}{2} \right. \\ & \left. + \frac{\left(A_{\text{Subject}}(t) + b_{\max,\text{Subject}}\right) \cdot \left(A_{\text{Subject}}(t) - b_{\max,\text{Subject}}\right)}{4J_{\text{Subject}}}\right] \\ & \cdot \frac{\left(A_{\text{Subject}}(t) - b_{\max,\text{Subject}}\right)}{J_{\text{Subject}}}, \end{aligned} \tag{8}$$

$$A_{\text{Leader}}^{\text{Hybrid}}(t) = \alpha \cdot \left(V_{i+1}^{\text{Infra}}(t) - V_i^{\text{Infra}}(t)\right), \tag{9}$$

$$V_{\text{Leader}}^{\text{Hybrid}}(t) = V_{\text{Subject}}(t) + H_i^{\text{Infra}}(t) \cdot \frac{V_{i+1}^{\text{Infra}}(t) - V_i^{\text{Infra}}(t)}{L_i}, \tag{10}$$

$$\text{DSSM}_{\text{Subject}}^{\text{Hybrid}}(t) = \frac{b_{\text{Subject}}(t)}{b_{\max.\text{Subject}}}, \tag{11}$$

where $b_{\text{Subject}}(t)$ is the required deceleration of the subject vehicle, $v_{\text{Subject}}(t)$ is the speed of the subject vehicle at time t, $A_{\text{Leader}}^{\text{Hybrid}}(t)$ is the estimated acceleration of the subject vehicle based on infrastructure data, $V_{\text{Leader}}^{\text{Hybrid}}(t)$ is the estimated velocity of the subject vehicle based on infrastructure data, $b_{\max,\text{Subject}}$ is the maximum braking performance of the subject vehicle, J_{Subject} is the maximum variation of subject vehicle acceleration, $\text{DSSM}_{\text{Subject}}^{\text{Indiv}}(t)$ is the collision risk of the subject vehicle at time t, $V_i^{\text{Infra}}(t)$ is the average speed at detector i over 30 s, $\text{H}_i^{\text{Infra}}$ is the average spacing at detector i over 30 s, and $A_{\text{Subject}}(t)$ is the acceleration of the leading vehicle at time t.

The ICWS is a collision warning system solely based on the macroscopic information collected by road sensors such as loop detectors [27]. The collision risk is calculated in the ICWS using the following equations:

$$b_i^{\text{Infra}}(t) = \frac{b_{\max} \cdot \left[V_{i+1}^{\text{Infra}}(t) + A_i^{\text{Infra}}(t) \cdot \tau\right]^2}{\left[2 \cdot K \cdot b_{\max,\text{Subject}} + V_{i+1}^{\text{Infra}}(t)^2\right]}, \tag{12}$$

$$\begin{aligned} K = & -H_i^{\text{Infra}} + \left[2 \cdot V_i^{\text{Infra}}(t) + A_i^{\text{Infra}}(t) \cdot \tau\right] \cdot \frac{\tau}{2} \\ & - \left[\frac{V_{i+1}^{\text{Infra}}}{2} + \left(A_{i+1}^{\text{Infra}}(t) + b_{\max}\right) \cdot \frac{\left(A_{i+1}^{\text{Infra}}(t) - b_{\max}\right)}{4J}\right] \\ & \cdot \frac{\left(A_{i+1}^{\text{Infra}}(t) - b_{\max}\right)}{J} \\ & + \left[V_i^{\text{Infra}}(t)/2 + A_i^{\text{Infra}}(t) \cdot \frac{\tau}{2} + \left(A_i^{\text{Infra}}(t) + b_{\max}\right) \right. \\ & \left. \frac{\left(A_i^{\text{Infra}}(t) - b_{\max}\right)}{4J}\right] \cdot \frac{\left(A_i^{\text{Infra}}(t) - b_{\max}\right)}{J}, \end{aligned} \tag{13}$$

$$A_i^{\text{Infra}}(t) = \alpha \cdot \left(V_{i+1}^{\text{Infra}}(t) - V_i^{\text{Infra}}(t)\right), \tag{14}$$

$$\text{DSSM}_i^{\text{Infra}}(t) = \frac{b_i^{\text{Infra}}(t)}{b_{\max}}, \tag{15}$$

where $b_i^{\text{Infra}}(t)$ is the required deceleration for infrastructure section i, $A_i^{\text{Infra}}(t)$ is the estimated acceleration for infrastructure section i, $b_{\max}$ is the representative maximum braking performance for all vehicles, J is the representative value for maximum variation in acceleration, and $\text{DSSM}_i^{\text{Infra}}(t)$ is the risk of collision in infrastructure section i over 30 s starting at time t.

3.2. Evaluation Method. To evaluate the different collision warning systems, the collision risk was calculated using the $\text{DSSM}(t)$ for the VCWS and SCWS, $\text{DSSM}_{\text{Subject}}^{\text{Hybrid}}(t)$ for the HCWS, and $\text{DSSM}_i^{\text{Infra}}(t)$ for the ICWS. When calculating the collision risk, a maximum deceleration rate of $-3.96\ \text{m/s}^2$ ($-13\ \text{ft/s}^2$) was assumed, extracted from the top 1% of the cumulative distribution of decelerations at the study site and representing the driver's maximum allowable value with reference to previous work [28]. Other required microscopic information describing vehicle movements, such as location, speed, space headway, and acceleration, as well as

macroscopic information (e.g., flow, density, and speed) was directly extracted from next generation simulation (NGSIM) trajectory data collected at highway US-101 in California, the United States, between 07 : 50 am and 08 : 35 am on June 15, 2005 [39]. The V2V and V2I communication delay was set to 0.1 s and data processing time was set to 0.1 s [40].

The performance of the proposed SCWS was obtained by calculating the collision risk based on averaged data collected from roadway vehicles by an RSU and microscopic data from the subject vehicle using equations (1)–(6). The performance of the ICWS was obtained by calculating the collision risk based only on the macroscopic data obtained from the road detection system using equations (12)–(15). The performance of the HCWS was obtained by calculating the collision risk based on both macroscopic data from infrastructure and microscopic data from the subject vehicle using equations (7)–(11). The performance of the VCWS was obtained by calculating the collision risk based only on the microscopic data from neighboring vehicles and the subject vehicle using equations (1)–(3). Table 1 provides details of the data sources and aggregation levels of the ICWS, HCWS, SCWS, and VCWS.

To evaluate the performance of the proposed SCWS, the collision risk estimated by the four systems was compared at two levels: the aggregation level and disaggregation level. In the aggregation level analysis, the average collision risks determined by the four systems were compared over 30 s. The performance of the collision warning systems at this level reflects their suitability for application as a macroscopic road control system, such as setting variable speed limits, variable message signs, and collision warnings for road sections with multiple links. In the disaggregation level analysis, the collision risks of the four systems are plotted in 0.1 s intervals, and the root mean square errors (RMSE) of the ICWS, HCWS, and SCWS are calculated under the assumption that the VCWS with 100% market penetration rate produces the most ideal estimation of collision risk.

4. Experiment Results

4.1. Comparison of Collision Warning Systems. Figure 4 shows comparisons of the RMSE values for the VCWS and ICWS, the VCWS and HCWS, and the VCWS and SCWS for three different cases, assuming that the results of the VCWS are the ideal values. It can be observed that, among the other collision warning systems, the SCWS provides the most similar performance to the VCWS: the RMSE of the SCWS is lower than that of the ICWS and HCWS. The average RMSE value of the SCWS when compared to the VCWS of 0.27 may initially seem too large to accept the former as a replacement for the latter. However, the difference in the results of the two systems may be attributed to the difference in the absolute quantity of the peak values of the VCWS and SCWS, as shown in the following results. When the warning threshold values for the two systems are adjusted, this difference may decrease and the potential for the SCWS to replace the VCWS may be even greater when the market penetration rate of the VCWS is low.

Figure 5 shows two examples of the calculated collision risk under the four different collision warning systems at the aggregation level. In both examples, the ICWS and HCWS underestimate the collision risk compared to the SCWS and VCWS because they average the speed, acceleration, and distance between vehicles. In terms of warning timing, the ICWS occasionally produces a later warning signal than the other collision warning systems. This late warning could be due to the system delay inherent to the ICWS due to the preprocessing of big-data sets and the data acquisition process. This delay in warning signal could be critical as a late signal could fail to prevent an accident, degrading the reliability of the collision warning system.

In contrast to the ICWS and HCWS, the collision risk estimated by the SCWS shows similar trends to that estimated by the VCWS: the low peaks and high peaks of the estimated collision risk occur at almost the same time. The similar timing and magnitude of estimated collision risk indicate that the SCWS has the potential to be used instead of the VCWS by simply replacing the actual leading vehicle's information with the average data from vehicles sampled on the road segment. Moreover, the SCWS can detect dangerous situations earlier than the VCWS in some cases. A possible reason for this is that the area across which the SCWS can gather data is larger than the collection range of the VCWS. To produce a collision risk between the leading vehicle and subject vehicle, the VCWS only considers the movement data from the leading vehicle, so only imminent risk is identified by the VCWS. However, the SCWS uses data gathered from multiple vehicles traveling along the same road section, allowing it to produce estimates of upcoming collision risk arising downstream based on the overall data and react to an impending collision risk faster than the VCWS.

Figure 6 shows a disaggregation level comparison of the collision risks estimated by the four different collision warning systems for a car-following example. Note that the ICWS shows a constant value for collision risk over a plot of 0.1 s time intervals, as it only provides collision warnings using 30 s averaged data. Thus, the ICWS produces a collision risk for the entire road segment, not for individual drivers. However, the SCWS, VCWS, and HCWS provide collision risks for individual vehicles and all generally show very similar trends except at several points in Figure 6(a). The difference in the values of the collision risk estimated by the SCWS and HCWS is due to the difference in the estimated velocity of the leading vehicle, as shown in Figure 6(c), in which the SCWS produces a leading vehicle speed somewhat similar to that determined by the VCWS. The differences between the SCWS and VCWS shown in Figure 6 are caused by the slight underestimation of collision risk using the SCWS due to the higher estimated speed of the leading vehicle. Overall, however, the SCWS shows a similar performance to the VCWS, especially when the leading vehicle exhibits a similar driving behavior to the surrounding traffic condition.

Table 1: Data source for four collision warning systems.

		ICWS	HCWS	SCWS	VCWS
Information of leading vehicle	Speed	Average (infrastructure)	Average (infrastructure)	Average (vehicle)	Individual (vehicle)
	Acceleration	Average (infrastructure)	Average (infrastructure)	Average (vehicle)	Individual (vehicle)
Information of subject vehicle	Speed	Average (infrastructure)	Individual (vehicle)	Individual (vehicle)	Individual (vehicle)
	Acceleration	Average (infrastructure)	Individual (vehicle)	Individual (vehicle)	Individual (vehicle)
	Space headway	Average (infrastructure)	Average (infrastructure)	Individual (vehicle)	Individual (vehicle)

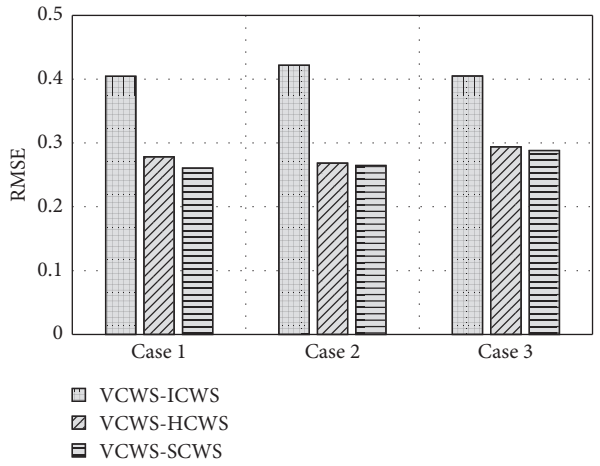

Figure 4: RMSE between the VCWS and the ICWS, HCWS, and SCWS for three cases.

5. Verification of SCWS Applicability

The proposed SCWS is based on the gathered data from the OBUs of the vehicles on the road, so the accuracy of this system will vary considerably according to different market penetration rates. To apply the SCWS in practice, the effect of market penetration rate on the collision warning accuracy must be understood. Figure 7 shows the results of this analysis. In all cases, the RMSE of the SCWS decreases as the market penetration rate increases, but the rate of decrease is different depending on the market penetration rate. When the market penetration rate less than 30%, the RMSE is significantly reduced with greater market penetration rate; when the market penetration rate is greater than 40%, the rate of decrease of the RMSE is slower and nearly constant with greater penetration rate. These results thus indicate that in practical application, the proposed SCWS can be effectively implemented with an approximately 30% market penetration rate. In other words, with an approximately 30% market penetration of vehicle OBUs, the proposed SCWS can provide similar performance to the VCWS with a 100% market penetration rate.

The proposed SCWS relies on edge computing in the RSU to gather and distribute the data among the OBUs. This system has enormous potential for data sharing but is also potentially limited in application as a collision warning system due to the possible time delay required for data transmission. To demonstrate the effects of this limitation on the practical application of the proposed SCWS, the effect of time delay on the accuracy of the SCWS was analyzed as shown in Figure 8. On average, the RMSE between the VCWS and SCWS slightly increases as the time delay increases from 0.2 s to 2 s. However, this increase in RMSE between the VCWS and SCWS is insignificant in all cases. This result accordingly shows that the SCWS is robust to the issues of time delay.

6. Conclusion

In this paper, we proposed a sectional information-based collision warning system (SCWS) that does not require exact information from the leading vehicle (e.g., exact location) but calculates the collision risks based only on the sectional data from an roadside unit (RSU) gathered using vehicle-to-infrastructure (V2I) communication. The SCWS calculates the collision risk based on the deceleration-based safety surrogate measure (DSSM), a measurement of collision risk between two vehicles, and issues a collision warning signal when the estimated value of collision risk is higher than the threshold value. Unlike previously proposed collision warning systems, in which the subject vehicle must directly communicate with its neighboring vehicles, the SCWS uploads the information describing the subject vehicle's operation (e.g., speed, acceleration, and braking performance) to the RSU and downloads the representative values for each road segment through V2I communication. The main concept underlying the SCWS is that the downloaded data, which represents the surrounding traffic situation, indirectly represents the status of the leading vehicle based on the assumption that the collision risk of the subject vehicle is significantly affected by the average movement of the surrounding vehicles and the traffic state of the road segment.

To demonstrate its capabilities, this paper compared the performance of the SCWS with that of three other systems, namely, the infrastructure-based collision warning system (ICWS), hybrid collision warning system (HCWS), and vehicle-to-vehicle communication-based collision warning system (VCWS). The results of the comparisons indicate that the SCWS produces a similar trend to the VCWS (assuming a 100% market penetration rate) and that the SCWS sometimes issues warning signals to the driver

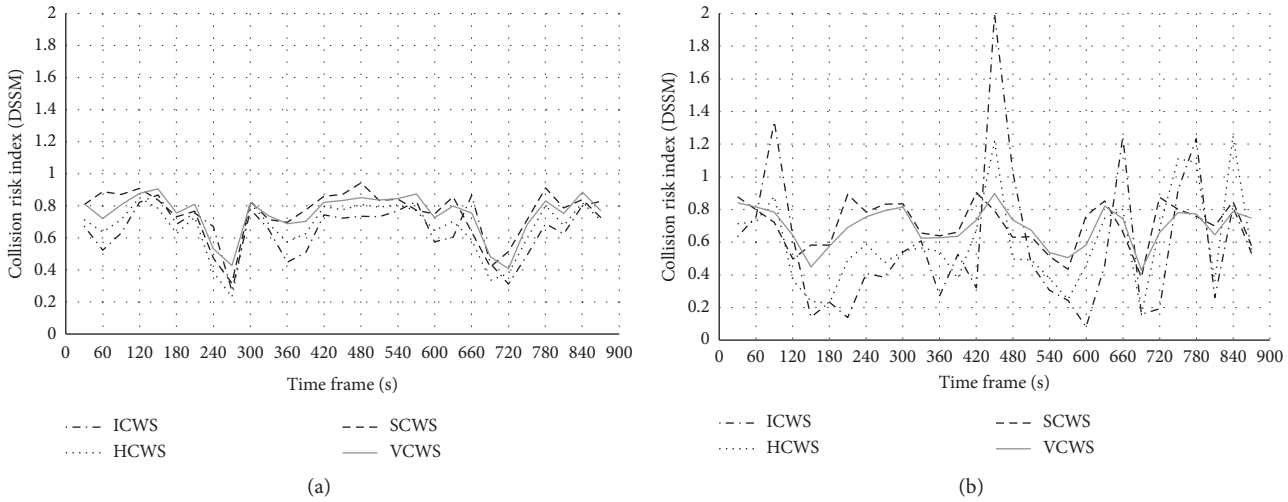

Figure 5: Aggregated level comparison of collision risk calculated using four different collision warning systems: (a) example 1; (b) example 2.

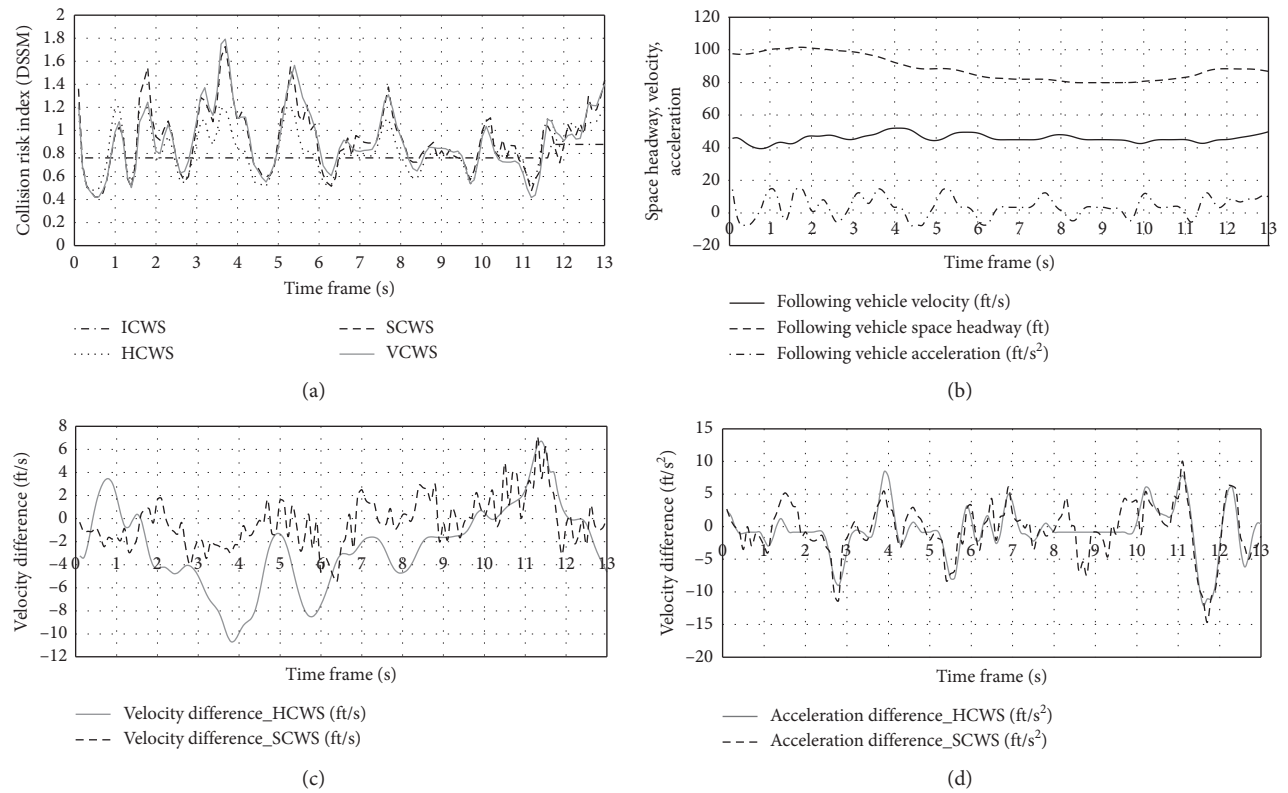

Figure 6: Disaggregation level comparison of collision risks calculated using four different collision warning systems for car-following Case 1 in terms of (a) DSSM, (b) driving data, (c) estimated velocity, and (d) estimated acceleration.

earlier than the VCWS in the aggregation level. The earlier warning signal issued by the SCWS is achieved through the use of a wider area of gathered data because data downloaded from the RSU contains indirect information describing the traffic conditions on the road further downstream. In the disaggregation level, the SCWS also shows a similar trend to the VCWS at most points. The observed difference between the SCWS and VCWS is possibly caused by the slightly higher leading vehicle speed estimated by the SCWS.

Furthermore, to demonstrate the practical application of the proposed SCWS, the effect of market penetration rate and time delay on the root mean square error when compared to the VCWS was analyzed for three cases. The result

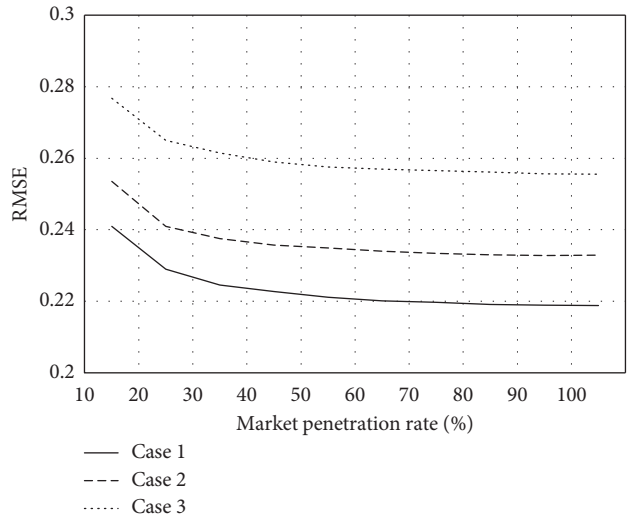

Figure 7: Effect of sampling rate on the RMSE for three cases of SCWS application.

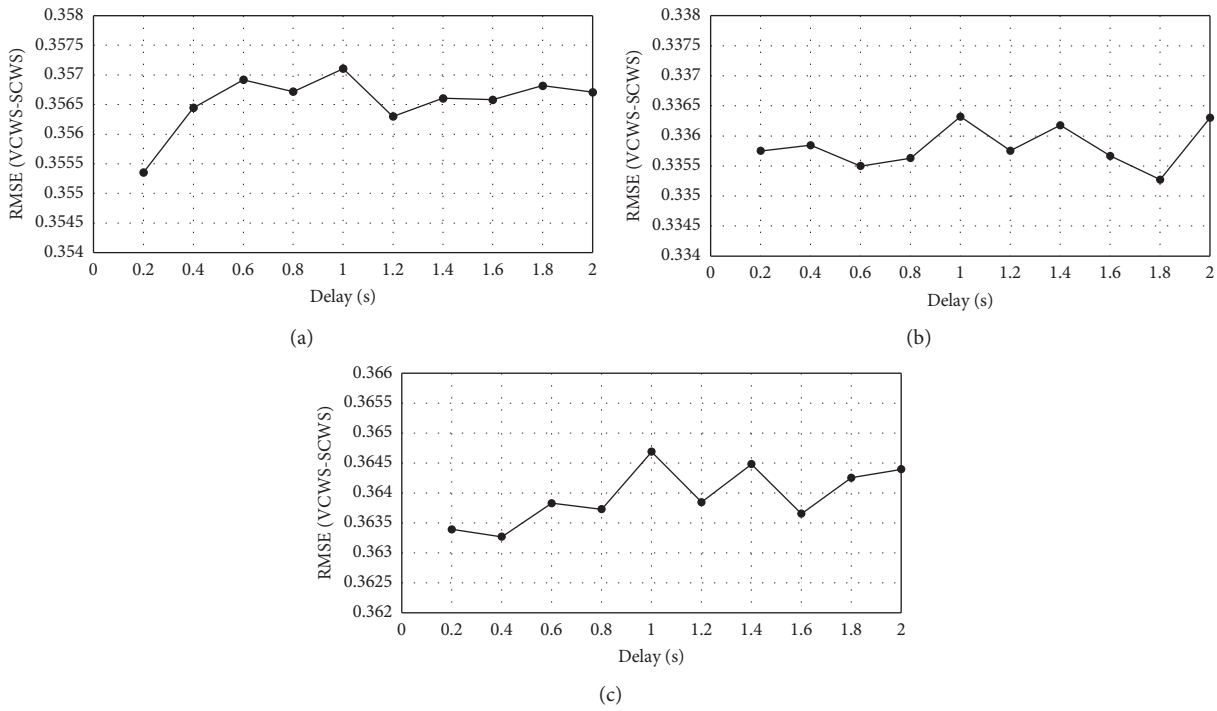

Figure 8: Effect of time delay on the RMSE between the VCWS and the SCWS for (a) Case 1, (b) Case 2, and (c) Case 3.

shows that the collision risk estimated by the proposed SCWS with a 30% market penetration rate is similar to the collision risk estimated by the VCWS with a 100% market penetration rate. This indicates that the proposed SCWS can overcome the limitations of current connected-vehicle (CV) technology requiring a high market penetration rate in order to produce accurate warning signals [41]. Indeed, by applying the proposed SCWS to current CVs, it appears possible to solve the problem of system performance degradation during the early stage of CV technology introduction.

Data Availability

The data used to support the findings of this study are available from NGSIM on the following web page: https://ops.fhwa.dot.gov/trafficanalysistools/ngsim.html.

Conflicts of Interest

The authors declare that there are no conflicts of interest regarding the publication of this article.

Acknowledgments

This research was supported by the Ministry of Land, Infrastructure, and Transport (MOLIT, Korea) under the Connected and Automated Public Transport Innovation National R&D Project (Grant no. 20TLRP-B146733-03).

References

[1] R. Knipling, M. Mironer, and D. Hendricks, "Assessment of ivhs countermeasures for collision avoidance: rear-end crashes," Final Report, 1993.

[2] K. Rumar, "The basic driver error: late detection," *Ergonomics*, vol. 33, no. 10-11, pp. 1281–1290, 1990.

[3] A. Lindgren and F. Chen, "State of the art analysis: an overview of advanced driver assistance systems (adas) and possible human factors issues," *Handbook of Human Factors and Ergonomics in Health Care*, pp. 38–50, 2006.

[4] ITSJPO, *What Public Officials Need to Know about Interoperability*, ITSJPO, Washington, DC, USA, 2003, https://www.its.dot.gov/factsheets/jpo_publicofficials.htm.

[5] R. Parasuraman, P. A. Hancock, and O. Olofinboba, "Alarm effectiveness in driver-centred collision-warning systems," *Ergonomics*, vol. 40, no. 3, pp. 390–399, 1997.

[6] J. D. Lee, D. V. McGehee, T. L. Brown, and M. L. Reyes, "Collision warning timing, driver distraction, and driver response to imminent rear-end collisions in a high-fidelity driving simulator," *Human Factors: The Journal of the Human Factors and Ergonomics Society*, vol. 44, no. 2, pp. 314–334, 2002.

[7] R. J. Kiefer, D. J. LeBlanc, and C. A. Flannagan, "Developing an inverse time-to-collision crash alert timing approach based on drivers' last-second braking and steering judgments," *Accident Analysis & Prevention*, vol. 37, no. 2, pp. 295–303, 2005.

[8] A. Polychronopoulos, "Dynamic situation and threat assessment for collision warning systems: the Euclide approach," in *Proceedings of the Intelligent Vehicles Symposium*, IEEE, Parma, Italy, June 2004.

[9] S. Wang and Y. Cheng, "A vehicle collision warning system employing vehicle-to-infrastructure communications," in *Proceedings of the Wireless Communications and Networking Conference*, IEEE, Las Vegas, NV, USA, pp. 3075–3080, March 2008.

[10] ERTRAC, "Ersosynthesis2016-Adas15_En," *European Commission*, 2016.

[11] F. de Ponte Müller, "Survey on ranging sensors and cooperative techniques for relative positioning of vehicles," *Sensors*, vol. 17, no. 2, pp. 271–327, 2017.

[12] K. Vogel, "A comparison of headway and time to collision as safety indicators," *Accident Analysis & Prevention*, vol. 35, no. 3, pp. 427–433, 2003.

[13] S. E. Shladover and S.-K. Tan, "Analysis of vehicle positioning accuracy requirements for communication-based cooperative collision warning," *Journal of Intelligent Transportation Systems*, vol. 10, no. 3, pp. 131–140, 2006.

[14] A. Stateczny, W. Kazimierski, D. Gronska-Sledz, and W. Motyl, "The empirical application of automotive 3D radar sensor for target detection for an autonomous surface vehicle's navigation," *Remote Sensing*, vol. 11, no. 10, pp. 1156–1218, 2019.

[15] N. Asselin-Miller, "Study on the deployment of c-its in europe," pp. 1–218, 2016, Final Report.

[16] Ministry of Land and Transportation and Inrfafstructure, *C-ITS Pilot Project Final Report*, Ministry of Land and Transportation and Inrfafstructure, 2017, http://www.molit.go.kr/portal.do.

[17] J. Harding, "Vehicle-to-vehicle communications : readiness of V2V technology for application," p. 327, Report No DOT HS 812 014, 2014.

[18] European Commission, *C-ITS Platform Phase 2*, European Commission, Brussels, Belgium, 2017.

[19] European Commission, *Commission Delegated Regulation directive 2010/40/EU*, European Commission, Brussels, Belgium, 2019.

[20] J. Chen, S. Tian, H. Xu, R. Yue, Y. Sun, and Y. Cui, "Architecture of vehicle trajectories extraction with roadside LiDAR serving connected vehicles," *IEEE Access*, vol. 7, pp. 100406–100415, 2019.

[21] J. Wu, H. Xu, Y. Zheng, and Z. Tian, "A novel method of vehicle-pedestrian near-crash identification with roadside LiDAR data," *Accident Analysis & Prevention*, vol. 121, pp. 238–249, 2018.

[22] K. Balke, H. Charara, and S. Sunkari, *Report on Dynamic Speed Harmonization and Queue Warning Algorithm Design*, pp. 1–79, FHWA, Washington, D.C., USA, 2014.

[23] ITSJPO, *Connected Vehicle Benefits*, ITSJPO, Washington, DC, USA, 2016, https://www.its.dot.gov/factsheets/connected_vehicle_benefits.htm.

[24] X. Zeng, K. Balke, and P. Songchitruksa, *Potential Connected Vehicle Applications to Enhance Mobility, Safety, and Environmental Security*, Texas A&M University System, College Station, TX, USA, 2012.

[25] V. Milanés, J. Villagra, J. Godoy, J. Simo, J. Perez, and E. Onieva, "An intelligent V2I-based traffic management system," *IEEE Transactions on Intelligent Transportation Systems*, vol. 13, no. 1, pp. 49–58, 2012.

[26] S. Tak, S. Woo, and H. Yeo, "Sampling-based collision warning system with smartphone in cloud computing environment," in *Proceedings of the IEEE Intelligent Vehicles Symposium*, Seoul, South Korea, June 2015.

[27] S. Tak, S. Woo, and H. Yeo, "Study on the framework of hybrid collision warning system using loop detectors and vehicle information," *Transportation Research Part C: Emerging Technologies*, vol. 73, pp. 202–218, 2016.

[28] S. Tak, S. Kim, and H. Yeo, "Development of a deceleration-based surrogate safety measure for rear-end collision risk," *IEEE Transactions on Intelligent Transportation Systems*, vol. 16, no. 5, pp. 2435–2445, 2015.

[29] J. Hayward, "Near-miss determination through use of a scale of danger," *Highw. Res. Rec.*vol. 384, pp. 22–34, 1972.

[30] A. Laureshyn, Å. Svensson, and C. Hydén, "Evaluation of traffic safety, based on micro-level behavioural data: theoretical framework and first implementation," *Accident Analysis & Prevention*, vol. 42, no. 6, pp. 1637–1646, 2010.

[31] Y. Kweon, "Development of crash prediction models using real time safety surrogate measures," *UVACTS*, vol. 104, 2008.

[32] S. Tak and H. Yeo, "The impact of predictive cruise control on traffic flow and energy consumption," in *Proceedings of the Computing In Civil Engineering*, pp. 403–410, Los Angeles, CA, USA, June 2013.

[33] S. Tak, S. Woo, and H. Yeo, "A Study of the Framework on Collision Risk Warning System Using Loop Detector and Vehicle Information," in *Proceedings of the Computing In Civil And Building Engineering*, pp. 1134–1141, Orlando, FL, USA, June 2014.

[34] A. R. Girard, J. de Sousa, J. B. de Sousa, J. A. Misener, and J. K. Hedrick, "A control architecture for integrated cooperative cruise control and collision warning systems," in *Proceedings of*

the 2001 40th IEEE Conference, pp. 1491–1496, Orlando, FL, USA, December 2001.

[35] T. ElBatt, S. Goel, and G. Holland, "Cooperative collision warning using dedicated short range wireless communications," in *Proceedings Of the 3rd International Workshop on Vehicular Ad Hoc Networks*, Los Angeles, CA, USA, September 2006.

[36] R. Sengupta, S. Rezaei, S. E. Shladover, D. Cody, S. Dickey, and H. Krishnan, "Cooperative collision warning systems: concept definition and experimental implementation," *Journal of Intelligent Transportation Systems*, vol. 11, no. 3, pp. 143–155, 2007.

[37] S. Song and H. Yeo, "Method for estimating highway collision rate that considers state of traffic flow," *Transportation Research Record: Journal of the Transportation Research Board*, vol. 2318, no. 1, pp. 52–62, 2012.

[38] H. Yeo, K. Jang, and A. Skabardonis, "Impact of traffic states on freeway collision frequency," *Safe Transp. Res. Educ. Cent.*, 2010.

[39] 2006 NGSIM-Next Generation Simulation.

[40] J. P. O. ITS, "Connected vehicle pilot deployment program phase 1, concept of operations (ConOps)-New York city," *Final ConOps*, vol. 8, pp. 16–299, 2016.

[41] J. Shelton, J. Wagner, S. Samant, G. Goodin, T. Lomax, and E. Seymour, "Impacts of connected vehicles in a complex, congested urban freeway setting using multi-resolution modeling methods," *International Journal of Transportation Science and Technology*, vol. 8, no. 1, pp. 25–34, 2019.

Hindawi
Journal of Advanced Transportation
Volume 2020, Article ID 4219562, 12 pages
https://doi.org/10.1155/2020/4219562

Research Article

Fatigue Driving Prediction on Commercial Dangerous Goods Truck Using Location Data: The Relationship between Fatigue Driving and Driving Environment

Shifeng Niu and Guiqiang Li

Automotive Transportation Safety Assurance Technology Key Laboratory of Transportation Industry, Chang'an University, Xi'an, Shaanxi 710064, China

Correspondence should be addressed to Shifeng Niu; nsf530@chd.edu.cn and Guiqiang Li; 1119084992@qq.com

Received 2 January 2020; Revised 31 May 2020; Accepted 13 June 2020; Published 9 July 2020

Academic Editor: Feng Chen

The approaches monitoring fatigue driving are studied because of the fact that traffic accidents caused by fatigue driving often have fatal consequences. This paper proposes a new approach to predict driving fatigue using location data of commercial dangerous goods truck (CDT) and driver's yawn data. The proposed location data are from an existing dataset of a transportation company that was collected from 166 vehicles and drivers in an actual driving environment. Six different categories of the predictor set are considered as fatigue-related indexes including travel time, day of week, road type, continuous driving time, average velocity, and overall mileage. The driver's yawn data are used as a proxy for ground truth for the classification algorithm. From the six different categories of the predictor set, we obtain a set of 17 predictor variables to train logistic regression, neural network, and random forest classifiers. Then, we evaluate the predictive performance of the classifiers based on three indexes: accuracy, F1-measure, and area under the ROC curve (AUROC). The results show that the random forest is more suitable for predicting fatigue driving using location data according to its best accuracy (74.18%), F1-measure (62.02%), and AUROC (0.8059). Finally, we analyze the relationship between fatigue driving and driving environment according to variable importance described by random forest. In summary, our results obviously exhibit the potential of location data for reducing the accident rate caused by fatigue driving in practice.

1. Introduction

The transportation volume of the CDT continues to rise throughout the world with the rapid development of the modern manufacturing and logistics industries [1]. Dangerous goods transportation has a high potential risk which refers to the possibility of incurring traffic accidents with disastrous consequences [2, 3]. For example, explosions in densely populated areas or the release of toxic chemicals can lead to casualties directly or indirectly through environmental degradation [4]. Dangerous goods usually have characteristics, such as flammable, explosive, volatile, easy-corrosive, and so on. Thus, the transportation accidents involving dangerous goods usually show the following features: unpredictability, severe losses, and sudden and long-term effects [5]. When the catastrophic accidents occur, the consequences cannot be often controlled and lowered [6]. Therefore, the safety of dangerous goods transportation has caught the attention of the public, transportation companies of dangerous goods, and decision makers and researchers within governmental and nongovernmental safety organization [7, 8].

Fatigue driving is one of the main reasons for fatal traffic accidents according to the causality analysis of traffic accidents [9, 10]. Up to 20 percent of traffic accidents are caused by fatigue driving [11–13]. Commercial truck drivers have relatively long driving time and are more prone to fatigue. Studies show that fatigue driving has been a major reason for commercial truck accidents [14–16]. Fatigue driving of commercial truck drivers increases the accident rate and leads to severe property loss, injuries, and fatalities [17–20].

Many previous researches have focused on the fatigue driving problem of commercial truck drivers [21–25]. Various sources and types of real-time data have been used in detecting driving fatigue. Physiological signals, being continuously available, objective, and fairly direct indicators, were often used to detect fatigue [26]. The electroencephalogram (EEG) and electrooculogram (EOG) are often used as a medium for detection [27–29]. However, EEG signals are very susceptible to noise and movements of the body [30]. EOG detection removes some problems of EEG; it only gives reasons for a certain aspect of the degree of human fatigue [28]. In addition, most physiological signal acquisition devices need to contact the driver's body, which may interfere with the normal operation of the driver and affect the driving safety. Thus, the alternative approaches without contacting the driver's body were developed using camera and other driving data. Fatigue may affect driver's behaviors including face and body activities [31]. The ocular and eyelid movements are often used to detect fatigue [32]. However, the image acquisition device is expensive and easy to be affected by the light. So, some other relative detection information was used to detect driving fatigue. The standard deviation of lane position (SDLP) or steering wheel movements are also often measured to detect the drivers' fatigue [33–35].

The above studies mainly focus on real-time detection of fatigue, which is a good approach to reduce the effects of fatigue driving. However, it may be not enough. When the fatigue is detected, the commercial driver is already on a transport mission and is difficult to abandon the mission or recover from a short rest [36]. If we can use historical data to predict the fatigue status of drivers before a new transportation mission, managers can select the drivers who are not prone to fatigue to undertake the more heavy transportation task by adjusting transportation plans. Fatigue driving is not only related to the driver's current driving, but also related to the driver's previous driving task intensity [37–39]. Long and hectic work schedules will increase the odds of driver fatigue [17, 21, 23, 25, 40–42]. Studies showed that the odds of driver fatigue increased heavily as the continuous days of driving increased [43, 44]. This might be a result of "accumulated fatigue" among the drivers due to long and continuous days of driving [44, 45]. The driver's recent driving tasks and driving environment can be used to predict the possibility of driver fatigue. The results can provide accurate information for driving tasks arrangement and early driver fatigue intervention.

The primary objective of this study is to propose an approach for predicting driver fatigue using characteristics of driver's recent driving task and driving environment extracted from location data and then use these characteristics to predict the possibility of driver fatigue. At present, studies focused on prediction of fatigue driving have emerged [26, 46, 47]. However, to the best knowledge of the authors, the approaches to predict fatigue using drivers' recent driving task and driving environment characteristics extracted from location data are yet to come. The contributions of this paper can be summarized as follows:

(1) Previous studies mainly used real-time data from drivers or vehicles to detect fatigue, but few studies used the historical data. In addition, previous studies have suggested that fatigue driving is intimately related to the driver's previous driving task intensity [37–39]. The proposed approach predicts fatigue driving using the drivers' recent driving task and driving environment characteristics

(2) There have been studies on the prediction of fatigue driving [26, 46, 47]; however, most studies focus on short-time forecasting. Few studies research on long-term prediction methods, specifically on commercial dangerous goods truck (CDT). At present, there is no research on prediction of fatigue driving of CDT within the scope of our literature review. The proposed approach can use the location data of CDT to predict fatigue driving of CDT

(3) At present, most studies on the prediction of fatigue driving mainly use physiological and behavioral indicators. However, physiological and behavioral measurements may interfere with the driver's normal driving, and the corresponding detection devices are relatively expensive and inconvenient to carry, which brings some difficulties to the future popularization and application of real driving conditions. To the best of our knowledge, there has not been a solution that is noninvasive and accurate. The proposed approach uses the location data of CDT to predict fatigue. The location data of CDT are available in many countries, so using location data makes the approach very scalable. In China, all CDTs are equipped with satellite positioning system and the data are uploaded to the national management system. However, we have not found any research on predicting fatigue driving using location data. The proposed approach is established based on six different categories of the predictor set only using raw location data

The paper is organized as follows. Section 2 details the study dataset. The overview for the methodology is described in Section 3. The obtained results are presented and discussed in Sections 4 and 5. Finally, conclusions to the paper are provided in Section 6.

2. Data

2.1. Data Description. We obtained data from the database of a transportation company in the south of China that currently comprises more than 200 CDTs. It has more than 580 drivers and more than 250 managers. The registered capital of the company is about 8 million dollars, with total assets of 32 million dollars. Each vehicle was equipped with devices which contains a GPS sensor, yawn detecting camera, and wireless transmission system. Because of the privacy restrictions of the database, we only took the location data and yawn data from the company's 166 CDT for 11 months in 2017. The location data were updated every 10 seconds, containing vehicle's plate number, speed, latitude, longitude, direction and location address, and time stamp. The yawn data included the vehicle's plate number and the specific time of yawning.

The mileage can be calculated from latitude and longitude data. Continuous driving time can be obtained using the time stamp and speed which is used to judge whether the vehicle is driving or not. The road type containing urban roads, highway except freeway, and freeway can be obtained using GIS systems. Some data were rejected due to the following reasons:

(i) The error in the data (e.g., the error in time or speed makes it impossible to accurately determine whether the vehicle is driving.)

(ii) Failure of the GPS sensor for a long time, so that the location data were not available

(iii) Failure of the yawn detecting device for a long time, so that the yawn data were not available

(iv) Too much location data were interrupted due to signal blocking (e.g., too much data of the latitude and longitude are interrupted, so that excessive mileage cannot be accurately calculated)

These cases finally led to a reduction of the location data by 5 vehicles to 161. The outliers were not further eliminated because we believed that their impact on the prediction results was insignificant due to the large data size.

2.2. Predictor Variables. The predictor variables are derived from raw location data. Traffic safety researchers have inferred some risk factors related to fatigue from observed-accident statistics, such as travel time, average velocity, mileage, road type, and so on [48, 49]. In addition, studies have shown that the risk factors such as travel time, average velocity, road type, and driving environment have significant impact on truck safety [50–52]. According to these risk factors, we designed six different categories of the predictor set including travel time, day of week, road type, continuous driving time, average velocity, and overall mileage. By accumulating mileage between every adjacent two data points of CDT, overall mileage M of each CDT can be calculated using latitude and longitude. Continuous driving time is an important index for predicting driver fatigue, so we take the average continuous driving time and the longest continuous driving time (C1-2) to measure driving time. Except for overall mileage and continuous driving time, we discretize the four other categories of the predictor set into a fixed number of intervals, where each interval corresponds to a predictor variable. Travel time is divided into five variables T1-5 that catch vehicle traveling at different times. Two other predictor variables catch vehicle traveling on weekdays and weekends (W1-2), while another variable triplet differentiates the three road types (R1-3). We separate average velocity into four variables V1-4, where the fourth interval includes mileage accumulated at velocities larger than 80 km/h (i.e., 80 km/h is the maximum speed limit for the CDT in China). The overview of predictor variables is shown in Table 1.

We assume that cumulative fatigue driving on the target day is strongly related to the task of the previous week. The predictor variables for specific target day were calculated using data from the previous week. We define the accumulated mileage of the previous week as the mileage accumulated from day $t-1$ to day $t-7$ on day t. The accumulated mileage of day t is described as

$$\mathrm{PAM}_t = \sum_{i=t-7}^{t-1} P_i, \tag{1}$$

where PAM_t represents the accumulated mileage of the day t, P_i represents the mileage of the ith day, and t is an integer greater than 7.

We use the location data of the 161 vehicles to calculate predictor variables of each day which was described in Table 1. Except for continuous driving time, values of the 15 predictor variables are the mileage accumulated in a week before target day (i.e., the predictor variables of day t are accumulated for day $t-1$ to day $t-7$ on the dependent variable). The predictor variables, which have different dimensions and change intervals, may result in some indicators to be ignored and affect the results of data analysis. Therefore, we normalize all predictor variables, where the normalized equation for all predictor variables except for overall mileage and continuous driving time is

$$X^* = \frac{X}{M}, \tag{2}$$

where X is the values of all predictor variables except for overall mileage and continuous driving time and M is the values of overall mileage.

The normalized equation for continuous driving time C is

$$C^* = \frac{C - C_{\min}}{C_{\max} - C_{\min}}, \tag{3}$$

where $C_{\max}$ is the values of the maximum continuous driving time, $C_{\min}$ is the values of the minimum continuous driving time, and their values are obtained across 161 vehicles in 11 months. And we furthermore normalize overall mileage M by taking the logarithm of M and dividing it by the logarithm of the M maximum:

$$M^* = \frac{\log_{10}(M)}{\log_{10}(M_{\max})}, \tag{4}$$

where the maximum of M is also obtained across 161 vehicles in 11 months. The descriptive statistics of all predictor variables are shown in Table 2.

Except for continuous driving time, values of the 15 predictor variables are the mileage accumulated in a week. It may cause the collinearity problem of the generated predictor variables at the same time. This problem is an unwanted property for most classifiers and is especially troublesome for logistic regression [53, 54].

Therefore, we select the method of factor analysis to solve the collinearity problem of logistic regression. Factor analysis is a multivariate analysis method that converts multiple variables into several integrated variables (or latent variables), which are mainly used to reduce the number of variables and classify variables with high correlation, using common factors instead. In this study, principal component analysis is used to extract factors with eigenvalues greater than 1 as common factor. Table 3 presents the eigenvalues, the percentage of variance, the

Table 1: Predictor variables.

Group	Variable description
Travel time (T)	$T1$: 0 am and 5 am
	$T2$: 5 am and 9 am
	$T3$: 9 am and 5 pm
	$T4$: 5 pm and 10 pm
	$T5$: 10 pm and 12 pm
Day of week (W)	$W1$: weekdays except Friday
	$W2$: weekends with Friday
Road type (R)	$R1$: urban roads
	$R2$: highway except the freeway
	$R3$: freeway
Continuous driving time (C)	$C1$: average continuous driving time
	$C2$: longest continuous driving time
Average velocity (V)	$V1$: 0 km/h–40 km/h
	$V2$: 40 km/h–60 km/h
	$V3$: 60 km/h–80 km/h
	$V4$: over 80 km/h (has only a lower bound)
Overall mileage (M)	M: mileage traveled per day

Table 2: Descriptive statistics of all predictor variables.

Variable	Mean	1st Q	2nd Q (median)	3rd Q
$T1$	0.076	0.000	0.034	0.123
$T2$	0.168	0.078	0.159	0.243
$T3$	0.496	0.395	0.484	0.604
$T4$	0.208	0.124	0.221	0.285
$T5$	0.052	0.000	0.040	0.092
$W1$	0.592	0.497	0.577	0.678
$W2$	0.408	0.321	0.423	0.503
$R1$	0.263	0.130	0.238	0.345
$R2$	0.227	0.072	0.136	0.355
$R3$	0.510	0.265	0.566	0.774
$C1$	0.501	0.333	0.487	0.669
$C2$	0.314	0.178	0.273	0.413
$V1$	0.213	0.084	0.153	0.260
$V2$	0.285	0.151	0.245	0.375
$V3$	0.497	0.292	0.538	0.699
$V4$	0.005	0.000	0.000	0.000
M	0.717	0.695	0.742	0.775

cumulative eigenvalue, and the cumulative percentage of variance associated with each factor. It reveals that the first four factors explain approximately 76.9% of total variance. Finally, the number of common factors is determined to be 4.

Fatigue may be determined according to the physical activities and human behavior [55]. The driver's yawn data are used as a proxy for ground truth for the classification algorithm. If the driver yawns in target day, the driver is considered to be fatigued in this day. In this paper, fatigue, indicated by yawning, is predicted by our approach using location data of CDT. According to Kiang's suggestions on classifier selection [56], our approach considers three types of classifiers, namely, logistic regression, neural networks, and random forest.

In a supervised classification problem, a training set is usually used to construct classification models and the independent testing set is used to testify the predictive performance of these models [57]. Therefore, for logistic regression, we randomly divided the dataset with 4 common factors into two subsets, in which 70% of the whole dataset were included in the training set and the remaining 30% were included in the testing set. For neural network, we randomly divided the normalized dataset with 17 predictor variables in Table 1 into two subsets, in which 70% of the whole dataset were used for training and 30% were used for testing. Cutler et al. suggested that the random forest algorithm included the interactions among the variables, so there was no collinearity problem faced by other models [58]. Therefore, for random forest, we randomly divided the unnormalized dataset with 17 predictor variables in Table 1 into two subsets, in which 70% of the whole dataset were used for training and 30% were used for testing.

3. Research Approach

3.1. Logistic Regression. This paper judges whether the driver is fatigued by whether the driver is yawning. Since the dependent variable is binary, we establish a binary logistic model:

Table 3: Eigenvalues, percent of variance, cumulative eigenvalue, and cumulative percent of variance for factor analysis.

Factor	Eigenvalue	Percentage of variance	Cumulative eigenvalue	Cumulative percentage of variance
1	6.343	37.313	6.343	37.313
2	2.860	16.826	9.203	54.139
3	2.413	14.192	11.616	68.331
4	1.458	8.574	13.074	76.905
5	0.931	5.479	14.005	82.384
6	0.658	4.028	14.663	86.412
7	0.519	3.052	15.182	89.465
8	0.445	2.616	15.627	92.080
9	0.392	2.307	16.019	94.387
10	0.345	2.029	16.364	96.416
11	0.259	1.523	16.623	97.939
12	0.245	1.443	16.868	99.382
13	0.104	0.610	16.972	99.992
14	0.001	0.006	16.973	99.998
15	0.000	0.002	17	100.000
16	$1.022E-13$	$6.010E-13$	17	100.000
17	$7.399E-14$	$4.317E-13$	17	100.000

$$\text{Logit}(P) = \ln\left(\frac{P}{1-P}\right) = \alpha + \sum \beta_j X_j + \varepsilon, \tag{5}$$

where P is the probability of the dependent variable $Y = 1$ (i.e., the probability of the driver yawning), the independent variable X_j is the various factors affecting the driver's fatigue (i.e., the common factor extracted by the factor analysis method), β_j is the regression coefficients of the independent variable X_j, α is a constant term, and ε is an error term.

3.2. Neural Network. In this paper, the multilayer perceptual neural network algorithm is used to train data samples. The multilayer perceptual neural network is a forward-structured artificial neural network that uses a backpropagation algorithm for training. The network consists of an input layer, hidden layers, and an output layer. The input layer corresponds generally to features to classify and is used to receive input data. The hidden layer may have multiple layers for learning data and storing training results. The output layer corresponds to the defined classes and each class corresponds to a node in the output layer. It is used to output results. Each layer consists of multiple nodes, each of which can be passed to the next layer up to the output layer. Excluding the input node, all other nodes multiply the input by its own weighting factor ω, plus the offset b, and then combine its own nonlinear activation function to produce the output [59].

The optimization algorithm of multilayer perceptual neural network adopts the adjusted conjugate gradient algorithm and the activation function of each layer is different. The middle layer node uses the hyperbolic tangent function as the activation function:

$$\tanh x = \frac{e^x - e^{-x}}{e^x + e^{-x}}. \tag{6}$$

The output layer node uses the Softmax function as the activation function:

$$f(x_i) = \frac{e^{x_i}}{\sum_{n=1}^{N} e^{x_n}}, \tag{7}$$

where x_i represents the input from the previous layer and N represents the total number of nodes in the previous layer.

We use the 17 predictor variables normalized in Table 1 as the network input and choose to use a layer of hidden neurons based on the data characteristics. In order to determine the optimal number of nodes in the hidden layer, we first make the number of nodes in the hidden layer equal to the number of nodes in the input layer. Then, we gradually reduce the number of nodes and simultaneously calculate generalization errors, training errors, deviations, and variances. The number of nodes at this point is our choice when the generalization error has dropped and before it begins to increase again. We finally determined that the optimal number of nodes in the hidden layer is 13. Figure 1 shows the structure of the established neural network model. The comparison between neural network and logistic regression is common, and related studies have found that neural network is superior to logistic regression due to its complex model structure [60, 61].

3.3. Random Forest. Random forest proposed by Breiman is an ensemble learning algorithm which constructs multiple decision trees through bootstrap aggregation [62]. Each tree is a standard Classification or Regression Tree (CART) that uses the so-called Decrease of Gini Impurity (DGI) as a splitting standard of the node [63]. Instead of using all input variables, random forest selects at random a subset of the input variables to split each node when growing a CART [64]. Each tree predicts a classification independently and "votes" for the corresponding class. The majority of the votes determine the optimal result of the random forest model [65]. The operating principle of random forest is summarized as follows and shown in Figure 2.

(i) k subsets of the sample $D1$, $D2$,. . ., Dk are drawn from the total sample set D using the bagging technique. The sample size of subsets Dk is the same as the total sample set D.

(ii) k decision trees are constructed according to the k subsets and obtain k classification results.

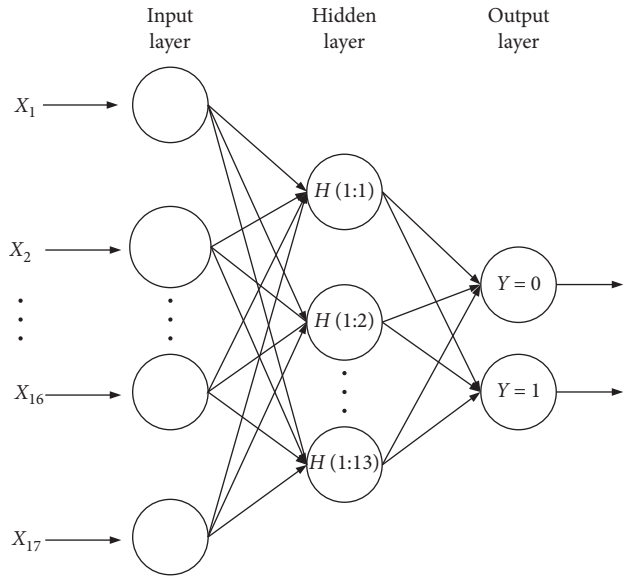

Figure 1: Schematic diagram of multilayer perceptual neural network structure.

(iii) Optimal results are obtained by voting.

To execute the random forest algorithm, the open source software, Python, which provides a language and environment for statistical calculation, was used. Before training the random forest model, tuning its hyperparameter is necessary to obtain random forest model with the best predictive performance. Two important hyperparameters, namely, the number of classification trees (ntree) and the number of variables tried at each split (mtry), have a significant effect on the performance of the model. Regarding the hyperparameters mtry, many studies use the value recommended by Breiman mtry = sqrt (M), where M is the number of predictor variables [66]. In this study, mtry = 4. Therefore, we only tuned the hyperparameters ntree and its tuning range was 10–4000. We compared the random forest models with different hyperparameters $n$tree using the average error rate from 5-fold cross-validation. As shown in Figure 3, the average error rate decreased sharply when ntree increased from 10 to 60. When ntree increased from 60 to 2200, the average error rate had slightly different trends; however, generally, the average error rate decreased slightly. When increased from 2200 to 4000, the average error rate almost remained stable. Therefore, $n$tree = 2200 was determined as the optimal value. Finally, the optimum hyperparameters were determined to be 2200 trees with the number of variables tried at each split being 4.

3.4. Model Evaluation. For the training results, three indexes including accuracy, F1-measure, and area under the ROC curve (AUROC) are used to evaluate the predictive performance of the classifiers. Although more indexes can be used to evaluate the predictive performance of the classifiers, we believe that these three indexes can complete the comparison between logistic regression and neural network classifiers. The numbers of true negatives (TN), true positives (TP), false positives (FP), and false negatives (FN) are used as a

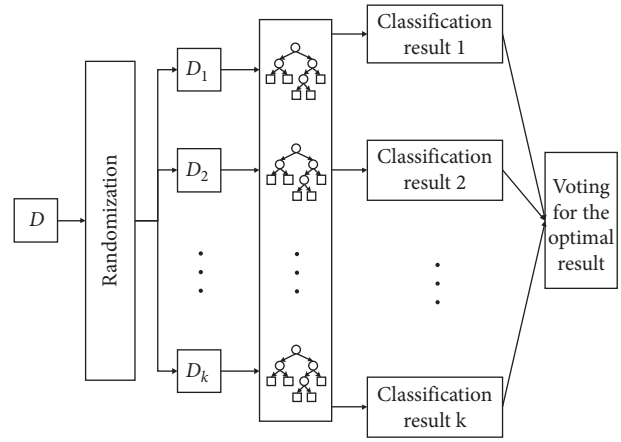

Figure 2: The operating principle of random forest.

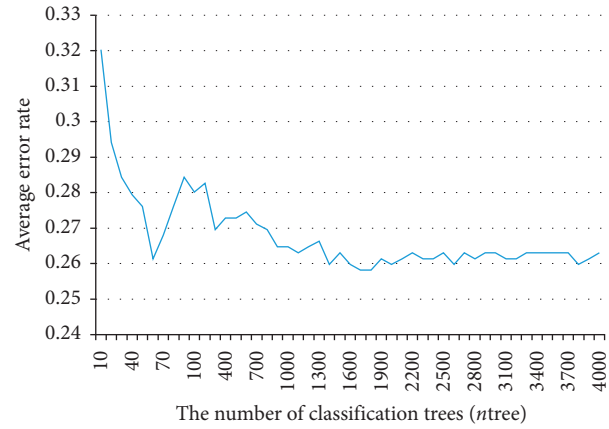

Figure 3: Average error rate of hyperparameter tuning.

measurement to assess the performance of classifiers. Different terms are used in different domains. Accuracy is the most basic index for assessing the performance of classifiers. It is used as an overall measure and calculated as

$$\text{accuracy} = \frac{\text{TP} + \text{TN}}{\text{TP} + \text{TN} + \text{FP} + \text{FN}}, \tag{8}$$

where TP and TN indicate correctly classified cases and FP and FN indicate the incorrectly classified cases. However, the skewed class distribution of samples, in reality, makes traditional metrics such as accuracy unable to properly reflect the performance of the classifiers [67]. Therefore, another index, F1-measure, is proposed to evaluate performance and calculated as

$$\text{F1} - \text{measure} = \frac{2\text{TP}}{2\text{TP} + \text{FP} + \text{FN}}. \tag{9}$$

Accuracy and F1-measure evaluate the performance of the classifiers by comparing predicted class labels. In this sense, they can actually be thought to measure different aspects of the same coin, and show recognized disadvantages [68]. Therefore, the receiver operating characteristic (ROC) curve is used to measure the performance of classifiers. The curve is generated by plotting true positives as the percentage of all positives and negative ones in the sample [69]. We hope to reduce ROC performance to a single scalar value

representing expected performance to evaluate the performance of classifiers, so the AUROC is considered as an additional index. AUROC gives a single measure of overall accuracy that is independent of any particular threshold [70, 71]. Larger AUROC value indicates that better predictive model is a generally accepted rule for determining a model's performance when comparing various models.

4. Results

4.1. Model Comparison and Selection. We trained logistic regression, neural network, and random forest using the training set and calculated accuracy, F1-measure, and AUROC value of every model based on the testing set.

Figure 4 depicts the results for classification performance of logistic regression, neural network, and random forest models. Obviously, the accuracy, F1-measure, and AUROC of the random forest are higher than the logistic regression and neural network (i.e., the predictive performance of the random forest is better). Therefore, the random forest is more suitable to use location data to predict fatigue driving than logistic regression and neural network. It can be seen from Figure 4 that the accuracy of the random forest is 74.18%. Although this accuracy is not too high, it can be accepted compared to other fatigue driving detection methods based on vehicle information. In addition, more than 60% of F1-measure reveals its ability to detect real yawn, which means the number of a missed yawn is reduced using the random forest classification. The random forest was selected to predict fatigue driving using predictor variables.

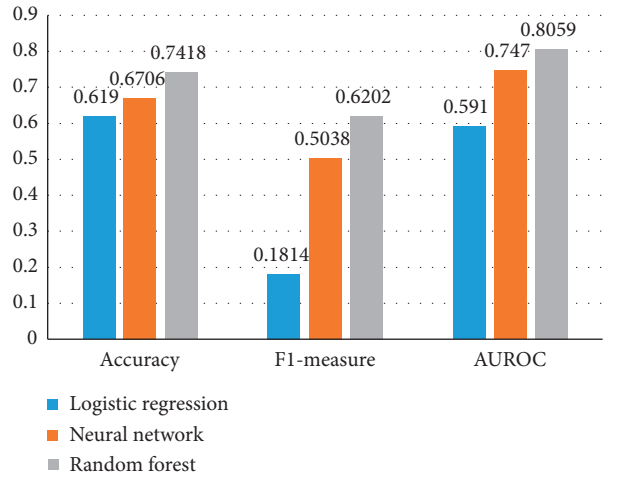

Figure 4: Prediction accuracy, F-measure, and AUROC for every model.

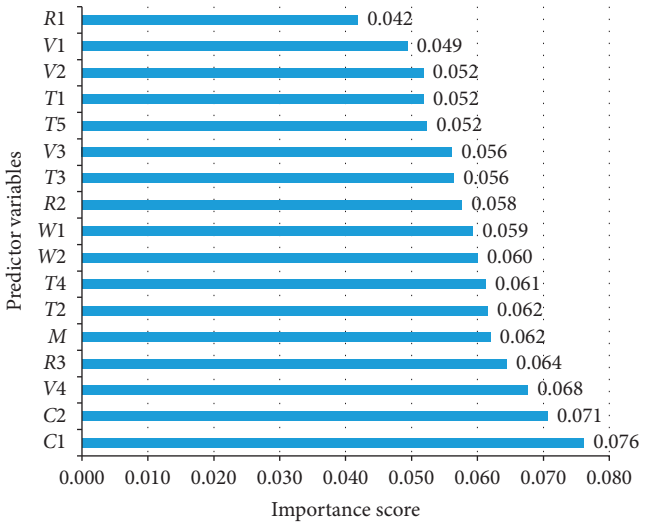

Figure 5: Relative importance of predictor variables.

4.2. Variable Importance Analysis. After determining the random forest model as the optimal prediction model, we analyzed the relationship between fatigue driving and driving task of last week according to variable importance described by random forest.

Variable importance (called "variable importance score" in this study) reflects every predictor variable's contribution to the total risk. The random forest model computes variable importance scores by assessing the importance of every predictor variable using the Gini decrease index [72]. The computation was implemented based on the "feature_importances_" in the random forest package of open source software, Python. Figure 5 provides the normalized variable importance scores (i.e., the sum of the importance scores for all variables is one).

Fatigue driving has a close relationship with the driving task of last week. By comparing the variable importance in Figure 5, the paper draws the following conclusions:

(1) It is not difficult to see from Figure 5 that the importance scores of average continuous driving time ($C1$) and longest continuous driving time ($C2$) are the highest among all the predictor variables. This shows that continuous driving time is closely related to fatigue driving. Fatigue driving refers to the phenomenon that the driver produces dysfunction of physiology and mental function after driving for a long time so that driving skills decline objectively. Prolonged driving will make driver mental overload and cause task-related fatigue [45]. Therefore, the continuous driving time of the driver must be strictly controlled to avoid accidents caused by prolonged driving.

(2) During the predictor variables of travel time group, the importance scores of travel time between 5 am and 9 am ($T2$) and travel time between 5 pm and 10 pm ($T4$) are the highest. This shows that the driver is more likely to be fatigued when driving in these two time periods for a long time, which is basically consistent with the previous research results [73, 74]. In addition, it has been extensively proven that the number of accidents related to fatigue driving increase in the early morning and late evening [45, 75]. The time period indicated by $T4$ is extremely fragile. This is because, after a day of hard work, the driver will have a series of tired symptoms such as dry eyes, dry throat, and yawning. The time period indicated

by $T2$ is early morning, which is the time period when fatigue driving and traffic accidents are most likely to occur. During this time, the human circadian rhythm is in a state of slow brain reaction, lower blood pressure, and stiff and paralyzed blood vessels in the hands and feet. Therefore, in order to avoid fatigue driving, the driver's driving time should be reasonably arranged and the driver should try to avoid driving in these two periods. The importance scores of travel time between 10 pm and 12 pm ($T5$) and travel time between 0 am and 5 am ($T1$), in contrast, were found to be lower than all other variables of travel time (T). Apparently it seems surprising. But we can see from Table 2 that the mean of these two time periods is relatively small, which indicates that the driver rarely travels during these two time periods. One reason for this may be due to the relatively higher accident rate compared to other time periods; the company deliberately controls the driver not to drive during this time period.

(3) It is not surprising to observe that the importance scores of the average velocity (V) consistently decrease from average velocity over 80 km/h ($V4$) to average velocity between 0 and 40 km/h ($V1$). Therefore, the importance scores for $V4$ (0.104) > $V3$ (0.040) > $V2$ (0.036) > $V1$ (0.035). This shows that the driver is more likely to be fatigued when driving at a high speed for a long time. It has been extensively proven that the higher the driving speed is, the easier the driver is to be fatigued [76]. The higher the driving speed, the greater the degree of tension or concentration of the driver's central nervous system and the greater the mental and physical energy consumed. At the same time, the driver's field of vision narrows as the speed of the vehicle increases, and the information that is missed increases, making the driver more nervous. It is worth mentioning that the importance scores of average velocity between 40 and 60 km/h ($V2$) and average velocity between 0 and 40 km/h ($V1$) are relatively lower than other predictor variables and the importance of average velocity over 80 km/h ($V4$) is relatively higher. This shows that when the driver drives in the environment in which the speed is lower than 60 km/h for a long time, the driver is not prone to fatigue, but once the driver drives in the environment where the speed exceeds 80 km/h for a long time, the driver is more likely to be fatigued. Therefore, the driving speed of the vehicle should be reasonably controlled to avoid the driver driving at a high speed for a long time.

(4) It can be seen from Figure 5 that the importance scores of the road type (R) consistently increase from urban roads ($R1$) to freeway ($R3$). This shows that the driver is more likely to be fatigued when driving on the freeway for a long time, which is consistent with previous research [74, 76, 77]. In addition, it has been reported that 40 percent of the accidents caused by fatigue driving occur on freeways [78]. The freeway has neither traffic signal control nor pedestrians, nonmotor vehicles, and other low-speed motor vehicles. Driving on this road for a long time is easy to cause the driver to sleep. In addition, when driving on the freeway, the driver's energy is always in a state of high tension, and the physical exertion is increased, and the speed of the vehicle will be unconsciously increased, and even the brake deceleration consciousness will be lost. Driving in such an environment for a long time can also make the driver feel tired. Therefore, it is necessary to adopt the fatigue warning device when the driver is driving on the freeway.

(5) We can also find that the importance score of weekends with Friday ($W2$) is higher than the importance score of weekdays except Friday ($W1$) from Figure 5. This indicates that the driver is more likely to be fatigued when driving on weekends for a long time. This is because the driver will continue to accumulate fatigue as he drives on weekdays, which makes the driver's fatigue index relatively higher on weekends. This provides a basis for a reasonable arrangement of driver travel time.

5. Discussion

This paper has offered a brand new approach to predict driving fatigue using location data of CDT. The existing approach to predict driving fatigue mainly uses physiological and behavioral indicators. However, physiological and behavioral measurements may interfere with the driver's normal driving, and the corresponding detection devices are relatively expensive. Our approach predicts fatigue using the location data of CDT which are collected without interfering with the driver's normal driving. Location data acquisition equipment is relatively inexpensive and is generally installed in commercial trucks. These are beneficial to the future popularization and application of real driving conditions. In addition, most studies on the prediction of fatigue driving focus on short-time forecasting. Few studies research on long-term prediction methods, specifically on commercial trucks. Our approach addresses the long-term prediction of fatigue driving in commercial trucks.

5.1. Model Application Illustration. The proposed approach can be used not only for driving fatigue prediction of commercial dangerous goods transport vehicles but also for other transport vehicles. In addition, our approach can directly use the location data of the vehicle to predict fatigue, which not only solves the problem that most domestic commercial transport vehicles do not have the image acquisition device installed, but also has no disadvantages of other detection approaches that interfere with the driver. Our approach can also aid decision making and is a useful complement to real-time monitoring. Even if the transport vehicles are equipped with the image acquisition device, our approach is also necessary to help prevent fatigue. What is also worth noting about our approach is that it can not only be used to predict fatigue, but also provide a basis for transportation companies to arrange transportation mission reasonably. Figure 6 depicts the application of the prediction approach.

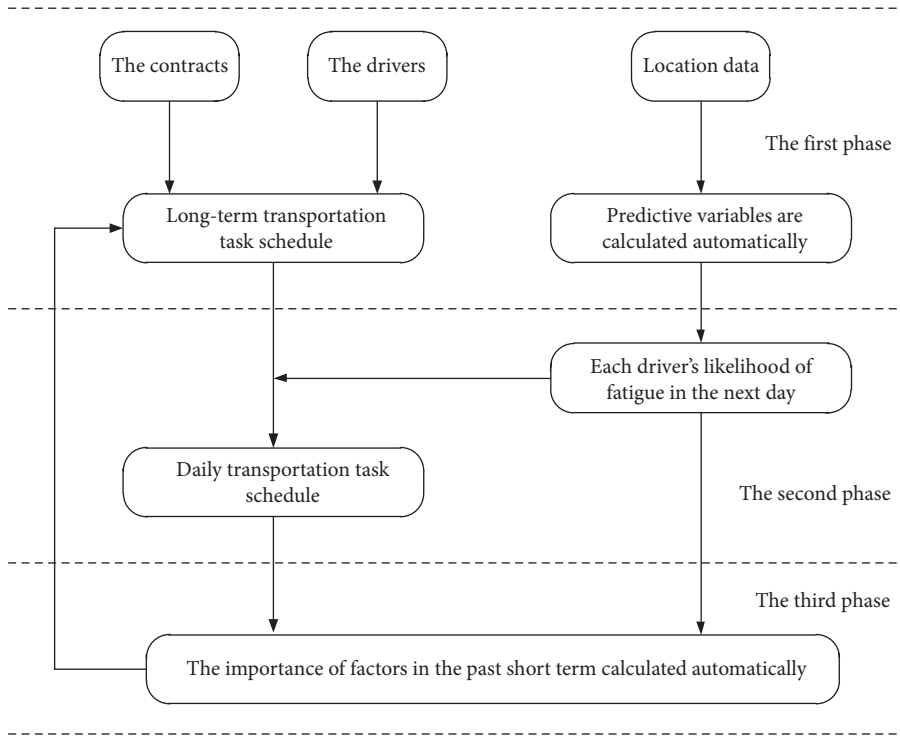

Figure 6: Application of the prediction approach.

The proposed approach can be used to optimize the daily task arrangement of the transportation company. In the first phase, the transportation company will complete a long-term transportation task schedule, which may be used for a week or a month, based on the contracts signed and the number of drivers. At the same time, the location data of the driver during the transportation task are automatically collected.

In the second phase, 17 indicators can be calculated automatically and each driver's likelihood of fatigue in the next day was dynamically predicted. The prediction results can help optimize the daily schedule of transportation tasks.

In the third phase, the importance of each factor in the past short term can help the transportation company managers to formulate the long-term task schedule. Do your best to avoid long hours in which drivers are prone to fatigue.

5.2. Research Limitations and Future Research Needs. Some methodological and conceptual limitations should be considered in the interpretation of our results. These limitations make us consider using other models to further improve prediction accuracy in future research. This would involve the combination of different classifiers [79]. We should also use the data from other dangerous goods transportation companies to verify our results. Due to the limited data acquisition properties, our approach only analyzes the influence of six predictor sets. In the future, other available related variables should also be considered to extend the set of predictor variables and yield further improvements to predictive performance and the guidance of analysis results. Driver's physique, lifestyle, stress, and other factors have a certain impact on the predictive performance of our model. Therefore, if the driver's relevant information can be obtained and used as predictor variables, the accuracy of the model will be further improved. In addition, seasonal changes have a significant impact on our approach; future efforts should be made to eliminate the effects of the seasons, thus making our approach more complete.

6. Conclusion

In order to solve the fatigue driving problem of dangerous goods transportation, this paper proposed an approach that used location data obtained from a transportation company to predict fatigue driving and further analyzed the relationship between fatigue driving and driving environment. The proposed approach can be used to predict fatigue driving using the location data of CDT which were collected without interfering with the driver's normal driving and provide a basis for transportation companies to arrange transportation mission reasonably. The main findings were concluded as follows:

(1) We used logistic regression, neural network, and random forest techniques to predict fatigue driving from the location data. To choose a more suitable classifier as a predictive model, we obtained a set of 17 predictor variables from the six different categories of the predictor set related to fatigue to train and compare logistic regression, neural network, and random forest

classifiers. By analyzing and comparing the classification performance results of logistic regression, neural networks, and random forest models, we found that accuracy (74.18%), F1-measure (62.02%), and AUROC (0.8059) of random forest were separately best, so random forest was more suitable for predicting fatigue driving using location data

(2) To provide a basis for the transportation company to arrange transportation reasonably, after determining the random forest model as the optimal prediction model, we analyzed the relationship between fatigue driving and driving environment according to variable importance described by random forest. We found that fatigue driving was closely related to driving conditions such as travel time, continuous driving time, driving speed, road type, and so on. The period extremely prone to fatigue driving is early morning and the evening, and the driver is more prone to fatigue on weekdays than on weekends. The higher the driving speed is, the easier the driver is to be fatigued. The probability of fatigue driving on the freeway is higher than that of highway and urban road. These conditions can provide a basis for the company to avoid driver fatigue driving, thereby reducing traffic accidents.

Data Availability

The data used to support the findings of this study are included within the article.

Conflicts of Interest

The authors declare no potential conflicts of interest with respect to the research, authorship, and/or publication of this article.

Acknowledgments

This work was supported by the National Key R&D Program of China (2019YFB1600500).

References

[1] Q. Yang, K.-S. Chin, and Y.-L. Li, "A quality function deployment-based framework for the risk management of hazardous material transportation process," *Journal of Loss Prevention in the Process Industries*, vol. 52, no. 52, pp. 81–92, 2018.

[2] Y. Leung, R. Li, and N. Ji, "Application of extended Dempster-Shafer theory of evidence in accident probability estimation for dangerous goods transportation," *Journal of Geographical Systems*, vol. 19, no. 3, pp. 249–271, 2017.

[3] E. Erkut, S. A. Tjandra, and V. Verter, "Hazardous materials transportation," in *Handbooks in Operations Research and Management Science*, G. Laporte and C. Barnhart, Eds., vol. 14, pp. 539–621, Elsevier, Haarlem, Netherlands, 2007.

[4] M. H. Laarabi, A. Boulmakoul, R. Sacile, and E. Garbolino, "A scalable communication middleware for real-time data collection of dangerous goods vehicle activities," *Transportation Research Part C: Emerging Technologies*, vol. 48, pp. 404–417, 2014.

[5] P. Leonelli, S. Bonvicini, and G. Spadoni, "New detailed numerical procedures for calculating risk measures in hazardous materials transportation," *Journal of Loss Prevention in the Process Industries*, vol. 12, no. 6, pp. 507–515, 1999.

[6] A. M. Tomasoni, *Models and Methods of Risk Assessment and Control in Dangerous Goods Transportation (DGT) Systems*, École Nationale Supérieure des Mines de Paris, Paris, France, 2010.

[7] G. Landucci, G. Antonioni, A. Tugnoli, S. Bonvicini, M. Molag, and V. Cozzani, "HazMat transportation risk assessment: a revisitation in the perspective of the Viareggio LPG accident," *Journal of Loss Prevention in the Process Industries*, vol. 49, no. SI, pp. 36–46, 2017.

[8] R. Bubbico, G. Maschio, B. Mazzarotta, M. F. Milazzo, and E. Parisi, "Risk management of road and rail transport of hazardous materials in Sicily," *Journal of Loss Prevention in the Process Industries*, vol. 19, no. 1, pp. 32–38, 2006.

[9] R. Fu, H. Wang, and W. Zhao, "Dynamic driver fatigue detection using hidden Markov model in real driving condition," *Expert Systems with Applications*, vol. 63, pp. 397–411, 2016.

[10] A. Williamson and R. Friswell, "The effect of external non-driving factors, payment type and waiting and queuing on fatigue in long distance trucking," *Accident Analysis & Prevention*, vol. 58, no. 3, pp. 26–34, 2013.

[11] I. D. Brown, "Prospects for technological countermeasures against driver fatigue," *Accident Analysis & Prevention*, vol. 29, no. 4, pp. 525–531, 1997.

[12] G. Maycock, "Driver sleepiness as a factor in car and HGV accidents," Trl Report, The Royal Society for the Prevention of Accidents, Birmingham, UK, 1995.

[13] G. Zhang, K. K. W. Yau, X. Zhang, and Y. Li, "Traffic accidents involving fatigue driving and their extent of casualties," *Accident Analysis & Prevention*, vol. 87, pp. 34–42, 2016.

[14] America USO, *Safety Study: Fatigue, Alcohol, Other Drugs, and Medical Factors in Fatal-to-the-Driver Heavy Truck Crashes*, Vol. 1, Bureau of Justice Statistics, Washington, DC, USA, 1990.

[15] P. C. Morrow and M. R. Crum, "Antecedents of fatigue, close calls, and crashes among commercial motor-vehicle drivers," *Journal of Safety Research*, vol. 35, no. 1, pp. 59–69, 2004.

[16] Federal Motor Carrier Safety Administration, *Report to Congress on the Large Truck Crash Causation Study*, U.S. Department of Transportation, Washington, DC, USA, 2006.

[17] M. J. M. Sullman, M. L. Meadows, and K. B. Pajo, "Aberrant driving behaviours amongst New Zealand truck drivers," *Transportation Research. Part F: Traffic Psychology and Behaviour*, vol. 5, no. 3, pp. 1–232, 2002.

[18] D. Blower, P. E. Green, and A. Matteson, "Condition of trucks and truck crash involvement," *Transportation Research Record: Journal of the Transportation Research Board*, vol. 2194, no. 1, pp. 21–28, 2010.

[19] F. Sagberg, "Road accidents caused by drivers falling asleep," *Accident Analysis & Prevention*, vol. 31, no. 6, pp. 639–649, 1999.

[20] B. C. Tefft, "Prevalence of motor vehicle crashes involving drowsy drivers, United States, 1999–2008," *Accident Analysis & Prevention*, vol. 45, no. 45, pp. 180–186, 2012.

[21] G. Tzamalouka, M. Papadakaki, and J. E. Chliaoutakis, "Freight transport and non-driving work duties as predictors of falling asleep at the wheel in urban areas of Crete," *Journal of Safety Research*, vol. 36, no. 1, pp. 75–84, 2005.

[22] H. M. Kanazawa, T. Onoda, and N. Yokozawa, "Excess workload and sleep-related symptoms among commercial long-haul truck drivers," *Sleep and Biological Rhythms*, vol. 4, no. 2, pp. 121–128, 2006.

[23] M. Suzuki, T. Kontogiannis, G. Tzamalouka, C. Darviri, and J. Chliaoutakis, "Exploring the effects of lifestyle, sleep factors and driving behaviors on sleep-related road risk: a study of Greek drivers," *Accident Analysis & Prevention*, vol. 40, no. 6, pp. 2029–2036, 2008.

[24] J. Duke, M. Guest, and M. Boggess, "Age-related safety in professional heavy vehicle drivers: a literature review," *Accident Analysis & Prevention*, vol. 42, no. 2, pp. 364–371, 2010.

[25] F. Meng, S. Li, L. Cao et al., "Driving fatigue in professional drivers: a survey of truck and taxi drivers," *Journal of Crash Prevention and Injury Control*, vol. 16, no. 5, p. 10, 2015.

[26] C. J. de Naurois, C. Bourdin, C. Bougard et al., "Adapting artificial neural networks to a specific driver enhances detection and prediction of drowsiness," *Accident Analysis & Prevention*, vol. 121, pp. 118–128, 2018.

[27] Y. Wang, Y. Zhang, D. Liu et al., "Driving fatigue detection based on EEG signal," in *Proceedings of the Fifth International Conference on Instrumentation & Measurement, Computer, Communication, and Control (IMCCC)*, IEEE, Qinhuangdao, China, pp. 714–717, September 2015.

[28] X. Q. Huo, W. L. Zheng, and B. L. Lu, "Driving fatigue detection with fusion of EEG and forehead EOG," in *Proceedings of the International Joint Conference on Neural Networks (IJCNN)*, IEEE, Vancouver, Canada, pp. 897–904, July 2016.

[29] Z. Li, J. Peng, L. Chen et al., "Fatigue driving detecting method based on time-space features in real driving conditions," in *Proceedings of the 10th IEEE Conference on Industrial Electronics and Applications Industrial Electronics and Applications*, IEEE, Auckland, New Zealand, pp. 183–187, June 2015.

[30] Y. Wang, X. Liu, Y. Zhang et al., "Driving fatigue detection based on EEG signal," in *Proceedings of the Fifth International Conference on Instrumentation & Measurement*, IEEE, Shenzhen, China, September 2016.

[31] Y. Dong, Z. Hu, K. Uchimura et al., "Driver inattention monitoring system for intelligent vehicles: a review," in *Proceedings of the IEEE Intelligent Vehicles Symposium*, IEEE, Xi'an, China, 2009.

[32] J. Chen and Q. Ji, "Drowsy driver posture, facial, and eye monitoring methods," in *Handbook of Intelligent Vehicles*, A. Eskandarian, Ed., pp. 913–940, Springer, London, UK, 2012.

[33] C. C. Liu, S. G. Hosking, and M. G. Lenné, "Predicting driver drowsiness using vehicle measures: recent insights and future challenges," *Journal of Safety Research*, vol. 40, no. 4, pp. 239–245, 2009.

[34] Y. J. Zhong, L. P. Du, K. Zhang et al., "Localized energy study for analyzing driver fatigue state based on wavelet analysis," in *Proceedings of the International Conference on Wavelet Analysis & Pattern Recognition*, IEEE, Hong Kong, China, 2008.

[35] Y. Takei and Y. Furukawa, "Estimate of driver's fatigue through steering motion," in *Proceedings of the IEEE International Conference on Systems*, IEEE, Los Angeles, CA, USA, 2006.

[36] L. Wang and Y. Pei, "The impact of continuous driving time and rest time on commercial drivers' driving performance and recovery," *Journal of Safety Research*, vol. 50, pp. 11–15, 2014.

[37] G. X. Chen, Y. Fang, F. Guo, and R. J. Hanowski, "The influence of daily sleep patterns of commercial truck drivers on driving performance," *Accident Analysis & Prevention*, vol. 91, pp. 55–63, 2016.

[38] Y. Wang, C. Ma, and Y. Li, "Effects of prolonged tasks and rest patterns on driver's visual behaviors, driving performance, and sleepiness awareness in tunnel environments: a simulator study," *Iranian Journal of Science and Technology, Transactions of Civil Engineering*, vol. 42, no. 2, pp. 143–151, 2018.

[39] K. Mahajan, N. R. Velaga, A. Kumar, A. Choudhary, and P. Choudhary, "Effects of driver work-rest patterns, lifestyle and payment incentives on long-haul truck driver sleepiness," *Transportation Research Part F: Traffic Psychology and Behaviour*, vol. 60, no. 60, pp. 366–382, 2019.

[40] A. T. Mccartt, J. W. Rohrbaugh, M. C. Hammer, and S. Z. Fuller, "Factors associated with falling asleep at the wheel among long-distance truck drivers," *Accident Analysis & Prevention*, vol. 32, no. 4, pp. 493–504, 2000.

[41] M. M. Ohayon, "Demographic factors, fatigue, and driving accidents: an examination of the published literature," *Accident Analysis and Prevention*, vol. 43, no. 2, pp. 516–532, 2011.

[42] K. Sadeghniiat-Haghighi, Z. Yazdi, and A. M. Kazemifar, "Sleep quality in long haul truck drivers: a study on Iranian national data," *Chinese Journal of Traumatology*, vol. 4, no. 19, pp. 225–228, 2016.

[43] P. K. Arnold, L. R. Hartley, A. Corry, D. Hochstadt, F. Penna, and A. M. Feyer, "Hours of work, and perceptions of fatigue among truck drivers," *Accident Analysis & Prevention*, vol. 29, no. 4, pp. 471–477, 1997.

[44] T. Åkerstedt, A. Knutsson, P. Westerholm, T. Theorell, L. Alfredsson, and G. Kecklund, "Sleep disturbances, work stress and work hours," *Journal of Psychosomatic Research*, vol. 53, no. 3, pp. 741–748, 2002.

[45] J. F. May and C. L. Baldwin, "Driver fatigue: the importance of identifying causal factors of fatigue when considering detection and countermeasure technologies," *Transportation Research Part F: Traffic Psychology and Behaviour*, vol. 12, no. 3, pp. 1–224, 2009.

[46] A. Watson and G. Zhou, "Microsleep prediction using an EKG capable heart rate monitor," in *Proceedings of the 2016 IEEE First International Conference on Connected Health: Applications, Systems and Engineering Technologies (CHASE)*, 2016.

[47] C. Jacobé de Naurois, C. Bourdin, A. Stratulat, E. Diaz, and J.-L. Vercher, "Detection and prediction of driver drowsiness using artificial neural network models," *Accident Analysis & Prevention*, vol. 126, pp. 95–104, 2019.

[48] J. Paefgen, T. Staake, and F. Thiesse, "Evaluation and aggregation of pay-as-you-drive insurance rate factors: a classification analysis approach," *Decision Support Systems*, vol. 56, pp. 192–201, 2013.

[49] D. Lord and F. Mannering, "The statistical analysis of crash-frequency data: a review and assessment of methodological alternatives," *Transportation Research Part A*, vol. 44, no. 5, pp. 0–305, 2010.

[50] F. Chen, H. Peng, X. Ma, J. Liang, W. Hao, and X. Pan, "Examining the safety of trucks under crosswind at bridge-tunnel section: a driving simulator study," *Tunnelling and Underground Space Technology*, vol. 92, Article ID 103034, 2019.

[51] S. Niu and S. V. Ukkusuri, "Risk Assessment of Commercial dangerous -goods truck drivers using geo-location data: a case study in China," *Accident Analysis & Prevention*, vol. 137, Article ID 105427, 2020.

[52] F. Chen and S. Chen, "Injury severities of truck drivers in single- and multi-vehicle accidents on rural highways," *Accident Analysis & Prevention*, vol. 43, no. 5, pp. 1677–1688, 2011.

[53] F. Chen, M. Song, and X. Ma, "Investigation on the injury severity of drivers in rear-end collisions between cars using a random parameters bivariate ordered probit model," *International Journal of Environmental Research and Public Health*, vol. 16, no. 14, p. 2632, 2019.

[54] H. Midi, S. K. Sarkar, and S. Rana, "Collinearity diagnostics of binary logistic regression model," *Journal of Interdisciplinary Mathematics*, vol. 13, no. 3, pp. 253–267, 2010.

[55] M. Littner, C. A. Kushida, W. M. Anderson et al., "Practice parameters for the role of actigraphy in the study of sleep and circadian rhythms: an update for 2002," *Sleep*, vol. 26, no. 3, pp. 337–341, 2003.

[56] M. Y. Kiang, "A comparative assessment of classification methods," *Decision Support Systems*, vol. 35, no. 4, pp. 441–454, 2003.

[57] C. Qi, A. Fourie, X. Du, and X. Tang, "Prediction of open stope hangingwall stability using random forests," *Natural Hazards*, vol. 92, no. 2, pp. 1179–1197, 2018.

[58] D. R. Cutler Jr., T. C. Edwards, K. H. Beard et al., "Random forests for classification in ecology," *Ecology*, vol. 88, no. 11, pp. 2783–2792, 2007.

[59] F. K.-H. Chun, P. I. Karakiewicz, A. Briganti et al., "A critical appraisal of logistic regression-based nomograms, artificial neural networks, classification and regression-tree models, look-up tables and risk-group stratification models for prostate cancer," *BJU International*, vol. 99, no. 4, pp. 794–800, 2007.

[60] B. Swiderski, J. Kurek, and S. Osowski, "Multistage classification by using logistic regression and neural networks for assessment of financial condition of company," *Decision Support Systems*, vol. 52, no. 2, pp. 539–547, 2012.

[61] O. E. Askin and F. Gokalp, "Comparing the predictive and classification performances of logistic regression and neural networks: a case study on timss 2011," *Procedia-Social and Behavioral Sciences*, vol. 106, pp. 667–676, 2013.

[62] T. Shaikhina, D. Lowe, S. Daga, D. Briggs, R. Higgins, and N. Khovanova, "Decision tree and random forest models for outcome prediction in antibody incompatible kidney transplantation," *Biomedical Signal Processing and Control*, vol. 52, pp. 456–462, 2019.

[63] A.-L. Boulesteix, S. Janitza, J. Kruppa, and I. R. König, "Overview of random forest methodology and practical guidance with emphasis on computational biology and bioinformatics," *Wiley Interdisciplinary Reviews: Data Mining and Knowledge Discovery*, vol. 2, no. 6, pp. 493–507, 2012.

[64] J.-H. Huang, H.-L. Xie, J. Yan, H.-M. Lu, Q.-S. Xu, and Y.-Z. Liang, "Using random forest to classify T-cell epitopes based on amino acid properties and molecular features," *Analytica Chimica Acta*, vol. 804, pp. 70–75, 2013.

[65] R. J. Marshall, "The use of classification and regression trees in clinical epidemiology," *Journal of Clinical Epidemiology*, vol. 54, no. 6, pp. 603–609, 2001.

[66] D. C. Duro, S. E. Franklin, and M. G. Dubé, "A comparison of pixel-based and object-based image analysis with selected machine learning algorithms for the classification of agricultural landscapes using SPOT-5 HRG imagery," *Remote Sensing of Environment*, vol. 118, pp. 259–272, 2012.

[67] J. Shreve, H. Schneider, and O. Soysal, "A methodology for comparing classification methods through the assessment of model stability and validity in variable selection," *Decision Support Systems*, vol. 52, no. 1, pp. 247–257, 2012.

[68] P. A. Flach, J. Hernández-Orallo, and C. F. Ramirez, "A coherent interpretation of AUC as a measure of aggregated classification performance," in *Proceedings of the 28th International Conference on Machine Learning*, pp. 657–664, Washington, DC, USA, July 2011.

[69] E. Gokgoz and A. Subasi, "Comparison of decision tree algorithms for EMG signal classification using DWT," *Biomedical Signal Processing and Control*, vol. 18, pp. 138–144, 2015.

[70] F. Chen, S. Chen, and X. Ma, "Analysis of hourly crash likelihood using unbalanced panel data mixed logit model and real-time driving environmental big data," *Journal of Safety Research*, vol. 65, pp. 153–159, 2018.

[71] A. Subasi, "Classification of EMG signals using PSO optimized SVM for diagnosis of neuromuscular disorders," *Computers in Biology and Medicine*, vol. 43, no. 5, pp. 576–586, 2013.

[72] F.-f. Ai, J. Bin, Z.-m. Zhang et al., "Application of random forests to select premium quality vegetable oils by their fatty acid composition," *Food Chemistry*, vol. 143, pp. 472–478, 2014.

[73] J. A. Horne and L. A. Reyner, "Driver sleepiness and sleep disorders, with particular reference to Parkinson's disease," in *Proceedings of the Meeting on Causes and Management of Sleep Disturbances in Parkinsons Disease*, pp. 15–20, Cannes, France, January 2000.

[74] D. J. Beirness, H. M. Simpson, and K. Desmond, *The Road Safety Monitor 2004: Drowsy Driving*, Ottawa: Traffic Injury Research Foundation, Ottawa, Canada, 2005.

[75] A. I. Pack, A. M. Pack, E. Rodgman, A. Cucchiara, D. F. Dinges, and C. W. Schwab, "Characteristics of crashes attributed to the driver having fallen asleep," *Accident Analysis & Prevention*, vol. 27, no. 6, pp. 769–775, 1995.

[76] P.-H. Ting, J.-R. Hwang, J.-L. Doong, and M.-C. Jeng, "Driver fatigue and highway driving: a simulator study," *Physiology & Behavior*, vol. 94, no. 3, pp. 448–453, 2008.

[77] D. H. Li, Q. Liu, W. Yuan et al., "Relationship between fatigue driving and traffic accident," *Journal of Traffic and Transportation Engineering*, vol. 10, no. 2, pp. 104–109, 2010.

[78] A. T. Mccartt, S. A. Ribner, A. I. Pack, and M. C. Hammer, "The scope and nature of the drowsy driving problem in New York state," *Accident Analysis & Prevention*, vol. 28, no. 4, pp. 511–517, 1996.

[79] J.-Y. Yeh, T.-H. Wu, and C.-W. Tsao, "Using data mining techniques to predict hospitalization of hemodialysis patients," *Decision Support Systems*, vol. 50, no. 2, pp. 439–448, 2011.

Hindawi
Journal of Advanced Transportation
Volume 2020, Article ID 7475682, 12 pages
https://doi.org/10.1155/2020/7475682

Research Article

Risk Modeling and Quantification of a Platoon in Mixed Traffic Based on the Mass-Spring-Damper Model

Luo Jiang,[1] Jie Ji,[1] Yue Ren,[1] Hong Wang,[2] and Yanjun Huang[3]

[1]*College of Engineering and Technology, Southwest University, Chongqing 400715, China*
[2]*School of Vehicle and Mobility, Tsinghua University, Beijing 100084, China*
[3]*Department of Mechanical and Mechatronics Engineering, University of Waterloo, Waterloo, Ontario N2L3G1, Canada*

Correspondence should be addressed to Jie Ji; jijiess@swu.edu.cn

Received 3 January 2020; Revised 30 May 2020; Accepted 11 June 2020; Published 8 July 2020

Academic Editor: Feng Chen

Connected and automated vehicle (CAV) technologies have great potential to improve road safety. However, an emerging type of mixed traffic flow with human-driven vehicles (HDVs) and CAVs has also arisen in recent years. To improve the overall safety of this mixed traffic flow, a novel car-following model is proposed to control the driving behaviors of the above two types of vehicles in a platoon from the perspective of a mechanical system, mass-spring-damper (MSD) system. Furthermore, a quantitative index is proposed by incorporating the psychological field theory into the MSD model. The errors of spacing and speed in the car-following processes can be expressed as the accumulation of the virtual total energy, and the magnitude of the energy is used to reflect the danger level of vehicles in the mixed platoon. At the same time, the optimization model of minimum total energy is solved under the constraints of vehicle dynamics and the mechanical characteristics of the MSD system, and the optimal solutions are used as the parameters of the MSD car-following model. Finally, a mixed platoon composed of 3 CAVs and 2 HDVs without performing lane changing is tested using the driver-in-the-loop test platform. The test results show that, in the mixed platoon, CAVs can optimally adjust the intervehicle spacing by making full use of the braking distance, which also provides sufficient reaction time for the driver of HDV to avoid rear-end collisions. Furthermore, in the early stage of the emergency braking, the spacing error is the dominant factor influencing the car-following behaviors, but in the later stage of emergency braking, the speed error becomes the decisive factor of the car-following behaviors. These results indicate that the proposed car-following model and quantitative index are of great significance for improving the overall safety of the mixed traffic flow with CAVs and HDVs.

1. Introduction

Due to the slow expansion of the road network, traffic oscillations, and traffic accidents occur frequently in road traffic. The emerging connected and automated vehicle technologies, however, offer great potential for enhancing traffic operations and improving the roadway capacity under existing road infrastructure, which helps make traffic flow more stable, more efficient, and safer. This is because CAVs are able to share driving information with others in real time, which makes the motion of CAVs more cooperative [1]. Vehicle platooning is a typical application that stands out in the domain. Thus, it has obtained extensive research interests and a great variety of research is indicating that platooning of CAVs can tremendously improve traffic safety [2–5] and energy efficiency [6]. It is worth noting that most research is focusing on the pure platoon of CAVs, but CAVs and HDVs will coexist in the near future [7–10]. Therefore, the most likely formation of vehicular platoons will be a mixture of CAVs and HDVs. This complex traffic environment will bring huge challenges to traffic flow modeling, control, and management when considering the stochastic driving characteristics of humans and the uncertainty of the interaction between CAVs and HDVs. Thus, how to make these two types of vehicles operate coordinately is the key to enhance traffic safety.

Modeling the mixed traffic flow is a feasible way to solve this problem. Many scholars have carried out in-depth research on the car-following models of vehicular platoons, which are mainly divided into the following categories: stimulus-response models [11], safety distance models [12], psycho-physical models [13], artificial intelligence model [14], optimal velocity model [15], intelligent driver model [16], and cellular automata model [17]. The advantages of these car-following models have been widely recognized in the field of transportation. More recently, some researchers have proposed car-following models combined with two different models to capture the driving behaviors of CAVs and HDVs, respectively. For example, Gong et al. [8] proposed a cooperative control method for mixed platoons to ensure the stability and safety of the platoons. In addition, the CAVs and HDVs adopted the MPC model and Newell model, respectively. The results indicate that this novel platoon control method can dampen traffic oscillation propagation and stabilize the traffic flow more efficiently for the entire mixed platoon. Zhu et al. [9] proposed a novel car-following model with adjustable sensitivity and smoothing factor for mixed traffic flow. The car-following model of HDVs selected optimal velocity model (OVM), while the car-following model of CAVs reduced its sensitivity factor on the basis of OVM. The numerical simulation results show that the proposed model is able to stabilize the mixed traffic flow and suppress the traffic jam. Zhao et al. [18] proposed a cooperative eco-driving model for mixed platoons, where HDVs were modeled by the OVM and CAVs are controlled by the MPC model. This model achieves better performance for the overall traffic. In these above-mentioned research studies, HDVs and CAVs used different car-following models under the mixed traffic environment, and they have achieved good results in improving mixed traffic efficiency and safety to a certain extent. However, the stochastic vehicle performance and driving behavior of CAVs and HDVs are not considered and employing two models will make the control system more complicated. Furthermore, it is uncoordinated for an integrated platoon system to use two different models to capture the motion of vehicles in the mixed platoon.

Furthermore, considering the similarity between the acceleration or deceleration behavior in traffic flow and the scaling properties of spring [19], some scholars modeled the traffic flow from the perspective of a mechanical system—the mass-spring (MS) system. For instance, Wang et al. [20] established a car-following model by regarding both the stopping (deceleration) process and the starting (acceleration) process as spring systems. Compared with traditional stimulus-response car-following models, the proposed model can better explain traffic flow phenomena and drivers' behavior. In the actual car-following process, the relative spacing and speed of two adjacent vehicles are two important indices. Therefore, some scholars applied the MSD theory to describe the interaction between vehicles in a platoon [21–23], and the MSD model was capable of enhancing traffic safety and increasing roadway capacity. However, all the proposed MSD models were only applicable to the platoons that are entirely made up of HDVs or CAVs. Because the MSD system has natural stability characteristics and is widely used to represent interactions with uncertain environments [24], we propose a novel car-following model for the mixed platoon under the same simplified framework based on the virtual MSD theory, which has a great advantage over the traditional platoon model in both the stability analysis and the stable operation. Unlike the previous models, both HDVs and CAVs share the identical framework in the proposed model and it takes both the spacing errors and speed errors into account, which can more accurately describe the car-following behaviors of CAVs and HDVs.

Another problem of traffic flow is how to quantify the level of risk in car-following processes, which has a significant impact on driving behaviors. K. Vogel [25] compared with two safety indices "time headway (TH)" and "time to collision (TTC)" in different traffic situations. However, when the speed of the following vehicle is near or equal to that of the preceding vehicle, TTC changes sharply; when the speed of the preceding vehicle changes relatively large, TH will underestimate the danger of the car-following process. In other words, it is insufficient for TTC and TH to quantify the risk level of car-following. Lu et al. [26] proposed safety margin (SM) as a suitable quantitative index of risk perception based on the risk homeostasis theory. Compared with TTC and TH, SM more suitably quantifies the level of risk in car-following processes. Inspired by it, in this manuscript, combining with the psychological field theory, we utilize the magnitude of virtual total energy as a quantitative index of danger in the car-following processes based on the MSD car-following model.

The remainder of this paper is organized as follows: Section 2 presents the modeling, car-following rules, and spacing policy of a mixed vehicular platoon. Section 3 presents a novel car-following model of mixed platoons from the perspective of a mechanical system, and the string stability of the mixed platoon is analyzed based on the MSD model. In Section 4, the virtual total energy is proposed as a quantitative index based on the psychological field theory and MSD model to reflect the danger level of vehicles in the car-following processes. The optimization model of minimum total energy is solved under the constraints of vehicle dynamics and the mechanical characteristics of MSD system in Section 5. In Section 6, a mixed platoon is tested in the driver-in-the-loop test platform to verify the validity of the proposed MSD car-following model. Finally, conclusions are made.

2. Control of Vehicular Platoon

2.1. Modeling of Mixed Platoon. As shown in Figure 1, a mixed platoon consisting of n cars travels on the highway in a single lane, where the i^{th} vehicle is a HDV. In this platoon, x_i is the position of the i^{th} vehicle and v_i is the speed of the i^{th} vehicle. Therefore, for the i^{th} vehicle, the spacing errors can be defined as

$$\delta_i = x_{i-1} - x_i - L - d_s, \tag{1}$$

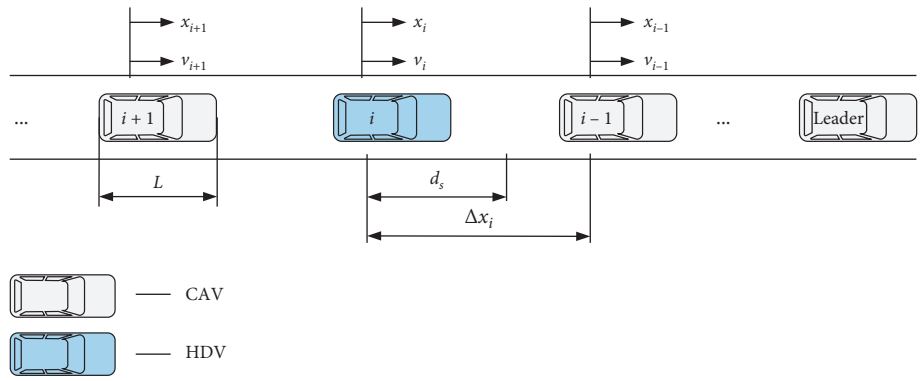

Figure 1: Model of a mixed platoon.

where L denotes the length of the vehicle and d_s represents the desired distance between the i^{th} and $i-1^{\text{th}}$ vehicles.

The kinematic differential equation of the intervehicle spacing error is

$$\dot{\delta}_i = \dot{x}_{i-1} - \dot{x}_i - \dot{d}_s = v_{i-1} - v_i - \dot{d}_s. \tag{2}$$

The control target of the platoon model is that the intervehicle spacing errors and the relative speed of any adjacent vehicles tend to be zero.

2.2. Car-Following Rules. String stability should be guaranteed when vehicles travel in a fleet. Because the spacing error is not expected to be zero when the preceding vehicle accelerates or decelerates, it is necessary to describe how the spacing error is propagated along the platoon when using the same spacing policy. The stable driving of a platoon needs to ensure that the spacing error does not amplify along the platoon [27]. Therefore, the desired characteristic of the transmission attenuation of spacing errors can be described as

$$\left\|\delta_i\right\|_\infty \le \left\|\delta_{i-1}\right\|_\infty. \tag{3}$$

Let $G(S)$ be the transfer function related to the spacing errors of consecutive vehicles in a fleet, we obtain

$$G_i(s) = \frac{\delta_i(s)}{\delta_{i-1}(s)}. \tag{4}$$

When

$$\left\|G(s)\right\|_\infty \le 1, \tag{5}$$

we obtain

$$\left\|\delta_i\right\|_2 \le \left\|\delta_{i-1}\right\|_2. \tag{6}$$

Equation (6) ensures that the energy of the output error is less than that of the input error. However, it is difficult for this condition to fully meet the desired characteristics of the transmission attenuation of spacing errors.

The ∞-norm of $G(S)$ and the 1-norm of $g(t)$ can make the output value of the system correlate with the input value of the system:

$$\left\|g\right\|_1 = \sup_{x \in L_\infty} \frac{\left\|\delta_i\right\|_\infty}{\left\|\delta_{i-1}\right\|_\infty}. \tag{7}$$

To satisfy equation (3), the formula below needs to be satisfied.

$$\left\|g\right\|_1 \le 1. \tag{8}$$

According to the theory of linear systems, we obtain

$$\left|G(0)\right| \le \left\|G(j\omega)\right\|_\infty \le \left\|g\right\|_1. \tag{9}$$

When $g(t) > 0$, we get

$$\left|G(0)\right| = \left|\int_0^\infty g(t)\mathrm{d}t\right| \le \int_0^\infty g(t)\mathrm{d}t = \left\|g\right\|_1. \tag{10}$$

Therefore, equation (8) that satisfies the desired characteristics of the transmission attenuation of spacing errors can be replaced by the following two conditions:

$$\begin{cases} \left\|G(s)\right\|_\infty \le 1, \\ g(t) > 0, \quad \forall t \ge 0, \end{cases} \tag{11}$$

where $G(S)$ is the transfer function of the spacing error of consecutive vehicles in the fleet and $g(t)$ is the impulse response function.

2.3. Spacing Policy. The spacing policy for longitudinal control of vehicular platoons is mainly divided into two types: constant spacing [28] and variable spacing [29]. When adopting the constant spacing, the distance between two adjacent vehicles in the platoon does not change with driving conditions, which can tremendously increase the traffic density. However, adopting this spacing policy requires more complicated communication methods, and in the case of external interference or large communication delay, this spacing policy will seriously affect the stability and safety of the platoon. Therefore, in order to ensure the string stability of the mixed platoon, we adopt the constant time-headway (CTH) policy.

For the CTH policy, the desired spacing between two consecutive vehicles varies linearly with speed:

$$d_s = h\dot{x}_i + s_0, \tag{12}$$

where h is the time headway and s_0 represents the minimum safety spacing.

It can be seen from formula (12) that when the speed of the host vehicle increases, the corresponding distance between the adjacent vehicles also increases. When the preceding vehicle brakes urgently, it can provide sufficient braking distance for the following vehicle to avoid collision.

Therefore, the spacing error can be expressed as

$$\delta_i = x_{i-1} - x_i - L - h\dot{x}_i - s_0. \tag{13}$$

When $h = 0$, the CTH policy will become a constant spacing policy.

3. MSD Car-Following Model and Stability Analysis of Mixed Platoon

In this section, we build the car-following model of a platoon from the perspective of a mechanical system, the mass-spring-damper system, to describe the car-following behaviors. We consider the vehicle as a mass and assume that there are a spring and a damper between every two adjacent masses. In the MSD model for HDVs (Figure 2(a)), $k_{t,i}$ is the spring stiffness between the i–1$^{\text{th}}$ vehicle and the i^{th} vehicle and $c_{t,i}$ is the damping coefficient between the i–1$^{\text{th}}$ vehicle and the i^{th} vehicle. Likewise, in the MSD model for CAVs (Figure 2(b)), $k_{a,i}$ is the spring stiffness between the i–1$^{\text{th}}$ vehicle and the i^{th} vehicle and $c_{a,i}$ is the damping coefficient between the i–1$^{\text{th}}$ vehicle and the i^{th} vehicle. When a fast-moving CAV/HDV is approaching a slow-moving CAV/HDV, the MSD model will exert a force on the fast-moving CAV/HDV to decelerate. On the contrary, when the speed of the following CAV/HDV is smaller than that of the preceding CAV/HDV, the MSD model will exert a reactive force on the following CAV/HDV to accelerate.

For the upcoming mixed traffic flow composed of CAVs and HDVs, we extend the MSD system to establish a car-following model for mixed platoons. At the same time, in order to reduce the complexity of the model, the following assumptions are made:

(1) Vehicles travel on a straight, dry, and flat road without performing lane changing

(2) Vehicle weight, maximum deceleration, aerodynamic drag coefficient, and rolling resistance coefficient are known

Based on the above assumptions, the MSD car-following model for a mixed platoon is shown in Figure 2(c), where the leading vehicle and the i^{th} vehicle are HDVs and the other vehicles are CAVs. In addition, $k_{a,i}$ and $c_{a,i}$ represent the spring stiffness and damping coefficient between CAVs. Furthermore, $k_{t,i}$ and $c_{t,i}$ represent the spring stiffness and damping coefficient between CAV and HDV, respectively.

The differential equation of motion for a mixed platoon can be expressed as

$$\mathbf{M}\ddot{\mathbf{x}} = \mathbf{f}(\mathbf{t}) + \mathbf{C}\dot{\mathbf{x}} + \mathbf{K}\mathbf{x}. \tag{14}$$

Therefore,

$$\ddot{\mathbf{x}} = \frac{1}{\mathbf{M}}\mathbf{f}(\mathbf{t}) + \frac{\mathbf{C}}{\mathbf{M}}\dot{\mathbf{x}} + \frac{\mathbf{K}}{\mathbf{M}}\mathbf{x}, \tag{15}$$

where $\mathbf{M}$ is the mass matrix, $\mathbf{K}$ is the spring stiffness matrix, $\mathbf{C}$ is the damping coefficient matrix, $\mathbf{f(t)}$ is the force matrix, $\mathbf{x}$ is the displacement matrix, and $\dot{\mathbf{x}}$ and $\ddot{\mathbf{x}}$ are the first derivative and the second derivative of $\mathbf{x}$ versus time, respectively:

$$\mathbf{x} = \begin{pmatrix} x_0 & x_1 & \cdots & x_{i-1} & x_i & x_{i+1} & \cdots & x_{n-2} & x_{n-1} \end{pmatrix}^{\mathrm{T}},$$

$$\mathbf{f}(\mathbf{t}) = \begin{pmatrix} f & 0 & \cdots & 0 & 0 & 0 & \cdots & 0 & 0 \end{pmatrix}^{\mathrm{T}},$$

$$\mathbf{M} = \begin{pmatrix} m_H & & & & & & \\ & \ddots & & & & & \\ & & m_C & & & & \\ & & & m_H & & & \\ & & & & \ddots & & \\ & & & & & m_C & \end{pmatrix},$$

$$\mathbf{K} = \begin{pmatrix} -k_a & k_a & \cdots & 0 & 0 & 0 & 0 & \cdots & 0 & 0 \\ \vdots & \vdots & \ddots & \vdots & \vdots & \vdots & \vdots & \cdots & \vdots & \vdots \\ 0 & 0 & \cdots & k_a & -k_a - k_t & k_t & 0 & \cdots & 0 & 0 \\ 0 & 0 & \cdots & 0 & k_t & -k_a - k_t & k_a & \cdots & 0 & 0 \\ \vdots & \vdots & \cdots & \vdots & \vdots & \vdots & \vdots & \ddots & \vdots & \vdots \\ 0 & 0 & \cdots & 0 & 0 & 0 & 0 & \cdots & k_a & -k_a \end{pmatrix},$$

$$\mathbf{C} = \begin{pmatrix} -c_a & c_a & \cdots & 0 & 0 & 0 & 0 & \cdots & 0 & 0 \\ \vdots & \vdots & \ddots & \vdots & \vdots & \vdots & \vdots & \cdots & \vdots & \vdots \\ 0 & 0 & \cdots & c_a & -c_a - c_t & c_t & 0 & \cdots & 0 & 0 \\ 0 & 0 & \cdots & 0 & c_t & -c_a - c_t & c_a & \cdots & 0 & 0 \\ \vdots & \vdots & \cdots & \vdots & \vdots & \vdots & \vdots & \ddots & \vdots & \vdots \\ 0 & 0 & \cdots & 0 & 0 & 0 & 0 & \cdots & c_a & -c_a \end{pmatrix}, \tag{16}$$

where m_H is the mass of HDV and m_C is the mass of CAV.

In the car-following processes, spacing error and speed error are two important factors for the stability analysis of a platoon. Therefore, we introduce the spacing error and speed error into equation (14) simultaneously, and it can be expressed as

$$\mathbf{M}'\ddot{\boldsymbol{\delta}} = \mathbf{f}'(\mathbf{t}) + \mathbf{C}'\dot{\boldsymbol{\delta}} + \mathbf{K}'\boldsymbol{\delta}, \tag{17}$$

where $\mathbf{M}'$ is the mass matrix, $\mathbf{K}'$ is the spring stiffness matrix, $\mathbf{C}'$ is the damping coefficient matrix, $\mathbf{f}'\mathbf{(t)}$ is the force matrix, $\boldsymbol{\delta}$ is the spacing error matrix, and $\dot{\boldsymbol{\delta}}$ and $\ddot{\boldsymbol{\delta}}$ are the speed error matrix and the acceleration error matrix, respectively:

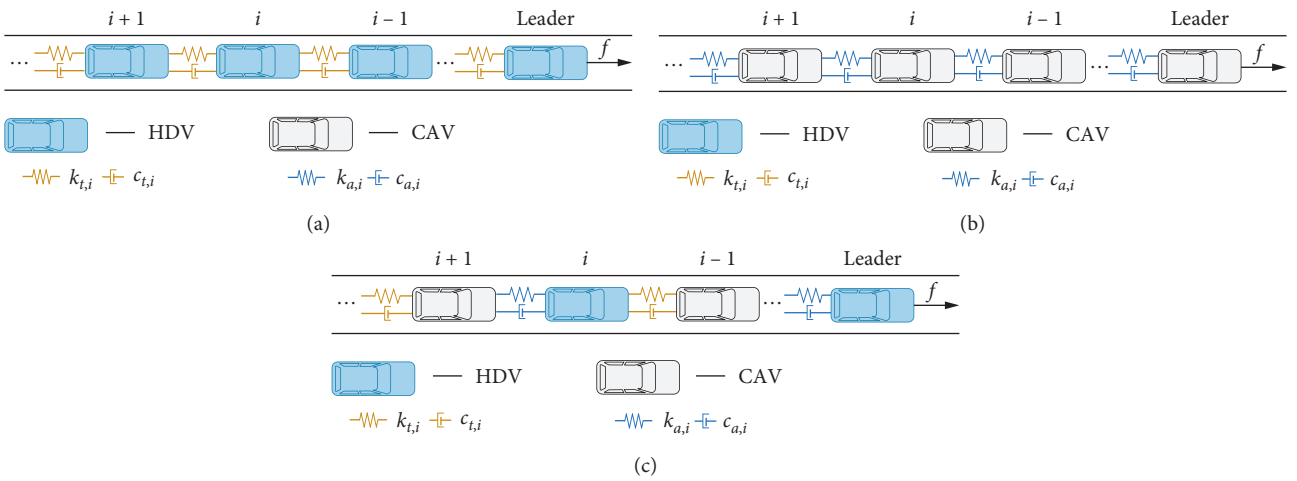

Figure 2: MSD car-following models. (a) MSD model for HDVs. (b) MSD model for CAVs. (c) Mixed MSD model.

$$\boldsymbol{\delta} = \begin{pmatrix} \delta_1 & \delta_2 & \dots & \delta_{i-1} & \delta_i & \delta_{i+1} & \dots & \delta_{n-2} & \delta_{n-1} \end{pmatrix}^{\mathrm{T}},$$

$$\mathbf{f}\prime(\mathbf{t}) = \begin{pmatrix} m_C f & 0 & \dots & 0 & 0 & 0 & \dots & 0 & 0 \end{pmatrix}^{\mathrm{T}},$$

$$\mathbf{M}' = \begin{pmatrix} m_H m_C & & & & & \\ & \ddots & & & & \\ & & m_H m_C & & & \\ & & & \ddots & & \\ & & & & m_C \end{pmatrix},$$

$$\mathbf{K}' = \begin{pmatrix} -(m_H+m_C)k_a & m_H k_a & 0 & 0 & 0 & 0 & 0 & 0 & 0 \\ \vdots & \vdots & \ddots & \vdots & \vdots & \vdots & \vdots & \vdots & \vdots \\ 0 & 0 & 0 & m_H k_a & -(m_H+m_C)k_t & m_C k_a & 0 & 0 & 0 \\ \vdots & \vdots & \vdots & \vdots & \vdots & \vdots & \ddots & \vdots & \vdots \\ 0 & 0 & 0 & 0 & 0 & 0 & 0 & k_a & -2k_a \end{pmatrix}, \tag{18}$$

$$\mathbf{C}' = \begin{pmatrix} -(m_H+m_C)c_a & m_H c_a & 0 & 0 & 0 & 0 & 0 & 0 & 0 \\ \vdots & \vdots & \ddots & \vdots & \vdots & \vdots & \vdots & \vdots & \vdots \\ 0 & 0 & 0 & m_H c_a & -(m_H+m_C)c_t & m_C c_a & 0 & 0 & 0 \\ \vdots & \vdots & \vdots & \vdots & \vdots & \vdots & \ddots & \vdots & \vdots \\ 0 & 0 & 0 & 0 & 0 & 0 & 0 & c_a & -2c_a \end{pmatrix}.$$

In the mixed MSD system, the last vehicle only receives unidirectional force. Therefore, starting from the last vehicle of the platoon, we can obtain the transfer function of spacing error:

$$G_1(s) = \frac{\delta_n(s)}{\delta_{n-1}(s)} = \frac{(c/m_C)s + (k/m_C)}{s^2 + (2c/m_C)s + (2k/m_C)}. \tag{19}$$

Going one step forward, we obtain

$$G_i(s) = \frac{\delta_{n-i}(s)}{\delta_{n-i-1}(s)} = \frac{G_1(s)}{1 - G_1(s)G_{i-1}(s)}. \tag{20}$$

Therefore, to ensure the driving stability of a mixed platoon, it is necessary to meet the condition as follows:

$$\left\| G_{1,n}(s) \right\|_\infty = \left\| G_1(s) \cdot G_2(s), \dots, G_n(s) \right\|_\infty \le 1. \tag{21}$$

4. Risk Quantification

In car-following processes, the driving behaviors of vehicles are mainly affected by the surroundings. On the one hand, to reduce the travel time, the host vehicle intends to accelerate; on the other hand, the danger of collision with the preceding vehicle forces it to constantly adjust the speed to ensure

safety. Therefore, a precise and suitable risk index plays an important role in car-following processes.

4.1. Risk Quantification for HDVs. Driving behavior is the result of the driver's judgment based on his/her psychological expectations under the stimulation of external environmental information. There is a psychological field during the HDV car-following processes [30]. When the external traffic environment changes, it will exert the forces on the psychological field, thereby adjusting the speed and direction of the vehicle. To describe the car-following behaviors of HDVs, in this manuscript, we propose a quantitative index, virtual total energy, based on the MSD car-following model and psychological field theory. We divide the drivers' psychological status into three zones, which are shown in Figure 3. When the virtual total energy varies with car-following errors, drivers' psychological status will be in different zones. Correspondingly, they will perform different vehicle maneuvers, as shown in Figure 4. For example, when the platoon is disturbed during driving, such as the sudden deceleration of the leading vehicle, this will cause the spacing errors Δx and speed errors Δv of the following vehicles to suddenly increase. Correspondingly, in the MSD system, the energy generated by springs and dampers will be greater, which will produce a sense of depression for the driver, forcing him/her to perform braking until his/her psychological depression has disappeared. When the leading vehicle accelerates, the driver's psychology depression is fully released, and the following vehicle will also accelerate until it travels at the desired speed. Ideally, when the following vehicle travels exactly as the preceding vehicle, the driver will maintain the vehicle's speed. Therefore, it is appropriate for the virtual total energy to quantify the level of danger during the car-following processes.

In the MSD model, when the distance between two adjacent cars is less or greater than the desired distance, the spring will be compressed or stretched. According to Hooke's law, the force generated by a spring is proportional to its deformation variable Δx. From the relationship of work and energy, we know that when the spacing error is Δx, the energy generated by the spring is

$$V_{t,i} = \int_{\Delta x} kx \, \mathrm{d}x. \tag{22}$$

When the speed of the following car is less than or greater than that of the leading car, the energy consumption of the damper is

$$D_{t,i} = \int_{\Delta v} cv \, \mathrm{d}v. \tag{23}$$

Therefore, in the MSD system, when the platoon is disturbed by external environment, the virtual energy generated by the i^{th} vehicle can be expressed as

$$E_{t,i} = V_{t,i} + D_{t,i}. \tag{24}$$

At the same time, the virtual total energy of the entire platoon can be expressed as

$$E_{T,t} = \sum V_{t,i} + \sum D_{t,i}. \tag{25}$$

4.2. Risk Quantification for CAVs. CAVs can quickly obtain the driving information (speed and position) from other vehicles within the communication range. Therefore, the CAVs can detect abnormal driving behaviors in the platoon earlier and take actions in advance. Although there is no psychological field during the car-following process of CAVs, in the MSD system, they still use the spacing errors and speed errors of adjacent vehicles as the control reference index. Therefore, in this manuscript, we consider the virtual total energy as a proper index to reflect the risk of a platoon based on the MSD car-following model:

$$E_{T,a} = \sum V_{a,i} + \sum D_{a,i}. \tag{26}$$

5. Parameter Optimization Based on Minimum Total Energy

In the mixed MSD system, k_{a} and c_{a} represent the control gains of relative position and relative speed between adjacent CAVs; k_t and c_{t} represent the control gains of relative position and relative speed between CAV and HDV, respectively. For the vehicle in the mixed platoon, the virtual energy generated by the interference from the external environment can be expressed as

$$E_{T,i} = \frac{1}{2}\omega(k) \cdot \Delta x_i^2 + \frac{1}{2}\omega(c) \cdot \Delta v_i^2, \tag{27}$$

where $\omega(k) = \begin{cases} k_a, & k \quad \text{between CAVs} \\ k_t, & k \quad \text{between CAV and HDV} \end{cases}$ and $\omega(c) = \begin{cases} c_a, & c \quad \text{between CAVs} \\ c_t, & c \quad \text{between CAV and HDV} \end{cases}$.

It can be seen from equation (27) that the values of k_{a} (k_t) and c_{a} (c_{t}) will directly affect the energy accumulation of CAVs and HDVs during the car-following processes, so it is necessary to optimize their values to get a better control effect of the mixed platoon.

The magnitude of E represents the virtual energy generated by the corresponding car-following errors. When a vehicle collides, we assume that $E = \infty$, which means that the vehicle's car-following errors reach the maximum. In the car-following processes without an accident, as E gradually becomes smaller, the vehicle's car-following errors also become smaller. When $E = 0$, it means that the vehicle is driving at the desired speed and intervehicle spacing completely, and the driving status is in absolute safety. When the leading vehicle performs emergency braking, the CAVs in the platoon can obtain the driving information of the leading vehicle and the preceding vehicle in real time through V2X technology and immediately apply the brakes. At this point, the virtual energy generated by the car-following errors from CAVs is small. However, if it is followed by a HDV, the driver needs a certain reaction time to take

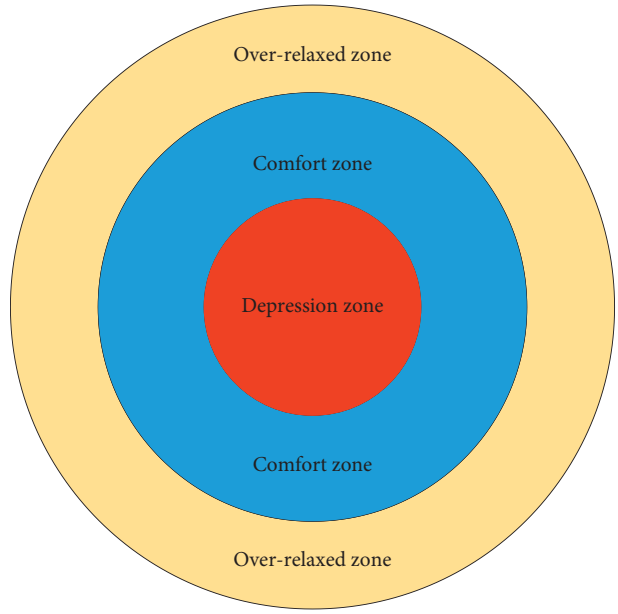

Figure 3: Three zones of drivers' psychological status.

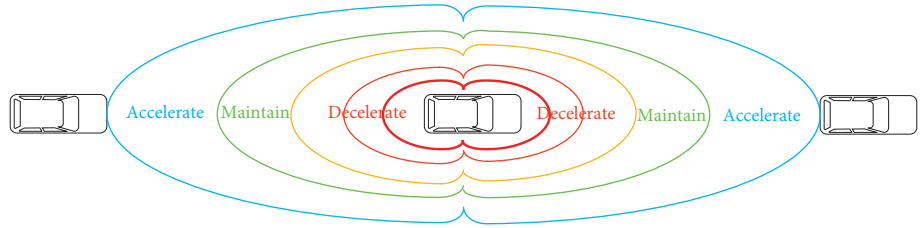

Figure 4: Vehicle maneuvers based on drivers' psychological status.

corresponding measures. Obviously, the virtual energy generated by the pair of HDV and CAV will be relatively large, which will cause the vehicles to be unstable or even have a collision. The ideal situation is that when the CAVs brake, they will not only consider their own driving conditions but also reserve a certain braking distance for the HDVs that follow them. Although this will increase the CAVs' accumulated energy, the increased braking distance can greatly improve the driving safety for the following HDVs, which also reduces the energy accumulation. Overall, the total energy of the platoon will be reduced because collisions are avoided. Therefore, for the mixed vehicular platoon based on the MSD system, we propose taking the minimum total energy as the optimization objective of the car-following model:

$$\min \sum \frac{1}{2}\omega(k)\cdot \Delta x_i^2 + \sum \frac{1}{2}\omega(c)\cdot \Delta v_i^2. \tag{28}$$

Based on the assumptions of Section 3, the mass $m_C(m_H)$ and the maximum deceleration $d_{\max}$ of each vehicle in the platoon are known. The platoon when only considering the spring is shown in Figure 5, and its dynamic equation is

$$m_C d_{\max} = k_{\max}\Delta x_{\max}. \tag{29}$$

Therefore,

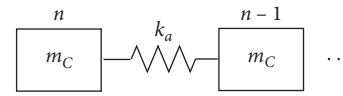

Figure 5: MS car-following model.

$$k_{\max} = \frac{m_C d_{\max}}{\Delta x_{\max}}. \tag{30}$$

Similarly, when the platoon only considers the effect of the damper, we obtain

$$c_{\max} = \frac{m_C d_{\max}}{\Delta v_{\max}}. \tag{31}$$

In addition, for realistic control, vehicles in a mixed platoon need to consider their actual performance and dynamic constraints:

$$\begin{cases} \dot{x}_i = v_i, \\ \dot{v}_i = a_i, \\ m_H a_i = k_t \Delta x_{i-1} + c_t \Delta v_{i-1} - k_a \Delta x_i + c_a \Delta v_i, \end{cases} \tag{32}$$

where a_i is the acceleration of the i^{th} vehicle.

Therefore, the parameter optimization problem based on the minimum total energy can be expressed as

$$
\begin{cases}
\min f(x) = \sum \frac{1}{2}\omega(k)\cdot \Delta x_i^2 + \sum \frac{1}{2}\omega(c)\cdot \Delta v_i^2, \\
s.t.\ \dot{x}_i = v_i, \\
\dot{v}_i = a_i, \\
m_H a_i = k_t \Delta x_{i-1} + c_t \Delta v_{i-1} - k_a \Delta x_i + c_a \Delta v_i, \\
a_{i,\min} \le a_i \le a_{i,\max}, \quad i = 1, 2, \ldots, n, \\
0 < k_a < k_{a,\max}, \\
0 < c_a < c_{a,\max}, \\
0 < k_t < k_{t,\max}, \\
0 < c_t < c_{t,\max}, \\
k_t - k_a < 0, \\
c_t - c_a < 0.
\end{cases} \tag{33}
$$

For the above-mentioned multidimensional constrained nonlinear programming problem, we solve it in Matlab. As shown in Figure 6, the red point represents the optimal solution of the spring stiffness (k) and damping coefficient (c).

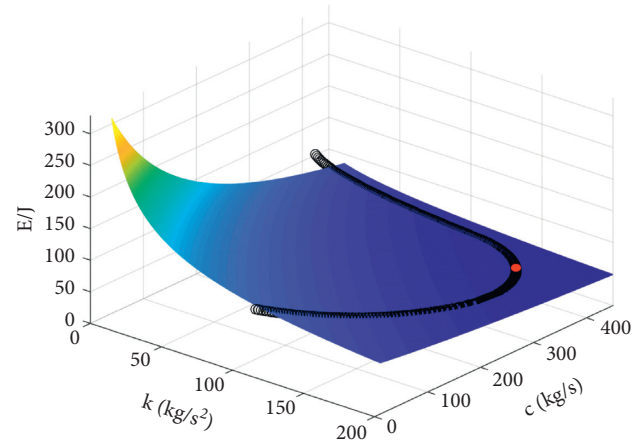

Figure 6: Parameter optimization based on minimum total energy.

Figure 7: Driver-in-the-loop test platform.

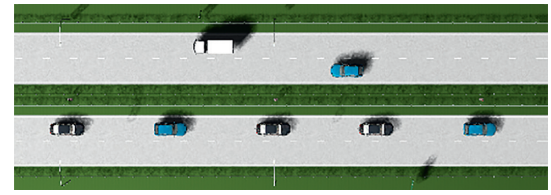

Figure 8: Test scenario for the mixed platoon.

6. Driver-in-the-Loop Test and Results Analysis

6.1. Establishment of Driver-in-the-Loop Platform and Test Scenarios. In view of the high cost and high risk of actual vehicle tests, driving simulators are widely used for research on traffic safety and driving behaviors [31]. The driver-in-the-loop test platform built in this manuscript is shown in Figure 7. It mainly includes a Logitech G29 vehicle controller (steering wheel, pedal, and gear lever) and two sorts of simulation software (PreScan and Matlab/Simulink). PreScan provides a rich set of scene elements to restore real-life driving conditions to a high degree, and its built-in vehicle dynamics model supports Logitech G29 to control the vehicle in real time. In addition, we build the MSD car-following model in Matlab/Simulink, and the joint simulation is performed with PreScan to verify the validity of the proposed MSD car-following model for mixed platoons.

As shown in Figure 8, the mixed vehicular platoon involved in the driver-in-the-loop test consists of 3 CAVs and 2 HDVs. The first and fourth vehicles are HDVs, and the rest are CAVs. The first HDV and the fourth HDV are controlled by drivers through Logitech G29. At the same time, the initial speed of each vehicle in the vehicular platoon is set to 30 m/s plus ±5%, and it is made to fluctuate randomly. The distance between two consecutive vehicles varies according to different velocity. At time $t = 0$, human factors cause the leading vehicle to perform emergency braking.

6.2. Simulation Parameters. To make the simulation close to the real scene, we assume that the mass and length of each vehicle in the mixed platoon are different. During the car-following processes, the deceleration of the vehicle is limited by the vehicle's motion characteristics and road environment. In this manuscript, all the vehicles travel straight on a dry and flat road. Therefore, we assume that the peak rolling adhesion coefficient is 0.85, and the maximum deceleration of the vehicle is detailed in Table 1, where the other vehicle simulation parameters are also expanded. To improve the

Table 1: Vehicle simulation parameters.

Vehicle number	Mass (kg)	Length (m)	Maximum deceleration (m/s^2)	Initial speed (m/s)	Initial position (m)
1	1570	5.48	−7.9	30.0	147.52
2	1240	4.84	−8.3	29.2	110.04
3	1350	5.12	−8.1	30.7	74
4	1680	5.68	−7.7	28.5	36.18
5	1430	5.35	−8.0	30.3	0

traffic capacity, we set the minimum safety distance to 2 m. In addition, the values of k (k_t) and c (c_t) will directly affect the car-following behaviors. Thus, by adjusting the values of k (k_t) and c (c_t) in the MSD car-following model, we can simulate the driving characteristics of different drivers. The specific parameters in this manuscript are shown in Table 2.

After setting the parameters, the car-following test can be completed through the cyclic process shown in Figure 9.

Table 2: MSD system parameters.

Vehicle number	Spring stiffness (kg/s^2)	Damping coefficient (kg/s)
1-2	96	196
2-3	83	173
3-4	176	382
4-5	81	169

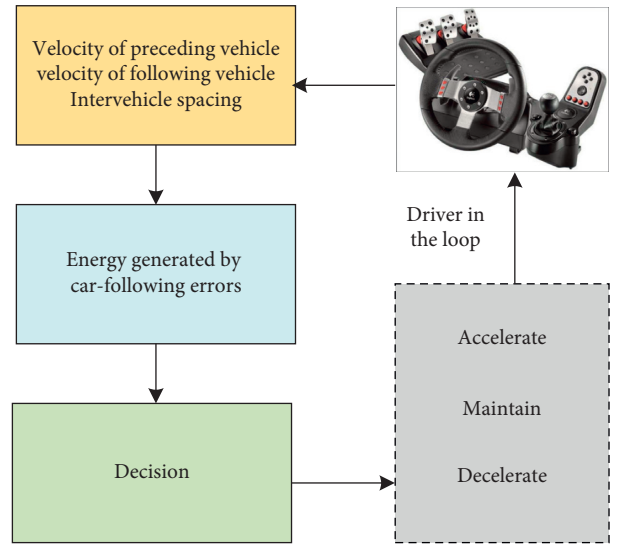

Figure 9: Test process of the mixed platoon.

6.3. Results Analysis. The optimal parameters in the previous section are used to verify the validity of the MSD model for a mixed platoon in the driver-in-the-loop test platform, and the test results are shown in Figure 10. It can be seen from Figure 10(a) when the leading vehicle performs emergency breaking, each following vehicles take corresponding measures to brake. In particular, the CAV in the middle position (the third vehicle) maintains the same deceleration as the preceding vehicle in the early stage of braking. However, in the later stage of breaking (the red circles in Figure 10(a)), the deceleration of the third vehicle changes sharply under the premise of ensuring safe driving, which reserves enough time for the following HDV to brake. At the same time, it can be seen intuitively from Figure 10(b) that there are no collisions between all vehicles in the mixed platoon and the intervehicle spacing between the three CAVs and their preceding vehicle is always within a reasonable error range. When the CAVs stop, the minimum distance between them is 2.05 m, which is slightly greater than the minimum safety distance ($s_0 = 2$ m). However, the minimum distance between the fourth HDV and the CAV in the middle position is 3.39 m. The above results indicate that each CAV in the mixed platoon can make full use of the braking distance and adjust the gap between each vehicle optimally, which can provide the driver of HDV with sufficient reaction time and braking distance to effectively avoid rear-end collisions.

According to the analysis of the above test results, it can be considered that the proposed MSD model can capture the car-following behaviors of CAVs with high accuracy. However, the MSD car-following model for HDVs needs further analysis. Therefore, we compare the MSD model with the traditional mass-spring (MS) model [19] using the driver-in-the-loop test platform. We establish the test scenarios that are the same as that in Figure 8, and all the initial conditions of the vehicles are also the same. The results are shown in Figure 11.

As shown in Figure 11(a), in the early stage of braking (0~6.2 s), the maximum speed error between the MSD model and the driver is 0.30 m/s, and the variance is 0.135 m^2/s^2; the maximum speed error between the MS model and the driver is 0.77 m/s, and the variance is 0.227 m^2/s^2. In the later stage of braking (6.2~15 s), the maximum speed error between the MSD model and the driver is 0.27 m/s, and the variance is 0.187 m^2/s^2. However, the maximum speed error between the MS model and the driver is 1.02 m/s with a variance of 0.673 m^2/s^2. Overall, both car-following models can accurately describe the driver's driving behavior during the braking process, but the MSD car-following model is more accurate than the MS car-following model. This is because the MS model only considers the spacing errors of the platoon. Similarly, it can be intuitively seen from Figure 11(b) that the spacing errors of the MSD car-following model are smaller than that of the MS car-following model, so the MSD car-following model can accurately describe the drivers' driving behaviors.

In the car-following processes, the virtual energy caused by the car-following errors in the mixed platoon is shown in Figure 12. Figure 12(a) shows the virtual total energy generated by the errors of spacing and speed of all

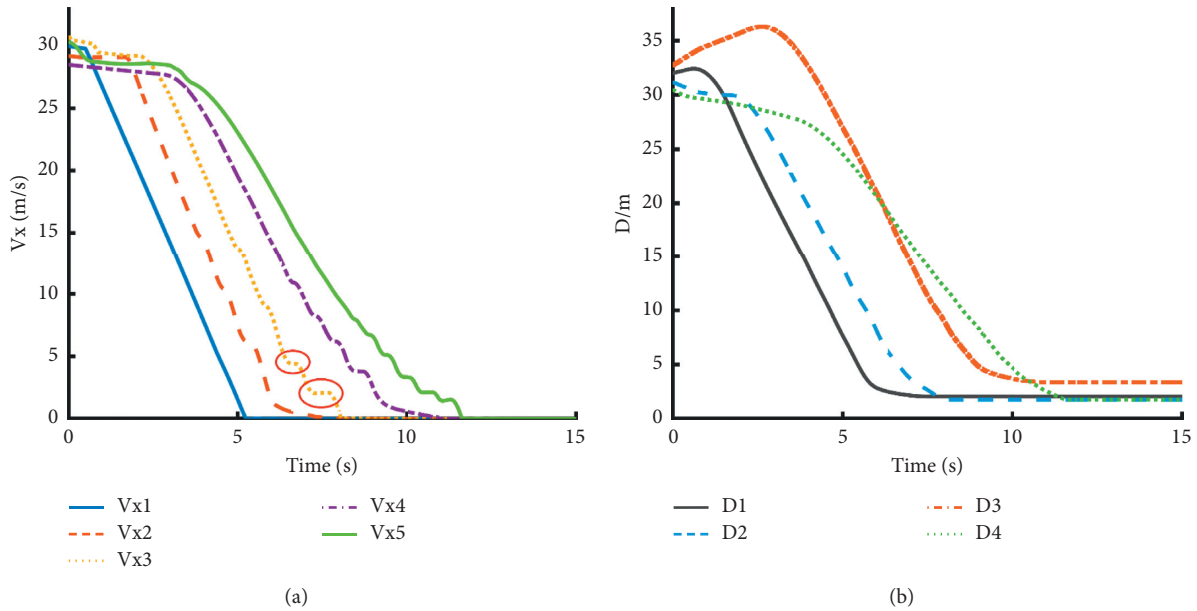

Figure 10: Test results of the mixed platoon. (a) Longitudinal velocity. (b) Intervehicle spacing.

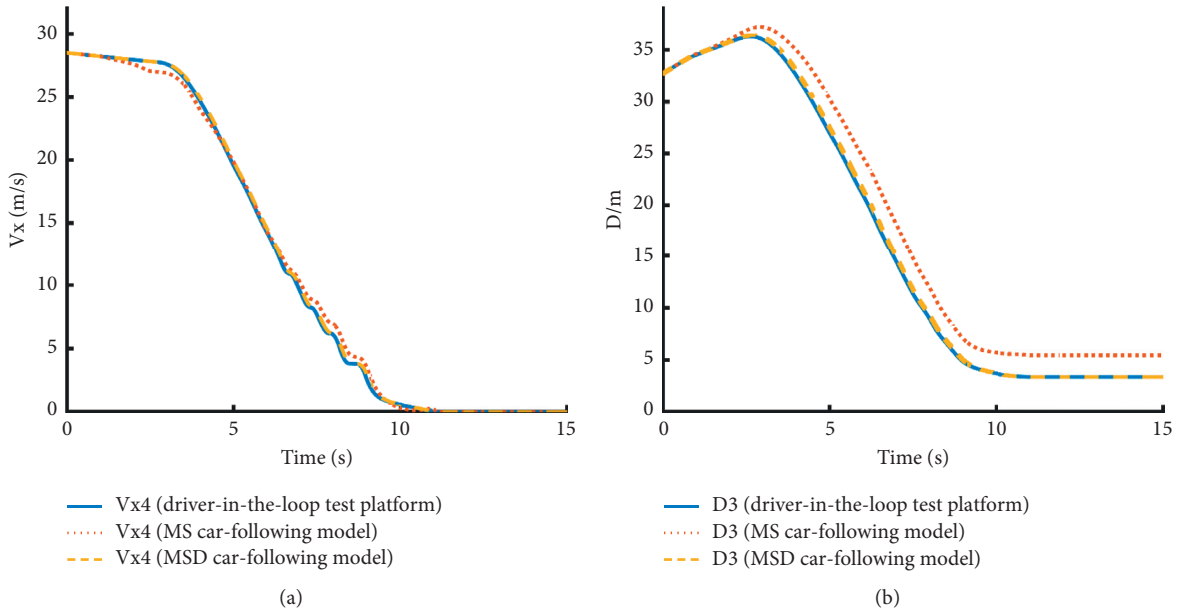

Figure 11: Results of comparison test. (a) Longitudinal velocity. (b) Intervehicle spacing.

vehicles in the platoon. Figure 12(b) and Figure 12(c) show the energy generated by the spacing errors and speed errors between adjacent vehicles, respectively. It can be seen from these figures that 67.2% of the energy in the mixed platoon is caused by the HDV (the fourth vehicle), and the energy of spacing error and the energy of speed error have not achieved peak simultaneously. The peak energy of speed error (7878 J) is more than triple that of spacing error (2477 J). Furthermore, in the early stage of the emergency braking, the spacing error is the dominant factor influencing the car-following behaviors, but in the later stage of the emergency braking, the speed error becomes the decisive factor of the car-following behaviors. Overall, CAVs possess good car-following characteristics, and the errors of spacing and speed between them are small. However, errors of spacing and speed between HDV and CAV are relatively large during the emergency braking processes.

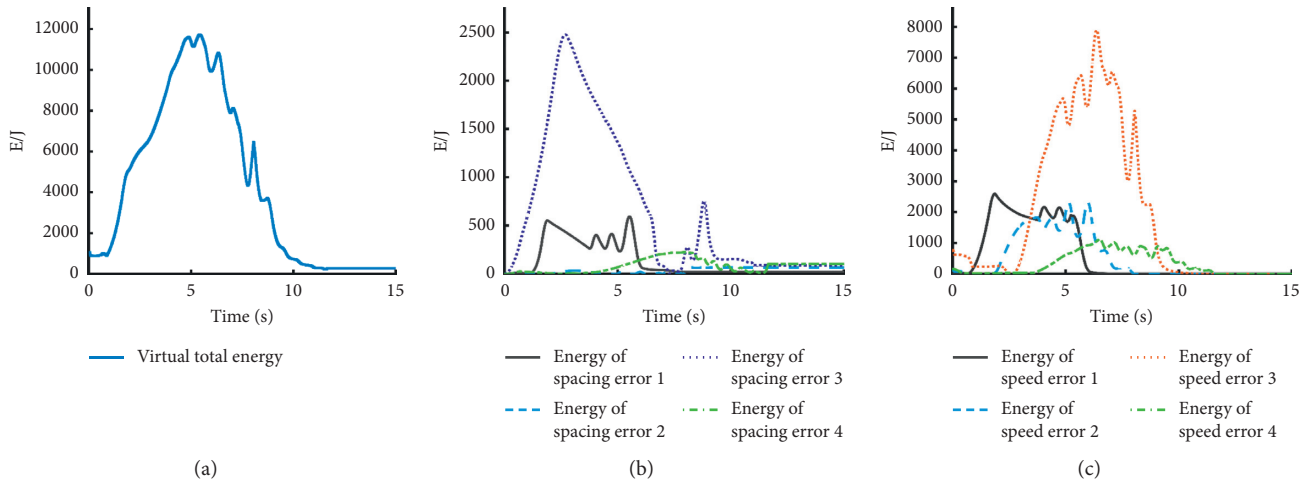

Figure 12: Energy accumulation of the mixed platoon. (a) Total energy accumulation. (b) Energy generated by spacing errors. (c) Energy generated by speed errors.

7. Conclusions

In this paper, from the perspective of a mechanical system, a novel car-following model for mixed platoons with CAVs and HDVs was established based on the mass-spring-damper theory. Both relative speed and intervehicle spacing were taken into account in this MSD car-following model, which can effectively capture the car-following behaviors of CAVs and HDVs. Furthermore, the driving characteristics of different vehicles can be described by adjusting the magnitude of the spring stiffness and damping coefficient. At the same time, a quantitative index was proposed in this paper based on the psychological field theory and MSD model, which can indicate the virtual total energy caused by car-following errors of a mixed platoon. Therefore, the magnitude of the energy can be used to quantificationally reflect the danger level of vehicles in the car-following processes. The driver-in-the-loop test was conducted to verify the validity of the proposed MSD car-following model, and the key parameters in the MSD system were determined by the optimal solution based on minimum total energy. Compared with the traditional MS car-following model, the proposed MSD model possesses higher accuracy and it can better describe the car-following behaviors of CAVs and HDVs. Meanwhile, the virtual total energy is an acceptable index to quantify the risk of a mixed platoon. Most of the energy generated by the car-following errors of the mixed platoon is caused by the HDV. In the early stage of emergency braking, the spacing error is the dominant factor of the car-following behaviors and the decisive factor of those in the later stage of emergency braking is the speed error. An obvious conclusion is that the proposed MSD car-following model has great potential to enhance the overall safety of the mixed traffic flow with CAVs and HDVs.

While the MSD car-following model can effectively describe the longitudinal behavioral interactions of a mixed platoon, some future research is still needed. First, this research only conducted driver-in-the-loop tests on CAVs and HDVs with the emergency braking maneuvers. In the subsequent research, more complicated and real-life driving conditions will be fully considered, and the effectiveness of the MSD car-following model will be further verified. Second, an expansion of the lateral driving behaviors based on the MSD theory will be explored in the future.

Data Availability

The data used to support the findings of this study are available from the corresponding author upon request.

Conflicts of Interest

The authors declare that there are no conflicts of interest regarding the publication of this paper.

Acknowledgments

This work was supported by the National Natural Science Foundation of China (Grant no. 61304189), Fundamental Research Funds for the Central Universities (Grant no. XDJK2019B053), and Open Foundation from Chongqing Key Laboratory of Automotive Active Safety Testing Technology (Grant no. 19AKC8).

References

[1] Z. J. Gao, J. F. Wang, X. Zhang et al., "Traffic oscillations mitigation in vehicle platoon using a car-following control model for connected and autonomous vehicle," *Journal of Advanced Transportation*, vol. 2019, Article ID 3067291, 12 pages, 2019.

[2] Z. Huang, D. Chu, C. Wu, and Y. He, "Path planning and cooperative control for automated vehicle platoon using hybrid automata," *IEEE Transactions on Intelligent Transportation Systems*, vol. 20, no. 3, pp. 959–974, 2019.

[3] L. H. Li, J. Gan, and W. Q. Li, "A separation strategy for connected and automated vehicles: utilizing traffic light information for reducing idling at red lights and improving fuel economy," *Journal of Advanced Transportation*, vol. 2018, Article ID 5679064, 10 pages, 2018.

[4] A. Petrillo, A. Pescapé, and S. Santini, "A collaborative approach for improving the security of vehicular scenarios: the case of platooning," *Computer Communications*, vol. 122, pp. 59–75, 2018.

[5] J. Lioris, R. Pedarsani, F. Y. Tascikaraoglu, and P. Varaiya, "Platoons of connected vehicles can double throughput in urban roads," *Transportation Research Part C: Emerging Technologies*, vol. 77, pp. 292–305, 2017.

[6] L. L. Zhang, F. Chen, X. X. Ma et al., "Fuel economy in truck platooning: a literature overview and directions for future research," *Journal of Advanced Transportation*, vol. 2020, Article ID 2604012, 10 pages, 2020.

[7] D. V. Marco, F. Giovanni, P. Alberto et al., "Cooperative shock waves mitigation in mixed traffic flow environment," *IEEE Transactions on Intelligent Transportation Systems*, vol. 20, no. 12, pp. 4339–4353, 2019.

[8] S. Gong and L. Du, "Cooperative platoon control for a mixed traffic flow including human drive vehicles and connected and autonomous vehicles," *Transportation Research Part B: Methodological*, vol. 116, pp. 25–61, 2018.

[9] W. X. Zhu and H. M. Zhang, "Analysis of mixed traffic flow with human-driving and autonomous cars based on car-following model," *Physica A: Statistical Mechanics and its Applications*, vol. 496, pp. 274–285, 2017.

[10] F. Li and Y. Wang, "Cooperative adaptive cruise control for string stable mixed traffic: benchmark and human-centered design," *IEEE Transactions on Intelligent Transportation Systems*, vol. 18, no. 12, pp. 3473–3485, 2017.

[11] R. E. Chandler, R. Herman, and E. W. Montroll, "Traffic dynamics: studies in car following," *Operations Research*, vol. 6, no. 2, pp. 165–184, 1958.

[12] M. Brackstone and M. Mcdonald, "Car-following: a historical review," *Transportation Research Part F: Traffic Psychology and Behaviour*, vol. 2, no. 4, pp. 181–196, 1999.

[13] W. Wang, W. Zhang, D. Li et al., "Improved action point model in traffic flow based on driver's cognitive mechanism," in *Proceedings of the Intelligent Vehicles Symposium*, pp. 447–452, Parma, Italy, October 2004.

[14] M. Zhou, X. Qu, and X. Li, "A recurrent neural network based microscopic car following model to predict traffic oscillation," *Transportation Research Part C: Emerging Technologies*, vol. 84, pp. 245–264, 2017.

[15] D. Yang, P. Jin, Y. Pu, and B. Ran, "Stability analysis of the mixed traffic flow of cars and trucks using heterogeneous optimal velocity car-following model," *Physica A: Statistical Mechanics and its Applications*, vol. 395, pp. 371–383, 2014.

[16] M. F. Zhou, X. B. Qu, and S. Jin, "On the impact of cooperative autonomous vehicles in improving freeway merging: a modified intelligent driver model-based approach," *IEEE Transactions on Intelligent Transportation Systems*, vol. 18, no. 6, pp. 1422–1428, 2017.

[17] X. Y. Ni and H. Huang, "A new cellular automaton model accounting for stochasticity in traffic flow induced by heterogeneity in driving behavior," *Chinese Physics B*, vol. 28, no. 9, Article ID 28098901, 2019.

[18] W. Zhao, D. Ngoduy, S. Shepherd, R. Liu, and M. Papageorgiou, "A platoon based cooperative eco-driving model for mixed automated and human-driven vehicles at a signalised intersection," *Transportation Research Part C: Emerging Technologies*, vol. 95, pp. 802–821, 2018.

[19] Y. F. Li, W. B. Chen, S. Peeta et al., "An extended microscopic traffic flow model based on the spring-mass system theory," *Modern Physics Letters B*, vol. 31, no. 9, Article ID 1750090, 2017.

[20] D. H. Wang, S. H. Yang, and L. Y. Chu, "Modeling car-following dynamics during the starting and stopping process based on a spring system model," *Tsinghua Science and Technology*, vol. 9, no. 6, pp. 643–652, 2004.

[21] A. Ali, G. Garcia, and P. Martinet, "The flatbed platoon towing model for safe and dense platooning on highways," *IEEE Intelligent Transportation Systems Magazine*, vol. 7, no. 1, pp. 58–68, 2015.

[22] C. R. Munigety, "A spring-mass-damper system dynamics-based driver-vehicle integrated model for representing heterogeneous traffic," *International Journal of Modern Physics B*, vol. 32, no. 11, Article ID 1850135, 2018.

[23] C. R. Munigety, ""Conformity and stability analysis of a modified spring–mass–damper system dynamics-based car-following model," *International Journal of Modern Physics B*, vol. 33, no. 6, Article ID 1950025, 2019.

[24] S.-Y. Yi and K.-T. Chong, "Impedance control for a vehicle platoon system," *Mechatronics*, vol. 15, no. 5, pp. 627–638, 2005.

[25] K. Vogel, "A comparison of headway and time to collision as safety indicators," *Accident Analysis & Prevention*, vol. 35, no. 3, pp. 427–433, 2003.

[26] G. Lu, B. Cheng, Q. Lin, and Y. Wang, "Quantitative indicator of homeostatic risk perception in car following," *Safety Science*, vol. 50, no. 9, pp. 1898–1905, 2012.

[27] Y. G. Liu and C. Pan, "Cooperative spacing control for autonomous vehicle platoon with input delays," in *Proceedings of the Control And Decision Conference*, pp. 6238–6243, Yinchuan, China, August 2016.

[28] X. G. Guo, J. L. Wang, F. Liao et al., "String stability of heterogeneous leader-following vehicle platoons based on constant spacing policy," in *Proceedings of the IEEE Intelligent Vehicles Symposium*, pp. 761–766, Gothenburg, Sweden, August 2016.

[29] Q. Xin, N. Yang, R. Fu, S. Yu, and Z. Shi, "Impacts analysis of car following models considering variable vehicular gap policies," *Physica A: Statistical Mechanics and its Applications*, vol. 501, pp. 338–355, 2018.

[30] S. K. Amezquita, C. Y. Chen, W. H. Chen et al., "Stimuli-induced equilibrium point: a psychological field theory application in ramp merging systems," in *Proceedings of the 17th International Conference On Control, Automation and Systems (ICCAS)*, pp. 825–830, Jeju, South Korea, October 2017.

[31] F. Chen, H. R. Peng, X. X. Ma et al., "Examining the safety of trucks under crosswind at bridge-tunnel section: a driving simulator study," *Tunnelling and Underground Space Technology*, vol. 92, Article ID 103034, 2019.

Hindawi
Journal of Advanced Transportation
Volume 2020, Article ID 2793150, 11 pages
https://doi.org/10.1155/2020/2793150

Research Article

Risk Analysis of Vehicle Rear-End Collisions at Intersections

Sheng Dong,[1] **Minjie Zhang**,[1] **and Zhenjiang Li**[2]

[1]*School of Civil and Transportation Engineering, Ningbo University of Technology, Fenghua Rd. #201, Jiangbei District, Ningbo, Zhejiang Province, 315211, China*
[2]*The State Key Laboratory for Management and Control of Complex Systems, Institute of Automation, Chinese Academy of Sciences, Beijing 100190, China*

Correspondence should be addressed to Sheng Dong; dongsheng@nbut.edu.cn

Received 3 January 2020; Revised 24 March 2020; Accepted 22 May 2020; Published 1 July 2020

Academic Editor: Feng Chen

Aiming at solving a typical problem of past research using accident experience statistics of being unable to adapt to changing traffic flows, this paper provides an evaluation method of the risk of vehicle rear-end collisions at red-light-camera (RLC) intersections based on theoretical probabilities. Taking advantage of trajectory data of vehicles at the two similar intersections, which are Cao'an Road and Lvyuan Road with RLCs and Cao'an Road and Anhong Road without RLCs in Shanghai, a binary logit (BL) model of stop-and-go decision-making is established. Using the model and adjusting the headway and potential travel time, we can perform simulation and analysis of rear-end collisions. The result shows that this method is feasible to analyse the influence of RLCs on rear-end collisions. The analysis indicates that RLCs can cause higher speeds for vehicles passing the RLC intersection and more abnormal driving behaviors, which increase the difficulty of stop-and-go decision-making. RLCs do not always lead to an increase of rear-end collisions. For vehicles close to or far from intersection at the decision-making time, RLCs will significantly reduce the possibility of rear-end collisions; however, for vehicles in the potential travel time of 2 s~3 s, RLCs will increase the probability of rear-end collisions.

1. Introduction

In the past, running a red light during signal changes was a common phenomenon at intersections, which had a significant impact on the traffic safety of intersection. To effectively solve the problem of red-light violations, red-light cameras (RLCs) should be installed. RLCs have been widely used worldwide for more than 20 years. RLCs are also widely used in some large- and medium-sized cities in China. RLCs have played a huge role in reducing intentional red-light running. However, RLCs affect the driver's driving state and decision-making behavior at the intersection, and many potential safety problems that may be caused by RLCs have not been fully explored. Therefore, it is important to evaluate the impact of RLC installation on vehicle operation safety. Research on RLCs can not only find and eliminate the potential safety hazards presented by RLCs but also provide the basis for the future introduction of RLC installation national standards and use principles.

In China, the following problems and challenges still exist in the study of the safety impact of RLCs on vehicles at intersections:

(1) The limitations of RLC evaluation methods in mixed traffic: the environment and driving characteristics of mixed urban traffic are quite different from those of foreign countries. Red-light violations and accidents are affected by mixed traffic conditions. The evaluation of RLC effects in mixed traffic is more complex.

(2) Taking the accident rate as the metric of the evaluation method: the implementation of traffic accident collection systems is late, and there are many problems facing accident records. Simultaneously, the degree of urban renewal is quickly leading to frequent changes in facilities, which affects the occurrence of accidents, making the performance of RLC evaluation methods based on accident experience statistics in China questionable.

This paper provides a method of evaluating the effect of RLCs on driver's traffic behavior based on mathematical simulation to solve the above problems. Using driving characteristic data of vehicles at the intersection decision-making time, the impact analysis and evaluation of RLCs on drivers' stop-and-go decision-making and rear-end hazards can be realized, therein avoiding the error and cost brought by accident statistics. This method can adjust the traffic parameters in the sensitivity analysis of the risk of rear-end accidents due to RLCs; thus, it can be applied to intersections with different traffic conditions and thus has portability. This method can be used to set the speed limit of the road after the installation of RLCs and can effectively reduce the potential safety hazards of the intersection after the installation of RLCs.

The organizational structure of this paper is as follows: first, the relevant background of this paper is introduced. Then, the literature review part summarizes the previous relevant research results and presents the focus of this study. The data collection methods used in this study appear in the "Field Observation and Data Collection" part, mainly including vehicles with and without RLCs, analysis of speed characteristics, decision-making behavior, and safety conditions. Based on the above data, the driving behavior model is constructed. First, the stop-and-go model is constructed and verified. Based on this, the rear-end collision risk model is constructed, and the rear-end collision probability is determined by changing the two key parameters of headway and potential travel time. The last part of this paper discusses the influence of RLCs on decision-making behavior during driving and in the risk of rear-end collisions.

2. Literature Review

There have been many research efforts on the application of RLCs, most of which focused on the occurrence of accidents related to RLC [1–6]. Chin's research shows that RLCs just applied in Singapore could effectively reduce red-light violations [7]. South, Hillier, Andreassen, Retting, and others, through accident comparisons before and after the installation of RLCs at intersections and the horizontal comparison of incidences of rear-end collisions, frontal collisions, and side collisions, analysed the impact of RLCs on traffic safety. The conclusions of these researchers are relatively consistent; that is, RLCs may increase rear-end collisions while reducing vehicle frontal collision and side collision accidents [8–15].

In addition, several studies have performed behavioral studies concerning RLCs. Helai Huang, Zeng. et al., through the analysis of the decision-making process, found that RLCs significantly affect the decision-making behavior of drivers. Although RLCs can reduce the red-light violation rates of vehicles, their effect on rear-end accidents at intersections is more complex. The possibility of RLCs increasing or reducing rear-end accidents is closely related to the speed of the following vehicle and the headway between the front vehicle and the following vehicle [16–20]. Lum et al. analysed two T-intersections and one cross-intersection and found that the RLC can effectively increase drivers' stopping tendency; in addition, the RLC can accentuate the distance to the stop line to affect the stopping propensity. However, one drawback of this study was that the possible accident risk caused by RLCs was not included [21]. According to simulation analysis, Sun et al. found that RLCs can significantly reduce frontal accidents and may increase rear-end collisions. In addition, RLCs can affect a driver's comfort [22].

Generally speaking, past research on RLCs mainly has the following two problems: First, the safety impact analysis of RLCs is mostly based on accident experience statistics, where the accident data collection cycle is long and the time span is large, during which changes in other road traffic parameters will lead to reductions in the credibility of the final evaluation result. Thus, the RLC evaluation method based on accident experience statistics has serious defects. Second, the conclusion that RLCs can reduce the right-angle accidents and increase the rear-end accidents at intersections is unanimously accepted; however, the quantitative analysis of the rear-end collision risk by RLCs under limited conditions has not been carried out. Therefore, it is necessary to make a systematic analysis of the driver's behavior characteristics, the stop-and-go decision-making behavior, and the risk of traffic safety in the case of RLCs.

3. Field Observation and Data Collection

3.1. Site Descriptions. One of the best ways to analyse the influence of RLCs on drivers' driving behavior is to find two similar intersections: one is RLC intersection and the other is non-RLC intersection. The two intersections have similar characteristics in terms of geometric parameters, traffic flow composition and traffic volume, traffic management measures such as speed limit, and signal timing parameters such as phase number and the type of transition signals. It is very difficult to select the intersection meeting the above conditions. After a large-scale survey of intersections in Shanghai urban area, two adjacent signal intersections of Cao'an Road and Lvyuan Road and Cao'an road and Anhong Road are finally determined. The location of the two intersections is shown in Figure 1; the characteristics of intersections investigated are shown in Table 1.

3.2. Data Collection. In order to obtain all the traffic data related to driving behavior and ensure the accuracy of the data, video recording is used in this study. Take through lanes of the east import way as the research object. Two synchronous cameras need to be set, among which a far side camera was set 80 m upstream of the intersection, so as to capture the whole decision-making process of the vehicle in the approach. The other camera is used to record traffic signals.

Image processing software was used to process the video. The software can extract high-precision vehicle trajectory data, such as vehicle speed, acceleration, position coordinates, and traffic signal status at every time step. In order to meet the need of the study on stop-and-go decision-making

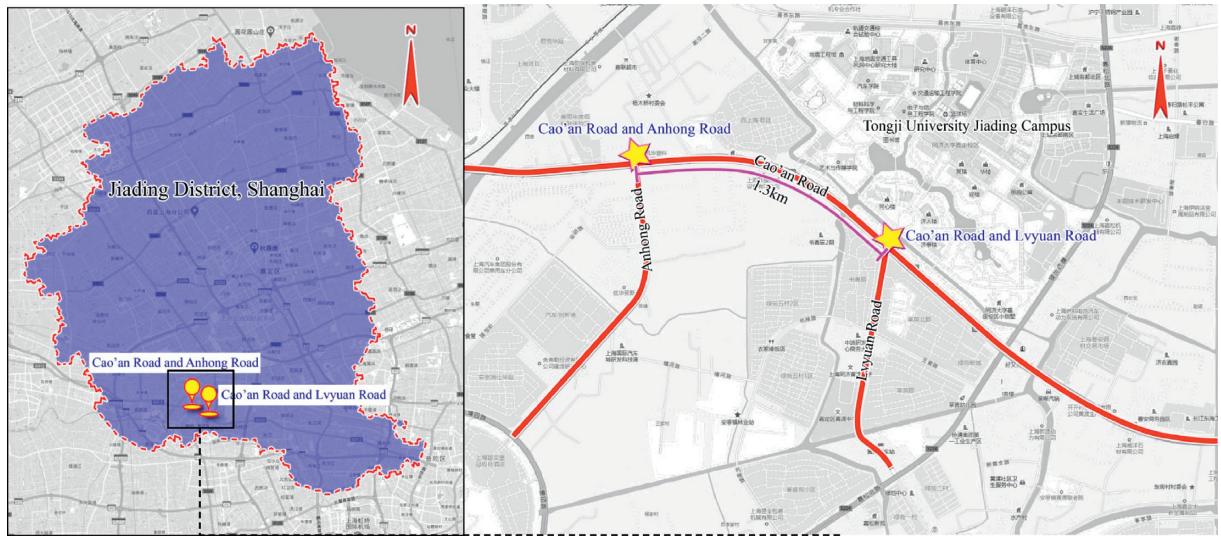

Figure 1: Location of the observed intersections in Shanghai.

Table 1: Key parameters of the observed intersections.

Description		Lvyuan Road	Anhong Road
Geometry parameters	Intersection layout	"T"	"T"
	Width of intersection	45 m	42 m
	Adjacent bound level	Low	Low
	Adjacent land use	University	Factory
	Number of through lanes (westbound)	5	4 (include 1 through-right lane)
	Lane length	3 m	3 m
	Pedestrian crossing	Yes	Yes
Signal timings	Cycle	72 s	90 s
	No. of phases	3 s	3 s
	Yellow time	3 s	3 s
	Flash green	3 s	3 s
	Transition signal	Green countdown (i) Flash green-amber	Green countdown (i) Flash green-amber
Traffic management	RLC installation	Yes	No
	Posted speed limit	80 km/h	80 km/h
Traffic flow	Flow composition	Percentage of car is 54%	Percentage of car is 59%
	Traffic volume	719 pcu/h	748 pcu/h

and rear-end accidents and to avoid the interference of other vehicles in driving behavior, trajectory data of the last-to-stop and the first-to-go through-ahead vehicles after the start of the green flashing light are extracted as the most important part. Data collection and video camera coverage are shown in Figure 2.

The method can also determine the time when the yellow light is on, the vehicle arrival information, the position of the vehicle in the fleet, the position of the vehicle when the yellow light is on, the decision-making behavior of the driver (stop, yellow light pass or violation), and so forth. The video processing is applied to 99 vehicles stopping and 251 vehicles passing with RLCs, among which 208 vehicles encounter yellow lights and 25 vehicles perform red-light violations, including 21 vehicles 3 seconds before the red lights start. A total of 20 vehicles stop under non-RLC conditions, 351 vehicles pass, 162 vehicles encounter yellow lights, and 157 vehicles violate red lights, including 85 vehicles 3 seconds before the red lights start.

3.3. Data Reduction

3.3.1. Statistical Analysis of Speed. Speed is an important indicator of driving behavior; thus, this study compares the speed of vehicles with and without the RLC from multiple perspectives. The time of vehicles arriving at the intersection can be divided into three categories: arrival during the tail of green time (i.e., less than 5 s from the end of green time, EG), arrival during the yellow-light time (3 s, AT), and arrival at the beginning of red time (i.e., the initial 3 s, BR). The statistical characteristics of the instantaneous speed of vehicles passing through the parking line in the above time intervals are shown in Figure 3.

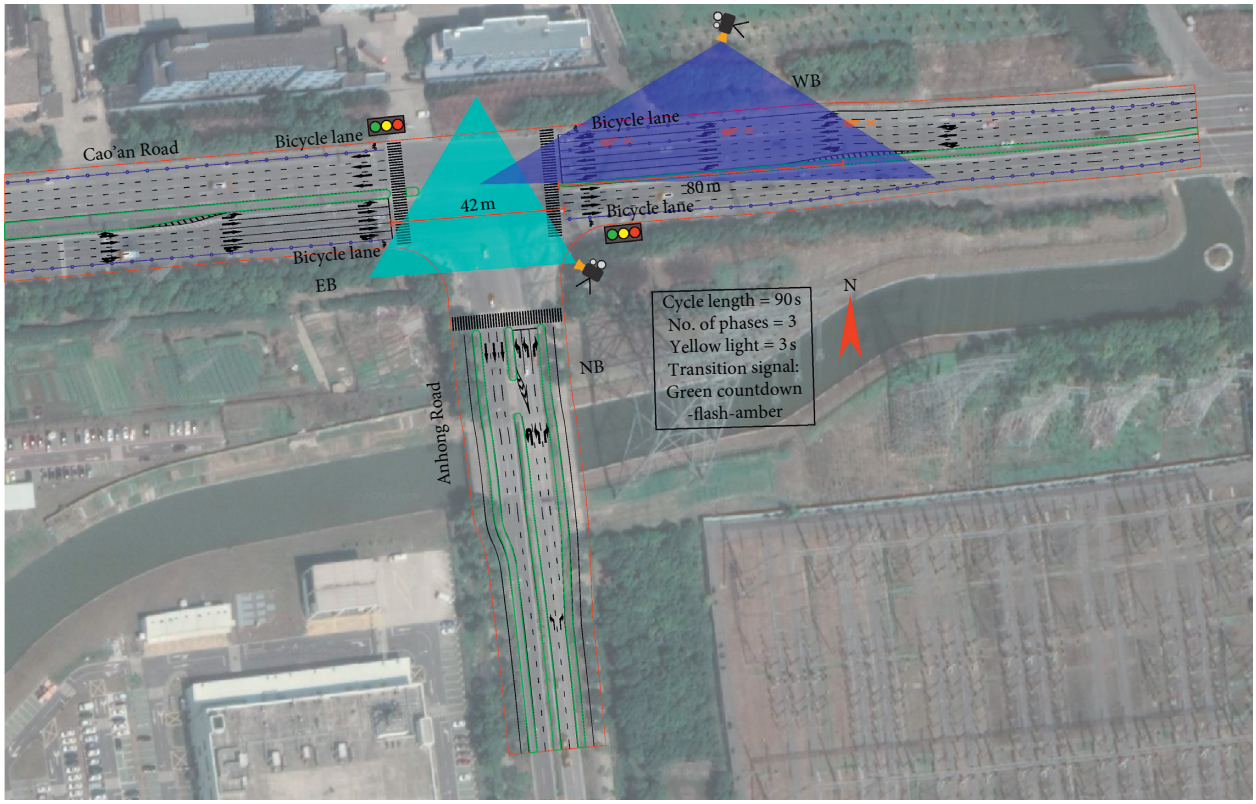

Figure 2: Camera setting and data collection at the study intersections.

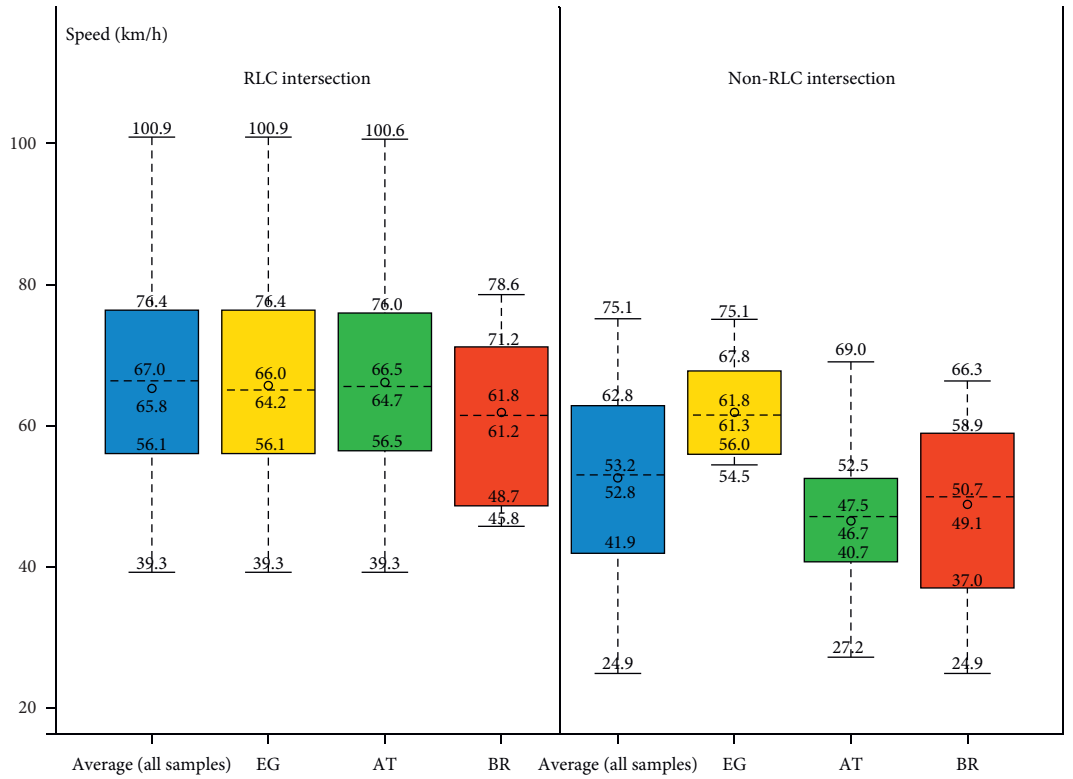

Figure 3: Statistical features of speed in different period.

By comparing the passing speed of vehicles during EG, AT, and BR, it is found that the speed of the vehicles with RLCs, such as the mean, minimum, maximum, and 15th percentile, 50th percentile, and 85th percentile speeds, are relatively large compared with those of the vehicles without RLCs. Compared with the intersection without RLCs, the average speed with RLCs is lower when the yellow light is on; however, the mean, minimum, maximum, and 15th percentile, 50th percentile, and 85th percentile speeds all increase when the vehicle enters the intersection. From the speed analysis, RLCs have an important impact on the driver's speed. Compared to the case without RLCs, RLCs enable the driver to have a higher speed to leave the intersection entrance faster.

3.3.2. Abnormal Driving Behavior. According to previous studies [23], the driver makes a decision after the yellow light comes on (if the green flash or countdown is set before the yellow light, the decision-making time will be ahead of the yellow light) and estimates the distance from the current position to the stop line. Therefore, the distance from the stop line (actually reflected as the estimated time to the stop line) is the main judgment basis for deciding on passing or stopping. The driver's decision-making is mainly based on the estimated time to the stop line, while the estimated time difference refers to the difference between the actual running time from the decision-making time to the end of the yellow light and the estimated time to the stop line. The main reason for the abnormal decision-making is the estimated time difference. A negative difference means that the vehicle will enter the intersection at the current speed within the red time, so the driver should choose to stop; on the contrary, a positive difference means that the vehicle could safely pass the stop line at the current speed before the end of the yellow light, so the driver should do so. This is calculated as follows:

$$\mathrm{ETD} = T_a - T_e, \tag{1}$$

$$T_e = \frac{D_d}{V_d}, \tag{2}$$

where ETD is the estimated time difference, T_e is the estimated time to stop line, that is, the potential travel time, T_a is the actual duration from the decision point (i.e., start of amber/start of the flash green light) to the end of yellow light, D_d is the distance from the position making decision point to the stop line, and V_d is the instantaneous speed of the vehicle at the current decision point. For a random sample, the speed remains constant during the period from making decision to passing through the stop line.

If the result of the decision does not match the estimated time difference, it can be considered as an abnormal driving behavior, and its statistical results can reflect the change in the driver's state during the decision-making process. The difference in the driver's judgment of the distance results in the difference in driving behavior when passing or stopping. After making a decision, the driver will find that he cannot enter the intersection before the onset of red time at the current speed; thus, he will continue to accelerate. If the judgment error of the distance is large, the driver cannot pass. According to the matching results of the estimated time difference and the stop-and-go decision, the decision-making behavior can be divided into four types: normal pass, incorrect pass, normal stop, and abrupt stop. The decision-making mechanism is shown in Figure 4.

We analyse the stopping vehicles and passing vehicles during a yellow light and the initial stage of red time (3 s after the red light starts) and calculate the decision-making behavior data under RLC and non-RLC conditions, respectively, according to formulas (1) and (2), as shown in Table 2.

It can be seen from Table 3 that, in the case of non-RLC conditions, the proportion of incorrect pass during passing decisions and the proportion of abrupt stop during stopping decisions are significantly larger than those of the intersection with RLCs. It can be seen that installing RLCs can effectively reduce the occurrence of incorrect pass and abrupt stop.

4. Driving Behavior Model Based on Data Simulation

First, data were collected to establish an effective mathematical model, and then the analysis of various parameters was realized via mathematical simulation. The main advantage of mathematical simulation is its universality; that is, with the same set of computer equipment and different simulation software, various types of systems can be simulated and tested. This paper focuses on the impact of RLCs on rear-end collisions during decision-making through mathematical simulation. The main work of the simulation model is to build the stop-and-go decision-making model and rear-end collision probability model.

4.1. Stop-and-Go Decision-Making Model. The decision-making model of intersection driving behavior is the stop-and-go model. A BL model (binary logit model, BL model for short) is easy to understand from a mathematical point of view and provides a simple method to explain the random probability generated by the cumulative logic density function assumed in the basic formula. Therefore, the BL model is the most widely used in addressing the decision-making of a driver when deciding to stop at or pass an intersection when encountering a yellow light. Through this model, the impact can be realized via a sensitivity analysis of factors related to the driver's decision-making behavior [9]. The BL model used to simulate driver stop-and-go decision-making is calculated as follows:

$$\mathrm{Logit}\left(\pi_i\right) = \log\left(\frac{\pi_i}{1-\pi_i}\right) = \sum_{k=0}^{K} \beta_k x_{ik}. \tag{3}$$

In the formula, x_i is a group of vectors composed of k interpretable variables, such as the geometry, traffic volume, and other intersection elements that can affect the driver's decision-making. x_{ik} is the k-th variable, and β_k is the corresponding influence coefficient of the k-th variable.

Considering the influence of the RLC, this paper analyses the driver's choice behavior near the intersection during the signal change interval, herein fully considering factors such as the vehicle speed, the distance to the stop line when the

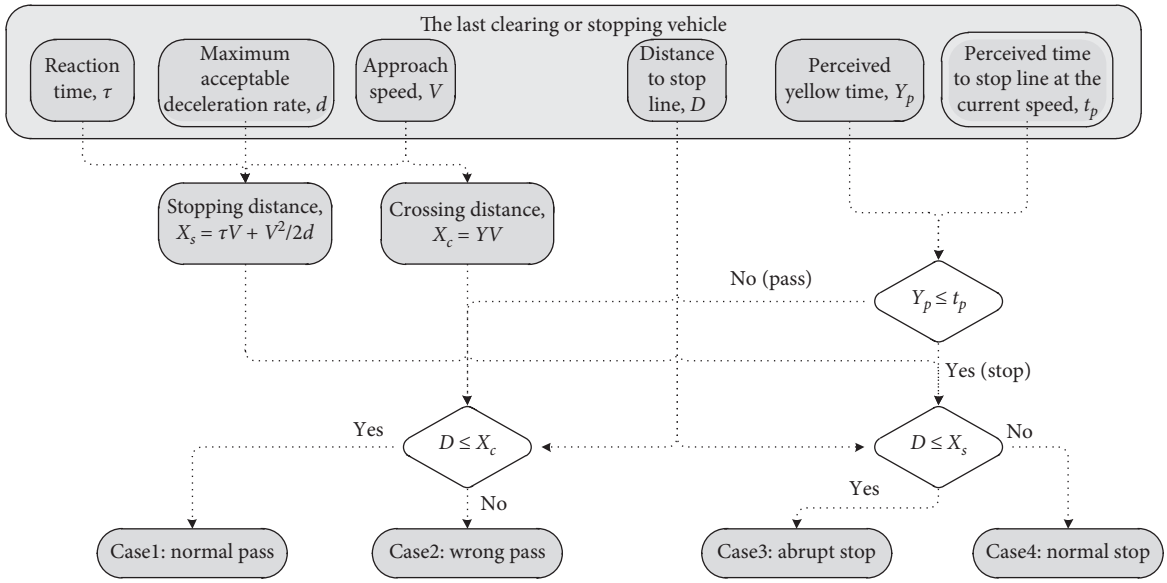

Figure 4: Classification of decision-making behavior.

Table 2: Comparison of abnormal decision behavior with RLC and without RLC.

Abnormal decision	Pass decision			Stop decision		
	Normal	Wrong	Wrong percentage (%)	Normal	Abrupt	Abrupt percentage (%)
RLC	94	15	13.8	93	6	6.1
Non-RLC	109	33	23.2	18	2	10.0

Table 3: Stopping probability models for stop-and-go decision.

Model	Explanatory variable	Coeff.	S.E.	Wald test	df	Sig.	Exp (B)
Category 1: presence of RLC = 1	Potential time (s)	2.445	0.423	33.432	1	0.000	11.528
	Constant	−6.620	1.190	30.946	1	0.000	0.001
Category 2: presence of RLC = 0	Potential time (s)	1.296	0.252	26.473	1	0.000	3.655
	Constant	−6.709	1.093	37.713	1	0.000	0.001
All samples	Potential time (s)	1.183	0.218	69.451	1	0.000	6.129
	Presence of RLC	3.940	0.600	43.094	1	0.000	51.435
	Constant	−8.876	1.003	78.282	1	0.000	0.000

Note: log likelihood (fitting results of model) = 447.892. Hosmer and Lemeshow test of goodness of fit (p) = 0.329 ($p = 0.329 > 0.05$ indicates good result). Area under receiver operating curve = 0.979, which gives validity of model with lower bound of 0.968 and the upper bound of 0.990 (95% confidence interval). Percentage correct = 0.923. Coeff. = coefficient; S.E. = standard error; df = degrees of freedom; Sig. = significance. RLC is dummy variable (0 = non-RLC, 1 = RLC).

yellow light is on, and whether an RLC is installed. Table 3 shows each analysis index and index value.

Table 3 shows the −2log likelihood and two pseudo-decision coefficients, that, the Cox and Snell R squared and the Nagelkerke R squared of the current model. The smaller the -2log likelihood is, the closer it is to 0 and the better the model fit is. The greater the pseudodeterminate coefficient is, the closer it is to 1 and the higher the model precision is. The prediction accuracy of the model shows that correct prediction records account for 91.3% of all samples, among which the prediction rate of the stopping decisions is 85.7%, and the prediction rate of the passing decisions is 94.0%. The model predictions are highly accurate.

The stopping probability can be expressed as

$$P_{\text{stop}} = \frac{1}{1 + e^{8.876 - 1.183 * \text{potential time} - 3.940 * \text{RLC (1 or 0)}}}, \quad (4)$$

where RLC = 1 represents RLCs installation and 0 is opposite; P_{stop} is the probability of making a decision to pass.

In the model, the regression coefficient of speed is positive, the regression coefficient of distance is negative, and the regression coefficient of whether there is an RLC installed (i.e., installed RLC = 1) is negative. This shows that the greater the speed of the vehicle, the smaller the distance from the stop line and the higher the probability of making the pass decision when an RLC is not installed. Comparing the absolute values of the coefficient of each influencing factor, we can see that the

coefficient value of the RLC is far greater than those of speed and distance, which shows that RLCs' installation has a significant impact on the decision-making process of passing, which is consistent with the actual situation.

4.2. Rear-End Collision Probability Model

4.2.1. Determination of Key Influencing Parameters. For drivers approaching the stop line when the yellow light is on, they must decide whether to go through or to stop. If the driving speed is high and the vehicle is very close to the stop line, the driver should choose to cross the intersection before red light onset. On the contrary, if the distance is far, the driver should make a decision to brake. Two types of abnormal driving behaviors often occur when drivers make decisions. One is when they are far away from the intersection, they make a decision to pass, which makes them unable to pass the intersection smoothly at a normal speed. In this case, the driver tends to speed up to pass the stop line as fast as possible. This inappropriate action is likely to lead to running a red light and then cause the right-angle collisions with the cross traffic flow. Another situation is when the driver makes a decision to stop when he is close to the intersection, which results in a failure to stop safely in front of the stop line with normal braking. Such decision-making for emergency stopping readily leads to rear-end collisions.

When the trailing car follows the leading car, an incorrect decision by the leading car will lead to rear-end collisions. The necessary condition for rear-end collisions is that the leading car chooses to stop and then the car makes a pass decision. When a yellow light or green light is active, the leading vehicle fails to slow down sufficiently due to an incorrect judgment or perception error, resulting in emergency deceleration. However, if the distance between the following car and the leading car is small and the driving speed exceeds that of the leading car, the possibility of rear-end collisions increases.

The stop-and-go decisions made by the driver of the leading vehicle mainly consider the distance to the stop line and the current speed, that is, the potential travel time. Some scholars, such as Mahalel, Zaidel, and Hayward, have clearly pointed out that speed and distance, that is, the potential travel time, have a significant impact on the driver's stop-and-go decision-making. Hence, the potential travel time was used to study the driver's behavior during the period from green to yellow lights [23–25]. In addition, some studies have shown that changes in headway will have an important impact on the decision-making of the following vehicle and thus indirectly affect the possibility of rear-end collisions [16]. Therefore, the headway and the potential travel time are selected as the key influencing factor for rear-end hazard analysis for the process of vehicle decision-making. Under two key traffic parameters, the risk of vehicle rear-end collision under different traffic flow conditions is discussed.

4.2.2. Probability Analysis of Rear-End Collisions. Headway refers to the time interval between two consecutive vehicles in a vehicle queue operating in the same lane passing through a certain section. Obviously, headway, as the time difference between two vehicles passing through the parking line, has an impact on rear-end accidents. Therefore, headway will be used as an important variable in the probability analysis of rear-end collisions.

Using the developed decision model and mathematical simulation method, the theoretical probability of rear-end collisions at the RLC intersection under the combination of headway and the potential travel time is obtained, as shown in Figure 5.

Figure 5 shows that the changing trend of the probability of rear-end collisions under different headways is the same, and the maximum occurrence rate is potential travel time value of 2–3 s, which shows that the possibility of inconsistent decision-making between the leading and following vehicles is the largest within 2 s~3 s from stopping line. In other intervals, the leading and following vehicles tend to make the same decision.

When the potential travel time takes on a certain fixed value, the smaller the headway is, the greater the incidence of rear-end collisions is. This indicates that the smaller the following distance is, the greater the influence of the leading car is. After being influenced by the driving behavior tendency of the leading car, the following car will take a while to make corresponding adjustments on the driving state. During the reaction time period, the driving speed of the following car may be much faster than that of the leading car, and the time to collision (TTC) decreases sharply, which corresponds to an increased possibility of collision.

5. Risk Impact Analysis of RLC on Driving Behavior

5.1. The Influence of RLCs on Drivers' Decision-Making Behavior. The dilemma zone is caused in the process of stop-and-go decision-making, which has always been an important index to evaluate the safety of intersections. There are two types of difficult areas which lead to incorrect decisions [26]. Type I dilemma zone occurs when the intergeen time is insufficient, which leads to the driver being unable to not only achieve a safe stop before the red light turns on but also pass through the intersection safely. Type I dilemma zone is mainly eliminated by the design of the yellow time and all-red time. Type II dilemma zone reflects a region in which it is difficult for drivers to make stop-and-go decisions. Therefore, Type II dilemma zone is also called the "indecision zone." The most typical definition of Type II dilemma zone is the zone between the 10% probability stop and 90% probability stop when the yellow light is on. [26–30]. Based on the stop-and-go decision model, Type II dilemma zone of the intersection with or without RLC is established, as shown in Figure 6.

Figure 4 shows that the indecision zone of the RLC intersection is 2 s–3.9 s, and the indecision zone of the non-RLC intersection is 3.5 s–6.9 s. Compared with the non-RLC intersection, the potential travel times corresponding to 10% stop probability and 90% stop probability are 1.5 s and 3 lower, respectively. This shows that the presence of RLC helps to reduce the difficulty of decision-making by

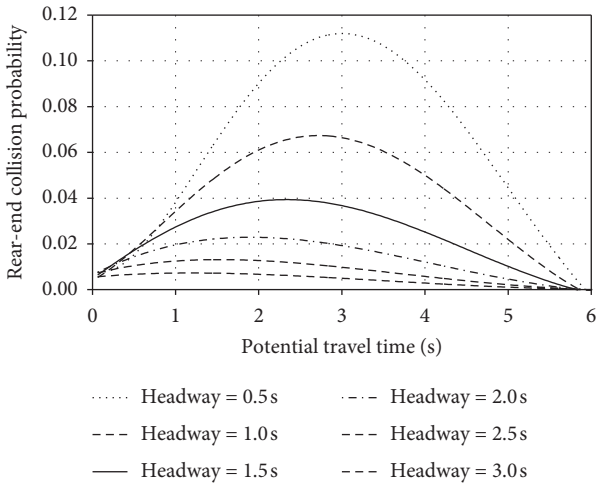

Figure 5: Probability of rear-end collisions with different headway.

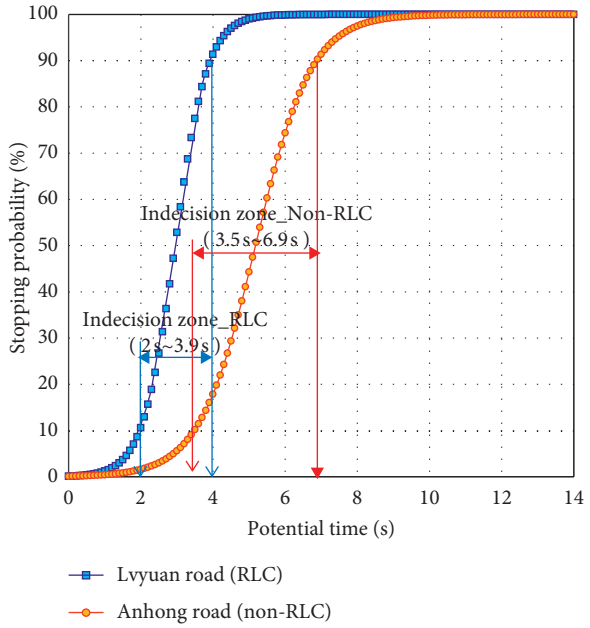

Figure 6: Indecision zones of the RLC intersection and the non-RLC intersection.

drivers. This finding is consistent with the results of previous studies [21]; that is, during green or yellow lights, RLCs is very effective in increasing the tendency of drivers to stop.

From the perspective of the time span of the indecision zone, RLCs can help drivers to make decisions more quickly and decisively, which greatly increases the tendency of the leading vehicle to choose to brake. However, the leading vehicle's stop decision is a necessary condition for the occurrence of rear-end accidents. Therefore, although setting RLCs greatly reduces the indecision zone, it brings more possibility to the rear-end accident. The further analysis of the impact of RLCs on rear-end collisions is described in the following content of the paper [31].

5.2. The Influence of RLCs on Risk of Rear-End Collisions. According to the actual observation, the headway of continuous saturated traffic flow is about 2 s. Therefore, taking the headway as 2 s, this paper analyses the impact of different potential travel time on the rear-end collision probability, as shown in Figure 7.

(i) RLCs can effectively reduce the rear-end collision probability in ranges close to or far from the intersection.

(ii) For vehicles with low driving speeds, RLCs will effectively reduce the rear-end collision risk, which indicates that the decision-making tendency of these drivers is greatly affected by RLCs. For vehicles with high driving speeds, RLCs have no obvious influence on the rear-end collision probability because most of these drivers are aggressive, and their decision-making tendency is generally affected by RLCs.

(iii) According to the previous speed analysis, the driving speed of most vehicles is in the range of 30 km/h to 70 km/h; therefore, in the range of potential traffic times of 2 s~3 s, RLCs will increase the probability of rear-end collisions for most vehicles.

In this study, estimated time to stop line (ETSL) proposed by Huang et al. was used to analyse the effect of RLCs on the rear-end collision probability with different speeds [16]. Through mathematical simulation, the cut-off speed curves corresponding to the ETSL are obtained when the headway is taken as 2 s. The area above the curve indicates an increase in the rear-end collision probability, as shown in Figure 8.

From Figure 8, it can be seen that 80% of the vehicles at non-RLC intersections fall on the top of the curve, while 91% of the vehicles at RLC intersections fall on the top. On the whole, RLCs can lead to greater probability of rear-end collisions, but the effect of RLCs on the risk of rear-end collision is not obvious in a specific range.

6. Conclusions

In this study, aiming at typical problems, such as lag and large errors in accident statistics research methods for analysing the rear-end collision risk with RLCs installed, a simulation analysis method of rear-end collisions based on the probability of collision theory is proposed, and the feasibility of this method is verified using two adjacent, similar intersections in Shanghai. This study mainly considers the driving characteristics, decision-making behavior, and safety status of vehicles with and without RLCs. The study not only analyses these three aspects separately but also discusses the relevance of each analysis conclusion to provide a comprehensive understanding of the impact of RLCs on vehicles at intersections. The following conclusions are drawn in this study:

(1) The method of rear-end collision risk assessment based on mathematical simulation and calculation can determine the rear-end collision probability at

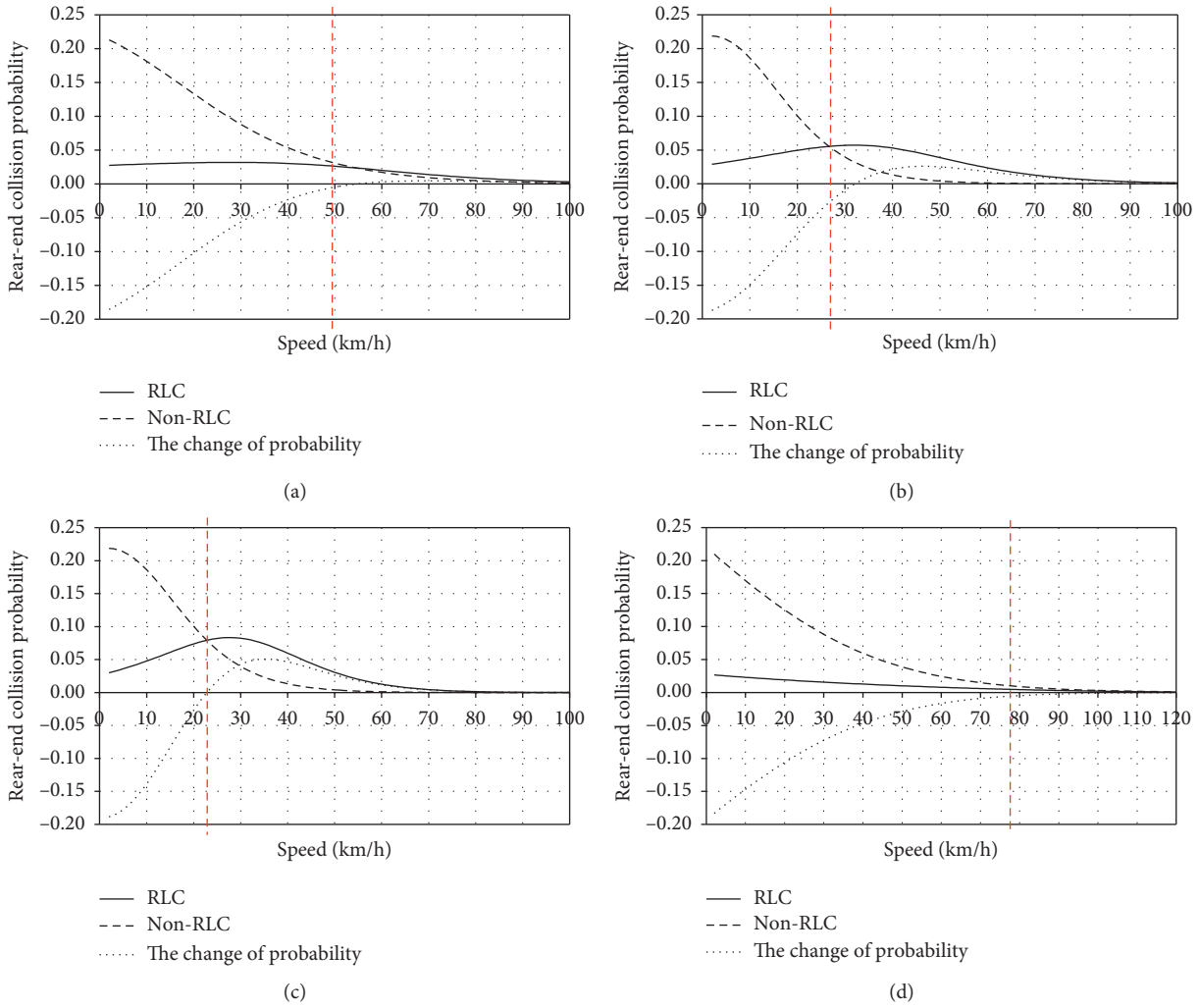

Figure 7: Probability of rear-end collisions with different potential travel time. Through the analysis of the above probability curve, the following can be found: (a) Potential travel time = 1.0 s. (b) Potential travel time = 2.0 s. (c) Potential travel time = 3.0 s. (d) Potential travel time = 4.0 s.

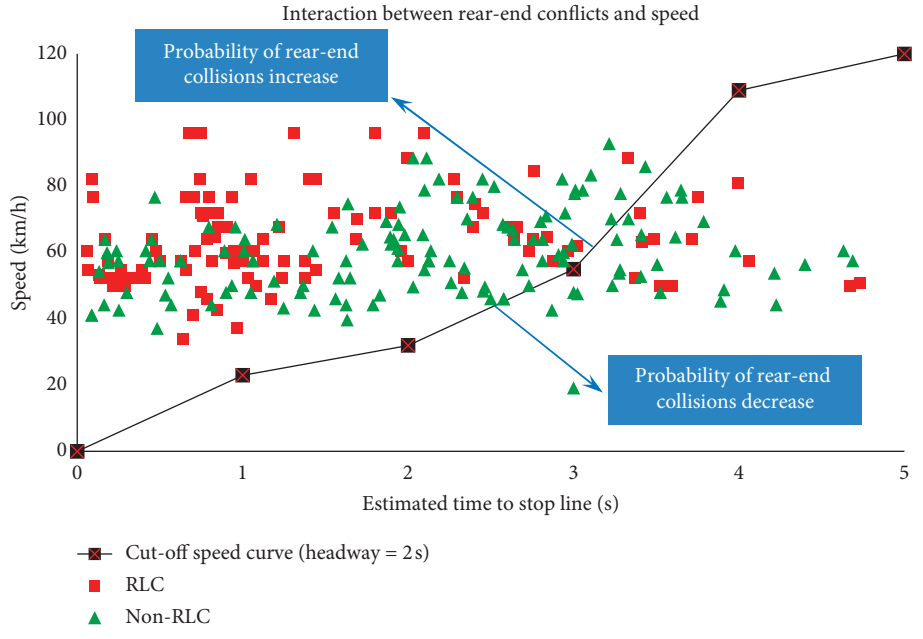

Figure 8: The rear-end collision probability distribution with ETSL.

intersections before and after the installation of RLCs. This method has wide applicability.

(2) RLCs have an important impact on the driver's speed. They can cause the vehicle speed at the intersection to increase and cause more abnormal driving behaviors, which increase the difficulty of driver's stop-and-go decision-making.

(3) RLCs are helpful for drivers to make the stop-and-go decision, reduce the difficulty of decision, and increase the tendency of stopping and the complexity and possibility of rear-end collision.

(4) Unlike previous studies, we find that RLCs do not always lead to an increase of rear-end collisions. For the vehicle close to or far from the intersection at the decision-making time, the RLC will significantly reduce the rear-end collision probability; however, for the vehicle at the potential travel time of 2 s~3 s, RLCs will cause an increase of rear-end collisions. RLCs have minimal effects on aggressive drivers who drive at high speed at decision-making time.

(5) The probability distribution of rear-end collisions under different traffic flow states shows that strict speed limit management can lower the rear-end collision risk caused by RLCs.

Data Availability

The data used to support the findings of this study are available from supplemental files.

Conflicts of Interest

The authors declare that there are no conflicts of interest regarding the publication of this paper.

Acknowledgments

This study was supported by Public Technology Research Program of Zhejiang Province (no. LGF20F030004), Natural Science Foundation of Ningbo Municipality (no 2019A610044), and Opening Foundation of the State Key Laboratory for Management and Control of Complex Systems (no. 20190102). The authors are grateful to Professor Hideki Nakamura at Nagoya University for providing the image-processing software for data reduction in this study. Thanks are also due to Dr. Jibiao Zhou at Ningbo University of Technology for data collection and reduction as well as the construction of stop-and-go decision-making model.

Supplementary Materials

This section includes two Excel tables. Table S1: data for building indecision zone models of the RLC intersection and the non-RLC intersection (Figure 6 in the article). Table S2: all simulation data of rear-end probability calculation. Using these data, we can build the probability of rear-end collision models (Figures 5, 7, and 8 in the article). (*Supplementary Materials*)

References

[1] H. W. McGee and K. A. Eccles, "Impact of red light camera enforcement on crash experience," *ITE Journal*, vol. 73, no. 3, pp. 44–48, 2003.

[2] Safety Evaluation of Red-Light Cameras, *RRPORT FHWA-HRT-05-048*, Federal Highway Administration, Washington, DC, USA, 2005.

[3] F. Chen, M. Song, and X. Ma, "Investigation on the injury severity of drivers in rear-end collisions between cars using a random parameters bivariate ordered probit model," *International Journal of Environmental Research and Public Health*, vol. 16, no. 14, Article ID 2632, 2019.

[4] F. Chen and S. Chen, "Injury severities of truck drivers in single- and multi-vehicle accidents on rural highways," *Accident Analysis & Prevention*, vol. 43, no. 5, pp. 1677–1688, 2011.

[5] C. Ma and Y. Dong, "Public transit network planning in small cites considering safety and convenience," *Advances in Mechanical Engineering*, vol. 12, no. 1, pp. 1–12, 2020.

[6] C. Ma, Y. Dong, J. Zhou, Z. Feng, and Y. Quan, "Risk riding behaviors of urban E-bikes: a literature review," *International Journal of Environmental Research and Public Health*, vol. 16, no. 13, Article ID 2308, 2019.

[7] H. C. Chin, "Effect of automatic red-light cameras on red running," *Traffic Engineering and Control*, vol. 30, no. 4, pp. 175–179, 1989.

[8] C. H. Ng, Y. D. Wong, and K. M. Lum, "The impact of red light surveillance cameras on road safety in Singapore," *Road and Transport Research*, vol. 6, no. 2, pp. 72–81, 1997.

[9] G. E. Maisey, "The effects of mechanical surveillance device on urban signalized intersection accidents," Research and Statistics Report no. 17, Road Traffic Authority, Perth, Australia, 1981.

[10] D. R. South, W. A. Harrison, I. Portans, and M. King, *Evaluation of the Red Light Camera Program and the Owner Onus Legislation*, Victoria Transport: Road Traffic Authority, Hawthorn, Victoria, Australia, 1998.

[11] W. Hillier, J. Ronczka, and F. Schnerring, *An Evaluation of Red Light Cameras in Sydney*, Road Safety Bureau, Roads and Traffic Authority, New South Wales, Australia, Research Note RN 1/93, 1993.

[12] D. A. Andreassen, *Long Term Study of Red Light Cameras and Accidents*, Research Report ARR No. 261, ARRB Transport Research Ltd., Victoria, Australia, 1995.

[13] R. A. Retting and S. Y. Kyrychenko, *Crash Reductions Associated with Red Light Camera Enforcement in Oxnard, California*, Insurance Institute for Highway Safety, Arlington, VA, USA, 2001.

[14] P. B. Farradyne, *City of San Diego Photo Enforcement System Review Final Report*, City of San Diego Police Department, Los Angeles, CA, USA, 2002.

[15] U.S. House of Representatives, *The Red Light Running Crisis, Is it Intentional, Office of the Majority Leader*, U.S. House of Representatives, Washington, DC, USA, 2001.

[16] H. L. Huang, H. C. Chin, and A. H. H. Heng, ""Effect of red light cameras on accident risk at intersections", transportation research record," *Journal of the Transportation Research Board*, vol. 1969, pp. 18–26, 2006.

[17] Q. Zeng, W. Gu, X. Zhang, H. Wen, J. Lee, and W. Hao, "Analyzing freeway crash severity using a Bayesian spatial generalized ordered logit model with conditional autoregressive priors," *Accident Analysis & Prevention*, vol. 127, pp. 87–95, 2019.

[18] Q. Zeng, H. Wen, H. Huang, and M. Abdel-Aty, "A Bayesian spatial random parameters Tobit model for analyzing crash rates on roadway segments," *Accident Analysis & Prevention*, vol. 100, pp. 37–43, 2017.

[19] J. Sun, T. Li, F. Li, and F. Chen, "Analysis of safety factors for urban expressways considering the effect of congestion in Shanghai, China," *Accident Analysis & Prevention*, vol. 95, pp. 503–511, 2016.

[20] B. Dong, X. Ma, F. Chen, and S. Chen, "Investigating the differences of single- and multi-vehicle accident probability using mixed logit model," *Journal of Advanced Transportation*, Article ID 2702360, 9 pages, 2018.

[21] K. M. Lum and Y. D. Wong, "A before-and-after study of driver stopping propensity at red light camera intersections," *Accident Analysis and Prevention*, vol. 35, no. 2, pp. 111–120, 2003.

[22] J. Sun, X. S. Dong, and Y. Ni, "Comparative study of impacts of red light cameras in China," *Transportation Research Record: Journal of the Transportation Research Board*, vol. 2317, no. 1, pp. 68–75, 2012.

[23] H. Köll, M. Bader, and K. W. Axhausen, "Driver behavior during flashing green before yellow: a comparative study," *Accident Analysis and Prevention*, vol. 36, no. 2, pp. 273–280, 2004.

[24] D. Mahalel and D. M. Zaidel, "Safety evaluation of a flashing-green light in a traffic signal," *Traffic Engineering and Control*, vol. 26, no. 2, pp. 79–81, 1985.

[25] J. C. Hayward, "Near-miss determination through use of a scale of danger," *Highway Research Record*, vol. 384, pp. 24–34, 1972.

[26] T. J. Gates, D. A. Noyce, and L. Laracuente, "Analysis of dilemma zone driver behavior at signalized intersections," in *Proceedings of the Transportation Research Board 85th Annual Meeting*, Transportation Research Board, Washington, DC, USA, 2006.

[27] B. James and K. Zimmerman, *Red-Light-Running Handbook: An Engineer's Guide To Reducing Red-Light-Related Crashes*, Texas Department of Transportation and the Federal Highway Administration, Austin, TX, USA, 2004.

[28] B. E. Porter and T. D. Berry, "A nationwide survey of self-reported red light running: measuring prevalence, predictors, and perceived consequences," *Accident Analysis & Prevention*, vol. 33, no. 6, pp. 735–741, 2001.

[29] C. V. Zegeer, *Effectiveness of Green-Extension Systems at High-Speed Intersections*, Kentucky Transportation Center at the University of Kentucky, Lexington, KY, USA, 1977.

[30] A. D. May, *Clearance Interval at Flashing Systems*, Highway Research Board, National Research Council, Washington, DC, USA, Highway Research Record 221, 1968.

[31] S. Dong, J. Zhou, and S. Zhang, "Determining E-bike drivers' decision-making mechanisms during signal change interval using the hidden markov driving model," *Journal of Advanced Transportation*, vol. 2019, Article ID 7341097, 10 pages, 2019.

Hindawi
Journal of Advanced Transportation
Volume 2020, Article ID 8573232, 12 pages
https://doi.org/10.1155/2020/8573232

Research Article

Exploring Factors Affecting the Yellow-Light Running Behavior of Electric Bike Riders at Urban Intersections in China

Jing Cai,[1] Jianyou Zhao ,[1] Jing Liu ,[1,2] Ke Shen,[1] Xun Li,[1] and Yuntao Ye[1]

[1]*School of Automobile, Chang'an University, Xi'an 710064, Shaan Xi, China*
[2]*School of Mechanical and Electrical Engineering, Anhui Jianzhu University, Hefei 230601, China*

Correspondence should be addressed to Jianyou Zhao; jyzhao@chd.edu.cn

Received 13 November 2019; Revised 30 January 2020; Accepted 25 February 2020; Published 10 June 2020

Academic Editor: Jaeyoung Lee

Electric bikes play an important role in the urban transportation system in China. Yellow-light running behavior of riders is one of the most critical factors for e-bike riders involved in traffic crashes at intersection. The main purpose of this study is to explore how a variety of factors affect e-bike riders' yellow-light running behaviors at intersection by a field observation conducted in Xi'an, China. Based on 396 e-bike riders who faced yellow-light samples, two analytical methods, the principle component analysis logistics model and a base logistics model, were employed to evaluate the impacts of contributing factors on e-bike riders' yellow-light running behavior. The modeling results showed that seven variables significantly affect the e-bike riders' yellow-light running behavior, which were the approaching speed of e-bike, the distance to stop line, riders' age and gender attributes, type of e-bike, and the characteristics of intersection including the width of intersection and the existence of physical barriers. This study can provide valuable insights into understanding e-bike riders' yellow-light running behavior and may also help decision makers propose countermeasures to reduce e-bike rider-related crashes at intersection.

1. Introduction

Electric bike as one of the flexible transportation modes is popular in China and other Asian countries, which constitutes about 34% proportion among all travel modes in China [1]. Due to the convenience in congestion traffic, energy efficiency, and high manoeuvrability [2], the electric bike (e-bike) has experienced a tremendous growth in China and its total number was more than 250 million according to the China Bicycle Industry Information Center in 2018 [3]. This trend is likely to continue with the soaring prices of fuel and the traffic jam due to the growing ownership of motor vehicles. More e-bikes traffic accidents may be incurred by the surging number of e-bikes which has attracted some safety concerns around the world. Riders are considered as vulnerable road users since they are not protected by any metal structures of vehicles in traffic crashes [4]. In 2015, e-bike accidents accounted for more than 70% of nonmotorized traffic accidents which involved 14471 casualties [5]. The total number of road e-bike traffic accidents from 2016 to 2017 was 25990, which resulted in 4070 deaths and 28509 injuries [6]. Wu et al. revealed that over 60% of fatal crashes involving two-wheelers resulted from violation of signal rules [7]. According to the Chinese road rules, nonmotorized traffic including regular bicycles and electric bikes should obey the same signal as motor vehicles at signalized intersections. Because of lower speed and inappropriate signal controlling, e-bike riders may do an inappropriate go-stop decision when facing signal changes. Due to the insufficient clearance time, riders may meet the opposite vehicles, thus causing a right-angle collision when doing a go-decision at the onset of yellow-light. Therefore, a study focusing on e-bike riders' crossing behavior at intersection in yellow-light interval is imperative.

Although the growing violation in e-bikes has attracted widespread interest of researchers to model the signal violation behavior, few studies have investigated e-bike riders yellow-light running behavior. Therefore, this study mainly reviewed the red-light running behavior of e-bike riders and the yellow-light running behaviors of motor vehicle drivers.

Several researchers have studied associated factors, which may influence the e-bike riders' red-light running (RLR) behavior. Wu et al. [7–9] focused on the rider characteristics such as gender and age group, which were proven to have significant impact on the RLR behavior. Wu et al. studied that the young and middle-aged riders were more likely to run against a red-light than the old ones and males were more likely to act in a risk-taking manner than females [7]. Some studies examined the effects of environment factors on the RLR behavior. Yan et al. found that the type of day (weekday, weekend, and holiday) and period per day (peak and off-peak hours) had effects on RLR violation rate. And the result showed that the RLR rate of e-bike riders was high in off-peak hours but low on weekends and holidays [10]. Yu et al. found that riders were more likely to stop at the intersection with pedestrian countdown signal devices [11]. The study conducted by Zhang and Wu suggested that the sunshields installed at intersection can reduce RLR violation rates of e-bikes on both sunny and cloudy days [8]. Bai et al. found that the type of vehicle had a significant effect on red-light running behavior occurrences [9].

Most of yellow-light running (YLR) behavior studies focused on motor vehicles. Some useful reviews of existing research studies on vehicle YLR behavior can be seen as follows. A number of studies have conducted to explore effects of driver's personal attributes on YLR behavior violation. The finding of the study conducted by Papaioannou indicated that drivers' age and gender significantly impacted their YLR violation behavior [12]. Consistent conclusions were found by Rakha and Haque et al. [13, 14]. Many scholars studied the effects of vehicle operation characteristics on yellow-light running behavior. Köll et al. concluded that drivers were likely to pass through intersection rather than stop with a higher approaching speed and shorter distance [15]. Similar conclusions were found by Papaioannou, Bharat, Hurwitz, and Ding et al. [12, 16–18]. Elmitiny et al. [19] and Pathivada, and Perumal [16] focused on the exposures affecting the violation behavior and they found that vehicle type had a statistically influence on the YLR behavior.

The existing signal violation research studies have similarities and differences in the contributing factors that are explained in terms of the following aspects: (a) General summarization: drivers' characteristics including gender and age were proved to have significant impact on the e-bike riders' red-light running and vehicle drivers' yellow-light running violation behaviors, and in both violations, vehicle type is a significant exposure. (b) Differences of exposures: compared with the vehicle YLR studies, the researchers studying e-bike RLR focused on the environment exposures (e.g., the type of day, the weather, and facilities in the intersection). However, the vehicle operation characteristics (e.g., the approaching speed and the distance to stop line) were the crucial factors which have been proved to affect the YLR violation in many vehicle YLR research studies. However, till now, rare studies addressed that the operation characteristics of the e-bike impacted the riders' crossing behavior in yellow-light interval. The crucial factors of approaching speed and distance to the stop line are taken into consideration about how they affect the intersection crossing behavior of riders in this study.

Modeling techniques were explored by many researchers to explain the e-bike rider's and vehicle driver's signal violation behavior at the signalized intersections. The logistic regression model was the most commonly used model to explain the signal violation behavior in studies conducted by Wu, Zhang, Tang, and Bharat et al. [7, 8, 11, 16]. Yan et al. used the Poisson model to describe the e-bike cyclist's and bicyclist's RLR behavior [10]. Elmitiny et al. proposed a decision tree model to classify the driver's stop-go decision behavior in yellow-light interval [19]. Hurwitz et al. [17] and Tang et al. [20] developed a fuzzy logic model to explain the probability of a driver's go-stop decision at the intersection when facing the signal changes. In this study, the principle component analysis logistics model is proposed to investigate e-bike riders' yellow-light running behavior. This approach can be used to describe how various factors affect the violation behavior and to eliminate the multicollinearity in the observed data, further improving the measurement accuracy. PCA logistics models have been widely applied in biometrics [21], engineering application [22], economics [23], and management [24] fields to determine causality from collected data. Results of these studies indicated that the PCA model had high model accuracy.

In summary, the objective of this paper is twofold. The first aim is to examine the effects of a set of contributing factors on yellow-light running behavior, which included e-bike rider characteristics (gender, age group, and the type of vehicle), the e-bike riders' operation characteristics (approaching speed, distance to the stop line), and the characteristics of intersection (the width and the facility of intersection). The second aim is to compare the PCA logistics model and base logistics model, further revealing the contribution of variables excluded or omitted by the base model and improving the model performance in e-bike riders' yellow-light running behavior analysis. The results of this paper would explain why e-bikers infringe the traffic signal at intersections and might help propose some suggestions on enhancing the safety of e-bike riders, which is a major issue in China and other developing countries.

2. Methodology

2.1. Intersection Selected. The signal intersection chosen to conduct this observation was in Xi'an, the provincial capital city of Shaan Xi province, China, where the total number of electric bikes has been estimated to be more than 3 million [25]. The selected intersection shared the following characteristics:

(1) The electric bike traffic flow is smooth and not queueing

(2) An exclusive nonmotorized lane exists

(3) Before the onset of yellow-light, the signal device has 3-second green-light countdown flashing

(4) To clearly record the approaching behaviors of e-bike at intersection by using a UAV camera, the landscape trees do not exist on the side of nonmotorized lane

Details and characteristics of the selected intersection are shown in Table 1.

2.2. Data Collection Using UAV. In this study, the field observation approach was used to record the yellow-light running behavior of e-bike riders, which has been commonly used to investigate the red-light running violation [7, 8, 10, 11] and yellow-light running behavior of road users at urban intersections [16, 20, 26]. An unmanned aerial vehicle which has been applied in traffic behavior analysis [27–29] recorded e-bike riders' crossing behaviors, and synchronized cameras were used to collected riders' individual characteristics. The location of two cameras is listed in Figure 1. The unmanned aerial vehicle, also called drone, was operated to hover for 50 m altitude over the nonmotorized lane located in upstream intersection. The fight altitude ensured that it would not be visible and audible for the riders and that the rider's entire crossing process could be recorded. To avoid being spotted by subjective riders and consequently causing changes in crossing behaviors, the synchronized camera installed was hidden behind telegraph poles and pointed towards the riders to observe their detail characteristics. This field survey was conducted during weekday's peak hour periods (8:00 a.m.9:00 a.m.; 5:30 p.m.6: 30 p.m.) in good weather conditions for 3 weeks in April 2019.

2.3. Data Extraction. All road users' crossing behaviors were recorded on the camera videos, but only the behaviors of e-bike riders were extracted when they entered the scope of the UAV camera in 6 seconds prior to the onset yellow-light to the end of yellow-light. We restricted the coding process to only include e-bikes straightly passing through at intersections. Right-turn e-bikes were ignored because they could not subject to the traffic signal controlling on the basis of the road law in China. Meanwhile, left-turn e-bikes were also excluded due to having dedicated left signal light for them. After the coding process, video analysis software was applied to extract trajectory information. The software could mark the objective e-bike and automatically track its position at the frame rate of 25 frames per second. The Cartesian coordinate was established with the cross point of the pavement and the stop bar as the origin which can be regarded as a reference to extract the X and Y of e-bikes' position (see in Figure 2). Hence, the approaching speed and the distance to the stop line of e-bikes could be obtained. Then, the riders' individual characteristics coded by the synchronized camera including gender, estimated age group, and vehicle type were extracted and are listed in Table 2.

In order to avoid data recording mistake, two trained graduate students independently extracted the data from collected videos. The recoding reliability was calculated by Cohen's Kappa for categorical variables and intraclass correlation for continuous variables. All the coefficients ranged from 0.79 to 0.99, which ensured the reliability of extracting process.

2.4. Modeling Rider Behavior. Some limitations may exist in predicting the result by the linear regression model due to the binary response variables frequently involved in traffic behavior. The logistics regression has been widely applied and proven to be successful to model traffic safety research, such as evaluating the contributing factors for vehicle accident [31], especially in examination of risk factors involved in red-light running and yellow-light running behavior [7, 8, 11, 16]. In our model, $Y = 1$ denoted yellow-light running behavior of e-bike riders and $Y = 0$ denoted that riders stopped their riding behavior in the yellow-light interval. The YLR behavior model was formulated as follows:

$$\log it\left(\frac{p_i}{1-p_i}\right) = \alpha + \beta_0 x_0 + \beta_1 x_1 + \cdots + \beta_n x_n, \quad (1)$$

where p_i is the probability that events occurred, α is a constant term, and β_i are the corresponding coefficient of x_i estimated by the method of maximum likelihood.

The probability of the rider i running against the yellow-light was obtained in the following equation:

$$p_i\left(y_i = 1 \mid x_0, x_1, \ldots, x_n\right) = \frac{\exp\left(\alpha + \beta_0 x_0 + \beta_1 x_1 + \cdots + \beta_n x_n\right)}{1 + \exp\left(\alpha + \beta_0 x_0 + \beta_1 x_1 + \cdots + \beta_n x_n\right)}. \quad (2)$$

2.5. Method of Estimating Variables' Multicollinearity. The logistics model presented in equations (1) and (2) assumes that explanatory variables are independent. However, the observed variables had a multicollinearity problem. Multicollinearity may result in prejudices in the estimation of the model and the interpretation of its parameters. In this paper, we used two variable selection methods to eliminate the multicollinearity problem.

2.5.1. Stepwise Regression Selection Model. The stepwise regression has been commonly used to deal with multicollinearity in logistics regression process. The stepwise regression selection method was used to extract possible combination of explanatory variables affecting the rider behavior at the yellow-light onset, and the final combination of variables was decided based on whether those were significant at a 95% confidence level using a T-test in the SPSS 22.0 software.

2.5.2. Principle Component Analysis Selection Model. In order to obtain an accurate estimation of explanatory variables under multicollinearity, principal component analysis (PCA) was proposed to extract features of explanatory variable. The Kaiser–Meyer–Olkin (KMO) test is shown whether the sample data met the requirements for PCA. Since PCA is suitable for continuous variables, categorical principal component analysis (CATPCA) was used in this study to transform the categorical variables into numerical

Table 1: Characteristics of study intersections.

Intersection	Wenyi North rd.–Huangheng South rd. (W-H intersection)	Hanguang North rd.–Xiaozhai West rd. (H-X intersection)	Taibai North rd.–Keji rd. (T-K intersection)
Type of intersection	Four-arm	Four-arm	Four-arm
Approaches[a]	SB	SB	E-WB
Width of intersection[b] (m)	60	50	75
Width of nonmotorized lane (m)	2.7	3.0	2.7
Length of yellow-light (s)	3	3	3
Flashing countdown green-light time	3	3	3

[a]NB: south-bound approach; E-WB: east-west approach. [b]Width of intersection: the distance between the stop line in the entrance of the intersection and the other invisible stop line in the exit of the intersection which is the extension cord of the opposite nonmotoried lane's stop line.

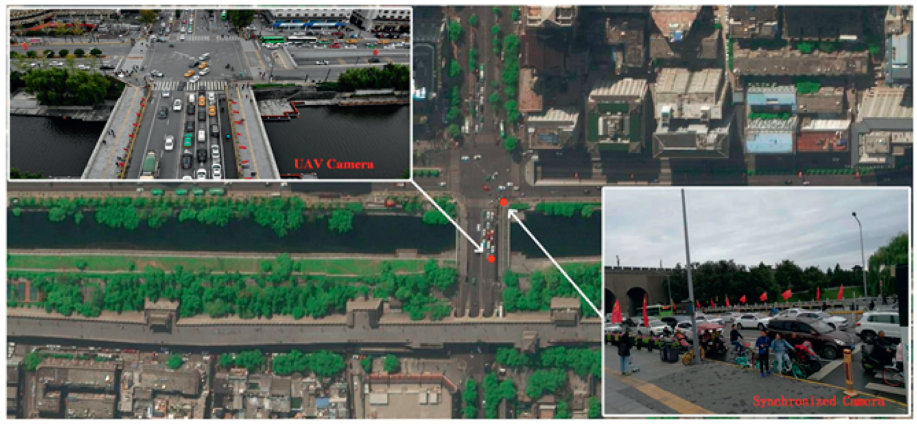

Figure 1: Bird's eye view and two photos of camera view of W-H intersection.

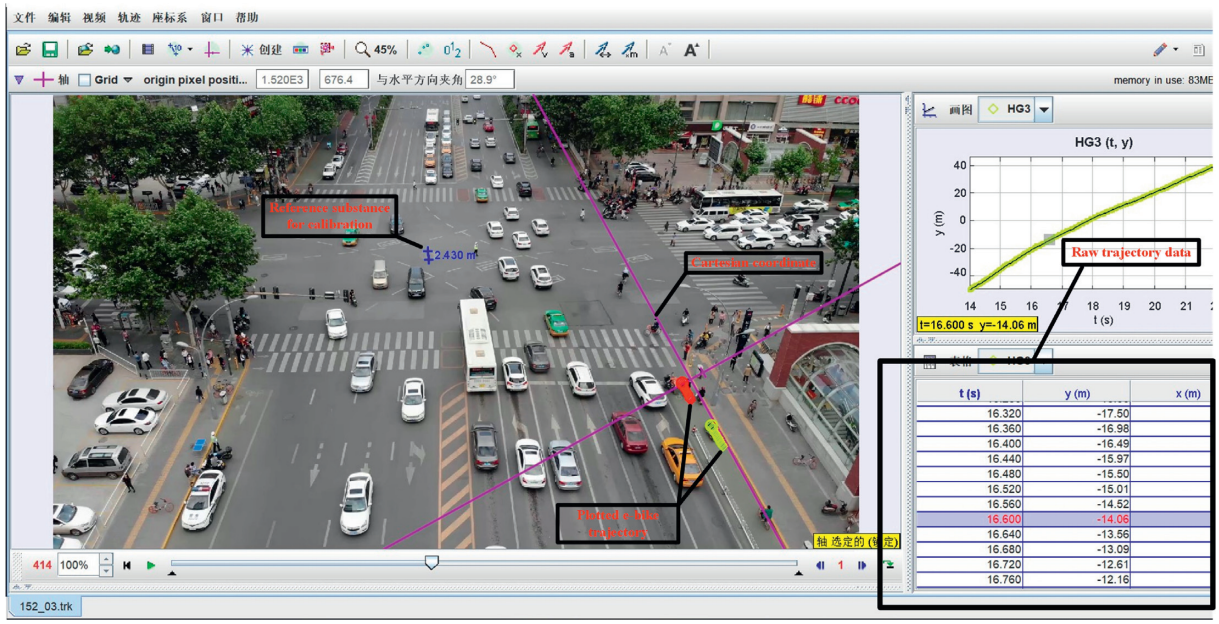

Figure 2: Image of software for data extraction.

values [32]. The CATPCA process is briefly described as follows:

Assuming that measurements of n individuals on m variables scores were given in an $n \times m$ scores matrix $\mathbf{H}$ where each variable was dedicated by $\mathbf{X}_j$, $j = 1, \ldots, m$, that was the j^{th} column of $\mathbf{H}$, $\mathbf{X}_j$ was measured in nominal or ordinal level. Equation (3) transformed the score into category quantification:

Table 2: Definition of variables coded.

Variable	Definition	Type of variable
Gender (GEN)	0 for female; 1 for male	Categorical
Estimated age group[a] (AGE)	0 for young group (<30) 1 for middle-age group (30–50) 2 for old group (>50)	Categorical
Vehicle type[b] (VT)	0 for bicycle-style electric bike 1 for scooter-style electric bike	Categorical
Physical barrier (PB)	0 for without physical barriers between motorized vehicle lane and nonmotorized vehicle lane 1 for with physical barriers between motorized vehicle lane and nonmotorized vehicle lane	Categorical
Approaching speed (AS)	The approaching speed of vehicle at the onset of the yellow	Continuous
Distance to the stop bar (DTS)	Vehicle's distance to the stop bar at the onset of the yellow indication	Continuous
Width of intersection (WI)	The distance between the stop line in the entrance of the intersection and the other invisible stop line in the exit of the intersection which is the extension cord of the opposite nonmotoried lane's stop line	Continuous

[a]The rider's age information extracted from the recorded videos using the estimated age group could be more effective, and the group-dividing method was reported by Wu et al. [7]. [b]Bicycle-style e-bike can be solely electric-powered or require pedal assistance, while the power of scooter-style e-bike only comes from the electromotor. The speed of the scooter-style e-bike is faster than the bicycle-style ones, and the features of each type are shown in Figure 3 [30].

(a) (b)

Figure 3: (a) Bicycle-style e-bike. (b) Scooter-style e-bike.

$$\mathbf{q}_j = \varphi_j\left(\mathbf{X}_j\right). \tag{3}$$

The loss function was defined as

$$F(\mathbf{Q}, \mathbf{A}, \mathbf{B}) = n^{-1} \sum_{j}^{m} tr\left(\mathbf{q}_j \mathbf{a}_j^T - \mathbf{B}\right)^T \left(\mathbf{q}_j \mathbf{a}_j^T - \mathbf{B}\right), \tag{4}$$

where $\mathbf{Q}$ is the matrix of category quantifications. $\mathbf{A}$ is the $m \times p$ matrix of the component loadings where the j^{th} column is denoted by $\mathbf{a}_j$. $\mathbf{B}$ is the $n \times p$ matrix of object scores, which are the individuals on the principal component. tr is the trace function.

The score matrix $\mathbf{H}$ is replaced by the matrix $\mathbf{Q}$ that has the categorical variables into numerical values [23]. Then, the PCA analysis was conducted by software SAS 9.4 to replace the original corrected variables by uncorrelated principal components to regress the logistics model [21, 33, 34].

Two logistics models based on different methods (e.g., stepwise regression for the base logistics model and principle component analysis for the PCA logistics model) were employed to deal with multicollinearity. The results about e-bike riders' YLR behaviors were estimated and compared.

Furthermore, the Hosmer–Lemeshow test and some goodness-of-fit measure were used for model comparison.

3. Results

3.1. Descriptive Statistics. In 28 h high-resolution videos, a total of 396 valid clearing intersection behaviors in the yellow-light interval events were observed, among which 248 riders had yellow-light running behaviors. YLR riders were divided into different characteristic groups, as summarized in Table 3.

Table 3: Yellow-light running by each subcategory.

Intersection site	Number of YLR rider			
	W-H intersection	H-X intersection	T-K intersection	Total
Gender				
Male	62.6% (52/83)	75% (33/44)	85.4% (76/89)	74.5% (161/216)
Female	34.8% (24/69)	45.8% (11/24)	59.8% (52/87)	48.3% (87/180)
Age group				
Young	59% (36/61)	82.9% (29/35)	82.1% (55/67)	73.6% (120/163)
Middle-age	42.9% (21/49)	42.9% (12/28)	69.6% (64/92)	57.4% (97/169)
Old	45.2% (19/42)	60% (3/5)	52.9% (9/17)	48.4% (31/64)
Vehicle type				
Bicycle-style electric-bike	29.7% (19/64)	42.9% (12/28)	47.4% (36/76)	39.9% (67/168)
Scooter-style electric-bike	64.8% (57/88)	80% (32/40)	92% (92/100)	79.4% (181/228)
Overall	50% (76/152)	64.7% (44/68)	72.7% (128/176)	62.6% (248/396)

The overall proportion of riders who cross against yellow-light was 62.6%, and it varied with the intersections (from 50% to 72.7%). The majority of observed riders were male (216) and were aged under 50 years (332). Scooter-style e-bike accounted for more than 57% of the total vehicles in all intersections. The chi-square test was used to analyze the number of YLR behavior riders in different gender, age, and vehicle type groups. It was observed that male riders were prone to YLR behaviors (161 vs. 87, $p = 0.01$). In addition, riders who drove scooter-style e-bikes were more likely to go against yellow-light than bicycle-style e-bike riders (181 vs. 76, $p < 0.01$). A higher proportion of yellow-light runners were observed in young and middle-age riders than in old ones (73.6% and 57.4% vs. 48.4%); however, marginal difference can be observed from the result of the chi-square test for the number of YLR riders in the age group ($p = 0.167$).

Table 4 lists the vehicle's approaching speed and distance to the stop line extracted from the acquired trajectory data.

The data were tested by the Levene test ($F = 3.307$, $p < 0.05$) prior to Student's t-test. The result indicated that the mean approaching speed of YLR riders at the onset of yellow-light was 18.9 km, significantly higher than the non-YLR ones ($t = -5.248$, $p < 0.05$) Furthermore, the distance to the stop line was different between the YLR group and non-YRL group ($F = 8.814$, $p < 0.05$; $t = 4.02$, $p < 0.01$). The YLR riders were closer to the stop line than non-YLR riders (8.0 m vs. 14.9 m).

3.2. Characteristic Parameters Analysis of the YLR Behavior Model. In order to further study the correlation of each driver's own characteristics in different stages, the strength of a relationship between variables should be quantitatively measured. Pearson correlation coefficients were evaluated by continuous variables, and the categorical variables were estimated by Cramer's V coefficient by the chi-square test. The results are listed in Table 5.

AS and VT and GEN and VT had significant positive correlation with each other, the value of correlation coefficient reaching 0.767 and 0.612, respectively. The positive correlation coefficient illustrated that scooter-style e-bike riders had a higher approaching speed to clear the intersection at the onset of yellow-light and male riders were more likely to ride a scooter-style e-bike than bicycle-style. In addition, gender had a significantly positive influence on the approaching speed and the distance to the stop line ($r = 0.506$ and $r = 0.350$, respectively). That is to say, at the onset of yellow-light, in comparison with female riders, males rode faster and were closer to the stop line. The value of correlation coefficients between AS and AGE and AS and DTS were negative, reaching −0.495 and −0.05, respectively. The negative correlation between AS and these two parameters showed that the faster the approaching speed riders had, the younger they were, and that riders with faster approaching speed could be closer to the stop line. Furthermore, the DTS had slight negative correlation between WI and PB ($r = -0.266$, $r = -0.370$ respectively), which indicated that the riders were far away from the stop line at the onset of yellow-light when the crossing distance was longer or when there existed physical barriers separating the motorized vehicle lane and nonmotorized vehicle lane.

The variance inflation factory (VIF) was calculated to confirm multicollinearity among the explanatory variables in the following equation:

$$\mathrm{VIF}_i = 1 - \frac{1}{R_i^2}, \tag{5}$$

where R_i^2 is the model determination coefficient.

The results were as follows: VIF = [12.629, 11.396, 1.355, 1.540, 12.087, 1.637, 2.946]. Three VIF values were greater than 5 (12.629, 11.396, and 12.087), which indicated that the multicollinearity problem existed in explanatory variables.

3.3. Principle Component Analysis of Explanatory Variables. Principal component analysis was used to eliminate the multicollinearity problem of explanatory variables mentioned above. Four explanatory variables, physical barriers, gender, age group and vehicle type, are the categorical variables in this study. Therefore, we utilized CATPCA to transform categorical variables into continuous ones. The Kaiser–Meyer–Olkin (KMO) test was used to calculate the four transformed variables and three original variables, and the value of the test was 0.7 which suggested that the sample

Table 4: Descriptive statistical of operation parameters.

	Mean	Std. deviation	Minimum	Maximum	The 80th percentile of speed
AS of YLR vehicle (km/h)	18.9	7.6	6.0	36.8	25.7
AS of Non-YLR vehicle (km/h)	11.3	5.9	1.7	24.9	15.8
DTS of YLR vehicle (m)	8.0	7.0	−0.468	33.2	13.5
DTS of Non-YLR vehicle (m)	14.9	9.9	−5.4	38.2	23.8

Table 5: Correlation coefficient matrix.

	AS	DTS	WI	PB	GEN	AGE	VT
AS	1						
DTS	−0.05*	1					
WI	0.029	−0.266**	1				
PB	0.156	−0.370**	0.491**	1			
GEN	0.506**	0.350**	0.60	0.007	1		
AGE	−0.495**	−0.148	0.051	0.138	0.549**	1	
VT	0.767**	0.109	0.05	0.056	0.612**	0.503**	1

*Correlation is significant at the 0.05 level (2-tailed). **Correlation is significant at the 0.01 level (2-tailed).

data met the requirements for PCA. Then, seven variables were subjected to PCA. A two-factor structure was identified which explained 65.435% of the total variance (Cattell's scree plot presented in Figure 4). Table 6 shows the results of component score coefficient by PCA with the Varimax rotation method.

The object scores corresponding to each observed variable on the components were achieved in the following equations:

$$\text{factor}_1 = 0.306\text{AS} + 0.065\text{DTS} + 0.015\text{WI} + 0.069\text{PB} + 0.288\text{GEN} - 0.274\text{AGE} + 0.316\text{VT}, \quad (6)$$

$$\text{factor}_2 = 0.087\text{AS} - 0.385\text{DTS} + 0.420\text{WI} + 0.460\text{PB} - 0.103\text{GEN} - 0.004\text{AGE} + 0.017\text{VT}. \quad (7)$$

AS, GEN, AGE, and VT had a strong absolute value of lodging in factor_1 (loading values of 0.1 were used as a cutoff point), this means that there was a strong correlation between these explanatory variables and the factor_1. All the three variables related to cycling characteristics and individual characteristics of e-bike riders could define factor_1 as e-bike riders' characteristics. PB and WI had a positive projection on factor_2, and GEN had a negative projection on it. The value of GEN (−0.103) was excluded not only because it caused interpretation difficulties but also because of its small absolute value of loading compared with the loading values of PB and WI. The explanatory variables of PB and WI to factor_2 were related to characteristics of intersection.

3.4. Model Estimation. The two binomial logistics models of rides' yellow-light running behavior which was based on the field observation were established by the forward stepwise (likelihood ratio) and PCA methods, respectively.

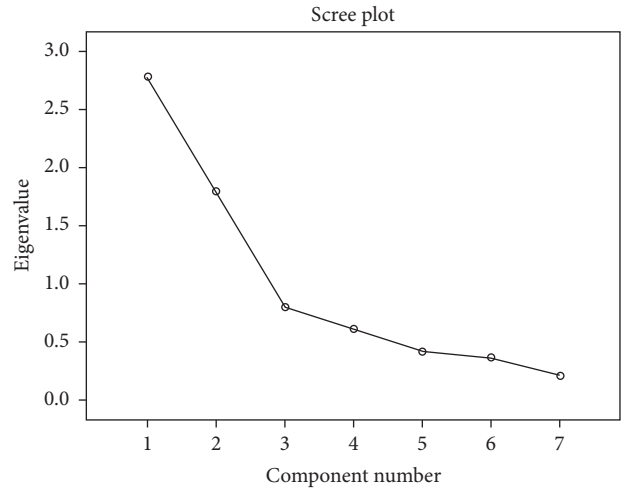

Figure 4: Cattell's scree plot.

3.4.1. Base Logistics Model. Based on the previous study, seven explanatory variables were selected to explore riders' yellow-light running behavior. Among those variables, only the estimated age group is a three-category variable. Two dummy variables and a consultative valuable were set for the base logistics model, which are shown in Table 7.

Through the forward stepwise (likelihood ratio) method, the yellow-light running behavior using the base logistics model was established. The result is reported in Table 8. Estimation step terminated at step[c] because the change in parameter estimations is less than 0.01.

The probability prediction of YLR behavior function was given by

$$p = \frac{\exp\ (-1.040 + 0.191\text{AS} - 0.2\text{DTS} + 1.826\text{GEN})}{1 + \exp\ (-1.040 + 0.191\text{AS} - 0.2\text{DTS} + 1.826\text{GEN})}. \quad (8)$$

The Hosmer–Lemeshow test and the value of prediction accuracy are summarized in Table 9, respectively, to access goodness of fit in the proposed model.

3.5. PCA Logistics Model. As mentioned earlier, we applied principle component analysis to eliminate the multicollinearity of explanatory variables. The result of the PCA logistics model, obtained from the output of the logistics model with the uncorrelated factors, is listed in Table 10. Hence, the PCA logistics model is given as follows:

$$\log it\ (p_{i=1}) = 0.704 + 1.027\ \text{factor}_1 + 0.868\ \text{factor}_2. \quad (9)$$

Table 6: Matrix of component loadings.

Variables	Component	
	$Factor_1$	$Factor_2$
Approaching speed at the onset of yellow-light (AS)	0.306	0.087
Distance to the stop line at the onset of yellow-light (DTS)	0.065	−0.385
The width of intersection (WI)	0.015	0.420
Physical barrier (PB)	0.069	0.460
Gender (GEN)	0.288	−0.103
Age (AGE)	−0.274	−0.004
Vehicle type (VT)	0.316	0.017

Table 7: Categorical variables coding.

Variable		Parameter coding	
		(1)	(2)
Estimated age	Age ≤30	1	0
	30< age ≤50	0	1
	Age >50	0	0

Table 8: Base logistics regression values of the predicting variables.

		β	SE	Wald	df	Sig.	Exp (β)	95% CI for exp (β)	
								Lower	Upper
Step[a]	AS	0.173	0.042	17.422	1	0.000	1.189	1.096	1.290
	Constant	−2.042	0.618	10.901	1	0.001	0.130		
Step[b]	AS	0.239	0.055	18.613	1	0.000	1.270	1.140	1.416
	DTS	−0.145	0.038	14.730	1	0.000	0.865	0.803	0.931
	Constant	−1.327	0.684	3.766	1	0.052	0.265		
Step[c]	AS	0.191	0.058	10.831	1	0.001	1.210	1.080	1.356
	DTS	−0.200	0.052	14.702	1	0.000	0.819	0.739	0.907
	GEN	1.826	0.860	4.511	1	0.034	6.212	1.151	33.511
	Constant	−1.040	0.695	2.242	1	0.134	0.353		

[a]Variables entered on step 1: AS, [b]variable(s) entered on step 2: DTS, and [c]variable(s) entered on step 3: GEN.

Substituting equations (6) and (7) into equation (8), the probability prediction of YLR behavior PCA logit function is given by

$$p = \frac{\exp\ (0.704 + 0.39\text{AS} - 0.267\text{DTS} + 0.38\text{WI} + 0.47\text{PB} + 0.206\text{GEN} - 0.285\text{AGE} + 0.339\text{VT})}{1 + \exp\ (0.704 + 0.39\text{AS} - 0.267\text{DTS} + 0.38\text{WI} + 0.47\text{PB} + 0.206\text{GEN} - 0.285\text{AGE} + 0.339\text{VT})}. \quad (10)$$

Table 9 summarizes the result of goodness of fit for the base logistics and PCA logistics models. Prediction accuracy of the PCA logistics model was 77.8%, and the value of chi-square calculated by the Hosmer–Lemeshow test was 5.72, while the two values of base model were 74.7% and 6.398, respectively.

4. Discussion

Electric bike is a critic transportation mode in China and other developing Asian countries, while it is involved in massive casualties at intersections. The objective of this study was to explore e-bike riders' behavior when facing the yellow-light interval. The results indicated that 62.6% (248/396) of e-bike riders arriving during the yellow-light period run against the traffic signal at intersection. This finding was higher than that of Bharat [16]. The difference in ratio of the number of yellow-light running behaviors may be caused by different collecting data time.

Two types of yellow-light running behavior analytical modelss for e-bike riders were developed, with different multicollinearity eliminating method (forward stepwise and PCA). Table 9 lists goodness-of-fit measures for the base logistics model and PCA logistics model, respectively. Results revealed that the principle component analysis model improved in overall fit as measured by the Hosmer–Lemeshow test and percentage correct compared to the base model. As shown in Table 9, the PCA logistics model's chi-square value was smaller than that of the base model's which indicated that the variance between model prediction and origin data was small ($p > 0.1$). In addition, the

Table 9: Goodness-of-fit statistics for logistics regression.

	Base logistics model	PCA logistics model
Hosmer–Lemeshow test		
Chi-square	6.398	5.720
df	8	8
Sig.	0.603	0.679
Percentage correct	74.7	77.8

Table 10: PCA logistics regression values of the predicting variables.

	β	SE	Wald	df	Sig.	Exp (β)	95% CI for exp (β)	
							Lower	Upper
$Factor_1$	1.027	0.272	14.209	1	0.000	2.791	1.637	4.760
$Factor_2$	0.868	0.268	10.456	1	0.001	2.382	1.408	4.032
Constant	0.704	0.251	7.850	1	0.002	2.021		

percentage correct also proved that the PCA logistics model was statistically superior, which had a higher percentage correct of 3.1%. The results suggested that stepwise regression could obtain an optimal combination of variables, but those combinations of variables may eliminate some variables due to the small interpretation which should not be omitted in the YLR behavior model. Therefore, the following analysis was mainly based on PCA logistics model.

4.1. Effect of e-Bike Riders' Operation Characteristics. The result of the PCA model indicated that the approaching speed had a significant positive impact on the YLR decision. The odds ratio was 1.477($e^{0.39}$) which suggested that the rider, who traveled 1 km/h faster than the other ones, was 1.477 times likely to do a go-decision against yellow-light signal. The result was consistent with the result in a motor vehicle observation study reported by Papaioannou [12]. One possible reason would be that the riders traveling in a fast approaching speed may think they can pass the stop line in the remanent yellow-light time and quickly cleared the intersection to avoid waiting for the next green light signal. Therefore, effectively lowering riders' approaching speed at the approach to the intersection may result in a significantly less YLR violation.

The effect of distance to the stop line (DTS) on the YLR violation was significantly negative (−0.276). The odds ratio value was 0.765 which indicated that the riders, who were 1 m farther than the others, was 0.765 times more liable to run against yellow-light, that was to say riders who are closer to the stop line at the onset of yellow-light will be more likely to cross the intersection than the one who was far away from the stop bar. The GHM model proposed by Gazis et al. proved that a smaller distance to the stop distance than the vehicle's minimum stopping line could lead to a rear-end accident [35]. Riders may feel they cannot safely stop before the stop line so that they prefer continuously running against the yellow-light. This result was in line with the previous study [16], proving that a shorter distance to the stop line reduced the likelihood of stopping in the yellow-light period. With respect to the appropriate measures aiming at improving the current situation, speed limit measure should urgently be carried out in e-bike vehicle and strict law enforcement related to riders violate in yellow-light signal should be considered.

4.2. Effect of e-Bike Riders' Characteristics. According to the model in equation (8), gender was found to be a significant variable to estimate the YLR behavior. Male riders had 1.299 times yellow-light running violation than female riders at signal intersection (the odds ratio = $e^{0.206}$), which meant that males had more propensity to running against yellow-light than females. Consistent result showed that the female drivers had lower rates of signal infringement than male drivers [36]. Also, Wu et al. analyzed information recorded by video cameras, which implied that males were more likely to cross the intersection in a risk-taking manner among 451 e-bikers and bicyclists [7]. The previous study conducted by Parker et al. found that males reacted with more inconsiderate driving and impatient driving than females when they faced impede progress such as the signal light changing into yellow-light or red-light [37], which may explain the gender difference in the yellow-light running behavior.

The estimated age group was found to be significant for prediction of the YLR behavior and had a negative effect on it. The young group had higher violation behaviors than middle-aged and old riders. This tied in with the findings of Chung and Wong [38] and Zamani-Alavijeh et al. [39] that compared to other drivers, the young driver was more likely to engage in risky driving behavior and involved in severe accidents. However, the result was not consistent with the result in which the age group failed to be a significant variable for predicting signal violation proposed by Wu et al. [7]. One possible reason was that researchers used the stepwise regression method in the logistics model, and the method of stepwise regression could obtain an optimal combination of variables, but this combination of variables may eliminate some variables due to the small interpretation.

It was clearly observed that the probability of YLR was influenced by the vehicle type. The running yellow-light probability of scooter-style e-bike riders was 1.4 times more than the running yellow-light probability of bicycle-style e-bike riders (the odds ratio = $e^{0.339}$). This conformity tendency was also reported in the study conducted by Bai et al. which indicated that compared to bicycle-style riders, e-scooter riders were more likely to show risky behavior [9]. This may be due to that the two types of e-bikes have great difference in power performance, among which the scooter style has a powerful engine to provide faster speed than the bicycle style. Scooter-style e-bike riders had the ability to clear the intersection with the strong power before the opposite vehicle came to the intersection.

In terms of the abovementioned views, much attention should be paid to road safety interventions for e-bike riders; the riders need to enforce safety attitudes to change the belief that they could safely clear the intersection with yellow-light running in a fast speed. In addition, the punishment should

be carried out in practice to avoid yellow-light running behavior so that riders would take YLR behavior as an illegal behavior rather than a normal riding behavior.

4.3. Effect of the Characteristics of Intersection. The width of intersection had a significant positive impact on the yellow-light running behavior. The odds ratio was 1.462 ($e^{0.38}$) which suggested that 1 m longer width may result in the rider having 1.462 times to go against the yellow-light signal. One possible reason was that the gap in the cross traffic is larger in a big intersection than that in a small one; therefore, riders consider that they may have a chance to safely cross the intersection in an enough gap.

The probability of riders running against yellow-light in an intersection with physical barriers was 1.6 times higher than in intersections without physical barriers (the odds ratio = $e^{0.47}$). One possible explanation was that the existence of a barrier between motorized vehicle lane and nonmotorized vehicle lane might increase speed among riders due to the separation from motorized traffic; thus, riders may run against the yellow-light in fast speed.

4.4. Limitation. There are several limitations in the present study. First, the data collection in this study is performed in a single city and in the four-leg intersection which may not be representative of Chinese complicated intersection environments. More data should be collected at multiple intersections in other cities to validate the findings in further study. Second, the various types of traffic light devices and phase of traffic light may impact e-bike riders' behavior, which were not considered in present research. Future research studies including traffic light devices and phase are required to better understand how these variables influence the YLR behavior. Third, the current study focused on individual e-bike rider's yellow-light running behavior while ignoring the impacts of platoons. E-bike riders' yellow-light running behavior could be affected by the behaviors of other people, and future research is required to take these effects into consideration.

5. Conclusion

This study sought to examine the effects of factors on e-bike riders' yellow-light running behavior. 396 samples were collected using field observation in Xi'an, China, for model development. Except for riders' attributes, the type of e-bikes, operation characteristics related to approaching speed, distance to stop line, and characteristics of intersection including the width of intersection and the existence of physical barriers are also considered as explanatory variables. Given that riders have two choices either to pass or to stop at the intersection when facing the yellow-light, two logistics regression models, PCA logistics model and base logistics model, have been developed to explain this behavior.

The empirical analysis revealed a number of findings. First, results of the PCA logistics model showed that seven factors had significant effect on YLR behavior, while results of the base logistics model showed that just two factors significantly affected YLR violation. The comparison between the results of two established models revealed that omission of effective variables would result in lower prediction accuracy of the model and misunderstanding in riders' YLR behavior. Second, the characteristics of operation were found to have effect on e-bike riders YLR behavior. It was observed that the probability of stopping decreased with the increase in the approaching speed of the e-bike and riders' stopping probability decreased with the increase in their distance from the stop line when green traffic light çhanged to yellow. Third, e-bike riders' attributes were important factors affecting YLR behaviors. Female riders demonstrated a more obedient behavior to signals than male riders. Riders in the old age group were more likely to stop at the onset of yellow-light compared to other age groups. Also, scooter-style e-bike riders were less likely to stop at the intersection. Last but not the least, e-bike riders' violation behavior was affected by the intersection characteristics. The existence of physical barrier decreased the riders' stopping probability. And an intersection with a shorter crossing distance may increase the stopping probability of e-bike riders.

Based on the findings of this study, some countermeasures to improve e-bike riders' yellow-light running violation should be adopted. Adjustment of the signal time may be necessary to reflect the e-bike operation characteristics. In addition, YLR infringement education must be given repeatedly in a rider's daily life. Moreover, a license system should be required to e-bike riders; thus, penalization for those YLR riders can link YLR violation with their individual credits under a stricter enforcement at intersection. Improvements for the existing road infrastructure as well as some other countermeasures are required for crossing safety of e-bike riders.

Data Availability

The data used to support the findings of this study have not been made available because we have no right to share it.

Conflicts of Interest

The authors declare that there are no conflicts of interest with respect to the research, authorship and/or publication of this article.

Acknowledgments

This work was jointly supported by the National Key R & D Plan of China (No. 2018YFC0807500), the National Nature Science Foundation of China (No. 51878066), and Funds for Central Universities and Colleges of Chang'an University (No. 300102229201).

References

[1] Chinese Electric Vehicle News, "Six strategies to improve the management of e-bikes in China," 2018, https://news.ddc.net.cn/newsview_76563.html.

[2] S. Das and A. K. Maurya, "Modelling of motorised two-wheelers: a review of the literature," *Transport Reviews*, vol. 38, no. 2, pp. 209–231, 2018.
[3] China News, "Electric bikes increased by 250 million in China," 2018, http://www.chinanews.com/cj/2018/10-28/8661930.shtml.
[4] D. Shinar, "Safety and mobility of vulnerable road users: pedestrians, bicyclists, and motorcyclists," *Accident Analysis & Prevention*, vol. 44, no. 1, p. 2, 2012.
[5] Traffic Administration Bureau of the Ministry of Public Security of China, *China Road Traffic Accidents Statistics Report*, Traffic Management Research Institute of the Ministry of Public Security, Beijing, China, 2015.
[6] Z. Wang, R. L. Neitzel, X. Xue, W. Zheng, and G. Jiang, "Awareness, riding behaviors, and legislative attitudes toward electric bikes among two types of road users: an investigation in Tianjin, a municipality in China," *Traffic Injury Prevention*, vol. 20, no. 1, pp. 72–78, 2019.
[7] C. Wu, L. Yao, and K. Zhang, "The red-light running behavior of electric bike riders and cyclists at urban intersections in China: an observational study," *Accident Analysis & Prevention*, vol. 49, pp. 186–192, 2012.
[8] Y. Zhang and C. Wu, "The effects of sunshields on red light running behavior of cyclists and electric bike riders," *Accident Analysis & Prevention*, vol. 52, pp. 210–218, 2013.
[9] L. Bai, P. Liu, Y. Guo, and H. Yu, "Comparative analysis of risky behaviors of electric bicycles at signalized intersections," *Traffic Injury Prevention*, vol. 16, no. 4, pp. 424–428, 2015.
[10] F. Yan, B. Li, W. Zhang, and G. Hu, "Red-light running rates at five intersections by road user in Changsha, China: an observational study," *Accident Analysis & Prevention*, vol. 95, pp. 381–386, 2016.
[11] R. Yu, H. Zhao, C. Zhang, and Z. Wang, "Analysis of risk-taking behaviors of electric bicycle riders in response to pedestrian countdown signal devices," *Traffic Injury Prevention*, vol. 20, no. 2, pp. 182–188, 2019.
[12] P. Papaioannou, "Driver behaviour, dilemma zone and safety effects at urban signalised intersections in greece," *Accident Analysis & Prevention*, vol. 39, no. 1, pp. 147–158, 2007.
[13] H. Rakha, I. El-Shawarby, and J. R. Setti, "Characterizing driver behavior on signalized intersection approaches at the onset of a yellow-phase trigger," *IEEE Transactions on Intelligent Transportation Systems*, vol. 8, no. 4, pp. 630–640, 2007.
[14] M. M. Haque, A. D. Ohlhauser, S. Washington, and L. N. Boyle, "Decisions and actions of distracted drivers at the onset of yellow lights," *Accident Analysis & Prevention*, vol. 96, pp. 290–299, 2016.
[15] H. Köll, M. Bader, and K. W. Axhausen, "Driver behaviour during flashing green before amber: a comparative study," *Accident Analysis & Prevention*, vol. 36, no. 2, pp. 273–280, 2004.
[16] B. K. Pathivada and V. Perumal, "Analyzing dilemma driver behavior at signalized intersection under mixed traffic conditions," *Transportation Research Part F: Traffic Psychology and Behaviour*, vol. 60, pp. 111–120, 2019.
[17] D. S. Hurwitz, H. Wang, M. A. Knodler Jr., D. Ni, and D. Moore, "Fuzzy sets to describe driver behavior in the dilemma zone of high-speed signalized intersections," *Transportation Research Part F: Traffic Psychology and Behaviour*, vol. 15, no. 2, pp. 132–143, 2012.
[18] Y. X. Ding, "A comparitive analysis of stop/go driving behavior during the amber light at city signalized intersecdtions," *Applied Mechanics and Materials*, vol. 744-746, pp. 2045–2048, 2015.
[19] N. Elmitiny, X. Yan, E. Radwan, C. Russo, and D. Nashar, "Classification analysis of driver's stop/go decision and red-light running violation," *Accident Analysis & Prevention*, vol. 42, no. 1, pp. 101–111, 2010.
[20] K. Tang, Y. Xu, F. Wang, and T. Oguchi, "Exploring stop-go decision zones at rural high-speed intersections with flashing green signal and insufficient yellow time in China," *Accident Analysis & Prevention*, vol. 95, pp. 470–478, 2016.
[21] B. D. Marx and E. P. Smith, "Principal component estimation for generalized linear regression," *Biometrika*, vol. 77, no. 1, pp. 23–31, 1990.
[22] L. P. Qu, W. Yang, M. Sun, and W. X. Zheng, "Research on the main controlling index of deep seam mining damage index based on comprehensive principal-component analysis," *Safety in Coal Mines*, vol. 44, no. 1, pp. 203–207, 2013.
[23] G. Kemalbay and Ö. B. Korkmazoğlu, "Categorical principal component logistic regression: a case study for housing loan approval," *Procedia-Social and Behavioral Sciences*, vol. 109, pp. 730–736, 2014.
[24] H. Li and J. Sun, "Empirical research of hybridizing principal component analysis with multivariate discriminant analysis and logistic regression for business failure prediction," *Expert Systems with Applications*, vol. 38, no. 5, pp. 6244–6253, 2011.
[25] San Qin News, "The new national standard publicity and standardized management of electric bike industry conference was held in Xi'an," 2019, http://www.sanqin.com/2019/0412/415656.shtml.
[26] A. Najmi, A.-A. Choupani, and I. Aghayan, "Characterizing driver behavior in dilemma zones at signalized roundabouts," *Transportation Research Part F: Traffic Psychology and Behaviour*, vol. 63, pp. 204–215, 2019.
[27] G. Salvo, L. Caruso, and A. Scordo, "Urban traffic analysis through an UAV," *Procedia-Social and Behavioral Sciences*, vol. 111, pp. 1083–1091, 2014.
[28] G. Salvo, L. Caruso, and A. Scordo, "Gap acceptance analysis in an urban intersection through a video acquired by an UAV," *Recent Advances in Civil Engineering and Mechanics*, pp. 199–205, 2014.
[29] M. Khan, W. Ectors, T. Bellemans, D. Janssens, and G. Wets, "Unmanned aerial vehicle-based traffic analysis: a case study for shockwave identification and flow parameters estimation at signalized intersections," *Remote Sensing*, vol. 10, no. 3, pp. 458–474, 2018.
[30] E. Fishman and C. Cherry, "E-bikes in the mainstream: reviewing a decade of research," *Transport Reviews*, vol. 36, no. 1, pp. 72–91, 2015.
[31] J. Liu, J. Li, K. Wang, J. Y. Zhao, H. Cong, and P. He, "Exploring factors affecting the severity of night-time vehicle accidents under low illumination conditions," *Advances in Mechanical Engineering*, vol. 11, no. 4, p. 9, 2019.
[32] M. Linting and A. van der Kooij, "Nonlinear principal components analysis with CATPCA: a tutorial," *Journal of Personality Assessment*, vol. 94, no. 1, pp. 12–25, 2012.
[33] A. M. Aguilera, M. Escabias, and M. J. Valderrama, "Using principal components for estimating logistic regression with high-dimensional multicollinear data," *Computational Statistics & Data Analysis*, vol. 50, no. 8, pp. 1905–1924, 2006.
[34] I. Camminatie and A. Lucadamo, "Estimating multinomial logit model with multicollinear data," *Asian Journal of Mathematics & Statistics*, vol. 3, no. 2, pp. 93–101, 2010.

[35] D. Gazis, R. Herman, and A. Maradudin, "The problem of the amber signal light in traffic flow," *Operations Research*, vol. 8, no. 1, pp. 112–132, 1960.

[36] X. Yang, M. Huan, M. Abdel-Aty, Y. Peng, and Z. Gao, "A hazard-based duration model for analyzing crossing behavior of cyclists and electric bike riders at signalized intersections," *Accident Analysis & Prevention*, vol. 74, pp. 33–41, 2015.

[37] D. Parker, T. Lajunen, and H. Summala, "Anger and aggression among drivers in three European countries," *Accident Analysis & Prevention*, vol. 34, no. 2, pp. 229–235, 2002.

[38] Y.-S. Chung and J.-T. Wong, "Beyond general behavioral theories: structural discrepancy in young motorcyclist's risky driving behavior and its policy implications," *Accident Analysis & Prevention*, vol. 49, pp. 165–176, 2012.

[39] F. Zamani-Alavijeh, S. Niknami, M. Bazargan et al., "Risk-taking behaviors among motorcyclists in middle east countries: a case of Islamic Republic of Iran," *Traffic Injury Prevention*, vol. 11, no. 1, pp. 25–34, 2010.

Hindawi
Journal of Advanced Transportation
Volume 2020, Article ID 1250827, 13 pages
https://doi.org/10.1155/2020/1250827

Research Article

A Comparative Study on Drivers' Stop/Go Behavior at Signalized Intersections Based on Decision Tree Classification Model

Sheng Dong[1] **and Jibiao Zhou**[2,3]

[1]*School of Civil and Transportation Engineering, Ningbo University of Technology, Fenghua Rd. #201, Jiangbei District, Ningbo, Zhejiang 315211, China*
[2]*Department of Transportation Engineering, Tongji University, Caoan Rd. #4800, Shanghai 201804, China*
[3]*Intelligent Transport System (ITS) R&D Center, Shanghai Urban Construction Design and Research Institute (Group) Co., Ltd., Shanghai 200082, China*

Correspondence should be addressed to Jibiao Zhou; zhoujibiao@tongji.edu.cn

Received 27 December 2019; Revised 3 February 2020; Accepted 12 May 2020; Published 29 May 2020

Academic Editor: Qiang Zeng

The stop/go decisions at signalized intersections are closely related to driving speed during signal change intervals. The speed during stop/go decision-making has a significant influence on the dilemma area, resulting in changes of stop/go decisions and high complexity of the decision-making process. Considering that traffic delays and vehicle exhaust pollution are mainly caused by queuing at intersections, the stop-line passing speed during the signal change interval will affect both vehicle operation safety and the atmospheric environment. This paper presents a comparative study on drivers' stop/go behaviors when facing a transition signal period consisting of 3 s green flashing light (FG) and 3 s yellow light (Y) at rural high-speed intersections and urban intersections. For this study, 1,459 high-quality vehicle trajectories of five intersections in Shanghai during the transition signal period were collected. Of these five intersections, three are high-speed intersections with a speed limit of 80 km/h, and the other two are urban intersections with a speed limit of 50 km/h. Trajectory data of these vehicle samples were statistically analyzed to investigate the general characteristics of potential influencing factors, including the instantaneous speed and the distance to the intersection at the start of FG, the vehicle type, and so on. Decision Tree Classification (DTC) models are developed to reveal the relationship between the drivers' stop/go decisions and these possible influencing factors. The results indicate that the instantaneous speed of FG onset, the distance to the intersection at the start of FG, and the vehicle type are the most important predictors for both types of intersections. Besides, a DTC model can offer a simple way of modeling drivers' stopping decision behavior and produce good results for urban intersections.

1. Introduction

At signalized intersections in most cities of China, a 3 s green flashlight (FG) indicator and a 3 s yellow light (Y) indicator are the most common form of transition signal setting [1–3]. The current practice shows that it is reasonable to set the yellow light as 3 s for the intersection with a speed limit of less than 50 km/h. Once the speed limit is higher than 50 km/h, the vehicle will often fall into the dilemma zone (DZ) due to the higher driving speed and insufficient yellow light duration [4–8]. In most Chinese cities, the speed limit of high-speed intersections in rural areas is generally larger than 60 km/h. In comparison, in urban areas, the speed limit of high-speed intersections is usually smaller than 60 km/h. Thus, for the above two intersections with different areas, the setting of green flashlight (FG) can impose other effects on the stop/go decision-making behavior of drivers.

Tremendous research efforts have done to study the influence of FG on drivers' decision-making behaviors as well as to model such behaviors in response to signal change intervals. However, few studies have compared the impact of FG on the driver decision-making process at different types of intersections. Furthermore, there is no study on the specific combination of 3-second yellow light (Y) and 3-second green flashlight (FG). This kind of signal combination is a unique feature of signalized intersections in

Table 1: Characteristics and conditions of the investigated intersections.

Intersections	Cao'an Rd. and Jiasongbei Rd.	Cao'an Rd. and Xiangjiang Rd.	Cao'an Rd. and Caofeng Rd.	Siping Rd. and Dalian Rd.	Rende Rd. and Jipu Rd.
Speed limit	80 km/h			50 km/h	
Observed approaches	East-bound	East-bound	West-bound and east-bound	East-bound	North-bound
Lane layout	L-T-T-T-R	L-T-T-T-R	L-T-T-T-R	L-L-T-TR	L-TR
Size	72 m	72 m	48 m	64 m	40 m
Cycle length	161 s	160 s	104 s	200 s	86 s
Number of phases	4	4	3	4	2
Green time	38 s	45 s	45 s	77 s	45 s
FG	3 s	3 s	3 s	3 s	3 s
Y	3 s	3 s	3 s	3 s	3 s
All-red time	1 s	1 s	1 s	2 s	1 s
First-to-go vehicles (Passenger cars/ trucks)	201 (156/45)	153 (119/34)	303 (203/100)	112 (103/9)	33 (28/5)
Last-to-stop vehicles (Passenger cars/ trucks)	156 (111/45)	101 (77/24)	272 (175/97)	75 (68/7)	53 (37/16)

Note: L = exclusive left-turn lane; T = through-ahead lane; R = exclusive right-turn lane; TR = shared through and right-turn lane.

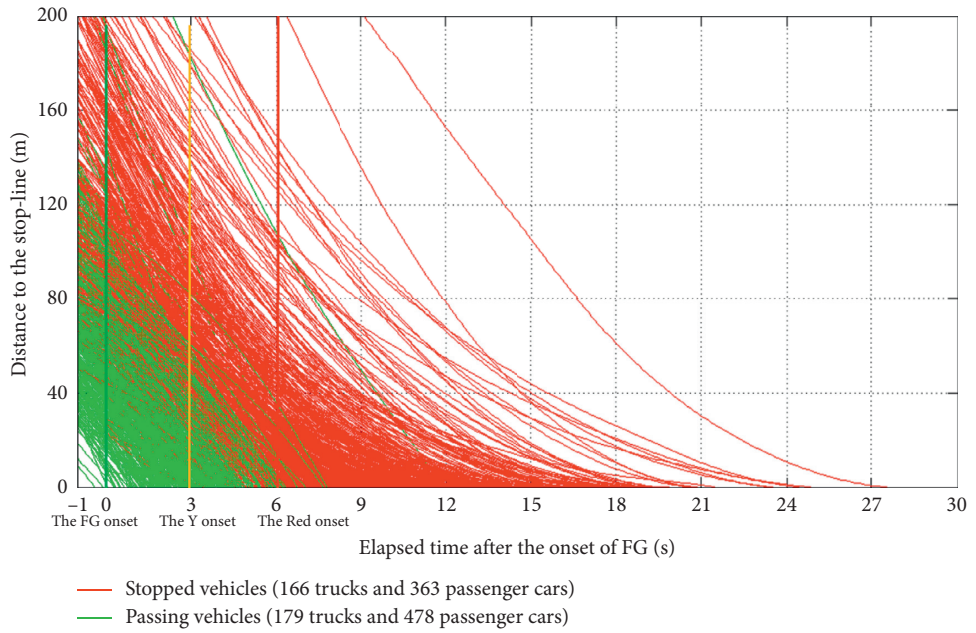

(a)

Figure 1: Continued.

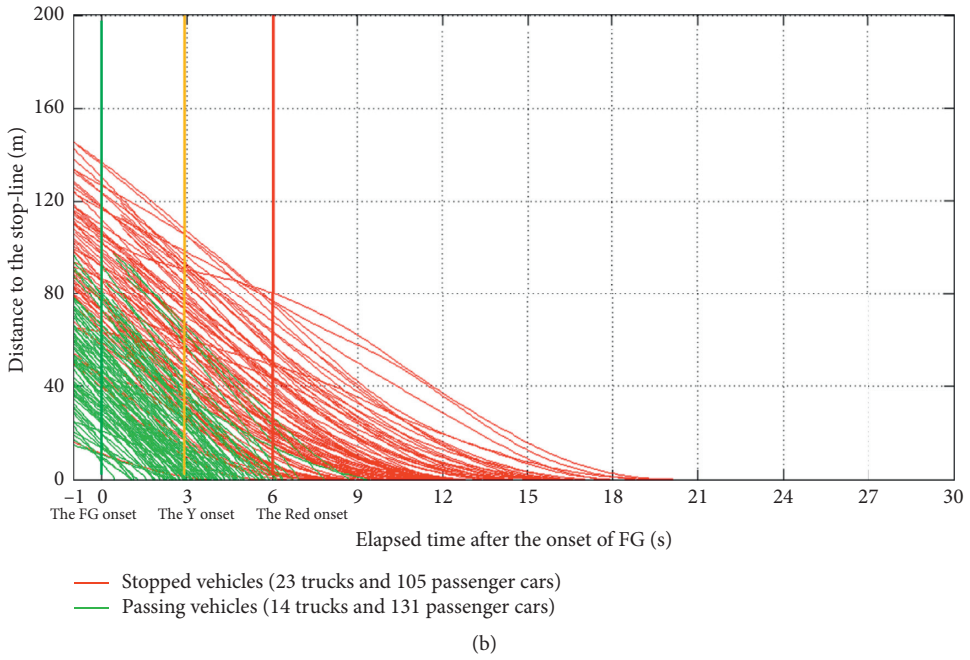

(b)

Figure 1: Vehicle trajectory data of the investigated intersections. (a) Rural intersections (the speed limit is 80 km/h) and (b) urban intersections (the speed limit is 50 km/h).

Table 2: Descriptive statistics for instantaneous speed at the onset of FG (unit: km/h).

Intersection types	Sublevel	Sublevel	Sample size	Mean	Std. dev	Min	Max
Rural intersections	Stop	Passenger cars	363	61.8	19.1	16.7	118.9
		Trucks	166	53.8	17.4	21.7	115.6
		Overall	529	59.3	18.9	16.7	118.9
	Go	Passenger cars	478	64.5	16.7	19.4	115
		Trucks	179	56.1	15.6	5.6	100.6
		Overall	657	62.2	16.8	5.6	115
Urban intersections	Stop	Passenger cars	105	39.2	8.9	16.4	64.5
		Trucks	23	38.9	8.1	23.3	56.2
		Overall	128	39.2	8.7	16.4	64.5
	Go	Passenger cars	131	45.4	10.3	15.2	68
		Trucks	14	46.6	8.7	21.4	57.2
		Overall	145	45.5	10.2	15.2	68

China. It provides a long time for the observation and determination of the driver before stop/go decision-making, i.e., 6 s. Therefore, this paper mainly focuses on the research gap.

In this study, the Decision Tree Classification (DTC) models are applied to analyze how drivers' stop decisions relate to potential influencing factors for two different types of intersections. Firstly, vehicle trajectory data, reflecting stop/go decision behavior of five intersections, are collected during the signal change interval. Three of which are high-speed intersections with a speed limit of 80 km/h in the rural area, and two of which are intersections with a speed limit of 50 km/h in the urban area. Secondly, we use these trajectory data, and we also carried out statistical analysis to summarize the general characteristics of the potential influencing factors of the two types of the intersection, including instantaneous speed, the vehicle type, and the distance to the intersection at the beginning of FG signal. Thirdly, the DTC model is built based on the description of the critical design decisions and parameters. Next, the results of the DTC model and the discussion of findings are given accordingly. Finally, we summarize the findings of the study, point out the contribution of this study, and suggest future directions of related research.

2. Literature Review

Many previous achievements have focused on the influence of FG on the driver's decision behavior and DZ. There are both positive and negative conclusions about the effect of FG in these kinds of literature studies. The positive results show that FG can warn the driver that the phase of green light is

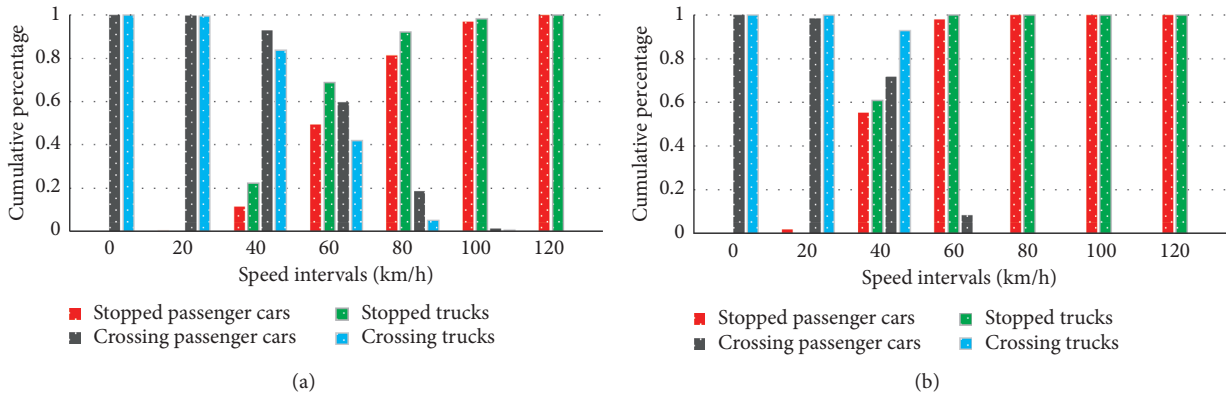

Figure 2: Stop/go decision distribution based on speed intervals. (a) Rural intersections and (b) urban intersections.

Table 3: Descriptive statistics for distance to the intersection at the beginning of FG (unit: m).

Intersection types	Sublevel	Sublevel	#	Mean	Std. dev	Min	Max
Rural intersections	Stop	Passenger cars	363	105.9	37.6	23.1	217.7
		Trucks	166	102.5	36.5	23.6	197.5
		Overall	529	104.8	37.2	23.1	217.7
	Go	Passenger cars	478	56.4	26.4	3.2	132.9
		Trucks	179	49.3	26.5	5.2	132.9
		Overall	657	54.5	26.6	3.2	132.9
Urban intersections	Stop	Passenger cars	105	95.7	24.9	39.8	163.1
		Trucks	23	96.7	35.5	40.4	155.6
		Overall	128	95.8	26.9	39.8	163.1
	Go	Passenger cars	131	46.2	19.5	7.5	95.2
		Trucks	14	60.3	23.3	16.7	97.7
		Overall	145	47.6	20.2	7.5	97.7

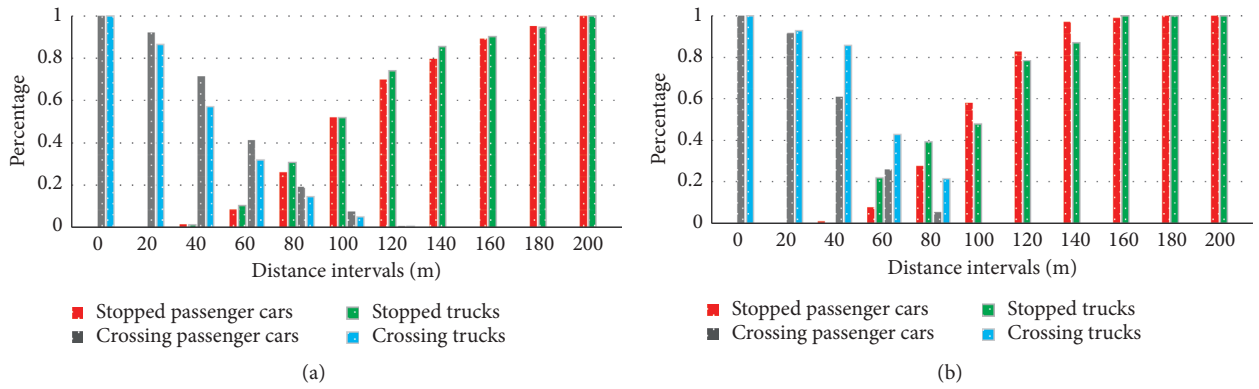

Figure 3: Distributions of stop/go decisions for distance interval from intersections. (a) Rural intersections and (b) urban intersections.

coming to an end, and the driver can reduce the incidence of DZ by reducing the driving speed, to avoid red light violations [1, 2, 9]. FG signal essentially plays a role in prolonging the duration of yellow light. Therefore, compared with the intersections without FG, the proportion of drivers running the red light at the intersections with FG is significantly reduced [10–13]. Among the negative aspects, it showed that FG could cause a significant increase in the proportion of stop decisions [10, 11, 14]. Besides, although FG can effectively reduce the DZ range caused by the yellow light, it enlarges the indecision zone and enormously increases the number of conservative stops and slightly encouraging aggressive passes slightly [13, 15]. Meanwhile, the presentation of an FG indicator before the Y indicator considered increasing the complexity of the driver's stop/go decision, leading to repeated decision-making [15, 16].

Table 4: Analysis of variance table for speed and distance of FG onset.

Variables	Source	Sum of square	df	Mean square	F	Sig.
Speed	Stop/go	5816.2	1	5816.2	17.9	0.000
	Vehicle type	7172.9	1	7172.9	22.1	0.000
	Area type	78365.9	1	78365.9	283.8	0.000
	Time of the day	52384.1	1	52384.1	179.2	0.000
Distance	Stop/go	895878.7	1	895878.7	958.8	0.000
	Vehicle type	0.0	1	0.0	0.0	0.998
	Area type	10098.6	1	10098.6	6.5	0.011
	Time of the day	4374.2	1	4374.2	2.8	0.093

Table 5: Precision of models for rural intersections and urban intersections.

Models		Observed	Predicted		
			Stop	Go	Hit ratios (%)
Rural intersections	Training	Stop	213	49	81.30
		Go	47	287	85.90
		Total	43.60%	56.40%	**83.90**
	Test	Stop	199	68	74.50
		Go	49	274	84.80
		Total	42%	58%	**80.20**
Urban intersections	Training	Stop	61	7	89.70
		Go	2	76	97.40
		Total	43.20%	56.80%	**93.80**
	Test	Stop	52	8	86.70
		Go	7	60	89.60
		Total	46.50%	53.50%	**88.20**

Notably, most of the studies listed above focused on the comparative study of FG installation or not and DZ occurrence and/or stopping probability.

Meanwhile, numerous studies have focused on the modeling of driver's decision-making behavior at the end of the green light [17–20], the most typical of which is the GHM model proposed by Gazis, Herman, and Maraddin [21]. A basic assumption of the GHM model is that the driver decides whether to stop or pass the intersection according to the relationship between the maximum passing distance and the minimum stopping distance at the beginning of the yellow light. Several notable variants have also been reported in the literature [22–25]. The GHM model assumes that all drivers will choose to stop, if possible. But Olson and Rothery [26] found that the yellow light is often used as an extension of the green time phase in the decision-making process. Research conducted by May [27] showed that some drivers avoid DZ by accelerating or decelerating. The study of Liu et al. and Wei et al. [23, 28] showed that the theoretical hypothesis could lead to differences in driving behavior. In general, the primary defect of the GHM model is the lack of description of the randomness of driving behavior. Because of this disadvantage, some other researchers have attempted to explain DZ behavior through stochastic approaches [15, 29, 30].

Many studies [12, 16, 17, 23, 31–34] believe that the decision-making behavior of drivers is random and obeys a specific probability distribution. The stopping probability, which is described as a function of the speed of the vehicle, the distance to the intersection, or the travel time to the stop-line at the beginning of the yellow light, the type of vehicle, etc., is expressed as binary logit model or Bayesian model. Meanwhile, other researchers, such as Rakha et al. [35], Hurwitz et al. [36], Kuo et al. [37], and Moore et al. [38], used fuzzy logic theory to analyze decision-making behavior. It should further point out that the behavioral parameters closely related to decision-making behavior may vary due to the influence of location conditions, driver behavior characteristics, vehicle performance, etc. Also, various potential influencing factors are often related to each other. Some research studies [16, 29, 30, 39–41] carried out in recent years have found that the distribution of decision-making areas may be dynamic, rather than the certainty described by traditional theories.

3. Data Collection and Reduction

3.1. Site Descriptions. Five intersections in Shanghai were selected to collect the necessary data, which were a 3 s FG signal and a 3 s Y signal. These intersections are divided into two categories, one with a speed limit of 80 km/h and the other with a speed limit of 50 km/h. The former is mainly located on the roads connecting the urban area and the suburban area, such as Cao'an highway, etc., which has a large traffic flow and a high proportion of large trucks in peak hours. The latter is mainly located in the urban area, and the traffic composition is mostly cars. The main characteristics and conditions of the investigated intersections are shown in Table 1.

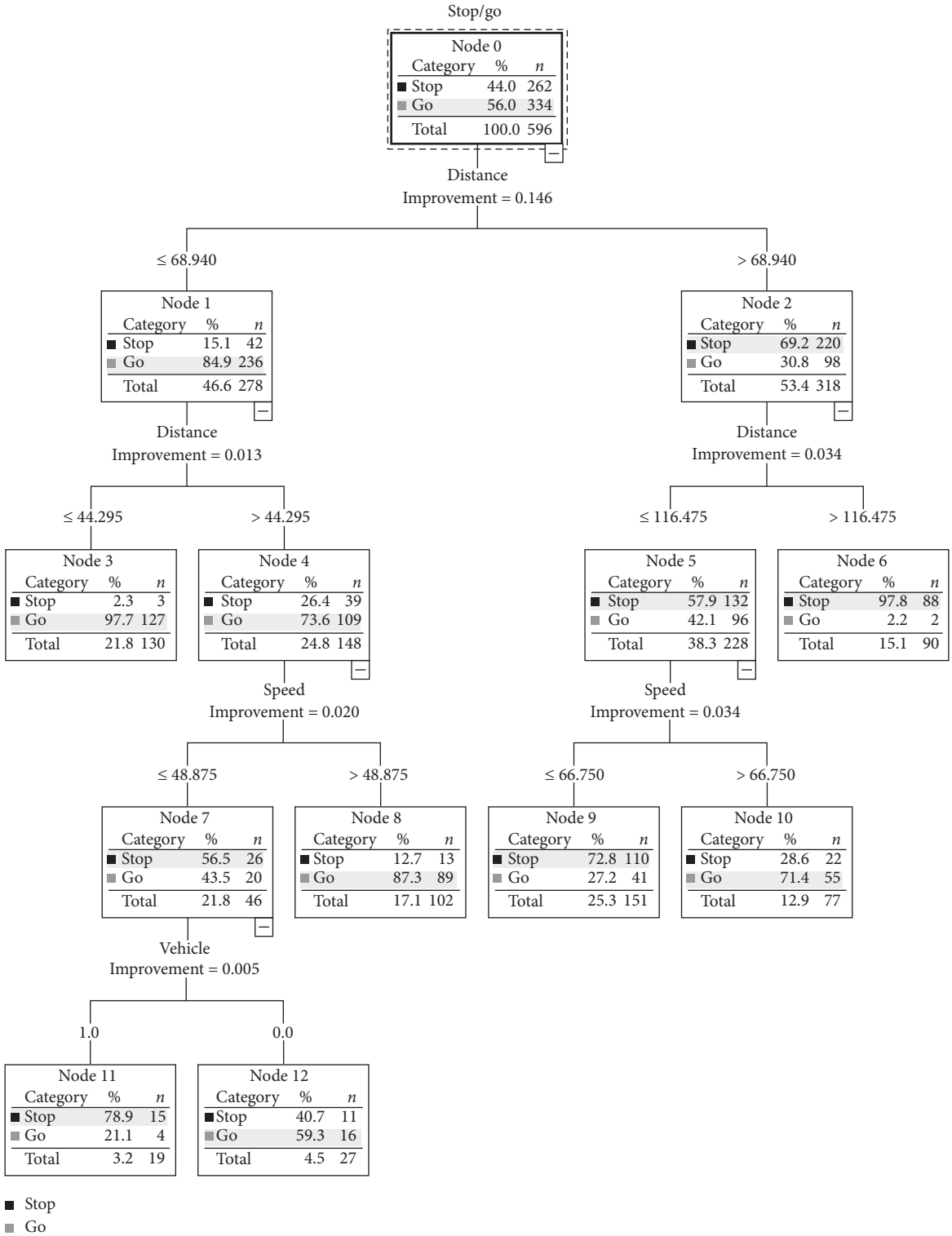

Figure 4: DTC analysis results for rural high-speed intersections (training model).

3.2. Field Surveys and Vehicle Trajectory Extraction. We select the sunny weekdays to carry out data collection, trajectory data of vehicles collected by video recording. Two high-definition cameras are required to record synchronously. One of the cameras is installed on the high building near the intersection, which can cover the 80 m long area upstream of the stop-line, to record the movement trajectory of the whole decision-making process. Another camera is set at the intersection to record traffic signals synchronously. The acquisition of travel trajectories relies on image processing software. It is located by the global coordinates of five related points in the shooting

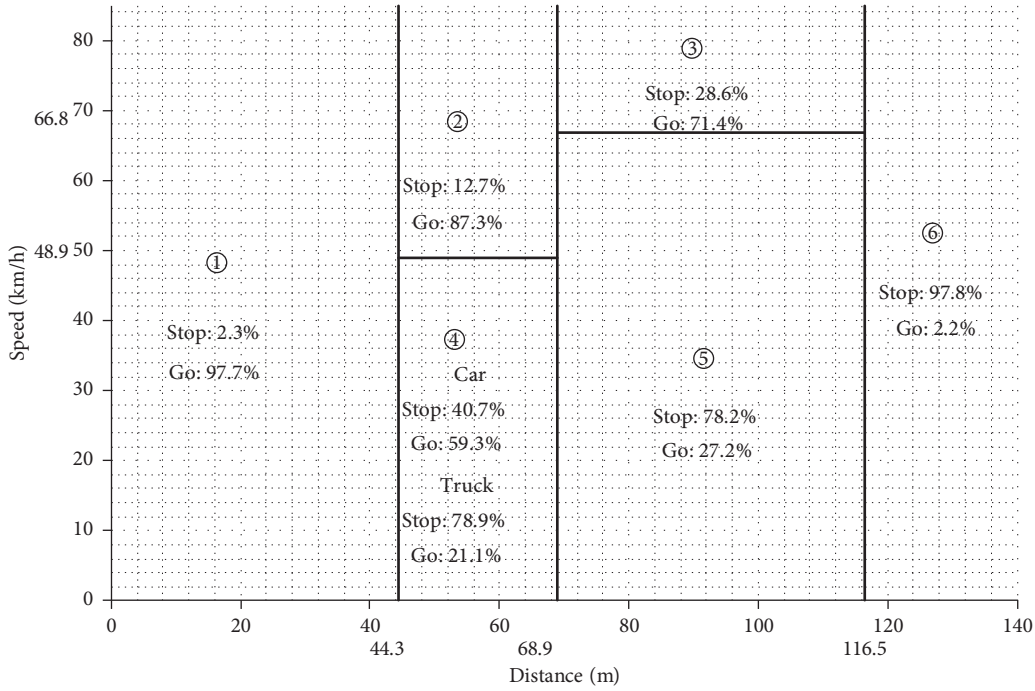

Figure 5: Partition for the stop/go decision model for rural high-speed intersections.

lens. Through residual analysis and *t*-test, it ensured that the accuracy error is not more than 0.15 m and 0.1 s. The time interval of the software-controlled is 0.1 s. Therefore, matching the trajectory data with the signal change timing, driving behavior parameters such as the speed, acceleration, and deceleration of vehicles, and the position of each step are obtained.

To avoid the influence of preceding vehicles, only the last-to-stop and first-to-go vehicles after the onset of FG are selected for analysis. The last-to-stop vehicle refers to the vehicle selected to stop in front of the stop-line before the start of the red light. The last means that the vehicle is the last vehicle to make a decision in the study period. The first-to-go vehicle refers to the first vehicle passing through the stop-line during the study period (i.e., from the end of green light time to the end of yellow light).

Eventually, the trajectories of 1,459 vehicles including 1,186 vehicles (345 trucks and 841 passenger cars) at the rural intersections and 273 vehicles (37 trucks and 236 passenger cars) at the urban intersections were obtained for use in subsequent statistical analysis and model development. As shown in Figure 1, the 1,186 vehicle trajectories collected at the rural intersections included the trajectories of 529 vehicles selected to stop and 657 vehicles selected to pass. In comparison, the 273 trajectories obtained from the urban intersections included the trajectories of 128 vehicles selected to stop and 145 vehicles selected to pass.

4. Statistical Analysis of Potential Influencing Factors

Past research has indicated that drivers' stopping decisions at signalized intersections may be influenced by the speed and distance to the stop-line immediately before the phase transition period as well as the vehicle type and time of day [14, 21, 22]. Therefore, statistical analysis was performed to explore the variability of these potential influencing factors as well as their relationships with stop/go decisions in response to the onset of FG.

4.1. Instantaneous Speed at the Start of FG. A statistical analysis of vehicles' instantaneous speeds at the observed approach lane at the start of FG is provided in Table 2. Comparisons between the rural and urban areas indicate that in both areas, the mean velocities of vehicles making go decisions are higher than those of vehicles making stop decisions. Besides, passenger cars typically have higher rates than trucks in both rural and urban areas. Figure 2 illustrates the distributions of the stop/go decisions relative to various FG-onset speed intervals in rural and urban areas. It finds that in a rural area, if the driver's speed is 60 km/h, the probabilities of stop and go decisions are equal. The same situation occurs in an urban area when the speed is 50 km/h, meaning that more truck drivers decide to stop than passenger car drivers given the same approach speed. In Figure 2(b), the situation is similar, with more truck drivers choosing to cross the intersection at a lower speed, which may be safer for large vehicles.

4.2. Distance to the Intersection at the Start of FG. Table 3 presents a statistical summary of distance to the intersection at the start of FG. It is found that the mean value of distance for crossing drivers is shorter than that for stopping drivers. Figure 3 illustrates the distributions of the stop/go decisions

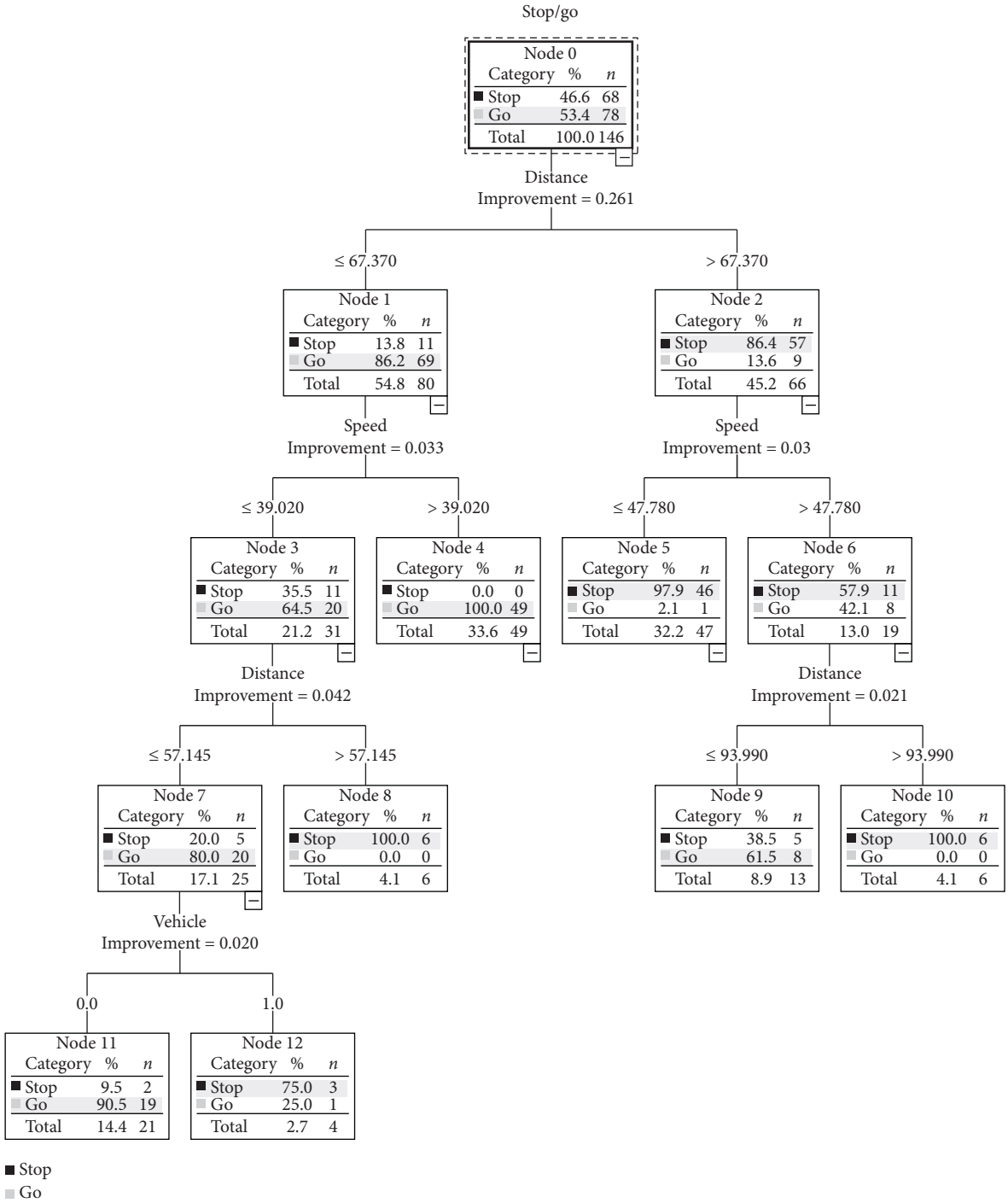

Figure 6: DTC analysis results for urban intersections (training model).

relative to various FG-onset distance intervals in rural and urban areas. This figure shows that it is more likely for a driver to make a go decision if he or she is farther from the stop-line, and vice versa. In rural areas, for drivers located in a distance interval of 60–100 m from the stop-line, the probability of stop decision or pass decision is close to 50%. The same situation is found for a distance interval of 60–80 m in urban areas. In these distance intervals, it is difficult for drivers to decide whether to stop or go. Moreover, among all drivers who make stop decisions, more truck drivers than passenger car drivers are inclined to stop when the distance to the intersection at the start of FG is shorter than 100 m.

4.3. Analysis of Variance of Potential Influencing Factors. Table 4 shows the analysis of variance (ANOVA) results for the speed and distance at FG onset, where this analysis is conducted to investigate the differences between every pair of factors. The ANOVA results show that multiple traffic factors,

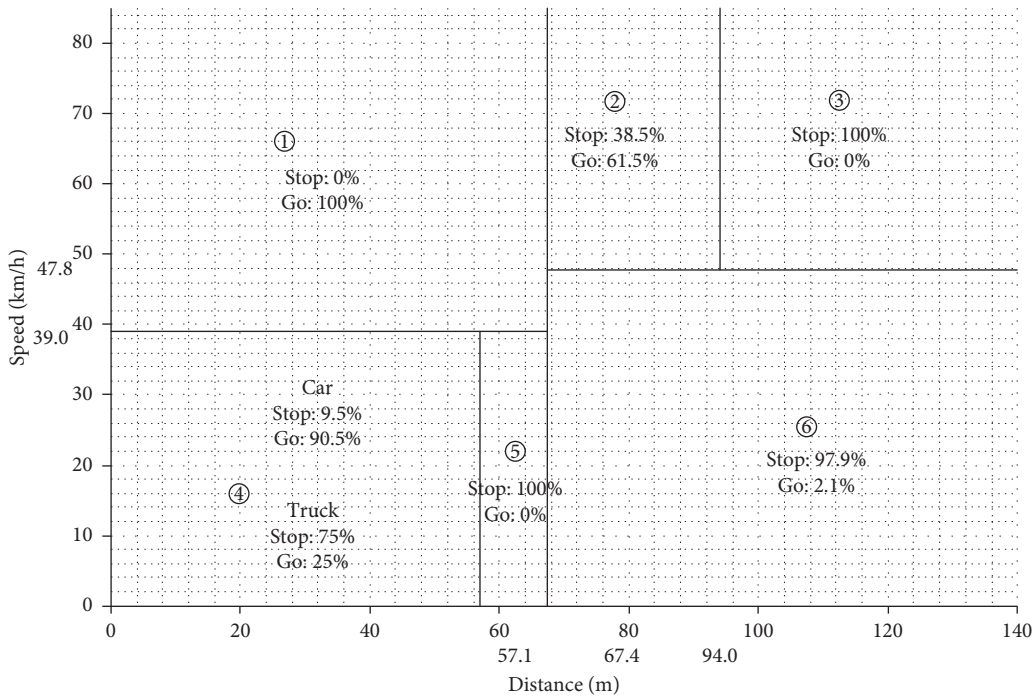

Figure 7: Partition for the stop/go decision model for urban intersections.

including stop/go decisions ($p < 0.01$), vehicle type ($p < 0.01$), and area type ($p < 0.01$), exhibit significant effects with respect to the approach speed of the vehicles at the onset of FG, but only the stop/go decisions ($p < 0.01$) exhibit significant effects with respect to the distance to the stop-line.

5. Development of Decision Tree Classification Models

5.1. Decision Tree Models. Because of its nonparametric nature and straightforward interpretation, DTC is proved in the field of traffic engineering [42]. For example, in the traffic safety evaluation, Abellán et al. [43] use DTC to analyze the relationship between stop/go decision, red light violation, and traffic parameters. Some researchers [44, 45] have used DTC methods to explore the relationship between the relevant traffic rules and accident severity.

In this study, the SPSS software package is used for the classification tree analysis. Based on the CART approach, a classification tree model was established, and the Gini criterion (or index) is used as the measure for splitting decisions. Because the data volume is not large, the minimum number of cases for the parent nodes was set to 30, and the minimum number of instances of the child nodes was set to 10. Besides, the cross-validation method (with ten folds) was used to evaluate how to extend the tree structure to a larger population. The three variables were expected to be closely related to the driver's stop/go decision, i.e., distance, speed, and vehicle type. The distance variable represents the distance from the vehicle to the stop-line at the start of FG, and the speed variable represents the vehicle's speed at the beginning of FG. Vehicle type variables are divided into two categories: passenger cars and trucks (0 = passenger cars and 1 = trucks).

Table 5 shows the precision of the two developed models. For the rural area model, the training and test accuracies are 83.9% and 80.2%, respectively, and the prediction of cross behavior is more accurate than that of stopping the behavior. For the urban area model, the training and test model accuracies are 93.8% and 88.2%, respectively. The model is correctly fitted.

5.2. Result Analysis at Rural High-Speed Intersections. Figure 4 shows the classification tree diagram used for training the stop/go decision model for rural areas.

Figure 5 shows the corresponding partitions, which are much finer-grained than those in Figure 4. When the distance to the stop-line is shorter than 44.3 m or more prolonged than 116.4 m, most of the vehicles make the same decision. When the distance is between 44.3 m and 116.4 m, the approach speed effects on the stop/go decision.

(i) For vehicles at FG-onset distances of less than 44.3 m, 97.7% of drivers will cross the intersection, as shown in Zone 1.

(ii) By contrast, for vehicles at FG-onset distances of more than116.5 m, the percentage of drivers that will cross the intersection is only 2.2%, whereas most drivers (97.8%) will stop, as shown in Zone 6.

(iii) For vehicles at FG-onset distances between 44.3 m and 68.9 m, the most critical factor affecting the drivers' stop/go decisions is speed. For vehicles with FG-onset rates higher than 48.9 km/h, most drivers (87.3%) will cross the intersection. By contrast, for vehicles with FG-onset speeds below than 48.9 km/h, the vehicle type plays an essential role in the stop/go

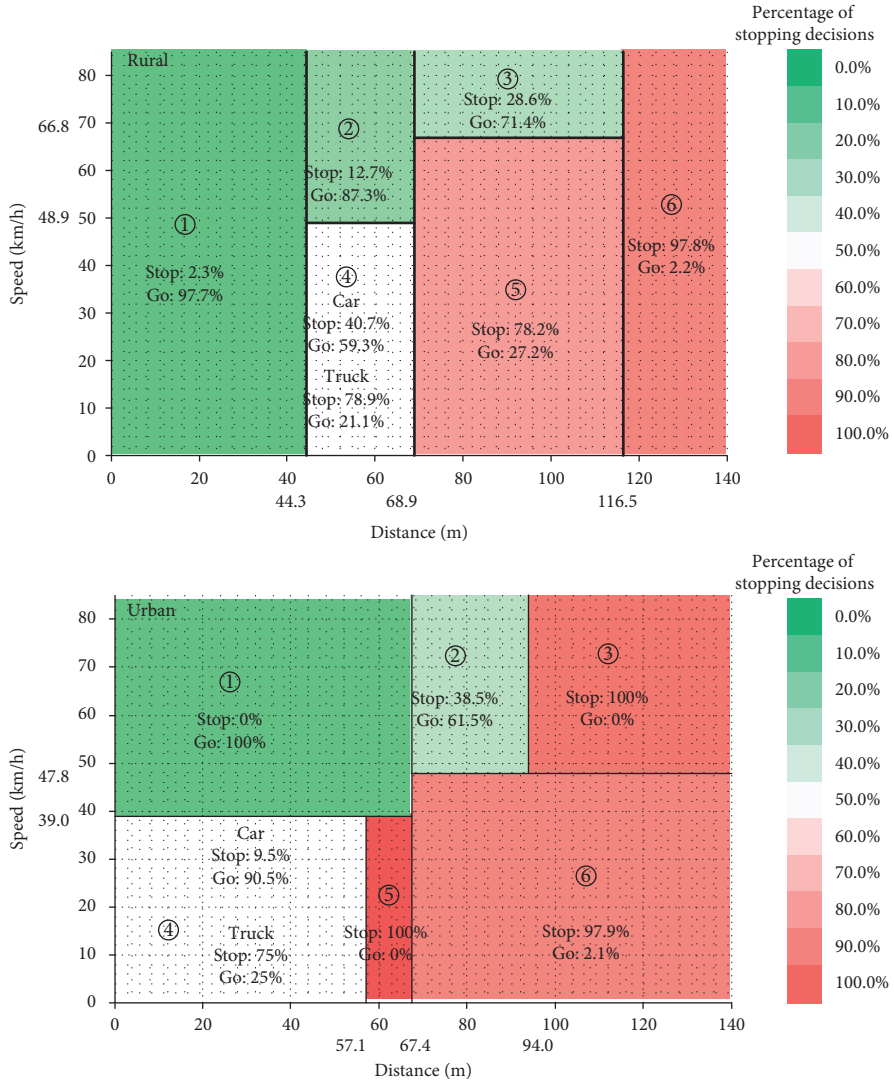

Figure 8: Comparison of the stop/go decision between rural and urban intersections.

decision. Trucks are more likely to stop than passenger cars. These behaviors above and below 48.9 km/h correspond to Zones 2 and 4, respectively.

(iv) Finally, for vehicles at FG-onset distances between 68.9 m and 116.5 m, the approach speed again plays a critical role. For vehicles with FG-onset rates higher than 66.8 km/h, most of the drivers (71.4%) will cross the intersection. However, for vehicles with FG-onset speeds below than 66.8 km/h, most drivers (72.8%) will stop, as indicated in Zone 5.

5.3. Result Analysis at Urban Intersections. Figure 6 shows the classification tree diagram used to train the stop/go decision model for urban areas. Similar to Figure 5, the corresponding partitions for the tree in Figure 6 are drawn in Figure 7. This graph is divided into six zones:

(i) As shown in Figure 7, all vehicle drivers in Zone 1 will choose to cross the intersection, while most drivers (97.9%) in Zone 6 will stop, since the distance to the stop-line is more significant than a particular threshold value, in this case, 67.4 m.

(ii) A situation similar to that found for rural intersections occurs in the classification tree for urban intersections. The vehicle type plays a vital role in the drivers' stop/go decisions for vehicles in Zone 4, where FG-onset distances are less than 57.1 m, and the FG-onset speeds are below 39 km/h.

(iii) For vehicles at FG-onset distances between 57.1 m and 67.3 m with FG-onset speeds below 39 km/h, all drivers will choose to stop (corresponding to Zone 5 in Figure 7).

(iv) For vehicles with FG-onset speeds higher than 47.8 km/h, there are two different situations: for vehicles at FG-onset distances between 67.4 m and 94 m, 61.5% of drivers will cross the intersection, while for vehicles at FG-onset distances greater than 94 m, 100% of drivers will choose to stop, as indicated in Zones 2 and 3, respectively.

5.4. Comparisons of Rural High-Speed Intersections and Urban Intersections. The percentages of stop decisions are shown through a color scale in Figure 8. This figure illustrates that drivers tend to make stop decisions when the vehicle is farther from the stop-line, and the approach speed is higher, whether the intersection is in a rural or urban area.

However, there are some differences between rural high-speed intersections and urban intersections:

(1) Truck drivers are more conservative at urban intersections, especially when they are nearer to the stop-line at modestly low speeds (below 39 km/h). Because of the higher speed limit at rural high-speed intersections, such conservative decision behavior emerges at these intersections at greater distances of 44.3~68.9 m and speeds below 48.9 km/h.

(2) Due to the difference between the speed limits, most drivers tend to stop rather than cross at urban intersections when the distance exceeds 57.1 m while at rural high-speed intersections, this distance threshold increases to 68.9 m.

(3) When the vehicles are at a sufficiently far distance, such as 116.5 m from the stop-line at a rural intersection, nearly all drivers choose to stop independent of the approach speed. However, this value is much smaller, specifically, 94 m at an intersection.

6. Conclusions and Future Works

This study generated two models: the first illustrates the conditions affecting stop/go decisions in rural areas, and the other explains the corresponding requirements in urban areas. The data analysis indicates that the vehicle speed and distance to the stop-line when FG is on as well as the vehicle type are the most significant factors affecting the driver's stop/go decision in both rural and urban areas. The normalized importance of the distance variable is 100% for both types of sites. In rural areas, the normalized importance of speed is higher than that in urban areas. For vehicles at FG-onset distances between 68.9 m and 116.5 m, the rate becomes the critical factor affecting drivers' behavior. The probability of stop decision is almost equal to that of pass decision, both of which are close to 0.5. The corresponding distance interval in urban areas is between 67.4 m and 94 m. An interesting finding of this study is that under the same conditions, regardless of whether the intersection is in a rural or urban area, most truck drivers tend to park more than car drivers.

This study presents a novel way to analyze stop/go decisions. The tree-based model provides a good verbal explanation, which makes it easier to examine other conditions. The classification tree provides a simple method to model the driver's behavior without any normal assumptions. The stop/go decision-making model based on DTC developed in this study can be used to improve the driver behavior model embedded in microscopic traffic simulation software.

Data Availability

The data used to support the findings of this study included in the article.

Conflicts of Interest

The authors declare that there are no conflicts of interest regarding the publication of this paper.

Acknowledgments

This study was supported by the Natural Science Foundation of Zhejiang Province (no. LQ19E080003), Philosophy and Social Science Program of Ningbo (no. G20-ZX37), Natural Science Foundation of Ningbo (nos. 2018A610127 and 2019A610044), and The Opening Foundation of the State Key Laboratory for Management and Control of Complex Systems (no. 20190102).

References

[1] K. Tang, Y. Xu, P. Wang, and F. Wang, "Impacts of flashing green on dilemma zone behavior at high-speed intersections: empirical study in China," *Journal of Transportation Engineering*, vol. 141, no. 7, Article ID 04015005, 2015.

[2] S. Dong, J. Zhou, L. Zhao, K. Tang, and R. Yang, "Feasibility analysis of phase transition signals based on e-bike rider behavior," *Advances in Mechanical Engineering*, vol. 7, no. 11, pp. 1–18, 2015.

[3] S. Dong, J. Zhou, and S. Zhang, "Determining E-bike drivers' decision-making mechanisms during signal change interval using the hidden Markov driving model," *Journal of Advanced Transportation*, vol. 2019, pp. 1–10, 2019.

[4] K. Tang, Y. Xu, F. Wang, and T. Oguchi, "Exploring stop-go decision zones at rural high-speed intersections with flashing green signal and insufficient yellow time in China," *Accident Analysis & Prevention*, vol. 95, pp. 470–478, 2016.

[5] P. Koonce and L. Rodegerdts, *Traffic Signal Timing Manual (No. FHWA-HOP-08-024)*, Federal Highway Administration, Washington, DC, USA, 2008.

[6] G. Britain and T. A. Unit, *General Principles of Traffic Control by Light Signals*, Department for Transport, London, UK, 2006.

[7] C. A. O'Flaherty, *Transport Planning and Traffic Engineering*, CRC Press, Boca Raton, FL, USA, 2018.

[8] X. Dou, X. Guo, X. Gong, and J. Yang, "Evaluating impacts of flashing green before amber on drivers' stop/cross decisions at signalized intersections in China: an empirical approach and comparative study," in *Proceedings of the 92nd Transportation Research Board Annual Meeting*, Washington, DC, USA, January 2013.

[9] M. Becker, *A Study of the Effect of a" Flashing Green" Phase in Traffic Signals at Urban Intersections*, Technion Research and Development Foundation Ltd., Haifa, Israel, 1971.

[10] D. Mahalel and D. M. Zaidel, "Safety evaluation of a flashing-green light in a traffic signal," *Traffic Engineering and Control*, vol. 26, no. 2, pp. 79–81, 1985.

[11] C. Newton, R. N. Mussa, E. K. Sadalla, E. K. Burns, and J. Matthias, "Evaluation of an alternative traffic light change anticipation system," *Accident Analysis & Prevention*, vol. 29, no. 2, pp. 201–209, 1997.

[12] Q. Zeng, W. Gu, X. Zhang, H. Wen, J. Lee, and W. Hao, "Analyzing freeway crash severity using a Bayesian spatial generalized ordered logit model with conditional autoregressive priors," *Accident Analysis & Prevention*, vol. 127, pp. 87–95, 2019.

[13] H. Köll, M. Bader, and K. W. Axhausen, "Driver behaviour during flashing green before amber: a comparative study," *Accident Analysis & Prevention*, vol. 36, no. 2, pp. 273–280, 2004.

[14] R. Factor, J. N. Prashker, and D. Mahalel, "The flashing green light paradox," *Transportation Research Part F: Traffic Psychology and Behaviour*, vol. 15, no. 3, pp. 279–288, 2012.

[15] K. Tang, Y. Xu, and F. Wang, "Dilemma zone occurrences at the rural high-speed intersections with flashing green and insufficient yellow time in China," in *Proceedings of the 94th Transportation Research Board Annual Meeting*, Washington, DC, USA, January 2015.

[16] F. Wang, K. Tang, Y. Xu, J. Sun, and K. Li, "Modeling risky driver behavior under the influence of flashing green signal with vehicle trajectory data," *Transportation Research Record: Journal of the Transportation Research Board*, vol. 2562, no. 1, pp. 53–62, 2016.

[17] K. Long, L. D. Han, and Q. Yang, "Effects of countdown timers on driver behavior after the yellow onset at Chinese intersections," *Traffic Injury Prevention*, vol. 12, no. 5, pp. 538–544, 2011.

[18] F. Chen, M. Song, and X. Ma, "Investigation on the injury severity of drivers in rear-end collisions between cars using a random parameters bivariate ordered probit model," *International Journal of Environmental Research and Public Health*, vol. 16, no. 14, p. 2632, 2019.

[19] X. Zhu, Z. Dai, F. Chen, X. Pan, and M. Xu, "Using the visual intervention influence of pavement marking for rutting mitigation-part II: visual intervention timing based on the finite element simulation," *International Journal of Pavement Engineering*, vol. 20, no. 5, pp. 573–584, 2019.

[20] G. Wu, F. Chen, X. Pan, M. Xu, and X. Zhu, "Using the visual intervention influence of pavement markings for rutting mitigation-part I: preliminary experiments and field tests," *International Journal of Pavement Engineering*, vol. 20, no. 6, pp. 734–746, 2019.

[21] D. Gazis, R. Herman, and A. Maradudin, "The problem of the amber signal light in traffic flow," *Operations Research*, vol. 8, no. 1, pp. 112–132, 1960.

[22] M. S. Chang, C. J. Messer, and A. J. Santiago, "Timing traffic signal change intervals based on driver behavior," *Transportation Research Record*, vol. 1027, pp. 20–30, 1985.

[23] C. Liu, R. Herman, and D. C. Gazis, "A review of the yellow interval dilemma," *Transportation Research Part A: Policy and Practice*, vol. 30, no. 5, pp. 333–348, 1996.

[24] J. Zhou, Y. Guo, S. Dong, M. Zhang, and T. Mao, "Simulation of pedestrian evacuation route choice using social force model in large-scale public space: comparison of five evacuation strategies," *PLoS one*, vol. 14, no. 9, pp. 1–18, 2019.

[25] J. Zhou, X. Mao, Y. Wang, M. Zhang, and S. Dong, "Risk assessment in urban large-scale public spaces using Dempster-shafer theory: an empirical study in Ningbo, China," *International Journal of Environmental Research and Public Health*, vol. 16, no. 16, p. 2942, 2019.

[26] P. L. Olson and R. W. Rothery, "Driver response to the amber phase of traffic signals," *Operations Research*, vol. 9, no. 5, pp. 650–663, 1961.

[27] A. D. May Jr., "Clearance interval at traffic signals," *Highway Research Record*, vol. 221, pp. 41–71, 1968.

[28] H. Wei, Z. Li, P. Yi, and K. R. Duemmel, "Quantifying dynamic factors contributing to dilemma zone at high-speed signalized intersections," *Transportation Research Record: Journal of the Transportation Research Board*, vol. 2259, no. 1, pp. 202–212, 2011.

[29] J. N. Prashker and D. Mahalel, "The relationship between an option space and drivers' indecision at signalized intersection approaches," *Transportation Research Part B: Methodological*, vol. 23, no. 6, pp. 401–413, 1989.

[30] P. Li and M. Abbas, "Stochastic dilemma hazard model at high-speed signalized intersections," *Journal of Transportation Engineering*, vol. 136, no. 5, pp. 448–456, 2010.

[31] P. Papaioannou, "Driver behaviour, dilemma zone and safety effects at urban signalised intersections in Greece," *Accident Analysis & Prevention*, vol. 39, no. 1, pp. 147–158, 2007.

[32] Q. Zeng, Q. Guo, S. C. Wong, H. Wen, H. Huang, and X. Pei, "Jointly modeling area-level crash rates by severity: a Bayesian multivariate random-parameters spatio-temporal Tobit regression," *Transportmetrica A: Transport Science*, vol. 15, no. 2, pp. 1867–1884, 2019.

[33] Y. Guo, Z. Li, P. Liu, and Y. Wu, "Modeling correlation and heterogeneity in crash rates by collision types using full Bayesian random parameters multivariate Tobit model," *Accident Analysis & Prevention*, vol. 128, pp. 164–174, 2019.

[34] Y. Guo, P. Liu, Y. Wu, and M. Yang, "Traffic conflict model based on Bayesian multivariate Poisson-lognormal normal distribution," *China Journal of Highway and Transport*, vol. 31, no. 1, pp. 101–109, 2018.

[35] H. Rakha, I. El-Shawarby, and J. R. Setti, "Characterizing driver behavior on signalized intersection approaches at the onset of a yellow-phase trigger," *IEEE Transactions on Intelligent Transportation Systems*, vol. 8, no. 4, pp. 630–640, 2007.

[36] D. S. Hurwitz, M. A. Knodler Jr., and B. Nyquist, "Evaluation of driver behavior in type II dilemma zones at high-speed signalized intersections," *Journal of Transportation Engineering*, vol. 137, no. 4, pp. 277–286, 2010.

[37] K. Y. Kuo, Y. J. Chen, and R. C. Hwang, "Calculation of the change and clearance intervals of traffic signal by fuzzy logic system," in *Proceedings of the Meeting of Joint Conference of International Computer Symposium*, Kaohsiung, Taiwan, 1996.

[38] D. Moore and D. S. Hurwitz, "Fuzzy logic for improved dilemma zone identification," *Transportation Research Record: Journal of the Transportation Research Board*, vol. 2384, no. 1, pp. 25–34, 2013.

[39] Y. J. Moon and F. Coleman III, "Dynamic dilemma zone based on driver behavior and car-following model at highway-rail intersections," *Transportation Research Part B: Methodological*, vol. 37, no. 4, pp. 323–344, 2003.

[40] K. Tang, S. Dong, F. Wang, Y. Ni, and J. Sun, "Behavior of riders of electric bicycles at onset of green and yellow at signalized intersections in China," *Transportation Research Record: Journal of the Transportation Research Board*, vol. 2317, no. 1, pp. 85–96, 2012.

[41] N. Elmitiny, X. Yan, E. Radwan, C. Russo, and D. Nashar, "Classification analysis of driver's stop/go decision and red-light running violation," *Accident Analysis & Prevention*, vol. 42, no. 1, pp. 101–111, 2010.

[42] L. Breiman, *Classification and Regression Trees*, Routledge Publisher, Taylor & Francis Group, Abingdon-on-Thames, UK, 2017.

[43] J. Abellán, G. López, and J. de Oña, "Analysis of traffic accident severity using decision rules via decision trees," *Expert*

Systems with Applications, vol. 40, no. 15, pp. 6047–6054, 2013.

[44] J. Zhou, Y. Wu, X. Mao, S. Guo, and M. Zhang, "Congestion evaluation of pedestrians in metro stations based on normal-cloud theory," *Applied Sciences*, vol. 9, no. 17, p. 3624, 2019.

[45] A. T. Kashani and A. S. Mohaymany, "Analysis of the traffic injury severity on two-lane, two-way rural roads based on classification tree models," *Safety Science*, vol. 49, no. 10, pp. 1314–1320, 2011.

Hindawi
Journal of Advanced Transportation
Volume 2020, Article ID 2817801, 8 pages
https://doi.org/10.1155/2020/2817801

Research Article

Analysis of Factors Affecting a Driver's Driving Speed Selection in Low Illumination

Jing Liu,[1,2] **Jing Cai**,[1] **Shanshan Lin**,[3] **and Jianyou Zhao**[1]

[1]*School of Automobile, Chang'an University, Xi'an, Shaanxi 710064, China*
[2]*School of Mechanical and Electrical Engineering, Anhui Jianzhu University, Hefei, Anhui, ST 230601, China*
[3]*School of Automobile and Traffic Engineering, Hefei University of Technology, Hefei 230009, Anhui, China*

Correspondence should be addressed to Jing Liu; liujing1102@ahjzu.edu.cn

Received 17 December 2019; Revised 8 February 2020; Accepted 14 February 2020; Published 21 April 2020

Guest Editor: Feng Chen

To better understand a driver's driving speed selection behaviour in low illumination, a self-designed questionnaire was applied to investigate driving ability in low illumination, and the influencing factors of low-illumination driving speed selection behaviour were discussed from the driver's perspective. The reliability and validity of 243 questionnaires were tested, and multiple linear regression was used to analyse the comprehensive influence of demographic variables, driving speed in a low-illumination environment with street lights and driving ability on speed selection behaviour in low illumination without street lights. Pearson's correlation test showed that there was no correlation among age, education, accidents in the past 3 years, and speed selection behaviour in low illumination, but gender, driving experience, number of night-driving days per week, and average annual mileage were significantly correlated with speed selection behaviour. In a low-illumination environment, driving ability has a significant influence on a driver's speed selection behaviour. Technical driving ability under low-illumination conditions of street lights has the greatest influence on speed selection behaviour on a road with a speed limit of 120 km/h ($\beta = 0.51$). Risk perception ability has a significant negative impact on speed selection behaviour on roads with speed limits of 80 km/h and 120 km/h ($\beta = -0.25$ and $\beta = -0.34$, respectively). Driving speed in night-driving environment with street lights also has a positive influence on speed selection behaviour in low illumination ($\beta = 0.61$; $\beta = 0.28$; $\beta = 0.37$).

1. Introduction

Night accidents are frequent and serious. Among the total number of traffic accidents, 46% to 54% of accidents occurred at night, while the traffic volume during this period was 10%~30% of that in the daytime, causing approximately 60% of the total number of deaths [1]. The probability and severity of traffic accidents in low-illumination environmental conditions at night are much higher than those in the daytime. A study on truck-involved accidents has found that the probability of severe injury increases in the low illumination condition [2].

The driver is in a dominant position in the transportation system. Studies have shown that motor vehicle drivers are one of the main factors leading to traffic accidents. According to statistics, 80 to 90% of road traffic accidents in China are caused by human factors, especially driving behaviours, as traffic accidents caused by driving errors constitute 70–80% [3].

A series of studies have been carried out on the effects of illumination on driving behaviours, especially drivers' visual characteristics. Previous studies have examined the effect of illumination on visual sensitivity. These studies found that visual sensitivities decrease linearly with a decrease in illumination [4]. Rackoff and Rockwell showed that the safety of driving at night could be improved by increasing environmental illumination to meet drivers' demands for visual information [5]. A comparative test of low illumination and normal illumination was conducted to analyse the effects of environmental illumination and speed on the recognition time of objects with different colors, and a measurement model of vehicle speed, dynamic low illumination, and

recognition time was built [6]. Driver's visual characteristics and cognitive ability are directly affected by insufficient illumination; thus, driving behaviour is also affected, showing a difference from normal illumination conditions.

In the process of driving, more than 90% of the information that the driver has is obtained by visual perception [7]. Through continuous perception of road environment information, the driver can make behavioural decisions and guide the cyclic feedback process of driving behaviour [8]. Most traffic accidents are caused by poor line-of-sight conditions [9]. In a dark night environment, it is difficult to form a clear image on the retina due to insufficient light entering the driver's eyes, so it is more difficult for the driver to perceive road environment information. Whether the driver can accurately visualize an obstacle in front, the difference between the brightness of the obstacle and the contrast of the environment, and the illumination of the environment in which the driver is located are important factors. As the illumination of the driver's environment increases, the driver's visibility of an obstacle will be reduced due to the high brightness of the surrounding environment [10].

The influence of illumination on the speed selection and safety of drivers has been studied by many scholars. A study found that illumination could affect a drivers' speed selection and attention during driving and that an increase in illumination could reduce the occurrence of accidents [11]. Haglund and Aberg found that 47%~58% of drivers overspeed at night, and their self-perceived speed is lower than the actual speed [12]. With insufficient lighting at night, the driver's perception of speed will be illusory. Suh and Park and other studies found that insufficient night lighting will make the driver feel that the speed of the vehicle is not fast, causing the driver to accelerate or even speed [13]. Baker found that night drivers underestimated speed and increased driving speed [14]. Read and others found that in the study of the effect of improving the brightness of street lamps on the driving performance of elderly individuals at night, the driver increased speed and reduced attention when road lighting was installed [15]. Under certain conditions, an increase in road brightness is helpful to some drivers, but in other cases, it has a negative impact on the driver. In addition, low illumination affects the driver's speed processing ability. A reduction in illumination seriously affects visual ability, reduces reaction time, and reduces speed processing capability.

Driving is a complex sensory movement task. Good driving ability is also a prerequisite for ensuring safe driving of drivers. Driving ability includes technical driving ability and risk perception ability. In low illumination, a driver's driving ability will also change to a certain extent, which in turn affects the driver's speed selection behaviour. However, there are few studies on driving ability and speed selection behaviour in low illumination at home and abroad.

Therefore, the purpose of this paper is to study the influence of driving ability on speed selection behaviour in low-illumination conditions and combine the driver's personal attributes to separately analyse speed selection behaviours under the two scenarios of street lights at night and no street lights at night. The corresponding data were obtained through a questionnaire survey, and a multiple regression model of driving speed selection in low illumination was established to provide a theoretical basis for road speed management in low illumination.

2. Research Methods

2.1. Measures. The existing methods of researching driver behaviours can be divided into driving simulator technology [16], real-time driving environmental big data [17], real vehicle experiment [18], mathematical model [19], and questionnaires [20]. Different from the former methods, the latter one measures the behaviours via psychological perspective. In the present study, a questionnaire instrument was used, which is a cost-effective way in examining driver behaviours based on psychological characteristics.

According to the purpose of this study, the "driver survey questionnaire in low illumination" consists of three parts: driver demographic information, speed selection behaviour, and driving ability scale in low illumination. The selection of items was mainly based on mature questionnaires that have been widely used in the industry and screening from the items of those questionnaires. In addition, drivers were interviewed, and the interview results showed that a driver's sensitivity to illumination was poor and that the perception and understanding of low illumination were different. Therefore, the questionnaire did not define low illumination by light intensity but described a low-illumination environment as a "night environment."

After the preliminary design and formation of the questionnaire, teachers and graduate students of the Traffic Safety Institute were invited to conduct evaluations, and 10 professional drivers were invited to pre-fill according to driving situations in low illumination in the past year and to propose amendments. Finally, some questions were adjusted, modified, and replaced. The specific design contents of the questionnaire were as follows:

2.1.1. Demographic Information. The demographic information included gender, age, driving experience, education, average annual mileage, number of night-driving days per week, number of traffic accidents that occurred at night in the past three years, deduction in 2017, deduction due to low illumination, and self-assessment of the influence of a low-illumination environment on driving performance and driving skills.

2.1.2. Speed Selection Behaviour. The speed limit value has a significant impact on driving speed, and a driver will choose to increase or decrease speed with a change in the road speed limit value [21]. Therefore, this study combines road classification and common speed limit values to classify roads into three types: urban roads/low-grade highways (speed limit: 60 km/h), high-grade highways (speed limit: 80 km/h), and expressways (speed limit: 120 km/h). Drivers were asked to answer six questions about speed selection: in night-driving environment with street lights, the driving speed

(WSL60) that is preferred on a road with a speed limit of 60 km/h; in night-driving environment without street lights, the driving speed (WOSL60) that is preferred on a road with a speed limit of 60 km/h; in night-driving environment with street lights, the driving speed (WSL80) that is preferred on a road with a speed limit of 80 km/h; in night-driving environment without street lights, the driving speed (WOSL80) that is preferred on a road with a speed limit of 80 km/h; in night-driving environment with street lights, the driving speed (WSL120) that is preferred on a road with a speed limit of 120 km/h; and in night-driving environment without street lights, the driving speed (WOSL120) that is preferred on a road with a speed limit of 120 km/h.

2.1.3. Driving Ability Scale in Low Illumination. Referring to the driving skills assessment questionnaire designed by Zheng [22], the traffic scenario was set as a low-illumination environment at night and was specifically divided into two scenarios of street lights at night and no street lights at night. The specific contents are shown in Tables 1 and 2. Drivers were required to self-report by scoring on the form to evaluate their driving ability in a low-illumination environment at night. Each item was scored in the form of a Likert 5-point scale, from "1 = completely inconsistent" to "5 = completely consistent." The items were set in the opposite direction; the lower the score was, the better the driving ability was.

2.2. Experimental Process. The questionnaire was conducted through a field survey, and drivers were required to fill in the questionnaire according to their actual driving conditions in low illumination at night. Participants participated in the survey voluntarily and anonymously, and it took approximately 10 minutes to complete the questionnaire. The driver will be paid 10 yuan after the investigation is completed.

2.3. Data Collection. A total of 266 questionnaires were collected in this survey, and 243 valid questionnaires were finally collected, excluding those that were incomplete or had less than one year of driving experience. Participants included 182 men and 61 women, with an average age of 31.9 years (SD = 7.319) and ages ranging from 20 to 55 years old; average driving experience of 5.6 years (SD = 5.127); and average annual mileage of 160.27 million kilometres (SD = 2.1119). The average number of night-driving days per week was 2.426 days (SD = 1.8644), the average deduction in 2017 was 2.35 (SD = 3.449), and the average deduction due to low illumination at night was 0.18 (SD = 0.72).

3. Results

3.1. Descriptive Analysis. Under the condition with street lights, the average driving speed of a driver is 58.61 km/h (SD = 8.795), 77.13 km/h (SD = 8.654), and 110.88 km/h (SD = 10.594) on roads with speed limits of 60 km/h, 80 km/h, and 120 km/h, and the corresponding speed reduction in night-driving environment with street lights is 14.09% (M = 50.35 km/h, SD = 10.139), 18.13% (M = 63.15 km/h, SD = 7.811), and 11.89% (M = 97.70 km/h, SD = 7.360), respectively; that is, a driver will drive at a speed approximately 15% lower than normal when driving in a low-illumination environment.

3.2. Reliability and Validity Analysis. To ensure the reliability and validity of the research results, it is necessary to test the reliability and validity of the self-compiled driving ability scale in low illumination. Among the results, the Kaiser–Meyer–Olkin (KMO) value of the driving ability scale in the case of street lights at night is 0.937, which is greater than the standard value of 0.5, and the Bartlett sphericity test result reaches the level of significance ($p < 0.01$). The KMO value of the driving ability scale in the case of no street lights at night is 0.948, which is greater than the standard value of 0.5, and the Bartlett sphericity test results reach the level of significance ($p < 0.01$), indicating that the data are suitable for factor analysis [23].

Principal component analysis was used to conduct the maximum rotation of variance for the driving ability scale with and without street lights at night. In the case of street lights at night, the driving ability scale obtains two factors with eigenvalues greater than 1, named "Technical Driving Ability 1" (TDA1) and "Risk Perception Ability 1" (RPA1). The questionnaire consists of 16 items, these two factors explain 81.62% of the total variance, and the load of each item is above 0.66. The specific results are shown in Table 1. The factor structure agrees with the theoretical conception, and the validity of the questionnaire structure is good.

In the case of no street lights at night, the driving ability scale obtains two factors with eigenvalues greater than 1, named "Technical Driving Ability 2" (TDA2) and "Risk Perception Ability 2" (RPA2). The questionnaire consists of 22 items, these two factors explain 76.34% of the total variance, and the load of each item is above 0.71. The specific results are shown in Table 2. The factor structure agrees with the theoretical conception, and the validity of the questionnaire structure is good.

Cronbach's α coefficients were used for reliability analysis of the scale to measure its reliability. When $\alpha > 0.7$, the questionnaire is acceptable. Cronbach's α coefficient of the driving ability scale for street lights at night used in this study is 0.976, and the combined reliability of the two factors is 0.962 and 0.969; Cronbach's α coefficient of the driving ability scale for no street lights at night is 0.975, and the combined reliability of the two factors is 0.961 and 0.975, indicating that the questionnaires have ideal reliability.

3.3. Correlation Analysis. The Pearson correlation coefficient method is adopted to measure the correlation between a driver's personal attributes and speed selection behaviour in low illumination without street lights. The specific results are shown in Table 3. The gender of the driver and average number of night-driving days per week are significantly correlated with speed selection behaviour on roads with speed limits of 60 km/h and 80 km/h, respectively, in night-driving environment without street lights; driving

Table 1: Factor structure and load of the driving ability scale in environments with street lights at night.

Item	Item content	TDA1	RPA1
1	When there are street lights at night, I can control the vehicle smoothly on the road	0.85	
2	When there are street lights at night, I can control the vehicle steadily on slippery roads	0.82	
4	When there are street lights at night, I can park safely and correctly on the ramp	0.84	
8	I have mastered the methods and techniques of emergency steering at night with street lights	0.67	
13	When there are street lights at night, I can always safely avoid in case of an emergency	0.82	
21	When there are street lights at night, I can drive reasonably by observing the movements of pedestrians and other vehicles	0.73	
23	When there are street lights at night, I can overtake safely and reasonably	0.82	
12	When there are street lights at night, I can plan or choose routes to avoid getting lost and taking long detours		0.70
14	When there are street lights at night, I can detect potential traffic dangers on the road		0.77
16	When there are street lights at night, I can keep a safe driving distance from the vehicle in front		0.85
17	When there are street lights at night, I can get a good grasp of the surrounding traffic situation when driving the vehicle		0.76
18	When there are street lights at night, I can react quickly in case of an emergency during driving		0.84
20	When there are street lights at night, I can make a quick decision when I encounter a choice during driving		0.83
22	When there are street lights at night, I can notice the dynamic state of the roadside		0.84
24	When there are street lights at night, I can judge the safe speed of the road according to different road conditions		0.81
25	When there are street lights at night, I can pay attention to the dynamics near my vehicle while driving		0.80

Table 2: Factor structure and load of the driving ability scale in environments with no street lights at night.

Item	Item content	TDA1	RPA1
28	When there is no street light at night, I can control the vehicle smoothly on the road	0.78	
29	When there is no street light at night, I can control the vehicle steadily on slippery roads	0.79	
31	When there is no street light at night, I can park safely and correctly on the ramp	0.78	
32	I can drive steadily and safely at night without street lights	0.82	
33	When there is no street light at night, I can drive the vehicle smoothly at night (such as slow acceleration and deceleration)	0.85	
35	I have mastered the methods and techniques of emergency steering at night without street lights	0.75	
36	I mastered the skills of braking quickly and controlling the car at night without street lights	0.73	
37	When there is no street light at night, I can still complete the necessary driving action in an emergency	0.76	
38	When there is no street light at night, I can skilfully use various electronic navigation equipment in the vehicle	0.75	
46	When there is no street light at night, I can change lanes reasonably in heavy traffic	0.76	
51	When there is no street light at night, I can overtake safely and reasonably	0.77	
30	When there is no street light at night, I will observe the surrounding traffic conditions before driving		0.79
34	When there is no street light at night, I can adjust the driving speed according to the driving situation		0.86
44	When there is no street light at night, I can get a good grasp of the surrounding traffic situation when driving the vehicle		0.82
45	When there is no street light at night, I can react quickly in case of an emergency during driving		0.81
47	When there is no street light at night, I can make a quick decision when I encounter a choice during driving		0.80
48	When there is no street light at night, I can drive reasonably by observing the movements of pedestrians and other vehicles		0.83
50	When there is no street light at night, I can notice the dynamic state of the roadside		0.72
52	When there is no street light at night, I can judge the safe speed of the road according to different road conditions		0.80
53	When there is no street light at night, I can pay attention to the dynamics near my vehicle while driving		0.87
54	When there is no street light at night, I can quickly detect dangerous behaviours of other drivers.		0.83
55	When there is no street light at night, I can quickly identify pedestrians crossing the road ahead		0.87

experience is significantly related to speed selection behaviour on a road with a speed limit of 80 km/h; total annual deduction is significantly related to speed selection behaviour on a road with a speed limit of 60 km/h; and the average annual mileage is significantly correlated with the speed selection behaviour on roads with speed limits of 60 km/h and 120 km/h. Speed selection behaviour in low illumination without street lights is significantly correlated with speed selection behaviour in night-driving environment with street lights with speed limits of 60 km/h, 80 km/h, and 120 km/h, respectively. Age, education, and accidents in the past 3 years are not correlated with speed selection behaviour in night-driving environment with street lights.

3.4. Difference Analysis. An independent *t*-test was used to analyse the differences in speed selection behaviour for different driving experience and average annual mileage in a low-illumination environment without street lights. The specific results are shown in Table 4. The results show that

Table 3: Correlation analysis between a Driver's personal attributes and speed selection behaviour in low illumination.

	WOSL60	WOSL80	WOSL120
Gender	0.143*	0.240**	0.096
Age	0.006	0.115	0.040
Education	0.004	−0.103	0.001
Driving experience	0.109	0.147*	0.090
Average annual mileage	0.182*	0.107	0.203**
Number of night-driving days per week	0.229**	0.129*	−0.074
Deduction in the past year	0.164*	0.086	0.121
Accidents in the past 3 years	0.031	−0.065	0.054
WSL60	0.665**	0.255**	0.220**
WSL80	0.566**	0.457**	0.328**
WSL120	0.398**	0.439**	0.388**

drivers tend to choose the speeds WOSL60, WOSL80, and WOSL120 in a low-illumination environment without street lights with road speed limits of 60 km/h, 80 km/h, and 120 km/h, respectively, that have significant differences in terms of driving experience and average annual mileage. Under the same speed limit conditions, the greater the driving experience and the higher the average annual mileage are, the higher the speed selection in a low-illumination environment.

3.5. Predictors of Speed Selection Behaviour. Since the driving ability of a driver in low illumination cannot be directly observed, multiple linear regression analysis is used in this paper to predict the preferred speeds WOSL60, WOSL80, and WOSL120 in a low-illumination environment without street lights with speed limits of 60 km/h, 80 km/h, and 120 km/h, respectively, as shown in Table 5. The driver's gender, age, education, driving experience, average annual mileage, number of night-driving days per week, total annual deduction, and accidents in the past 3 years are taken as demographic variables and included in the regression model as the first step. The driving speeds that a driver tends to choose on roads with the three different speed limit conditions in a low-illumination environment with street lights are gradually incorporated into the regression model in the second step. The driving skills under street lights at night and the driving skills under no street lights at night are gradually incorporated into the regression model in the third step.

The total explanatory power of the regression model for WOSL60 is 48.3%, among which the driver's number of night-driving days per week, WSL60, and WSL120 are significant predictors. Demographic variables have 10.9% explanatory power (F (8,234) = 3.581, p = 0.001), WSL60 has 38.1% explanatory power (F (9,233) = 24.847, p = 0.000), and WSL120 has 1.5% explanatory power (F (10,232) = 23.629, p = 0.000).

The total explanatory power of the regression model for WOSL80 is 37.4%, among which the driver's gender, education, total annual deduction, WSL80, WSL120, TDA1, and RPA1 are significant predictors. The explanatory power of demographic variables is 12.9% (F (8,234) = 4.318, p = 0.000). The explanatory power of WSL80 and WSL120 for WOSL80 is 16.9% (F (9,233) = 10.977, p = 0.000) and 4% (F (10,232) = 11.818, p = 0.000), respectively, indicating that the higher the driver's preferred speed is on a road with street lights and an 80 km/h or 120 km/h speed limit, the higher the driver's preferred speed on a road with an 80 km/h speed limit in a low-illumination environment. In addition, the explanatory power of RPA1 is 1.8% (F (12,230) = 13.026, p = 0.000), and the explanatory power of TDA1 to WOSL80 is 4.9% (F (11,231) = 13.223, p = 0.000), indicating that the stronger the driver's technical driving ability is under the condition of street lights at night, the higher the speed the driver tends to choose on a road with a speed limit of 80 km/h in a low-illumination environment. However, the stronger that risk perception ability is under the condition of street lights at night, the lower the speed selection is.

The driver's number of night-driving days per week, total annual deduction, WSL120, TDA1, and RPA2 are significant predictors of WOSL120, and the total explanatory power of the regression model is 30.9%. Among them, the explanatory power of demographic variables is 7.5% (F (8,234) = 2.373, p = 0.018), and the explanatory power of WSL120 to WOSL120 is 14.7% (F (9,233) = 7.371, p = 0.000), indicating that the higher the driver's preferred speed is on a road with street lights conditions and a speed limit of 120 km/h, the higher the driver's preferred speed on a road with a speed limit of 120 km/h in a low-illumination environment without street lights. The explanatory power of TDA1 is 6.8% (F (10,232) = 9.437, p = 0.000), indicating that the more skilled the driver is at driving with street lights at night, the higher the value of WOSL120. RPA2 has a minimum explanatory power of 5.1% (F (11,231) = 10.819, p = 0.000), indicating that the higher the driver's risk perception ability is under the condition of street lights at night, the lower the value of WOSL120 is.

4. Discussion

This study aims to explore the relationships between speed selection behaviour and demographic variables and driving ability in a low-illumination environment by questionnaires and analysis. The results show that there are significant differences in terms of driving experience and average annual mileage affecting drivers' preferred speeds in a low-illumination environment. Drivers' driving skills in a low-illumination environment have a significant predictive effect on speed selection behaviour. In addition, gender, driving experience, average annual mileage, average number of night-driving days per week, and total annual deduction were found to be significantly correlated with speed selection behaviour in low illumination without street lights.

4.1. Validation of the Driving Ability Scale. Based on previous questionnaire designed by Zheng [22], we confirmed the validation of the newly developed scale concerning a low-illumination environment at night and the scenarios of street lights at night/no street lights at night. In the case of street lights at night, it yielded 2 factors explaining 81.62% of the variance, Cronbach's α values of factors were above 0.9, and

Table 4: Difference analysis of speed selection behaviour in low illumination.

Variable	Driving experience M (SD)		T	Average annual mileage M (SD)		T
	<6 years	≥6 years		<15,000 km	≥15,000 km	
WOSL60	48.91 (10.450)	52.89 (9.080)	2.986***	48.39 (9.782)	53.41 (9.974)	3.878***
WOSL80	61.94 (7.674)	65.28 (7.632)	3.276***	62.09 (7.308)	64.79 (8.313)	2.657**
WOSL120	96.84 (7.253)	99.20 (7.346)	2.433*	96.45 (7.125)	99.63 (7.338)	3.354***

* $p < 0.05$, ** $p < 0.01$, and *** $p < 0.005$.

Table 5: Regression prediction model of speed selection behaviour in low illumination.

Variable	WOSL60		WOSL80		WOSL120	
	ΔR^2	β	ΔR^2	β	ΔR^2	B
Step 1: enter	0.109		0.129		0.075	
Gender		0.002		0.124*		0.049
Age		−0.06		−0.007		−0.1
Education		−0.068		−0.141**		−0.018
Driving experience		0.109		0.041		0.036
Average annual mileage		0.042		−0.086		0.047
Number of night-driving days per week		0.114*		−0.006		−0.204***
Deduction in the past year		0.066		−0.149**		0.136*
Accidents in the past 3 years		−0.042		−0.101		0.003
Step 2: stepwise						
WSL60	0.381	0.609***				
WSL80			0.169	0.277***		
WSL120	0.015	0.139**	0.04	0.223***	0.147	0.374***
Step 3: stepwise						
TDA1			0.049	0.445***	0.068	0.513***
RPA1			0.018	−0.248**		
TDA2						
RPA2					0.051	−0.343***
	$R^2 = 0.483$		$R^2 = 0.374$		$R^2 = 0.309$	

* $p < 0.05$, ** $p < 0.01$, and *** $p < 0.005$.

values of factor loading were above 0.66. Moving onto the other scale, it also yielded 2 factors explaining 76.34% of the total variance, Cronbach's α values of factors were above 0.9, and the load of each item is above 0.71. The results show that the two scales are effective; the items have high factorial weight and good internal consistency. The first dimension, "Technical Driving Ability," mainly examined the ability to operate and control the vehicles. The second one, "Risk Perception Ability," showed the drivers' ability to perceive environmental factors and potential risks. The findings were in line with previous studies relating to driving ability assessment [24, 25].

4.2. Factors Influencing Speed Selection Behaviours in Low Illumination. Driver characteristics have also been found to influence speed selection. In terms of demographic variables, gender was significantly correlated with speed selection behaviour, with men driving at a higher speed than their counterparts. This is in line with the results of Sadia et al., who suggested that the average speed of women are relatively lower than the men's and women showing a basic lower speed choice [26]. Research focused on demographic characteristics, finding that men drive generally faster than women, and the young drive faster than older ones [27, 28]. However, the impact of age on speed selection behaviour in low illumination without street lights was not significant in the present study. The importance of road safety education for males may promote safer driving.

There are significant differences in terms of driving experience and average annual mileage affecting drivers' speed selection behaviours in a low-illumination environment. Under the same speed limit conditions, the greater the driving experience and the higher the average annual mileage are, the higher the speed selection in a low-illumination environment is. This may be because the more experienced that drivers are, the more confident they are in themselves, believing that they can handle the handling of vehicles and emergencies well even in low-light environments. This is similar with previous findings, such as Spolander proposed that with increased experience, drivers perceive themselves as having higher skills [29] and Xu et al. suggested that the assessment of perceptual-motor skills improved with increased driving experience [30]. However, research shows that even for drivers with experience, safety education for driving at night still needs to be strengthened [31].

Under the low-illumination condition of street lights at night, the driver's technical driving ability TDA1 has a significant ability to predict the driver's preferred speed on roads with speed limits of 80 km/h and 120 km/h. The

stronger the technical driving ability is, the faster the speed that the driver tends to choose is, which indicates that a driver with better driving skills believes that he can also complete braking and collision avoidance in a short time and short distance in the case of emergency in a low-illumination environment. However, in low illumination, especially when there are no street lights at night, due to the shortening of the visual range, when a driver discovers obstacles or emergencies, the distance between them is greatly shortened compared with that of high-illumination conditions. It is difficult for drivers driving at a high speed to complete braking within this distance, resulting in collision accidents. Therefore, it is necessary to strengthen the safety education of drivers who have rich driving experience and often drive at night to clarify the dangers of high-speed driving in low illumination.

The risk perception ability in low-illumination conditions with street lights at night RPA1 and the risk perception ability in low-illumination conditions without street lights at night RPA2 are significant predictors of driver speed selection behaviour on roads with speed limits of 80 km/h and 120 km/h, respectively. The stronger the driver's risk perception ability is, the slower speed that the driver tends to choose is, which indicates that a driver with stronger risk perception ability is more cautious when driving in a low-illumination environment and will choose a slower driving speed. In addition, the research results show that in low-illumination conditions with street lights at night, the driver's technical driving ability and risk perception ability have significant predictive ability for speed selection behaviour: the better the technical driving ability is, the faster the speed that the driver tends to choose is; the stronger the risk perception ability is, the lower the speed that the driver tends to choose is. However, in low-illumination conditions without street lights at night, only risk perception ability has a significant predictive ability for speed selection behaviour. This may be because technical driving ability mainly depends on the driver's ability to control the vehicle; however, in the absence of street lights, the driver's visual range is severely limited, and he cannot effectively judge the surrounding environment, which leads to an inability to exert the original driving ability. However, risk perception ability is a psychological state that is more reflected in the driver's awe of traffic safety and subjective cognition. Therefore, for driving safety education at night, we should pay attention not only to the improvement of driving skills but also to the improvement of traffic safety awareness.

The driving speed in a low-illumination environment with street lights has a positive effect on speed selection behaviour in low illumination. The driving speed on a road with a speed limit of 120 km/h under a low-illumination environment with street lights has a significant positive effect on speed selection behaviour on roads with speed limits of 60 km/h, 80 km/h, and 120 km/h in low illumination without street lights. Therefore, speed management in a low-illumination environment with street lights should be strengthened, especially for expressways with 120 km/h speed limits, where the degree of traffic accident damage is relatively high, to severely punish speeding behaviour, strictly control driving speeds, reduce driving speeds under the condition of low illumination, and reduce the risk of accidents in low illumination and accident severity. Severe punishment for speeding behaviour and strict control of a driver's speed are conducive to reducing the driver's driving speed in low illumination, reducing the accident risk and accident severity in low illumination.

5. Conclusion

In this study, a "driver survey questionnaire in low illumination" effectively revealed the influencing factors of driver's speed selection behaviour in low illumination from the driver's perspective. The results show that the education and the total deduction score have a significant negative impact on speed selection behaviour in low illumination without street lights with a speed limit of 80 km/h, while gender have a significant positive impact. Night-driving days have a significant negative impact on speed selection behaviour in low illumination without street lights with a speed limit of 120 km/h, while deduction has a significant positive influence. Technical driving ability has a positive effect on peed selection behaviour in low illumination without street lights, while risk perception ability has a negative effect. The driving speed of a driver in a low-illumination environment with street lights has a positive influence on the choice of driving speed in low illumination without street lights, and the driving speed on a road with a speed limit of 120 km/h has a significant positive influence on speed selection behaviour on roads with speed limits of 60 km/h, 80 km/h, and 120 km/h under the condition of low illumination without street lights.

This study provides a theoretical foundation for the prevention of speed selection behaviours in a low-illumination environment. Regarding the design of further interventions, the emphasis on road safety education among males and experienced drivers may help promote safer driving in a low-illumination environment.

6. Limitations

There are some limitations in this study. This study suffers from the typical limitations of studies based on self-reported data, in which potential vulnerability to sources of bias are present. However, various existing studies have shown that self-reported data are basically consistent with actual data and can be used in experimental research [32]. Another limitation is that the survey was conducted only in Hefei, Anhui, China, and did not cover other cities. Future studies should compare several Chinese cities to validate the conclusions reported here.

Data Availability

The data used to support the findings of this study have not been made available because we have no right to share it.

Conflicts of Interest

The authors declare that they have no conflicts of interest.

References

[1] A. Gyakov, *Night Driving Safety of the Car*, China Communications Press, Beijing, China, 1990.

[2] F. Chen and S. Chen, "Injury severities of truck drivers in single- and multi-vehicle accidents on rural highways," *Accident Analysis & Prevention*, vol. 43, no. 5, pp. 1677–1688, 2011.

[3] Road Traffic Management Bureau of the Ministry of Public Security, *Statistical Annual Report on Road Traffic Accidents of the People's Republic of China*, Road Traffic Management Bureau of the Ministry of Public Security, Beijing, China, 2015.

[4] D. A. Owens, J. M. Wood, and J. M. Owens, "Effects of age and illumination on night driving: a road test," *Human Factors: The Journal of the Human Factors and Ergonomics Society*, vol. 49, no. 6, pp. 1115–1131, 2007.

[5] N. Rackoff and T. Rockwell, *Driver Search and Scan Patterns in Night Driving*, Transportation Research Board Special Report, Washington, DC, USA, 1975.

[6] Z. X. Feng, Y. W. Lei, H. Z. Yuan, W. H. Zhang, and N. N. Zhang, "Determination method of reasonable driving speed on highway in dynamic low illumination environment," *China Journal of Highway and Transport*, vol. 28, no. 10, pp. 105–111, 2015.

[7] M. Lyu, *The Connection Section between Tunnels and Bridges in Highway Traffic Safety Evaluation Model*, Tongji University, Shanghai, China, 2009.

[8] W. Wang, *Theory and Method of Driving Behavior in Road Traffic System*, Science Press, Berlin, Germany, 2001.

[9] X. Pang, H. Jiang, and A. Gao, "Cause and security counter measures of traffic accident in foggy expressway," *Communications Standardization*, vol. 10, pp. 200–203, 2006.

[10] W. Zhao, L. Wang, F. Ye et al., "Influence of environmental illuminance of drivers on visual recognition distance," *Traffic Information and Safety*, vol. 31, no. 6, 2013.

[11] F. Jørgensen and P. A. Pedersen, "Drivers' response to the installation of road lighting. an economic interpretation," *Accident Analysis and Prevention*, vol. 34, no. 5, pp. 601–608, 2002.

[12] M. Haglund and L. ABerg, "Speed choice in relation to speed limit and influences from other drivers," *Transportation Research. Part F: Traffic Psychology and Behaviour*, vol. 3, no. 1, pp. 0–51, 2000.

[13] W. Suh, P. Y.-J. Park, C. H. Park, and K. S. Chon, "Relationship between speed, lateral placement, and drivers' eye movement at two-lane rural highways," *Journal of Transportation Engineering*, vol. 132, no. 8, pp. 649–653, 2006.

[14] R. G. V. Baker, "On the quantum mechanics of optic flow and its application to driving in uncertain environments," *Transportation Research Part F: Traffic Psychology and Behaviour*, vol. 2, no. 1, pp. 27–53, 1999.

[15] M. Reed and S. Easa, "Effect of luminance on night driving performance of younger-old and older-old adults," *International Journal of Research & Reviews in Applied Sciences*, vol. 7, no. 3, pp. 218–227, 2011.

[16] A. Calvi, A. Benedetto, and F. D'Amico, "Investigating driver reaction time and speed during mobile phone conversations with a lead vehicle in front: a driving simulator comprehensive study," *Journal of Transportation Safety & Security*, vol. 10, no. 1-2, pp. 5–24, 2018.

[17] F. Chen, S. Chen, and X. Ma, "Analysis of hourly crash likelihood using unbalanced panel data mixed logit model and real-time driving environmental big data," *Journal of Safety Research*, vol. 65, pp. 153–159, 2018.

[18] Z. Feng, M. Yang, W. Zhang, Y. Du, and H. Bai, "Effect of longitudinal slope of urban underpass tunnels on drivers' heart rate and speed: a study based on a real vehicle experiment," *Tunnelling and Underground Space Technology*, vol. 81, pp. 525–533, 2018.

[19] F. Chen, M. Song, and X. Ma, "Investigation on the injury severity of drivers in rear-end collisions between cars using a random parameters bivariate ordered probit model," *International Journal of Environmental Research and Public Health*, vol. 16, no. 14, p. 2632, 2019.

[20] J. Shi, Y. Xiao, L. Tao, and P. Atchley, "Factors causing aberrant driving behaviors: a model of problem drivers in China," *Journal of Transportation Safety & Security*, vol. 10, pp. 288–302, 2018.

[21] S. Wu, X. Sun, and Y. He, "A study on the correlation between restricted speed and running speed of graded highways," *Traffic Standardization*, vol. 23, pp. 50–54, 2010.

[22] D. Zheng, *Study on Driver's Risk Perception and Influencing Factors*, Shanghai Jiaotong University, Shanghai, China, 2013.

[23] B. L. De Castro, F. J. Gracia, I. Tomás, and J. M. Peiró, "The safety culture enactment questionnaire (SCEQ): theoretical model and empirical validation," *Accident Analysis & Prevention*, vol. 103, pp. 44–55, 2017.

[24] K. Wang, W. Zhang, J. Liu et al., "Exploring the factors affecting myopic drivers' driving skills and risk perception in nighttime driving," *Cognition Technology and Work*, vol. 21, no. 2, pp. 275–285, 2018.

[25] W. Zhang, Z. Hu, Z. Feng, C. Ma, K. Wang, and X. Zhang, "Investigating factors influencing drivers' speed selection behavior under reduced visibility conditions," *Traffic Injury Prevention*, vol. 19, no. 5, pp. 1–20, 2018.

[26] R. Sadia, S. Bekhor, and A. Polus, "Speed variation for different drivers, situations, and road geometry: simulator and survey analysis," *Journal of Transportation Safety & Security*, vol. 10, no. 1-2, pp. 25–44, 2017.

[27] Stichting Wetenschap Onderzoek Verkeersveiligheid (SWOV), *SWOV Fact Sheet: Intelligent Speed Assistance (ISA)*, SWOV: Institute for Road Safety Research, Leidschendam, The Netherlands, 2010.

[28] P. Wasielewski, "Speed as a measure of driver risk: observed speeds versus driver and vehicle characteristics," *Accident Analysis & Prevention*, vol. 16, no. 2, pp. 89–103, 1984.

[29] K. Spolander, "Drivers' assessment of their own driving ability," Report No. 252, Swedish National Road and Transport Research Institute (VTI), Linköping, Sweden, 1983.

[30] J. Xu, J. Liu, X. Sun, K. Zhang, W. Qu, and Y. Ge, "The relationship between driving skill and driving behavior: psychometric adaptation of the driver skill inventory in China," *Accident Analysis & Prevention*, vol. 120, pp. 92–100, 2018.

[31] G. Cheng, H. Xu, and X. Mo, "The law of drivers' recognition of pedestrians crossing the street at night," *Journal of Harbin Institute of Technology*, vol. 45, no. 6, pp. 65–70, 2013.

[32] M. Ma, X. Yan, H. Huang, and M. Abdel-Aty, "Safety of public transportation occupational drivers: risk perception, attitudes, and driving behavior," *Transportation Research Record: Journal of the Transportation Research Board*, vol. 2145, no. 1, pp. 72–79, 2010.

Hindawi
Journal of Advanced Transportation
Volume 2020, Article ID 9263605, 11 pages
https://doi.org/10.1155/2020/9263605

Research Article

Vehicle Fuel Consumption Prediction Method Based on Driving Behavior Data Collected from Smartphones

Ying Yao,[1] Xiaohua Zhao,[1] Chang Liu,[1] Jian Rong,[1] Yunlong Zhang,[2] Zhenning Dong,[3] and Yuelong Su[3]

[1]*Beijing Key Laboratory of Traffic Engineering and the College of Metropolitan Transportation, Beijing University of Technology, Beijing 100124, China*
[2]*Zachry Department of Civil Engineering, Texas A&M University, College Station, TX 77843, USA*
[3]*Joint Laboratory for Future Transport and Urban Computing of Amap, AutoNavi Software Co., Ltd., Beijing 100102, China*

Correspondence should be addressed to Xiaohua Zhao; zhaoxiaohua@bjut.edu.cn

Received 26 December 2019; Revised 8 February 2020; Accepted 15 February 2020; Published 23 March 2020

Guest Editor: Feng Chen

Transportation is an important factor that affects energy consumption, and driving behavior is one of the main factors affecting vehicle fuel consumption. The purpose of this paper is to improve fuel consumption monitoring databases based on mobile phone data. Based on the mobile phone terminals and on-board diagnostic system (OBD) installed in taxis, driving behavior data and fuel consumption data are extracted, respectively. By matching the driving behavior data collected by a mobile phone with the fuel consumption data collected by OBD, the correlation between driving behavior and fuel consumption is explored, so that vehicle fuel consumption could be predicted based on mobile phone data. The fuel consumption prediction models are built using back propagation (BP) neural network, support vector regression (SVR), and random forests. The results show that the average speed, average speed except for idle (ASEI), average acceleration, average deceleration, acceleration time percentage, deceleration time percentage, and cruising time percentage are important indicators for fuel consumption evaluation. All three models could predict fuel consumption accurately, with an absolute relative error less than 10%. The random forest model is proved to have the highest accuracy and runs faster, making it suitable for wide application. This method lays a foundation for monitoring database improvement and fine management of urban transportation fuel consumption.

1. Introduction

Vehicle energy consumption and pollutant emissions are key problems for the healthy and sustainable development of urban transportation. With the continuous growth of car ownership in China, the energy consumption of its private cars increased 4.2 times, from 13.12 to 68.34 million tons of standard coal, from 2005 to 2015. Based on growth of the population, GDP, and the proportion of secondary and tertiary industries of China, the trend of future transportation energy consumption can be predicted. The energy consumption of private cars will continue to increase before 2020, when it is expected to reach 117.38 million tons of standard coal [1]. Therefore, reducing energy consumption has become one of the most important challenges in the transportation field.

Among many factors that affect the energy consumption of vehicles, driving behavior plays an important role. Research conducted by Ford Motor Company [2] shows that improvement of driving behavior could improve fuel economy by 25% in the short term. Providing drivers with continuous eco-driving feedback in the long term could lead to a 10% reduction in fuel consumption. Hiraoka et al. [3] studied the influence of ecological driving behavior on fuel consumption and found that giving feedback on fuel consumption information to drivers could improve fuel economy by 10%. In addition, the eco-driving instructions given to drivers could improve the fuel economy by approximately 15%. Ahn and Rakha [4] analyzed the influence of drivers' route choice on vehicle fuel consumption, and the results indicated that energy consumption and exhaust emissions

are significantly reduced by minimizing high-emission driving behavior. Thus, it is important to study the correlation between driving behavior and energy consumption and to use driving behavior to predict energy consumption.

At present, there is a significant volume of research on prediction models of energy consumption based on driving behavior. Hu et al. [5] conducted some real vehicle tests and a questionnaire survey to study the influence of driving style on the fuel consumption of electric vehicles on urban roads and constructed a prediction model for the fuel consumption of electric vehicles. Xu et al. [6] constructed two kinds of truck fuel consumption prediction models using driving behavior data obtained from the Internet of vehicles. The dynamic relationship between truck fuel consumption and truck drivers' driving behavior was described using an energy consumption index, and a generalized regression neural network model was established to predict truck fuel consumption. Zhao et al. [7] built a fuel consumption prediction model of urban road sections based on driving behavior by applying a machine learning algorithm, and the model could intuitively show the distribution characteristics of fuel consumption in basic sections of the Beijing expressway.

Data sources supporting the studies of fuel consumption prediction are mostly based on the data collected from the main controller of the vehicle, and an on-board diagnostic system (OBD) in conjunction with a questionnaire. The controller and OBD are limited by the equipment installation cost and drivers' installation willingness, so can only realize small-scale data management for small areas and with high uncertainty. The data collection form of a questionnaire also lacks flexibility, and it is difficult to guarantee the quality of the data.

With the rapid development of mobile terminal technology, the application of mobile phone sensors has been promoted. Mobile phone terminals have been used in the collection of driving behavior data and for the warning of dangerous driving. Johnson and Trivedi [8] proposed a system using dynamic time warping (DTW) and smartphone-based sensor fusion to detect nonaggressive and aggressive driving behavior, which gave audible feedback when it detected aggressive driving. Guido et al. [9] used the vehicle tracking data from smartphone sensors to estimate the safety performance of driving (including the deceleration rate to avoid crashes and the time to collision), and the crash risks in south-bound and north-bound lanes were analyzed. The application of the mobile phone terminal in driving safety has played an important role in the evaluation of vehicle fuel consumption. Because driving behavior data collected by mobile terminals are more detailed and easier to popularize, they lay a foundation for enriching urban road fuel consumption databases.

At present, the fuel consumption and emission data monitored by the statistical monitoring platform for the Beijing Municipal Transportation Administration are mostly based on OBD devices. The data collection objects are mainly taxi drivers, bus drivers, and truck drivers and do not cover all transportation enterprises. The mobile phone terminal provides a possibility for a larger scale of data collection. Fuel consumption cannot be directly collected by mobile phone terminals, but it could be predicted accurately by exploring the correlation between mobile phone and OBD data. At the same time, the driving behavior data collected by the mobile phone are influenced by the types, placement, shaking (caused by vehicle vibration), and drivers' usage of the phone, resulting in the instability of the driving behavior data, so a lot of calibration work needs to be done on the data. By constructing a fuel consumption prediction model, the application of mobile phone data could be used to calculate the fuel consumption of vehicles, which saves the installation cost of OBD equipment and provides a theoretical basis for traffic management departments to more accurately monitor urban traffic fuel consumption.

This study proposes a vehicle fuel consumption prediction method based on Global Positioning System (GPS) data collected from a smartphone. Taxi drivers participated in this experiment. By matching the driving behavior data of the mobile phone and the fuel consumption data of the OBD terminal, the driving behavior indexes that affect fuel consumption were screened, and the fuel consumption prediction models were constructed using machine learning algorithms. The prediction model of drivers' individual fuel consumption based on mobile phone data could not only further improve the real-time monitoring database of fuel consumption with strong error tolerance but also provide technical support for macro control of urban transportation energy consumption and effectiveness evaluation of the transportation energy policy.

2. Method

2.1. Analysis Framework. Since mobile phones cannot obtain the data of vehicles' fuel consumption directly, the driving behavior data collected from mobile phones and the fuel consumption collected from OBD were matched, and the fuel consumption prediction model was built. In the process of model construction, the data collected from mobile phones and OBD were both applied. After the model was built, larger-scale traffic fuel consumption was able to be predicted using only the driving behavior data collected from the mobile phones. The framework of model construction is shown in Figure 1. The steps of fuel consumption prediction are as follows:

(1) Data collection: natural driving behavior data of multiple drivers were collected based on GPS, linear accelerometer, gyroscope, and other sensors of mobile phones. At the same time, the real-time vehicle fuel consumption data were collected by the OBD terminal installed in the vehicle simultaneously.

(2) Index extraction: the data of mobile phones and OBD terminals were combined based on time. By comparing the consistency and difference of driving behavior data of the two terminals, the indexes for predicting vehicle fuel consumption based on mobile phone data were extracted.

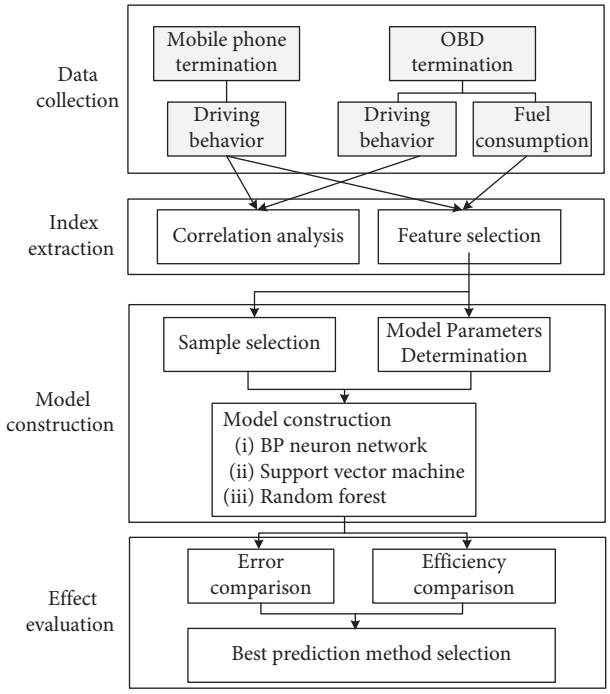

Figure 1: The framework of model construction. OBD means on-board diagnostic system and BP represents back propagation.

(3) Model construction: the training set and test set were selected randomly, and the fuel consumption prediction models were built using a back propagation (BP) neural network, a support vector machine, and a random forest.

(4) Effect evaluation: by building the fuel consumption prediction models several times and comparing the accuracy and efficiency of the three prediction models using different methods, the best method to predict vehicle fuel consumption based on mobile terminals is proposed.

2.2. Prediction Model. BP neural networks, support vector regression (SVR), and random forests are several common prediction methods with high accuracy and operation efficiency. This study built three types of prediction models, compared the difference in the prediction results, and finally we chose the best model for fuel consumption prediction.

2.2.1. BP Neural Network. An artificial neural network (ANN) is an operation model that mimics the process of neurons transmitting perceptual information to the human brain. This method has the characteristics of self-learning and high efficiency when processing nonlinear, unstructured, and large sample data. The error back propagation algorithm (BP neural network) [10] is one of the most widely used supervised learning algorithms in artificial neural networks. After the weights of the network are randomly selected, the BP neural network uses the back propagation method to update weights to minimize loss, and finally the connection weights of the network are determined. The structure of the vehicle fuel consumption prediction model based on a BP neural network is shown in Figure 2.

After screening the prediction indexes of fuel consumption, n indexes are determined as input variables. There are 5 neurons in the hidden layer, and the output y is the predicted fuel consumption. The connection weight between the input layer and the hidden layer is w_{ij}, and the connection weight between the hidden layer and the output layer is w_{jk}. First, the sample is transmitted through the input layer, and the data is converted into a nonlinear array within a certain range using the excitation function. Then, the nonlinear array reaches the output layer through weighting and outputs the results. If the error between the output fuel consumption and the actual fuel consumption exceeds the set of the expected error, the weight coefficient is corrected by back propagation. The network is repeat trained until the error is within the expected error, and the vehicle fuel consumption prediction model based on BP neural network is finally built.

2.2.2. Support Vector Regression (SVR). As a supervised machine learning algorithm, support vector machines are mainly applied to classification problems and regression problems [11]. The support vector machine algorithm transforms nonlinear problems into linear problems in high-dimensional space by constructing kernel functions, which gives the problem a geometrical explanation. The structure of the vehicle fuel consumption prediction model based on SVR is shown in Figure 3.

For a given set of samples $\{X_i, y_i\}$, $i = 1, 2, \ldots, m$, X is the n-dimensional input vector (including n driving behavior indicators) and y is the corresponding fuel consumption. The input vector is mapped to high-dimensional space, and the output y can be calculated as follows:

$$f(X) = w \cdot \varphi(X) + b, \tag{1}$$

where w is the weight vector, $\varphi(\cdot)$ is the mapping function that maps the input vector to the high-dimensional feature space, and b is the bias term.

By adding a convex optimization problem and relaxation factor, the support vector regression problem can be converted into the following equivalent solution:

$$\text{minimize} \quad \frac{1}{2}\|w\|^2 + C\sum_{i=1}^{n}\left(\xi_i + \widehat{\xi}_i\right)$$

$$\text{s.t.} \quad \begin{cases} f(X_i) - w^T \cdot \varphi(X_i) - b \le \varepsilon + \xi_i \\ w^T \cdot \varphi(X_i) + b - f(X_i) \le \varepsilon + \widehat{\xi}_i \\ \widehat{\xi}_i, \xi_i \ge 0 \\ i = 1, 2, \ldots, n \\ C > 0, \end{cases} \tag{2}$$

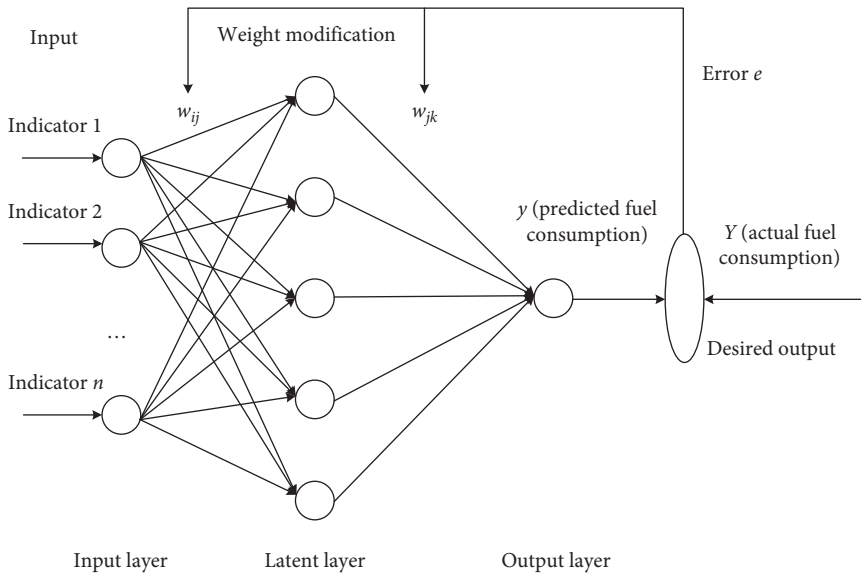

Figure 2: The structure of the vehicle fuel consumption prediction model based on the BP neural network.

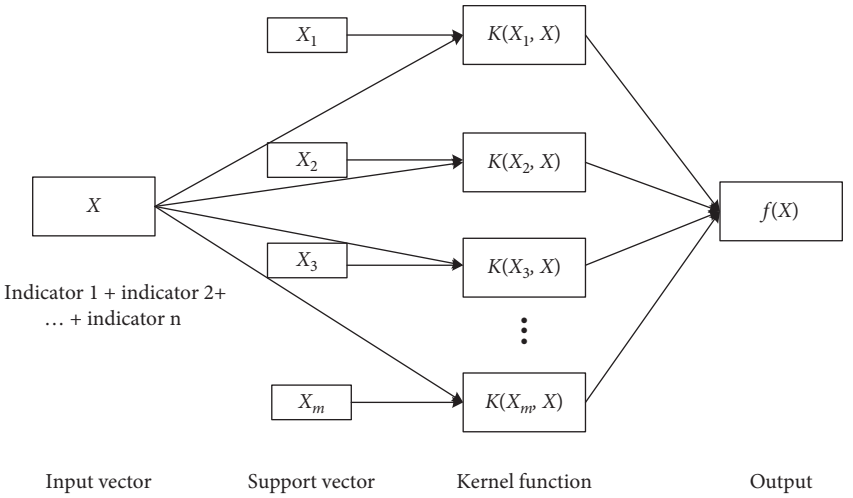

Figure 3: The structure of vehicle fuel consumption prediction model based on support vector regression (SVR).

where $\widehat{\xi}_i, \xi_i$ are the slack variables; C is the penalty-factor, which reflects the importance of outlier points; and ε is the insensitive loss function coefficients, which can ignore the error of the true value within a certain range and affect the final number of support vectors.

Three parameters, namely, ε, C, and the kernel function, should be determined when using the SVR algorithm to predict vehicle fuel consumption. The input vector is the n indicators required for fuel consumption prediction, and the output is vehicle fuel consumption. ε and C are determined by dividing them into several small cells according to certain rules. The model error corresponding to the variable value of each cell is calculated, and the variable values of the small cells with the minimum error are selected. The radial basis function (RBF) has a better performance in the application of SVR [12, 13]. Therefore, the kernel function adopted in this study is RBF, and the calculation method is as follows:

$$K(X, X') = e^{-||X - X'||^2/\sigma^2} \quad (3)$$

where σ is the hyperparameter of the RBF kernel, which is able to determine the range characteristics of input data and the correlation extent between support vectors.

2.2.3. Random Forest. A random forest (RF) is an effective classification method for prediction and classification [14]. A random forest is composed of a large number of decision trees. On the basis of decision trees, random processes are added to the row and column vectors, so as to avoid the potential overfitting problem of decision trees. For each tree, the training sample is sampled with replacement, and the

out-of-bag (OOB) data in each tree accounts for approximately 37% of the total data. The main calculation steps of the random forest regression algorithm are as follows:

First of all, k groups of training sample sets were selected by sampling with replacement. Secondly, m features were randomly selected from n features in each training sample set as splitting nodes, and k decision trees were generated. The node splitting of each decision tree adopted the principle of minimum mean square error, which minimizes the sum of mean square deviations of two groups of datasets after splitting. Finally, the predicted vehicle fuel consumption was obtained by averaging the predicted value of k decision trees. The structure of the vehicle fuel consumption prediction model based on the random forest is shown in Figure 4.

The three models have their advantages and disadvantages on the basis of different datasets. This study constructed three kinds of fuel consumption prediction models, and the most suitable and efficient model was chosen to predict fuel consumption.

3. Data Source and Index Extraction

3.1. Data Source. Experimental data were collected from OBD terminals installed in taxis and mobile phone terminals, and the sampling interval was 1 s. The data types that were collected are shown in Table 1.

The experiment was conducted in August 2017, and 20 drivers participated in the experiment to collect natural driving data for 15 days. All the taxicabs were Elantra with a 4-cylinder, 1.6-liter engine and were certified by the national-level-IV emission standard. On-board diagnostics (OBD) were installed in each taxicab during the experiment to collect driving behavior and fuel consumption data. The OBD devices have been widely used in Beijing taxi companies for over five years for monitoring the fuel consumption and emission data by the statistical monitoring platform for the Beijing Municipal Transportation Administration. The instantaneous fuel consumption of vehicles collected from OBD is calculated by relevant parameters such as engine load rate, engine speed, peak air inflow, and fuel correction factor. By comparing the fuel consumption calculated by OBD with the fuel consumption collected by CAN bus (calculated by fuel injection pulse width), the error of the instantaneous fuel consumption was within ±3% and the error of average fuel consumption per 100 km was 0.74% [15]. Meanwhile, drivers were asked to install software on their own mobile phone and keep the software running while driving to collect GPS data. The software is based on the android system and is specifically developed to collect GPS data from mobile phone sensors and calculate driving behavior. The two types of data were collected and uploaded to the cloud simultaneously.

Before the experiment, a mobile phone holder was given to each driver and held in the same position in the vehicle. The screen of the phone was placed perpendicular to the horizontal line. Mobile phone direction sensors were applied to the test to ensure that the location of the mobile phone is fixed and unified, and drivers were required to keep their phones in place while driving.

Although both the OBD and the mobile phone have GPS and drivers are required to place the mobile phone in a fixed position during driving, the output results of GPS data collected from OBD and mobile phone are different, which may be caused by the shaking of mobile phone when the vehicle vibrates or the differences of mobile phone type. In the actual driving process, mobile phone shaking and type differences are inevitable. Therefore, this study assumes that the construction of the fuel consumption prediction model could reduce the influence of data error collected by mobile phones and predict the fuel consumption accurately without the OBD device.

3.2. Index Extraction. By matching the data collected from the OBD and mobile phone terminals, the daily driving behavior of each driver and the corresponding fuel consumption could be obtained. There are many driving behavior factors that affect the fuel consumption of vehicles [16]. Seven indicators which could be calculated by mobile phone data were selected to predict fuel consumption. The types and definitions of the indicators are shown in Table 2. The acceleration condition is defined as acceleration greater than 0.1 m/s^2, the deceleration condition is defined as acceleration less than −0.1 m/s^2, and the condition of cruising is defined as the absolute value of acceleration less than 0.1 m/s^2. By averaging the driving behaviors of 20 drivers over 15 days, a total of 300 sets of data can be obtained.

Although road conditions, weather, and other factors also have a great influence on fuel consumption, they are not considered in this study. The main objective of this study is to evaluate the daily eco-driving level of taxi drivers, so as to help the traffic management department to monitor and improve the eco-driving skills of taxi drivers, and eco-driving training courses could be provided to drivers with poor eco-driving skills to reduce fuel consumption. Therefore, it is necessary to estimate the daily average fuel consumption (L/100 km) for taxi drivers. Since each taxi driver drives a different route each day, it is difficult to count all road types throughout the day. Although ignoring the influence of road conditions and other factors resulted in a decrease in the prediction accuracy of fuel consumption, the method adopted in this study is more applicable to a wider range of conditions and could estimate the daily ecological driving level of the drivers. The method also provides the feasibility demonstration for the future refined fuel consumption prediction. In the future research, the fuel consumption prediction results of drivers under different road conditions (such as ramps, curves, and intersections) would be analyzed and compared, so as to improve the accuracy of vehicle fuel consumption prediction.

Pearson correlation analysis was adopted to verify the correlation between driving behavior data from OBD and mobile phone terminals, and the results are shown in Table 3. It can be seen that, except for the cruising time

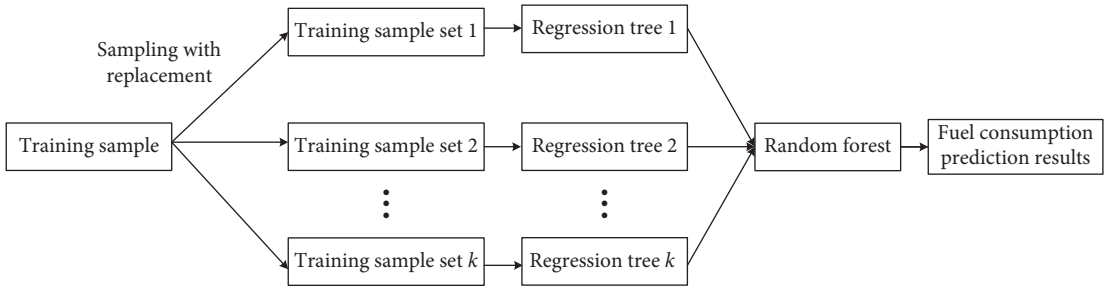

Figure 4: The structure of vehicle fuel consumption prediction model based on the random forest.

Table 1: Data types collected from the OBD terminal and mobile phone terminal.

OBD termination	Mobile phone termination
Time	Time
The global positioning system (GPS) latitude and longitude	The GPS latitude and longitude
GPS direction angle	Elevation
Speed in car dashboard	GPS speed
GPS speed	X-direction acceleration
Revolutions per minute (RPM)	Y-direction acceleration
Torque	Z-direction acceleration
State of air condition	X-direction angular acceleration
Oxygen sensor state	Y-direction angular acceleration
The instantaneous fuel consumption	Z-direction angular acceleration

Table 2: Related indexes to predict fuel consumption.

Indicators	Definition	Unit
Average speed V_{mean}	$V_{\text{mean}} = (1/T)\sum_{i=1}^{T} v_i$ where v_i is the speed of i second and T is the total driving time of one day	km/h
Average speed except for idle (ASEI) V'_{mean}	$V'_{\text{mean}} = (1/T')\sum_{i=1}^{T'} v_i$ where T' is the driving time of one day except idle	km/h
Average acceleration $\overline{a}_+$	$\overline{a}_+ = (1/t_a)\sum_{i=1}^{t_a} a_i$ where a_i is the acceleration of i second and t_a is the driving time of acceleration per day	m/s^2
Average deceleration $\overline{a}_-$	$\overline{a}_- = (1/t_d)\sum_{i=1}^{t_d} a_i$ where t_d is the driving time of deceleration per day	m/s^2
Acceleration time percentage P_a	$P_a = (t_a/T) \cdot 100\%$	%
Deceleration time percentage P_d	$P_d = (t_d/T) \cdot 100\%$	%
Cruising time percentage P_c	$P_c = (t_c/T) \cdot 100\%$ where t_c is the driving time of cruising per day	%
Fuel consumption FC	$\text{FC} = \sum_{i=1}^{T} \text{FC}_i/\text{distance}$ where FC_i is the instantaneous fuel consumption of i second and distance is the total driving distance per day	L/100 km

Table 3: Correlation analysis of driving behavior collected from OBD and mobile phone terminals.

	Pearson correlation coefficient	P value
Average speed V_{mean}	0.975	<0.001
ASEI V'_{mean}	0.936	<0.001
Average acceleration $\overline{a}_+$	0.793	<0.001
Average deceleration $\overline{a}_-$	0.670	<0.001
Acceleration time percentage P_a	0.662	<0.001
Deceleration time percentage P_d	0.662	<0.001
Cruising time percentage P_c	0.060	0.467

percentage, the other driving behavior indicators calculated by OBD and mobile phones are significantly correlated, with a correlation coefficient above 0.6. The reason for the difference in the cruising time percentage is that there are some differences in sampling accuracy between mobile phones and OBD, so the value of speed and acceleration calculated by GPS data collected from mobile phones and OBD are not exactly the same. The high correlation of multiple indicators indicates that the method of using mobile phone data to predict fuel consumption is feasible.

In order to verify the correlation between the data collected by mobile phone and the fuel consumption data collected by OBD and extract the relevant indexes for predicting fuel consumption, the relationship between different driving behavior indexes collected from mobile phones and fuel consumption collected from OBD were analyzed; the results are shown in Figure 5. As can be seen from Figure 5(a), the higher the average driving speed of the driver, the lower the fuel consumption. There is a strong correlation between average speed and fuel consumption. Since this study only considered the average driving speed of each day, the maximum average speed does not exceed 50, and the relationship between fuel consumption and speed is linear. From the perspective of instantaneous speed, fuel consumption increases when it exceeds 80 km/h, and the speed and fuel consumption are u-shaped curves [17]. The relationships between average acceleration/deceleration and fuel consumption are shown in Figures 5(b) and 5(c). The results show that a driver with heavy acceleration or deceleration during a day's driving would consume more fuel. Figure 5(d) shows the relationship between acceleration time percentage, deceleration time percentage, cruising time percentage, and fuel consumption. The results show that for a journey with lower fuel consumption, the driving time of cruising takes a larger proportion and the driver has less idle behavior, and a journey with high fuel consumption usually shows the driver as idle for a long time. Time percentage and fuel consumption also show a certain correlation, but these trends are not as obvious as the impact of the value of speed or acceleration on fuel consumption. In order to verify the influence of various driving behavior indexes on fuel consumption and select the related indexes of fuel consumption prediction, correlation analyses are examined in the following section.

Pearson correlation is a common filter-based feature selection method. By analyzing the Pearson correlation between driving behavior data collected by mobile phones and fuel consumption data collected by OBD, the key driving behavior indexes that affect vehicle fuel consumption can be selected through filtering. The results are shown in Table 4. All the driving behavior indexes are significantly correlated with fuel consumption ($P < 0.05$). Therefore, the indicators of average speed, ASEI, average acceleration, average deceleration, acceleration time percentage, deceleration time percentage, and cruising time percentage are selected to predict fuel consumption.

4. Results and Discussion

4.1. Model Training. The process of building the fuel consumption prediction model based on taxi drivers' daily driving behavior data is shown in Figure 6. On the one hand, the indicators of average speed, ASEI, average acceleration and deceleration, acceleration time percentage, deceleration time percentage, and cruising time percentage of each driver during each day were calculated using the driving behavior data collected from the mobile phone terminal. On the other hand, the instantaneous fuel consumption data of the vehicle were collected through the OBD terminal and converted into daily fuel consumption data. The two sources of data (driving behavior data and daily fuel consumption data) were matched through the collection time. Of all data collected, 75% were randomly selected as training samples and the remaining data were test samples. The fuel consumption prediction models were constructed based on the BP neural network, SVR, and random forest. To ensure the accuracy and stability of the prediction model, sample selection and model training were conducted 10 times. By comparing the difference in predicted fuel consumption and actual fuel consumption between the three models, the accuracy of using mobile phone data to predict vehicle fuel consumption was evaluated.

In the fuel consumption prediction model based on BP neural network, the "trainlm" algorithm was used for training, the logarithmic function "tansig" was used for the exciting function, and the linear function "purelin" was used for the node transfer function. The training times of the model were set as 100 times, and the convergence condition was set as the error of the model which is less than 0.001.

Based on the fuel consumption prediction model of SVR, the determination of the value of the insensitive loss function and penalty parameter was based on the exhaustive method, and the optimal value of the two coefficients was calculated by limiting the number of iterations to make the error less than a certain absolute value. The radial basis function (RBF) was taken as the kernel function of the SVR model.

Based on the fuel consumption prediction model of the random forest, 50 regression trees were set for training. The relationship between the number of regression trees and the out-of-bag error is shown in Figure 7. It can be seen that with the increase in the number of regression trees, the model error decreases, and the model is converged when there are about 50 regression trees.

4.2. Evaluation Results. The fuel consumption prediction results of one training process are shown in Figure 8. The figure shows the approximation degree between the three fuel consumption prediction results (BP neural network, SVR, and random forest) and the actual fuel consumption. As can be seen from Figure 8, some points with a larger deviation are the prediction results of the BP neural network model. However, in general, the three prediction models

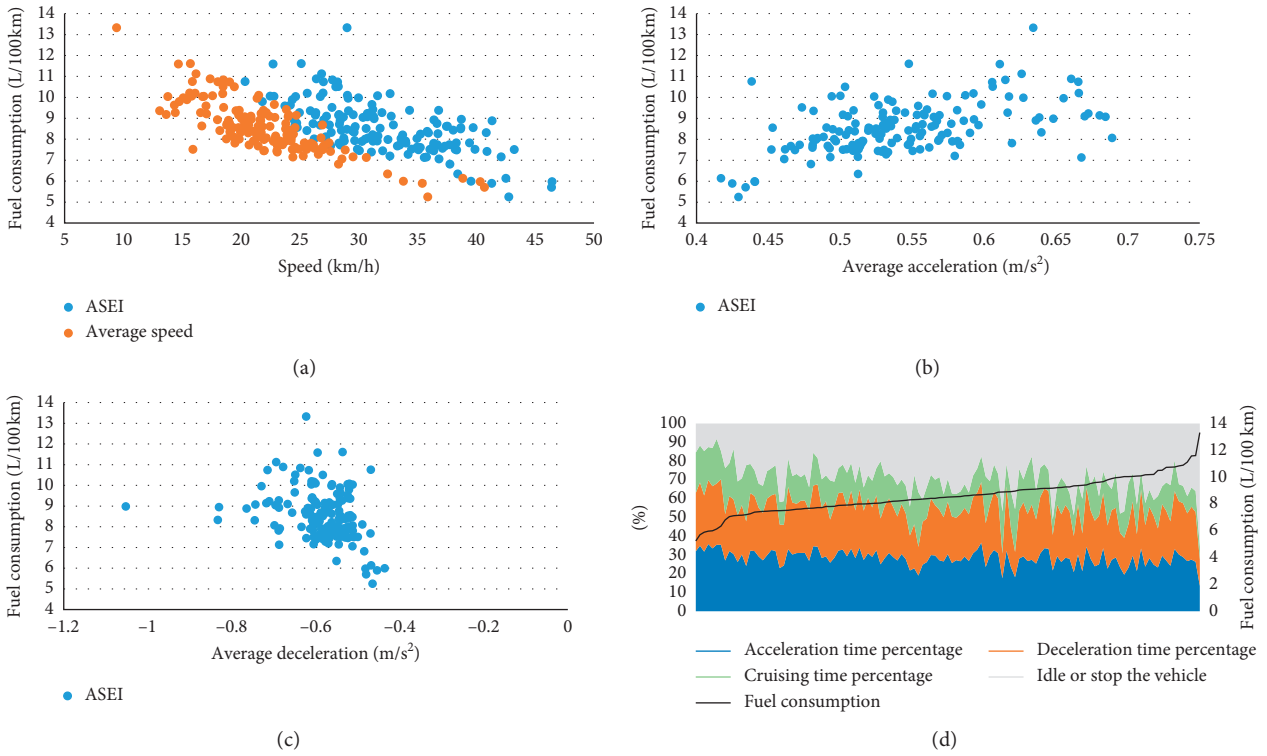

Figure 5: Fuel consumption distribution based on different driving behavior indexes. (a) The relationship between average speed and fuel consumption. (b) The relationship between average acceleration and fuel consumption. (c) The relationship between average deceleration and fuel consumption. (d) The relationship between time percentage and fuel consumption.

Table 4: Correlation analysis of driving behavior collected from mobile phone termination and fuel consumption collected from OBD.

	Fuel consumption	
	Pearson correlation coefficient	P value
Average speed V_{mean}	−0.8	<0.001
ASEI V'_{mean}	−0.659	<0.001
Average acceleration $\overline{a}_+$	0.515	<0.001
Average deceleration $\overline{a}_-$	−0.314	<0.001
Acceleration time percentage P_a	−0.363	<0.001
Deceleration time percentage P_d	−0.293	<0.001
Cruising time percentage P_c	−0.229	0.005

have a good fitting degree; the prediction results are basically distributed on both sides of $y = x$ with a high approximation degree.

In order to evaluate the accuracy and efficiency of the three fuel consumption prediction models, four indexes, namely, the root-mean-square error (RMSE), mean absolute percentage error K, R-squared, and model running time, were compared. The calculation methods of the first three of these indexes are as follows:

$$\text{RMSE} = \sqrt{\frac{\sum (f_i - y_i)^2}{n}},$$
$$K = \left| \frac{f_i - y_i}{y_i} \times 100\% \right|, \tag{4}$$
$$R^2 = 1 - \frac{\sum_{i=1}^{n} (y_i - f_i)^2}{\sum_{i=1}^{n} (y_i - \overline{y})^2},$$

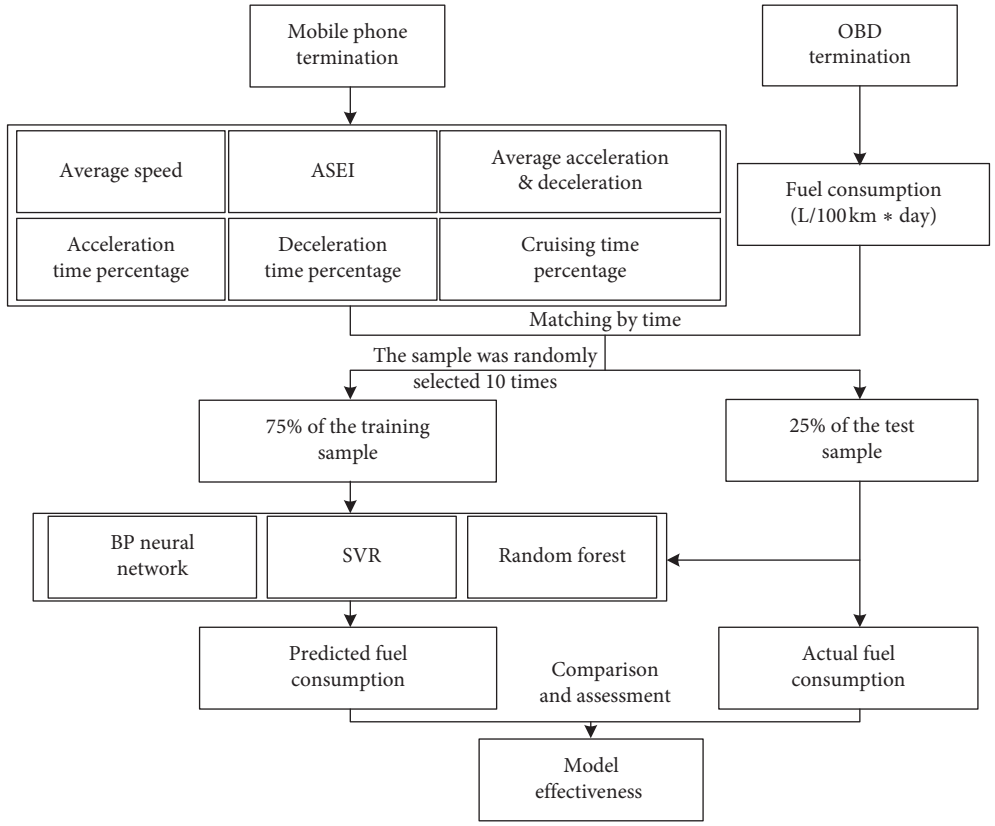

Figure 6: The process of building the fuel consumption prediction model.

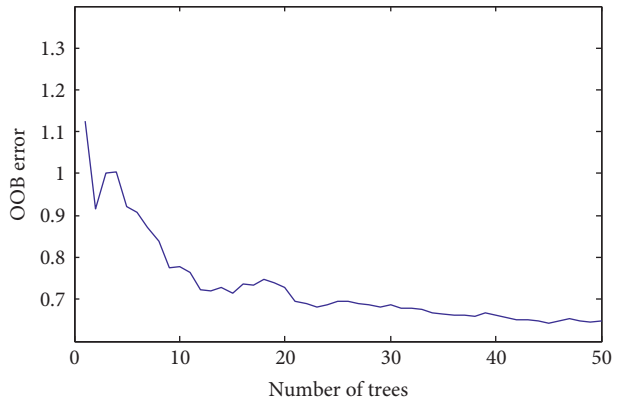

Figure 7: Out-of-bag error of the random forest model.

where f_i is the predicted fuel consumption, y_i is the actual fuel consumption, $\overline{y}$ is the average fuel consumption, and n is the number of samples.

The model evaluation results are shown in Table 5. It can be seen that the three models all show high prediction accuracy. The RMSE is 0.78–0.89 L/100 km, the absolute relative error (K) is 6.9%–7.5%, and the R-squared is greater than 0.5, indicating that the three models can accurately predict the fuel consumption of vehicles with the data collected by mobile phones. By comparing the errors and efficiency among the three models, it can be seen that the model based on the random forest has higher accuracy than BP neural network or SVR, and the running time of the random forest model is far lower than that of the BP neural network and SVR models. Therefore, the fuel consumption prediction model based on the random forest is effective and efficient for predictions based on individual driving behavior collected from mobile phones and is more suitable for practical applications to larger sample datasets.

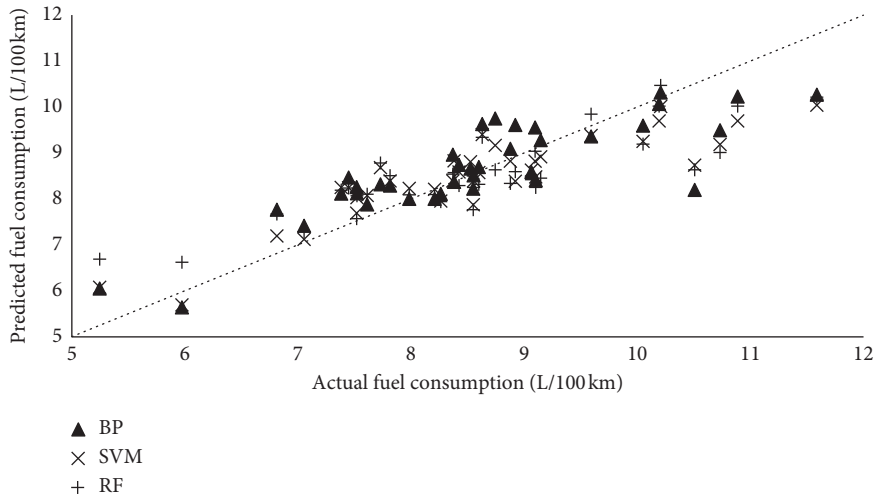

Figure 8: Fuel consumption prediction results.

Table 5: Model evaluation results.

Prediction method	Root-mean-square error (RMSE)	K	R-squared	Time (s)
BP neural network	0.872	0.075	0.547	0.724
Support vector regression	0.888	0.073	0.519	0.933
Random forest	0.783	0.069	0.635	0.140

5. Conclusion

In this study, driving behavior data and fuel consumption data of taxi drivers collected from OBD and mobile phone terminals, respectively, were matched. The correlation between driving behavior and fuel consumption was analyzed, and relevant driving behavior indicators affecting fuel consumption were extracted through the filter-based feature selection method. Using the seven selected driving behavior indicators (namely, average speed, ASEI, average acceleration, average deceleration, acceleration time percentage, deceleration time percentage, and cruising time percentage), three fuel consumption prediction models based on a BP neural network, SVR, and a random forest were constructed.

The results of model error and the run time comparison analysis show that the three models could predict fuel consumption accurately, and the random forest model had the highest accuracy and efficiency, with an RMSE of 0.783 L/100 km, mean absolute percentage error (K) of 6.9%, and model running time of 0.14 s. This finding is consistent with the research of Wickramanayake and Bandara [15], which also shows that random forest models are most effective in predicting fuel consumption based on driving behavior data. The research object of Wickramanayake and Bandara is the fuel consumption prediction of the bus, and this study focuses on the fuel consumption of the taxicabs. At the same time, the driving behavior data of this study are collected from mobile phones with higher flexibility and complexity rather than a fixed GPS device. This method could predict vehicle fuel consumption with high accuracy and efficiency based on cell phone data and provide strong support for traffic management departments to monitor the ecological levels of driving behavior of taxi drivers.

It is worth emphasizing that in the early stage of model construction, driving behavior data collected by mobile phones and fuel consumption data collected by OBD are applied. After the prediction model is built, mobile phone data can be directly used to predict the daily fuel consumption of drivers without installing OBD devices. Application of this method could change the traditional way of fuel consumption acquisition, and the use of mobile phone data to evaluate the ecological impacts of individual driving behavior could save the cost of equipment installation. At the same time, since not all taxi drivers are willing to install OBD devices in their taxicabs, this method could help increase the user data source, which could greatly improve the database size of taxi fuel consumption. Therefore, the method in this study could improve the depth, breadth, and refinement level of fuel consumption monitoring and management of taxi drivers' driving behavior, thus laying a theoretical foundation and providing technical support for the city to reduce fuel consumption.

This study aims to propose a method to predict vehicle energy consumption using mobile phone data. Although the sample size used in this study is limited, it provides a basis for larger scale and more accurate fuel consumption prediction. In future research, the collection of samples will be further expanded, and the fuel consumption under various road conditions, traffic conditions, and weather conditions would be considered. Through the data enrichment, model optimization, and improvement of the prediction indicators, the method could lay a theoretical foundation for the precise energy consumption supervision of taxi enterprises.

Meanwhile, since taxicabs are relatively homogenous, the fuel consumption prediction model in this study was fixed, taking only taxi drivers as the research object. In future study, more types of vehicles, such as buses and trucks, could be considered. Differentiated fuel consumption prediction models based on different vehicle types could be constructed to further improve the monitoring and management of urban energy consumption.

Data Availability

The driving behavior and fuel consumption data used to support the findings of this study are available from the corresponding author upon request.

Conflicts of Interest

The authors declare that they have no conflicts of interest.

Acknowledgments

This study is supported by the National Key R&D Program of China (Grant no. 2018YFB1601000), National Natural Science Foundation of China (Grant no. 61672067), Natural Science Foundation of Beijing Municipality (Grant no. 17JH0001), Joint Laboratory for Future Transport and Urban Computing of Amap, and Beijing Engineering Research Center of Urban Transport Operation Guarantee, Beijing University of Technology.

References

[1] H. Wang, "Energy consumption in transport: an assessment of changing trend, influencing factors and consumption forecast," *Journal of Chongqing University of Technology (Social Science)*, vol. 7, 2017.

[2] J. N. Barkenbus, "Eco-driving: an overlooked climate change initiative," *Energy Policy*, vol. 38, no. 2, pp. 762–769, 2010.

[3] T. Hiraoka, Y. Terakado, S. Matsumoto, and S. Yamabe, "Quantitative evaluation of eco-driving on fuel consumption based on driving simulator experiments," in *Proceedings of the 16th ITS World Congress and Exhibition on Intelligent Transport Systems and Services*, Stockholm, Sweden, September 2009.

[4] K. Ahn and H. Rakha, "The effects of route choice decisions on vehicle energy consumption and emissions," *Transportation Research Part D: Transport and Environment*, vol. 13, no. 3, pp. 151–167, 2008.

[5] K. Hu, J. Wu, and M. Liu, "Modelling of EVs energy consumption from perspective of field test data and driving style questionnaires," *Journal of System Simulation*, vol. 30, no. 11, pp. 83–91, 2018.

[6] Z. Xu, T. Wei, S. Easa, X. Zhao, and X. Qu, "Modeling relationship between truck fuel consumption and driving behavior using data from internet of vehicles," *Computer-Aided Civil and Infrastructure Engineering*, vol. 33, no. 3, pp. 209–219, 2018.

[7] X.-h. Zhao, Y. Yao, Y.-p. Wu, C. Chen, and J. Rong, "Prediction model of driving energy consumption based on PCA and BP network," *Journal of Transportation Systems Engineering and Information Technology*, vol. 5, pp. 185–191, 2016.

[8] D. A. Johnson and M. M. Trivedi, "Driving style recognition using a smartphone as a sensor platform," in *Proceedings of the 2011 14th International IEEE Conference on Intelligent Transportation Systems (ITSC)*, pp. 1609–1615, Toronto, Canada, October 2011.

[9] G. Guido, A. Vitale, V. Astarita, F. Saccomanno, V. P. Giofré, and V. Gallelli, "Estimation of safety performance measures from smartphone sensors," *Procedia—Social and Behavioral Sciences*, vol. 54, pp. 1095–1103, 2012.

[10] W. J. Zhang, S. X. Yu, Y. F. Peng, Z. J. Cheng, and C. Wang, "Driving habits analysis on vehicle data using error back-propagation neural network algorithm," in *Computing, Control, Information and Education Engineering*, vol. 55, CRC Press, Guilin, China, 2015.

[11] H. Drucker, J. C. Chris, L. Kaufman, A. Smola, and V. Vapnik, "Support vector regression machines," in *Advances in Neural Information Processing Systems*, pp. 155–161, MIT Press, Cambridge, MA, USA, 1997.

[12] H.-l. Feng, "Study on prediction model of ecological security index in Chongqing city based on SVR model," *Computer Science*, vol. 40, no. 8, pp. 245–248, 2013.

[13] Z. Ramedani, M. Omid, A. Keyhani, S. Shamshirband, and B. Khoshnevisan, "Potential of radial basis function based support vector regression for global solar radiation prediction," *Renewable and Sustainable Energy Reviews*, vol. 39, pp. 1005–1011, 2014.

[14] L. Breiman, "Random forests," *Machine Learning*, vol. 45, no. 1, pp. 5–32, 2001.

[15] S. Wickramanayake and H. M. N. D. Bandara, "Fuel consumption prediction of fleet vehicles using machine learning: a comparative study," in *Proceedings of the 2016 Moratuwa Engineering Research Conference (MERCon)*, pp. 90–95, IEEE, Moratuwa, Sri Lanka, April 2016.

[16] M. Kuhler and D. Karstens, "Improved driving cycle for testing automotive exhaust emissions," in *Proceedings of the SAE International*, Dearborn, MI, USA, 1978.

[17] D. Yang, M. Li, and X. Ban, "Real-time on-board monitoring method of gasoline vehicle fuel consumption based on OBD system," *Journal of Automotive Safety and Energy*, vol. 7, no. 1, pp. 108–114, 2016.

Hindawi
Journal of Advanced Transportation
Volume 2020, Article ID 7539829, 14 pages
https://doi.org/10.1155/2020/7539829

Research Article

The Impact of Violations of Bicycles and Pedestrians on Vehicle Emissions at Signalized Intersections

Jianchang Huang, Guohua Song, Jianbo Zhang, Chenxu Li, Qiumei Liu, and Lei Yu

Key Laboratory of Transport Industry of Big Data Application Technologies for Comprehensive Transport, Beijing Jiaotong University, Beijing 100044, China

Correspondence should be addressed to Guohua Song; ghsong@bjtu.edu.cn

Received 23 September 2019; Revised 10 January 2020; Accepted 5 February 2020; Published 21 March 2020

Guest Editor: Young-Ji Byon

An intersection is a typical emission hot spot in the urban traffic network. And frequent violations such as running the red light have been a critical social problem at signalized intersections in developing countries. This article aimed to quantify the impact of violations (behaviors which will block the fleet) on emissions at signalized intersections. Increased emissions of vehicles affected by violations are of two levels: (1) trajectory level for the first four affected vehicles and (2) traffic flow level for the subsequent vehicles. At the trajectory level, the study focuses on the second-by-second activities of the first four affected vehicles. First, the trajectory model of the first affected vehicle is developed. Then, the trajectory of the other three vehicles is constructed using the Gipps car-following model. At the traffic flow level, a linear emission model is developed to describe the relationship between emission factors and idling time in the one-stop (vehicle stop once) and two-stop (vehicle stop twice) scenarios based on the global position system (GPS)-collected data at 44 intersections in Beijing. Based on the linear emission model, increased emissions at the traffic flow level are calculated as knowing the number of stops and idling time before and after violations. The analysis of the subsequent vehicles is divided into unsaturated and saturated conditions. Under the unsaturated condition, the emissions have barely increased due to the increase of idling time for one-stop vehicles caused by the violations. Under the saturated conditions, the emission increment increases sharply as the one-stop vehicle gradually transforms to a two-stop vehicle because of violations, and the maximum emission increment reaches 45% in half an hour in the case. The increment of emissions decreases steadily as the proportion of two-stop vehicles reaches 100% after violations, while the proportion before violations keeps increasing.

1. Introduction

In recent years, urban vehicle pollution has threatened human health. Air pollutants can cause pulmonary and cardiovascular diseases and chronic obstructive pulmonary disease, and decrease lung function [1]. According to the WHO report, air pollution resulted in 3.7 million premature deaths worldwide in 2012 [2]. In the United States, motorized vehicles are responsible for 57% of emissions [3].

An intersection is a typical emission hot spot in the urban traffic network [4], especially in a densely populated metropolis like Beijing. Extensive studies have been carried out on vehicle emissions around intersections, and illustrate that high emissions at intersections mainly resulted from unstable traffic operation and stop-and-go vehicle activity [5–7] and lead to high pollutant exposure, particularly to pedestrians and cyclists around the intersections.

When vehicles, pedestrians, and cyclists arrive at the intersection, each traffic subject follows the corresponding rules and passes through the intersection orderly. However, violation behaviors, one of the core factors, are frequently observed in developing countries such as China [8]. Frequent violations will not only aggravate traffic risk but also worsen the stop-and-go condition of vehicles. Four typical violations at intersections are shown in Figure 1 frequent violations of pedestrians and bicycles block the vehicle fleet, aggravating stop-and-go behaviors at intersections. In this article, the critical problem of quantifying emission increments caused by violations has been discussed.

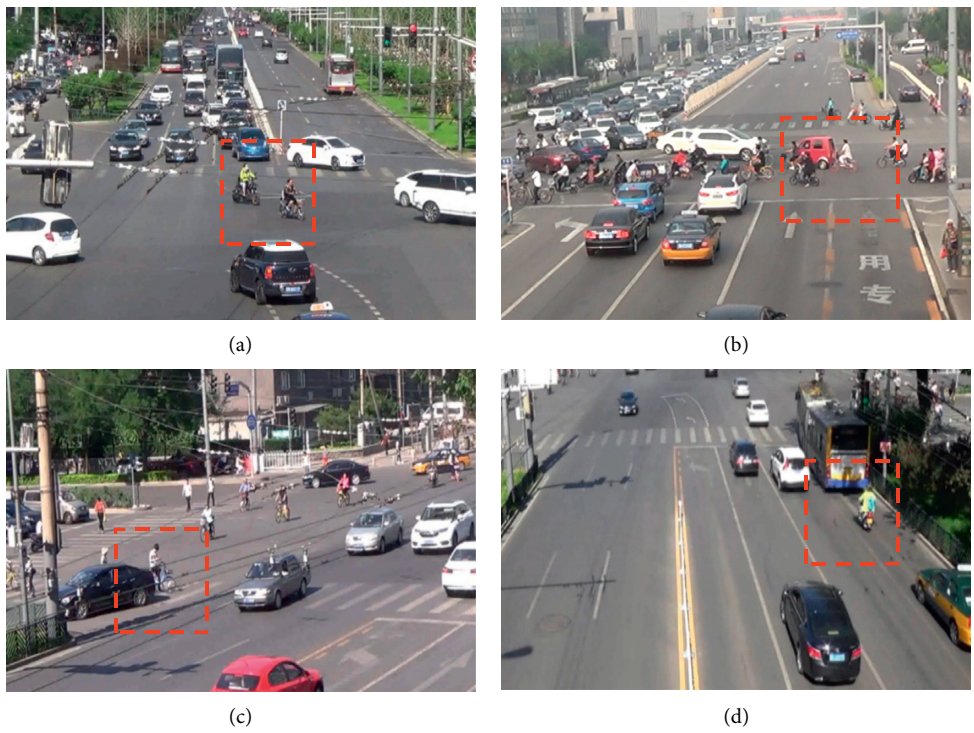

(a) (b) (c) (d)

Figure 1: Violations at signalized intersections under mixed traffic in Beijing. (a) Crossing the intersection diagonally. (b) Running the red light. (c) Waiting in front of the motorway. (d) Intruding into the lane.

Motor vehicles, bicycles, and pedestrians are three typical traffic components of mixed traffic flow intersections. Their relationships are variable and complex due to the conflict in time and space. Existing studies indicated that violations were frequently observed in developing countries and had a significant impact on driving operation [7]. Researches on the impact of violations on emissions can be summarized into two categories: (1) intersection emission estimation and (2) violation characteristics and impact analysis.

In terms of intersection emission estimation, existing studies indicated that steady speed, shortest delays, and fewest stops are the best operations for emission reduction [9, 10]; nonsmooth traffic operations and stop-and-go activity were the main reasons for high emissions at intersections; and much more time was spent in the acceleration mode after highly interrupted movements of vehicles [11–13]. During the acceleration period, an engine operates at a high level, which leads to excessive fuel consumption and emissions [14, 15]. In existing studies, extensive studies have been carried out on vehicle emission around intersections. Rakha and Ding analyzed the impact of stops on vehicle fuel consumption and emissions and found that vehicle fuel consumption was more sensitive to cruise-speed levels [13]. Papson et al. used a time-in-mode model with MOVES to analyze vehicle emissions at congested and uncongested signalized intersections [16]. Zhang et al. developed the SIDRA model to estimate intersection emissions with MOVES, and acceleration mode included constant acceleration and linearly decreasing acceleration (3). Gokhale and Pandian developed a semi-empirical box model to predict CO concentration based on the assumed traffic flow pattern at intersections [17]. Braven et al. estimated vehicle emissions at a signalized intersection by using VISSIM [18].

In terms of violation characteristic analysis, it can be summarized into two categories. (1) Violation characteristics mainly include two aspects: (a) for the influencing factors (waiting time, group size of pedestrians, gender, nonmotor vehicle type, and so on), existing studies indicated that these factors had an obvious impact on intersection violations [19–21], and (b) for the frequency model, violation probability model [22] and violation waiting time model [23] were developed to predict the frequency of violations. (2) Impact of interference has an impact on vehicles, both at the trajectory level and the traffic flow level. At the trajectory level, Przybyla established a dynamic car-following model for driving distraction [24]. At the traffic flow level, interference has an impact on vehicle speed [25] and further influences intersection capacity [26–28].

The mechanism of the trajectory and emission characteristics affected by interference has not been fully understood. Further investigation is thus necessary. Hence, this article was aimed at quantifying the impact of violations on emissions at intersections. The content of this article is divided based on the following two aspects. (1) Variations in vehicle operating affected by violations. Variations of vehicle headways and trajectories are analyzed based on manual investigation data. (2) Based on the analysis above, increased emissions of vehicles affected by violations included two levels: (a) modeling at the trajectory level for second-by-second activities of the first four affected vehicles and (b) modeling at the traffic flow level for the aggregated

parameters (number of stops and idling time) of the subsequent vehicles after the first four vehicles. A numerical simulation is conducted to assess the impact of violations on emissions based on the existing study.

2. Materials and Methods

In this study, violations are defined as the behavior that will block the vehicle fleet. Pedestrians and cyclists are the objectives of violations.

Increased emissions of vehicles affected by violations include two levels (see Figure 2): (1) trajectory level for the first four affected vehicles and (2) traffic flow level for the subsequent vehicles. At the trajectory level, the study focused on second-by-second activities of the first four affected vehicles. First, the trajectory model of the first affected vehicle is developed. Then, the trajectory of the other three vehicles is constructed by using the Gipps car-following model. At the traffic flow level, a linear emission model that can describe the relationship between emission factors and idling time in the one-stop and two-stop scenarios is developed by using Global Position System (GPS)-collected data at 44 intersections in Beijing. Increased emissions are calculated by the number of stops and idling time before and after violations based on the linear emission model. Finally, a case study is conducted to assess the impact of violations on vehicle emissions at signalized intersections.

2.1. Data Collection. This article includes two types of data. (1) Manual investigation data are used for describing the vehicle operating characteristics under violation. (2) Emission data are used for developing the linear emission model, which can explain the relationship between emission factors and idling time in the one-stop and two-stop scenarios.

2.1.1. Manual Investigation Data. Video data of 8 signalized intersections under mixed traffic were collected in Beijing, China, which are used to model the operating of vehicles affected by violations. The data include intersection attributes and violation data.

(1) Intersection attributes

(a) Channelization information
(b) Signal information

(2) Violation data: Violation data were acquired from videos frame by frame, which included three parts.

(a) Trajectories data. The crosswalk grid is constructed by crosswalks in the four directions of the intersection (see Figure 3). Based on the crosswalk grid in the video, positions of vehicles at each time step are collected, and 10 groups of trajectories are collected under the influence of violations.

(b) Headway. 171 groups of time headway are collected from video, and each group includes five headways of vehicle fleet after the violation with a precision of 0.02 s.

(c) Idling time of the first affected vehicle. The time precision is 0.02 s, and 66 groups of data are collected.

2.1.2. Emission Data. The emission data includes two parts.

(1) Emission rate. Vehicle emission data are derived from the local emission rate model for light-duty gasoline vehicles [29, 30]. The emission standard of China IV was selected to provide the emission rates for LDVs, which is more common in Beijing compared with other emission standards.

(2) Global positioning system (GPS) trajectory data. 1666 valid trajectories of data, whose range is 200 meters of the intersection radius, were selected from 44 arterial and collector intersections in Beijing. Vehicle specific power (VSP, kW/ton) is estimated after data quality control [31]. Other details about the data are listed as follows:

(i) Date, from April 25th, 2004, to April 16th, 2013;

(ii) Time, from 5:00 to 23:00; and

(iii) Speed, from 0 to 133 km/h (for the whole trajectory to ensure accuracy of the GPS device), with a precision of 0.1 km/h [32].

2.2. Variations of Vehicle Operating Affected by Violations. Increased emissions of vehicles affected by violations included two levels: (1) trajectory level for the first four affected vehicles and (2) traffic flow level for the subsequent vehicles. At the trajectory level, the study focused on second-by-second activities of the first four affected vehicles. At the traffic flow level, the study focused on the number of stops and idling time before and after violations of the subsequent vehicles after the first four vehicles. Increased emissions of the two levels are the total increased emissions under the violation condition.

The characteristics of headway under violations are shown in Figure 4. When the violation occurs, the headway of the first affected vehicle will increase obviously. From the first affected vehicle to the fourth, the headways gradually return to be stable. The impact of violations on the vehicle fleet disappears after the fourth vehicle. As a result, the first four vehicles are determined as vehicles affected by violations in the trajectory level.

$$t_{\text{lost}} = \sum_{i=1}^{4} \left(t_{\text{head,after},i} - t_{\text{head,before},i} \right), \tag{1}$$

where t_{lost} (s) is the total lost time of violation behaviors. i is the i^{th} vehicle after the violation location. $t_{\text{head,after}}$ (s) is the headway after the violation, and $t_{\text{head,before}}$ (s) is the time headway before the violation.

Vehicles trajectories under the violation are shown in Figure 5. The x-axis is time, and the y-axis is the distance. The negative y-axis is the location of the queuing vehicles, and the positive y-axis is downstream of the intersection.

The red point represents the location and time of the violation. τ is the reaction time plus braking time, and S_τ is the corresponding distance. The first affected vehicle will

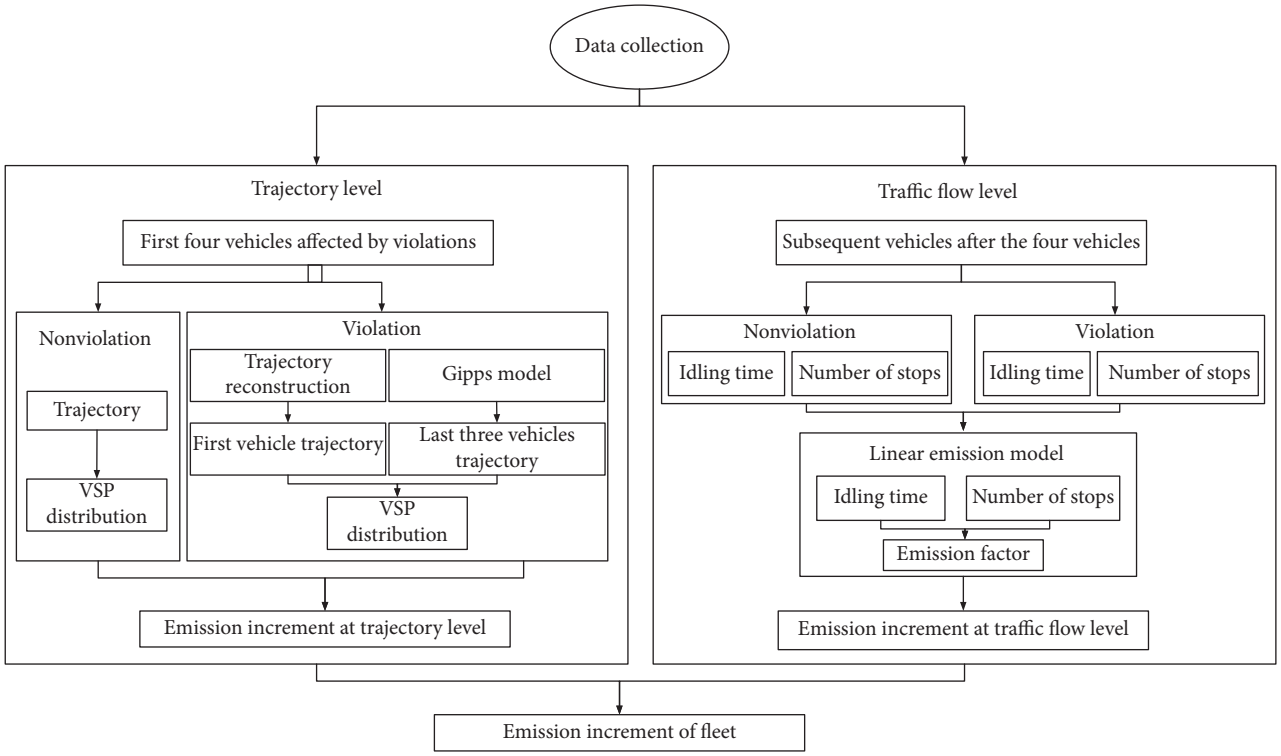

Figure 2: Overview of the methodology.

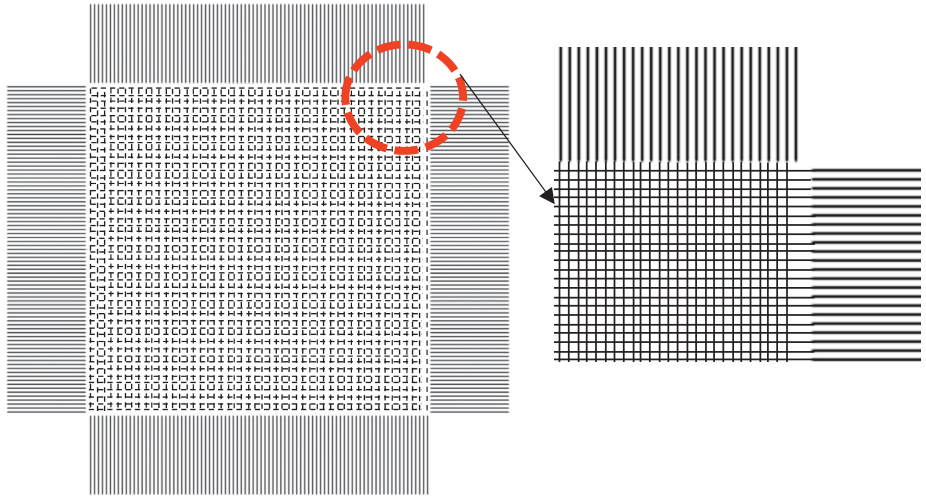

Figure 3: Intersection crosswalk grid in the video.

return to normal speed after the process of deceleration-idling-acceleration. The second vehicle starts to decelerate after the reaction time of D_r since the first affected vehicle began to decelerate. The deceleration of the second vehicle is less than the first vehicle as the interference decreases as the impact of the violation spreads in the vehicle fleet. The second vehicle begins to accelerate after the reaction time of A_r since the first affected vehicle accelerated. When the y-axis of D_r and A_r is the same, the second affected vehicle will have a second stop; the process of the second vehicle is deceleration-idling-acceleration; if not, the process is deceleration-acceleration.

The interference is gradually transmitted to the rear of the vehicle fleet, as described above. When the speed is low enough, the subsequent vehicles will extend the idling time to eliminate the interference as the fifth vehicle. Then, the subsequent vehicles will pass the intersection with the saturated time headway.

2.3. Trajectory Level. At the trajectory level, the objective is the first four affected vehicles after the violation. It is necessary to divide the model into two parts: (1) the trajectory model for the first vehicle and (2) the car-following model for the other three vehicles.

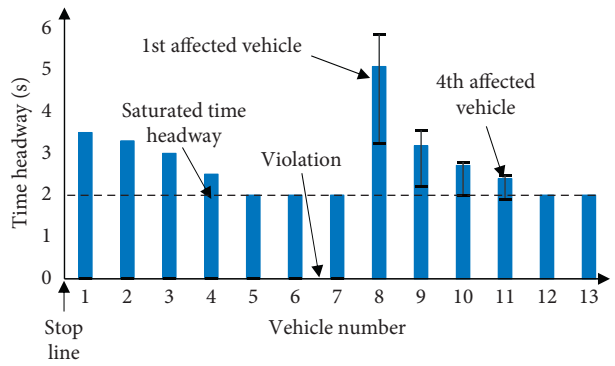

Figure 4: Time headway after violations (with the first and third quantiles).

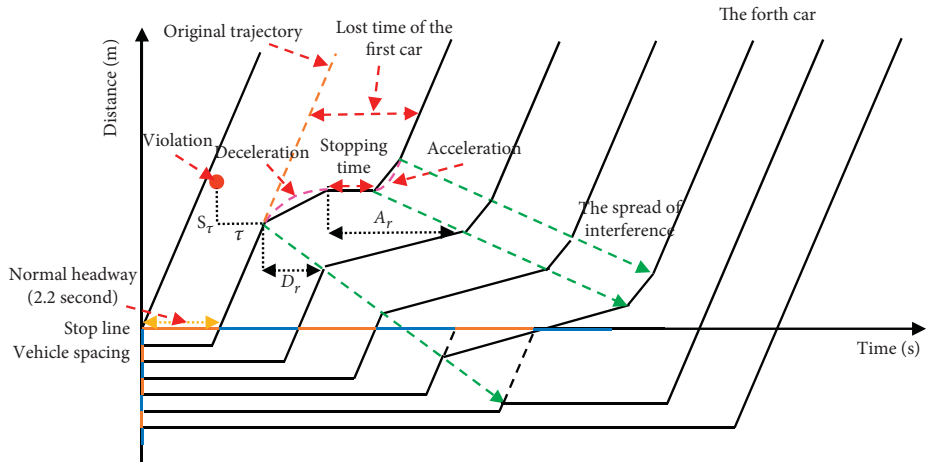

Figure 5: Vehicle trajectories affected by the violation.

2.3.1. The First Affected Vehicle. The trajectory of the first affected vehicle can be described when the following two factors are determined: (1) idling time and (2) acceleration and deceleration data.

For the idling time, sixty-six groups of idling time data in violation situations are collected. The average idling time is 2.08 s (standard deviation is 3.03).

For the acceleration and deceleration data, a corresponding relationship between vehicle speed and acceleration is developed in the low-speed range based on GPS trajectory data (see Figure 6).

As shown in Figure 6, based on the GPS trajectory data of 44 intersections, a total of 18,709 pieces of valid data of the first 10-s deceleration and 10-s acceleration around the idling time are extracted. At low speed, each speed corresponds to a group of accelerations. In other words, the process of acceleration and deceleration in violation conditions can be totally described after knowing the initial speed before violations. The acceleration of the first affected vehicle can be calculated as equations (2)–(3):

$$a_{s,t} = \text{random}\left(a_{\text{range}}\left(v_{s,t}\right)\right), \quad \text{when acceleration or deceleration,} \tag{2}$$

$$a = 0, v = 0, \quad \text{when idling,} \tag{3}$$

where $V_{s,t}$ are the speeds in the acceleration and deceleration states at time t; the states are acceleration and deceleration when s is a and d, respectively. a_{range} $(V_{s,t})$ are the corresponding acceleration range of $V_{a,t}$ and $V_{d,t}$. Each corresponding acceleration range has a database in which random values are taken by numerical simulation.

2.3.2. The Rear Three Vehicles of the First Four Affected Vehicles. The rear three vehicles decelerate after the sudden stop of the first affected vehicle. At the intersection, acceleration of the rear vehicle is closely related to the speed of the preceding vehicle, the speed of the rear vehicle, and the distance between the two vehicles. The Gipps car-following model can not only fulfill the above requirement but also generate rather realistic VSP distributions among the car-following models [33], which are calculated as equations (4)–(6):

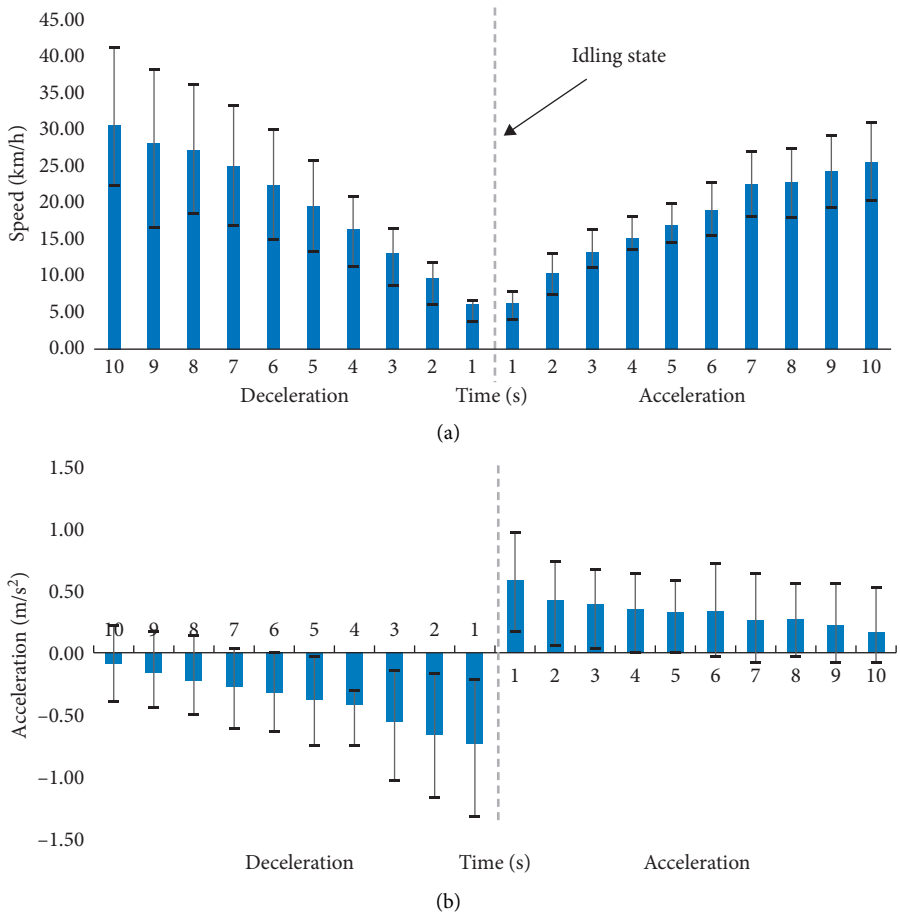

Figure 6: Speed and corresponding acceleration in the low-speed range (with the first and third quantiles). (a) Speed distribution under low-speed range of queuing. (b) Acceleration distribution under low-speed range of queuing.

$$v_n(t+\tau) = \min\left\{v_n^{\mathrm{acc}}(t+\tau), v_n^{\mathrm{dec}}(t+\tau)\right\}, \tag{4}$$

$$v_n^{\mathrm{acc}}(t+\tau) = v_n(t) + 2.5 \cdot a_n \tau\left(1 - \frac{v_n(t)}{v_n^d}\right)\sqrt{0.025 + \frac{v_n(t)}{v_n^d}}, \tag{5}$$

$$v_n^{\mathrm{dec}}(t+\tau) = -\tau d_n + \sqrt{\tau^2 d^2 + d_n\left\{2 \cdot \left[x_{n-1}(t) - x_n(t) - S_{n-1}\right] - \tau v_n(t) + \frac{v_{n-1}(t)^2}{d_{n-1}}\right\}}. \tag{6}$$

where a_n (m/s^2) is the maximum desired acceleration of the following vehicle; d_n (m/s^2) is the maximum desired deceleration of the following vehicle; $\widetilde{d}_{n-1}$ (m/s^2) is the estimation of the maximum desired deceleration of the leading vehicle; T (s) is the apparent reaction time; S_{n-1} is the effective length of a vehicle, which consists of the vehicle length and the minimum distance between the vehicles; θ is the additional delay for braking, which is 0.5; and α, β, and γ are parameters, which are 2.5, 0.025, and 0.5, respectively.

2.3.3. Emission Increment at Trajectory Level. At the trajectory level, the study focused on second-by-second activities of the first four affected vehicles. Two different models are developed: one is the trajectory model of the first vehicle, while the other is the Gipps car-following model of the three rear vehicles. The trajectory model of four vehicles affected has been developed above; thus, increased emission factors of the four vehicles can be calculated as follows:

$$\mathrm{EF}_{\mathrm{increased,trajectory},x} = 3600 \cdot \left(\frac{\sum_i \mathrm{ER}_i \cdot \mathrm{VSPBin}_{i,\mathrm{trajectory},x}}{v_{\mathrm{effected},x}} - \frac{\sum_i \mathrm{ER}_i \cdot \mathrm{VSPBin}_{i,\mathrm{normal},x}}{v_{\mathrm{normal},x}}\right), \quad x = 1, 2, 3, 4, \tag{7}$$

where $EF_{increased,trajectory,x}$ (g/km) is the increased emission factors of the x^{th} affected vehicle, VSP $Bin_{i,trajectory,x}$ is the time fraction in the i^{th} VSP bin of trajectory after violations, and $V_{effected,x}$ (km/h) is the average speed after violations.

2.4. Traffic Flow Level. At the traffic flow level, a linear emission model that can describe the relationship between emission factors and idling time in the one-stop and two-stop scenarios is developed by using GPS-collected data at 44 intersections in Beijing. Increased emissions are calculated by the number of stops and idling time before and after violations based on the linear emission model.

2.4.1. Linearly Emission Model. In this section, a linear emission model which can describe the relationship between emission factors and idling time in the one-stop and two-stop scenarios is developed. The emission model is developed based on the emission rate data and 85 VSP distributions, which are constructed based on the number of stops and idling time.

(1) VSP Distribution. Based on field measurements from the available research on emissions, there are three typical trajectories for a vehicle passing through an intersection (see Figure 7): (a) No stop, (b) one stop, and (c) multiple stops at the intersection (30, 31). It is hypothesized that each of these speed profiles generates different levels of emissions, with type three generating the highest amount of emission due to longer idling time and more acceleration and deceleration circles.

The equation for calculating VSP is provided by equation (8). VSP values are binned at an interval of 1 kW/ton. This article analyzes the VSP bins of −20 kW/ton to 20 kW/ton. More than 98% of the VSP data are in this range.

$$VSP_t = \frac{A \cdot v_t + B \cdot v_t^2 + C \cdot v_t^3}{m} + (a_t + g \cdot \sin\theta) \cdot v_t, \quad (8)$$

where a_t (m/s^2) is the acceleration, g (m/s^2) is the acceleration due to gravity, which is 9.8 m/s^2; and $\sin\theta$ is the road grade. A (kw·s/m), B (kw·s^2/m^2), and C (kw·s^3/m^3) are road load coefficients, representing rolling resistance, rotational resistance, and aerodynamic drag, respectively; the values of A, B, and C are 0.156461, 0.0020002, and 0.000493, respectively. m (ton) is the vehicle weight, and the value is 1.4788 ton.

Based on GPS trajectory data, idling time rarely exceeds 150 s for one-stop vehicles, or 275 s for two-stop vehicles. Thus, 85 VSP distributions are developed based on the number of stops, idling time, and division of upstream and downstream (see Table 1).

(2) Emission Rates. Vehicle emission rate data were derived from the local emission rate model for light-duty gasoline vehicles (see Figure 8), and the type of gasoline emission standard is China IV.

(3) Emission Factors. Idling time and number of stops are the most important changes under the violation. Therefore, the eimssion factors have two key parameters: number of stops and the idling time based on GPS data (see Figure 8). The

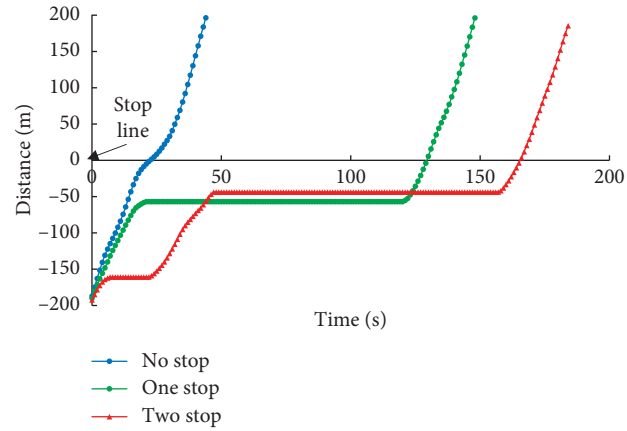

Figure 7: Three types of GPS trajectories at mixed-flow intersection.

Table 1: Information of the eighty-five VSP distributions.

Serial number	Spatial position	Number of stops	Idling time (s)
1	Downstream of intersection	0	0
2	Upstream of intersection	0	0~2
3	Upstream of intersection	1	2~5
4	Upstream of intersection	1	5~10
5	Upstream of intersection	1	10~15
.....			
30	Upstream of intersection	1	135~140
31	Upstream of intersection	1	140~145
32	Upstream of intersection	1	145~150
33	Upstream of intersection	2	10~15
34	Upstream of intersection	2	15~20
35	Upstream of intersection	2	20~25
.....			
83	Upstream of intersection	2	260~265
84	Upstream of intersection	2	265~270
85	Upstream of intersection	2	270~275

downstream emission factor is constant, as there is no stop. The emission factors are calculated as follows:

$$EF_v = \frac{3600 \cdot \sum_i ER_i VSPBin_i}{v}, \quad (9)$$

where EF_v (g/km) is the emission factor at the average speed of v (km/h). ER_i (g/s) is the mean emission rate of the i^{th} VSP Bin. VSP Bin_i is the fraction in the i^{th} VSP Bin.

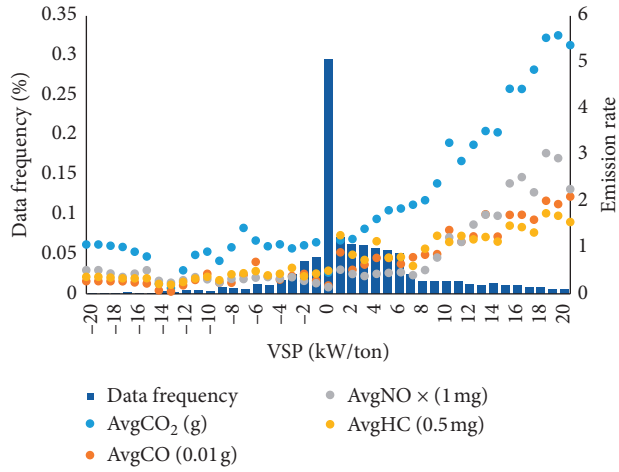

Figure 8: Mean emission rates in each VSP bin.

The emission factors increase linearly with the increase in idling time, as shown in Figure 9. The difference in emission factors between one-stop and two-stop vehicles is small under the same idling time. It is because the two-stop vehicle keeps a low speed and low acceleration, while the corresponding VSP value is concentrated around zero, and the corresponding emission rate is also small. But the range of the idling time of one-stop and two-stop vehicles is obviously different. The emission factor model is shown as follows:

$$\mathrm{EF}_{c,i} = a_{c,i} \cdot t_{\mathrm{idling}} + b_{c,i}, \quad c = 1, 2, i = 1, 2, 3, 4, \tag{10}$$

where EF_i, EF_j (g/km) are emissions of types i and j. When $i = 1$, 2, 3, 4, EF_i is the emission factor of CO_2, CO, NO_X, and HC of one-stop vehicles, respectively. When $c = 1$, 2, EF_j is the emission factor of one-stop and two-stop vehicles, respectively. t_{idling} is the idling time of the vehicle. a_i and b_i are parameters.

2.4.2. Variations of Vehicles Operating at Traffic Flow Level. At the traffic flow level, the study focused on the number of stops and idling time for the subsequent vehicles after the first four vehicles, which is divided into two scenarios (see Figure 10).

(1) Unsaturated condition of the vehicle fleet after being disturbed by violations;

(2) Saturated condition of the vehicle fleet after being disturbed by violations.

As shown in Figure 10, the total lost time of the first four affected vehicles is 4 s in the unsaturated condition. The idling time of subsequent vehicles increases by 4 s, and the number of stops is still one. Under the saturated condition, two vehicles will transform from one stop to two stops due to the increased idling time. And the idling time of two-stop vehicles increases by 4 s. Suppose that the maximum number of stops for all vehicles is two. Subsequent vehicles are divided into three types: (type A) one-stop vehicle, the increase in idling time is equal to the total lost time, (type B) transformation from one-stop vehicle to two-stop vehicle, and (type C) two-stop vehicle, the increase in idling time is equal to the total lost time of cycles.

Under the unsaturated condition, the subsequent vehicles are all type A. Under the saturated condition, vehicles that passing through the intersection are types A, B, and C at the beginning. As cycles pass, type A vehicles will disappear first, followed by type B vehicles. After all vehicles transform to two-stop vehicles, vehicles passing through the intersection are all type C.

As shown in Figure 11, VSP distributions of vehicles with and without violations are divided into three conditions, which corresponds to types A, B, and C (see Figure 11). For types A and C, the number of stops of affected vehicles is constant. Thus, the difference in VSP distributions of vehicles with and without violations is small. For type B, the number of stops transforms from one to two, and the idling time increment is the sum of the lost time and the red-light time. The frequency of VSP distributed above 0 kW/ton will be much highly affected by violations.

Take equation (10) as a reference. The emission model has been developed based on the number of stops and idling time. The operation change of subsequent vehicles, which are after the first four affected vehicles, is reflected in the number of stops and idling time. Therefore, increased emissions of the subsequent vehicles can be obtained by the emission model above. Based on equation (11), the numerical simulation method is used to calculate the emissions under violation conditions.

$$\begin{aligned}\mathrm{EF}_{\mathrm{increased,flow},y} = &\left(a_{\mathrm{cAfter},i} \cdot t_{\mathrm{after}} + b_{\mathrm{cAfter},i}\right) \\ &- \left(a_{\mathrm{cBefore},i} \cdot t_{\mathrm{before}} + b_{\mathrm{cBefore},i}\right),\end{aligned} \tag{11}$$

where $\mathrm{EF}_{\mathrm{increased,flow},y}$ (g/km) is the increased emission factors of subsequent vehicles. y is the y^{th} vehicle of vehicles going through the intersection in the cycle. t_{after} is the idling time after violations, and t_{before} (s) is the idling time without violations. cAfter and cBefore are stopping numbers before and after violations, respectively.

2.5. Increased Emissions Affected by Violations. The analysis of emissions affected by violations includes two levels. At the trajectory level, the study focused on second-by-

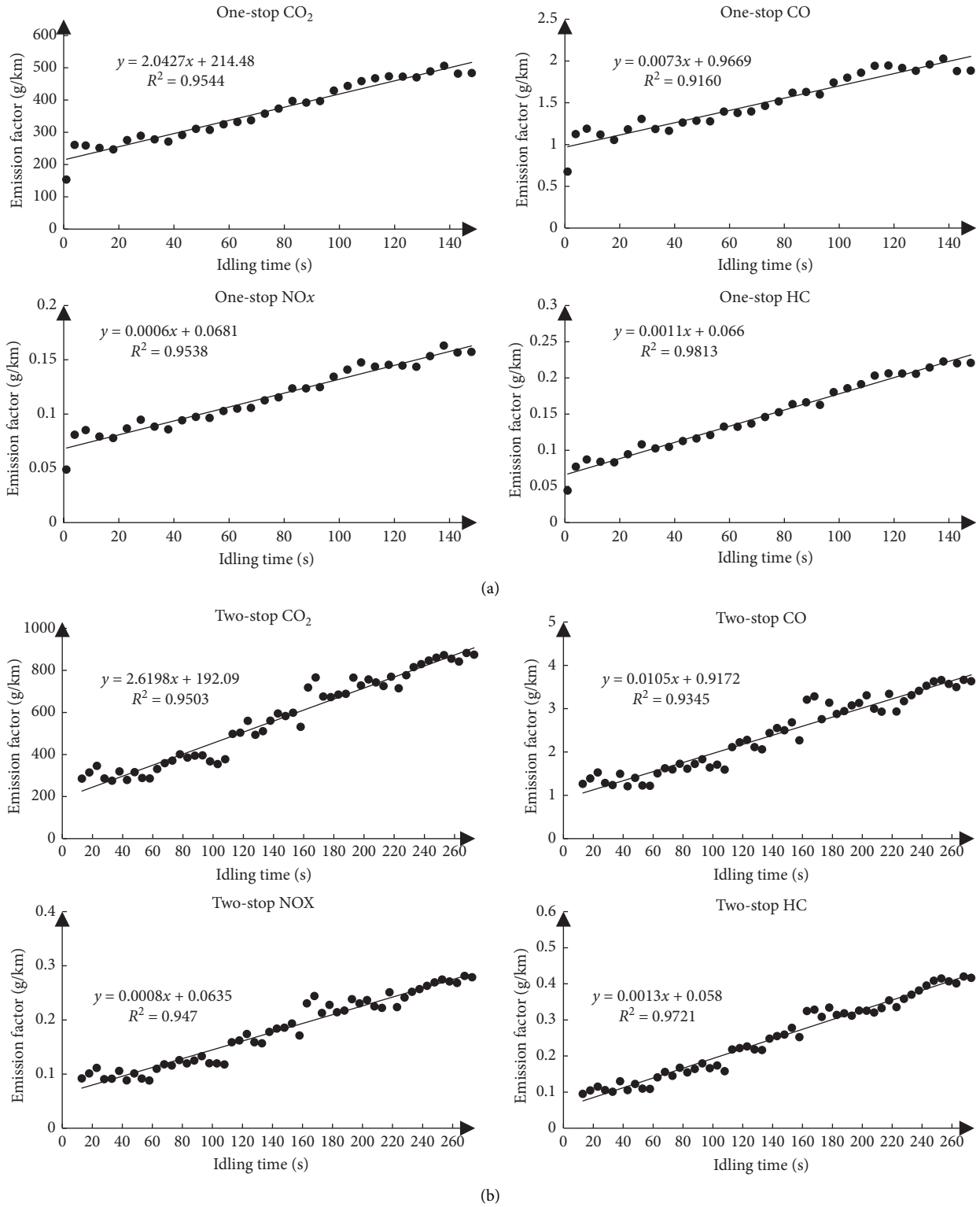

Figure 9: Emission factor model based on the number of stops and idling time.

second activities of the first four affected vehicles. At the traffic flow level, the study focused on the aggregated parameters (number of stops and idling) for the subsequent vehicles after the first four vehicles, and the conditions are divided into two categories: unsaturated and saturated conditions of the vehicle fleet disturbed by violations.

The sum of the increased emissions on these two levels is the total emission at intersections affected by violations, which can be calculated as follows:

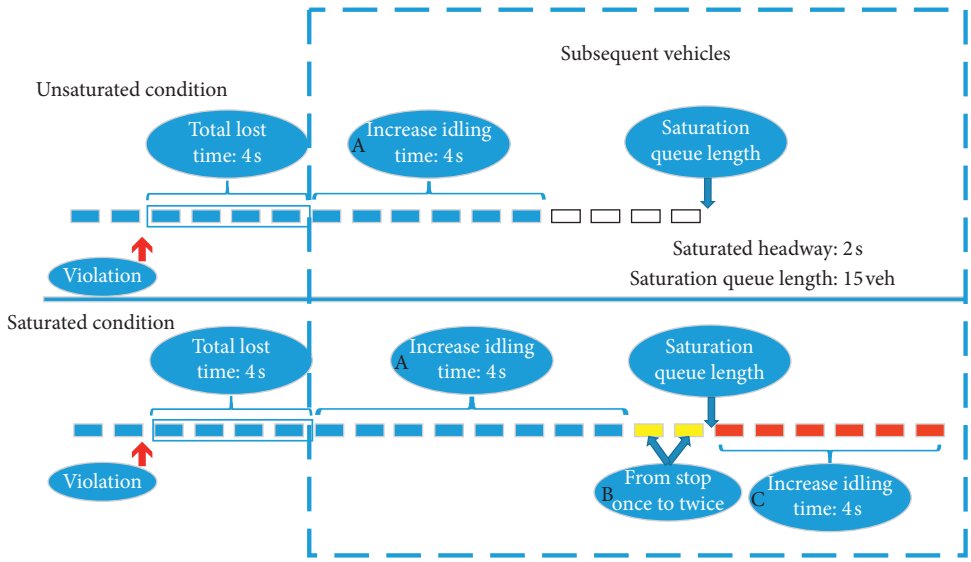

Figure 10: Characteristics of subsequent vehicles after violations.

$$\mathrm{AE} = \frac{\sum_{x=e}^{e+3} \mathrm{EF}_{\mathrm{increased,trajectory},x} + \sum_{x=e+4}^{n} \mathrm{EF}_{\mathrm{increased,flow},x}}{\sum_{i=1}^{n} \left(\mathrm{EF}_i + \mathrm{EF}_{\mathrm{downstream}}\right)} \cdot D, \tag{12}$$

where AE (%) is the increased emission increment of the cycle. e is the e^{th} vehicle, which is the location of the first affected vehicle. n is the vehicle number of the cycle. $\mathrm{EF}_{\mathrm{increased,trajectory},x}$ (g/km) is the increased emission factors of the first four affected vehicles. $\mathrm{EF}_{\mathrm{increased,flow},y}$ (g/km) is the increased emission factors of the subsequent vehicles after the first four affected vehicles. EF_i (g/km) is the normal emission factors of vehicles. $\mathrm{EF}_{\mathrm{downstream}}$ (g/km) is the emission factors downstream of the intersection. D (km) is the distance of the study range, which is 200 meters.

3. Case Study

Numerical simulations are designed in the case. The impact of violations on intersection emissions can be quantified based on the model built at the trajectory and traffic flow levels. The numerical simulation object of the case is the arterial (north-south) direction of the intersection. The seven simulation conditions are listed as follows:

(1) The average lost time is 5.52 s according to the violation data.

(2) Traffic flow arrival distribution conforms to Poisson distribution.

(3) The research scope is in 200 meters of the intersection.

(4) The maximum number of stops is two.

(5) The average speed of the normal vehicle at the intersection is 16.74 km/h according to the 1666 trajectories.

(6) The frequency of violations is 1 time/cycle/lane based on the actual statistics.

(7) The two objects to be compared are (1) vehicle emissions in this cycle before the violation and (2) the same vehicles after violations. The number of vehicles is the same.

3.1. Case Intersection. A typical intersection in Beijing (Anli and Huizhong North) is chosen as a reference for the case intersection, which is the arterial and collector protected intersection. The simulation object is the arterial (north-south) direction of the intersection. The signal information and channelization information are shown in Table 2.

3.2. Results and Discussion. When the volume is 38 veh/lane/cycle, for example, emission increment under violations in the case study is as shown in Figure 12 The x-axis indicates the cycle number, and the y-axis indicates the emission increment under the impact of violations. VSN means "the number of stops of vehicles is increasing after violations." Figure 12 explains the impact of violations on emissions at intersections under the volume from the following four aspects.

(1) The cycle number is less than 13: emission increment increases as VSN until the proportion of two-stop vehicles after violation reaches 100%.(saturated flow/(volume - saturated flow after violations) = 13).

(2) The cycle number is equal to 13: all vehicles have to stop twice after violations.

(3) The cycle number is between 13 and 26: the stopping number is two and the stopping time is increasing, the growth rate of emission after violations has a slower trend, and is even smaller than the growth rate of emission before violations.

(4) The cycle number is over 26: the three-stop vehicle will appear after violations.

Based on the analysis above, emission increment under violations in the case study is shown in Figure 13 The x-axis indicates the vehicle volume, and the y-axis indicates the

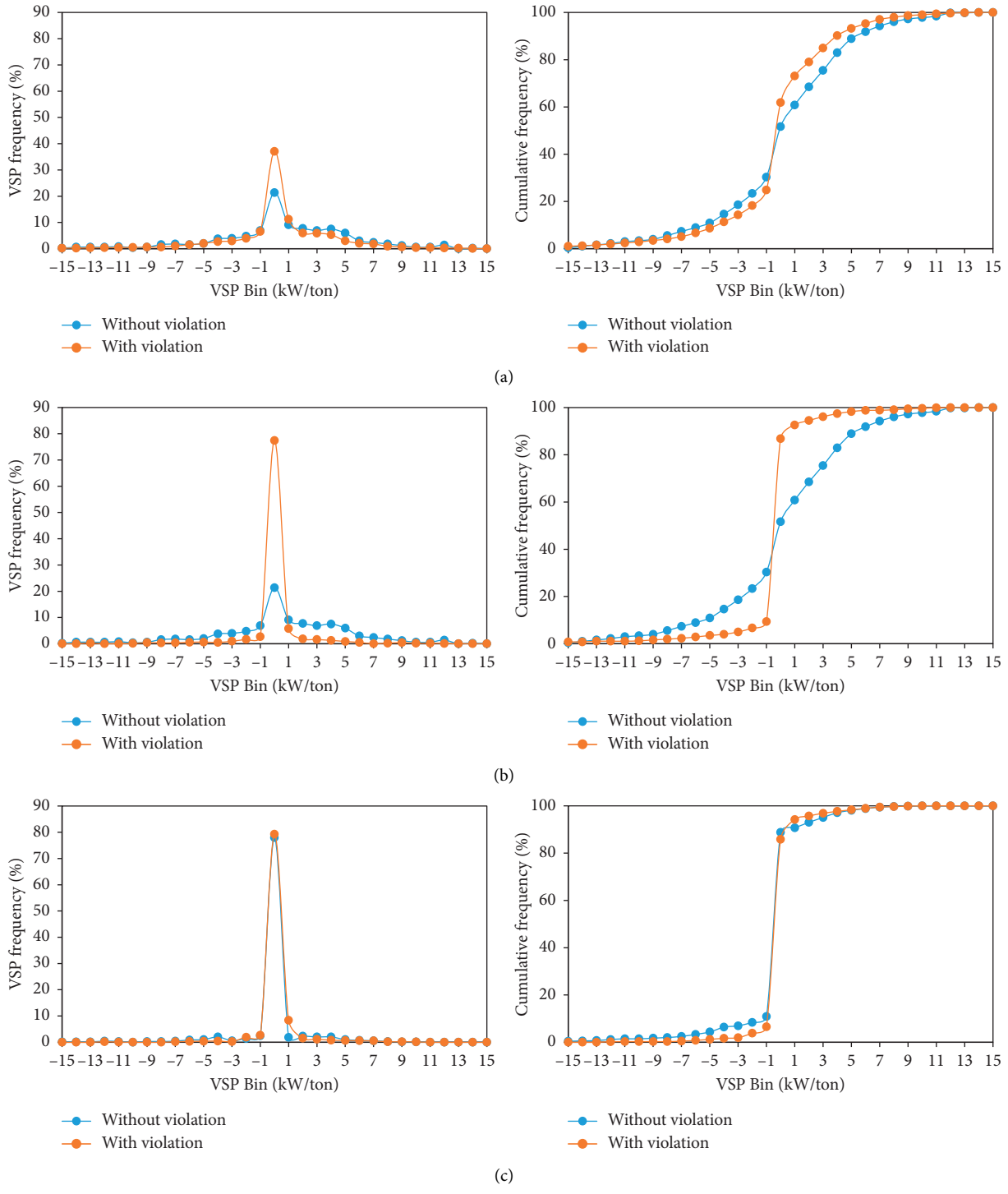

FIGURE 11: VSP distributions of vehicles with and without violations. (a) One-stop vehicle (type A). (b) The vehicle transforms from one stop to two stops (type B). (c) Two-stop vehicle (type C).

emission increment under the influence of violations. And different volumes will have different simulation cycles to avoid three-stop vehicles. Taking CO_2 as an example, the increment of CO_2 emissions can be divided into unsaturated and saturated states.

(1) Under the unsaturated condition, the emission increment is constant, and when the volume is 35 veh/lane/cycle, the emissions have barely increased (1.08%) because the stopping number is constant and the idling time only increases by 5.52 s.

Table 2: Signal and channelization information of case intersection.

Signal information (s)				Channelization information			
Phase	Green	Yellow	All red	Direction	Lane number		
North-south straight	74	3	2		Straight	Left	Right
North-south turn left	42	3	2	North	3	1	1
East phase	34	3	2	South	3	1	Straight-right
West phase	28	3	2	East	0	1	Straight-right
Cycle time		198		West	1	1	Straight-right

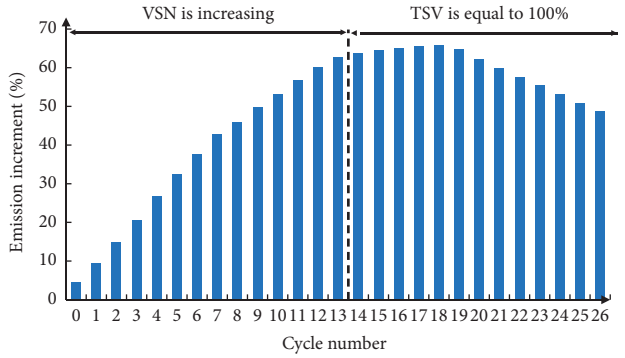

Cycle time (s)	Green time (s)	Lost time (s)
198	74	5.52
Volume (veh/cycle)	Saturated flow (veh/cycle)	Saturated flow after violations (veh/cycle)
38	37	35

Figure 12: Emission increment after violations such as cycle passing (volume = 38 veh/lane/cycle).

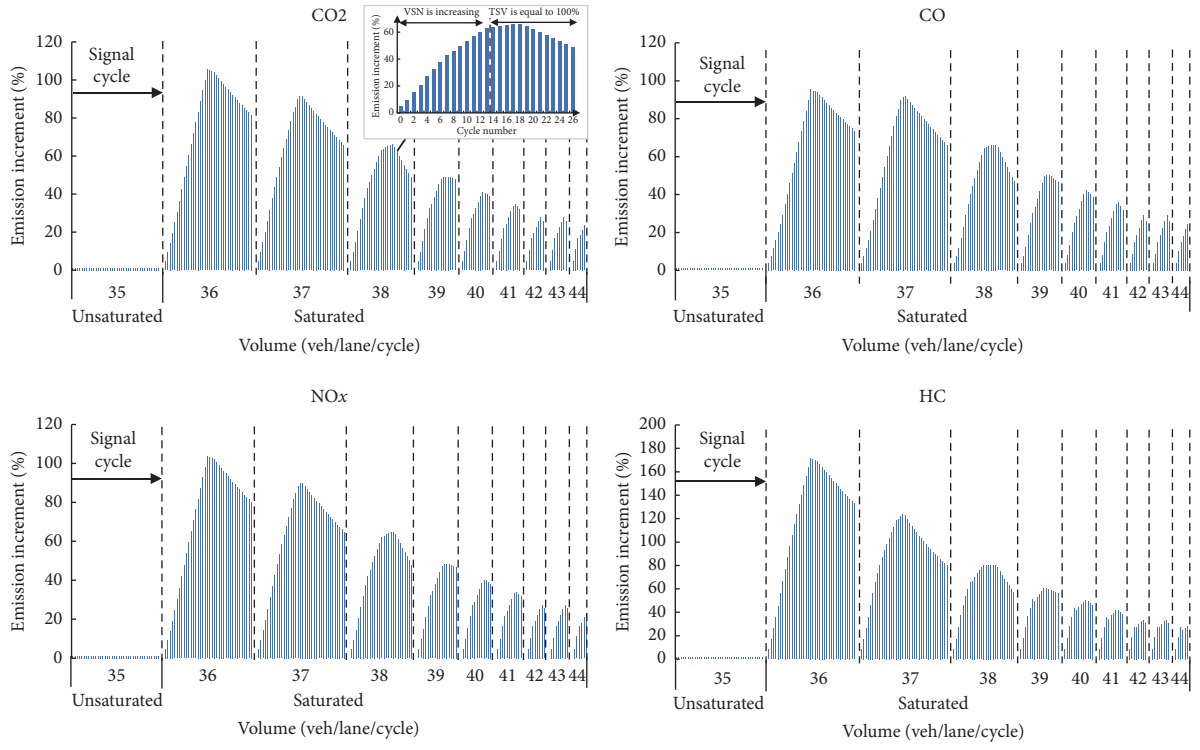

Cycle time (s)	Green time (s)	Saturated flow (veh)	Saturated flow after violations (veh)
198	74	37	35

Figure 13: Emission increment after violations for saturated/unsaturated conditions as cycle passing.

(2) Under the saturated condition, the emission increment increases sharply as the one-stop vehicle gradually transforms to the two-stop vehicle because of violations. As the proportion of two-stop vehicles after violations reaches 100%, and as the proportion before violations keeps increasing, the increment of emissions will decrease steadily. At the ninth cycle (half an hour), the emission increment is changed from 45% to 33% as the volume is changed from 36 to 42 veh/lane/cycle.

(3) As the cycle passes, the increment emissions of violations will have another increasing-decreasing process when three-stop vehicles appear. And a more increasing-decreasing process will appear when multiple-stop vehicles appear.

4. Conclusions

This paper studies the impact of violations on emissions at intersections based on the real-world driving trajectory data. First, the characteristics of vehicle operating affected by violations are analyzed. Second, a violation emission model is developed to evaluate emission increment under trajectory and traffic flow levels. Finally, a numerical simulation is conducted to assess the impact of violations on emissions based on the existing study. The main findings from the research can be summarized as follows.

The headway stabilized by the fourth affected vehicle, and the average total lost time caused by violations is 5.52 s. The effect of violations can be divided into trajectory and traffic flow levels.

The proposed emission model under trajectory and traffic flow levels can be used for estimating the impact of violations. The trajectory is modeled by the Gipps car-following model, and the proposed linear emission model based on the number of stops and idling time is used for the traffic flow level. At the trajectory level, the first four vehicles have obvious trajectory characteristics. The operating mode of the first affected vehicle is deceleration-idling-acceleration. The other three vehicles are modeled by the Gipps car-following model. At the traffic flow level, the proposed linear emission model based on the number of stops and idling time is used for estimating the emission of subsequent vehicles.

The emission increment is constant under the unsaturated condition and is 1.08% when the volume approaches saturated flow. The emission increment increases sharply as the one-stop vehicle gradually transforms to the two-stop vehicle because of violations under the saturated condition, and the maximum emission increment reaches 45% in half an hour in the case. The increment of emissions decreases steadily as the proportion of two-stop vehicles after violations reaches 100%, and the proportion before violations keeps increasing.

More emission numerical simulations for different types and frequencies of violations are recommended for further studies. In addition, three-stops and above should be considered in high-frequency violation scenarios.

Data Availability

Previously reported emission data were used to support this study and are available at https://doi.org/10.3141/2627-08 and https://doi.org/10.3141/2570-09. These prior studies (and datasets) are cited at relevant places within the text as references [30, 32]. The manual investigation data used to support the findings of this study are included within the article.

Disclosure

This paper was submitted for presentation at the annual meeting of the 98th Transportation Research Board.

Conflicts of Interest

The authors declare that there are no conflicts of interest regarding the publication of this paper.

Acknowledgments

This research was supported by the National Key R&D Program of China (#2018YFB1600701), the Fundamental Research Funds for the Central Universities (#2018YJS081), and the Natural Science Foundation of China (NSFC) (#51678045 and 51578052). The authors are thankful to all personnel who provided technical support and helped with data collection and processing.

References

[1] R. J. Laumbach, "Outdoor air pollutants and patient health," *American Family Physician*, vol. 81, no. 2, pp. 175–180, 2010.

[2] M. Krzyzanowski, B. Kunadibbert, J. S. Chneider et al., "Health effects of transport-related air pollution," *Journal of Health Effects of Transport-Related Air Pollution*, vol. 97, no. 5, pp. 418-419, 2005.

[3] F. Khalighi and E. Christofa, "Emission-based signal timing optimization for isolated intersections," *Transportation Research Record: Journal of the Transportation Research Board*, vol. 2487, no. 1, pp. 1–14, 2015.

[4] Federal Highway Administration, *Carbon Monoxide Categorical Hot-Spot Finding*, Federal Highway Administration, Washington, DC, USA, 2017.

[5] Y. Zhang, X. Chen, X. Zhang, G. Song, Y. Hao, and L. Yu, "Assessing effect of traffic signal control strategies on vehicle emissions," *Journal of Transportation Systems Engineering and Information Technology*, vol. 9, no. 1, pp. 150–155, 2009.

[6] L. Zhang, Y. Yin, and S. Chen, "Robust signal timing optimization with environmental concerns," *Transportation Research Part C: Emerging Technologies*, vol. 29, no. 1, pp. 55–71, 2013.

[7] M. Franklin, X. Yin, R. Urman, R. Lee, S. Fruin, and R. Mcconnell, "Environmental factors affecting stress in children: interrelationships between traffic-related noise, air pollution, and the built environment," in *Proceedings of the HEI Annual Conference*, Washington, DC, USA, May 2019.

[8] J. Xing, J. Hua, and P. Hao, "Study on pedestrian crossing rate at signal-controlled intersections," *Journal of Technology & Economy in Areas of Communications*, vol. 16, no. 5, pp. 14–19, 2014, Chinese article.

[9] C. Minh and K. Sano, "Analysis of motorcycle effects to saturation flow rate at signalized intersection in developing countries," *Journal of the Eastern Asia Society for Transportation Studies*, vol. 5, pp. 1211–1222, 2003.

[10] A. Stevanovic, J. Stevanovic, K. Zhang, and S. Batterman, "Optimizing traffic control to reduce fuel consumption and vehicular emissions: integrated approach with VISSIM, CMEM, and VISGAOST," *Transportation Research Record: Journal of the Transportation Research Board*, vol. 2128, no. 1, p. 105, 2009.

[11] X. Sun, X. Chen, Y. Qi, B. Mao, and L. Yu, "Analyzing the effects of different advanced traffic signal status warning systems on vehicle emission reductions at signalized intersections," in *Proceedings of the Presented at 95th Annual Meeting of the Transportation Research Board*, Washington, DC, USA, January 2016.

[12] K. Chen and L. Yu, "Microscopic traffic-emission simulation and case study for evaluation of traffic control strategies," *Journal of Transportation Systems Engineering and Information Technology*, vol. 7, no. 1, pp. 93–99, 2007.

[13] H. Rakha and Y. Ding, "Impact of stops on vehicle fuel consumption and emissions," *Journal of Transportation Engineering*, vol. 129, no. 1, pp. 23–32, 2002.

[14] H. C. Frey, N. M. Rouphail, and H. Zhai, "Speed- and facility-specific emission estimates for on-road light-duty vehicles on the basis of real-world speed profiles," *Transportation Research Record: Journal of the Transportation Research Board*, vol. 1987, no. 1, pp. 128–137, 2006.

[15] H. Zhai, H. C. Frey, and N. M. Rouphail, "A vehicle-specific power approach to speed- and facility-specific emissions estimates for diesel transit buses," *Environmental Science & Technology*, vol. 42, no. 21, pp. 7985–7991, 2008.

[16] A. Papson, S. Hartley, and K. Kuo, "Analysis of emissions at congested and uncongested intersections with motor vehicle emission simulation," *Transportation Research Record: Journal of the Transportation Research Board*, vol. 2270, no. 1, pp. 124–131, 2012.

[17] S. Gokhale and S. Pandian, "A semi-empirical box modeling approach for predicting the carbon monoxide concentrations at an urban traffic intersection," *Atmospheric Environment*, vol. 41, no. 36, pp. 7940–7950, 2007.

[18] K. Braven, A. Abdel-Rahim, K. Henrickson, and A. Battles, *Modeling Vehicle Fuel Consumption and Emissions at Signalized Intersection. Publication KLK721*, National Institute for Advanced Transportation Technology, University of Idaho, Moscow, Idaho, 2012.

[19] M. Brosseau, S. Zangenehpour, N. Saunier, and L. Miranda-Moreno, "The impact of waiting time and other factors on dangerous pedestrian crossings and violations at signalized intersections: a case study in montreal," *Transportation Research Part F: Traffic Psychology and Behaviour*, vol. 21, pp. 159–172, 2013.

[20] G. Ren, Z. Zhou, W. Wang, Y. Zhang, and W. Wang, "Crossing behaviors of pedestrians at signalized intersections: observational study and survey in China," *Transportation Research Record: Journal of the Transportation Research Board*, vol. 2264, no. 1, pp. 65–73, 2011.

[21] X. Wang, Y. Xu, P. J. Tremont, and D. Yang, "Moped rider violation behavior and moped safety at intersections in China," *Transportation Research Record: Journal of the Transportation Research Board*, vol. 2281, no. 1, pp. 83–91, 2012.

[22] V. Perumal, S. Marisamynathan, Study on pedestrian crossing behavior at signalized intersections," *Journal of Traffic and Transportation Engineering*, vol. 2, no. 1, pp. 103–110, 2014.

[23] M. Huan, M. Yang, and B. Jia, "Modeling cyclist violation behavior at signalized intersection in China," in *Proceedings of the 2012 Fifth International Joint Conference on Computational Sciences and Optimization*, IEEE, Harbin, China, June 2012.

[24] J. Przybyla, J. Taylor, J. Jupe, and X. Zhou, "Estimating risk effects of driving distraction: a dynamic errorable car-following model," *Transportation Research Part C: Emerging Technologies*, vol. 50, pp. 117–129, 2015.

[25] L. He, "Study on traffic efficiency of illegal lane change on signal intersection," Doctoral thesis, Chang'an University, Xi'an, China 2017. (Chinese article).

[26] J. B. Zhang, L. Yu, G. Song, J. Huang, and J. Guo, "Operational characteristics of signalized under mixed traffic: case in Beijing," in *Proceedings of the Presented at 98th Annual Meeting of the Transportation Research Board*, Washington, DC, USA, January 2019.

[27] Y. Guo, Q. Yu, Y. Zhang, and J. Rong, "Effect of bicycles on the saturation flow rate of turning vehicles at signalized intersections," *Journal of Transportation Engineering*, vol. 138, no. 1, pp. 21–30, 2012.

[28] X. Liang, Z. Liu, and Q. Kun, "Capacity analysis of signalized intersections under mixed traffic conditions," *Journal of Transportation Systems Engineering and Information Technology*, vol. 2, no. 11, pp. 91–99, 2011.

[29] D. Xie, G. Song, J. Guo, J. Sun, and L. Yu, "Development and application of an online dynamic emission model for traffic networks: a case study of Beijing," in *Proceedings of the Presented at 97th Annual Meeting of the Transportation Research Board*, Washington, DC, USA, January 2018.

[30] C. Li, L. Yu, W. He, Y. Cheng, and G. Song, "Development of local emissions rate model for light-duty gasoline vehicles: beijing field data and patterns of emissions rates in EPA simulator," *Transportation Research Record: Journal of the Transportation Research Board*, vol. 2627, no. 1, pp. 67–76, 2017.

[31] Report of Overall Architecture Design and Technical Difficult of the Distribution Regular Pattern of Traffic Emissions, *Technical Report for Center for Transportation Sector Energy Reduction and Emissions Mitigation of Beijing*, Beijing Jiaotong University, Beijing, China, 2014.

[32] J. Zhang, L. Yu, J. Guo, Y. Cheng, W. He, and G. Song, "Optimized adjustment of speed resolution and time alignment data for improving emissions estimations," *Transportation Research Record: Journal of the Transportation Research Board*, vol. 2570, no. 1, pp. 77–86, 2016.

[33] H. Lu, G. Song, and L. Yu, "A comparison and modification of car-following models for emission estimation," in *Proceedings of the Transportation Research Board 95th Annual Meeting, Transportation Research Board of the National Academies*, Washington, DC, USA, January 2016.

Hindawi
Journal of Advanced Transportation
Volume 2020, Article ID 6304651, 11 pages
https://doi.org/10.1155/2020/6304651

Research Article

Analysis of the Impact of Traffic Violation Monitoring on the Vehicle Speeds of Urban Main Road: Taking China as an Example

Fuquan Pan,[1] **Yongzheng Yang**,[1] **Lixia Zhang**,[1] **Changxi Ma**,[2] **Jinshun Yang**,[1] **and Xilong Zhang**[1]

[1]*School of Mechanical and Automotive Engineering, Qingdao University of Technology, Qingdao, Shandong 266520, China*
[2]*School of Traffic and Transportation, Lanzhou Jiaotong University, Lanzhou, Gansu 730070, China*

Correspondence should be addressed to Fuquan Pan; fuquanpan@yeah.net and Lixia Zhang; zlxzhanglixia@163.com

Received 3 January 2020; Accepted 12 February 2020; Published 20 March 2020

Guest Editor: Feng Chen

In recent years, there are more and more applications of traffic violation monitoring in some countries. The present work aims to analyze the vehicle speeds nearby road traffic violation monitoring area on urban main roads and find out the impact of road traffic violation monitoring on the vehicle speeds. A representative urban main road section was selected and the traffic flow was recorded by camera method. The vehicle speeds before, within, and after the road traffic violation monitoring area were obtained by the calculation method. The speed data was classified and processed by SPSS software and mathematical method to establish the vehicle speed probability density models before, within, and after the road traffic violation monitoring area. The results show that the average speed and maximum speed within the traffic violation monitoring area are significantly slower than those before and after the traffic violation monitoring area. 70.1% of the vehicles before the road traffic violation monitoring area were speeding, and 80.2% of the vehicles after the road traffic violation monitoring area were speeding, while within the road traffic violation monitoring area, the speeding vehicles were reduced to 15.9%. When vehicles pass through the road traffic violation monitoring area, the vehicle speeds tend to first decrease and subsequently increase. In its active area, road traffic violation monitoring can effectively regulate driving behaviors and reduce speeding, but this effect is limited to the vicinity of the traffic violation monitoring. The distribution of vehicle speeds can be calculated from vehicle speed probability density models.

1. Introduction

In many countries, with the development of the social economy, the number of automobiles has increased yearly, and a series of problems such as road congestion mess in traffic order and traffic accidents becomes frequent [1–7]. Traffic accidents can cause huge casualties and economic losses [8]. To maintain traffic order and reduce the occurrence of traffic accidents, traffic violation monitoring systems have been installed in some risk road sections (such as school sections and main road sections). A traffic violation monitoring system can capture and process various traffic violations such as speeding, illegal lane changes, and traffic sign violations in the active area. It primarily uses computer image processing technology and communication technology and obtains illegal vehicle information through an automatic detection device. It can regulate driving behaviors and ensure road traffic safety [9–13]. Some scholars have studied the effect of traffic violation monitoring on driving behaviors and vehicle speed. Zhu et al. [14] believed that traffic violation monitoring significantly affects driving behaviors. Traffic violation monitoring can effectively reduce the probability of traffic accidents. Traffic violation monitoring has a positive effect on road traffic safety. Pan et al. [15, 16] found that intersection traffic violation monitoring can effectively regulate the behavior of drivers and reduce the occurrence of speeding, which helps to reduce the occurrence of traffic accidents. Luo et al. [17] obtained drivers' opinions on traffic violation monitoring through a questionnaire survey, and they noted that traffic violation monitoring can alert the driver and reduce the occurrence of speeding, illegal lane changes, and other behaviors. Zhang

et al. [18] analyzed the effect of traffic violation monitoring on driving behaviors from the psychological point of view. They believe that traffic violation monitoring may negatively affect driving behaviors and that rear-end accidents significantly increase under traffic violation monitoring. Qian [19] studied driving behaviors under traffic violation monitoring at intersections and proposed that traffic violation monitoring helps to ensure traffic safety. Jiang et al. [20] studied the impact of traffic violation monitoring on traffic accidents at intersections in response to China's specific national conditions. They believe that traffic violation monitoring can reduce the occurrence but increase the severity of traffic accidents. Ahmed and Abdel-Aty [21] analyzed traffic accidents at intersections and found that traffic violation monitoring would reduce left-turn traffic accidents but increase traffic accidents in other directions. Chai et al. [22] believed that traffic violation monitoring has different effects on different types of traffic accidents. Traffic violation monitoring reduces the occurrence of collision accidents, but the probability of rear-end accidents increases. Pulugurtha and Otturu [23] analyzed traffic accidents with or without traffic violation monitoring at intersections and found that traffic violation monitoring at intersections increased rear-end accidents by 50% but reduced total traffic accidents by 16%. Higgins et al. [24] believed that traffic violation monitoring significantly affects driving behaviors and that most drivers and nondrivers support the installation of traffic violation monitoring.

At present, research on the impact of traffic violation monitoring on drivers is mostly concentrated at the intersection and focuses on the impact of traffic violation monitoring on traffic accidents. There are few studies on road traffic violation monitoring. In recent years, some countries such as China have implemented the large-scale installation of traffic violation monitoring facilities on urban roads to regulate driving behaviors, but the mechanism of the impact of traffic violation monitoring on drivers is not clear. To clarify the rationale and necessity of road traffic violation monitoring, we explore the impact of road traffic violation monitoring on driving behaviors and traffic safety. This work conducts field measurements through cameras, obtains vehicle speed data from different sections (before, within, and after the road traffic violation monitoring area), and studies the impact of road traffic violation monitoring on vehicle speeds.

2. Methodology

2.1. Data Collection Site. The road section selected in this study is a typical urban main road, Jialingjiang East Road, located in Huangdao District, Qingdao, Shandong Province, China. This traffic violation monitoring site is located on Jialingjiang East Road, specifically at 2000 m west of the intersection of Jialingjiang East Road and Hengshan Road in Huangdao District, Qingdao, and 500 m west of the south gate of Jialingjiang Road Campus of the Qingdao University of Technology. Its geographical location is shown in Figure 1.

Figure 1: Geographic location of the data collection area.

Jialingjiang East Road is a one-way three-lane road with an isolation barrier in the middle of the road to isolate the two-way traffic flow. The traffic violation monitoring device on this road is in the form of cantilever beams, which can completely cover 3 lanes, as shown in Figure 2.

2.2. Data Acquisition Method. The data acquisition devices are mainly cameras. The central point of the traffic violation monitoring area in this paper refers to the center point of the visual field of the traffic violation monitoring camera. One video device each is set up at the center of the traffic violation monitoring area as well as 100 m before and after it, and these devices are used to measure the speed of the same vehicle passing through the three places. Traffic violation monitoring is typically installed above the road. The installation height is generally 4.5 m, and the monitoring device is at an angle of approximately 60° to the road plane. Therefore, the center of the monitoring area is approximately 8 m ahead of the monitoring device.

The data collection took two days and was completed four times; each recording took thirty minutes. The collection time is concentrated in the common period. The data collection section is a representative urban main road section with a speed limit of 40 km/h. The vehicle speed measurement method is shown in Figure 3.

The speed measurement steps are as follows:

(1) Place cameras at points 1, 2, and 3, install and debug the cameras, and make preparations. Make sure that the camera has no visual field barrier at the shooting site.

(2) Set three background markers on the opposite side of the road and find three background markers on the camera screen.

(3) When the camera, vehicle, and background markers are aligned, make a vertical line from the vehicle to the roadside and record the vertical points as S_1, S_2, and S_3.

(4) After the data have been collected in the field, the video is processed, and the required data are recorded. The speed and acceleration of the vehicle cannot be directly obtained from the video but can be calculated based on the collected data.

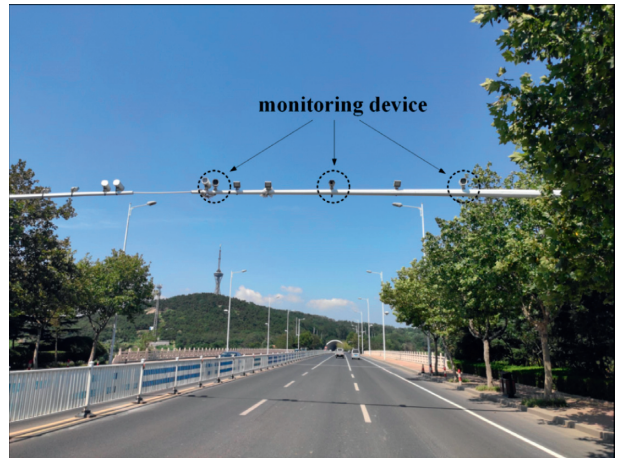

Figure 2: Actual road conditions of the data collection road section.

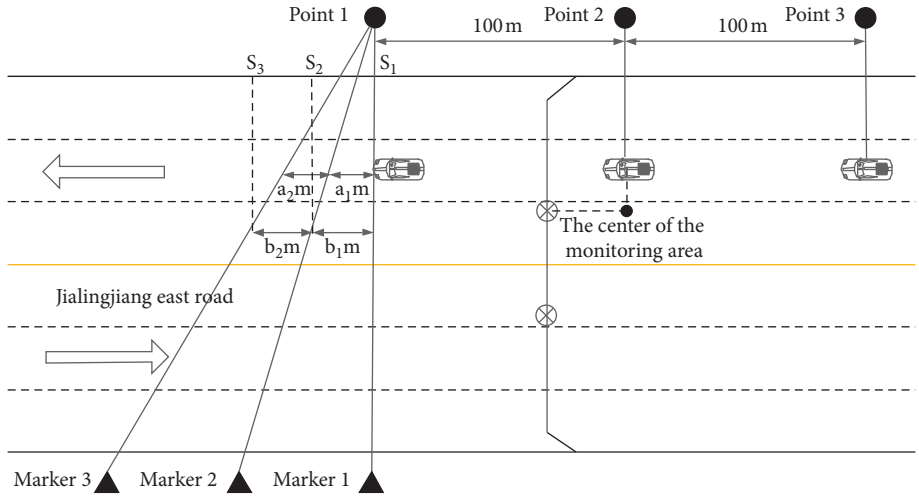

Figure 3: Vehicle speed measurement method.

$$V = \frac{S_{13}}{T_{13}},$$
$$a = \frac{(V_{23} - V_{12})}{T_{13}}. \quad (1)$$

In the formula, V is the average speed of the corresponding section. Because the distances among signs 1, 2, and 3 are relatively small, V can also be considered the instantaneous speed, S is the length of the corresponding section, T is the time difference between vehicles passing through the section, and a is the average acceleration of the vehicle passing the corresponding section. Since the distance between marker 1 and marker 3 is relatively small, the acceleration can be considered the instantaneous acceleration.

The data acquisition and data processing of measurement points 2 and 3 are identical to those of measurement point 1. After screening, 515 groups were obtained, totaling 1,545 valid vehicle data.

2.3. Sample Size Test of the Data. Due to the error of the measuring device and limited ability of the observer to identify the organ, there will be errors in the placement, sighting, and reading of the instrument

In addition, external conditions such as temperature, humidity, wind, and atmospheric refraction during the observation will directly affect the observed data. Therefore, to ensure the accuracy of the experimental results and reduce the impact of errors on the experimental results, the amount of measurement data must be guaranteed. Only when the sample size reaches the minimum sample size requirement do the experimental results become credible, and whether the sample size of the test data satisfies the requirements can be determined by the following formula:

$$N = \frac{Z^2 p(1-p)}{E^2}. \quad (2)$$

In the formula, N is the minimum number of samples required for the experiment; Z is the confidence coefficient, which is used to characterize the reliability. When the

confidence is 90%, $Z = 1.65$, and when the confidence is 95%, $Z = 1.96$; with higher confidence, a larger sample size is required; E is the maximum allowable error in data measurement. The smaller the allowable error, the larger the sample size required; and P is the ratio of the number of measured samples to the total traffic flow during the measurement period. In this paper, the maximum allowable error is 5%, and the confidence is 95%. After the calculation, the minimum sample size is 384. The sample size of this paper is much larger than the minimum sample size, so the sample size of this paper satisfies the requirements.

3. Data Analysis and Results

3.1. Speed Analysis. The vehicle speed statistics and vehicle speed distribution are shown in Table 1 and Figures 4 and 5.

Table 1 shows that the average speed and maximum speed within the traffic violation monitoring area are significantly slower than those before and after the traffic violation monitoring area. Thus, the road traffic violation monitoring system can effectively alert the driver to follow the traffic regulations and suppress the occurrence of speeding. In turn, the probability of traffic accidents decreases. When the vehicle passes through the sections before, within, and after the road traffic violation monitoring, the general trend of the average speed is first a reduction and subsequently an increase, which indicates that the road traffic violation monitoring interferes with the typical driving behavior and induces the occurrence of traffic accidents [25, 26]. The road traffic violation monitoring is not absolute for traffic safety. On the one hand, road traffic violation monitoring can reduce the probability of accidents in the active area; on the other hand, traffic violation monitoring may increase the probability of accidents within the transitional areas before and after the traffic violation monitoring.

Figure 4 shows that before the traffic violation monitoring area, the maximum speed is greater than 40 km/h in 70.1% of the cases; the second most common speed range is 30–40 km/h, occurring in 26.4% of the cases; and the least common speed range is less than 30 km/h, occurring in 3.5% of the cases. Within the traffic violation monitoring area, the most common maximum speed is 30–40 km/h (more than 70%), the second most common range is greater than 40 km/h (15.9%), and the least common range is less than 30 km/h (11.8%). After the traffic violation monitoring area, the most common maximum speed is greater than 40 km/h (80.2%), the second most common range is 30–40 km/h (18.4%), and the least common range is less than 30 km/h (1.4%). When a vehicle is driving within the traffic violation monitoring area, speeding is obviously reduced. Most drivers drive at a speed slightly lower than the speed limit standard. When they leave the traffic violation monitoring area, the frequency of speeding is the highest, which is related to factors such as the psychological relaxation of the driver immediately after leaving the traffic violation monitoring area and the personal characteristics of the drivers.

Figure 5 consists of 515 sets of vehicle speed data, arranged according to the order of data collection. Figure 5 shows that within a given set of speed data, the speed of the vehicle before and after the monitoring area is generally higher, and the speed of the vehicle within the monitoring area is generally the lowest. Thus, for a single vehicle, when it passes through the three sections before, within, and after the traffic violation monitoring area, the speed trend has a greater probability of first decreasing and subsequently increasing. According to statistics, among the 515 sets of data, 358 sets of data had the slowest speed in the monitoring area, which accounts for 70% of the total sample. Hence, 70% of the vehicles have the obvious behavior of first decelerating and subsequently accelerating when passing through the road traffic violation monitoring area. It can also be understood that when a vehicle passes through the road traffic violation monitoring area, there is a 70% probability that it will first decelerate and subsequently accelerate.

3.2. Hypothesis Test. Whether the road traffic violation monitoring significantly affects the driving behaviors and speeds is related to the rationale of road traffic violation monitoring installation. To determine whether the road traffic violation monitoring will affect vehicle speed, the single-factor hypothesis test is conducted for the data.

Test hypothesis

$$H_0: u_1 = u_2 = u_3. \tag{3}$$

In other words, road traffic violation monitoring has no significant impact on speeds:

$$H_1: u_1, u_2, u_3 \text{ not all equal.} \tag{4}$$

In other words, road traffic violation monitoring has a significant impact on speeds:

$$\begin{aligned} \text{SST} &= \sum_{j=1}^{S} \sum_{i=1}^{n_j} \left(X_{ij} - \overline{X}\right)^2, \\ \text{SSA} &= \sum_{j=1}^{S} \sum_{i=1}^{n_j} \left(X_{\cdot j} - \overline{X}\right)^2, \\ \text{SSE} &= \sum_{j=1}^{S} \sum_{i=1}^{n_j} \left(X_{ij} - \overline{X}_{\cdot j}\right)^2, \\ \text{MSA} &= \frac{\text{SSA}}{f_A}, \\ \text{MSE} &= \frac{\text{SSE}}{f_e}. \end{aligned} \tag{5}$$

In the formula, u_1, u_2, and u_3 are the speeds before, within, and after the road traffic violation monitoring area, respectively; SST is the total variation, which is the reflection of the difference among all test data; SSE is the error square sum, i.e., the sum of squares of deviations between the measured values of different measurement positions and the average values of the positions. SSE can reflect the fluctuations caused by the average errors; SSA is the sum of the squared effects, which is the sum of the squares of the deviations between the average of the measured values at

Table 1: Speed statistics.

Position	Before the traffic violation monitoring area	Within the traffic violation monitoring area	After the traffic violation monitoring area
Average (km/h)	48.0	37.8	50.3
Variance	100.0	49.0	94.1
Standard deviation	10.0	7.0	9.7
Range	46.0	46.0	45.0
Coefficient of variation	20.9	18.2	19.3
Skewness	0.6	1.4	0.4
Kurtosis	2.8	3.9	2.3
Maximum (km/h)	71.0	70.0	71.0
Minimum (km/h)	26.0	24.0	27.0

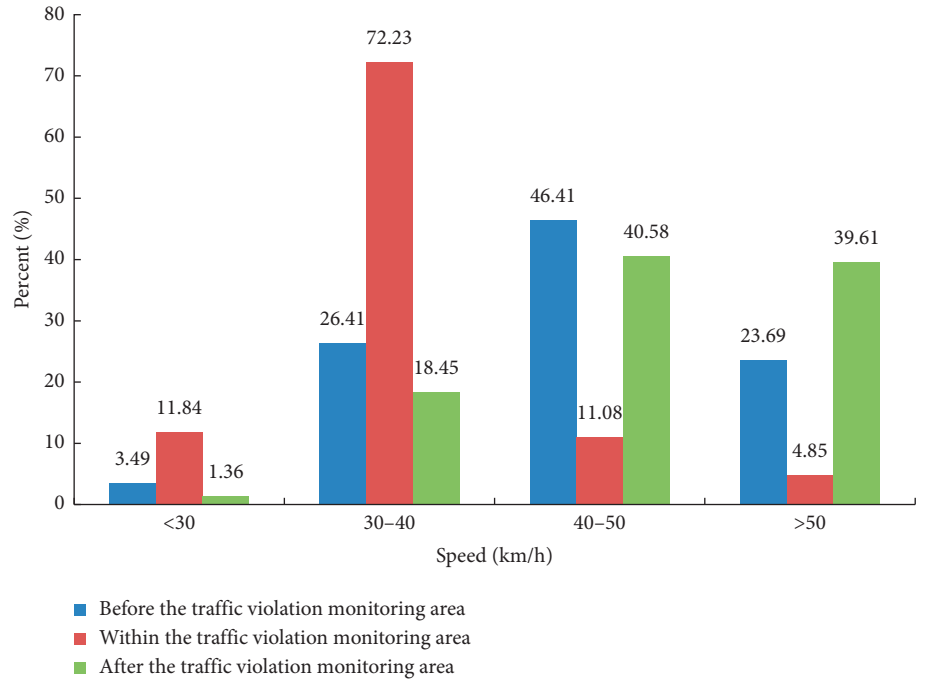

Figure 4: Vehicle speed distribution.

different points and the total average; n is the total number of vehicle speed data; s is the number of groups of vehicle speed data; f_T is the degree of freedom between groups, $f_T = n - 1$; f_e is the degree of freedom in the group, $f_e = n - s$; f_A is the overall degree of freedom, $f_A = S - 1$; MSA is the variance within the group; and MSE is the variance between groups.

The variance analysis table is obtained by processing the vehicle speed data using MATLAB software, as shown in Table 2.

Since $F_0 > F_{0.01}$ (2, 1542), H_0 is rejected; i.e., the road traffic violation monitoring has a significant impact on vehicle speeds.

3.3. Acceleration Analysis. The acceleration statistics and acceleration distribution are shown in Table 3 and Figures 6, and 7.

Table 3 shows that the average acceleration at different positions (before, within, and after the traffic violation monitoring area) is significantly different. Generally, before the road traffic violation monitoring area, the driver tends to slow down; in the road traffic violation monitoring area, the driver tends to travel at a constant speed; and after the road traffic violation monitoring area, the driver tends to accelerate. In addition, when the vehicle passes through the road traffic violation monitoring area, the overall trend of the vehicle speeds is first a decrease and subsequently an increase.

Figure 6 consists of 515 sets of acceleration data, arranged according to the order of acquisition. Figure 6 shows that the acceleration before the monitoring area is mostly distributed in (−1.3, −0.5), the acceleration in the monitoring area is mostly distributed in (−0.4, 0.4), and the acceleration after the monitoring area is mostly distributed in (0.6, 1.4). Hence, before the monitoring area, the driver tends to slow down; in the monitoring area, the driver tends to drive at a uniform speed; and after the monitoring area, the driver tends to accelerate. Taking any of the 515 sets of

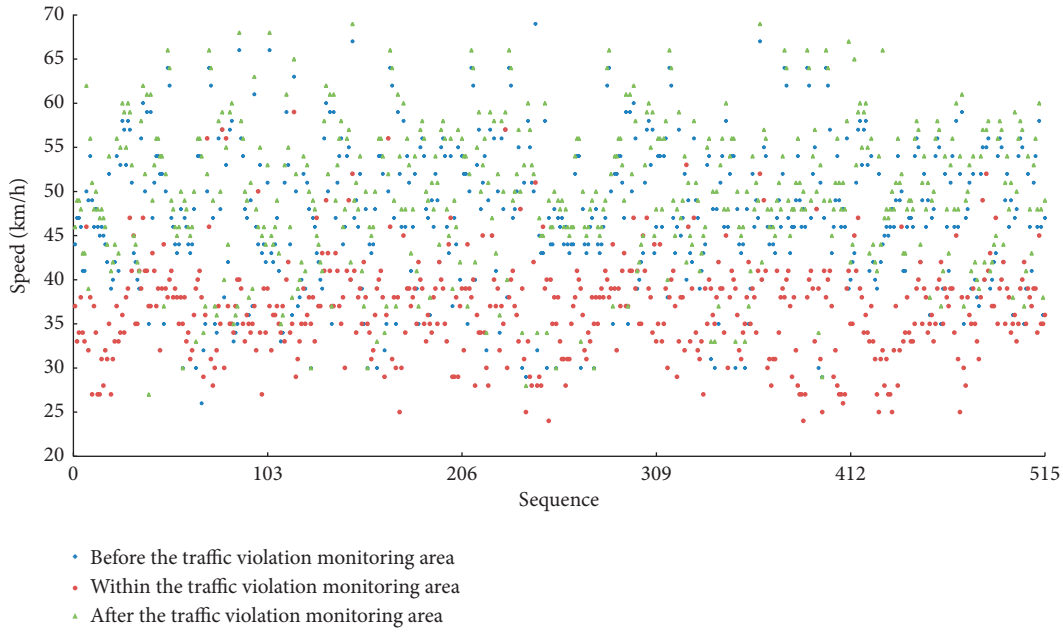

Figure 5: Vehicle speed distribution.

Table 2: Analysis of variance.

Source of variance	Square of deviance	Degree	Variance	F	F_α	Significance
Between groups	107.95	2	202.98	$F_0 = 4.55$	$F_{0.05}$ (2, 1542) = 3.00	Significant
Within group	67.91	1542	70.92	—	$F_{0.01}$ (2, 1542) = 4.61	—
Sum	175.86	1544	—	—	—	—

Table 3: Acceleration statistics.

Position	Before the traffic violation monitoring area	Within the traffic violation monitoring area	After the traffic violation monitoring area
Average (m/s^2)	−0.76	0.03	0.92
Variance	0.4	0.1	0.2
Standard deviation	0.6	0.3	0.4
Range	2.0	1.6	1.7
Coefficient of variation	−78.5	51.9	59.0
Skewness	−0.8	0.5	−0.3
Kurtosis	−0.3	2.6	−0.9
Maximum (m/s^2)	0.5	1.1	2.9
Minimum (m/s^2)	−2.7	−1.2	−0.6

data, the acceleration rate is very likely less than 0 before the monitoring area, approximately 0 in the monitoring area, and greater than 0 after the monitoring area. Thus, near the traffic violation monitoring area, a single driver has a high probability of first decelerating, subsequently driving at a constant speed, and finally accelerating.

Figure 7 shows that the acceleration range in the traffic violation monitoring area is the smallest, followed by that before the monitoring area and that after the monitoring area, where the acceleration is most dispersed. Thus, the traffic order within the traffic violation monitoring area of the road section is the best, the traffic violation monitoring area before the road section is second best, and the order after the traffic violation monitoring area of the road section is the most chaotic, which increases the probability of rear-end accidents before the road traffic violation monitoring area and the probability of speeding and illegal overtaking after the road traffic violation monitoring area.

3.4. Normality Test. The Kolmogorov–Smirnov test, also called the *K-S* test, is a commonly used method in statistical analysis. It compares the data required for statistical analysis with another set of standard data to obtain the deviation between it and the standard data. The Kolmogorov–Smirnov test is often used to test the normality of the data

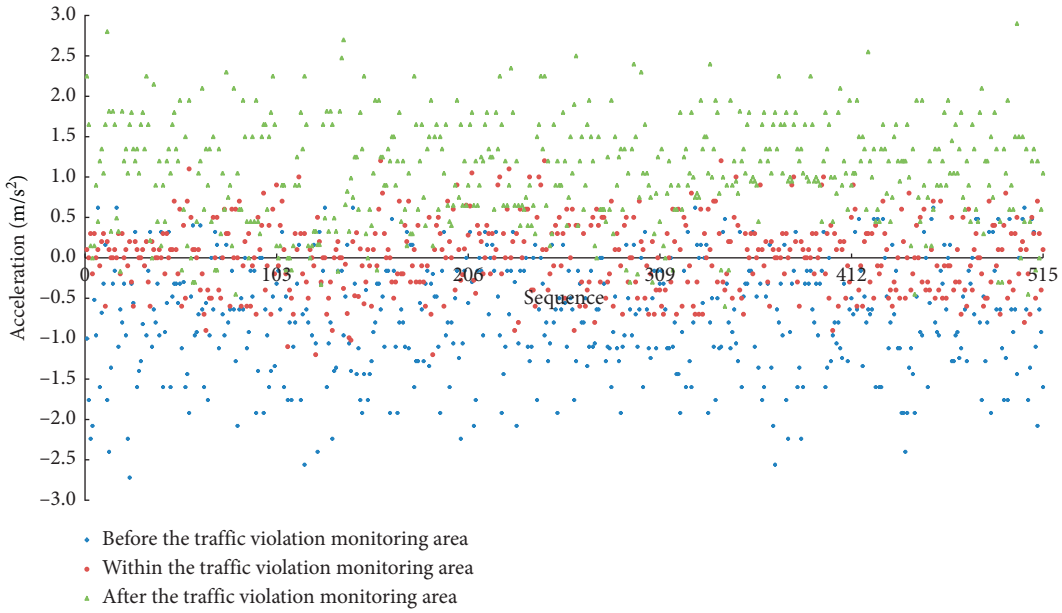

Figure 6: Acceleration distribution.

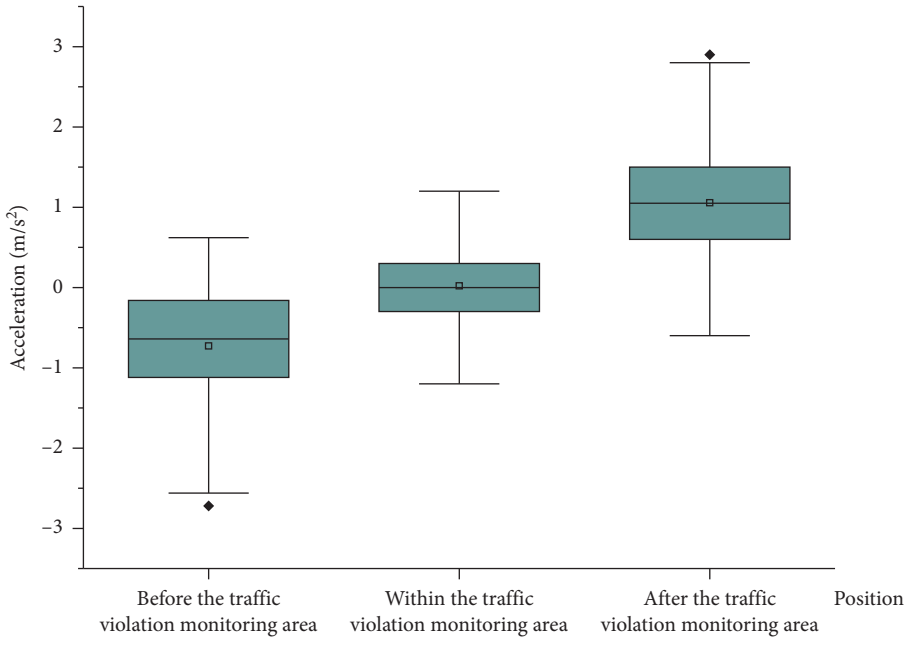

Figure 7: Acceleration box diagram.

distribution. When the P value is greater than 0.05, the measured data can be considered to obey a normal distribution [27].

The Shapiro–Wilk test, also called the S-W test, is a method of normal distribution testing for frequency data. When the P value is greater than 0.05, the measured data can be considered to obey a normal distribution [28].

The Kolmogorov–Smirnov test and the Shapiro–Wilk test are two commonly used methods for normal distribution detection. The largest difference between them is that the Kolmogorov–Smirnov test is suitable for the statistical analysis of a large number of data samples, and the Shapiro–Wilk test is suitable for the statistical analysis of a small number of data samples. In this paper, the sample number of vehicle speed data is moderate, so both test methods are used. The speed data are processed by SPSS software, and the results are shown in Table 4.

Table 4 shows that for both the Kolmogorov–Smirnov test and the Shapiro–Wilk test, the P values for vehicle speed before, within, and after the road traffic violation monitoring

area are greater than 0.05, which indicates that the distributions of vehicle speed before, within, and after the road traffic violation monitoring area obey a normal distribution.

3.5. Modeling and Analysis

(1) The vehicle speed distribution model within the road traffic violation monitoring area is as follows. Table 1 shows that the speeds nearby the road traffic violation monitoring area obey a normal distribution of N (37.8, 49) and that the probability density function is

$$f(x) = \frac{1}{\sqrt{98\pi}} e^{-\left((x-37.8)^2/98\right)}. \quad (6)$$

In equation (6), x is the vehicle speed. According to equation (6), the distribution curve is shown as Figure 8, and the average vehicle speed within the road traffic violation monitoring area is slightly lower than the maximum speed limit of the road.

By analogy, it can be concluded that the average speed within the monitoring area is approximately $0.95a$ on a road with a maximum speed limit of a km/h. Hence, on a road with the highest speed limit of a km/h, the vehicle speed probability density model within the road traffic violation monitoring area is

$$f(x) = \frac{1}{\sqrt{98\pi}} e^{-((x-0.95a)/98)}. \quad (7)$$

In equation (7), x is the vehicle speed. From equation (7), the distribution curve is shown as Figure 9, and it can be calculated that when a vehicle with a maximum speed limit of a km/h travels in the monitored area, there is a 68.2% probability that its speeds are in the range of $(0.95a - 7,\ 0.95a + 7)$ km/h, with a 95% probability in the range of $(0.95a - 14,\ 0.95a + 14)$ km/h.

(2) The model of vehicle speed distribution before the road traffic violation monitoring area, i.e., the vehicle speed distribution model within the transition zone before the road traffic violation monitoring area, is as follows. Table 1 shows that the vehicle speeds before the monitoring area obey the normal distribution of N (48,100), and compared with the values within the monitoring area, the average speed and standard deviation before the monitoring area are slightly higher. Assuming that the length of the transitional zone before the traffic violation monitoring area is 100 m and the transition is completed at 30 m in front of the center of the monitoring area, it is considered that the vehicle uniformly decelerates throughout the transitional area and the variance of the vehicle speed distribution has a positive correlation with the vehicle speed. Therefore, on a road with the maximum speed limit of a km/h, the vehicle speed probability density model at b m in front of the center of the road traffic violation monitoring area is inferred to be

$$f(x) = \frac{1}{\sqrt{2\pi(6.2 + 0.03b)^2}} e^{-\left([x-(0.84a+0.0035ab)]^2/2(6.2+0.03b)^2\right)},$$
$$30 < b < 130. \quad (8)$$

In equation (8), x is the vehicle speed. From equation (8), the distribution curve is shown as Figure 10, and it can be calculated that when a vehicle is about to enter the transition zone before the road traffic violation monitoring with a maximum speed limit of a km/h, there is a 68.2% probability that its speeds are in the range of $(1.3a - 10.1,\ 1.3a + 10.1)$ km/h and a 95% probability in the range of $(1.3a - 20.2,\ 1.3a + 20.2)$ km/h; for S_1 at any point in the former transition zone, the distance between S_1 and the center of the traffic violation monitoring area is L·m, and with 68.2% probability, the range of the vehicle speeds at that point is $(0.84a - 0.03L + 0.0035aL - 6.2,\ 0.84a + 0.03L + 0.0035aL + 6.2)$ km/h, and with 95% probability, the range of vehicle speeds is $(0.84a - 0.06L + 0.0035aL - 12.4,\ 0.84a + 0.06L + 0.0035aL + 12.4)$ km/h. When a vehicle is about to leave the former transition zone, there is a 68.2% probability that its speeds are in the range of $(0.95a - 7,\ 0.95a + 7)$ km/h and a 95% probability in the range of $(0.95a - 14,\ 0.95a + 14)$ km/h.

(3) The model of vehicle speed distribution after the road traffic violation monitoring area, i.e., the vehicle speed distribution model within the transition zone after the road traffic violation monitoring area, is as follows. Table 1 shows that the vehicle speed after the monitoring area obeys the normal distribution of N (50.3, 94), and compared with the values in the monitoring area, the average speed and standard deviation after the monitoring area are slightly higher. Assuming that the length of the transitional section after the traffic violation monitoring area is 100 m and the transition is completed at 30 m past the center of the monitoring area, it is considered that the vehicle is driving uniformly decelerating throughout the transitional area and the variance of the vehicle speed distribution is positively correlated with the vehicle speeds. Therefore, on a road with the maximum speed limit of a km/h, the vehicle speed probability density model at c·m past the center of the road traffic violation monitoring area is inferred to be

$$f(x) = \frac{1}{\sqrt{2\pi(6.2 + 0.03c)^2}} e^{-\left([x-(0.82a+0.0044ac)]^2/2(6.2+0.03c)^2\right)},$$
$$30 < c < 130. \quad (9)$$

In equation (9), x is the vehicle speed. From equation (9), the distribution curve is shown as Figure 11, and it can be

Table 4: Kolmogorov-Smirnov test and Shapiro-Wilk test results.

	Kolmogorov-Smirnov			Shapiro-Wilk		
	Statistical	Degree	Sig	Statistical	Degree	Sig
Before the traffic violation monitoring area	0.13	515	0.19	0.93	515	0.22
Within the traffic violation monitoring area	0.13	515	0.30	0.94	515	0.27
After the traffic violation monitoring area	0.06	515	0.17	0.98	515	0.11

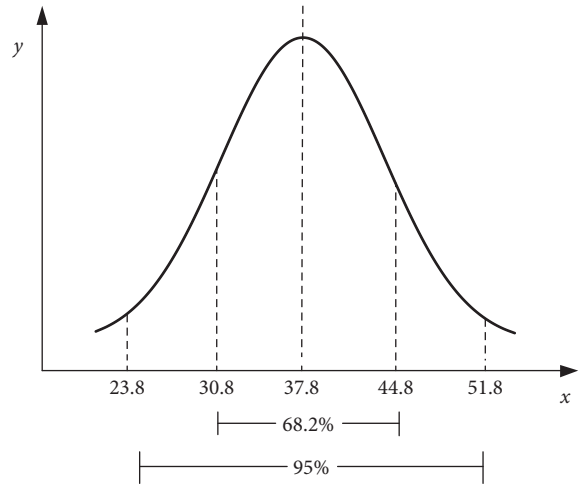

Figure 8: Distribution curve of equation (6).

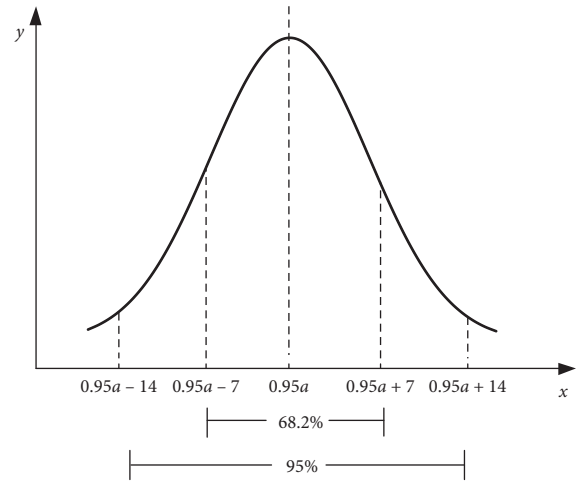

Figure 9: Distribution curve of equation (7).

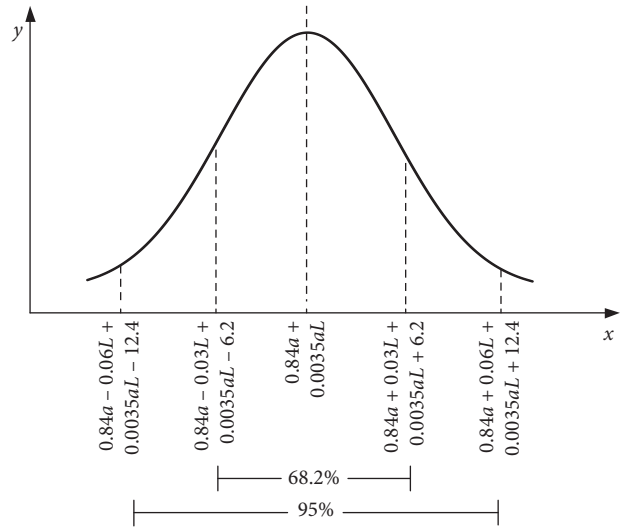

Figure 10: Distribution curve of equation (8).

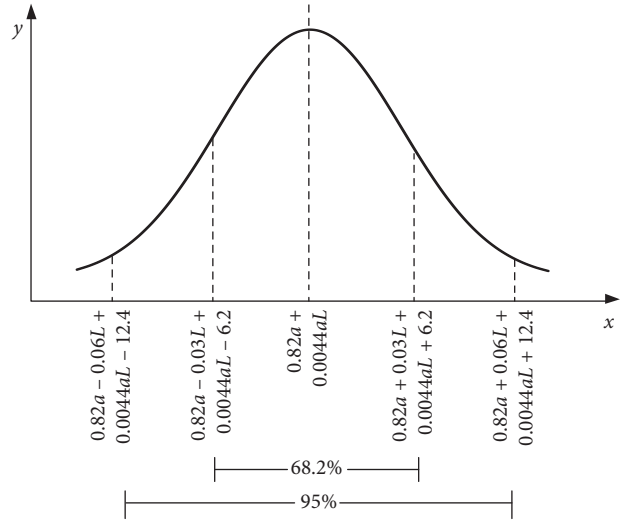

Figure 11: Distribution curve of equation (9).

calculated that when a vehicle is about to enter the transition zone after the road traffic violation monitoring area with a maximum speed limit of a km/h, there is a 68.2% probability that its speeds are in the range of $(0.95a - 7, 0.95a + 7)$ km/h and a 95% probability in the range of $(0.95a - 14, 0.95a + 14)$ km/h; for S_2 at any point in the posttransition zone, the distance between S_2 and the center of the traffic violation monitoring area is $L{\cdot}m$. With 68.2% probability, the vehicle speeds at that point are in the range of $(0.82a - 0.03L + 0.0044aL - 6.2,\ 0.82a + 0.03L + 0.0044aL + 6.2)$ km/h, and with a 95% probability, its speeds are in the range of $(0.82a - 0.06L + 0.0044aL - 12.4,\ 0.82a + 0.06L + 0.0044aL + 12.4)$ km/h. When a vehicle is about to leave the posttransition zone, there is a 68.2% probability that its speeds are in the range of $(1.39a - 10.1,\ 1.39a + 10.1)$ km/h and a 95% probability in the range of $(1.39a - 20.2,\ 1.39a + 20.2)$ km/h.

By comparing equations (8) and (9), we find that the entry of the road traffic violation monitoring area from the former transition zone and the entry of the posttransition zone following the road traffic violation monitoring area form a pair of approximately opposite processes.

4. Discussion and Conclusions

To further study the impact of road traffic violation monitoring on vehicle speeds, the following issues require further study:

(1) In the case of constant road facilities, weather conditions often affect vehicle speed distribution. The time period during which the data were collected by the institute had normal weather on sunny days. If the weather is raining, snowy, or foggy, the condition or pattern may differ from the results of this study.

(2) The concept of traffic safety among different drivers often varies. Therefore, the behavioral responses of different drivers who encounter traffic violation monitoring often vary. This study randomly collected vehicle data and cannot understand the drivers' traffic safety conceptions. In this case, there is a lack of understanding of the drivers' traffic safety conceptions.

(3) The road selected in this study is an urban main road. Traffic violation monitoring on different functional levels may have different effects on vehicle speeds. Other situations require further study.

By analyzing the impact of road traffic violation monitoring on the vehicle speeds, this paper produces the following conclusions:

(1) The vehicle speed distributions before, within, and after the road traffic violation monitoring area are all normally distributed. The average speed of vehicles within the monitoring area is slightly lower than the maximum speed limit of the road. The average speed of vehicles before and after the monitoring area is higher than the speed limit of the road of 40 km/h.

(2) Before and after the road traffic violation monitoring area, the traffic order is chaotic, and the probability of speeding and other behaviors is large. The road traffic violation monitoring is within its scope, which can effectively regulate driving behaviors and reduce the occurrence of illegal activities such as speeding, but its scope of action is limited to a small area. If a driver lacks safety awareness, deterrence that relies solely on traffic violation monitoring does not guarantee sustained traffic safety.

(3) The distribution of vehicle speeds can be calculated from vehicle speed probability density models. In the road with a maximum speed limit of a km/h, there is a 68.2% probability that the vehicle speeds are in the range of $(0.84a - 0.03L + 0.0035aL - 6.2,\ 0.84a + 0.03L + 0.0035aL + 6.2)$ km/h and a 95% probability in the range of $(0.84a - 0.06L + 0.0035aL - 12.4,\ 0.84a + 0.06L + 0.0035aL + 12.4)$ km/h before the traffic violation monitoring area; there is a 68.2% probability that the vehicle speeds are in the range of $(0.95a - 7,\ 0.95a + 7)$ km/h and a 95% probability in the range of $(0.95a - 14,\ 0.95a + 14)$ km/h within the traffic violation monitoring area; and there is a 68.2% probability that the vehicle speed is in the range of $(0.82a - 0.03L + 0.0044aL - 6.2,\ 0.82a + 0.03L + 0.0044aL + 6.2)$ km/h and a 95% probability in the range of $(0.82a - 0.06L + 0.0044aL - 12.4,\ 0.82a + 0.06L + 0.0044aL + 12.4)$ km/h after the traffic violation monitoring area.

(4) The traffic phenomena of vehicles entering the road traffic violation monitoring area from the former transition zone and vehicles entering the post-transition zone past the road traffic violation monitoring area are approximately opposite.

Data Availability

The data used to support the findings of this study are available from the corresponding author upon request.

Conflicts of Interest

The authors declare that they have no conflicts of interest.

Acknowledgments

The authors are grateful for the support of the Key Research and Development Project of Shandong, China (2018GGX105009), the Humanities and Social Science Fund Project under the Chinese Ministry of Education (18YJAZH067), the Natural Science Foundation of Shandong Province, China (ZR2016EEM14), and the National Natural Science Foundation of China (71861023 and 51505244).

References

[1] A. K. Lund, S. Y. Kyrychenko, and R. A. Retting, "Caution: a comment on Alena Erke's red light for red-light cameras? A meta-analysis of the effects of red-light cameras on crashes," *Accident Analysis and Prevention*, vol. 41, pp. 897–905, 2011.

[2] G. Lu, Y. Wang, X. Wu, H. X. Liu, and H. Liu, "Analysis of yellow-light running at signalized intersections using high-resolution traffic data," *Transportation Research Part A: Policy and Practice*, vol. 73, pp. 39–52, 2015.

[3] A. Erke, "Red light for red-light cameras?" *Accident Analysis & Prevention*, vol. 41, no. 5, pp. 897–905, 2009.

[4] R. Tay and A. de Barros, "Should traffic enforcement be unpredictable? The case of red light cameras in Edmonton," *Accident Analysis & Prevention*, vol. 43, no. 3, pp. 955–961, 2011.

[5] E. D. Pauw, S. Daniels, T. Brijs, E. Hermans, and G. Wets, "To brake or to accelerate? Safety effects of combined speed and red light cameras," *Journal of Safety Research*, vol. 50, pp. 59–65, 2014.

[6] G. Wu, F. Chen, X. Pan, M. Xu, and X. Zhu, "Using the visual intervention influence of pavement markings for rutting mitigation-part I: preliminary experiments and field tests," *International Journal of Pavement Engineering*, vol. 20, no. 6, pp. 734–746, 2019.

[7] X. Zhu, Z. Dai, F. Chen, X. Pan, and M. Xu, "Using the visual intervention influence of pavement marking for rutting mitigation-Part II: visual intervention timing based on the finite element simulation," *International Journal of Pavement Engineering*, vol. 20, no. 5, pp. 573–584, 2019.

[8] F. Chen, M. Song, and X. Ma, "Investigation on the injury severity of drivers in rear-end collisions between cars using a

random parameters bivariate ordered probit model," *International Journal of Environmental Research and Public Health*, vol. 16, no. 14, 2019.

[9] Z. Cheng, J. Lu, Z. Zu, and Y. Li, "Speeding violation type prediction based on decision tree method: a case study in Wujiang, China," *Journal of Advanced Transportation*, vol. 2019, Article ID 8650845, 10 pages, 2019.

[10] M. Huan and X. Yang, "A reliability-based analysis of bicyclist red-light running behavior at urban intersections," *Discrete Dynamics in Nature and Society*, vol. 2015, Article ID 794080, 7 pages, 2015.

[11] Y. Xia, J. Chen, X. Lu, C. Wang, and C. Xu, "Big traffic data processing framework for intelligent monitoring and recording systems," *Neurocomputing*, vol. 181, pp. 139–146, 2016.

[12] C. Ma, W. Hao, F. Pan, and W. Xiang, "Road screening and distribution route multi-objective robust optimization for hazardous materials based on neural network and genetic algorithm," *PLoS One*, vol. 13, no. 6, Article ID e0198931, 2018.

[13] H. Zheng, W. Chang, and J. Wu, "Traffic flow monitoring systems in smart cities: coverage and distinguishability among vehicles," *Journal of Parallel and Distributed Computing*, vol. 127, pp. 224–237, 2019.

[14] T. Zhu, P. Xie, C. Guo, and Y. Wang, "Effect of countdown of green light signal on vehicle speed at intersections," *Journal of Chang'an University (Natural Science Edition)*, vol. 4, pp. 70–75, 2012.

[15] F. Pan, L. Zhang, T. Liu, G. Kang, and M. Li, "Driver driving behavior modeling at countdown signal intersection considering vehicle value," *Transportation System Engineering and Information*, vol. 2, pp. 64–69, 2016.

[16] F. Pan, L. Zhang, C. Ma et al., "Impact of vehicular countdown signals on driving psychologies and behaviors: taking China as an example," *Journal of Advanced Transportation*, vol. 2017, Article ID 5838520, 11 pages, 2017.

[17] S. Luo, F. Pan, J. Wang, R. Qi, L. Zhang, and Q. Bing, "Investigation on the psychological and behavioral effects of traffic illegal monitoring on occupational and non-professional drivers," *Journal of Transport Information and Safety*, vol. 6, pp. 22–25, 2017.

[18] L. Zhang, T. Liu, F. Pan, T. Guo, and R. Liu, "Analysis on the influence of driver factors on road traffic accident index," *China Safety Science Journal*, vol. 5, pp. 79–84, 2014.

[19] H. Qian, "Study on the impact of vehicle green light countdown on traffic safety at intersections," *China Safety Science Journal*, vol. 3, pp. 9–13, 2010.

[20] X. Jiang, Z. Zhao, and Y. Pei, "Effect of electronic law enforcement on traffic illegality and traffic accidents at signalized intersections," *Journal of Harbin Institute of Technology*, vol. 10, pp. 84–87, 2011.

[21] M. Ahmed and M. Abdel-Aty, "Evaluation and spatial analysis of automated red-light running enforcement cameras," *Transportation Research Part C*, vol. 50, pp. 130–140, 2015.

[22] C. Chai, Y. D. Wong, and K. M. Lum, "Safety impacts of red light cameras at signalized intersections based on cellular automata models," *Traffic Injury Prevention*, vol. 16, no. 4, pp. 374–379, 2015.

[23] S. S. Pulugurtha and R. Otturu, "Effectiveness of red light running camera enforcement program in reducing crashes: evaluation using before the installation", "after the installation", and "after the termination" data," *Accident Analysis & Prevention*, vol. 64, pp. 9–17, 2014.

[24] L. M. Higgins, W. D. Shaw, and A. Egbendewe-Mondzozo, "Attributes affecting preferences for traffic safety camera programs," *Accident Analysis & Prevention*, vol. 43, no. 3, pp. 1042–1048, 2011.

[25] W. Wang, J. Xi, and H. Chen, "Modeling and recognizing driver behavior based on driving data: a survey," *Mathematical Problems in Engineering*, vol. 2014, Article ID 245641, 20 pages, 2014.

[26] F. Pan, Y. Dong, and L. Zhang, "Analysis and modeling of green lantern running behavior at countdown signal intersection," *China Safety Science Journal*, vol. 7, pp. 147–152, 2015.

[27] H. Zheng, A. kuang, and Q. Duan, "Empirical study on traffic arrival distribution at signalized intersections," *Journal of Transport Science and Engineering*, vol. 2, pp. 91–95, 2018.

[28] T. Zhu, C. Guo, C. Xie, and Y. Wang, "The impact of traffic signal countdown on vehicle speed and traffic safety," *China Safety Science Journal*, vol. 4, pp. 97–102, 2011.

Hindawi
Journal of Advanced Transportation
Volume 2020, Article ID 8523818, 8 pages
https://doi.org/10.1155/2020/8523818

Research Article

Predicting Crash Frequency for Urban Expressway considering Collision Types Using Real-Time Traffic Data

Hui Zhang[1,2] **Siyao Li**[1,2] **Chaozhong Wu**[1,2] **Qi Zhang**[1,2] **and Yafen Wang**[3]

[1]*Intelligent Transportation Systems Research Center, Wuhan University of Technology, Wuhan 430063, China*
[2]*Engineering Research Center of Transportation Safety, Wuhan 430063, China*
[3]*Road Traffic Safety Risk Prevention and Control Center, Wuhan Traffic Management Bureau, Wuhan Municipal Public Security Bureau, Wuhan, China*

Correspondence should be addressed to Chaozhong Wu; wucz@whut.edu.cn

Received 27 December 2019; Revised 28 January 2020; Accepted 4 February 2020; Published 20 March 2020

Guest Editor: Feng Chen

Current studies on traffic crash prediction mainly focus on the crash frequency and crash severity of freeways or arterials. However, collision type for urban expressway crash is rarely considered. Meanwhile, with the rapid development of urban expressway systems in China in recent years, traffic safety problems have attracted more attention. In addition, the traffic characteristics are considered to be a potentially important predictor of traffic accidents; however, their impact on crashes has been controversial. Therefore, a crash frequency predicting model for urban expressway considering collision types is proposed in this study. The loop detector traffic data and historical crash data were aggregated based on the similarities of the traffic conditions 5 minutes before crash occurrence, among which crashes were divided by collision type (rear-end collision and side-impact collision). The impact of traffic characteristics along with weather variables as well as their interactions on crash frequency was modelled by using negative binomial regression model. The results indicated that the influence of traffic and weather factors on two collision types shared similar trend, but different level. For rear-end collisions, crash frequency increased with lower average speed and high traffic volume under low speed limit. And when the speed limit is high, higher average speed coupled with larger volume increases the probability of crash. Higher average speed and traffic volume increase the probability of side-impact collisions, without being affected by the speed limit. The findings of the present study could help to determine efficient safety countermeasures aimed at improving the safety performance of urban expressway.

1. Introduction

With the rapid development of Chinese cities, residents' demand for travel and the increasing number of motor vehicles put forward higher requirements for the operation efficiency of cities. Urban expressway is a key part of the city roadway networks, which is of great significance to improve the travel efficiency. Compared with main arterial roads, urban expressway is characterized by large traffic volume and higher speed [1], resulting in frequent traffic crashes in recent years. In 2017, 6652 road crashes occurred causing 1673 deaths and 6862 injuries along the urban expressway [2]. Analysing the influence factors of urban expressway traffic crashes and establishing a crash prediction model play important roles for improving traffic safety.

A large number of studies on crash prediction models were mainly carried out from the aspects of crash frequency estimation and the crash severity prediction at the macro level (e.g., yearly, monthly) [3–6]. The Highway Safety Manual (HSM) prediction model represents the most widely used approach for road safety assessment, developing the safety prediction procedures for rural highways, urban and suburban arterials in the 2010 version of the HSM [7]. Taking factors such as traffic flow, road geometry, and so on into consideration, the HSM provides a prediction method for estimating the expected average frequency of single- and multiple-vehicle fatal-and-injury crashes.

Establishing the traffic crash model based on the historical crash data to analyse the relationship between crash frequency and the relevant risk factors such as roadway geometry variables has been a focus for a long time. Based on crash data of freeway, Ma et al. analysed the influence of road length, traffic environment, and other risk factors on crash rate [8]. Xie et al. analysed the relationship among crash probability and intersection characteristics and traffic volume based on the data of signalized intersections in Shanghai. The results showed that the number of lanes and average speed at intersections would have a significant impact on the crash probability [9]. There are also some scholars who have studied the prediction methods based on dividing crashes into single- and multivehicle crashes [10], but there are few studies conducted on the collision type (rear-end collision, side-impact collision, etc.), particularly in China. There is strong empirical evidence that the prediction model of crash frequency based on collision type can help better understand the influence of the crash occurrence contributing factors on specific collision type, especially in real-time risk assessment [11, 12].

Due to the impact of real-time driving environment data such as traffic flow on traffic accidents, and with the technology progress of traffic data detection and storage, real-time crash risk assessment has become a research hotspot in the field of traffic safety. Chen et al. adopted a zero-inflated, negative binomial regression model to estimate hourly crash frequency using real-time environmental and traffic data [13]. In order to explore the complex interactions among characteristics, the mixed logit model was adopted for his further research [14], which showed that environment and traffic were critical to the likelihood of collisions. Choudhary et al. explored the relationships between traffic characteristics and the occurrence of crashes based on traffic data collected through inductive loop detectors. The results indicated that crash probability is related to higher speeds, greater volume, and high between-lanes speed variation [15]. Shi et al. explored the impact of real-time traffic flow on urban expressway crash probability [16]. The crash risk analysis models were developed for total crashes and time-related crashes to reveal the significant factors that affect crash risk [17]. In addition, typical scenarios leading to an accident were found from the modelling results. In the following research, Yu et al. investigated the impacts of data aggregation schemes on the relationships between operating speed and traffic safety; additionally, a U-shaped relationship between operating speed and crash occurrence was identified [18].

Traffic characteristics are widely adopted as important indicators of crash frequency, but the research results on its safety effect are not consistent. The inconsistencies among the results may be relevant to the different data sources, low quality of data, and different analytical methods. Speed is considered to be one of the most important factors leading to crashes. Speed management interventions such as Variable Speed Limits (VSL) or fundamental speed limit settings are introduced to improve road capacity and safety. The application of speed limit settings relies on the in-depth understanding of the quantitative relationships between operating speeds and traffic safety to determine strategies to reduce the crash risk. Previous studies have shown positive associations of average speed with crashes [19], while single-vehicle crashes and fatal-and-injury crashes involving multiple vehicles increase with the increase of the average speed [20]. However, others have shown a negative or an insignificant relationship between average speed and crash risk [21, 22]. In addition, some scholars have suggested that the safety effect of average speed would vary with road types [23]. As for the impact of speed limit on crash risk, some studies have found that speed limit is positively correlated with crash frequency and severity [24], and high speed limit road sections are often associated with high crash risk. However, Gou et al. mentioned that the crash frequency may be reduced due to better road facilities with high speed limit sections [25]. What is more, the safety effect of speed seemed to be related to other traffic variables such as traffic flow. For example, Kononov et al. have shown that higher crash risk is associated with high-speed driving in high-density traffic flow [26].

In summary, most studies on traffic crash prediction mainly focus on the crash frequency and crash severity on freeway or intersections, while the study considering the collision type of urban expressway crash is rare. Moreover, the relationship between traffic characteristics and crash probability needs to be further discussed. Weather conditions have been found to be associated with accident risk, especially rainy weather [27]. This study explores the impact of traffic characteristics and weather variable on crash frequency. Data from Wuhan urban traffic management systems were utilized here and crashes are divided by collision type (rear-end collision, side-impact collision; collision type statistics reveal that rear-end collision and sideswipe collisions are the most common type of collision [28], and other collision types are excluded from the analysis because of the limited number). Data aggregated following a condition-based approach to reflect the conditions prior to crash occurrence are more accurate [18]. Finally, the relationships between relevant factors and traffic safety were conducted using negative binomial regression model.

The remaining of the paper is organized as follows. The data are collected and the negative binomial regression model is proposed for crash risk assessment. Sections 3 presented and discussed the results and the verification of the model. The paper ended with conclusions and limitations and looked forward for further study.

2. Data Collection and Preparation

To predict the crash frequency of urban expressway, historical crash, real-time traffic, and weather data have been utilized. Two urban expressways crossing over the river in Wuhan were chosen to be the data collection area, totalling 3,986 meters per direction. Inductive loop detectors and video monitoring were installed in the study area to provide real-time traffic flow data. Considering the design characteristics of urban expressways, the two-way lanes were considered to be independent of each other. Three datasets were used to build the database: (1) historical crash data

from January 1, 2018 to October 31, 2018. It was obtained from the traffic accident archives recorded by Wuhan Municipal Public Security Bureau in detail, including information concerning crash occurrence time, location, weather, and collision types. During the study, there were 536 crashes in total, in which 321 were rear-end collisions and 135 were side-impact collisions. Considering the high frequency of rear-end and side-impact collision, this study only discussed the impact of the crash occurrence contributing factors on these two kinds of collisions and finally obtained a total of 466 collision samples. Moreover, weather conditions were also extracted from this dataset, which were divided into two categories in this study to indicate whether it was rainy or not. When a crash occurs, its weather data is usually recorded accurately by professional traffic police based on the weather information collected by the nearest weather station; (2) roadway posted speed limit. The speed limit on the road, as the upper limit of real-time speed, has critical impact on crash risk. The speed limits of the urban expressway sections studied are 50 km/h and 70 km/h, respectively, and remained consistent during the study period; (3) traffic data detected by Loop Detectors (LDs) located along the study area. Lane-based average speed and total volume at 5-minute interval were provided by LDs data, which could provide analysis with high-quality traffic flow data. For each crash, Mile Maker (MM) or Chinese characters associated with the crash records were used to describe its location, and the traffic data can be exactly matched with crash data according to the occurrence location and time recorded.

In the raw data of the LDs, there are abnormal values caused by equipment problems and other random errors, which can be identified by setting appropriate value interval of parameters, so as to screen out the unrealistic value [29]. The invalid values of parameters include (1) speed < 0 km/h or speed > 100 km/h; (2) speed > 0 km/h and volume = 0; and (3) volume > 0 and speed = 0 km/h. Previous studies have shown that data aggregation has a significant impact on the results of the crash modelling. Abdel-Aty et al. compared the crash risk prediction effect of data aggregated at intervals of three minutes and five minutes and found that the latter provided more information for analysis and had better research significance [30]. The random noise can be effectively reduced by aggregating the data into five-minute intervals. Considering that the weather conditions generally do not change in a short period of time, the hourly collected weather conditions were matched with crashes to provide the weather information for model building [15]. In addition, traffic characteristics (average speed, traffic volume, etc.) 5 minutes just prior to the crash time had great contribution to their occurrence [29]. Therefore, the traffic data five minutes prior to the reported crash time and the weather conditions at the reported crash time were identified and defined as the precrash condition to construct the crash prediction model and finally obtain a total of 466 precrash conditions. For example, the crash occurred at 9 : 30; then traffic data from 9 : 20 to 9 : 25 (a 5-minute window) collected by the LDs closest to the crash occurrence location and the weather information extracted from the traffic accident archives were extracted to form the precrash condition as shown in Figure 1.

3. Methods

3.1. Variable Setting. Based on the impact of data aggregation on crash modelling, a scenario-based data aggregation approach of significance has been proposed to identify the traffic conditions just prior to the crashes which might lead to crashes. For the scenario-based analysis, crashes were aggregated based on the similarity of the traffic conditions just before the crashes as employed by Yu et al. [18]. Precrash conditions, coupled with speed limit, were used as the control variable to define the potential crash scenarios, which were classified into equal frequency categories [15]. Firstly, the average speed was divided into 25 equal groups with a 4-percentile step; then each speed quantile was divided into 3 categories with a 33-percentile step for traffic volume. Further, the sequence was followed by splitting the speed limit into two equal quantiles for each quantile of traffic volume. Similarly, the weather (rain/no rain) conditions were divided into two equal-frequency groups for each volume category. Finally, a total of 300 scenarios (i.e., $25 \times 3 \times 2 \times 2$) were created, representing all the possible traffic conditions just prior to the crashes.

The 300 condition-based scenarios were matched with crashes that occurred under these traffic conditions and the crash frequency of each scenario was expressed by collision types (rear-end collisions and side-impact collisions). Therefore, an analysis dataset was formed by aggregating crashes into the same scenario. The traffic characteristics of each scenario were represented by the median values of average speed and traffic volume. Since it makes sense to study the relationship between traffic variables and crashes further, the potential interaction among traffic variables also needs to be taken into account. In this study, multiple interaction terms were utilized to study their impact on crash frequency in addition to the individual traffic variables. Table 1 presents the summary statistics of the scenario-based dataset.

4. Modelling

Statistical counting models have been widely utilized for crash frequency prediction. The Poisson regression model is a basic model to analyse the impact of potential factors on crash frequency and requires the mean and variance of crash frequency to be equal [31]. However, the dispersion and low probability of traffic accidents do not satisfy the assumption of Poisson's distribution. This phenomenon of variance bigger than the mean value is usually called overdispersion. The negative binomial regression model is an extension of the Poisson regression model to handle this problem by introducing an error term that obeys Gamma distribution on the basis of Poisson's regression model. This study explored the relationship between independent variables and rear-end collision and side-impact collision by establishing two negative binomial regression models. The expected crashes can be expressed as follows:

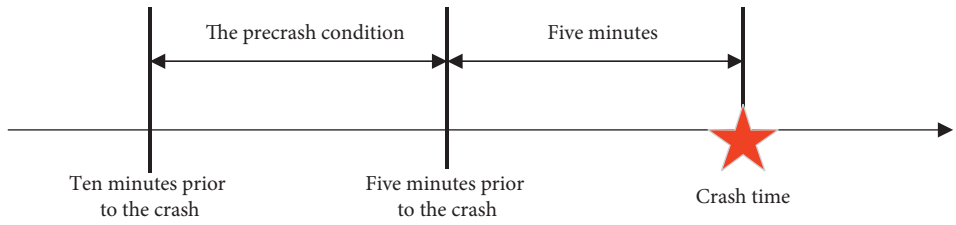

Figure 1: The precrash condition.

Table 1: Summary statistics of the scenario-based dataset.

Variable	Description	Mean	SD	Min	Max
Average speed (km/h)	Median speed for the crash occurrence scenario	37.68	8.04	20.98	80.77
Volume (vehicles in 5 min interval per lane, vehicles)	Median volume per lane for the crash occurrence scenario	126.97	44.19	12	209.875
Speed limit (km/h)	50 km/h or 70 km/h	60	60	50	70
Weather	=0 if rain; =1 otherwise	0.5	0.5	0	1
Average speed ∗ volume (km/h ∗vehicles)	—	4644.11	1565.61	547.68	8143.15
Average speed ∗ speed limit (km/h ∗ km/h)	—	2178.36	641.01	1049	5653.9
Volume ∗ speed limit (vehicles ∗ km/h)	—	7148.54	2283.65	840	10756.67
Crash frequency	Rear-end collisions	1.07	2.09	0	10
	Side-impact collisions	0.45	1.41	0	6

$$\lambda_{ik} = \exp\left(\beta_{\mu k} X_{\mu k} + \varepsilon_{ik}\right), \tag{1}$$

where λ_{ik} refers to the expected crash frequency for k collision type of the scenario i. $X_{\mu k}$ is a set of explanatory variables for k collision type, such as traffic volume, speed limit, etc. $\beta_{\mu k}$ is the corresponding regression parameters to be estimated for k collision type. ε_i is the error term, which follows the Gamma distribution, with a mean value of 1 and a variance of α^2. So, the variance of the crash frequency distribution is

$$\mathrm{VAR}[y_{ik}] = \mathrm{E}[y_{ik}][1 + \alpha \mathrm{E}[y_{ik}]] = \lambda_{ik}(1 + \alpha\lambda_{ik}), \tag{2}$$

where y_{ik} represents the observed crash frequency for k crash type of the scenario i, $\mathrm{VAR}[y_{ik}]$ represents its variance, and $\mathrm{E}[y_{ik}]$ is the expected crash frequency. Then, the probability density function of the negative binomial regression model is formulated as follows:

$$P(y_{ik}) = \frac{\Gamma(y_{ik} + (1/\alpha))}{\Gamma(y_{ik} + 1)\Gamma(1/\alpha)} \left(\frac{\alpha\lambda_{ik}}{1 + \alpha\lambda_{ik}}\right)^{y_{ik}} \left(\frac{1}{1 + \alpha\lambda_{ik}}\right)^{1/\alpha}. \tag{3}$$

Among them, $\Gamma(\cdot)$ is a Gamma function. When $\alpha = 0$, the negative binomial regression model is the same with Poisson's regression model; when $\alpha > 1$, the data deviation is large; when $\alpha < 1$, the data deviation is small. Since the large deviation of traffic crash data, the negative binomial model is widely used for traffic crash prediction.

5. Performance Evaluation of Prediction

Akaike Information Criterion (AIC) and Bayesian Information Criterion (BIC) were used to assess the overall goodness-of-fit. Note that lower values of these measures signify better statistical fit. To further evaluate the models, two forecasting accuracy measures were adopted: Mean Absolute Deviation (MAD) and Mean Squared Error (MSE) [32].

MAD describes the magnitude of average bias in model prediction:

$$\mathrm{MAD} = \frac{1}{n} \sum_{i=1}^{n} \left| y_{ik} - \lambda_{ik} \right|, \tag{4}$$

where y_{ik} is the observed crash frequency for k crash type of the scenario i and λ_{ik} is the predicted one.

On the other hand, MSE refers to the mean value of the square misprediction of the estimated models. MSE is computed as follows:

$$\mathrm{MSE} = \frac{1}{n} \sum_{i=1}^{n} (y_{ik} - \lambda_{ik})^2. \tag{5}$$

MSE and MAD can be used to describe the accuracy of the model fitting. In general, the lower the value indicated, the better the prediction of observed data. However, the range of their values is not limited, and the validity of the model is usually tested by artificially defining a reasonable range. Therefore, R^2 is further introduced to describe the accuracy of the model, and its value ranges from 0 to 1. The larger R^2, the better the model fitting effect, and when R^2 is greater than 0.4, the model is considered to have a good fit.

$$R^2 = \left(\frac{\sum_{i=1}^{n} \lambda_{ik} - \overline{y_{ik}})^2}{\sum_{i=1}^{n} \left(y_{ik} - \overline{y_{ik}}\right)^2}, \right. \tag{6}$$

where $\overline{y_{ik}}$ is the observed average crash frequency for k crash type of the scenario i.

6. Results and Discussion

Given the 0.05 significance level, the models were fitted by the Maximum Likelihood Estimation (MLE) method with the help of STATA 15.0 software. All the traffic variables along with their multiplicative interaction combinations and

rain were taken as explanatory variables in both multivariate models. The best fitted variable combination for crash frequency prediction included all traffic and weather variables plus the interaction between average speed and speed limit. The performance of prediction was evaluated and Table 2 presents the values of these measures.

The result shows that the negative binomial model has good prediction performance for the rear-end collision and the side-impact collision. The significant variables in the two models include average speed, traffic volume, weather, speed limit, and the interaction between average speed and speed limit. In Table 2, a positive (negative) sign for a variable in the crash count component indicates that an increase in the variable is likely to result in more (less) vehicle crashes. Some variables have similar influences on the two types of crashes. For instance, the parameter for traffic volume reveals a positive association with crash proportion in both models, indicating that the frequency of rear-end collisions and side-impact collisions will increase with the increase of traffic volume [7, 15, 18]. The estimated result of weather variable implies that the presence of rain has a negative effect on crash rates, which is consistent with previous studies [33–35]. The high crash risk in rainy weather may have a certain relationship with poor road conditions and reduced visibility, which leads to longer stopping distance and longer reaction time. However, the parameter estimate value of the same significance variable is different in the two models, indicating that the same variable has different effects on the two types of crash frequency. For example, in the rear-end collision prediction model, the weather coefficient is −1.4399, while being −0.9787 in the side-impact collision prediction model, indicating that compared with the side-impact collision, rainfall has a greater impact on the rear-end collisions. The probability of rear-end collisions in a rainy environment is relatively high. It can be explained that when driving in rainy days, the stopping distance becomes longer due to the wetness of pavement, which are more likely to lead to rear-end collision.

Further analysis of the impact of road average speed and speed limit on the crash frequency was conducted. Due to the existence in interaction terms, although the estimation results of these two parameters were negative, we cannot draw the conclusion that they are negatively related to the crash frequency. In order to observe the contribution of the interaction between average speed and speed limit to the crash frequency, the crash rates are plotted in Figures 2(a) and 2(b) for the rear-end collision and the side-impact collision, respectively. The speed limit design of urban expressway generally ranges from 60 km/h to 100 km/h in China. In addition, considering that there was a research object with speed limit of 50 km/h in this study, the range of speed limit range was determined to be 50 km/h–100 km/h, and the corresponding average speed range is 0 km/h–100 km/h. The results show that the influence of their interaction on rear-end collision and side-impact collision is different. For the rear-end collision, when the speed limit is low, the crash frequency will decrease with the increase of speed limit coupled with a low average speed. However, when the speed limit continues to increase, the crash frequency is positively related to the average speed. But for side-impact collision, no matter what the speed limit is, the average speed limit performs positive, indicating that the crash frequency increases with the rise of average speed.

Table 2: Estimation results of negative binomial model.

Variables	Rear-end collisions		Side-impact collisions	
	Mean	P value	Mean	P value
Intercept	11.4970	0.0000	13.1129	0.0015
Average speed	−0.1561	0.0080	−0.1236	0.0195
Volume	0.0027	0.0121	0.0044	0.0431
Rain	−1.4399	0.0000	−0.9787	0.0006
Speed limit	−0.1917	0.0000	−0.2565	0.0007
Average speed ∗ speed limit	0.0028	0.0067	0.0026	0.0134
AIC	490.61		392.37	
BIC	510.58		412.66	
MAD	1.42		1.23	
MSE	2.63		3.45	
R^2	0.75		0.63	

The relationship between average speed, traffic volume, and crashes is further analysed, and the surface relationship diagrams of average speed and traffic volume with rear-end collision and side-impact collision under different speed limit conditions were plotted, respectively, as shown in Figure 3. For rear-end collision, the curves show that high crash risk associates with low average speed when the speed limit is low. When the speed limit is low, vehicles tend to drive at a lower speed, which to some extent promotes the occurrence of traffic congestion. Many studies, including those of Golob et al. and Christoforou et al., have shown that traffic congestion is one of the most significant precursors of rear-end collisions [11, 13, 36]. In the case of traffic congestion, drivers must adjust the speed in short time and short distance, making it more likely to lead to a rear-end collision, which is consistent with the results of this paper. When the speed limit is high, crash seems to be triggered at higher average speed and volumes. The vehicle tends to drive at a high speed under high speed limit. The vehicle inertia is too large to brake within a safe distance, leading to higher probability of a rear-end collision crash. In addition, it is clear that rear-end collision potential increase when the traffic volume is higher. This may be due to more interaction between vehicles at higher flow conditions leading to an increased tendency for rear-end collisions. Similar findings are also found in other studies [37].

The results in Figure 4 show that for the side-impact collisions, when traffic volume increase, the frequency of side-impact collision increases, which may be related to more frequent lane change behaviour of vehicles in high-flow conditions. This finding is similar to the work of Christoforou et al. who reported that side-impact collisions are more likely to be positively correlated with traffic volume [11]. Further, side-impact collisions are more probable to occur for high levels of traffic average speed [38]. One possible explanation could be that side-impact collisions are usually associated with lane change operations, which are more prone to crash at high speeds. The relationship

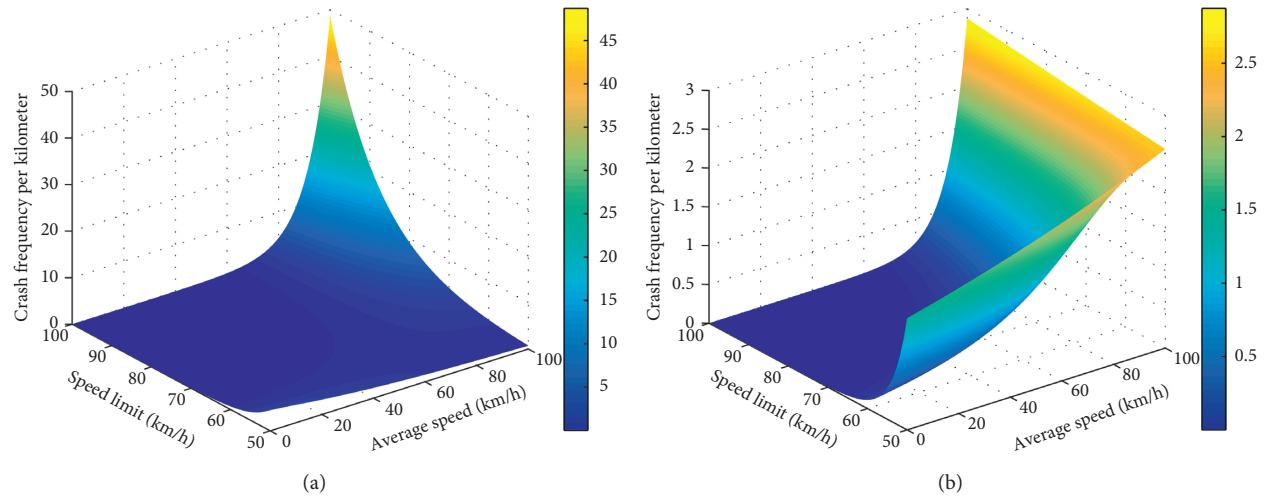

Figure 2: The impact of the interaction between average speed and speed limit on the crash frequency. (a) For the rear-end collision. (b) For the side-impact collision.

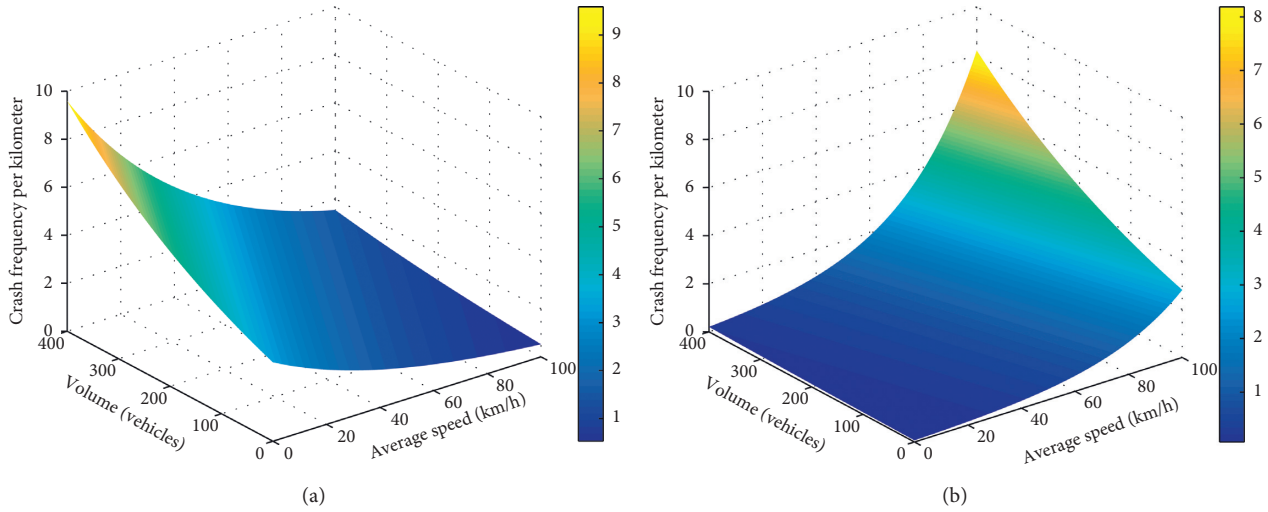

Figure 3: Relationships between speed, volume, and rear-end collision probability. (a) Speed limit = 50 km/h. (b) Speed limit = 70 km/h.

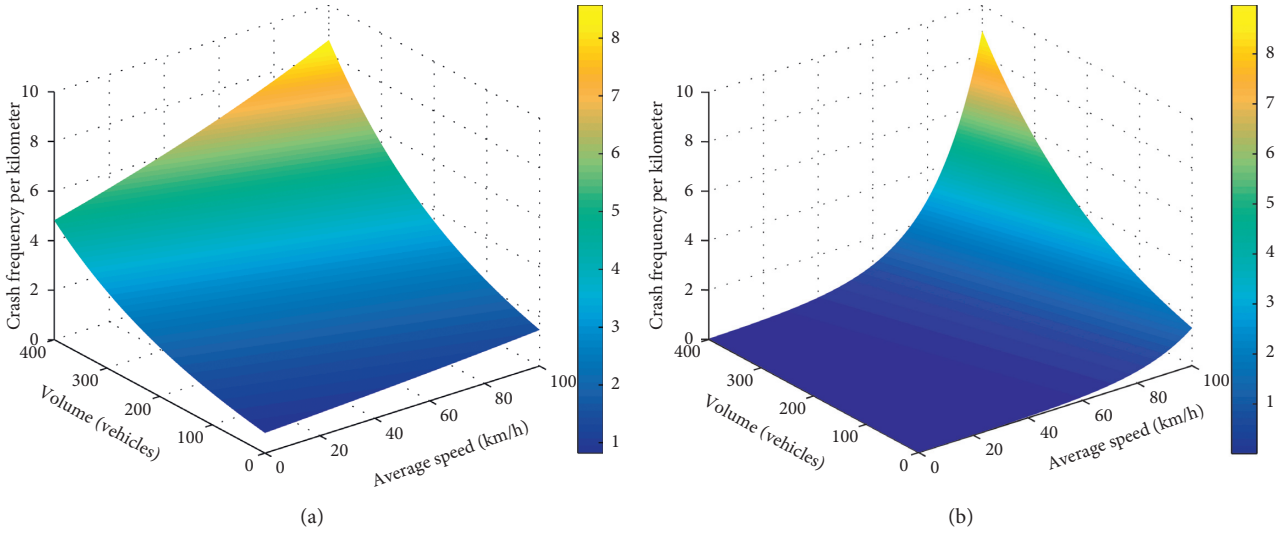

Figure 4: Relationships between speed, volume, and side-impact collision probability. (a) Speed limit = 50 km/h. (b) Speed limit = 70 km/h.

between these variables and the frequency of different crash types can be applied on safety improvement and management.

7. Conclusions

Traffic crash prediction is a hot topic in the field of traffic safety and keeps developing. In view of the shortage of urban expressway crash prediction and the controversial issue of the influence of speed on safety, the traffic and weather variables were used to predict the crash risk. This study developed crash risk analysis models for rear-end collision and side-impact collision with loop detector traffic data and historical crash data. For the purpose of exploring traffic conditions that leads to accidents, the data of Wuhan urban expressway were aggregated based on the similarity of traffic conditions in 5 minutes prior to crash occurrence. The impact of traffic variables along with their interactions and the weather condition on crash frequency was conducted by the negative binomial regression model. The results show that average speed, traffic volume, speed limit, and weather have significant impact on crash frequency and the influence of factors on two collision types is similar but with different degree. Specifically, the existence of rain increases the crash risk, especially for rear-end collisions. Higher traffic volume increases the crash risk. The impact of average speed on rear-end collision and side-impact collision on urban expressway is different. Specifically, under the lower speed limit, the probability of rear-end collision increases with the decrease of road average speed. At the higher speed limit, the probability of rear-end collision increases with the rise of road average speed. Regardless of the speed limit, with the increase of road average speed and traffic flow, the frequency of side-impact collision will increase.

In general, the specific combinations of traffic characteristics increase the probability of crash occurrences. These results are helpful to understand the crash risks under different traffic conditions and provide a basis for formulating traffic management countermeasures effectively. The results can be applied to real-time traffic management, where drivers can be warned via variable message sign once it is defined to be vulnerable to existing traffic conditions. In addition, the crash prediction model can also be applied to the evaluation and planning of road improvement projects when it is used to monitor the road safety level in real time. However, there are some limitations in this study. For example, due to the limited number of single-vehicle crashes, this study did not conduct the prediction model for it. Moreover, in order to better understand the impact of traffic characteristics on traffic crashes, further study of collision types is needed. At last, due to the existence of traffic heterogeneity, further crash risk analysis should consider the heterogeneous influence of various factors on traffic safety.

Data Availability

The crash data and traffic data are available upon request for research purpose.

Conflicts of Interest

The authors declare that there are no conflicts of interest regarding the publication of this paper.

Authors' Contributions

Chaozhong Wu and Hui Zhang conceived and designed the study. Siyao Li, Hui Zhang, and Yafen Wang collected the data. Siyao Li, Hui Zhang, and Qi Zhang analyzed and interpreted the results. Siyao Li and Hui Zhang prepared the manuscript draft. All authors reviewed the results and approved the final version of the manuscript.

Acknowledgments

This research was supported by the National Natural Science Foundation of China (61603282, u1624262) and the National Key Research and Development Program of China (2017YFC0804802). All authors also want to thank the staff from Wuhan Municipal Public Security Bureau for their kindly assistance in the data collection.

References

[1] C. Xu, X. Wang, H. Yang, K. Xie, and X. Chen, "Exploring the impacts of speed variances on safety performance of urban elevated expressways using GPS data," *Accident Analysis & Prevention*, vol. 123, pp. 29–38, 2019.

[2] Transportation Bureau, Ministry of Public Security, *The Road Traffic Accidents Statistics Report in China*, Transportation Bureau, Ministry of Public Security, Beijing, China, 2017.

[3] E. Sacchi and T. Sayed, "Bayesian estimation of conflict-based safety performance functions," *Journal of Transportation Safety & Security*, vol. 8, no. 3, pp. 266–279, 2016.

[4] T. Ahmed and S. Tarek, "Models to evaluate the severity of pedestrian-vehicle conflicts in five cities," *Transportmetrica A: Transport Science*, vol. 15, no. 2, pp. 354–375, 2019.

[5] H. L. Huang, P. P. Xu, M. Ma, and M. Abdel-aty, "Recent theoretical researches on transportation safety planning," *China Journal of Highway and Transport*, vol. 27, no. 09, pp. 90–118, 2014.

[6] Q. Zeng and H. Huang, "A stable and optimized neural network model for crash injury severity prediction," *Accident Analysis & Prevention*, vol. 73, pp. 351–358, 2014.

[7] AASHTO, *Highway Safety Manual*, American Association of State Highway and Transportation Officials, Washington, DC, USA, 2010.

[8] C. Ma, S. R. Zhang, Z. L. Ma, and J. Wang, "Nonlinear negative binomial regression model of expressway traffic accident frequency prediction," *China Journal of Highway and Transport*, vol. 31, no. 11, pp. 176–185, 2018.

[9] K. Xie, X. Wang, H. Huang, and X. Chen, "Corridor-level signalized intersection safety analysis in Shanghai, China using Bayesian hierarchical models," *Accident Analysis & Prevention*, vol. 50, pp. 25–33, 2013.

[10] B. W. Dong, X. X. Ma, F. Chen, and S. R. Chen, "Investigating the differences of single-vehicle and multivehicle accident probability using mixed logit model," *Journal of Advanced Transportation*, vol. 2018, Article ID 2702360, 9 pages, 2018.

[11] Z. Christoforou, S. Cohen, and M. G. Karlaftis, "Identifying crash type propensity using real-time traffic data on freeways," *Journal of Safety Research*, vol. 42, no. 1, pp. 43–50, 2011.

[12] T. Bhowmik, S. Yasmin, and N. Eluru, "Do we need multivariate modeling approaches to model crash frequency by crash types? A panel mixed approach to modeling crash frequency by crash types," *Analytic Methods in Accident Research*, vol. 24, p. 100107, 2019.

[13] F. Chen, S. Chen, and X. Ma, "Crash frequency modeling using real-time environmental and traffic data and unbalanced panel data models," *International Journal of Environmental Research and Public Health*, vol. 13, no. 6, p. 609, 2016.

[14] F. Chen, S. Chen, and X. Ma, "Analysis of hourly crash likelihood using unbalanced panel data mixed logit model and real-time driving environmental big data," *Journal of Safety Research*, vol. 65, pp. 153–159, 2018.

[15] P. Choudhary, M. Imprialou, N. R. Velaga, and A. Choudhary, "Impacts of speed variations on freeway crashes by severity and vehicle type," *Accident Analysis & Prevention*, vol. 121, pp. 213–222, 2018.

[16] Q. Shi, M. Abdel-aty, and R. Yu, "Multi-level Bayesian safety analysis with unprocessed automatic vehicle identification data for an urban expressway," *Accident Analysis & Prevention*, vol. 88, pp. 68–76, 2016.

[17] R. Yu, X. Wang, K. Yang, and M. Abdel-aty, "Crash risk analysis for shanghai urban expressways: a Bayesian semiparametric modeling approach," *Accident Analysis & Prevention*, vol. 95, pp. 495–502, 2016.

[18] R. Yu, M. Quddus, X. Wang, and K. Yang, "Impact of data aggregation approaches on the relationships between operating speed and traffic safety," *Accident Analysis & Prevention*, vol. 120, pp. 304–310, 2018.

[19] L. Aarts and I. van Schagen, "Driving speed and the risk of road crashes: a review," *Accident Analysis & Prevention*, vol. 38, no. 2, pp. 215–224, 2006.

[20] M.-I. M. Imprialou, M. Quddus, and D. E. Pitfield, "Predicting the safety impact of a speed limit increase using condition-based multivariate Poisson lognormal regression," *Transportation Planning and Technology*, vol. 39, no. 1, pp. 3–23, 2016.

[21] M. Quddus, "Exploring the relationship between average speed, speed variation, and accident rates using spatial statistical models and GIS," *Journal of Transportation Safety & Security*, vol. 5, no. 1, pp. 27–45, 2013.

[22] X. Wang, R. Yu, and C. Zhong, "A field investigation of red-light-running in Shanghai, China," *Transportation Research Part F: Traffic Psychology and Behaviour*, vol. 37, pp. 144–153, 2016.

[23] M. H. Cameron and R. Elvik, "Nilsson's Power Model connecting speed and road trauma: applicability by road type and alternative models for urban roads," *Accident Analysis & Prevention*, vol. 42, no. 6, pp. 1908–1915, 2010.

[24] A. Vadeby and Å. Forsman, "Traffic safety effects of new speed limits in Sweden," *Accident Analysis & Prevention*, vol. 114, pp. 34–39, 2018.

[25] Y. Guo, Z. Li, P. Liu, and Y. Wu, "Modeling correlation and heterogeneity in crash rates by collision types using full Bayesian random parameters multivariate Tobit model," *Accident Analysis & Prevention*, vol. 128, pp. 164–174, 2019.

[26] J. Kononov, C. Durso, D. Reeves, and B. K. Allery, "Relationship between traffic density, speed, and safety and its implications for setting variable speed limits on freeways," *Transportation Research Record: Journal of the Transportation Research Board*, vol. 2280, no. 1, pp. 1–9, 2012.

[27] F. Chen and S. Chen, "Injury severities of truck drivers in single- and multi-vehicle accidents on rural highways," *Accident Analysis & Prevention*, vol. 43, no. 5, pp. 1677–1688, 2011.

[28] C. Thanapong, J. Sajjakaj, C. Vuttichai, K. Ampol, and R. Vatanavongs, "Analysis of rear-end crash on Thai highway: decision tree approach," *Journal of Advanced Transportation*, vol. 2019, Article ID 2568978, 13 pages, 2019.

[29] Y. Kui, X. S. Wang, and R. J. Yu, "A Bayesian dynamic updating approach for urban expressway real-time crash risk evaluation," *Transportation Research Part C: Emerging Technologies*, vol. 96, pp. 192–207, 2018.

[30] M. Abdel-aty, A. Pande, A. Das, and W. J. Knibbe, "Assessing safety on Dutch freeways with data from infrastructure-based intelligent transportation systems," *Transportation Research Record: Journal of the Transportation Research Board*, vol. 2083, no. 1, pp. 153–161, 2008.

[31] Q. Hou, A. P. Tarko, and X. Meng, "Investigating factors of crash frequency with random effects and random parameters models: new insights from Chinese freeway study," *Accident Analysis & Prevention*, vol. 120, pp. 1–12, 2018.

[32] T. Bhowmik, S. Yasmin, and N. Eluru, "A joint econometric approach for modeling crash counts by collision type," *Analytic Methods in Accident Research*, vol. 19, pp. 16–32, 2018.

[33] C. Xu, W. Wang, and P. Liu, "Identifying crash-prone traffic conditions under different weather on freeways," *Journal of Safety Research*, vol. 46, pp. 135–144, 2013.

[34] F. Xing, H. Huang, Z. Zhan et al., "Hourly associations between weather factors and traffic crashes: non-linear and lag effects," *Analytic Methods in Accident Research*, vol. 24, p. 100109, 2019.

[35] S. Jung, X. Qin, and D. A. Noyce, "Rainfall effect on single-vehicle crash severities using polychotomous response models," *Accident Analysis & Prevention*, vol. 42, no. 1, pp. 213–224, 2010.

[36] T. F. Golob, W. W. Recker, and V. M. Alvarez, "Freeway safety as a function of traffic flow," *Accident Analysis & Prevention*, vol. 36, no. 6, pp. 933–946, 2004.

[37] L. Dimitriou, K. Stylianou, and M. A. Abdel-Aty, "Assessing rear-end crash potential in urban locations based on vehicle-by-vehicle interactions, geometric characteristics and operational conditions," *Accident Analysis & Prevention*, vol. 118, pp. 221–235, 2018.

[38] W. Wang, R. Chen, R. Y. Chen, and P. Liu, "Conditional inference tree-based analysis of hazardous traffic conditions for rear-end and sideswipe collisions with implications for control strategies on freeways," *IET Intelligent Transport Systems*, vol. 8, no. 6, pp. 509–518, 2014.

Hindawi
Journal of Advanced Transportation
Volume 2020, Article ID 8467152, 18 pages
https://doi.org/10.1155/2020/8467152

WILEY | Hindawi

Research Article

A Novel Methodology for Estimating the Capacity and Level of Service for the New Mega Elliptical Roundabout Intersection

Ahmed I. Z. Mohamed,[1,2] **Yusheng Ci**,[1,3] **and Yiqiu Tan**[1]

[1]*School of Transportation Science and Engineering, Harbin Institute of Technology, Harbin 150090, China*
[2]*Department of Construction and Utilities Engineering, Faculty of Engineering, Zagazig University, Zagazig 44519, Egypt*
[3]*Department of Civil & Environmental Engineering, University of Washington, Box 352700, Seattle, WA 98195, USA*

Correspondence should be addressed to Yusheng Ci; ciyusheng1999@126.com

Received 10 October 2019; Revised 19 December 2019; Accepted 21 January 2020; Published 12 March 2020

Guest Editor: Young-Ji Byon

Mega elliptical roundabout is a new intersection on rural multilane highways. This intersection was developed in a previous paper using simulation data, and the authors found that it is better than interchange (full cloverleaf) in most scenarios of traffic flow. Basically, there are no guidelines or procedures for designing mega elliptical roundabout in AASHTO Green Book, Federal Highway Administration guides, and Highway Capacity Manual. Thus, the purpose of this study is to analyze the traffic operation performance and propose a methodology for calculating the capacity of mega elliptical roundabout and also the level of service by gap acceptance theory. Moreover, this research studied the influence of different values of truck ratios and also different values of a major highway speed on geometric design and traffic operation performance for mega elliptical roundabout. To validate the thoroughness of the proposed methodology, VISSIM simulations were conducted. This research will assist practitioners in determining the appropriate geometric design, assessing mega elliptical roundabout intersections, and making comparisons with other alternatives.

1. Introduction

The designs of conventional intersections cannot often relieve congestion without incurring increased conflicts and also significant improvement costs. Thus, there is a great need for alternative intersections offering the potential to reduce delay, improve safety, and reduce the influence on the environment with fewer effects and a lower cost than traditional solutions [1–4]. Therefore, the authors proposed a new type of intersections which is called "mega elliptical roundabout" in a previous paper [5]. Totally, they analyzed 1134 scenarios by VISSIM software to analyze the initial feasibility and determine the best scenarios of geometric design for mega elliptical roundabout intersections. They compared mega elliptical roundabout with the interchange (full cloverleaf). They found that mega elliptical roundabout as an intersection is better than the interchange (full cloverleaf) in some scenarios of traffic flow, but mega elliptical roundabout as an interchange is better than the interchange (full cloverleaf) in all scenarios of traffic flow relative to delay time, fuel consumption, and emission.

Based on the previous studies, intersection analysis models generally fall into three categories: simulation models, empirical models, and analytical models. Simulation models are useful in the initial feasibility analysis of new types of intersections which do not have Highway Capacity Manual (HCM) procedures and in comparing them with current intersections [6–14]. Empirical models rely on field data to develop relationships between geometric design features and performance measures such as capacity and delay [15–18]. Analytical models are based on the concept of gap acceptance theory, conflict theory, or probability theory [19–29].

The empirical models are generally better but cannot be used to analyze mega elliptical roundabout at present because mega elliptical roundabout is a new type of

intersections, so no field data are available, while the initial feasibility analysis of mega elliptical roundabout has been introduced in another work by simulation models [5].

There are no guidelines or procedures for the design of mega elliptical roundabout in AASHTO Green Book, Federal Highway Administration (FHWA) guides, and Highway Capacity Manual (HCM). Therefore, this research analyzed the traffic operation performance and used the gap acceptance theory to propose a methodology for calculating the capacity of mega elliptical roundabout and also the level of service, to assist practitioners in determining the appropriate geometric design.

The remainder of this research is organized as follows. Section 2 introduces the literature review. Section 3 shows the basic concept of this study. Section 4 presents the proposed methodology. Section 5 shows the assumptions and built-up models. Section 6 presents the statistical analysis of built-up models. Section 7 demonstrates the case description and methodology validation. Section 8 introduces the sensitivity analysis. Section 9 gives the conclusions of this study and proposes future work.

2. Review of the Previous Studies

Mega elliptical roundabout is a new intersection. Its form is an elongated ellipse combining the best functions of the roundabout and the unconventional median U-turn (UMUT) intersection [5]. Therefore, the first efforts for this work looked at the studies related to estimating the capacity and level of service for roundabout, conventional median U-turn (MUT) intersection, and UMUT intersection to determine the ideal methodology to estimate the capacity and level of service for mega elliptical roundabout intersection.

2.1. Roundabout Intersection. Because vehicles enter the roundabout only when the gap in the circulating traffic is large enough, the capacity of the roundabout depends primarily on the circulating flow and the availability of gaps. Therefore, roundabout capacity is measured in terms of the entry capacity, whether by gap acceptance theory [30–32], empirical models [33–39], simulation models [40–43], conflict theory [44], or others [45–47].

Yap et al. [48] examined the worldwide state-of-the-art in roundabout capacity modeling, covering the three main methodologies on which models are based: fully empirical, gap acceptance, and simulation. They found that due to their limitations, each of these methodologies on its own cannot completely explain the complex behavioural and physical processes involved in roundabout entries; hence, all the models require strong semiempirical or fully empirical bases using data obtained from their countries of origin. Differences in driver behaviour and methodologies thus result in differences in predicted capacities by the various models, and although local calibration allows some transferability, it is often limited by the availability of data or an incomplete understanding of the relationships between model parameters and capacity.

Little research exists from the viewpoint of the weaving section in capacity estimation for the roundabout. Diah et al. [49] introduced a model to predict the weaving section flow at the weaving area of Malaysian conventional roundabout by regression models, while Diah et al. [50] studied the relation between the roundabout performance, geometric design of roundabout, and weaving section flow process using Paramics software. Wang and Yang [51] proposed a method to estimate the capacity of the roundabout by modeling weaving gap acceptance at the weaving sections, but they did not calibrate their method.

In the literature, only one paper by Wu and Brilon [52] treated the whole roundabout intersection as one entity. They believe that the total roundabout capacity can be obtained according to traffic volumes for the movements at the intersection by their method, but they did not calibrate their method by empirical data.

The Highway Capacity Manual [53] only provides a methodology for estimating the capacity of each entry lane and the level of service for the single-lane and multilane roundabout. However, HCM [53] neglected the weaving section when designing the roundabout.

2.2. MUT Intersection. Al-masaeid [54] used empirical and gap acceptance approaches to predict the capacity and the delay of U-turn movement at median openings of four lane-divided arterials. Florida Department of Transportation (FDOT) sponsored a lot of projects to develop a model to estimate delay and travel time for two alternatives: right turn followed by U-turn (RTUT) and direct left turn (DLT) [55–57]. Zhou et al. [58] assessed the operational effects of an RTUT and a DLT. They used field data from eight sites in the Tampa and Clearwater areas of Florida to develop delay and travel-time models. They found that vehicles making a DLT experienced longer delay and travel times than those that made an RTUT.

Zhou et al. [59] introduced the regression model for predicting the average weaving speed in weaving segments at RTUT. Also, they developed a theoretical equation to determine the optimal location of median openings on roadways. Liu et al. [60] analyzed the operational effects of RTUT as an alternative to DLT. They collected the field data from 34 sites in central Florida. They developed a binary logit model to the number of drivers who would like to make an RTUT instead of a DLT under different roadway geometric and traffic conditions.

Zhao et al. [61] proposed a lane-based optimization model for the integrated design of the MUT and formulated a multiobjective mixed-integer nonlinear programming problem to optimize the intersection design types, the layout of the intersection, and the signal timings simultaneously. They conducted a numerical analysis to evaluate the performance of the proposed design under various demand and layout scenarios, but they did not calibrate their method by empirical data. Dash et al. [62] used four different methods to estimate the critical gap of U-turns: modified Raff, maximum likelihood, macroscopic probability equilibrium,

and merging behaviour approach by collecting data at seven median openings in India.

The Highway Capacity Manual [53] provides a methodology for estimating the capacity and level of service for MUT intersection. However, HCM [53] neglected the weaving section when designing the MUT intersection.

2.3. UMUT Intersection. Shahi and Choupani [15] conducted traffic operation analysis of the UMUT design by the field data. They developed a regression model to calculate the travel time of the minor street through traffic, travel time of the left-turn traffic, speed of the nonweaving flows, weaving time, and speed of the U-turning vehicles. The developed models have been compared with the RTUT models which have been developed by FDOT [55–57]. They found that FDOT models always overestimate travel times.

3. Basic Concept

3.1. Mega Elliptical Roundabout Characteristics. As shown in Figure 1, the mega elliptical roundabout has two essential features.

The first feature is the central island that is elongated on the major highway for providing enough length for weaving sections. Moreover, the form of this island is an ellipse that has an ellipse element (b) for providing a suitable basic ellipse roadway radius in order to be appropriate for heavy vehicles that make a U-turn on basic ellipse roadway.

The second feature is the ellipse roadway, which has three parts: the basic ellipse roadway, weaving sections, and nonweaving sections [5].

3.2. The Operation Analysis of Mega Elliptical Roundabout. The mega elliptical roundabout reroutes both of the through and left-turning traffic coming from a minor highway through right turns in order to merge them with the traffic of a major highway on the weaving sections, followed by U-turn on a basic ellipse roadway. Left-turning traffic for a major highway must also make a U-turn on a basic ellipse roadway then a right turn on a minor highway. The conflict between merging the through traffic for a major highway and the traffic from cross-highway can be treated by putting a "Yield" sign on a minor highway and basic ellipse roadway. It gives the priority for a major highway through traffic, as shown in Figure 1.

3.3. The Weaving Pattern on Mega Elliptical Roundabout. To analyze mega elliptical roundabout intersection, it first needs to be broken down into four parts as shown in Figure 2. Second, it needs to convert the intersection turning movements into the weaving volumes. As shown in Figure 2 the volumes are V_1 to V_{12}.

Two weaving patterns are defined in the HCM [53]. According to HCM [53], in two-sided weaving sections, only the movement from ramp to ramp is considered a weaving movement, where the movement of the major highway does not need any lane change, while the minor highway movement needs more than one lane change.

The vehicle movement weaving pattern on mega elliptical roundabout is like a two-sided weaving section configuration where the right hand on-ramp is followed by the left hand off-ramp or vice versa. As shown in Figure 3, basic ellipse roadway-to-minor-highway vehicles must cross all the lanes in order to execute their desired maneuver, while the major highway vehicles do not need any lane change. Note that the movement in part 1 is like that in part 3. Also, as shown in Figure 4, the minor highway to basic ellipse roadway vehicles must cross all the lanes in order to execute their desired maneuver, while the nonweaving vehicles do not need any lane change. Note that the movement in part 2 is like that in part 4.

There are few studies concerning the operation of two-sided weaving sections. Lertworawanich and Elefteriadou [63–65] proposed a methodology for calculating the capacity for all weaving section types based on linear programing techniques and gap acceptance theory. They compared this methodology with the HCM [66] weaving sections model and field capacity. They found that this methodology provides capacity estimates nearer to the observed capacity values in the field than HCM [66, 67].

Also, in two papers by Zhang and Rakha [68, 69] and a doctoral thesis by Yihua Zhang, analytical models for calculating the capacity of all weaving section types were developed using simulated data collected by INTEGRATION software. They validated the analytical models against field observations gathered in Toronto. They found a high consistency between analytical models and field. Also, they found that the proposed analytical models calculate the capacity for weaving sections within 12% of the simulated data, while HCM [66] procedures exhibit errors within 114%.

However, in this research, we have decided to use the gap acceptance model proposed by HCM [53] with some modifications to suit estimation of the weaving section capacity for mega elliptical roundabout for the following reasons:

(1) As described in Section 2, most researchers estimated roundabout capacity in terms of entry capacity. However, the mega elliptical roundabout differs from a roundabout in traffic operations [5].

(2) Researchers who analyzed the roundabout from the viewpoint of the weaving section did not calibrate their method. Also, the weaving pattern on mega elliptical roundabout is like a two-sided weaving section, while the weaving pattern on the roundabout is like a one-side weaving section.

(3) Researchers who analyzed the MUT and UMUT intersections from the viewpoint of the weaving section did not estimate the weaving section capacity.

(4) HCM [53] neglected the weaving section when designing the roundabout and MUT intersection.

(5) Mega elliptical roundabout is new idea for intersections, so no field data are available at present.

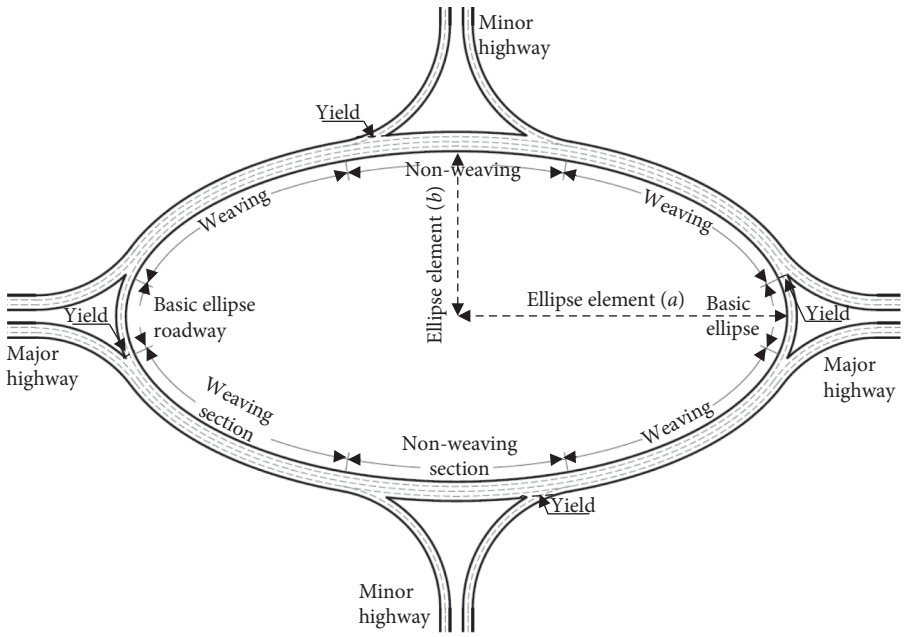

Figure 1: Geometric elements for mega elliptical roundabout.

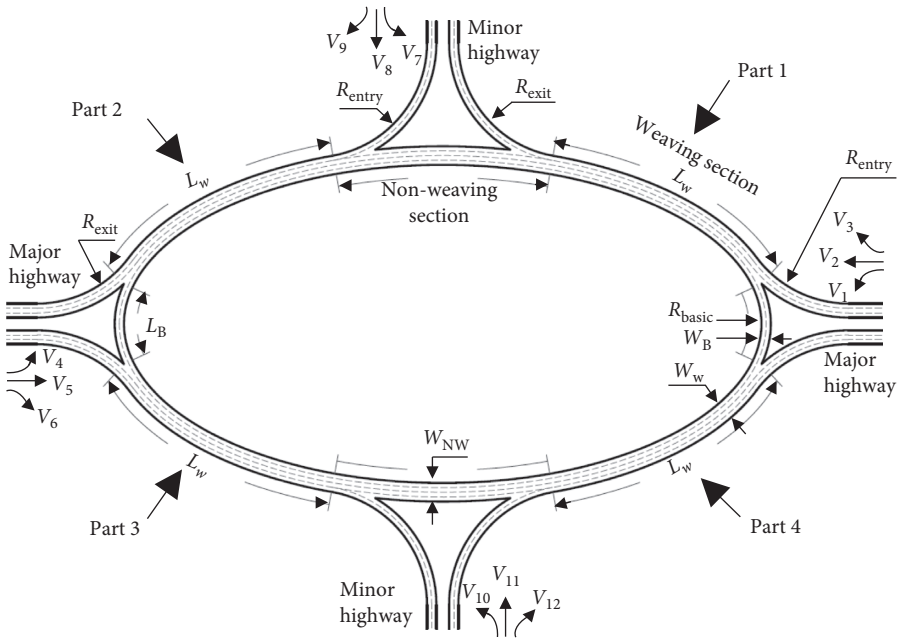

Figure 2: Flow stream definitions.

(6) HCM is an international reference manual supervised by an independent committee of experts in this field and therefore is often the basis for policy decisions when choosing an intersection.

4. Methodology

This section aims to propose a methodology for calculating the capacity of mega elliptical roundabout in addition to the level of service by gap acceptance theory. The general methodology for analyzing mega elliptical roundabout intersection operations is shown in the flowchart in Figure 5. These methodology steps are described in detail as follows:

Step 1: adjust volume.

HCM [53] proposed equation (1) to convert demand volumes to flow rates at equivalent ideal conditions.

$$v_i = \frac{V_i}{(\mathrm{PHF} * f_{\mathrm{HV}})}, \tag{1}$$

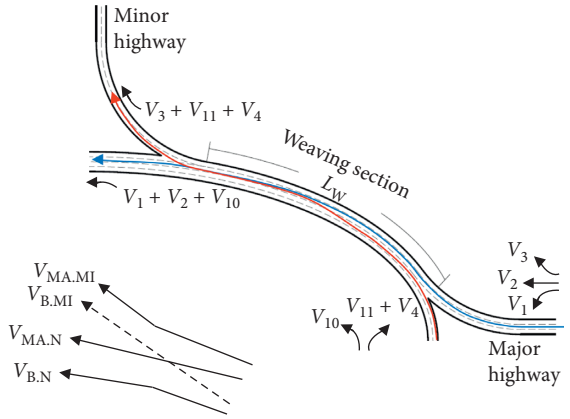

Figure 3: The weaving pattern for weaving section on mega elliptical roundabout (part 1). $V_{MA.MI}$ = traffic volume in outer lane from major highway to minor highway (veh/h)–V_3; $V_{MA.N}$ = traffic volume from major highway to nonweaving section (veh/h)–$V_2 + V_1$; $V_{B.MI}$ = conflicting volume from basic ellipse roadway to minor highway (veh/h)–$V_{11} + V_4$; $V_{B.N}$ = traffic volume in inner lane from basic ellipse roadway to nonweaving section (veh/h)–V_{10}; V_W = total weaving volume in the weaving section (veh/h)–$V_{B.MI}$; V_{NW} = total nonweaving volume in the weaving section (veh/h)–$V_{MA.MI} + V_{MA.N} + V_{B.N}$.

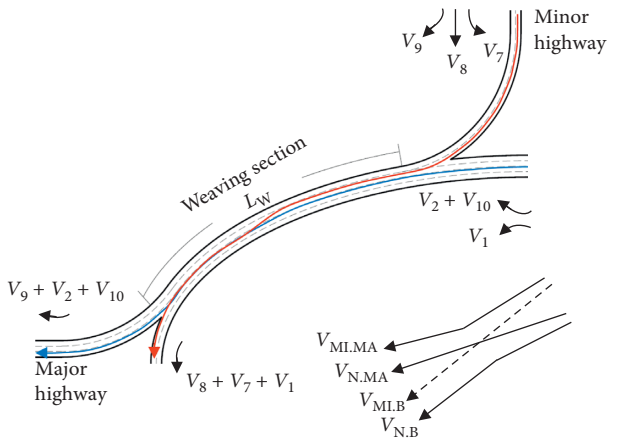

Figure 4: The weaving pattern for weaving section on mega elliptical roundabout (part 2). $V_{MI.MA}$ = traffic volume in outer lane from minor highway to major highway (veh/h)–V_9; $V_{MI.B}$ = conflicting traffic volume from minor highway to basic ellipse roadway (veh/h)–$V_8 + V_7$; $V_{N.MA}$ = traffic volume from nonweaving section to major highway (veh/h)–$V_2 + V_{10}$; $V_{N.B}$ = traffic volume in inner lane from nonweaving section to basic ellipse roadway (veh/h)–V_1; V_W = total weaving volume in the weaving section (veh/h)–$V_{MI.B}$; V_{NW} = total nonweaving volume in the weaving section (veh/h)–$V_{MI.MA} + V_{N.MA} + V_{N.B}$.

where v is the peak 15-minute flow rate in an hour (pc/h), V is the hourly volume (veh/h), PHF is the peak-hour factor, and f_{HV} is the heavy vehicle adjustment factor estimated in

$$f_{HV} = \frac{1}{1 + P_T\left(E_T - 1\right)}, \quad (2)$$

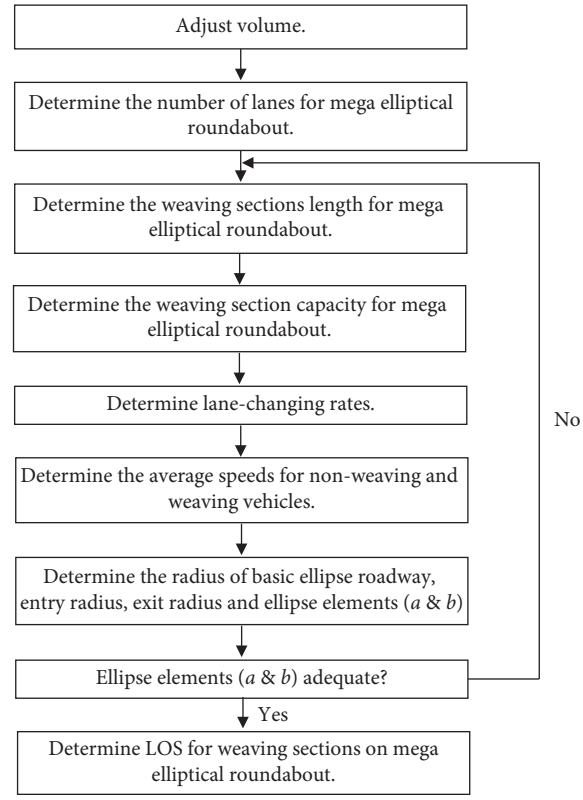

Figure 5: Methodology flowchart.

where P_T is the proportion of buses and trucks in a traffic stream and E_T is passenger car equivalents for buses and trucks. By following HCM [53], the E_T value is assumed as 1.5, which is the proposed value for intersections in the level area.

Step 2: determine the number of lanes for mega elliptical roundabout.

Mohamed et al. [5] found that the best scenarios of mega elliptical roundabout are the following: when the number of lanes of weaving section (W_W) equals the number of lanes of the nonweaving section (W_{NW}) and also equals the number of lanes of major highway plus one lane.

$W_W = W_{NW}$ = number of lanes of major highway +1

Moreover, the number of lanes of basic ellipse roadway (W_B) equals the number of lanes of minor highway.

W_B = number of lanes of minor highway

where W_W is the number of lanes of weaving section, W_{NW} is the number of lanes of the nonweaving section, and W_B is the number of lanes of basic ellipse roadway, as shown in Figure 2.

Step 3: determine the weaving sections length for mega elliptical roundabout.

HCM [53] defined the weaving section length (short length) as the distance between the end points of any barrier markings that prohibit or discourage lane

changing. Consequently, several geometric design scenarios for mega elliptical roundabout intersection were drawn using AutoCAD software to determine the relationship between the weaving section length (L_W) and ellipse elements (a) and (b), as described in Section 5. The following is a regression equation that can estimate the length of weaving section based upon ellipse elements (a) and (b).

If $b = 0.5a$

$$L_W = 0.868\,a - 7.271. \tag{3}$$

If $b = 0.75a$

$$L_W = 0.721\,a + 12.528, \tag{4}$$

where a is ellipse element (ft), b is ellipse element (ft), and L_W is the weaving section length for mega elliptical roundabout intersection (ft), as shown in Figure 2.

Step 4: determine weaving section capacity.

The HCM [53] proposed equation (5) to estimate the capacity. It is important to mention that the N_{WL} term in the equation of HCM [53] has been deleted because it equals zero for two-sided weaving sections.

$$C = \left[C_H - \left[438.2\ (1 + \mathrm{VR})^{1.6}\right] + \left(0.0765 * L_W\right)\right] * W_W * f_{HV}, \tag{5}$$

where C is the capacity for weaving section (veh/h/ln), C_H is the capacity for major highway under ideal conditions and free-flow speed (pc/h/ln), and VR is the weaving ratio. It is the ratio of the weaving flow rate to the total flow rate in weaving section (pc/h) estimated in

$$\mathrm{VR} = \frac{v_W}{\left(v_W + v_{NW}\right)}, \tag{6}$$

where v_W is the total weaving flow rate (pc/h) and v_{NW} is the total nonweaving flow rate in weaving section (pc/h).

Step 5: determine lane-changing rates.

Lane changes fall into three different categories: (1) Lane-changes which must be made by the weaving vehicles to complete a weaving maneuver successfully happen when the weaving vehicles leave weaving section on the lane nearest to their entry point and enter weaving section on the lane nearest to their desired destination. (2) Additional lane changes which may be made by the weaving vehicles happen when weaving vehicles enter weaving section on the lane next to the lane nearest to their desired destination or these vehicles leave on the lane next to the lane nearest to their entry point. These lane changes are based upon driver choices because these are optional. (3) Lane changes which may be made by nonweaving vehicles in weaving section are generally made for avoiding weaving turbulence. These lane changes are based upon driver choices because these are always optional [67].

As shown in Figure 3, the basic ellipse roadway to minor highway vehicles must make one required lane change, assuming they enter the weaving section on the right lane of basic ellipse roadway. Thus, $\mathrm{LC_{BM}} = 1$. As shown in Figure 4, the minor highway to basic ellipse roadway vehicles must also make one required lane change, assuming they enter the weaving section on the left lane of minor highway. Thus, $\mathrm{LC_{MB}} = 1$. The following lane-changing values can be computed from equations (7) and (8)

For part 1 or part 3

$$\mathrm{LC_{MIN}} = \mathrm{LC_{BM}} * v_{B.MI}. \tag{7}$$

For part 2 or part 4

$$\mathrm{LC_{MIN}} = \mathrm{LC_{MB}} * v_{MI.B}, \tag{8}$$

where $\mathrm{LC_{MIN}}$ is the minimum number of the lane changes (lc/h), $\mathrm{LC_{BM}}$ is the minimum number of the required lane changes for basic ellipse roadway to minor highway (lc/h), $v_{B.MI}$ is the flow rate of basic ellipse roadway to minor highway (pc/hr), $\mathrm{LC_{MB}}$ is the minimum number of the required lane changes for minor highway to basic ellipse roadway, and $v_{MI.B}$ is the flow rate of minor highway to basic ellipse roadway (pc/hr).

The total number of the lane changes made within the weaving section can be predicted by expanding the value of $\mathrm{LC_{MIN}}$ to include the number of optional lane changes which are made by both the weaving vehicles and the nonweaving vehicles. The total number of the lane changes which are made by weaving vehicles is calculated as

$$\mathrm{LC_W} = \mathrm{LC_{MIN}} + 0.39\left[\left(L_W - 300\right)^{0.5} W_W^2\ (1 + \mathrm{ID})^{0.8}\right], \tag{9}$$

where $\mathrm{LC_W}$ is the total number of lane changes made by weaving vehicles (pc/h) and ID is interchange density (int/mi).

The total number of the lane changes which are made by the nonweaving vehicles is calculated as follows.

Firstly, estimate the index

$$\mathrm{INDEX} = \frac{\left(L_W * \mathrm{ID} * v_{NW}\right)}{10000}. \tag{10}$$

Then, select the equation from Table 1 based upon the index value.

Table 1: The equations for estimating the number of nonweaving lane changes [53].

Index	Equation for LC_{NW}
≤1300	$LC_{NW1} = (0.206 v_{NW}) + (0.542 L_W) - (192.6 W_W)$
>1300 and <1950	$LC_{NW} = W_W + [(LC_{NW2} - LC_{NW1}) * [\text{INDEX} - 1300/650]]$
≥1950	$LC_{NW2} = 2135 + 0.233 (v_{NW} - 2000)$

Here, LC_{NW} is the total number of the lane changes which are made by the nonweaving vehicles (pc/h). The value of LC_{NW} must be equal to or greater than zero.

The total number of lane changes occurring in weaving section (LC_{All}) is estimated as

$$LC_{ALL} = LC_W + LC_{NW}. \tag{11}$$

Step 6: determine the average speeds for nonweaving and weaving vehicles.

The average speeds for nonweaving and weaving vehicles are estimated by the following regression-based equations proposed by HCM [53]:

$$S_W = 15 + \left[\frac{(FFS - 15)}{(1 + WI)}\right],$$

$$S_{NW} = FFS - (0.0072 * LC_{MIN}) - \left(\frac{(0.0048 * v)}{W_W}\right),$$

$$WI = 0.226\left(\frac{LC_{ALL}}{L_W}\right)^{0.789},$$

$$S = \left(\frac{v_W + v_{NW}}{(v_W/s_W) + (v_{NW}/s_{NW})}\right), \tag{12}$$

where S_W is the average speed of the weaving vehicles (mi/h), FFS is the free-flow speed of the major highway (mi/h), WI is the weaving intensity factor of the weaving speed, S_{NW} is the average speed of the nonweaving vehicles (mi/h), v is the total nonweaving and weaving flow rate (pc/h), and S is the average speed of all the vehicles in weaving sections (mi/h).

Step 7: determine the radius of basic ellipse roadway, entry radius, exit radius, and ellipse elements (a and b).

AASHTO [70] proposed equation (13) to estimate the radius of basic ellipse roadway, entry radius, and exit radius.

$$R = \frac{S\text{^}2}{15 (f + 0.01e)}, \tag{13}$$

where R is radius of basic ellipse roadway which is equal to the entry radius as well the exit radius (ft), as shown in Figure 2. f is side friction factor, and e is rate of basic ellipse roadway superelevation.

As described in Section 5, the ellipse elements (a) and (b) can be estimated based upon the radius of basic ellipse roadway (R) by the following regression equations.

If $b = 0.5a$

$$a = 3.954 R - 27.427. \tag{14}$$

If $b = 0.75a$

$$a = 1.778 R - 8.846. \tag{15}$$

Step 8: determine LOS for weaving sections on mega elliptical roundabout.

The HCM [53] proposed equation (16) to estimate the density from the average speed.

$$D = \left(\frac{(v/W_W)}{S}\right), \tag{16}$$

where D is average density within the weaving section (pc/mi/ln) and v is the total nonweaving and weaving flow rate (pc/h). From Table 2, we can determine the LOS.

5. Built-Up Models

By using AutoCAD software, several geometric design scenarios for mega elliptical roundabout intersection were drawn. The linear regression analysis was also used to determine the following relationships:

The relationship between the weaving section length (L_W) and the ellipse elements (a) and (b)—equations (3) and (4)

The relationship between the radius of basic ellipse roadway (R_{basic}) and the ellipse elements (a) and (b)—equations (14) and (15)

The relationship between the length of basic ellipse roadway (L_B) and the ellipse elements (a) and (b)—equations (17) and (18)

The mega elliptical roundabout provides appropriate storage lanes for vehicles making a U-turns by providing a sufficient length of basic ellipse roadway. The length of basic ellipse roadway (L_B) can be estimated based upon the ellipse elements (a) and (b) by the following regression equations:

If $b = 0.5a$,

$$L_B = 0.235 a - 29.365. \tag{17}$$

If $b = 0.75a$,

Table 2: Level of service for weaving sections on mega elliptical roundabout intersection [53].

Level of service	Density range (pc/mi/ln)
A	0–12
B	>12–24
C	>24–32
D	>32–36
E	>36–40
F	>40

$$L_B = 0.524\,a - 44.016, \tag{18}$$

where L_B is the length of basic ellipse roadway (ft), as shown in Figure 2.

The regression models were developed using AutoCAD data with the following assumptions and characteristics:

The entry radius of major highway (R_{entry}) equals the entry radius of minor highway, as shown in Figure 2

The entry radius (R_{entry}) equals the radius of basic ellipse roadway (R_{basic}) and also equals the radius of exit (R_{exit}) whether for the minor or major highway, as shown in Figure 2

Lane width equals 12.00 ft

Median width of the major and minor highway equals 32.80 ft

The minimum value for an ellipse element (a) in all scenarios equals 328 ft

The maximum value for an ellipse element (a) in scenarios when ($b = 0.5a$) equals 4920 ft

The maximum value for an ellipse element (a) in scenarios when ($b = 0.75a$) equals 2130 ft

The intersection is four-legged

The intersection is a six-lane-divided highway with a four-lane-divided highway

6. Statistical Analysis of Built-Up Models

The regression models were developed using the data that were compiled by the AutoCAD software, and a linear regression method was accomplished using SPSS software. Regression results of the relationship between the weaving section length (L_W) and ellipse element (a) and also of the relationship between the length of basic ellipse roadway (L_B) and ellipse element (a) when ($b = 0.5a$) and also when ($b = 0.75a$) are shown in Table 3. Moreover, regression results of the relationship between the ellipse element (a) and the radius of basic ellipse roadway (R) when ($b = 0.5a$) and also when ($b = 0.75a$) are shown in Table 4.

R-square value of all linear models is very high (99.9%), which means that 99.9% of the variation independent variables can be explained by these models. Also, for all models, the value of the standard error of the estimate (positive square root of variance of the errors), which typically measures the difference between dependent variables value with the "true" value, is relatively small.

Similar to the standard error of the estimate, the standard error presents the standard error of the coefficient estimates. Essentially, they measure how these coefficients vary from sample to sample. The models are more reliable as the standard error decreases. The t-statistic is the coefficient divided by its standard error. This is based on the following assumption: if the standard errors of the estimate (population errors) are normally distributed, then it can be shown that the sample estimates for coefficients of the model follow *a* t-distribution [71]. The t-statistic represents the size of the standard error relative to the estimated coefficient; therefore, the model quality improves as the absolute value of t-statistic increases. For those reasons, we can conclude that these models are adequate for predicting the dependent variables.

7. Model Validation and Analysis

7.1. Case Description. To validate the thoroughness of the proposed methodology, VISSIM simulations were conducted. Mega elliptical roundabout intersection which was analyzed was the intersection of the six-lane-divided highway with the four-lane-divided highway, where the intersection was four-legged. The study used hypothetical values of traffic volumes. Traffic volumes of the major highway approaches were varied from 1000 to 2500 veh/h/approach with 500 veh/h/approach increments (i.e., 4 volume levels). Also, traffic volumes of the minor highway were varied from 500 to 1000 veh/h/approach with 500 veh/h/approach increments (i.e., 2 volume levels). The left-turn volume percentage, the right-turn volume percentage, and the proportion of trucks and buses were considered equal to 20%. The major highway speed was considered 62 mi/h, the peak-hour factor (PHF) equals 0.95, the basic ellipse roadway superelevation equals 2%, and the ellipse element (b) equals 0.75 ellipse element (a). In total, seven scenarios of traffic volume combination for the mega elliptical roundabout design were analyzed, including different levels of the major highway volume and minor highway volume.

7.2. Methodology Validation. To test the accuracy of the proposed methodology, the simulation models for each scenario listed above were built with the VISSIM software package. The parameters were obtained based on the observation of the real two-sided weaving sections in Harbin to ensure its rationality, and the parameters of the VISSIM simulation model must be modified accordingly. Seven simulations of different random seeds were conducted, and the final results were the average values over seven simulations. The results of the estimation models and simulations for density and average speed are given in Table 5 when the traffic volume for the minor highway equals 500 veh/h. Moreover, these results are given in Table 6 when the traffic volume for the minor highway equals 1000 veh/h.

For all traffic volume cases on the major highway and minor highway, there was no significant difference in methodology results and simulation for estimating average

Table 3: Regression results of the relationship between L_W, L_B, a, and b.

Equation number	Dependent variables		Independent variables		Std. error of the estimate	R^2
			Constant	a (ft)		
If $b = 0.5a$						
		Coefficients	−7.271	0.868		
3	L_W	Standard error	2.658	0.001	5.027	1.00
		t-statistics	−2.735	849.058		
		Coefficients	−29.365	0.235		
20	L_B	Standard error	5.219	0.002	9.869	0.999
		t-statistics	−5.627	117.287		
If $b = 0.75a$						
		Coefficients	12.528	0.721		
4	L_W	Standard error	2.357	0.002	3.321	1.00
		t-statistics	5.315	382.886		
		Coefficients	−44.016	0.524		
21	L_B	Standard error	4.736	0.004	6.673	1.00
		t-statistics	−9.294	138.455		

Table 4: Regression results of the relationship between a, R, and b.

Equation number	Dependent variables		Independent variables		Std. error of the Estimate	R^2
			Constant	R (ft)		
If $b = 0.5a$						
		Coefficients	−27.427	3.954		
17	a	Standard error	3.715	0.006	6.968	1.00
		t-statistics	−7.383	705.367		
If $b = 0.75a$						
		Coefficients	−8.846	1.778		
18	a	Standard error	1.128	0.002	1.580	1.00
		t-statistics	−7.84	1115.688		

Table 5: Results of methodology, simulations, and relative error when the traffic volume for the minor highway equals 500 veh/h.

Traffic volume for the major highway		Part 1 or part 3			Part 2 or part 4		
		Average speed (mi/h)	Density (pc/mi/ln)	LOS	Average speed (mi/h)	Density (pc/mi/ln)	LOS
	VISSIM	52.85	7.6	A	52.7	6.7	A
1000	Methodology	55.2	8.4	A	56.2	7.2	A
	Relative error	4.4%	10.5%		6.6%	7.4%	
	VISSIM	51.9	10.7	A	51.88	8.7	A
1500	Methodology	53.9	11.8	A	55.8	9.3	A
	Relative error	3.8%	10.28%		7.5%	6.9%	
	VISSIM	49.5	14.2	B	50.2	11.03	A
2000	Methodology	52.4	15.5	B	55.4	11.5	A
	Relative error	5.8%	9.1%		10.3%	4.2%	
	VISSIM	43.7	19.6	B	45.9	14.2	B
2500	Methodology	51	19.3	B	54.9	13.7	B
	Relative error	16.7%	−1.5%		19.6%	−3.5%	

speed as well as density. The relative error range was [1.5%, 19.6%] for the average speed, while the relative error range was [−3.5%, 13.4%] for the density. The main cause of the existing relative error was the random VISSIM simulation results which led to some deviations from the average speed and density in the estimated models.

8. Sensitivity Analysis

8.1. Impact of Trucks Proportion on the Value of Ellipse Element (a), Density, and Average Speed. To study the influence of different ratios of trucks on geometric design and traffic operation performance for mega elliptical roundabout, the

Table 6: Results of methodology, simulations, and relative error when the traffic volume for the minor highway equals 1000 veh/h.

Traffic volume for the major highway		Part 1 or part 3			Part 2 or part 4		
		Average speed (mi/h)	Density (pc/mi/ln)	LOS	Average speed (mi/h)	Density (pc/mi/ln)	LOS
1000	VISSIM	52	9.7	A	49.6	10.2	A
	Methodology	52.8	11	A	52.8	11	A
	Relative error	1.5%	13.4%		6.4%	7.8%	
1500	VISSIM	49.8	13.2	B	44.9	13.57	B
	Methodology	51.4	14.6	B	52.3	13.3	B
	Relative error	3.2%	10.6%		16.4%	−1.9%	
2000	VISSIM	46.6	16.75	B	44.3	16.2	B
	Methodology	50	18.5	B	51.8	15.7	B
	Relative error	7.3%	10.4%		16.9%	−3%	

proposed methodology was used to predict the value of an ellipse element (a), density, and average speed at different ratios of trucks. The used scenarios are the same scenarios described in Section 7.1, but with different values of truck ratios which are 2, 5, 10, 15, and 20%.

The relationships between major highway traffic volume and the value of an ellipse element (a), density, and average speed for vehicles on the weaving sections for mega elliptical roundabout at different ratios of trucks when minor highway traffic volume equals 500 veh/h and 1000 veh/h are presented in Figures 6 and 7, respectively. The figures show that the average speed for vehicles decreases with the increase in truck ratios, but the differences are not significant. The decrease in average speed may be because of traffic interaction that occurs due to increasing the truck proportion, while the fact that the differences are not significant may be because mega elliptical roundabout is not conventional intersection. It gives priority to the vehicles entering from the major highway. Therefore, the movement on the weaving sections of mega elliptical roundabout intersection is like the movement on the two-sided weaving sections of any highway.

Moreover, the density increases with the increase in truck ratios, but the differences are not significant. This is most likely because the average speed decreases with the increase in truck ratios, thereby increasing the density, as described in equation (16).

In addition, the value of an ellipse element (a) decreases with the increase in truck ratios, but the differences are not significant. This is most likely because the average speed decreases with the increase in truck ratios that can lead to decreasing the value of radius of basic ellipse roadway, as described in equation (13), thereby decreasing the ellipse element (a), as described in equations (14) and (15).

Based on the above analysis, the influence of the different ratios of trucks on geometric design and traffic operation performance for mega elliptical roundabout is not significant.

8.2. Impact of Major Highway Speed on the Value of Ellipse Element (a), Density, and Average Speed. To study the influence of different values of a major highway speed on geometric design and traffic operation performance for mega elliptical roundabout, the proposed methodology was used to predict the value of an ellipse element (a), density, and average speed at different values of a major highway speed. The used scenarios are the same scenarios described in Section 7.1, but with different values of a major highway speed which were 30, 40, 45, 50, and 62 mi/h.

The relationships between major highway traffic volume and the value of an ellipse element (a), density, and average speed for vehicles on the weaving sections for mega elliptical roundabout at different values of a major highway speed when minor highway traffic volume is equal to 500 veh/h and 1000 veh/h are presented in Figures 8 and 9, respectively. The figures show that the average speed for vehicles increases with the increase in major highway speed, but the density decreases. This is probably because mega elliptical roundabout gives priority to the vehicles entering from the major highway. Therefore, the movement on the weaving sections of mega elliptical roundabout is like the movement on the two-sided weaving sections of any highway.

Also, the value of an ellipse element (a) increases with the increase in major highway speed because the average speed for vehicles increases, which can lead to increasing the value of radius of basic ellipse roadway, thereby increasing the ellipse element (a), as described in equations (13)–(15). Moreover, the value of an ellipse element (a) has doubled when the major highway speed increased from 30 mi/h to 40 mi/h, 40 mi/h to 50 mi/h, and 50 mi/hr to 62 mi/h. This is probably because mega elliptical roundabout island has an ellipse element (b) for providing a suitable radius for basic ellipse roadway in order to be appropriate for heavy vehicles that make a U-turn on basic ellipse roadway. This radius is calculated based on the average speed for vehicles on weaving sections from equation (13).

Furthermore, the average speed on part 2 or part 4 is greater than the average speed on part 1 or part 3 for mega elliptical roundabout in all scenarios. This is probably because total weaving volume on part 2 or part 4 is lower than total weaving volume on part 1 or part 3, as shown in Figures 3 and 4, thereby increasing the average speed. For the same reason, the value of an ellipse element (a) is always calculated according to the average speed on part 2 or part 4 from equations (14) and (15)

By analyzing Figure 8, it is possible to confirm the following.

In the case of the value of major highway speed equal to 30 mi/hr, minor highway volume = 500 veh/h, ellipse element (a) = 410 ft, and major highway volume ≤ 1500 veh/h, density is lower than 32 pc/mi/ln (level of service A-B-C).

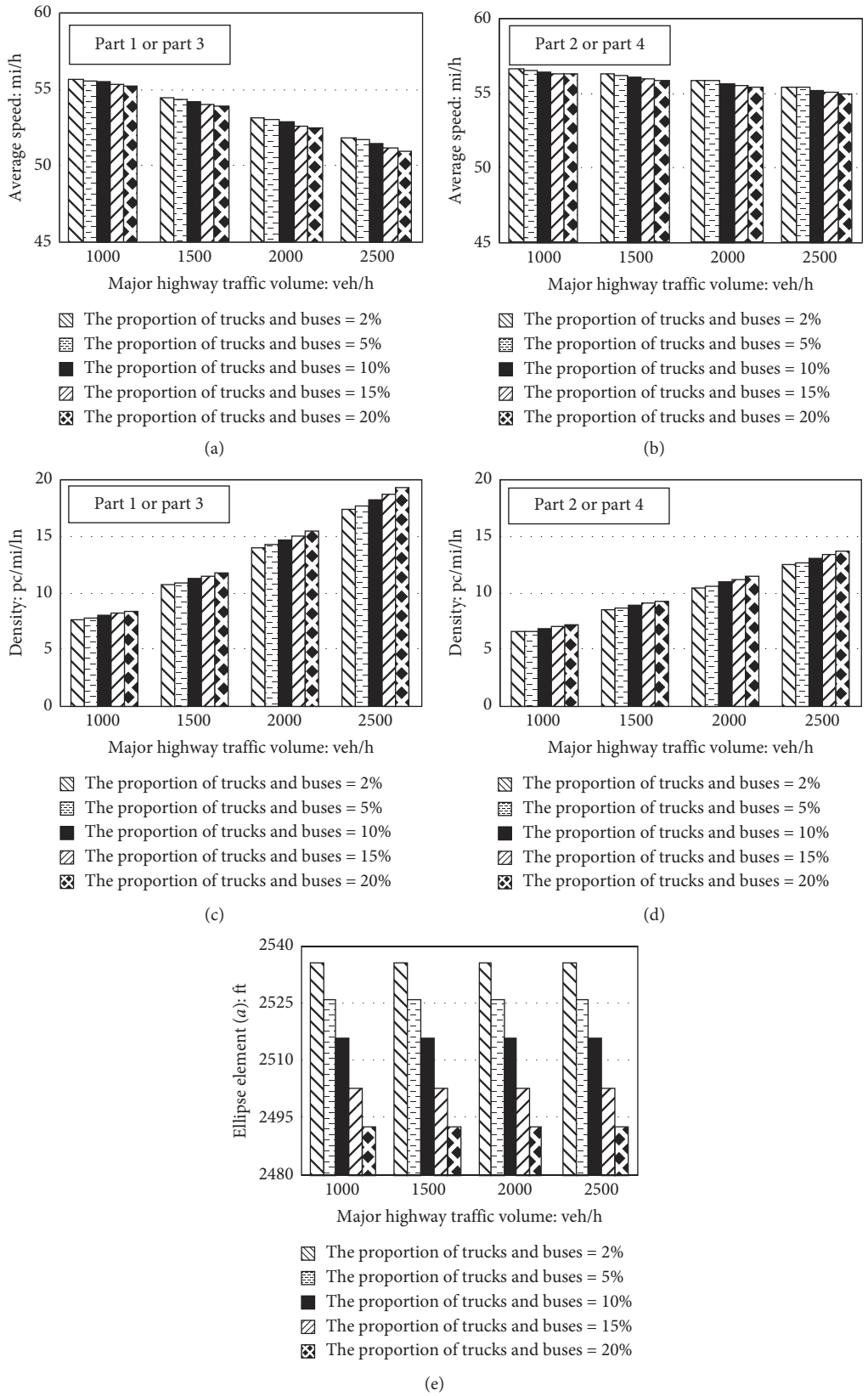

Figure 6: Relationships between major highway traffic volume and the value of an ellipse element (a), density, and average speed at different ratios of trucks when the minor highway traffic volume = 500 veh/h. (a) Average speed for part 1 or part 3, (b) average speed for part 2 or part 4, (c) density for part 1 or part 3, (d) density for part 2 or part 4, (e) ellipse element (a) for mega roundabout.

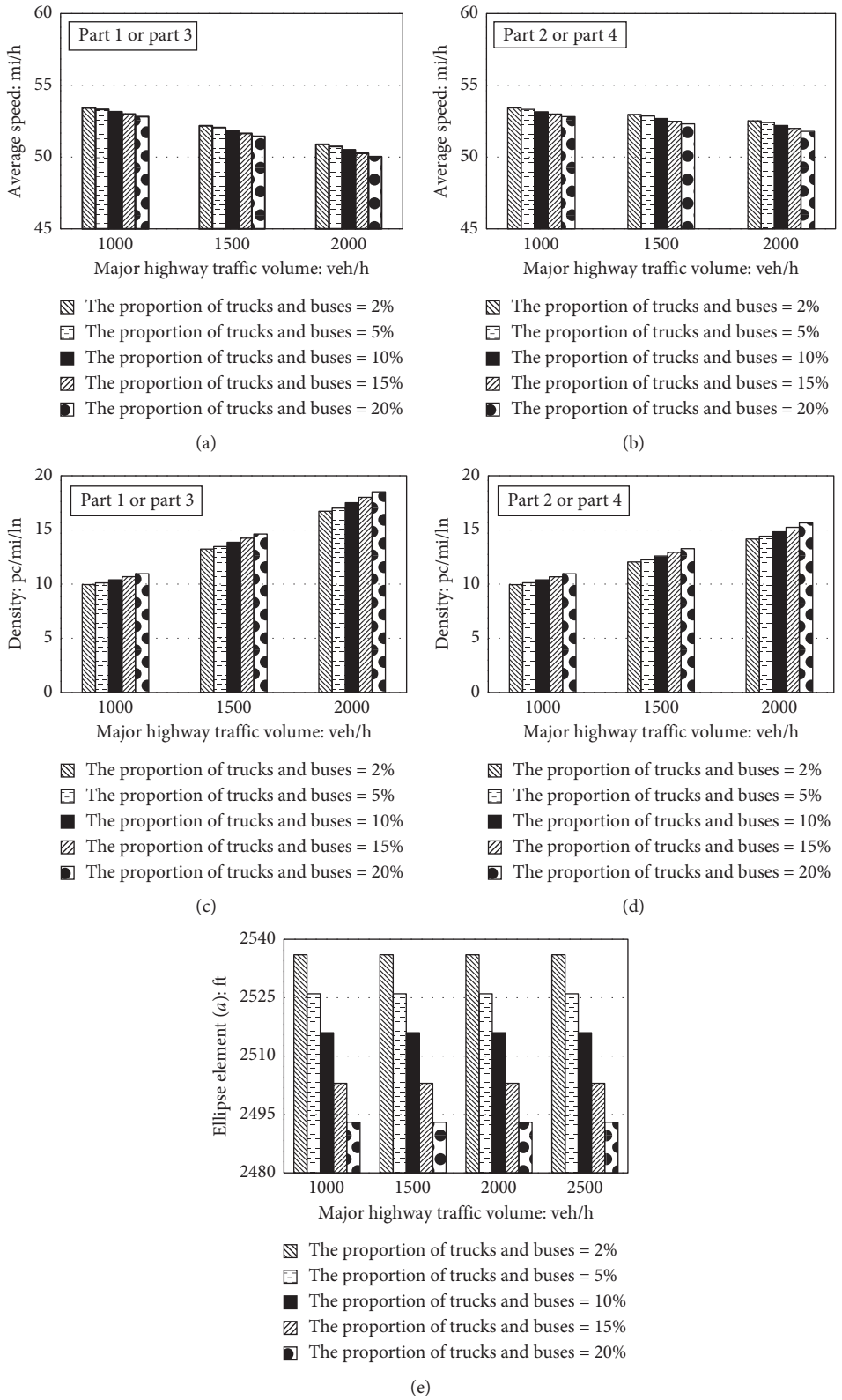

Figure 7: Relationships between major highway traffic volume and the value of an ellipse element (a), density, and average speed at different ratios of trucks when the minor highway traffic volume = 1000 veh/h. (a) Average speed for part 1 or part 3, (b) average speed for part 2 or part 4, (c) density for part 1 or part 3, (d) density for part 2 or part 4, (e) ellipse element (a) for mega roundabout.

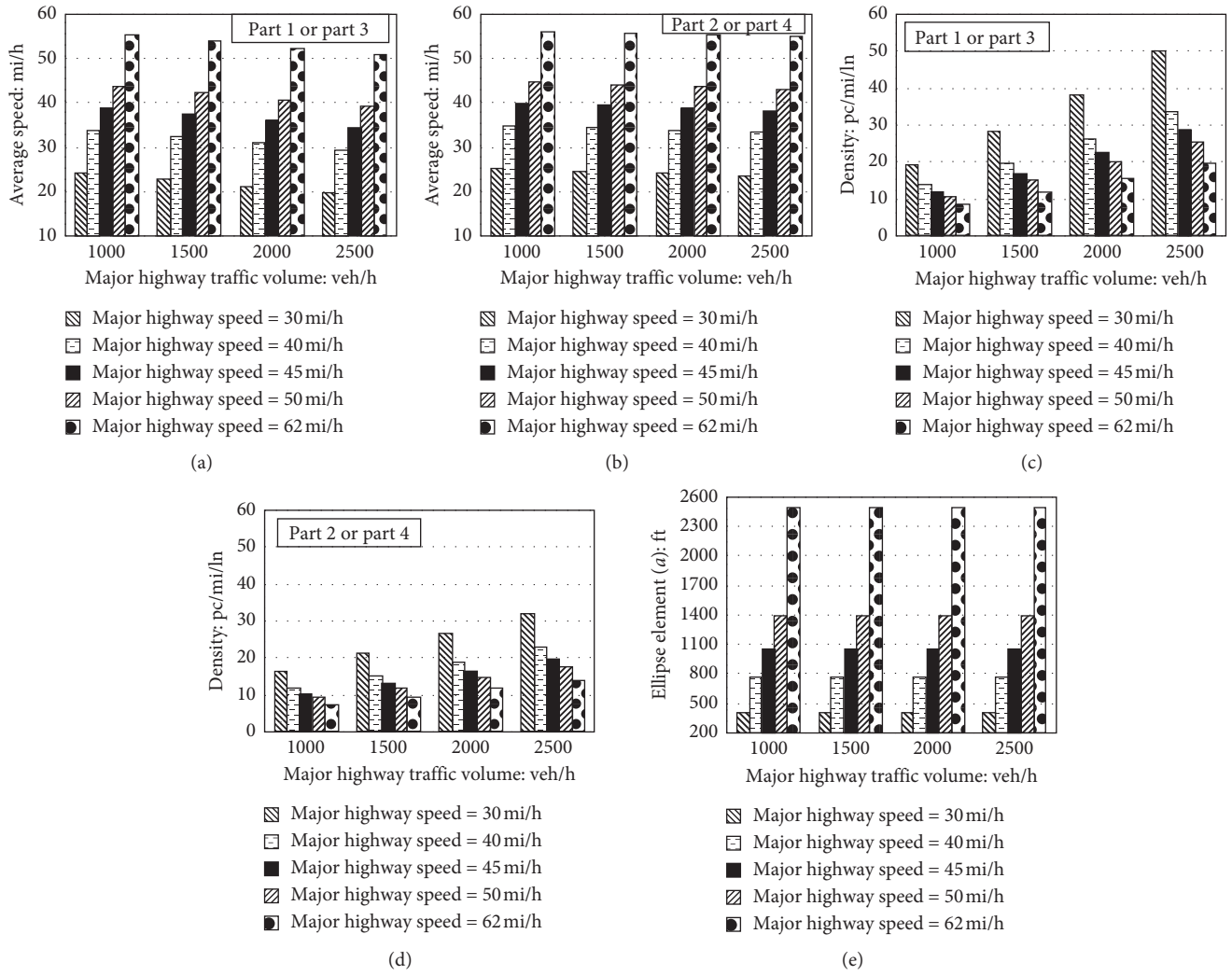

Figure 8: Relationships between major highway traffic volume and the value of an ellipse element (a), density, and average speed at different values of a major highway speed when minor highway traffic volume = 500 veh/h. (a) Average speed for part 1 or part 3, (b) average speed for part 2 or part 4, (c) density for part 1 or part 3, (d) density for part 2 or part 4, (e) ellipse element (a) for mega roundabout.

Also, in the case of the value of major highway speed equal to 40 mi/hr, minor highway volume = 500 veh/h, ellipse element (a) = 771 ft, and major highway volume ≤ 2000 veh/h, density is lower than 32 pc/mi/ln (level of service A-B-C).

By analyzing Figure 9, it is possible to confirm the following.

In the case of the value of major highway speed equal to 30 mi/hr, minor highway volume = 1000 veh/h, ellipse element (a) = 410 ft, and major highway volume ≤ 1000 veh/h, density is lower than 32 pc/mi/ln (level of service A-B-C). Also, in the case of the value of major highway speed equal to 40 mi/hr, minor highway volume = 1000 veh/h, ellipse element (a) = 771 ft, and major highway volume ≤ 1500 veh/h, density is lower than 32 pc/mi/ln (level of service A-B-C).

Based on the above analysis, in highways that have a speed equal to 30 mi/hr, the suitable design of mega elliptical roundabout is ellipse element (a) = 410 ft and ellipse element (b) = 308 ft. This is suitable in the following cases: the values of a major highway volume ≤ 1500 veh/h and minor highway volume ≤ 500 veh/h; or the values of a major highway volume ≤ 1000 veh/h and minor highway volume ≤ 1000 veh/h. Also, in highways that have a speed equal to 40 mi/hr, the suitable design of mega elliptical roundabout is ellipse element (a) = 771 ft and ellipse element (b) = 578 ft. This is suitable the following cases: the values of a major highway volume ≤ 2000 veh/h and minor highway volume = 500 veh/h; or the values of a major highway volume ≤ 1500 veh/h and minor highway volume = 1000 veh/h. Moreover, in highways that have a speed equal to 45, 50 and 62 mi/hr, the suitable design of mega elliptical roundabout is ellipse element (b) = 0.75 ellipse element (a), and ellipse element (a) = 1053, 1398, and 2493 ft, respectively. This is suitable in the following cases: the values of a major highway volume ≤ 2500 veh/h and minor highway volume ≤ 500 veh/h; or the values of a major highway volume ≤ 2000 veh/h and minor highway volume ≤ 1000 veh/h.

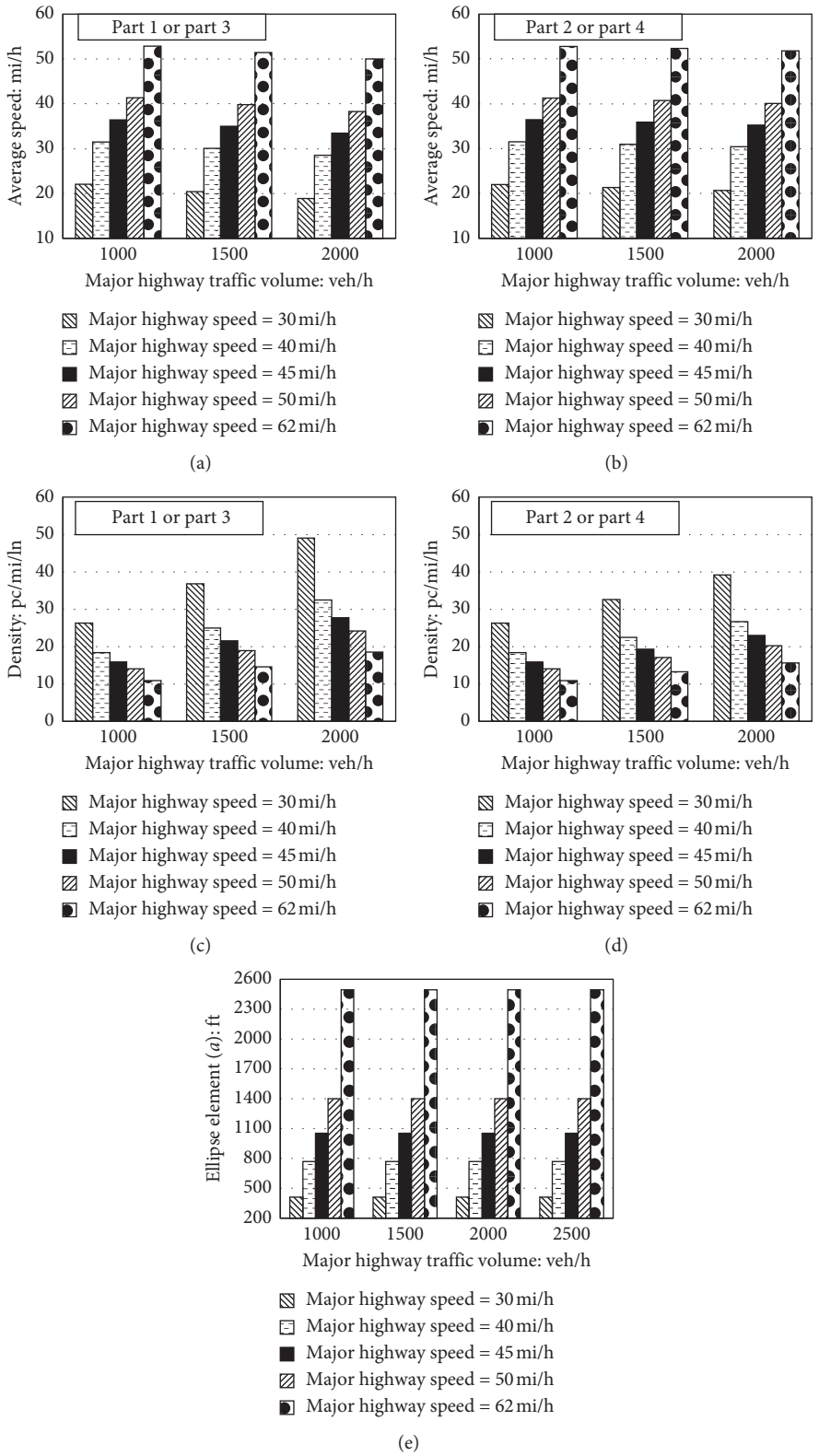

Figure 9: Relationships between major highway traffic volume and the value of an ellipse element (a), density, and average speed at different values of a major highway speed when minor highway traffic volume = 1000 veh/h. (a) Average speed for part 1 or part 3, (b) average speed for part 2 or part 4, (c) density for part 1 or part 3, (d) density for part 2 or part 4, (e) ellipse element (a) for mega roundabout.

9. Conclusions

In this paper, the performance of traffic operations was analyzed for mega elliptical roundabout intersection. Moreover, this paper proposed a methodology for estimating the capacity and level of service for mega elliptical roundabout intersections by gap acceptance theory. Furthermore, explicit VISSIM simulations were performed after calibrating them with field data from real two-sided weaving sections in Harbin to verify the accuracy of the proposed methodology. In addition, regression analysis was implemented by SPSS software to obtain the relationships of ellipse elements with the radius of basic ellipse roadway, the length of basic ellipse roadway, and the length of weaving section. Regression models were developed using the data that were compiled by the AutoCAD software for several geometric design scenarios for mega elliptical roundabout intersection. Also, the influence of different values of truck ratios and also different values of a major highway speed on geometric design and traffic operation performance for mega elliptical roundabout was studied. Based on the regression analysis, methodology validation, and sensitivity analysis, the following can be concluded:

(1) In mega elliptical roundabout intersection, the weaving sections are the key to the efficiency of the intersection as a whole

(2) The models built up in this study are adequate to predict the dependent variables

(3) Estimation methodology of the average speed and the density on the weaving sections of mega elliptical roundabout was confirmed to have a reasonable accuracy

(4) The influence of the different ratios of trucks on geometric design and traffic operation performance for mega elliptical roundabout is not significant, while the influence of the different ratios of a major highway speed is significant

In conclusion, it is clear that this study analyzed the performance of traffic operations and suggested a method for designing mega elliptical roundabout intersections to assist practitioners in determining the appropriate geometric design. Based on the previous studies, the traffic operation and safety are the main measures for assessing the intersections [72–76]. Therefore, further research will be needed to assess the safety performance of mega elliptical roundabout. We plan to use a surrogate safety assessment model developed by FHWA to compare safety aspects of the proposed intersection with those of other alternative intersections.

Data Availability

The basic data used to support the findings of this study are available from the corresponding author upon request.

Conflicts of Interest

The authors declare that there are no conflicts of interest.

Authors' Contributions

Ahmed I. Z. Mohamed and Yusheng Ci collected the data and analyzed and interpreted the results. Ahmed I. Z. Mohamed and Yiqiu Tan prepared the manuscript draft. All authors contributed to study conception and design, reviewed the results, and approved the final version of the manuscript.

Acknowledgments

The first author thanks the Ministry of Education of China for the Ph.D. scholarship they provided under CSC grant (no. 2017GBJ001910). Also, this project was financially supported by grants from the National Key R&D Program of China (no. 2017YFC0803907) and the MOE Project of Humanities and Social Sciences, China (no. 16YJCZH114).

References

[1] FHWA (Federal Highway Administration), *Diverging Diamond Interchange Informational Guide*, Federal Highway Administration Office of Safety, Washington, DC, USA, 2014.

[2] FHWA, *Displaced Left Turn Intersection Informational Guide*, Federal Highway Administration Office of Safety, Washington, DC, USA, 2014.

[3] FHWA, *Median U-Turn Intersection Informational Guide*, Federal Highway Administration Office of Safety, Washington, DC, USA, 2014.

[4] FHWA, *Restricted Crossing U-Turn Intersectional Information Guide*, Federal Highway Administration Office of Safety, Washington, DC, USA, 2014.

[5] A. I. Z. Mohamed, Y. Ci, and Y. Tan, "Mega elliptical roundabouts versus grade-separation interchange," *Proceedings of the Institution of Civil Engineers-Transport*, pp. 1–21, 2019.

[6] V. Tabernero and T. Sayed, "Upstream signalized crossover intersection: an unconventional intersection scheme," *Journal of Transportation Engineering*, vol. 132, no. 11, pp. 907–911, 2006.

[7] E. K. Shin, J. H. Lee, J. H. Kim, J. S. Kim, and Y. W. Jeong, "Two-level signalized intersection," *Transportation Research Record: Journal of the Transportation Research Board*, vol. 2060, no. 1, pp. 53–64, 2008.

[8] J. Reid, F. Ngai, and D. VanMeter, "Introduction of the dual-system urban interchange design," *Transportation Research Record: Journal of the Transportation Research Board*, vol. 2065, no. 1, pp. 27–35, 2008.

[9] M. E. Esawey and T. Sayed, "Unconventional USC intersection corridors: evaluation of potential implementation in Doha, Qatar," *Journal of Advanced Transportation*, vol. 45, no. 1, pp. 38–53, 2011.

[10] M. A. Sultana, A. Tarko, and M. Romero, "Evaluating the operational footprint of alternative diamond interchanges," *Journal of Transportation Engineering, Part A: Systems*, vol. 144, no. 9, pp. 1–11, 2018.

[11] L. F. Sutherland, D. J. Cook, and K. K. Dixon, "Operational effects of the displaced partial cloverleaf interchange," *Transportation Research Record: Journal of the Transportation Research Board*, vol. 2672, no. 17, pp. 108–119, 2018.

[12] A. M. Molana and J. E. Hummer, "Travel time evaluation of synchronized and milwaukee B as new interchange designs,"

Journal of Transportation Engineering, Part A: Systems, vol. 144, no. 2, pp. 1–8, 2018.

[13] N. Mitrovic, I. Dakic, and A. Stevanovic, "Using analytical models to calibrate a dual-roundabout intersection in microsimulation," *Put I Saobraćaj*, vol. 64, no. 2, pp. 13–19, 2018.

[14] A. M. Molan, J. E. Hummer, and K. Ksaibati, "Introducing the super DDI as a promising alternative service interchange," *Transportation Research Record: Journal of the Transportation Research Board*, vol. 2673, no. 3, pp. 586–597, 2019.

[15] J. Shahi and A.-A. Choupani, "Modelling the operational effects of unconventional U-turns at a highway intersection," *Transportmetrica*, vol. 5, no. 3, pp. 173–191, 2009.

[16] P. Liu, J. Wan, W. Wang, and Z. Li, "Evaluating the impacts of unconventional outside left-turn lane design on traffic operations at signalized intersections," *Transportation Research Record: Journal of the Transportation Research Board*, vol. 2257, no. 1, pp. 62–70, 2011.

[17] C. Yeom, B. J. Schroeder, C. Cunningham, C. Vaughan, N. M. Rouphail, and J. E. Hummer, "Lane utilization at two-lane arterial approaches to double crossover diamond interchanges," *Transportation Research Record: Journal of the Transportation Research Board*, vol. 2461, no. 1, pp. 103–112, 2014.

[18] C. Yeom, J. E. Hummer, B. Schroeder, C. M. Cunningham, C. L. Vaughan, and N. M. Rouphail, "Empirical before-after comparison of the operational performance of diverging and conventional diamond interchanges," *Journal of Transportation of the Institute of Transportation Engineers (ITE)*, vol. 7, no. 1, pp. 35–55, 2015.

[19] N. Wu, "Determination of capacity at all-way stop-controlled intersections," *Transportation Research Record: Journal of the Transportation Research Board*, vol. 1710, no. 1, pp. 205–214, 2000.

[20] M. Kyte and G. List, "A capacity model for all-way stop-controlled intersections based on stream interactions," *Transportation Research Part A: Policy and Practice*, vol. 33, no. 3-4, pp. 313–335, 1999.

[21] W. Brilon and N. Wu, "Capacity at unsignalized intersections derived by conflict technique," *Transportation Research Record: Journal of the Transportation Research Board*, vol. 1776, no. 1, pp. 82–90, 2001.

[22] W. Brilon and T. Miltner, "Capacity at intersections without traffic signals," *Transportation Research Record: Journal of the Transportation Research Board*, vol. 1920, no. 1, pp. 32–40, 2005.

[23] H. Li, W. Deng, Z. Tian, and P. Hu, "Capacities of unsignalized intersections under mixed vehicular and nonmotorized traffic conditions," *Transportation Research Record: Journal of the Transportation Research Board*, vol. 2130, no. 1, pp. 129–137, 2009.

[24] A.-Z. Li, X.-H. Song, X.-S. Song, and B.-H. Wu, "Capacity of urban road unsignalized T-intersection," in *Proceedings of the 2010 International Conference On Computational Intelligence and Software Engineering*, Wuhan, China, December 2010.

[25] H. Li, Z. Tian, and W. Deng, "Capacity of TWSC intersection with multilane approaches," *Procedia—Social and Behavioral Sciences*, vol. 16, pp. 664–675, 2011.

[26] Y. Pei, F. Chuanyun, and P. Ting, "Theory model for traffic capacity of unsignalized roundabout in urban road," in *Proceedings of the Third International Conference on Transportation Engineering (ICTE)*, Chengdu, China, July 2011.

[27] S. I. Guler and M. Menendez, "Methodology for estimating capacity and vehicle delays at unsignalized multimodal intersections," *International Journal of Transportation Science and Technology*, vol. 5, no. 4, pp. 257–267, 2016.

[28] W. Ma, Y. Liu, J. Zhao, and N. Wu, "Increasing the capacity of signalized intersections with left-turn waiting areas," *Transportation Research Part A: Policy and Practice*, vol. 105, pp. 181–196, 2017.

[29] L. Wu, Y. Ci, Y. Wang, and P. Chen, "Fuel consumption at the oversaturated signalized intersection considering queue effects: a case study in Harbin, China," *Energy*, vol. 192, Article ID 116654, , 2020.

[30] O. Hagring, "Derivation of capacity equation for roundabout entry with mixed circulating and exiting flows," *Transportation Research Record: Journal of the Transportation Research Board*, vol. 1776, no. 1, pp. 91–99, 2001.

[31] Z. Qu, Y. Duan, X. Song, H. Hu, H. Liu, and K. Guan, "Capacity prediction model based on limited priority gap-acceptance theory at multilane roundabouts," *Mathematical Problems in Engineering*, vol. 2014, Article ID 490280, 11 pages, 2014.

[32] A. N. Arshi, W. K. M. Alhajyaseen, H. Nakamura, and X. Zhang, "A comparative study on the operational performance of four-leg intersections by control type," *Transportation Research Part A: Policy and Practice*, vol. 118, pp. 52–67, 2018.

[33] L. Mussone, M. Matteucci, M. Bassani, and D. Rizzi, "An innovative method for the analysis of vehicle movements in roundabouts based on image processing," *Journal of Advanced Transportation*, vol. 47, 2011.

[34] J. Dahi and C. Lee, "Empirical estimation of capacity for roundabouts using adjusted gap-acceptance parameters for trucks," *Transportation Research Record: Journal of the Transportation Research Board*, vol. 2312, no. 1, pp. 34–45, 2012.

[35] T. Wei and J. L. Grenard, "Calibration and validation of highway capacity manual 2010 capacity model for single-lane roundabouts," *Transportation Research Record: Journal of the Transportation Research Board*, vol. 2286, no. 1, pp. 105–110, 2012.

[36] C. Lee and M. N. Khan, "Prediction of capacity for roundabouts based on percentages of trucks in entry and circulating flows," *Transportation Research Record: Journal of the Transportation Research Board*, vol. 2389, no. 1, pp. 30–41, 2013.

[37] A. Ahmad and R. Rastogi, "Regression model for entry capacity of a roundabout under mixed traffic condition—an Indian case study," *Transportation Letters*, vol. 9, no. 5, pp. 243–257, 2016.

[38] A. K. Patnaik, A. R. Ranjan, and P. K. Bhuyan, "Investigating entry capacity models of roundabouts under heterogeneous traffic conditions," *Transportation Research Record: Journal of the Transportation Research Board*, vol. 2672, no. 15, pp. 35–43, 2018.

[39] R. Chen and J. Hourdos, "Evaluation of the roundabout capacity model in HCM6 edition and HCM 2010 on a multilane roundabout," *Transportation Research Record: Journal of the Transportation Research Board*, vol. 2672, no. 15, pp. 23–34, 2018.

[40] E. Chevallier and L. Leclercq, "Microscopic dual-regime model for single-lane roundabouts," *Journal of Transportation Engineering*, vol. 135, no. 6, pp. 386–394, 2009.

[41] M. Martin-Gasulla, A. Garcia, A. T. Moreno, and C. Llorca, "Capacity and operational improvements of metering roundabouts in Spain," *Transportation Research Procedia*, vol. 15, pp. 295–307, 2016.

[42] W. Suh, J. I. Kim, H. Kim, J. Ko, and Y.-J. Lee, "Mathematical analysis for roundabout capacity," *Mathematical Problems in Engineering*, vol. 2018, Article ID 4310894, 8 pages, 2018.

[43] O. Giuffrè, A. Granà, M. L. Tumminello, and A. Sferlazza, "Capacity-based calculation of passenger car equivalents using traffic simulation at double-lane roundabouts," *Simulation Modelling Practice and Theory*, vol. 81, pp. 11–30, 2018.

[44] Z. Qu, Y. Duan, H. Hu, and X. Song, "Capacity and delay estimation for roundabouts using conflict theory," *The Scientific World Journal*, vol. 2014, Article ID 710938, 12 pages, 2014.

[45] J. Bie, H. K. Lo, and S. C. Wong, "Capacity evaluation of multi-lane traffic roundabout," *Journal of Advanced Transportation*, vol. 44, no. 4, pp. 245–255, 2010.

[46] A.-S. A. Al-Sobky and I. H. Hashim, "A generalized mathematical model to determine the turning movement counts at roundabouts," *Alexandria Engineering Journal*, vol. 53, no. 3, pp. 669–675, 2014.

[47] A. K. Patnaik, Y. Krishna, S. Rao, and P. K. Bhuyan, "Development of roundabout entry capacity model using INAGA method for heterogeneous traffic flow conditions," *Arabian Journal for Science and Engineering*, vol. 42, no. 9, pp. 4181–4199, 2017.

[48] Y. H. Yap, H. M. Gibson, and B. J. Waterson, "An international review of roundabout capacity modelling," *Transport Reviews*, vol. 33, no. 5, pp. 593–616, 2013.

[49] J. M. Diah, M. Y. A. Rahman, M. A. Adnan, and I. Atan, "Weaving section flow model at the weaving area of Malaysian conventional roundabout," *Journal of Transportation Engineering*, vol. 136, no. 8, pp. 782–792, 2010.

[50] J. M. Diah, M. Y. A. Rahman, M. A. Adnan, and K. H. Ling, "Modeling the relationship between geometric design and weaving section flow process of conventional roundabouts," *Journal of Transportation Engineering*, vol. 137, no. 12, pp. 980–986, 2011.

[51] W. Wang and X. Yang, "Research on capacity of roundabouts in beijing," *Procedia—Social and Behavioral Sciences*, vol. 43, pp. 157–168, 2012.

[52] N. Wu and W. Brilon, "Total capacity of roundabouts analyzed by a conflict technique," *Transportation Research Record: Journal of the Transportation Research Board*, vol. 2672, no. 15, pp. 9–22, 2018.

[53] HCM (Highway Capacity Manual), *Highway Capacity Manual 6th Edition/A Guide for Multimodal Mobility Analysis*, Transportation Research Board, Washington, DC, USA, 2016.

[54] H. R. Al-masaeid, "Capacity of U-turn at median openings," *Journal of Transportation of the Institute of Transportation Engineers (ITE)*, vol. 69, no. 6, pp. 28–30, 1999.

[55] J. Lu, S. Dissanayake, H. Zhou, and X. K. Yang, *Operational Evaluation of Right Turns Followed by U-Turns as an Alternative to Direct Left Turns*, Vol. III, Florida Department of Transportation, Tallahassee, FL, USA, 2001.

[56] J. Lu, P. Liu, J. Fan, and J. Pernia, *Operational Evaluation of Right Turns Followed by U-Turns at Signalized Intersections (6 or More Lanes) as an Alternative to Direct Left Turns*, Florida Department of Transportation, Tallahassee, FL, USA, 2004.

[57] J. J. Lu and P. Liu, *Operational Evaluation of Right Turns Followed by U-Turns (4-Lane Arterials) as an Alternative to Direct Left Turns*, Florida Department of Transportation, Tallahassee, FL, USA, 2005.

[58] H. Zhou, J. Lu, X. Yang, S. Dissanayake, and K. M. Williams, "Operational effects of U-turns as alternatives to direct left turns from driveways," *Transportation Research Record: Journal of the Transportation Research Board*, vol. 1796, no. 1, pp. 72–79, 2002.

[59] H. Zhou, P. Hsu, J. J. Lu, and J. E. Wright, "Optimal location of U-turn median openings on roadways," *Transportation Research Record: Journal of the Transportation Research Board*, vol. 1847, no. 1, pp. 36–41, 2003.

[60] P. Liu, J. J. Lu, H. Zhou, and G. Sokolow, "Operational effects of U-turns as alternatives to direct left-turns," *Journal of Transportation Engineering*, vol. 133, no. 5, pp. 327–334, 2007.

[61] J. Zhao, W. Ma, K. L. Head, and X. Yang, "Optimal intersection operation with median U-turn: lane-based approach," *Transportation Research Record: Journal of the Transportation Research Board*, vol. 2439, no. 1, pp. 71–82, 2014.

[62] S. Dash, S. S. Mohapatra, and P. P. Dey, "Estimation of critical gap of U-turns at uncontrolled median openings," *Transportation Letters*, vol. 11, no. 5, pp. 229–240, 2017.

[63] P. Lertworawanich and L. Elefteriadou, "Capacity estimations for type B weaving areas based on gap acceptance," *Transportation Research Record: Journal of the Transportation Research Board*, vol. 1776, no. 1, pp. 24–34, 2001.

[64] P. Lertworawanich and L. Elefteriadou, "A methodology for estimating capacity at ramp weaves based on gap acceptance and linear optimization," *Transportation Research Part B: Methodological*, vol. 37, no. 5, pp. 459–483, 2003.

[65] P. Lertworawanich and L. Elefteriadou, "Generalized capacity estimation model for weaving areas," *Journal of Transportation Engineering*, vol. 133, no. 3, pp. 166–179, 2007.

[66] HCM (Highway Capacity Manual), *Highway Capacity Manual*, Transportation Research Board, Washington, DC, USA, 2000.

[67] R. P. Roess and E. S. Prassas, "The highway capacity manual: a conceptual and research history volume 1: uninterrupted flow," in *Springer Tracts on Transportation and Traffic (STTT)*, vol. 5Berlin, Germany, Springer, 2014.

[68] H. Rakha and Y. Zhang, "Analytical procedure for estimating capacity of type B weaving sections," in *Proceedings of the Presented at 84th Annual Meeting of the Transportation Research Board*, Washington, DC, USA, January 2005.

[69] H. Rakha and Y. Zhang, "Systematic analysis of capacity of weaving sections," in *Proceedings of the Presented at 84th Annual Meeting of the Transportation Research Board*, Washington, DC, USA, 2005.

[70] AASHTO (American Association of State Highway and Transportation Officials), "Green book," in *A Policy On Geometric Design Of Highways and Streets*, American Association of State Highway and Transportation Officials, Washington, DC, USA, 2011.

[71] P. T. Vo, "Capacity estimation of two-sided type C weaves on freeways," Doctoral dissertation, University of Texas at Arlington, Arlington, TX, USA, 2007.

[72] A. M. Molan and J. E. Hummer, "Safety analysis of the new synchronized and milwaukee B interchanges in comparison to existing designs," *Accident Analysis & Prevention*, vol. 109, pp. 29–35, 2017.

[73] F. Chen and S. Chen, "Injury severities of truck drivers in single- and multi-vehicle accidents on rural highways," *Accident Analysis & Prevention*, vol. 43, no. 5, pp. 1677–1688, 2011.

[74] F. Chen, S. Chen, and X. Ma, "Analysis of hourly crash likelihood using unbalanced panel data mixed logit model and real-time driving environmental big data," *Journal of Safety Research*, vol. 65, pp. 153–159, 2018.

[75] F. Chen, M. Song, and X. Ma, "Investigation on the injury severity of drivers in rear-end collisions between cars using a

random parameters bivariate ordered probit model," *International Journal of Environmental Research and Public Health*, vol. 16, no. 14, p. 2632, 2019.

[76] A. M. Molana, J. E. Hummerb, and K. Ksaibatia, "Modeling safety performance of the new super DDI design in terms of vehicular traffic and pedestrian," *Accident Analysis and Prevention*, vol. 127, pp. 198–209, 2019.

Hindawi
Journal of Advanced Transportation
Volume 2020, Article ID 6326953, 8 pages
https://doi.org/10.1155/2020/6326953

Research Article

Optimal Parameters of Service in a Public Transportation Market with Pricing

Hongwei Gao,[1] **Vladimir V. Mazalov**,[2] **and Juan Xue**[1]

[1]*School of Mathematics and Statistics, Qingdao University and Institute of Applied Mathematics of Shandong, Qingdao 266071, China*
[2]*Institute of Applied Mathematical Research, Karelian Research Center, Russian Academy of Sciences, Pushkinskaya 11, Petrozavodsk 185910, Russia*

Correspondence should be addressed to Vladimir V. Mazalov; vmazalov@krc.karelia.ru

Received 5 December 2019; Accepted 12 February 2020; Published 10 March 2020

Guest Editor: Young-Ji Byon

The problem of choosing the optimal parameters of service by carriers in public transport passenger flows is considered. This problem is modeled as a two-stage game. At the first stage, the players (carriers) select the parameters of their service (the number and schedule of vehicles, etc.). At the second stage, the players announce the prices of service and the consumers choose an appropriate service. The Wardrop equilibrium is applied to the competition model with rational consumers preferring the carriers with minimum cost, where the cost of service includes the price and also the expected trip time. The equilibrium in the pricing game is found and the optimal parameters of service as a solution to a noncooperative game are determined. Some results of computer simulations are presented.

1. Introduction

Traffic control is the subject of many studies. Since the 1950s, models with different optimality principles and corresponding numerical methods have been used in this area of research. In 1952, Wardrop hypothesized that any transport system reaches equilibrium after a certain period of time and also formulated two principles of an equilibrium distribution of traffic flows [1]. In accordance with the Wardrop principles, the trip time on all existing routes is the same for all road users and less than the trip time of any road user deviating from his route; moreover, the average trip time is minimized. At present, the concept of Wardrop equilibrium is the main tool in the theory of transport flows [2, 3].

In this paper, we investigate the problem of equilibrium traffic flows for passengers of urban public transport, which includes buses, trolleybuses, trams, subway, taxis, and bicycles.

In the Wardrop approach, the cost of a transport service for users (passengers) is the trip time when using a corresponding carrier. This principle can be generalized by considering the costs composed of the trip time and also the total costs of road users on all routes. Similar to the Wardrop model, users are assumed to be rational agents who compare the costs from using a particular service and choose a service with the lowest costs. The cost function may include the price of a service, the average trip time, risks, and other relevant factors.

As an illustration to this problem, the choice of routes around the city of Qingdao can be considered, see Figure 1. At the end of lectures, students of Qingdao University (point A) move to the Qingdao railway station (point B). They can choose one of the three bus routes shown in the diagram. All buses have different schedules and different ticket prices. Being guided by these parameters, students are distributing themselves among the routes in accordance with the Wardrop principle or its generalization.

In [4], this generalization was made for the cost function that includes the price of service plus the trip time spent. Equations for calculating the equilibrium in this model were obtained using the Karush–Kuhn–Tucker theorem.

The behavior of users was taken into account in a number of other research works as well. For example, in [5], part of the users was considered to be oblivious; while the

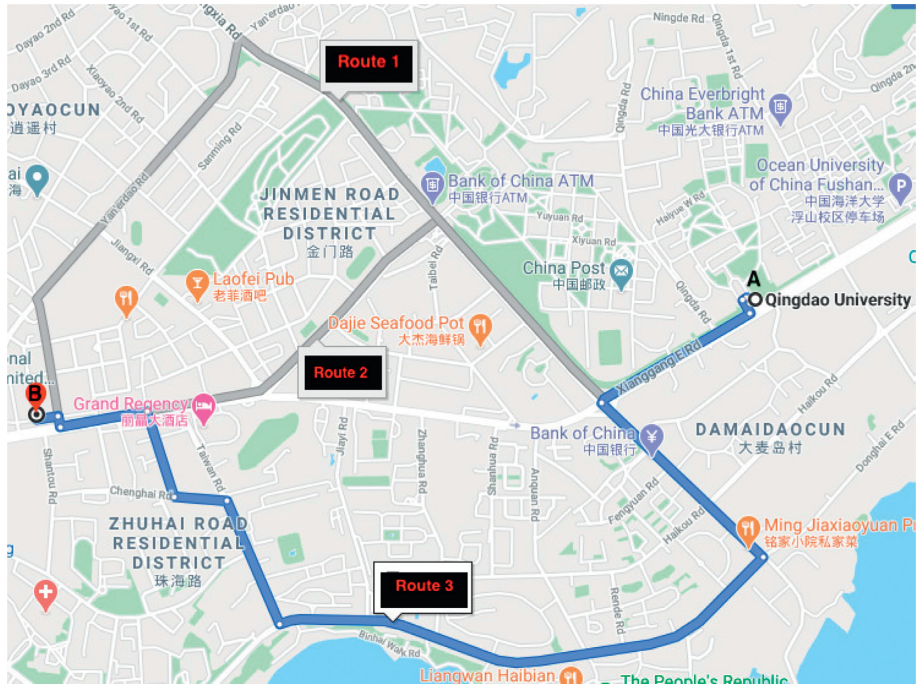

Figure 1: Routes in city of Qingdao.

rational users follow a strategy that minimizes their individual cost, an oblivious user prefers cheapest routes.

It is also important to consider the case in which users can choose a free mode of transportation, such as bicycles or motorcycles. Now this way of transportation is given a lot of attention [6]. In addition, many local authorities subsidize public transport, and then tickets for some municipal transport become much cheaper than for commercial transport. This can greatly affect the equilibrium in the distribution of passenger flows.

Note that the type of latency functions for public transport can be selected in different ways. Some publications followed this approach within the framework of queueing theory, see [7–11].

For a transport flow of intensity λ, the cited authors defined the latency as the average service time $1/(\mu - \lambda)$, i.e., as the expected sojourn time of a user in a queueing system $M/M/n$. In paper [11], the Wardrop principle was applied to networks of general topology and the BPR (Bureau of Public Road) latency functions [12].

The efficiency of a city traffic control system can be evaluated through the *price of anarchy*, initially introduced by Koutsopias and Papadimitriou [13]. This is the ratio of the social costs of the traffic system in the competitive and cooperative cases. The price of anarchy was evaluated for different classes of latency functions. Roughgarden showed that the price of anarchy is exactly 4/3 in the case of linear latency functions [11]. For the polynomial latency functions of maximum degree d, Roughgarden [11] established that the price of anarchy is $(d+1)^{1+1/d}/((d+1)^{1+1/d} - d)$. The price of anarchy was also studied for latency functions that involve a delay function of $M/M/1$ queues [8, 11, 14]. These results were obtained for the Wardrop model, where the consumers minimize the expected trip time. For a generalized case in which the costs include the trip time and price of service, in paper [15] it was demonstrated that the price of anarchy can be infinite. The influence of oblivious users on the price of anarchy was analyzed in [5].

In addition to the problem of finding equilibrium flows in a transport system, for each carrier, it is important to determine the optimal parameters of passenger service, such as schedule, the number, type and size of vehicles, and the time interval and speed of vehicles.

In the following, we formulate this problem as a two-stage game-theoretic model. At the first stage, the players choose the parameters of their service. At the second stage, the players announce the prices of service and the consumers select an appropriate service. We consider rational consumers for whom the cost of service includes the price and trip time. The Wardrop equilibrium is applied to determine the optimal flow in the network. Since the payoffs of the players are known, we return to the first stage and find the optimal parameters of service as the equilibrium in the new game.

This game can be considered as a variant of the multileader multifollower Stackelberg game [16, 17]. In such games, multiple Stackelberg leaders compete in a noncooperative game following which followers play a noncooperative game amongst themselves, taking the decisions of leaders as fixed. Under this approach, each player in our transportation game can be represented by two agents, a leader, and a follower. The leading agent is responsible for the service parameters, which may include the number of transport units and schedule, and the follower is responsible for the service prices.

The paper is organized in the following way. In Section 2, we give a formalization of the two-stage transportation game

with pricing. In Section 3, we construct equilibrium in the two-player game on two parallel routes with the linear latency function. In Section 4, we introduce an externality into this model and calculate equilibrium in the two-stage game. In Section 5, we find equilibrium for a transportation system with a possible use of service free of charge. We analyze this model for the latency function of the form $M/M/1$. In Section 6, we outline further research.

2. Two-Stage Game

Consider a two-stage noncooperative nonzero-sum game of n players, which is associated with a queueing system that operates on a transportation network. Denote a transportation n player game by $\Gamma = \langle N, G, \{Z_i\}_{\{i\in N\}}, \{H_i\}_{\{i\in N\}}\rangle$, where $N = \{1, \ldots, n\}$ means the set of players (carriers) serving passengers on a graph $G = \langle V, E\rangle$ with a node set $V(|V| = m)$ and an edge set E. For each player i, there exists a set of routes Z_i from a starting node $v_s \in V$ to a destination node $v_t \in V$ served by player i. Therefore, $Z_i = \{R_{st}\colon v_s, v_t \in V\}$, $i = 1, \ldots, n$. Each route represents a path, i.e., a sequence of nodes connected by edges $R_{st} = (v_s, v_{s+1}, \ldots, v_t)$ so that the end of one edge is the beginning of another edge $(v_s, v_{s+1}), \ldots, (v_{t-1}, v_t) \in E$.

We assume that the passenger flows over this graph are Poisson processes of some intensity. We introduce the matrix of flow intensities $\{\lambda_{st}\}$ from node v_s to node v_t for different $s, t = 1, \ldots, m$.

The game is organized as follows. At the first stage, the players determine the parameters of service on each route, such as schedule, the number and size of vehicles, and the time interval and speed of vehicles. Denote these control parameters by q^i for each player $i = 1, \ldots, n$.

Thus, at the first stage, each player i determines the control parameters $q^i_{st}, R_{st} \in Z_i$, and a strategy profile $\{q^i, i \in N\}$ is formed accordingly.

At the second stage, each player i establishes prices p_i^R of its service on each route $R \in Z_i$. As a result, a strategy profile $p^Z = \{p_i^R, R \in Z_i, i = 1, \ldots, n\}$ is formed. We assume that the passengers minimize their expected costs, which include the price of service and also the expected sojourn time (trip time). The expected trip time is a nondecreasing function of traffic intensity that takes the form $f_{st}(\lambda)$ on each route R_{st}. The latency function $f_{st}(\lambda_e)$ can be described by $1/(\mu_{st} - \lambda_{st})$ (in accordance with queueing theory) [9–11] or can have the linear $t_{st}(1 + \alpha_{st}\lambda_{st}/c_{st})$ or polynomial $t_{st}(1 + \alpha_{st}(\lambda_{st}/c_{st})^{\beta})$ forms (the well-known BPR latency function) [11]. Here, t_{st} is the trip time on an unoccupied route; c_{st} specifies the capacity of a route; the constants α_{st} and β_{st} capture route-specific features that may affect the impact of the flow-to-capacity ratio on the trip time.

Denote by $u(p, t)$ the costs of passengers who used a service with a ticket price p and a trip time t. In papers [4, 15], the costs were expressed as the ticket price plus the expected trip time, and the customers were assumed to choose the cheapest service. In this case, the incoming Poisson flow of intensity λ_{st} is decomposed into n subflows of intensities λ^i_{st}, where $\sum_{i=1}^n \lambda^i_{st} = \lambda_{st}$. Note that $\lambda^i_{st} = 0$ if the set Z_i of player i has no path R_{st}.

The costs of a passenger preferring service i on some route $R_{st} \in Z_i$ include the price of the service and also the expected trip time:

$$u\left(p^i_{st}, \lambda^i_{st}\right). \tag{1}$$

Following the Wardrop principle, we assume that the equilibrium costs of all passengers on competing directions coincide for all services. This feature allows evaluating the intensities λ^i_{st} for all services $i = 1, \ldots, n$ and routes R_{st}. That is,

$$u\left(p^i_{st}, \lambda^i_{st}\right) = u\left(p^j_{st}, \lambda^j_{st}\right), \tag{2}$$

for all i, j such that $R_{st} \in Z_i$ and $R_{st} \in Z_j$. If the price of some service on a route turns out to be too high, the passenger flow is distributed among other services, and the former service does not compete. In other words, equilibrium prices should be found among balanced prices.

The payoff of player $i \in N$ can be defined by its income per unit time from serving all flows on all routes of this player minus the operating costs, i.e.,

$$H_i\left(p_i^Z\right) = \sum_{(st):R_{st}\in Z_i} \lambda^i_{st} p^i_{st} - C_i\left(q^i\right), \quad i \in N. \tag{3}$$

Thus, we have a two-stage game of n players. First, we fix the parameters of service $\{q^i, i \in N\}$. Next, we find a Nash equilibrium in the pricing game with the payoff function (1), where the cost $C_i(q^i)$ is excluded. Let $\{p_i^*, i \in N\}$ be the equilibrium in the pricing game. The prices and flows in the equilibrium will depend on the service parameters $q = \{q^i, i \in N\}$.

Then, we return to the first stage and find a Nash equilibrium in the game with payoffs (1) among the strategies $q = \{q^i, i \in N\}$.

3. Game of Two Players on Two Parallel Routes with Linear Latency Function

Our analysis begins with the transportation game of two carriers rendering their services between two points v_1 and v_2. We assume that carriers 1 and 2 (players 1 and 2) are operating on two parallel routes.

Let the service time of player i have the linear BPR latency function:

$$t_i\left(1 + \alpha_i\left(\frac{\lambda_i}{c_i}\right)\right), \tag{4}$$

where $i = 1, 2$. For player i, the parameter t_i corresponds to the speed along a route, c_i is a capacity of the route, and α is some parameter. At the second stage, we fix the parameters $q^1 = (t_1, c_1, \alpha_1)$ and $q^2 = (t_2, c_2, \alpha_2)$, but we will return to the problem of their choice later.

The incoming flow is a Poisson process with an intensity λ. At the second stage, the players announce the prices of service, p_1 and p_2, respectively. The passengers select the minimum-cost service. As a result, the incoming flow is decomposed into two subflows with intensities λ_1 and λ_2, where $\lambda_1 + \lambda_2 = \lambda$.

The costs of passengers include the price of service and the expected trip time. We assume that the costs are a convex combination of these criteria:

$$u(p,\lambda) = kp + (1-k)t\left(1+\alpha\left(\frac{\lambda}{c}\right)\right), \tag{5}$$

where k: $0 \le k \le 1$. Because the parameters k, α, and c are constant, without loss of generality we may simplify the expression of the costs:

$$u(p,\lambda) = p + t\left(1+\frac{\lambda}{c}\right). \tag{6}$$

In accordance with the Wardrop principle, in an equilibrium the intensities of subflows λ_1 and λ_2 satisfy the balance equation:

$$\begin{gathered} u_1(p_1,p_2,\lambda_1,\lambda_2) = u_2(p_1,p_2,\lambda_1,\lambda_2) \\ \text{or } p_1 + t_1\left(1+\frac{\lambda_1}{c_1}\right) = p_2 + t_2\left(1+\frac{\lambda_2}{c_2}\right), \\ \lambda_1 + \lambda_2 = \lambda. \end{gathered} \tag{7}$$

From these equations, we obtain

$$\begin{aligned} \lambda_1 &= \frac{p_2 - p_1 + t_2 - t_1 + (t_2/c_2)\lambda}{(t_1/c_1)+(t_2/c_2)}, \\ \lambda_2 &= \frac{p_1 - p_2 + t_1 - t_2 + (t_1/c_1)\lambda}{(t_1/c_1)+(t_2/c_2)}. \end{aligned} \tag{8}$$

Consider the pricing game with the payoffs:

$$\begin{aligned} h_1(p_1,p_2) &= \lambda_1 p_1, \\ h_2(p_1,p_2) &= \lambda_2 p_2. \end{aligned} \tag{9}$$

This is a convex game with the equilibrium:

$$\begin{aligned} p_1^* &= \frac{1}{3}\left(t_2 - t_1 + \lambda\left(\frac{t_1}{c_1} + 2\frac{t_2}{c_2}\right)\right), \\ p_2^* &= \frac{1}{3}\left(t_1 - t_2 + \lambda\left(2\frac{t_1}{c_1} + \frac{t_2}{c_2}\right)\right). \end{aligned} \tag{10}$$

The intensities of subflows in the equilibrium are

$$\begin{aligned} \lambda_1^* &= \frac{t_2 - t_1 + \lambda(t_1/c_1 + 2t_2/c_2)}{3(t_1/c_1 + t_2/c_2)}, \\ \lambda_2^* &= \frac{t_1 - t_2 + \lambda(2t_1/c_1 + t_2/c_2)}{3(t_1/c_1 + t_2/c_2)}. \end{aligned} \tag{11}$$

Now, we return to the first stage of the game. The equilibrium payoffs (2) of players, $H_1(p_1^*, p_2^*)$ and $H_2(p_1^*, p_2^*)$, depend on the parameters of service, $q_1 = (t_1, c_1)$ and $q_2 = (t_2, c_2)$. Choosing specific values of these parameters, we may adjust the costs. This leads to a new game with the payoff functions:

$$\begin{aligned} H_1(q_1,q_2) &= \frac{(t_2 - t_1 + \lambda(t_1/c_1 + 2t_2/c_2))^2}{9(t_1/c_1 + t_2/c_2)} - C_1(t_1,c_1), \\ H_2(q_1,q_2) &= \frac{(t_1 - t_2 + \lambda(2t_1/c_1 + t_2/c_2))^2}{9(t_1/c_1 + t_2/c_2)} - C_2(t_2,c_2), \end{aligned} \tag{12}$$

where C_1 and C_2 are the operating costs of players for these parameters of service.

3.1. Computer Simulations. In this section, the results of computer simulations in which we find the equilibrium parameters (t_1^*, t_2^*) for the cost functions $C_1(t_1) = r_1/t_1^2$ and $C_2(t_2) = r_2/t_2^2$ are presented.

Table 1 shows the equilibrium parameters (t_1^*, t_2^*) calculated for the fixed values $c_1 = c_2 = 1$ and the costs $C_1(t_1) = r_1/t_1^2, C_2(t_2) = r_2/t_2^2$, where $r_1 = 1$ and $r_2 = 1.5$.

In this case, the capacities of both routes are equal and the only difference concerns the costs. Since $r_1 < r_2$, the second service is more expensive.

Clearly, if the incoming flow is increasing, the prices and the payoffs in the equilibrium are also increasing. However, there is some irregularity in the behavior of equilibrium operating times (speeds) of services as follows. Under increasing the incoming flow, the equilibrium operating time t_1 of the first service is decreasing; however, the equilibrium operating time t_2 of the second service is first decreasing and then, after some instant, starts increasing.

The second service is more expensive; therefore, the equilibrium payoff of the first service is higher than that of the second service.

4. Game of Two Players with Externalities

Consider a transportation network composed of two parallel routes with the linear latency functions:

$$\begin{aligned} f_1(\lambda) &= t_1(1 + a_1\lambda_1 + b_1\lambda_2), \\ f_2(\lambda) &= t_1(1 + a_2\lambda_2 + b_2\lambda_1). \end{aligned} \tag{13}$$

Two carriers (players) are serving consumers on the two parallel routes with prices p_1 and p_2, respectively. The incoming flow λ is decomposed into two subflows λ_1 and λ_2, $\lambda_1 + \lambda_2 = \lambda$, on routes 1 and 2, respectively. We assume that the flow λ is sufficiently large that all routes are used by the consumers.

Here, the parameters a_1 and a_2 describe an internal effect of the subflows λ_1 and λ_2 on routes 1 and 2, respectively. By analogy, the parameters b_1 and b_2 describe an external effect of the subflows λ_2 and λ_1 on routes 1 and 2.

We assume that $a_i > b_i, b_j, i \ne j$; the internal effect is more important than the external one for traffic control. However, the external parameters may significantly affect the traffic delays and can be a goal of improvement in a transportation system.

Following the same considerations as in Section 3, we obtain the equilibrium prices and flows in the pricing game. In accordance with the Wardrop principle, in equilibrium,

Table 1: Optimal parameters of services in equilibrium.

λ	t_1	t_2	p_1^*	p_2^*	λ_1^*	λ_2^*	H_1^*	H_2^*
1	1.772	2.656	2.656	1.772	0.6	0.4	1.274	0.496
1.1	1.732	2.610	2.841	1.934	0.654	0.445	1.526	0.642
1.2	1.696	2.582	3.039	2.094	0.710	0.489	1.811	0.800
1.3	1.660	2.572	3.252	2.249	0.768	0.531	2.138	0.969
1.4	1.624	2.587	3.493	2.402	0.829	0.570	2.519	1.146
1.5	1.585	2.632	3.773	2.552	0.894	0.605	2.978	1.327

the intensities of the subflows λ_1 and λ_2 satisfy the balance equation $p_1 + f_1(\lambda) = p_2 + f_2(\lambda)$. This yields

$$\lambda_1 = \frac{p_2 - p_1 + t_2 - t_1 + (a_2 t_2 - b_1 t_1)\lambda}{\Delta},$$
$$\lambda_2 = \frac{p_1 - p_2 + t_1 - t_2 + (a_1 t_1 - b_2 t_2)\lambda}{\Delta}, \tag{14}$$

where $\Delta = a_1 t_1 + a_2 t_2 - b_1 t_1 - b_2 t_2$.

For the pricing game with the payoffs,

$$h_1(p_1, p_2) = \lambda_1 p_1,$$
$$h_2(p_1, p_2) = \lambda_2 p_2, \tag{15}$$

we find equilibrium

$$p_1^* = \frac{1}{3}\left(t_2 - t_1 + \lambda\left(a_1 t_1 - b_2 t_2 + 2\left(a_2 t_2 - b_1 t_1\right)\right)\right),$$
$$p_2^* = \frac{1}{3}\left(t_1 - t_2 + \lambda\left(2\left(a_1 t_1 - b_2 t_2\right) + a_2 t_2 - b_1 t_1\right)\right). \tag{16}$$

The intensities of subflows in the equilibrium are

$$\lambda_1^* = \frac{p_1^*}{\Delta},$$
$$\lambda_2^* = \frac{p_2^*}{\Delta}. \tag{17}$$

Now, consider the game at the first stage. The equilibrium payoffs of the players, $H_1(p_1^*, p_2^*)$ and $H_2(p_1^*, p_2^*)$, depend on the parameters $q_1 = (t_1, a_1, b_1)$ and $q_2 = (t_2, a_2, b_2)$ of the latency functions. Changing these parameters, the players can improve the transportation system. However, this procedure can be rather expensive.

Let the players be interested in reducing the external influence on their own traffic. In other words, player 1 seeks to minimize b_1 while player 2 seeks to minimize b_2. In this case, we arrive in the game with the payoff functions:

$$H_1(b_1, b_2) = \frac{\left(t_2 - t_1 + \lambda\left(a_1 t_1 - b_2 t_2 + 2\left(a_2 t_2 - b_1 t_1\right)\right)\right)^2}{9\Delta} - C_1(b_1),$$
$$H_2(b_1, b_2) = \frac{\left(t_1 - t_2 + \lambda\left(2\left(a_1 t_1 - b_2 t_2\right) + a_2 t_2 - b_1 t_1\right)\right)^2}{9\Delta} - C_2(b_2), \tag{18}$$

where C_1 and C_2 the operating costs of players for these parameters of service.

4.1. Computer Simulations. We assume that the latency functions have form

$$f_1(\lambda) = 2\left(1 + 3\lambda_1 + b_1\lambda_2\right),$$
$$f_2(\lambda) = 3\left(1 + 2\lambda_2 + b_2\lambda_1\right). \tag{19}$$

Hence, the first route is faster than the second one for small traffic, but the latency is increasing more intensively for large traffic.

Then, the equilibrium prices are

$$p_1^* = \frac{1}{3}\left(1 + \lambda\left(18 - 3b_2 - 4b_1\right)\right),$$
$$p_2^* = \frac{1}{3}\left(-1 + \lambda\left(18 - 6b_2 - 2b_1\right)\right). \tag{20}$$

As a result, the payoff functions in this game are given by

$$H_1(b_1, b_2) = \frac{\left(1 + \lambda\left(18 - 3b_2 - 4b_1\right)\right)^2}{9\left(12 - 2b_1 - 3b_2\right)} - C_1(t_1, a_1, b_1),$$
$$H_2(b_1, b_2) = \frac{\left(1 + \lambda\left(18 - 6b_2 - 2b_1\right)\right)^2}{9\left(12 - 2b_1 - 3b_2\right)} - C_2(t_2, a_2, b_2). \tag{21}$$

For example, if the cost functions have the form $C_i(b_i) = c_i/b_i$, $i = 1, 2$ and the intensity of traffic is $\lambda = 1$, we obtain the following equilibrium values in this game, see Table 2.

Clearly, increasing the cost yields gives higher equilibrium values for b_1 and b_2. At the same time, the prices of both services (and hence the payoffs) are decreasing accordingly. Also, we may conclude that the parameters $t_i, i = 1, 2$ are more important for the payoffs than $a_i, i = 1, 2$. Here, $t_1 < t_2$ and $a_1 > a_2$, but in equilibrium, we obtain $H_1 > H_2$.

5. Transportation Game with Possible Use of Service Free of Charge

Our analysis proceeds to the transportation game with externality in which two carriers are rendering their services between two points v_1 and v_2, and, in addition, the consumers can use a cheap transportation service with a fixed price p_0.

It can be a free-of-charge way of personal transportation, e.g., biking (which matches the case $p_0 = 0$). Also, in some cities, the local government is supporting public transport and the price of bus tickets is sufficiently small.

A usual way of transportation in a city is presented in Figure 2. A person who has to travel from a starting point v_1 to a destination point v_2 can choose bike or public transport (bus or taxi). Both means of public transport are faster than bike but costly. Thus, the choice depends on personal preferences.

We assume that the service time of player i has the exponential probability density function with an intensity μ_i on the route (v_1, v_2), $i = 1, 2$. These parameters form a strategy profile (q^1, q^2) of the players at the first stage of the game.

Table 2: Optimal parameters of services in equilibrium.

	$c_2 = 0.03$	$c_2 = 0.06$	$c_2 = 0.09$	$c_2 = 0.12$
$c_1 = 0.03$	$b_1 = 0.187$ $b_2 = 0.157$ $p_1 = 5.925$ $p_2 = 5.227$ $H_1 = 2.988$ $H_2 = 2.259$	$b_1 = 0.187$ $b_2 = 0.223$ $p_1 = 5.861$ $p_2 = 5.096$ $H_1 = 2.974$ $H_2 = 2.101$	$b_1 = 0.187$ $b_2 = 0.273$ $p_1 = 5.811$ $p_2 = 4.996$ $H_1 = 2.964$ $H_2 = 1.979$	$b_1 = 0.187$ $b_2 = 0.316$ $p_1 = 5.768$ $p_2 = 4.910$ $H_1 = 2.955$ $H_2 = 1.877$
$c_1 = 0.06$	$b_1 = 0.265$ $b_2 = 0.157$ $p_1 = 5.823$ $p_2 = 5.176$ $H_1 = 2.856$ $H_2 = 2.444$	$b_1 = 0.265$ $b_2 = 0.222$ $p_1 = 5.758$ $p_2 = 5.046$ $H_1 = 2.842$ $H_2 = 2.086$	$b_1 = 0.265$ $b_2 = 0.273$ $p_1 = 5.707$ $p_2 = 4.944$ $H_1 = 2.831$ $H_2 = 1.965$	$b_1 = 0.265$ $b_2 = 0.315$ $p_1 = 5.665$ $p_2 = 4.859$ $H_1 = 2.822$ $H_2 = 1.863$
$c_1 = 0.09$	$b_1 = 0.326$ $b_2 = 0.157$ $p_1 = 5.742$ $p_2 = 5.135$ $H_1 = 2.754$ $H_2 = 2.233$	$b_1 = 0.325$ $b_2 = 0.222$ $p_1 = 5.678$ $p_2 = 5.006$ $H_1 = 2.740$ $H_2 = 2.075$	$b_1 = 0.325$ $b_2 = 0.273$ $p_1 = 5.627$ $p_2 = 4.904$ $H_1 = 2.729$ $H_2 = 1.953$	$b_1 = 0.324$ $b_2 = 0.315$ $p_1 = 5.586$ $p_2 = 4.820$ $H_1 = 2.720$ $H_2 = 1.852$
$c_1 = 0.12$	$b_1 = 0.376$ $b_2 = 0.157$ $p_1 = 5.675$ $p_2 = 5.102$ $H_1 = 2.669$ $H_2 = 2.224$	$b_1 = 0.375$ $b_2 = 0.222$ $p_1 = 5.611$ $p_2 = 4.972$ $H_1 = 2.654$ $H_2 = 2.066$	$b_1 = 0.375$ $b_2 = 0.272$ $p_1 = 5.561$ $p_2 = 4.872$ $H_1 = 2.644$ $H_2 = 1.944$	$b_1 = 0.375$ $b_2 = 0.315$ $p_1 = 5.518$ $p_2 = 4.786$ $H_1 = 2.635$ $H_2 = 1.842$

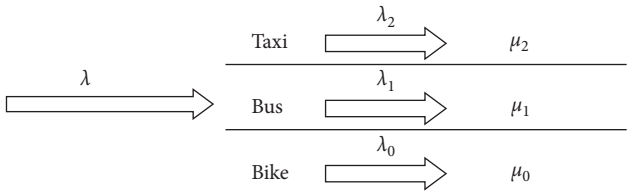

Figure 2: Scheme of public urban transport.

The incoming flow is a Poisson process with an intensity λ. In accordance with queueing theory, for the Poisson flow λ and a traffic flow μ on the route (v_1, v_2), the expected trip time is given by $1/(\mu - \lambda)$. Consequently, for a consumer selecting the service μ_1 or μ_2 (or deciding to use bike, μ_0), the expected trip time is $\mu_j - \lambda_j$, where λ_j is a flow in this route $j = 0, 1, 2$.

We assume that the parameters $\mu_i, i = 0, 1, 2$ are fixed and consider the second stage of the game. At the second stage, players 1 and 2 announce the prices of service, p_1 and p_2, respectively. Let the passengers be rational and select the minimum-cost service. Then, the incoming flow is decomposed into three subflows with intensities λ_1, λ_2, and λ_0, where $\lambda_0 + \lambda_1 + \lambda_2 = \lambda$.

We assume that the costs of passengers are described by a convex combination of the price of service and the expected trip time. Without loss of generality, we define the cost of service i by

$$u_i(p, t) = p_i + \frac{c}{\mu_i - \lambda_i}, \quad i = 1, 2, \tag{22}$$

where p_i is the price of service i; $1/(\mu_i - \lambda_i)$ is the expected trip time on the route i; c is some constant. The equilibrium intensities of the subflows λ_0, λ_1, and λ_2 satisfy the balance equation:

$$p_0 + \frac{c}{\mu_0 - \lambda_0} = p_1 + \frac{c}{\mu_1 - \lambda_1} = p_2 + \frac{c}{\mu_2 - \lambda_2}, \tag{23}$$

$$\lambda_0 + \lambda_1 + \lambda_2 = \lambda, \tag{24}$$

where p_0 is fixed.

Consider the pricing game with the payoff functions:

$$\begin{aligned} h_1(p_1, p_2) &= \lambda_1 p_1, \\ h_2(p_1, p_2) &= \lambda_2 p_2. \end{aligned} \tag{25}$$

Let $\lambda < \mu_0 \le \mu_1 \le \mu_2$ and also let p_2 be fixed. We find the best response of player 1. To calculate a maximum of the function $h_1(p_1, p_2)$, consider the Lagrange function:

$$L_1(p_1, \lambda_1, \lambda_2) = p_1\lambda_1 + k_1\left(p_1 + \frac{c}{\mu_1 - \lambda_1} - p_0 - \frac{c}{\mu_0 - (\lambda - \lambda_1 - \lambda_2)}\right) + k_2\left(p_2 + \frac{c}{\mu_2 - \lambda_2} - p_0 - \frac{c}{\mu_0 - (\lambda - \lambda_1 - \lambda_2)}\right). \tag{26}$$

The first-order optimality conditions yield:

$$\begin{aligned} &\frac{\partial L_1}{\partial p_1} = \lambda_1 + k_1 = 0, \\ &\frac{\partial L_1}{\partial \lambda_1} = p_1 + k_1\left(\frac{c}{(\mu_1 - \lambda_1)^2} + \frac{c}{(\mu_0 - \lambda_0)^2}\right) + k_2\frac{c}{(\mu_0 - \lambda_0)^2} = 0, \\ &\frac{\partial L_1}{\partial \lambda_2} = k_1\frac{1}{(\mu_0 - \lambda_0)^2} + k_2\left(\frac{1}{(\mu_2 - \lambda_2)^2} + \frac{1}{(\mu_0 - \lambda_0)^2}\right) = 0. \end{aligned} \tag{27}$$

Hence,

$$\begin{aligned} k_1 &= -\lambda_1, \\ k_2 &= \frac{\lambda_1(\mu_2 - \lambda_2)^2}{(\mu_2 - \lambda_2)^2 + (\mu_0 - \lambda_0)^2}. \end{aligned} \tag{28}$$

Substituting this result into (27) gives

$$p_1^* = \lambda_1 c\left(\frac{1}{(\mu_1 - \lambda_1)^2} + \frac{1}{(\mu_2 - \lambda_2)^2 + (\mu_0 - \lambda_0)^2}\right). \tag{29}$$

The best response of player 2 is obtained by analogy:

$$p_2^* = \lambda_2 c\left(\frac{1}{(\mu_2-\lambda_2)^2}+\frac{1}{(\mu_1-\lambda_1)^2+(\mu_0-\lambda_0)^2}\right). \quad (30)$$

Equations (23), (24), (29), and (30) determine the equilibrium prices and equilibrium flows for the given values μ_1 and μ_2.

Let us return back to the first stage of the game. At the first stage, we have the game with the payoff functions:

$$H_1(\mu_1,\mu_2) = \lambda_1 p_1^* - C_1(\mu_1) = \lambda_1^2 c\left(\frac{1}{(\mu_1-\lambda_1)^2}+\frac{1}{(\mu_2-\lambda_2)^2+(\mu_0-\lambda_0)^2}\right) - C_1(\mu_1),$$
$$H_2(\mu_1,\mu_2) = \lambda_2 p_2^* - C_2(\mu_2) = \lambda_2^2 c\left(\frac{1}{(\mu_2-\lambda_2)^2}+\frac{1}{(\mu_1-\lambda_1)^2+(\mu_0-\lambda_0)^2}\right) - C_2(\mu_2), \quad (31)$$

where λ_1 and λ_2 satisfy (23) and (24).

5.1. Computer Simulations. Consider a passenger flow with intensity $\lambda = 3$. Let the passengers choose among three possibilities for reaching a destination point: biking, using a bus, and hailing a taxi. Three capacities μ_0, μ_1, and μ_2 correspond to these cases. For example, if $\mu_0 = 2$, $\mu_1 = 2.1$, and $\mu_2 = 2.5$, from equations (23), (24), (29), and (30), we find the optimal equilibrium prices:

$$p_1^* = 0.685,$$
$$p_2^* = 0.793. \quad (32)$$

The flows which correspond to these prices are

$$\lambda_0 = 1.302,$$
$$\lambda_1 = 0.762, \quad (33)$$
$$\lambda_2 = 0.936.$$

The payoffs of the players are $h_1^* = 0.5223$ and $h_2^* = 0.7426$.

We assume that the costs for supporting the service of these players are described by

$$c_1(\mu_1) = c_1\mu_1^2,$$
$$c_2(\mu_2) = c_2\mu_2^2, \quad (34)$$

with $c_1 = 0.025$ and $c_2 = 0.022$. Then, the payoffs of the players calculated with the costs are

$$H_1 = 0.4121,$$
$$H_2 = 0.6051. \quad (35)$$

Now, for this flow $\lambda = 3$, let the biking capacity be the same, $\mu_0 = 2$, and also let the players invest some money to change the capacities μ_1 and μ_2

We assume the first player decides to change the intensity from $\mu_1 = 2.1$ to $\mu_1 = 2.2$. In new equilibrium, we find that the optimal prices are

$$p_1^* = 0.669,$$
$$p_2^* = 0.746. \quad (36)$$

The flows which correspond to these prices are

$$\lambda_0 = 1.276,$$
$$\lambda_1 = 0.796, \quad (37)$$
$$\lambda_2 = 0.927.$$

The payoffs of the players calculated with the costs are

$$H_1 = 0.4124,$$
$$H_2 = 0.5546. \quad (38)$$

Clearly, the strategy $\mu_1 = 2.2$ is more profitable for the first player than $\mu_1 = 2.1$. Applying the sequence of best responses of players, we obtain the Nash equilibrium for this case. We find the equilibrium intensities for the service:

$$\mu_1^* = 2.225,$$
$$\mu_2^* = 2.436, \quad (39)$$

with the payoffs

$$H_1^* = 0.438,$$
$$H_2^* = 0.545. \quad (40)$$

Table 3 presents the resulting equilibrium μ_1^* and μ_2^* calculated for different values of the flow $\lambda = 2, 2.1, \ldots, 3$ and the free-of-charge flow $\mu_0 = 2$ and the costs of service in the form $c_1(\mu_1) = c_1\mu_1^2$ and $c_2(\mu_2) = c_2\mu_2^2$, where $c_1 = 0.025$ and $c_2 = 0.022$.

Clearly, for higher flows, at equilibrium, the players increase the prices of services p_1^* and p_2^*. But the picture is not the same for the equilibrium capacities μ_1^* and μ_2^*. The capacities are firstly increasing and after some instant start decreasing. The equilibrium capacity of the carrier with smaller cost is larger than the capacity with higher cost, i.e., $\mu_2^* > \mu_1^*$. Interestingly, for higher flows the difference between these capacities $\mu_2^* - \mu_1^*$ is reduced.

Table 3: Optimal parameters of services in equilibrium.

λ	λ_0^*	λ_1^*	λ_2^*	μ_1^*	μ_2^*	p_1^*	p_2^*	H_1	H_2
2.0	0.822	0.478	0.701	2.168	2.681	0.257	0.344	0.005	0.083
2.1	0.843	0.529	0.728	2.245	2.700	0.281	0.357	0.023	0.099
2.2	0.868	0.577	0.755	2.307	2.716	0.305	0.373	0.043	0.120
2.3	0.896	0.620	0.784	2.356	2.731	0.330	0.392	0.066	0.143
2.4	0.928	0.660	0.812	2.393	2.740	0.356	0.414	0.092	0.171
2.5	0.963	0.698	0.839	2.420	2.744	0.384	0.439	0.121	0.203
2.6	1.003	0.730	0.866	2.430	2.740	0.415	0.470	0.156	0.242
2.7	1.047	0.765	0.888	2.440	2.720	0.452	0.504	0.197	0.284
2.8	1.102	0.792	0.906	2.420	2.680	0.499	0.550	0.249	0.340
2.9	1.171	0.812	0.917	2.370	2.610	0.563	0.615	0.317	0.414
3.0	1.282	0.813	0.905	2.230	2.440	0.688	0.742	0.435	0.541

6. Conclusion

The central point in the model is the concept of rational consumers. It has been assumed that after announcing prices of services, the consumers select the minimum-cost service in the expected sense. The cost includes the price of service and also the expected trip time. It has been assumed that the consumers consider two criteria and make a decision taking both criteria into account. For example, if the incoming flow λ is decomposed into subflows $\lambda_i, i \in N$, the passengers joining the flow λ_i will pay p_i for this service and waste some time $f_i(\lambda_i), i \in N$.

In future research we plan to consider the role of boundedly rational consumers in the sense of being oblivious to other consumers' influences on traffic flows, in a competitive transport system, where prices motivate the equilibrium between all players in the market, firms, and consumers. In this approach while the rational users follow a strategy that minimizes their individual cost, an oblivious user prefers fast routes.

A quite appropriate hypothesis is that the choice of consumers is balanced by an objective function. In this paper, the convolution of criteria has been adopted. It is possible to use other approaches as well. For multicriteria problems, the Nash Bargaining Solution (NBS) approach is widespread. In this case, NBS corresponds to an optimal allocation $\lambda_i, i \in N$, that minimizes an objective function. This issue will be considered in further research.

Data Availability

All data used can be obtained from the sources throughout the paper.

Conflicts of Interest

The authors declare that they have no conflicts of interest.

Acknowledgments

This research was supported by the Shandong Province "Double-Hundred Talent Plan" (no. WST2017009).

References

[1] J. G. Wardrop, "Road paper. Some theoretical aspects of road traffic research," *Proceedings of the Institution of Civil Engineers*, vol. 1, no. 3, pp. 325–362, 1952.

[2] J. R. Correa and N. E. Stier-Moses, "Wardrop equilibria," in *Wiley Encyclopedia of Operations Research and Management Science*, pp. 1–12, Springer, Berlin, Germany, 2011.

[3] Y. Sheffy, *Urban Transportation Networks: Equilibrium Analysis with Mathematical Programming*, Methods Prentice-Hall, Englewood Cliffs, NJ, USA, 1985.

[4] V. V. Mazalov and A. V. Melnik, "Equilibrium prices and flows in the passenger traffic problem *J*," *International Game Theory Review*, vol. 18, pp. 1–19, 2016.

[5] G. Karakostas, T. Kim, A. Viglas, and H. Xia, "On the degradation of performance for traffic networks with oblivious users," *Transportation Research Part B: Methodological*, vol. 45, no. 2, pp. 364–371, 2011.

[6] W. Ford, J. W. Lien, V. V. Mazalov, and J. Zheng, "Riding to wall street: determinants of commute time using citi bike," *International Journal of Logistics Research and Applications*, vol. 22, no. 5, pp. 473–490, 2019.

[7] R. Hassin and M. Haviv, *To Queue or Not to Queue. Equilibrium Behavior in Queueing Systems*, Springer, Berlin, Germany, 2003.

[8] Y. A. Korillis, A. A. Lazar, and A. Orda, "Capacity allocation under noncooperative routing," *Journal of IEEE Transactions on Automatic Control*, vol. 42, pp. 309–325, 1997.

[9] I. Luski, "On partial equilibrium in a queuing system with two servers," *The Review of Economic Studies*, vol. 43, no. 3, pp. 519–525, 1976.

[10] D. Levhari and I. Luski, "Duopoly pricing and waiting lines," *European Economic Review*, vol. 11, no. 1, pp. 17–35, 1978.

[11] T. Roughgarden, "The price of anarchy is independent of the network topology," *Journal of Computer and System Sciences*, vol. 67, no. 2, pp. 341–364, 2003.

[12] US Bureau of Public Roads, *Traffic Assignment Manual*, US Department of Commerce, Washington, DC, USA, 1964.

[13] E. Koutsoupias and C. Papadimitriou, "Worst-case equilibria," *STACS 99*, vol. 1563, pp. 404–413, 1999.

[14] A. Orda, R. Rom, and N. Shimkin, "Competitive routing in multiuser communication networks," *IEEE/ACM Transactions on Networking*, vol. 1, no. 5, pp. 510–521, 1993.

[15] J. W. Lien, V. V. Mazalov, A. V. Melnik, and J. Zheng, "Wardrop equilibrium for networks with the BPR latency function," in *Lecture Notes in Computer Science*, vol. 9869, pp. 37–49, Springer, Berlin, Germany, 2016.

[16] A. A. Kulkarni and U. V. Shanbhag, "A shared-constraint approach to multi-leader multi-follower games," *Set-Valued and Variational Analysis*, vol. 22, no. 4, pp. 691–720, 2014.

[17] A. A. Kulkarni and U. V. Shanbhag, "An existence result for hierarchical Stackelberg v/s Stackelberg games," *IEEE Transactions on Automatic Control*, vol. 60, no. 12, pp. 3379–3384, 2015.

Hindawi
Journal of Advanced Transportation
Volume 2020, Article ID 5868379, 8 pages
https://doi.org/10.1155/2020/5868379

Research Article

Factors Affecting Crash Involvement of Commercial Vehicle Drivers: Evaluation of Commercial Vehicle Drivers' Characteristics in South Korea

Jooyoung Lee[1], **Jiho Yeo**[1], **Ilsoo Yun**[2] **and Sanghyeok Kang**[3]

[1]*The Cho Chun Shik Graduate School of Green Transportation, Korea Advanced Institute of Science and Technology, Daejeon 34051, Republic of Korea*
[2]*Department of Transportation System Engineering, Ajou University, Suwon 443-749, Republic of Korea*
[3]*Department of Civil and Environmental Engineering, Incheon National University, Incheon 22012, Republic of Korea*

Correspondence should be addressed to Sanghyeok Kang; lifesine@inu.ac.kr

Received 10 December 2019; Revised 10 February 2020; Accepted 11 February 2020; Published 3 March 2020

Guest Editor: Qiang Zeng

The aim of this study was to evaluate the effects of driver-related factors on crash involvement of four different types of commercial vehicles—express buses, local buses, taxis, and trucks—and to compare outcomes across types. Previous studies on commercial vehicle crashes have generally been focused on a single type of commercial vehicle; however, the characteristics of drivers as factors affecting crashes vary widely across types of commercial vehicles as well as across study sites. This underscores the need for comparative analysis between different types of commercial vehicles that operate in similar environments. Toward these ends, we analyzed 627,594 commercial vehicle driver records in South Korea using a mixed logit model able to address unobserved heterogeneity in crash-related data. The estimated outcomes showed that driver-related factors have common effects on crash involvement: greater experience had a positive effect (diminished driver crash involvement), while traffic violations, job change, and previous crash involvement had negative effects. However, the magnitude of the effects and heterogeneity varied across different types of commercial vehicles. The findings support the contention that the safety management policy of commercial drivers needs to be set differently according to the vehicle type. Furthermore, the variables in this study can be used as promising predictors to quantify potential crash involvement of commercial vehicles. Using these variables, it is possible to proactively identify groups of accident-prone commercial vehicle drivers and to implement effective measures to reduce their involvement in crashes.

1. Introduction

Commercial vehicles have a high risk of traffic injury because they are driven long distances, which often leads to driver fatigue [1]. Moreover, when involved in traffic crashes, the heavy weight of such vehicles generates greater impact damage on the occupants of other vehicles or pedestrians [2, 3]. In South Korea in the year 2018, commercial vehicles—buses, taxis, and trucks—were involved in 43,632 traffic accidents, resulting in 67,262 injuries (20.8% of total traffic injuries) and 692 deaths (18.3% of total traffic injuries) [4]. Considering that commercial vehicles account for only 6.2% of total registered vehicles in South Korea, the proportions of traffic injuries and deaths involving commercial vehicles are substantially higher than those of other vehicle classes. While controlling for driving distance, commercial vehicles had 792.7 traffic accidents and 12.6 traffic deaths per one billion km, both of these values were 1.5 times greater than the values for noncommercial vehicles. In general, a large portion of traffic crashes is caused by driver-related factors [5].

Previous studies have mainly used two approaches to evaluate the effect of driver-related factors on traffic accidents. One approach used questionnaires or interviews to

evaluate psychological factors deriving from latent driver characteristics such as personality and attitude [6–12]. The use of self-reported data had the advantage of allowing the collection of enough samples to adopt statistical models, but it raised concerns about what are called "dishonest biases" and that the variables were unobservable in practical use. Due to these limitations, safety practitioners and scholars turned to the analysis of more measurable traffic-crash data. Such studies were generally performed with a focus on a single type of commercial vehicle [1, 13–19]. Although the vehicle types were different, driver characteristic variables such as age, gender, education, driving experience, license type, violation history, crash history, and job change history were commonly specified as explanatory variables [1, 10, 14–18, 20]. On the other hand, coefficient estimates of those common variables varied widely across types of commercial vehicles, as well as across study sites [21]. This underscores the need for a comparative analysis of different types of commercial vehicles operated in comparable environments. Such research would reveal the differential effects of driver characteristics on commercial vehicle safety while controlling for site-specific effects.

In the field of traffic-crash research, logistic regression has proven to be a popular and reliable way to reveal the relationships between response variables and explanatory variables [22–24]. However, in the case of logistic regression, a fixed, unique coefficient represents the effect of a particular factor on all individuals. This could lead to bias in the interpretation of the results, given that the incidence of one individual's crash is inherently heterogeneous [25]. Therefore, for the analysis of crash-related data, it is necessary to use a model that can explain unobserved heterogeneity. To address the issue, previous researchers used other, more promising approaches: several statistical and econometric methods are available to account for unobserved heterogeneity [26–29]. In many recent studies, mixed logit models have been used to account for unobserved heterogeneity of variables by applying individual-specific coefficients to standard logit models [30–33].

In this context, the aim of the present study was to evaluate the effect of driver characteristics on traffic crashes of four different types of commercial vehicles—express and local buses, taxis, and trucks—and to compare outcomes across types. Toward these ends, we analyzed commercial vehicle driver records in South Korea using a mixed logit model that could address unobserved heterogeneity in crash-related data. This study is distinct in that long-term driver characteristic variables were used for the crash analysis. A total of 627,594 commercial vehicle driver data were processed and the accumulated crash counts, traffic violations, and job changes from driver license acquisition date were used in the model. Furthermore, to control for site-specific effects, which set limitations on many previous studies in which only one type of commercial vehicle was analyzed, a comparative analysis of four vehicle types that operate in the same environment was executed to reveal the differences according to vehicle type. The results of this study can be used to establish traffic safety improvement policies by the characteristics of each commercial vehicle type.

2. Data Description

Records on 627,594 commercial vehicle drivers without identifiable personal information were obtained from the Korea Transportation Safety Authority (KTSA). The dataset contains driver information including date of birth, gender, issue date of commercial driver's license, violation records, previous job changes, license type (i.e., type of commercial vehicle), and crash records. In this study, only data for male drivers were used due to the insufficient sample size of female commercial vehicle drivers.

The dependent variable is binary: whether the drivers had been involved in traffic accidents for the recent three years between July 2014 and June 2017. Independent variables include driver's age, driving experience (in years), violation rate (numbers of violations per 10 years), job change rate (numbers of job changes per year), and previous crash involvement rate (numbers of crashes per 10 years). Driver age was discretized into several levels for convenience of analysis, while other variables remained as continuous variables. Descriptive statistics of variables are provided for each vehicle type from Tables 1–4.

Overall, the proportion of crash involvement was found to vary across types of commercial vehicles. Higher crash involvement was observed in local buses and taxis, which is presumed to be because they operate mainly in urban environments. The distribution patterns are also different. The proportion of recent crash involvement of trucks ranged from approximately 5% to 10%, while taxis ranged from 15% to 30%, showing an almost threefold difference. This trend was similar for other variables. The proportion of crash involvement tended to increase as age increased; however, taxi and truck drivers showed the highest rate at 21–30, and there was no clear trend of crash rate increase with age. The proportions of recent crash involvement of local bus, express bus, and taxi drivers were highest at 5–15 years of driving experience. For truck drivers, the rate was highest at 1–5 years. As traffic violation rate increased, the proportion of recent crash involvement tended to increase. However, the levels that had the highest proportions were different depending on the vehicle type. Local bus and express bus drivers had the highest traffic violation rates of 0.15–0.2. Taxi drivers had values of 0.1–0.15 and truck drivers have values above 0.2. The higher the job change rate, the higher the proportion of recent crash involvement. There is also a tendency similar to that of job change rate for past crash rates.

3. Methods

In this study, a mixed logit model was used to unveil significant factors that affect the crash involvement of commercial vehicle drivers in South Korea. The mixed logit model assumes that the effects of the parameters on the logit model are different for each individual [31]. Thus, the model can account for unobserved factors that are not captured directly through the data. To compare the explanatory power of the mixed logit model, we performed the log-likelihood ratio test with the logistic regression model that is using only

Table 1: Descriptive statistics of variables for local bus.

Variable description		Number of samples	Minimum	Maximum	Mean	SD
Dependent variable						
Recent crash involvement	0 = not involved in the crash for three years	63,256	—	—	—	—
	1 = involved in the crash for three years	12,179	—	—	—	—
Independent variables						
Driver age	21–30	316	0	1	0	0.06
	31–40	4,250	0	1	0.06	0.23
	41–50	20,640	0	1	0.27	0.44
	51–60	36,744	0	1	0.49	0.5
	More than 61	13,485	0	1	0.18	0.38
Driving experience	Years of driving	75,435	0.04	59.33	16.26	9.72
Violation rate	Total number of violations per 10 years	75,435	0	7.5	0.08	0.22
Job change rate	Total number of job changes per year	75,435	0	48	0.27	0.8
Crash rate	Total number of crashes per 10 years	75,435	0	4.44	0.38	0.4

Table 2: Descriptive statistics of variables for express bus.

Variable description		Number of samples	Minimum	Maximum	Mean	SD
Dependent variable						
Recent crash involvement	0 = not involved in the crash for three years	42,730	—	—	—	—
	1 = involved in the crash for three years	4,109	—	—	—	—
Independent variables						
Driver age	21–30	290	0	1	0.01	0.07
	31–40	2,054	0	1	0.04	0.2
	41–50	10,011	0	1	0.21	0.41
	51–60	24,574	0	1	0.4	0.49
	More than 61	85,021	0	1	0.33	0.47
Driving experience	Years of driving	46,839	0.04	50.75	16.47	10.29
Violation rate	Total number of violations per 10 years	46,839	0	9.11	0.12	0.21
Job change rate	Total number of job changes per year	46,839	0	48	0.34	0.98
Crash rate	Total number of crashes per 10 years	46,839	0	3.44	0.35	0.38

Table 3: Descriptive statistics of variables for taxi.

Variable description		Number of samples	Minimum	Maximum	Mean	SD
Dependent variable						
Recent crash involvement	0 = not involved in the crash for three years	182,557	—	—	—	—
	1 = involved in the crash for three years	37,287	—	—	—	—
Independent variables						
Driver age	21–30	161	0	1	0	0.02
	31–40	2,839	0	1	0.01	0.11
	41–50	24,574	0	1	0.11	0.31
	51–60	86,748	0	1	0.39	0.48
	More than 61	105,522	0	1	0.48	0.5
Driving experience	Years of driving	219,844	0.04	55.25	18.94	9.86
Violation rate	Total number of violations per 10 years	219,844	0	14.5	0.09	0.21
Job change rate	Total number of job changes per year	219,844	0	96	0.2	0.81
Crash rate	Total number of crashes per 10 years	219,844	0	4.41	0.32	0.34

fixed parameters. In the logistic regression model, the coefficient β value is fixed. The probability that driver i belongs to recent crash category n, consisting of two categories that are involved or not involved, is shown in the following equation:

$$P_{n,i} = \frac{e^{\beta X_{n,i}}}{\sum_j e^{\beta X_{j,i}}}. \quad (1)$$

In the mixed logit model, it is assumed that the coefficient is not fixed to β but is individual-specific β_i, and the probability of crash involvement could be expressed as shown in the following equation:

$$P_{n,i} = \frac{e^{\beta_i X_{n,i}}}{\sum_j e^{\beta_i X_{j,i}}}. \quad (2)$$

Table 4: Descriptive statistics of variables for truck.

Variable description		Number of samples	Minimum	Maximum	Mean	SD
Dependent variable						
Recent crash involvement	0 = not involved in the crash for three years	268,245	—	—	—	—
	1 = involved in the crash for three years	17,231	—	—	—	—
Independent variables						
Driver age	21–30	2,704	0	1	0.01	0.09
	31–40	31,887	0	1	0.11	0.31
	41–50	85,021	0	1	0.3	0.45
	51–60	102,815	0	1	0.36	0.48
	More than 61	63,049	0	1	0.22	0.41
Driving experience	Years of driving	285,476	0.04	58.25	12.66	9.51
Violation rate	Total number of violations per 10 years	285,476	0	11.43	0.12	0.29
Job change rate	Total number of job changes per year	285,476	0	48	0.13	0.62
Crash rate	Total number of crashes per 10 years	285,476	0	3.65	0.22	0.29

In order to derive a consistent estimated value through the above equation, it is necessary to use various data for each individual. That is, it is difficult to use the above equation with limited crash data. In the mixed logit model, it is assumed that β_i is a random parameter that is estimated for each individual. Therefore, given β_i, the probability of having a crash experience for driver i could be expressed by the following equation:

$$\frac{P_{n,i}}{\beta_i} = \frac{e^{\beta_i X_{n,i}}}{\sum_j e^{\beta_i X_{j,i}}}. \tag{3}$$

Since the above equation is a conditional probability, the unconditional probability is derived as equation (4) through integration using the probability density function of β_i:

$$P_{n,i} = \int_{\beta_i} \left(\frac{P_{n,i}}{\beta_i}\right) f\left(\frac{\beta_i}{\varphi}\right) \mathrm{d}\beta_i, \tag{4}$$

where $f(\beta_i/\varphi)$ is a probability density function for β_i having a parameter of φ. The normal distribution is most widely used as a function of the probability density of random parameters, and a uniform distribution is appropriate for dummy variables [34]. In this study, the multidimensional integration of β_i is necessary because the factors related to driver characteristics are reflected by several variables instead of one. It is difficult to calculate a multidimensional integral because of the complicated processes of numerical integration, such as the quadrature method, but this integral can be calculated by a simulation-based maximum likelihood method. In many works in the literature, Halton draws have proven to be the most efficient way of estimating coefficients [35–37]. We used a free statistical package R to implement the mixed logit model in this study. The risk factors include driver characteristics such as age, driving experience, traffic violation rate, job change rate, and previous crash rate. The response variable is a binary variable: whether or not a driver had a crash experience in the period from July 2014 to June 2017.

4. Results and Discussion

The results of the mixed logit model derived in this study successfully converged for all vehicle types, and the variables with random parameters showed statistically significant results. Heterogeneity variables have statistically significant results for standard deviation. In the derived model, there were significant differences among commercial vehicle types. Variables with heterogeneity were different for each vehicle type, and the sizes of statistically significant coefficients were also different. First, compared to the model using only fixed parameters, the log-likelihood ratio test was used to verify the explanatory power of the mixed logit model. The test results are shown in Table 5.

In the results of the log-likelihood ratio test, it was found that all models in this study that applied random parameters were superior to models using fixed parameters. The express bus model was statistically significant at the level of 95% confidence and the other models were significant at the level of 99.9% confidence. This is because random parameters applied to each model were able to reflect driver heterogeneity, which could not be considered in the fixed-parameter model.

The coefficient estimation results of the variables obtained using the mixed logit model are provided in Table 6. Among the eight variables used in this study, the variables that showed statistical significance differed between commercial vehicle types. Driving experience, traffic violation rate, and crash rate were statistically significant at a 99% confidence level in all models, and job change rate was statistically significant in all vehicle types except local bus. The driver's age was statistically significant at the level of 95% confidence in all models for the age group of 61 and older. There were differences in statistical significance for the other age groups by vehicle type. Heterogeneous variables also had different levels of statistical significance depending on the vehicle type. In the case of traffic violation rate, all vehicle types showed heterogeneity according to drivers, and the driving experience variable exhibited heterogeneity for all vehicle types except express bus. The age group of 31 to 40 years exhibited heterogeneity in groups of truck and taxi, while the older driver group (51 to 60 years) and job change rate variables exhibited heterogeneity only in a taxi.

The coefficient of the oldest age group for all vehicle types is positive. This could be interpreted showing that the oldest group of drivers had increased risk of crash involvement compared to drivers in the reference group (21 to

Table 5: Log-likelihood ratio test result for the fixed and random parameter logit models.

	Local bus		Express bus		Taxi		Truck	
	Fixed	Random	Fixed	Random	Fixed	Random	Fixed	Random
Degrees of freedom	9	17	9	17	9	17	9	17
Log-likelihood at convergence	−32,778	−32,743	−13,616	−13,608	−94,393	−93,665	−63,042	−62,856
χ^2	69.356		15.812		1,457.9		370.83	
p value	<0.001***		0.045*		<0.001***		<0.001***	

Table 6: Model estimation results for significant independent variables.

Variable	Local bus		Express bus		Taxi		Truck	
	Coef.	St. dev.	Coef.	St. dev.	Coef.	St. dev.	Coef.	St. dev.
Driver age (ref.: 21–30)								
31–40	−0.83		−1.76		−1.61*	5.20*	−1.47***	3.49***
41–50	0.08		−0.11		−0.34		−0.31	
51–60	0.77***		0.14		1.19*	0.87*	−0.03	
61 and above	0.97***		0.53*		1.70***		0.25**	
Violation rate	0.83***	1.59***	0.90***	0.59**	1.45***	1.51***	0.92***	1.33***
Driving experience	−0.03***	0.01*	−0.02***		−0.04***	0.01·	−0.03***	0.02***
Job change rate	0.01		0.04**		−0.44***	5.65***	0.06***	
Crash rate	0.60***		0.72***		1.25***		1.00**	
Constant	−2.20***		−2.69***		−3.02***		−2.89***	
Number of observations	75,435		46,839		285,476		219,844	

Note. Coef. = coefficient, st. dev. = standard deviation, ***$p < 0.001$, **$p < 0.01$, *$p < 0.05$, and ·$p < 0.1$.

30 years). This finding was consistent with the findings reported in previous studies [38–43]. Similarly, Valent et al. [39] reported that drivers aged 65 and above had a significantly increased risk of fatal injury for most kinds of transportation modes. As is well known, as people age, their cognitive and perceptual faculties deteriorate, which could increase crash risk [44–46]. Especially, local bus drivers in their 51 s and 60 s also had positive coefficients, while results for this age group with other vehicle types were not significant. Unlike other types of vehicles, local buses have tightly spaced schedules, which means they have to speed up and cut other vehicles off in order to meet the intervals, which leads to high labor intensity on the part of the driver. Therefore, for local bus drivers, the older driver management age range should be wider than for other vehicle drivers.

On the other hand, truck and taxi drivers in their 30 s and 40 s exhibited heterogeneity. Among heterogeneous variables that have different effects on traffic crashes, the probability of the positive impact of the crash involvement could be calculated if the standard deviation of the coefficients derived from each variable was statistically significant. The traffic violation rate, a variable that is heterogeneous for all vehicle types, with values of 69.89%, 93.67%, 75.53%, and 83.28%, affects involvement in crashes as it increases. Generally, traffic violations are a major risk to road safety, as confirmed by the results of many previous studies. The results of this study also show that up to 93% of drivers increase the risk of crashes, depending on the type of vehicles, when traffic violation rates increase if all other variables are kept constant. Similarly, many researchers have found a positive relationship between traffic violations and crash occurrence [6, 47–50]. However, most of the studies have been conducted on general drivers; only a few studies have been conducted on commercial vehicle drivers [10]. In the case of a commercial vehicle driver, heterogeneity in traffic violations occurred because the vehicle type and driving environment are different from those of general drivers. Especially for local buses, about 30% of drivers have an effect of reducing crash involvement when the violation rate increases. This is because the violation rate used in this study is the count value of all traffic violations. Not all traffic violations, as defined by national law, are directly related to crashes. Traffic violations that include violations that increase the risk of a crash, as found in the previous literature, are speeding and drunk driving; however, violations also include items not directly related to crash involvement such as parking violations or designated lane violations. Therefore, a more detailed analysis of traffic violations is required to identify crash-related violations of commercial vehicle drivers.

For driving experience, express buses had a fixed coefficient of −0.02; local buses, trucks, and taxis exhibited heterogeneity. For vehicle types with heterogeneity in the driving experience, the probability values for drivers who reduced the risk of crashes as driving experience increases were as follows: 99.77% for local bus, 95.66% for truck, and 99.99% for a taxi. This indicates that most drivers with short driving experience are likely to have recently been involved in a crash, regardless of vehicle type. This is in line with the fact that accident rates tend to diminish with experience [9, 51, 52]. Cooper et al. [52] revealed that crash rates of novice drivers aged 16 to 55 decreased with increasing

experience. McCartt et al. [9] used survival analysis to determine that the risk of a first crash during the first month of licensure was much higher than during any of the next 11 months. As has been previously found, the driving experience has a positive effect on driving skills [53, 54].

For express bus and truck drivers, the relationship between job change rate and crashes was found to be statistically significant, with positive coefficients, meaning that a job change increases the risk of crash involvement. The job change rate is a variable that represents a comprehensive measure of overall driver behavior. Frequent job changes imply that the duration of driving experience at a job position is not sufficient for that driver to be fully adept at the job and that the driver's overall skills and adaptation to the commercial vehicle industry may not be satisfactory. However, little research has been conducted to evaluate job change as a predictor of crash involvement of commercial vehicle drivers. Corsi and Fanara [55] reported that motor carriers with high driver turnover had significantly higher crash rates than those with lower turnover rates. Extending this research, Staplin and Gish [56] estimated the risk of crash involvement as a function of job change rate among truck drivers. However, these studies were based on univariate analysis, which might have caused confounding issues.

Meanwhile, taxi drivers, as examined in this study, exhibited heterogeneity in job change rate, with 46.9% affecting the increase of crash involvement and 53.1% affecting the decrease. In this context, the outcomes of this study provide solid evidence that the job change rate is a reliable crash predictor for express bus and truck drivers. For taxi and local bus drivers, it is not clear that job change rate increases the risk of a crash; it is found that when using job change rates for commercial vehicle driver safety management, it needs to be applied to specific vehicle types.

In contrast, a driver's previous safety performance, represented by the variable of crash rate, has a statistically significant effect on crash involvement for all commercial vehicle drivers. This is consistent with previous findings [1, 57]. Since the coefficient of the crash rate was not heterogeneous for all vehicle types, intensive safety management is needed for drivers who have higher crash rates, regardless of vehicle type.

5. Conclusions

The present study provides the first report on crashes of commercial vehicle drivers operating four different types of vehicles in Korea. The information in 627,594 driver records obtained from the Korea Transportation Safety Authority was used in this study to evaluate the effects of driver-related factors on crash involvement of four types of commercial vehicles: local buses, express buses, taxis, and trucks. Then, the outcomes were compared across vehicle types. We selected a mixed logit model able to account for unobserved heterogeneity in the driver data and revealed the relationships between commercial vehicle driver characteristics and crash involvement. The dependent variable was the crash involvement of commercial vehicle drivers for the most recent three years, and five driver-related factors were specified as explanatory variables.

The log-likelihood ratio test showed that the mixed logit model derived from this study was superior to the logit model using fixed parameters. The estimated outcomes showed that driver-related factors have common effects on crash involvement: driver experience diminished driver crash involvement, while driver traffic violations, job change, and previous crash involvement had negative effects. However, the magnitude of the effects and heterogeneity varied across different types of commercial vehicles. In the case of local buses, unlike other vehicle types, the job change rate was not statistically significant and the range of ages that increased the risk of crash involvement was wider than other types. Moreover, the crash rate increased the crash involvement in all vehicle types, and taxis, in particular, had a higher coefficient than other vehicle types. Therefore, the result of this study supports the contention that the safety management policy of commercial drivers needs to be set differently according to the vehicle type. Furthermore, because all the variables used in this study were measurable, the expected crash involvement could be estimated using commercial vehicle driver records by vehicle type. By properly using the outcomes, it should, therefore, be possible to proactively identify groups of accident-prone commercial vehicle drivers and to implement effective measures such as education and, if necessary, enforcement.

There are also several limitations of this study related to limitations in the data available. This study did not reflect other variables that might affect crash involvement, such as the average daily driving time related to labor intensity. In addition, it is necessary to study further the relationship between lists of traffic violations by vehicle type and crash involvement. If more information is available about commercial drivers in the future, more in-depth research to improve traffic safety will be possible.

Data Availability

The data used to support the findings of this study have not been made available because of KTSA's policy reasons.

Conflicts of Interest

The authors declare no conflicts of interest.

Acknowledgments

This work was supported by an Incheon National University Research Grant in 2016. The authors would like to thank the staff of the Big Data Center at the Korea Transportation Safety Authority for their kind assistance in providing the data used in this study.

References

[1] D. E. Cantor, T. M. Corsi, C. M. Grimm, and K. Özpolat, "A driver focused truck crash prediction model," *Transportation Research Part E: Logistics and Transportation Review*, vol. 46, no. 5, pp. 683–692, 2010.

[2] K. Jang, S. H. Park, S. Kang, K. H. Song, S. Kang, and S. Chung, "Evaluation of pedestrian safety: pedestrian crash hot spots and risk factors for injury severity," *Transportation Research Record: Journal of the Transportation Research Board*, vol. 2393, no. 1, pp. 104–116, 2013.

[3] C. Ma, W. Hao, F. Pan, and W. Xiang, "Road screening and distribution route multi-objective robust optimization for hazardous materials based on neural network and genetic algorithm," *PLoS One*, vol. 13, no. 6, Article ID e0198931, 2018.

[4] Korea Transportation Safety Authority, *2018 Statistics of Vehicle Travel*, Korea Transportation Safety Authority, Gimcheon, Gyeongsangbuk-do, South Korea, 2019.

[5] L. Evans, *Traffic Safety*, Science Serving Society, Bloomfield Hills, MI, USA, 2004.

[6] D. Parker, R. West, S. Stradling, and A. S. R. Manstead, "Behavioural characteristics and involvement in different types of traffic accident," *Accident Analysis & Prevention*, vol. 27, no. 4, pp. 571–581, 1995.

[7] R. West and J. Hall, "The role of personality and attitudes in traffic accident risk," *Applied Psychology*, vol. 46, no. 3, pp. 253–264, 1997.

[8] M. L. Meadows, S. G. Stradling, and S. Lawson, "The role of social deviance and violations in predicting road traffic accidents in a sample of young offenders," *British Journal of Psychology*, vol. 89, no. 3, pp. 417–431, 1998.

[9] A. T. McCartt, V. I. Shabanova, and W. A. Leaf, "Driving experience, crashes and traffic citations of teenage beginning drivers," *Accident Analysis & Prevention*, vol. 35, no. 3, pp. 311–320, 2003.

[10] Q. N. La, A. H. Lee, L. B. Meuleners, and D. Van Duong, "Prevalence and factors associated with road traffic crash among taxi drivers in Hanoi, Vietnam," *Accident Analysis & Prevention*, vol. 50, pp. 451–455, 2013.

[11] L. Mallia, L. Lazuras, C. Violani, and F. Lucidi, "Crash risk and aberrant driving behaviors among bus drivers: the role of personality and attitudes towards traffic safety," *Accident Analysis & Prevention*, vol. 79, pp. 145–151, 2015.

[12] Q. N. La, D. V. Duong, A. H. Lee, and L. B. Meuleners, "Factors underlying bus-related crashes in Hanoi, Vietnam," *Transportation Research Part F: Traffic Psychology and Behaviour*, vol. 46, pp. 426–437, 2017.

[13] S. Kaplan and C. G. Prato, "Risk factors associated with bus accident severity in the United States: a generalized ordered logit model," *Journal of Safety Research*, vol. 43, no. 3, pp. 171–180, 2012.

[14] S. Choi, C. Oh, and M. Kim, "Risk factors related to fatal truck crashes on Korean freeways," *Traffic Injury Prevention*, vol. 15, no. 1, pp. 73–80, 2014.

[15] K. Goh, G. Currie, M. Sarvi, and D. Logan, "Factors affecting the probability of bus drivers being at-fault in bus-involved accidents," *Accident Analysis & Prevention*, vol. 66, pp. 20–26, 2014.

[16] S. Feng, Z. Li, Y. Ci, and G. Zhang, "Risk factors affecting fatal bus accident severity: their impact on different types of bus drivers," *Accident Analysis & Prevention*, vol. 86, pp. 29–39, 2016.

[17] R. Tay and J. Choi, "Factors associated with crashes involving taxi owners and non-owners: a case of moral hazard and adverse selection?" *Accident Analysis & Prevention*, vol. 87, pp. 78–82, 2016.

[18] Z. Zheng, P. Lu, and B. Lantz, "Commercial truck crash injury severity analysis using gradient boosting data mining model," *Journal of Safety Research*, vol. 65, pp. 115–124, 2018.

[19] F. Chen and S. Chen, "Injury severities of truck drivers in single- and multi-vehicle accidents on rural highways," *Accident Analysis & Prevention*, vol. 43, no. 5, pp. 1677–1688, 2011.

[20] C. Ma, D. Yang, J. Zhou, Z. Feng, and Q. Yuan, "Risk riding behaviors of urban e-bikes: a literature review," *International Journal of Environmental Research and Public Health*, vol. 16, no. 13, p. 2308, 2019.

[21] H.-C. Park, D.-K. Kim, S.-Y. Kho, and P. Y. Park, "Cross-classified multilevel models for severity of commercial motor vehicle crashes considering heterogeneity among companies and regions," *Accident Analysis & Prevention*, vol. 106, pp. 305–314, 2017.

[22] J. Zhang, J. Lindsay, K. Clarke, G. Robbins, and Y. Mao, "Factors affecting the severity of motor vehicle traffic crashes involving elderly drivers in Ontario," *Accident Analysis & Prevention*, vol. 32, no. 1, pp. 117–125, 2000.

[23] R. Harb, E. Radwan, X. Yan, A. Pande, and M. Abdel-Aty, "Freeway work-zone crash analysis and risk identification using multiple and conditional logistic regression," *Journal of Transportation Engineering*, vol. 134, no. 5, pp. 203–214, 2008.

[24] H. Chen, L. Cao, and D. B. Logan, "Analysis of risk factors affecting the severity of intersection crashes by logistic regression," *Traffic Injury Prevention*, vol. 13, no. 3, pp. 300–307, 2012.

[25] M. Sarrias, "Discrete choice models with random parameters in R: the Rchoice Package," *Journal of Statistical Software*, vol. 74, no. 10, pp. 1–31, 2016.

[26] P. T. Savolainen, F. L. Mannering, D. Lord, and M. A. Quddus, "The statistical analysis of highway crash-injury severities: a review and assessment of methodological alternatives," *Accident Analysis & Prevention*, vol. 43, no. 5, pp. 1666–1676, 2011.

[27] F. Chen, M. Song, and X. Ma, "Investigation on the injury severity of drivers in rear-end collisions between cars using a random parameters bivariate ordered probit model," *International Journal of Environmental Research and Public Health*, vol. 16, no. 14, p. 2632, 2019.

[28] J. Weng, X. Gan, and J. Chen, "A separate analysis of crash frequency for the highways involving traffic hazards and involving no traffic hazards," *Journal of Transportation Safety & Security*, pp. 1–20, 2019.

[29] J. Weng, X. Gan, and G. Du, "Random coefficient models for work zone headway distribution," *Journal of Transportation Engineering, Part A: Systems*, vol. 145, no. 10, Article ID 04019042, 2019.

[30] B. Dong, X. Ma, F. Chen, and S. Chen, "Investigating the differences of single-vehicle and multivehicle accident probability using mixed logit model," *Journal of Advanced Transportation*, vol. 2018, Article ID 2702360, 9 pages, 2018.

[31] F. Chen, S. Chen, and X. Ma, "Analysis of hourly crash likelihood using unbalanced panel data mixed logit model and real-time driving environmental big data," *Journal of Safety Research*, vol. 65, pp. 153–159, 2018.

[32] C. Ma, W. Hao, W. Xiang, and W. Yan, "The impact of aggressive driving behavior on driver-injury severity at highway-rail grade crossings accidents," *Journal of Advanced Transportation*, vol. 2018, Article ID 9841498, 10 pages, 2018.

[33] J. Weng, G. Du, D. Li, and Y. Yu, "Time-varying mixed logit model for vehicle merging behavior in work zone merging areas," *Accident Analysis & Prevention*, vol. 117, pp. 328–339, 2018.

[34] D. A. Hensher and W. H. Greene, "The mixed logit model: the state of practice," *Transportation*, vol. 30, no. 2, pp. 133–176, 2003.

[35] C. R. Bhat, "Simulation estimation of mixed discrete choice models using randomized and scrambled Halton sequences," *Transportation Research Part B: Methodological*, vol. 37, no. 9, pp. 837–855, 2003.

[36] J. C. Milton, V. N. Shankar, and F. L. Mannering, "Highway accident severities and the mixed logit model: an exploratory empirical analysis," *Accident Analysis & Prevention*, vol. 40, no. 1, pp. 260–266, 2008.

[37] K. E. Train, *Discrete Choice Methods with Simulation*, Cambridge University Press, Cambridge, UK, 2009.

[38] S. Lyman, S. A. Ferguson, E. R. Braver, and A. F. Williams, "Older driver involvements in police reported crashes and fatal crashes: trends and projections," *Injury Prevention*, vol. 8, no. 2, pp. 116–120, 2002.

[39] F. Valent, F. Schiava, C. Savonitto, T. Gallo, S. Brusaferro, and F. Barbone, "Risk factors for fatal road traffic accidents in Udine, Italy," *Accident Analysis & Prevention*, vol. 34, no. 1, pp. 71–84, 2002.

[40] D. R. Mayhew, H. M. Simpson, and S. A. Ferguson, "Collisions involving senior drivers: high-risk conditions and locations," *Traffic Injury Prevention*, vol. 7, no. 2, pp. 117–124, 2006.

[41] X. Yan and E. Radwan, "Analyses of rear-end crashes based on classification tree models," *Traffic Injury Prevention*, vol. 7, no. 3, pp. 276–282, 2006.

[42] K. A. Braitman, B. B. Kirley, S. Ferguson, and N. K. Chaudhary, "Factors leading to older drivers' intersection crashes," *Traffic Injury Prevention*, vol. 8, no. 3, pp. 267–274, 2007.

[43] A. Theofilatos, D. Graham, and G. Yannis, "Factors affecting accident severity inside and outside urban areas in Greece," *Traffic Injury Prevention*, vol. 13, no. 5, pp. 458–467, 2012.

[44] K. Ball, C. Owsley, M. E. Sloane, D. L. Roenker, and J. R. Bruni, "Visual attention problems as a predictor of vehicle crashes in older drivers," *Investigative Ophthalmology & Visual Science*, vol. 34, no. 11, pp. 3110–3123, 1993.

[45] K. Ball, C. Owsley, B. Stalvey, D. L. Roenker, M. E. Sloane, and M. Graves, "Driving avoidance and functional impairment in older drivers," *Accident Analysis & Prevention*, vol. 30, no. 3, pp. 313–322, 1998.

[46] C. Owsley, K. Ball, G. McGwin Jr et al., "Visual processing impairment and risk of motor vehicle crash among older adults," *Jama*, vol. 279, no. 14, pp. 1083–1088, 1998.

[47] L. Evans and P. Wasielewski, "Do accident-involved drivers exhibit riskier everyday driving behavior?" *Accident Analysis & Prevention*, vol. 14, no. 1, pp. 57–64, 1982.

[48] P. J. Cooper, "The relationship between speeding behaviour (as measured by violation convictions) and crash involvement," *Journal of Safety Research*, vol. 28, no. 2, pp. 83–95, 1997.

[49] G. Zhang, K. K. W. Yau, and G. Chen, "Risk factors associated with traffic violations and accident severity in China," *Accident Analysis & Prevention*, vol. 59, pp. 18–25, 2013.

[50] R. Factor, "The effect of traffic tickets on road traffic crashes," *Accident Analysis & Prevention*, vol. 64, pp. 86–91, 2014.

[51] G. Maycock, C. R. Lockwood, and J. Lester, *The Accident Liability of Car Drivers*, Transport and Road Research Laboratory, Wokingham, UK, 1991.

[52] P. J. Cooper, M. Pinili, and W. Chen, "An examination of the crash involvement rates of novice drivers aged 16 to 55," *Accident Analysis & Prevention*, vol. 27, no. 1, pp. 89–104, 1995.

[53] D. D. Clarke, P. Ward, C. Bartle, and W. Truman, "Young driver accidents in the UK: the influence of age, experience, and time of day," *Accident Analysis & Prevention*, vol. 38, no. 5, pp. 871–878, 2006.

[54] P. Konstantopoulos, P. Chapman, and D. Crundall, "Driver's visual attention as a function of driving experience and visibility. using a driving simulator to explore drivers' eye movements in day, night and rain driving," *Accident Analysis & Prevention*, vol. 42, no. 3, pp. 827–834, 2010.

[55] T. M. Corsi and P. Fanara Jr., "Driver management policies and motor carier safety," *Logistics and Transportation Review*, vol. 24, no. 2, p. 153, 1988.

[56] L. Staplin and K. W. Gish, "Job change rate as a crash predictor for interstate truck drivers," *Accident Analysis & Prevention*, vol. 37, no. 6, pp. 1035–1039, 2005.

[57] M. C. Mejza, R. E. Barnard, T. M. Corsi, and T. Keane, "Driver management practices of motor carriers with high compliance and safety performance," *Transportation Journal*, vol. 42, no. 4, pp. 16–29, 2003.

Hindawi
Journal of Advanced Transportation
Volume 2020, Article ID 5215479, 11 pages
https://doi.org/10.1155/2020/5215479

Research Article

Model of Driver's Eye Movement and ECG Index under Tunnel Environment Based on Spatiotemporal Data

Weiwei Qi[1], **Bin Shen**[1] **and Linhong Wang**[2]

[1]*School of Civil Engineering and Transportation, South China University of Technology, Guangzhou, Guangdong 510641, China*
[2]*School of Transportation, Jilin University, Changchun, Jilin 130012, China*

Correspondence should be addressed to Linhong Wang; wanghonglin0520@126.com

Received 17 October 2019; Revised 7 December 2019; Accepted 18 January 2020; Published 17 February 2020

Academic Editor: Jaeyoung Lee

In order to improve the driver's physiological and psychological state, the driver's mental load which is caused by sight distance, lighting, and other factors in the tunnel environment should be quantified via modeling the spatiotemporal data. The experimental schemes have been scientifically designed based on methods of traffic engineering and human factor engineering, which aims to test the driver's spatiotemporal data of eye movement and ECG (electrocardiogram) index in the tunnel environment. Firstly, the changes in the driver's spatiotemporal data are analyzed to judge the changing trend of the driver's workload in the tunnel environment. The results show that the cubic spline interpolation function model can fit the dynamic changes of average pupil diameter and heart rate (HR) growth rate well, and the goodness of fit for the model group is above 0.95. So, tunnel environment makes the driver's typical physiological indicators fluctuate in the coordinates of time and space, which can be modeled and quantified. Secondly, in order to analyze the classification of tunnel risk level, a fusion model has been built based on the functions of average pupil diameter and HR growth rate. The tunnel environmental risk level has been divided into four levels via the fusion model, which can provide a guidance for the classification of tunnel risk level. Furthermore, the fusion model allows tunnel design and construction personnel to adopt different safety design measures for different risk levels, and this method can effectively improve the economy of tunnel operating safety design.

1. Introduction

Tunnel is a typical bad visual environment, and driving in tunnel environment is a relatively dangerous activity. Amundsen and Ranes analyzed the traffic accident data in Norway and pointed out that the accident severity in the tunnel is higher than that in the highway [1]. A survey from Italy shows that severe accident rates and cost rates in tunnels were higher than those on the corresponding motorways [2]. Driving performance in tunnels is different from freeway driving, and darker lighting conditions and enclosed space will make drivers nervous and increase the effort required to maintain lateral control of the vehicle, which will affect drivers' psychological state and driving behavior [3, 4]. Related research shows that visual intervention is an effective method in vehicle trajectories' intervention [5, 6], and the tunnel safety can be improved by using visual intervention method to affect the driver's driving behavior in tunnel section. Therefore, it is of practical significance to study the driver's physiological and psychological state in tunnel environment, which reduces the accident rate in tunnel environment.

There are many factors that affect the safety of tunnel driving: road alignment, transition of antisliding performance, traffic states, and differences in internal and external environments [7]. In recent years, scholars have carried out lots of research about the highway traffic safety to improve the driving safety, especially for the tunnel environment [8, 9]. Manser and Hancock studied how the type of visual pattern and presence of texture applied to transportation tunnel walls differentially affected driving performance based on simulated driving experiment [10]. Meng et al. proposed a novel quantitative risk assessment model to assess the risks in the nonhomogeneous urban road tunnels

in 2011, and the inverse Gaussian regression model had been used to estimate the rear-end vehicle crash frequency in road tunnels; then the relationship between the time to collision and its contributing factors had been establish in 2012 [11–13]. Calvi and D'Amico analyzed the driver's speed characteristics and speed control in tunnel environment based on simulated driving [14]. Rudin-Brown et al. explored the influence of mobile phone use on driving safety in the tunnel based on the method of simulated driving [15]. Kircher and Ahlstrom investigated the impact of tunnel illumination and design on driving performance; then Kircher and Ahlstrom discovered that the driver's attention had a higher impact on performance than tunnel design [16]. Moretti et al. proposed a life-cycle cost analysis method to maximize energy saving and road safety via LED (Light-Emitting Diode) technology [17, 18].

Scientific research on the driver's physiology and psychology began in the early nineteenth century. In recent years, with the improvement of medical research and the use of advanced instruments, scholars have continuously explored the integration of physiology and traffic engineering [19, 20]. Many scholars have studied the physiological and psychological characteristics of drivers in tunnel environment, which can provide experience for the selection of indicators and data analysis in this paper. Cho et al. calibrated the threshold of illumination intensity in tunnels based on the driver's visual characteristics [21]. He et al. recorded the eye movement parameters of drivers passing through the tunnel and analyzed the influence of tunnel lighting environment on driving safety [22]. Feng et al. studied changes in physiological and behavioral characteristics in longitudinal segments of urban underpass tunnels by conducting a real-vehicle experiment [23]. Kening et al. conducted the real-vehicle experiment with participants under different tunnels, in order to study the driver mental workload variation in exit of super long tunnel on expressway [24]. Chen et al. carried out a driving simulator experiment based on a box truck module, in order to investigate the safety of the truck under crosswind at the bridge-tunnel section [25]. It can be seen that eye movement index, electrocardiogram index, electroencephalogram index, workload, and mental load are commonly used by scholars [26, 27]. Because the tunnel environment mainly affects the driver's vision and the enclosed space will bring tension and anxiety, this paper mainly chooses two indicators of eye movement and electrocardiogram.

At present, the research of the driver safety in tunnel environment mainly focuses on the analysis of the driver's speed, vision, and ECG characteristics in tunnel environment. On the basis of scientific experiment design and data acquisition, scholars use statistical methods to analyze the distribution of the driver's physiological and psychological indicators in tunnel environment, which provides a reference for the experimental design and statistical analysis of this paper. However, the existing research cannot reflect the temporal and spatial distribution of drivers' physiological and psychological state in tunnel environment and cannot evaluate the risk level of different road section in tunnel environment. Thus, this paper aims to explore the spatiotemporal distribution of driver's physiological and psychological indicators and study the classification of the risk level in tunnel environment. Firstly, the driver's spatiotemporal data of eye movement and ECG index are tested in the tunnel environment. Secondly, models of average pupil diameter and HR growth rate change trend are constructed in different spatial nodes of tunnel. Lastly, a classification model of tunnel risk level is constructed to effectively evaluate the risk level of different road sections in tunnel environment.

The remainder of this paper is organized as follows. Section 2 describes the methodology of the simulated driving experiment. Section 3 gives some experimental results for eye movement characteristics and ECG index. Then, models of the driver's average pupil diameter and HR rate are illustrated in Section 4, and the classification model of tunnel risk level is also achieved. Finally, this paper ends with some conclusions in Section 5.

2. Method

2.1. Participant. A total of 31 participants participated in the experiment; all drivers who are involved in the test hold a driver license and already have driving experience in the tunnel. Due to the age and gender of the test subjects' unbalanced distribution, the driver's age and gender differences are ignored during the process of data analysis.

2.2. Experimental Equipment and Scenario. The main experimental equipment of this experiment is as shown in Figure 1, including the six-degree-of-freedom traffic safety simulation driving device for constructing the simulated driving environment, MP36R physiological tester for collecting the driver's ECG index, SMI wireless glasses for collecting the driver's eye movement index, and other related auxiliary equipment, such as laptops, timers, etc.

The objective of this study is to investigate the temporal and spatial distribution of drivers' physiological and psychological indicators in tunnels. To this end, a common section of highway was designed according to the Technical Standard of Highway Engineering (2014). The test scenes are based on the two-lane straight highway with design speed of 80 km/h. The cross section of the highway comprises two 3.75-meter-wide lanes and two 2.5-meter-wide shoulders. The total length of the highway is 10.1 km, including 3 tunnels, of which, each tunnel is 700 m long, and the interval between the two adjacent tunnels is 2 km (Figure 2). To ensure that the simulated environment is consistent with the real highway environment, there was some simulated vehicles moving in the same direction as the test vehicle, so that the traffic conditions are free-flow during the simulation. Trees, vertical speed limit signs, and traffic barriers were also added in the roadside to ensure drivers have the same feeling as real highway environment when driving in the test scenes.

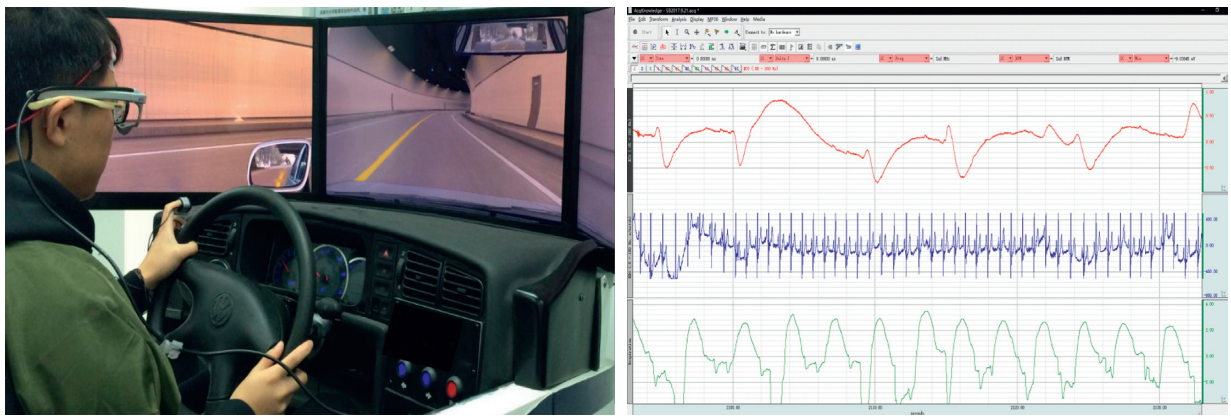

Figure 1: Main test equipment and data analysis interface.

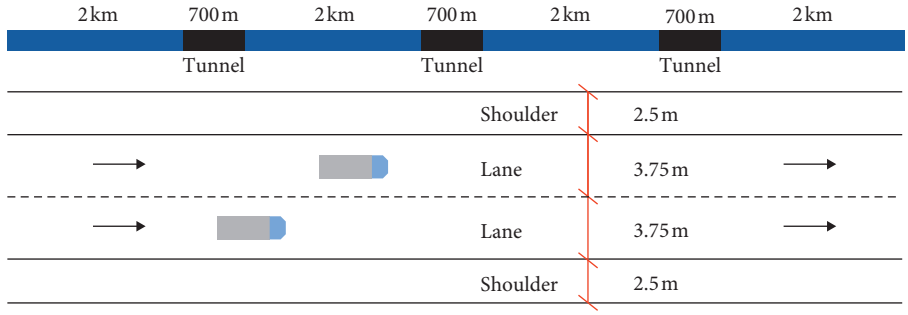

Figure 2: Experimental road conditions.

2.3. Experimental Procedure. The experiment has been carried out according to the following steps:

Step 1. The time of the experimental equipment has been checked to ensure that the time of all equipment is unified, and then a preliminary experiment has been conducted to ensure the reliability of the whole experiment.

Step 2. The SMI wireless glasses and the physiological instrument have been worn and calibrated for the test drivers. Then, the drivers have one hour to operate the driving stimulation to ensure the reliability of experimental data, so that drivers' strangeness on the simulated driving platform can be eliminated.

Step 3. The official experiment has been carried out, drivers in the test run normally according to the experimental design route, and the start time of the vehicle was used as the time base point to record the arrival and departure time of the driver in each tunnel section.

Step 4. The experimental data has been saved and the validity of the data has been checked after the experiment. Then, all the drivers completed the experiment according to the process strictly.

2.4. Data Collection. According to the experimental results, eye movement and ECG data of different drivers fluctuates greatly when the driver passes the first tunnel and the third tunnel, due to that different drivers have different adaptability to the simulated driving scenario. Some drivers have not adapted to the simulated driving platform fully during the first tunnel, and some drivers have adapted to the environmental parameters of the tunnel during the third tunnel. Therefore, the following research is based on the eye movement and ECG data of the second tunnel.

According to the switching time of the experimental scene recorded by the experimenter, the eye movement data analysis software can directly derive the fixation duration, the average pupil diameter, the blink duration, et al. Part of the eye movement data during the second tunnel is shown in Table 1.

Similar to eye movement data, the heart rate (HR) value during the second tunnel can be directly derived from the physiological data analysis software. Because of the individual differences between drivers, simply analyzing for the HR values is likely to cause large errors. Therefore, this paper uses the driver's HR growth rate for analysis and modeling. The calculation formula for heart rate indicators is shown in (1); the HR value and HR growth rate data is shown in Table 2.

$$N_i = \frac{n_i - n_p}{n_p} \times 100\%. \quad (1)$$

In this formula, N_i indicates the driver's heart rate at a certain moment, n_i indicates the HR value of the driver at a certain moment, and n_p indicates the average HR value of the driver in a calm state.

Table 1: Eye movement data during the second tunnel.

Item	Fixation duration (ms)	Average pupil diameter (mm)	Blink duration (ms)	...	Average pupil size (px) X	Average pupil size (px) Y	Dispersion Y
1	199	4.9	99		82	67.5	12
2	98	3.4	166		70.7	47.7	3
3	232	3.2	129		72.1	47.1	27
4	66	3.3	365		69	48	2
5	66	3.4	199		72	47.5	5
...							

Table 2: Data of the HR value and HR growth rate.

	Participant 1		Participant 2		...	Participant 31	
	Heart rate	HR growth rate	Heart rate	HR growth rate		Heart rate	HR growth rate
1	103.448	0.293	85.714	0.143		90.634	0.208
2	101.351	0.267	87.977	0.173		88.757	0.183
3	100.334	0.254	84.746	0.130		87.719	0.170
4	99.338	0.242	79.576	0.061		81.967	0.093
...							

3. Results

3.1. Analysis of Eye Movement Characteristics. As shown in Table 3, the eye movement data of the driver in the tunnel environment is counted within a time window of 30 s. By comparing the driving concentration and mental load of drivers in the tunnel and normal driving environment, it is found that the number of blinks of the driver in the tunnel is significantly smaller than the number of blinks in the normal environment ($P < 0.05$), and the average blink time in the tunnel (306.93 ms) is also smaller than the average blink time in the normal environment (323.87 ms), which indicates that drivers are more attentive and have a higher mental load in the tunnels due to the dim light and poor visual distance. In addition, the numbers of gazes and scans in the tunnel are significantly less than those of driving in normal situations ($P < 0.01$), while the average gaze time is higher than normal (219.60 ms). There is no significant difference in average scan time between the two groups (the tunnel is 79.79 ms, normal 80.24 ms), which indicates that the driving environment in the tunnel is more monotonous than in the normal environment [22], and drivers need to observe the surroundings more frequently in the normal environment than in the tunnel environment, and their sight will move more frequently.

The pupil diameter is an important indicator of the driver's sensitivity to light source [22]. The size of the pupil is affected by the illuminance: the larger the illuminance value, the smaller the pupil diameter. The average pupil diameter data is selected from the 60 s before entering the tunnel to the 60 s after leaving the tunnel. The result is shown in Figure 3.

According to Figure 3, drivers need to be more focused in the tunnel because of the poor sight, and the pupil diameter is larger than the pupil diameter in the normal environment. During the process of entering tunnel, the diameter of the driver's pupil shows a trend of gradual increase. The driver's concentration and mental load are increasing. During the process of leaving the tunnel, the diameter of the driver's pupil shows a trend of sharp decrease due to the sudden increase of light. At the same time, the driver's line of sight is severely obstructed, and appropriate measures (such as reducing the speed) are needed to prevent accidents. After leaving the tunnel, the diameter of the driver's pupil gradually rises and returns to the normal level.

Table 3: Analysis of the driver's eye movement data in the tunnel environment.

Items		Mean	Sd	T	P
Blink count	Tunnel	12.00	7.979	−2.10	0.049
	Freeway	22.29	10.193		
Blink duration average (ms)	Tunnel	306.93	106.464	−0.39	0.706
	Freeway	323.87	41.923		
Fixation count	Tunnel	37.86	11.423	−5.73	0.000
	Freeway	72.86	11.452		
Fixation duration average (ms)	Tunnel	227.51	103.510	0.18	0.864
	Freeway	219.60	59.490		
Saccade count	Tunnel	36.00	14.900	−3.81	0.003
	Freeway	71.14	19.308		
Saccade duration average (ms)	Tunnel	79.79	4.591	−0.16	0.875
	Freeway	80.24	5.930		

3.2. Analysis of Driver's ECG Index in the Tunnel Environment

3.2.1. The Driver's HR Growth Rate. The HR growth rate from the 60 s before entering the tunnel to the 60 s after leaving the tunnel is selected as the analysis data. The result is shown in Figure 4.

Previous studies have shown that the change in heart rate is a direct reflection of the driver's psychological tension. The changes of HR growth rate indicate that the driver's psychological tension is tight, which will lead to the driver's misjudgment and misoperation, thus causing traffic accidents. From Figure 4, we can see that the driver's HR growth rate increases in the tunnel section ranging from 12% to 27%; the HR growth rate in the normal section is maintained at a relatively stable level. When the driver begins to enter

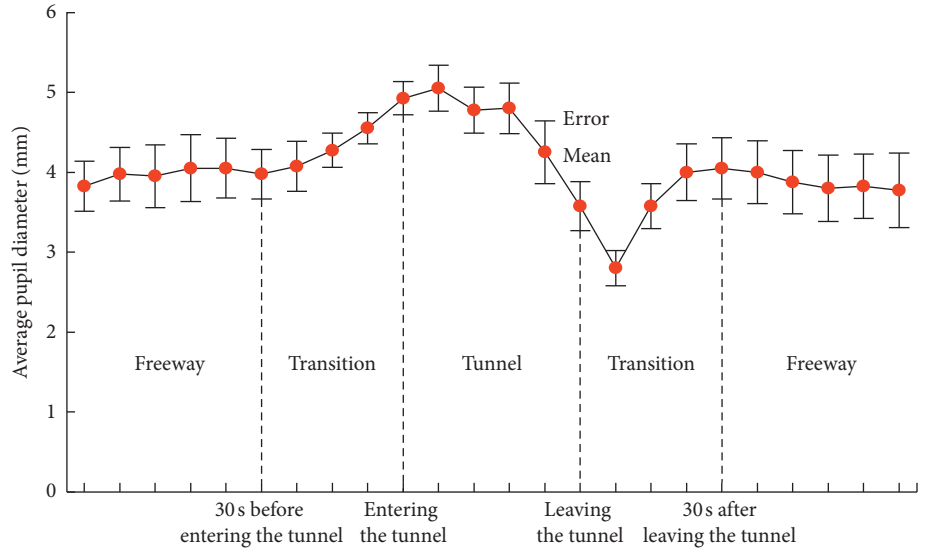

Figure 3: Changes in average pupil diameter during driving through a tunnel.

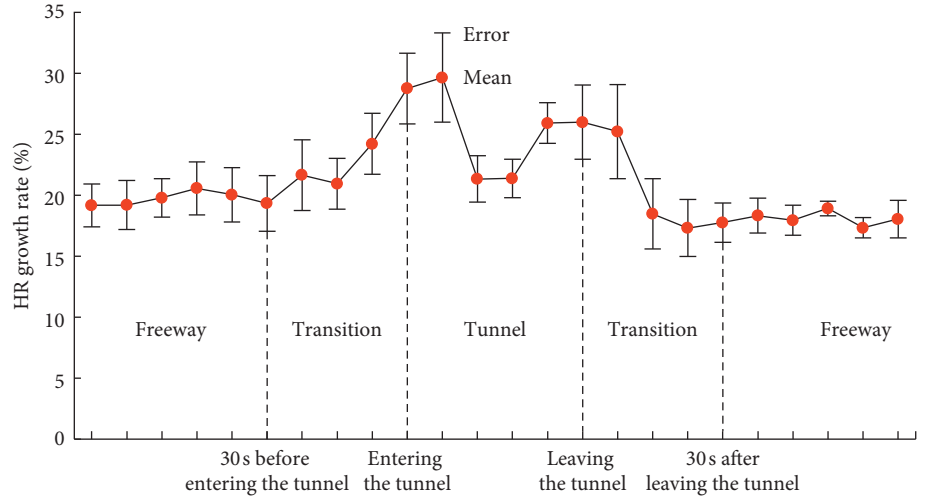

Figure 4: Changes of HR growth rate during driving through a tunnel.

the tunnel, the driver's HR growth rate increases. The driver's heart rate is maintained at a certain level in the tunnel. When the driver is about to leave the tunnel, the driver's heart rate rises. As the vehicle leaves the tunnel, the driver's heart rate gradually returns to a stable value. It is worth noting that the driver's heart rate does not suddenly become stable after entering the tunnel; it is a gradual process. The main reason for the change in the driver's heart rate during the process of passing the tunnel is the sudden change of sight distance and lighting conditions. After vehicle enters the tunnel, the driver gradually adapts to the sight distance and lighting conditions inside the tunnel, so the driver's heart rate gradually changes to a stable level.

3.2.2. Heart Rate Variability. HRV (heart rate variability) is a method that has been widely used in the academic literature. It reflects the state of ANS (autonomic nervous system) [28]. It is therefore a good objective tool for assessing emotional responses [29]. There are a number of different measurements which are derived from the interval between heartbeats (RR).

Time-domain analysis of HRV mainly included the following:

(i) MEAN: mean value of the RR intervals

(ii) SDNN: standard deviation of the RR intervals

(iii) RMSSD: root mean square of successive differences

(iv) SDSD: standard deviation of difference between adjacent RR intervals.

Frequency-domain analysis of HRV mainly included the following:

(i) HF: high frequency

(ii) LF: low frequency

(iii) LF/HF: the low frequency and high frequency ratio.

The driver's heart is innervated by both sympathetic and vagal nerves. Under normal conditions, the excitability of vagus nerve is dominant. Under fatigue, excitation, and tension, sympathetic nerve is dominant. In terms of time-domain index, according to the data in Table 3, the average MEAN of RR interval of drivers decreases after entering the tunnel section; that is, the number of inner jumps of drivers in the tunnel section increases, which indicates that drivers have a certain degree of tension because of the bad visual distance. In the tunnel section, the SDNN index value of drivers increased, which indicates that the sympathetic nerve activity increases, the parasympathetic nerve activity decreases, and the mental load increases. The trend of RMSSD and SDSD is the same as that of SDNN. After entering the tunnel, drivers are affected by bad sight distance and the index values increases.

In terms of frequency-domain indicators, according to the data in Table 4, after the driver entered the tunnel section, the driver's LF value increases and the HF value decreases due to the deterioration of the driving environment, indicating that the driver's vagus nerve activity is weakened during this process, sympathetic activity is enhanced, the driver's mental condition is increasingly unstable, and physiological indicators vary greatly. On the one hand, because the visibility of the road is low in this environment, the driver's line of sight is smaller than the safe distance of the vehicle, and the driver needs to constantly adjust the speed and the nerves are tight. On the other hand, in order to prevent the driver from colliding with other vehicles, it is necessary to concentrate, and therefore the tunnel conditions have greater mental stress on the driver.

4. Modeling

4.1. Driver's Average Pupil Diameter Modeling. The tunnel environment has a significant impact on the driver's eye movement and ECG indicators. In order to quantify the trend of this influence, the variation of the average pupil diameter has been obtained by the interpolation method. First, a certain number of data points are selected from the driving process from 30 seconds before entering the tunnel to 30 seconds after leaving the tunnel. Then the interpolation function of the driving process is obtained by using cubic spline interpolation method, and the function $f(x)$ is drawn with the help of MATLAB, as shown in Figure 5(a). According to the different functional areas of the tunnel, the function is divided into three stages: before entering the tunnel (f_1), inside the tunnel (f_2), and after leaving the tunnel (f_3); time axes of functions f_1 and f_2 are coordinate origins at the start of entering the tunnel, and the time axis of function f_3 is coordinate origins at the start of leaving the tunnel.

The fitted models are shown in (2)–(4). The R-square and RMSE of each model are shown in Table 5. The results of the cubic spline interpolation function fitting of each model are shown in Figures 5(b)–5(d). According to Table 4 and Figure 5, it can be clearly seen that the R-square value of the model is greater than 0.95, and the RMSE values are all less than 0.1, which satisfies the accuracy requirements in statistics, indicating that the goodness of fit of each model is higher.

Table 4: Time- and frequency-domain indicators of the driver's heart rate variability.

Items	Freeway		Tunnel	
	Mean	Sd	Mean	Sd
MEAN	0.732	0.116	0.683	0.112
SDNN	0.052	0.043	0.067	0.076
RMSSD	0.062	0.092	0.082	0.101
SDSD	0.037	0.050	0.065	0.087
HF	0.821	0.095	0.797	0.078
LF	0.179	0.090	0.206	0.078
LF/HF	0.218	0.156	0.258	1.580

$$f_1(x) = 0.000757x^2 + 0.05438x + 4.917, \tag{2}$$

$$f_2(x) = 1.989\exp\left(-\left(\frac{x-0.5788}{8.871}\right)^2\right) + 4.802\exp\left(-\left(\frac{x-20.14}{28.89}\right)^2\right), \tag{3}$$

$$f_3(x) = 3.488 - 0.3046\cos(0.1751x) - 0.5425\sin(0.1751x). \tag{4}$$

4.2. Driver's HR Growth Rate Modeling. According to the ideas in part 4.1, the variation of the average pupil diameter has been obtained by the interpolation method, and the function $g(x)$ is drawn with the help of MATLAB as shown in Figure 6(a). According to the different functional areas of the tunnel, the image is divided into three stages: before entering the tunnel (g_1), inside the tunnel (g_2), and after leaving the tunnel (g_3). The fitting model of the driver's HR growth rate in different functional sections of the tunnel is shown in (5)–(7). The R-square and RMSE of each model are shown in Table 6; the results of the cubic spline interpolation function fitting of each model are shown in Figures 6(b)–6(d). According to Table 6 and Figure 6, it can be clearly seen that the R-square value of the model is greater than 0.99, and the RMSE values are all less than 0.5, which satisfies the accuracy requirements in statistics, indicating that the goodness of fit of each model is higher.

$$g_1(x) = 28.18\exp\left(-\left(\frac{x-5.366}{24.84}\right)^2\right) + 13.76\exp\left(-\left(\frac{x+27.06}{11.38}\right)^2\right), \tag{5}$$

$$g_2(x) = -0.0001704x^4 + 0.01292x^3 - 0.2877x^2 + 1.432x + 27.98, \tag{6}$$

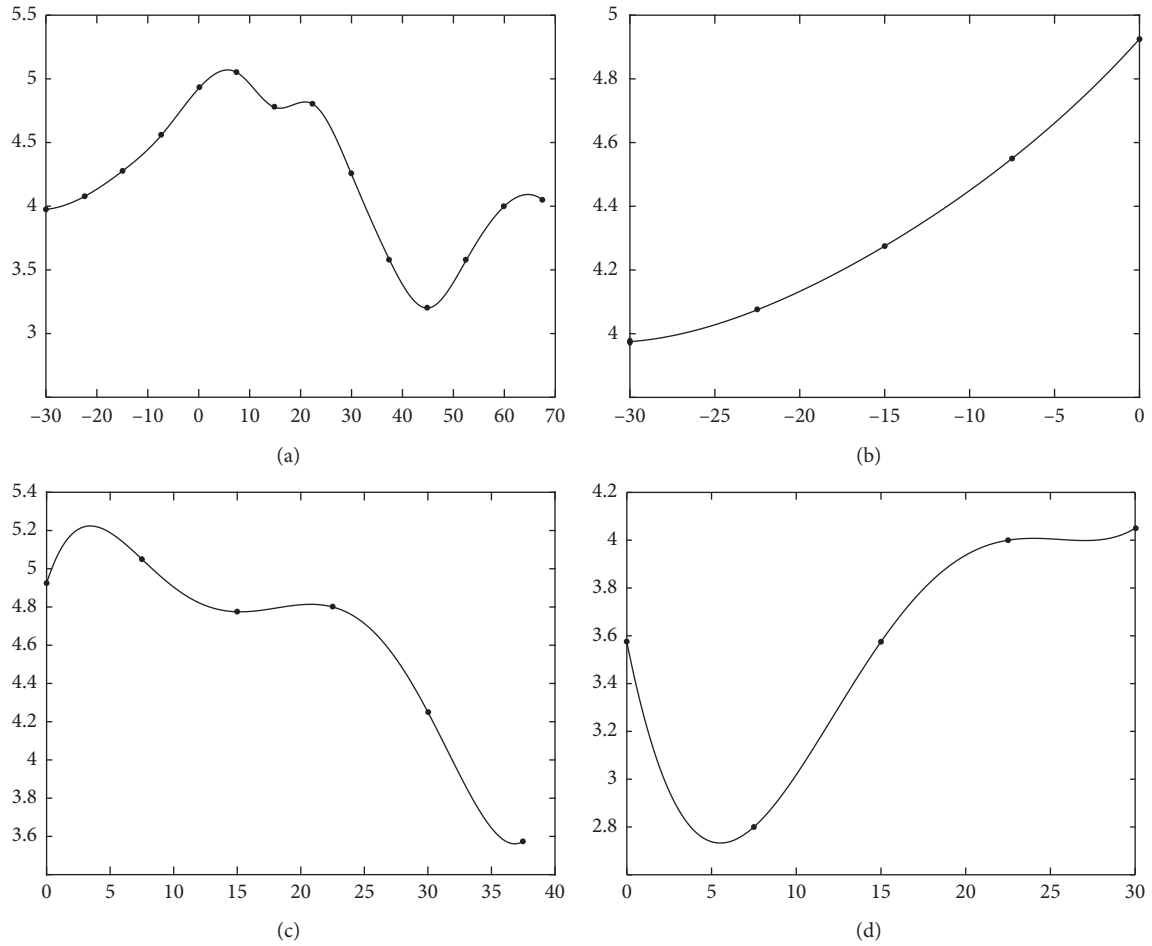

Figure 5: Piecewise cubic spline interpolation function model of average pupil diameter. (a) Piecewise cubic spline interpolation function. (b) Function f_1 fitting. (c) Function f_2 fitting. (d) Function f_3 fitting.

Table 5: Evaluation index of the driver's average pupil diameter fitting model in tunnel environment.

Evaluation index	f_1	f_2	f_3
R-square	0.9999	0.9928	0.9578
RMSE	0.002563	0.04015	0.09991

$$g_3(x) = -1.985e+04 \exp\left(-\left(\frac{x-14.1}{17.51}\right)^2\right) + 1.986e+0.4 \exp\left(-\left(\frac{x-14.09}{17.52}\right)^2\right). \quad (7)$$

4.3. Classification Model of Tunnel Risk Level. Tunnels are typical bad sight distance environments; driving in tunnels is very dangerous and easy to cause traffic accidents. In order to improve the driving safety in the tunnel environment, the tunnel design and construction personnel will optimize the safety of the tunnel, which needs so much of money and so many of material resources. Therefore, it is necessary to establish a classification model of tunnel risk level, which allows tunnel design and construction personnel to adopt different safety design measures for road sections on different risk levels. Tunnel manager can effectively improve the design economics of tunnel environmental safety.

In order to classify the risk level of the tunnel environment, a fusion model $T(x)$ needs to be built based on the functions $f(x)$ and $g(x)$. In the fusion model, $T(x)$ is the risk assessment value of tunnel environments, α is the weight coefficient of the driver's HR growth rate, $(1-\alpha)$ is the weight coefficient of the driver's average pupil diameter, $f'(x)$ is the dimensionless form to $f(x)$, and $g'(x)$ is the dimensionless form to $g(x)$. Then, the fusion model is shown as

$$T(x) = \alpha f'(x) + (1-\alpha) g'(x). \quad (8)$$

According to the research results in 4.1 and 4.2, the functions $f(x)$ and $g(x)$ need dimensional standardization. The models for dimensional standardization are shown as

$$f'(x) = \frac{f(x) - f(x)_{\max}}{f(x)_{\max} - f(x)_{\min}}, \qquad g'(x) = \frac{g(x) - g(x)_{\max}}{g(x)_{\max} - g(x)_{\min}}. \quad (9)$$

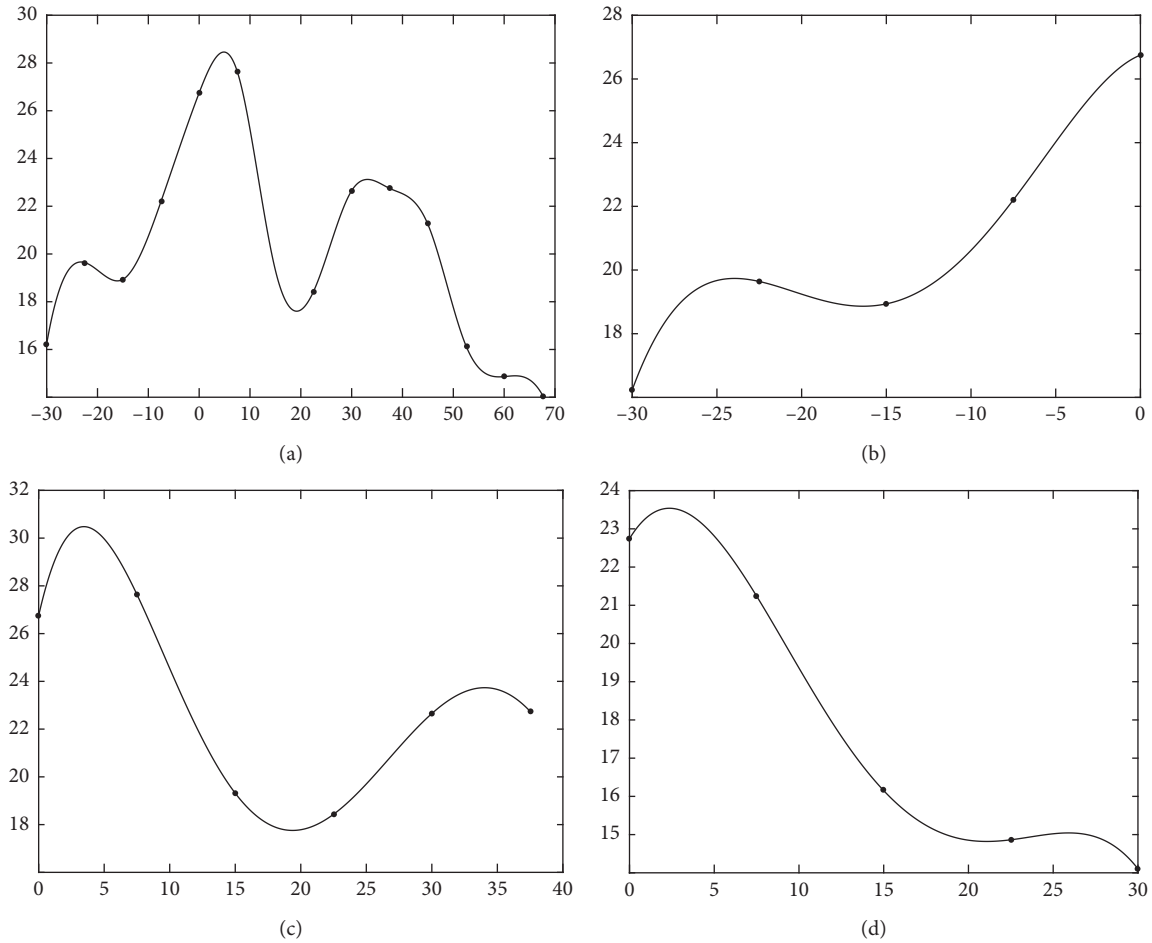

Figure 6: HR growth rate piecewise cubic spline interpolation function model. (a) Piecewise cubic spline interpolation function. (b) Function g_1 fitting. (c) Function g_2 fitting. (d) Function g_3 fitting.

Table 6: Evaluation index of the driver's HR growth rate fitting model in tunnel environment.

Evaluation index	g_1	g_2	g_3
R-square	0.9992	0.991	0.9996
RMSE	0.07524	0.3807	0.06458

Based on (8), T_n is defined to represent the risk assessment value of the common road section without tunnel or bridge, and the time interval (a, b) is defined as the time for driving in the common road section without tunnel or bridge; then T_n can be calculated by

$$T_n = \frac{1}{b-a} \int_a^b T(x)\mathrm{d}x. \tag{10}$$

The determination of the classification criteria of tunnel environmental risk level needs large amounts of traffic accident data, the experimental data that obtained in this study cannot be used to determine the classification criteria accurately, and there is no relevant research that has defined this criterion as well. Thus, for ease of use, the tunnel environmental risk level has been divided into four levels in this study, which are normal state, light danger, moderate danger, and severe danger. So, when the value of $T(x)$ is less than or equal to T_n, tunnel environmental risk level is normal; when the value of $T(x)$ is more than T_n and less than or equal to $1.5T_n$, tunnel environmental risk level is light danger; when the value of $T(x)$ is more than $1.5T_n$ and less than or equal to $2T_n$, tunnel environmental risk level is moderate danger; and when the value of $T(x)$ is more than $2T_n$, tunnel environmental risk level is severe danger. The classification criteria of tunnel environmental risk level are shown in Table 7.

To verify the validity of the classification model, this research selects the road section of 30 seconds before entering the second tunnel to 30 seconds after leaving the second tunnel as the studied area. As there is no relevant research to prove the weight coefficient relationship between the driver's HR growth rate and the average pupil diameter in the tunnel environment at present, this paper takes $\alpha = 0.5$ as an example to study the tunnel environment risk classification. T_n can be calculated according to (10), and $T_n = 0.7495$; the results are shown in Figure 7.

As shown in Figure 7, the tunnel area can be divided into nine road sections according to classification model of tunnel risk level. Among the nine road sections, risk level of

Table 7: Classification criteria of tunnel environmental risk level.

Level	Normal state	Light danger	Moderate danger	Severe danger
Criterion	$T(x) \le T_n$	$T_n < T(x) \le 1.5T_n$	$1.5T_n < T(x) \le 2T_n$	$T(x) > 2T_n$

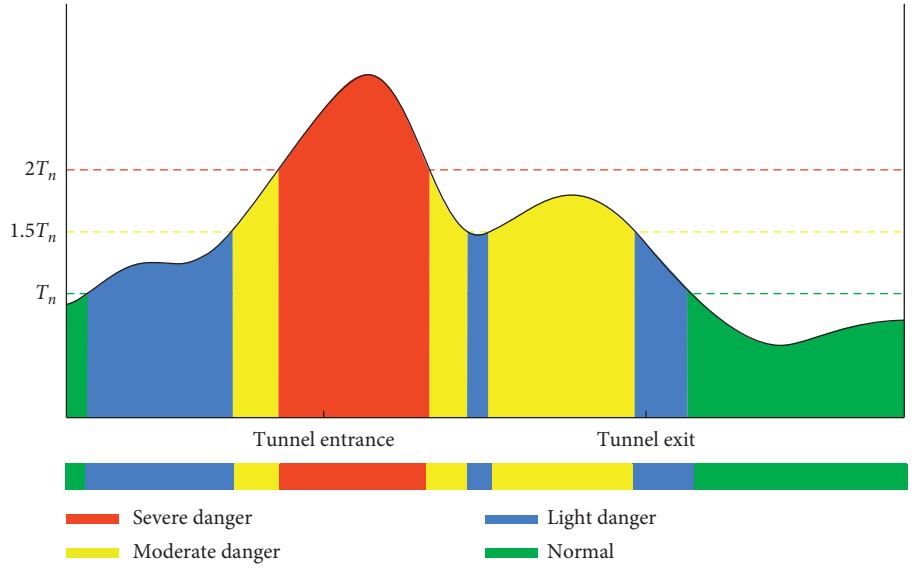

Figure 7: The results of tunnel environment risk level classification.

one road section is severe danger, risk level of three road sections is moderate danger, risk level of three road sections is light danger, and risk level of two road sections is normal. Compared with the total length of the tunnel area that has been studied in this paper, the lengths of road sections at different risk level are 17.8% (severe danger), 27.4% (moderate danger), 27.0% (light danger), and 27.8% (normal). So, if tunnel managers focus on optimizing road sections with risk level of severe danger (17.8%), nearly 82.2% of the construction funds can be saved and the economic benefits in the tunnel construction can be greatly improved.

5. Conclusions

This paper has tested the eye movement and ECG indicators in the tunnel environment and constructed the cubic spline interpolation function modeling. The main conclusions are as follows:

(1) The driver's blinking times and average blinking time in tunnels are lower than the normal level, but the average fixation time is higher than the normal level. In the process of entering the tunnel, the driver's pupil diameter shows a trend of gradual increase, and in the process of leaving the tunnel, the driver's pupil diameter shows a trend of sharp decrease. Results show that the tunnel environment has a significant impact on the driver's eye movement index, with abnormal fluctuations in blinking times, average blinking time, and pupil diameter.

(2) The driver's HR growth rate changes significantly during the tunnel section, which ranges from 12% to 27%. In the process of entering tunnel, the HR growth rate increases continuously and then maintains a relatively stable level in the tunnel. In the process of leaving the tunnel, the HR growth rate begins to decline and gradually returns to normal value. The results show that the tunnel environment also has a significant impact on the driver's heart rate index.

(3) The time-domain and frequency-domain indicators of the driver's heart rate variability fluctuate in varying degrees during driving in tunnels, among which the SDSD index changes obviously, and the maximum fluctuation range is 75.6%, which indicates that the driver's mental load increases greatly in this environment and results in a strong sense of tension, panic, and fatigue.

(4) Based on the statistical analysis of the driver's eye movement and ECG index, the cubic spline interpolation function is introduced to accurately fit the dynamic trend of the driver's physiological index in the 30 s interval before and after entering and exiting the tunnel. The goodness of fit of each model is above 0.95, which indicates that the impact of the tunnel environment on the driver's eye movement and ECG indicators can be quantified and predicted.

(5) A fusion model is constructed based on the models of the driver's average pupil diameter and HR growth rate to classify the risk level of the tunnel environment. According to this fusion model, the risk level of the tunnel environment can be divided into four levels, and the lengths of road sections with different risk level are 17.8% (severe danger), 27.4% (moderate danger), 27.0% (light danger), and 27.8% (normal).

(6) The classification model of tunnel risk level can provide guidance for the classification of tunnel risk level, and tunnel personnel for design and construction can adopt different safety design measures for different risk levels, which can effectively improve the economy of tunnel operating safety design.

Data Availability

The driver's spatiotemporal data of eye movement and ECG (electrocardiogram) index in the tunnel environment that are used to support the findings of this study are currently under embargo, while the research findings are commercialized. Requests for data, 12 months after publication of this article, will be considered by the corresponding author.

Disclosure

The funders played no role in the design of the study or in the collection and interpretation of the data.

Conflicts of Interest

The authors declare no conflicts of interest.

Acknowledgments

This research was funded by the National Natural Science Foundation of China under grants numbers 71701070 and 71971097, the Science and Technology Project of Guangzhou City under grant number 201804010466, the Fundamental Research Funds for the Central Universities under grant number 2019MS120, Jilin Scientific and Technological Development Program under grant number 20180520180JH, and Jilin Education Planning Program under grant number JJKH20180149KJ.

References

[1] F. H. Amundsen and G. Ranes, "Studies on traffic accidents in Norwegian road tunnels," *Tunnelling and Underground Space Technology*, vol. 15, no. 1, pp. 3–11, 2000.

[2] C. Caliendo and M. L. De Guglielmo, "Accident rates in road tunnels and social cost evaluation," *Procedia—Social and Behavioral Sciences*, vol. 53, pp. 166–177, 2012.

[3] A. C. Beall and J. M. Loomis, "Visual control of steering without course information," *Perception*, vol. 25, no. 4, pp. 481–494, 1996.

[4] Y. Li and Y. Chen, "Driver vision based perception-response time prediction and assistance models on mountain highway curve," *International Journal of Environmental Research and Public Health*, vol. 14, no. 1, p. 31, 2016.

[5] G. Wu, F. Chen, X. Pan, M. Xu, and X. Zhu, "Using the visual intervention influence of pavement markings for rutting mitigation-part I: preliminary experiments and field tests," *International Journal of Pavement Engineering*, vol. 20, no. 6, pp. 734–746, 2019.

[6] X. Zhu, Z. Dai, F. Chen, X. Pan, and M. Xu, "Using the visual intervention influence of pavement marking for rutting mitigation II: visual intervention timing based on the finite element simulation," *International Journal of Pavement Engineering*, vol. 20, no. 5, pp. 573–584, 2019.

[7] S. Bassan, "Overview of traffic safety aspects and design in road tunnels," *IATSS Research*, vol. 40, no. 1, pp. 35–46, 2016.

[8] C. Xu, P. Liu, W. Wang, and Z. Li, "Evaluation of the impacts of traffic states on crash risks on freeways," *Accident Analysis & Prevention*, vol. 47, pp. 162–171, 2012.

[9] H. Wen, J. Sun, Q. Zeng, X. Zhang, and Q. Yuan, "The effects of traffic composition on freeway crash frequency by injury severity: a Bayesian multivariate spatial modeling approach," *Journal of Advanced Transportation*, vol. 2018, Article ID 6964828, 7 pages, 2018.

[10] M. P. Manser and P. A. Hancock, "The influence of perceptual speed regulation on speed perception, choice, and control: tunnel wall characteristics and influences," *Accident Analysis & Prevention*, vol. 39, no. 1, pp. 69–78, 2007.

[11] Q. Meng, X. Qu, X. Wang, V. Yuanita, and S. C. Wong, "Quantitative risk assessment modeling for nonhomogeneous urban road tunnels," *Risk Analysis*, vol. 31, no. 3, pp. 382–403, 2011.

[12] Y. Bie, X. Xiong, Y. Yan, and X. Qu, "Dynamic headway control for high-frequency bus line based on speed guidance and intersection signal adjustment," *Computer-Aided Civil and Infrastructure Engineering*, vol. 35, no. 1, pp. 4–25, 2020.

[13] Q. Meng and X. Qu, "Estimation of rear-end vehicle crash frequencies in urban road tunnels," *Accident Analysis & Prevention*, vol. 48, pp. 254–263, 2012.

[14] A. Calvi and F. D'Amico, "A study of the effects of road tunnel on driver behavior and road safety using driving simulator," *Advances in Transportation Studies*, vol. 30, pp. 59–76, 2013.

[15] C. M. Rudin-Brown, K. L. Young, C. Patten, M. G. Lenné, and R. Ceci, "Driver distraction in an unusual environment: effects of text-messaging in tunnels," *Accident Analysis & Prevention*, vol. 50, pp. 122–129, 2013.

[16] K. Kircher and C. Ahlstrom, "The impact of tunnel design and lighting on the performance of attentive and visually distracted drivers," *Accident Analysis & Prevention*, vol. 47, pp. 153–161, 2012.

[17] L. Moretti, G. Cantisani, and P. Di Mascio, "Management of road tunnels: construction, maintenance and lighting costs," *Tunnelling and Underground Space Technology*, vol. 51, pp. 84–89, 2016.

[18] L. Moretti, G. Cantisani, P. Di Mascio, and S. Caro, "Technical and economic evaluation of lighting and pavement in Italian road tunnels," *Tunnelling and Underground Space Technology*, vol. 65, pp. 42–52, 2017.

[19] C. Ma, D. Yang, J. Zhou, Z. Feng, and Q. Yuan, "Risk riding behaviors of urban E-bikes: a literature review," *International Journal of Environmental Research and Public Health*, vol. 16, no. 13, p. 2308, 2019.

[20] L. Zhang, B. Cui, M. Yang, F. Guo, and J. Wang, "Effect of using mobile phones on driver's control behavior based on naturalistic driving data," *International Journal of Environmental Research and Public Health*, vol. 16, no. 8, p. 1464, 2019.

[21] W. B. Cho, J. H. Jeong, D. G. Kim, and W. I. Park, "Comparison of safety level between driver's ages by threshold zone luminance level of vehicular traffic tunnel," *Journal of the Korean Society of Road Engineers*, vol. 17, no. 1, pp. 129–142, 2015.

[22] S. He, B. Liang, G. Pan, F. Wang, and L. Cui, "Influence of dynamic highway tunnel lighting environment on driving safety based on eye movement parameters of the driver,"

Tunnelling and Underground Space Technology, vol. 67, pp. 52–60, 2017.

[23] Z. Feng, M. Yang, W. Zhang, Y. Du, and H. Bai, "Effect of longitudinal slope of urban underpass tunnels on drivers' heart rate and speed: a study based on a real vehicle experiment," *Tunnelling and Underground Space Technology*, vol. 81, pp. 525–533, 2018.

[24] Z. Kening and G. Bo, "Research on driver mental load in exit of super long tunnel," *Technology & Economy in Areas of Communications*, vol. 19, no. 3, pp. 6–9, 2017.

[25] F. Chen, H. Peng, X. Ma, J. Liang, W. Hao, and X. Pan, "Examining the safety of trucks under crosswind at bridge-tunnel section: a driving simulator study," *Tunnelling and Underground Space Technology*, vol. 92, Article ID 103034, 2019.

[26] E. Rendon-Velez, P. M. van Leeuwen, R. Happee, I. Horváth, W. F. van der Vegte, and J. C. F. de Winter, "The effects of time pressure on driver performance and physiological activity: a driving simulator study," *Transportation Research Part F: Traffic Psychology and Behaviour*, vol. 41, pp. 150–169, 2016.

[27] H. Wiberg, E. Nilsson, P. Lindén, B. Svanberg, and L. Poom, "Physiological responses related to moderate mental load during car driving in field conditions," *Biological Psychology*, vol. 108, pp. 115–125, 2015.

[28] K.-H. Choi, J. Kim, O. S. Kwon, M. J. Kim, Y. H. Ryu, and J.-E. Park, "Is heart rate variability (HRV) an adequate tool for evaluating human emotions?A focus on the use of the international affective picture system (IAPS)," *Psychiatry Research*, vol. 251, pp. 192–196, 2017.

[29] G. Valenza, P. Allegrini, A. Lanatà, and E. P. Scilingo, "Dominant Lyapunov exponent and approximate entropy in heart rate variability during emotional visual elicitation," *Frontiers in Neuroengineering*, vol. 5, no. 3, pp. 1–7, 2012.

Hindawi
Journal of Advanced Transportation
Volume 2020, Article ID 3654130, 10 pages
https://doi.org/10.1155/2020/3654130

Research Article

Exploring the Factors Associated with Car Use for Short Trips: Evidence from Kunming, China

Mingwei He, Yi Fei, and Min He

Faculty of Transportation Engineering, Kunming University of Science & Technology, Jingming Road 727, Kunming 650500, China

Correspondence should be addressed to Mingwei He; hmwei01@163.com

Received 8 October 2019; Revised 7 December 2019; Accepted 26 December 2019; Published 1 February 2020

Academic Editor: Jaeyoung Lee

The purpose of this study is to explore the factors associated with car use for short trips. Using the data collected from a travel survey conducted with car users in Kunming, the structural equation model is employed to explore the structural relationships between car use for short trips, attitudes toward cars and alternative travel modes, sociodemographics, and the built environment. The results show that instrumental and symbolic attitudes toward cars are positively related to the affective attitude, and these three attitudes have a significant effect on car use for short trips. The symbolic attitude of drivers is negatively associated with their walking and cycling attitudes. Drivers with a better cycling attitude use a car less frequently for short trips. Concurrently, the effects of sociodemographics and the built environment on the attitudes and car use for short trips are also identified. The findings may contribute to understanding the car use behavior and help policy makers to identify methods for reducing car use more clearly.

1. Introduction

In recent decades, with the rapid economic development and urbanization in China, cars are being increasingly used by families. Statistics from the National Bureau of Statistics of China in 2018 show that the number of private cars has reached 20.6 million [1]. Cars have gradually become an important travel mode in urban residents' daily life. Increased car use brought a series of negative problems, such as traffic congestion and air pollution, which have put tremendous pressure on energy crisis and climate change.

There is a general consensus that we need to reduce car trips to minimize these negative impacts [2]. Although it should be admitted that car use is necessary in response to some certain needs, unnecessary usage of cars must be reduced, particularly for some short trips. In fact, a majority of our daily trips by cars are proved to be short [3]. A study in Sydney showed that nearly a quarter of the car trips were less than 5 min in duration [4]. According to the fourth Comprehensive Traffic Survey in Beijing in 2010, car trip distances of less than 5 km accounted for more than 40% of the total number of car trips [5]. Short-distance car trips may require more fuel and generate more harmful emissions, such as carbon monoxide (CO), because they are always driven in urban areas with cold engines, compared with long-distance trips [6, 7]. Unlike long-distance trips, short trips in a car can be more easily replaced by other travel modes, such as walking and cycling. This is more likely to reduce car use for short trips. Moreover, promoting drivers to substitute car use with active travel modes also benefits public health and contributes to a low-carbon society [8].

Existing studies have analyzed the determinants of car use from different perspectives. These include sociodemographics of the traveler [9, 10], attitudes and perceptions toward cars [11, 12], built environment [13, 14], and the instrumental function of the car itself [15–17]. However, only a few studies have focused on car use for short trips. A Dutch study [6] investigated short car trips from a long-term travel survey of 35 car drivers. The results attributed the usage of cars for short trips to the transport of heavy goods and passengers. Another study [18] showed that the convenience of parking a car induced the park and ride demand,

and weather influenced the decisions of drivers to use cars for short trips. Additional influencing factors such as the individual and household socioeconomic status of the traveler, availability of cars and alternative modes, trip purpose, and the built environment of their residence also play an essential role in choosing the mode for short trips [19, 20].

Overall, the influencing mechanism of car use for short trips is not well understood, and several issues need to be further explored. First, the attitudes of travelers toward cars play an important role in explaining car use. Although the existing studies have investigated the instrumental, affective, and symbolic attitudes toward cars and their effects on car use [21–23], it is necessary to verify the effects of these attitudes on car use for short trips further. Second, besides the attitudes of car users toward their cars, we should also pay attention to their attitudes toward alternative travel modes. This may help to understand the reasons they select cars instead of alternative modes. Third, the effects of sociodemographics and the built environment on car use for short trips require further exploration. Examining these issues will contribute to a more comprehensive understanding of car use for short trips. In this study, using data collected from a travel survey conducted with car users in Kunming, the structural equation model (SEM) is employed to explore the structural relationships between the car use for short trips, attitudes toward different travel modes, sociodemographics, and the built environment.

The remainder of this article is structured as follows. The next section introduces the conceptual model. Section 3 presents the data collection, key variables, and method. Section 4 discusses the model results. Our conclusions are presented in the final section.

2. Conceptual Model

Existing studies have generally proven that attitudes have a significant impact on car use. Attitudes toward cars mainly consist of three components: instrumental aspect, symbolic aspect, and affective aspect [22–24]. The instrumental function of the car leads people to prefer using cars than other travel modes because they move faster and are always available for the trips [25]. Symbolic function could display drivers' social identity and express their self-concept to some extent [23]. Affective function refers to drivers' emotional feelings, such as the pleasure of driving and the passion for speed [12, 24]. In exploring the relationship among instrumental function, symbolic function, and affective function of the car, Steg and Tertoolen [21] proposed a theoretical model that car use depended on social, affective, and instrumental motivations; meanwhile, instrumental and symbolic motivations have an effect on affective motivation. Steg and his colleagues further verified this model empirically [22, 23]. Gatersleben [26] also reported that affective function of a car depended on its instrumental function and symbolic function.

The initial conceptual model structure of the interrelationships is presented in Figure 1. According to the theoretical model proposed by Steg and Tertoolen [21], the model assumed that car use depended on instrumental, symbolic, and affective attitudes, and the affective attitude was a consequence of the instrumental and symbolic attitude. These three attitudes affect car use in the meanwhile.

Considering that walking and cycling are the main alternatives to cars for short trips, we also included the impact of drivers' attitudes toward walking and cycling. In our hypothesis, walking and cycling attitudes directly influence car use for short trips, and the awareness of drivers about the environmental problems is considered to affect the car use, walking, and cycling attitudes. Besides the interrelationships between the three attitudes toward cars, the walking and cycling attitudes of car users are also verified. In the model, these attitudes are included as latent variables, which are measured by a series of attitude indicators. All these attitudes and car use for short trips are assumed to be influenced by sociodemographics and the built environment.

3. Research Design

3.1. Data Collection. The data for this study were obtained through a short-distance travel survey conducted in May 2019 in Kunming. Kunming is the capital of the Yunnan province in southwest China. Kunming is a representative of numerous Chinese cities with a hierarchical center structure and comparative size. The urban region of Kunming, which consists of the five districts: Chenggong, Wuhua, Panlong, Xishan, and Guandu, is shown in Figure 2. Approximately 3.6 million individuals live in the urban area of Kunming, the population density in 2018 was 10902 inhabitants/km^2.

Given the objectives of the study, we only selected respondents who are car users. The questionnaire included questions about their sociodemographic characteristics, driving information, attitudes, perceptions toward different travel modes, and information about their last 5 short trips (less than 4 km). The respondents were approached at multiple automobile 4S shops, garages, and public parking lots located in the five districts. All the respondents were given a reward of 10 CNY. In each district, we planned to obtain approximately 70 random samples. A total of 341 car users completed the questionnaires, and 26 questionnaires were eliminated owing to incomplete responses. Overall, the database used for this study included 315 valid samples. In general, the survey captured various car users in Kunming, and the sample was representative of the car users with respect to gender, age, household income, and employment status. A description of the sample is provided in Table 1.

3.2. Key Variables. The variables used in the analysis include personal and household characteristics, built environment, attitudes, and car use for short trips. The definition of short trip varies between studies [7, 27–29]. Lee et al. defined 8 km as the maximum distance for a short round trip (4 km for a one-way trip) [7]. de Nazelle et al. used 3 miles (4.8 km) as the threshold value for a short trip [27]. According to the report of the 2016 Kunming Urban

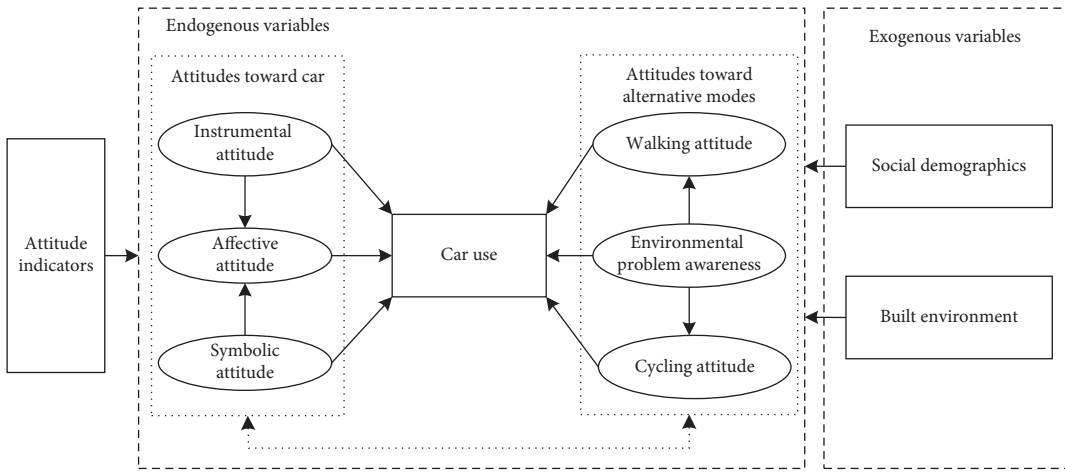

Figure 1: Conceptual model structure.

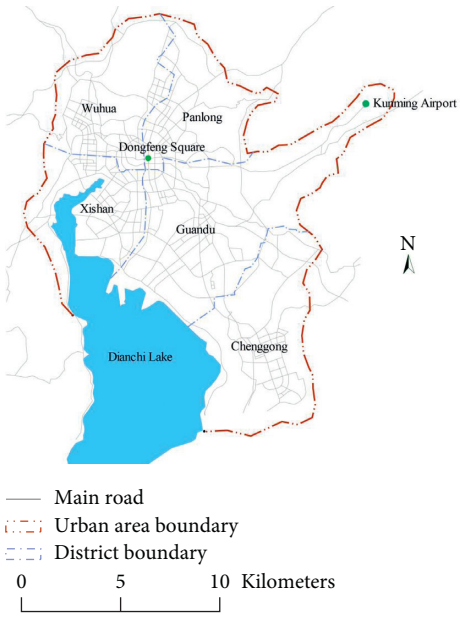

Figure 2: Map of the urban area of Kunming.

Residents Travel Survey [30], the average distance cycled is 2.9 km, and 75.6% of all cycling trips are less than 4 km. Almost all walking trips are within 4 km. Considering walking and cycling are potential alternatives to short car trips, a short trip is defined as a one-way trip within 4 km. Car use for short trips is an outcome variable. In our model, the percentage of trips made by a car in the past five short trips is the measure of car use. Consequently, the values range from 0 to 1, and the mean is 0.49.

The personal and household characteristics included gender, age, education level, employment status, driving experience, annual household income, and car ownership. Age is classified into three categories: 18–30, 31–50, and older than 50. Education level is classified into two categories: high school or less, and college or higher. Two categories are differentiated for employment status: staff and others, where staff mainly includes being an employee in an enterprise, a public institution staff or civil servant. The driving experience of a participant is classified into two categories: less than and greater than 10 years. The annual household income is divided into three categories: low (less than 100,000 CNY), medium (100,000–200,000 CNY), and high (more than 200,000 CNY). Two categories are differentiated for car ownership: households owning one car, and households owning two or more cars. Furthermore, the dominance of the car in a family, which may affect car use of a participant for short trips, is also considered. The dominance of a car in a family is classified into three categories: fully dominated by yourself, used more by yourself, and used more by your family members.

In this study, the built environment variables only include the number of bus stops around the residences of the respondents and the linear distance from their residence to the city center. Because the average pedestrian distance to bus stops is generally approximately 500 m [31, 32], we searched for the number of bus stops within a radius of 500 m from the residences of the participants. The average number of bus stops around their residences is 9.17, and the standard deviation is 4.60. Considering the overall layout of Kunming, this study adopted the Dongfeng Square (marked in Figure 1) as the city center. The average linear distance from respondents' residences to Dongfeng Square is 10.02 km, and the standard deviation is 7.62.

According to the theoretical model proposed by Steg and Tertoolen [21], the attitudes toward a car include instrumental, symbolic, and affective attitudes. In this study, these attitudes were the latent variables and measured by their indicators. The participants indicated the degree of agreement on a Likert scale ranging from 1 (totally disagree) to 7 (totally agree) for each statement. The statements were designed in accordance with the studies exploring how attitudes influence car use [2, 18, 23, 24] and with actual situations of the survey area.

The instrumental attitude is measured by five statements: "Using a car allows me to choose my own route," "Using a car can protect me against bad weather," "A car can make it easy to go out at any time," "A car can make it easy to reach

Table 1: Sample characteristics.

Variables	Classification	Cases	Percentage (%)
Gender	Male	200	63.5
	Female	115	36.5
Age	18–30	156	49.5
	31–50	141	44.8
	>50	18	5.7
Education level	High school or less	63	20.0
	College or higher	252	80.0
Employment status	Staff	210	66.7
	Others	105	33.3
Annual household income (CNY)	<100,000	133	42.2
	100,000–200,000	121	38.4
	>200,000	61	19.4
Car ownership	1	206	65.4
	≥2	109	34.6
Dominance of the car	Fully dominated by yourself	110	34.9
	Used more by yourself	108	34.3
	Used more by your family	97	30.8
Driving experience (years)	0–10	258	81.9
	>10	57	18.1

any place directly," and "A car can pick up passengers and carry capacity." The symbolic attitude is measured by four statements: "A car can distinguish me from the rest of people," "A car can express my taste and hobby," "A car can show my success to others," and "A car can make me more confident." The affective attitude is measured by four statements: "Driving can make me enthusiastic," "Driving is enjoyable," "I'm fond of my car," and "I feel everything is under control when I drive."

Considering that walking and cycling are the main alternatives to car use for short trips, we also investigated the attitudes of the participants toward walking and cycling. The Statements are "Cycling can benefit my health" and "Cycling is enjoyable" are designed for measuring the attitude toward cycling. Statements "Walking can benefit my health" and "Walking is enjoyable" are for measuring the attitude toward walking [33]. Moreover, the environmental problem awareness is measured using the following statements: "Car emission is an important cause of air pollution" [34] and "I think transportation has a huge impact on the environment, and I support low-carbon travel." Descriptive statistics of all the attitude statements are shown in Table 2.

3.3. Method. The structural equation model (SEM) has been widely used for exploring the travel behavior [35, 36]. In this study, the SEM was employed to explore the structural relationships between the car use for short trips, attitudes toward different travel modes, sociodemographics, and the built environment. SEM was chosen for its ability to capture both the effects of exogenous variables on endogenous variables, and the effects of endogenous variables on each other [37].

The model was developed by using MPLUS Version7 software. In this study, the attitude indicators were collected on a seven-point Likert scale and were treated as categorical variables. The sociodemographic attributes were also grouped to be included in the model. Therefore, we used an available method named weighted least square parameter estimator (WLSMV), which is a robust estimator designed for processing categorical-dependent variables with robust standard errors and does not require a large sample size [38].

The final model was modified in two phases. First, based on the conceptual model, all the variables and relationships were included in the model. Second, based on the model output, except the direct links between the attitudes toward the travel modes and car use for short trips, we discarded the links when the direct effects were not significant.

4. Results

4.1. Model Fit Indices. Table 3 lists the model-fitted indices from several aspects. The χ^2 statistic is used to measure the discrepancy between the model-based and observed covariance matrices. Because the χ^2 statistic increases with the sample size, it is not considered as a good measure of the goodness of fit. To reduce the sensitivity of the χ^2 statistic to the sample size, it can be divided by the degrees of freedom. The value of χ^2/df is 2.55, which is lower than the cutoff value of 3.0; values of 3 or less indicate a good fit [36]. The comparative fit index (CFI) and Tucker–Lewis index (TLI) are used to evaluate he improvement of the hypothesized model compared with the independence model with unrelated variables [39]. The value of the CFI is 0.926, and TLI is 0.917, indicating that the model has an acceptable fit. The value of the root-mean-square error of approximation (RMSEA) is 0.070, which exhibits a reasonable fit.

4.2. Measurement of Attitude Latent Variables. In the structural equation context, the measurement model specifies how the latent variables are measured by the observed variables. In our model, the attitude latent variables are measured by a series of attitudinal statements (mentioned in chapter 3.2.2). Table 4 lists the statements included in each

Table 2: Descriptive statistics of the attitudes.

Attitudes	Number of statements	Mean	SD	Cronbach alpha
Instrumental attitude	5	5.75	1.28	0.82
Symbolic attitude	4	3.23	2.32	0.79
Affective attitude	4	4.41	1.81	0.82
Cycling attitude	2	5.41	1.44	0.71
Walking attitude	2	5.68	1.30	0.74
Environmental awareness	2	5.36	1.47	0.70

Table 3: Model fit result.

	χ^2 (df) p	χ^2/df	CFI	TLI	RMSEA
Desired values	$p > 0.05$	<3.0	>0.9	>0.9	<0.08
Model-based values	1022.825 (165) 0.00	2.55	0.926	0.917	0.070

Table 4: The results of measurement model.

Latent variables	Attitude statements	Standardized factor loading	S.E.	Two-tailed p value
Instrumental attitude towards car	Using the car allows me to choose my own route.	0.772	0.029	<0.001
	Using the car could protect me against bad weather.	0.707	0.030	<0.001
	The car could make me easy to go out at any time.	0.868	0.021	<0.001
	The car could make me easy to reach any place directly.	0.713	0.029	<0.001
	The car could pick up passengers and carry capacity.	0.706	0.031	<0.001
Symbolic attitude towards car	The car can distinguish me from the rest of people.	0.880	0.015	<0.001
	The car could express my taste and hobby.	0.869	0.016	<0.001
	The car could show my success to others.	0.916	0.012	<0.001
	The car could make me more confident.	0.923	0.012	<0.001
Affective attitude towards car	Driving could bring me enthusiasm.	0.907	0.024	<0.001
	Driving is enjoyable.	0.714	0.029	<0.001
	I'm fond of my car.	0.534	0.038	<0.001
	I feel everything under control when I drive.	0.549	0.039	<0.001
Attitude towards cycling	Cycling could benefit my health.	0.901	0.024	<0.001
	Cycling is enjoyable.	0.754	0.028	<0.001
Attitude towards walking	Walking could benefit my health.	0.860	0.025	<0.001
	Walking is enjoyable.	0.895	0.024	<0.001
Environmental problem awareness	Car emission is an important reason for air pollution.	0.714	0.034	<0.001
	I think transportation has a great impact on environment and I support the low-carbon travel.	0.583	0.038	<0.001

attitude latent variable and the standardized factor loadings for each statement. All the statements in the measurement model have standardized factor loadings larger than 0.5, and all of them are significant at $p < 0.001$.

4.3. Structural Relationships and Effects between Endogenous Variables. Figure 3 displays the relationships between the endogenous variables, along with the corresponding standardized weights. Both the instrumental and symbolic attitudes have statistically significant positive effects on the affective attitude. The magnitude of the effect on the affective attitude by the instrumental attitude is smaller than that by the symbolic attitude. The environmental problem awareness shows a significant positive impact on both the walking and cycling attitudes. Car users with a better environmental awareness have a higher evaluation of the benefits brought by walking and cycling. We also find significant negative effects of the symbolic attitude on walking and cycling attitudes. These results indicate that car users who care more about the symbolism of a car have a lower evaluation of walking and cycling.

The direct and indirect effects of the attitude variables on car use for short trips are listed in Table 5. The affective attitude has a significant positive direct effect on car use for short trips. The direct effect of the instrumental attitude is not statistically significant. However, the instrumental attitude has a significant indirect effect on car use for short trips based on the affective attitude. In terms of the symbolic attitude, it has a significant positive total indirect effect on

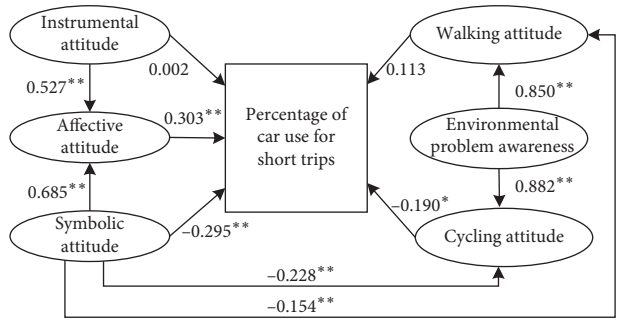

Figure 3: Structural relationships between the endogenous variables (note: $^{*}p < 0.1$ and $^{**}p < 0.05$).

Table 5: Standardized direct, indirect, and total effects of the attitudes on car use.

Attitudes	Direct effect	Indirect effect	Total effect
Instrumental attitude	0.002	0.160**	0.162**
Symbolic attitude	−0.295**	0.234**	−0.061**
Affective attitude	0.303**		0.303**
Cycling attitude	−0.190*		−0.190*
Walking attitude	0.113		0.113
Environmental problem awareness		−0.06	−0.06

Note: $^{*}p < 0.1$ and $^{**}p < 0.05$.

car use for short trips via three mediating variables. In detail, it has a significant positive indirect effect on car use for short trips via the affective attitude. Moreover, the symbolic attitude has a significant positive indirect effect on car use for short trips based on the cycling attitude and none through the walking attitude. Different from our expectations, the symbolic attitude has a negative direct and total effect on car use for short trips. In terms of the individual attitude toward the alternative modes, the cycling attitude has a negative effect on car use for short trips. This indicates that drivers with a better cycling attitude use a car less for short trips. However, the walking attitude is less related to car use for short trips.

4.4. Effects of the Exogenous Variables on Attitudes and Car Use. Table 6 lists the direct, indirect, and total effects of the exogenous variables on the attitudes and car use for short trips. The total effect is the sum of the direct and indirect effects. In terms of personal characteristics, age is negatively related to the affective attitude. It appears the affection of an individual for a car decreases with increasing age. Age also has a significant negative indirect effect on car use for short trips through the affective attitude. Gender has a significant positive direct effect on the affective attitude and positive indirect effect on car use for short trips. This indicates that men have a deeper affection for a car and are more likely to use cars for short trips when compared with women. The education level has a significant negative direct effect on the symbolic attitude and negative indirect effect on the affective attitude via the symbolic attitude. Simultaneously, car users with a college education are more are likely to have a higher evaluation of the benefits of walking and cycling when compared with those with a high school education or less. Nevertheless, the total effect of the education level on car use is not significant. Compared with others, staff is positively related to car use for short trips. The driving experience is positively related to the instrumental attitude and has a positive indirect effect on the affective attitude through the instrumental attitude. Although the indirect effect of the driving experience on car use for short trips is positive, the total effect is negative.

In terms of the household characteristics, compared with the reference group with an annual household income below 100,000 CNY, the group with an annual household income above 200,000 CNY has a significant positive direct effect on the symbolic attitude. It also has a significant positive indirect effect on the affective attitude and negative indirect effect on the cycling and walking attitudes through the symbolic attitude. Moreover, both the higher income groups have a significant negative direct effect on the cycling attitude. According to the total effect, people belonging to the group with an annual household income above 200,000 CNY are more likely to use a car for short trips. Car use is also positively related to the car ownership in a household and car dominance.

In terms of the built environment, people living in a residential area with more bus stops are less likely to use a car for short trips. The linear distance to the city center has a significant positive direct effect on the instrumental attitude and positive indirect effect on the affective attitude through the instrumental attitude. According to the total effect, car use is positively related to the linear distance to the city center.

Table 6: Standardized direct, indirect, and total effects of the exogenous variables on the attitudes and car use.

Effect	Instrumental attitude	Symbolic attitude	Affective attitude			Cycling attitude			Walking attitude			Percentage of car use		
	Total	Total	Direct	Indirect	Total	Direct	Indirect	Total	Direct	Indirect	Total	Direct	Indirect	Total
Age, 18–30 (ref.)														
Age, 30–50			−0.197**		−0.197**								−0.060*	−0.060*
Age, 50+			−0.257**		−0.257**								−0.078**	−0.078**
Gender, female (ref.)														
Gender, male			0.249**		0.249**								0.075**	0.075**
Education, high school or less (ref.)														
Education, college or higher		−0.133**		−0.091**	−0.091**	0.177**	0.030*	0.207**		0.020*	0.020*		−0.025	−0.025
Employment state, others (ref.)														
Employment state, staff												0.139**		0.139**
Income, 0–100,000 CNY (ref.)														
Income, 100,000–200,000 CNY		−0.005		−0.003	−0.003	−0.163**	0.001	−0.162**		0.001	0.001	0.070	0.031	0.101
Income, 200,000+ CNY		0.154**		0.105**	0.105**	−0.176**	−0.035**	−0.211**		−0.024*	−0.024*	0.144**	0.033	0.177**
Number of cars, 1 (ref.)														
Number of cars, 2+												0.205**		0.205**
Car dominance, family use (ref.)														
Car dominance, you use more													0.152**	
Car dominance, completely controlled												0.152**	0.166**	
By yourself												0.166**		
Driving experience, 0–10 years (ref.)														
Driving experience, 10+ years	0.139**			0.073**	0.073**							−0.116**	0.023**	−0.093**
Number of bus stops												−0.255**		−0.255**
Linear distance to city center	0.137**			0.072**	0.072**								0.022**	0.022**

Note: * $p < 0.1$ and ** $p < 0.05$.

5. Conclusion and Discussion

This aim of this study is to explore the reasons why car use is attractive for short trips. Using the data collected from a travel survey conducted with car users in Kunming, the SEM is employed to explore the structural relationships between the car use for short trips, attitudes toward different travel modes, sociodemographics, and the built environment.

This study emphasizes the effects of the affective, instrumental, and symbolic attitudes toward cars on car use for short trips. The results indicate that the instrumental and symbolic attitudes toward cars have a significantly positive direct effect on affective attitude. This result is consistent with that of Lois and López-Sáez [24], which confirmed that drivers with high evaluation of the instrumental and symbolic effects of a car will increase their affection for their cars. The affective attitude has a significant positive direct and total effect on car use for short trips. Coincident with the finding of Steg [23], in our model, the instrumental attitude is not directly related to car use. The results reflect that compared with the instrumental function provided by cars, drivers' affection of cars seems to play a more important role in their car use for short trips.

It is noteworthy that although the symbolic attitude has a positive indirect effect on car use, the total effect is negative because the magnitude of the negative direct effect is relatively larger. To explain this result, we offer several possible reasons. First, the dominance of a car in a family is related to the individual car use. We compared the average scores of the symbolic attitude statements of the drivers who have different car dominances in their families. The average scores of the three categories are as follows: fully dominated by yourself (3.10), used more by yourself (3.05), and used more by your family members (3.35). This result shows that the drivers with more car dominance, which usually implies more car use, have a lower evaluation of the symbolic function. It may also indicate a psychological phenomenon that the more you lack something, the more you care about it. Second, the subjective biases of the respondents may also lead to this result. The average score of the symbolic attitude statements is the lowest among all the attitude statements. This may be the same situation as in the study by Steg et al. [22] in which when people were asked to evaluate the attractiveness of the aspects of car use, they deliberately avoided the symbolism of a car. We believe that the effect of the symbolic attitude on car use for short trips requires further verification and explanation by empirical and theoretical studies.

In agreement with Lois and López-Sáez [24], the affective attitude and car use are positively related to men and young drivers. Young drivers' higher evaluation of the affective effect of a car may lead their short trips use cars more. Education and the annual household income are also related to these attitudes, except the instrumental attitude. Concurrently, the number of bus stops around the residences has a negative effect on car use for short trips. These results confirm that people living in neighborhoods who are easily accessible by transit tend to reduce car use [39, 40]. Moreover, as the distance to the city center increases, drivers will have a higher evaluation of the instrumental and affective attitudes toward a car and will use a car more for short trips. This result is similar to the previous study in China [41] that people being close to city center tend to reduce the car use. In addition, the employment status, driving experience, car dominance, and car ownership in a household have significant effects on car use for short trips.

Encouraging people to choose walk and cycle is one way to reduce unnecessary car use and improve individual health outcomes [42]. In this study, we also investigate the attitudes of car users toward walking and cycling, to gain a more comprehensive understanding of the views on the active modes of people who use cars in their daily lives. The results show significant negative effects of the symbolic attitude on the walking and cycling attitudes. Furthermore, the cycling attitude of drivers is negatively related to car use for short rips. However, the walking attitude has no significant effect on car use for short trips.

All of these findings may contribute to understanding car use behavior for short trips. Our research fills the gaps in the study of short car trips from a psychological perspective. Several implications for policymakers may be drawn from this study. Our results demonstrate the attitudes play an important role in car use for short trips. Greater attention should be given to psychological strategies to change the perceptions and attitudes toward cars. Furthermore, in order to promote a modal shift from short car trips to cycling, it may be worthwhile to make car users aware of the benefits of cycling through education and publicity. Our results demonstrate that the attitudes and car use for short trips are related to the sociodemographics of car users. Therefore, policies should be tailored toward specific targeted groups to make them more effective [23]. In addition, our results also claim that improving the accessibility of public transport can effectively reduce car use.

The current study also has several limitations. First, our data were based on the perception of the participants of their short trips. The difficulty of recalling past behaviors and their perceptions of travel information may have led to a certain bias. Second, this study only included a few built environment factors. Other factors such as the walking and cycling environment, neighborhood design, and land use are also essential factors influencing people to choose active modes [42]. In the future, we will consider more built environment factors to promote the shift of drivers from cars to active modes for short trips.

Data Availability

The data for this study was obtained through a short-distance travel survey conducted in May 2019 in Kunming, Yunnan province, China. The data will be available to the scientific community by a data article, which will be submitted to an appropriate journal in the near future.

Conflicts of Interest

The authors declare no conflicts of interest.

Acknowledgments

The authors thank all research assistants for data collection and processing. This research was funded by the National Natural Science Foundation of China (No. 71861017, No. 71661020) and the Talent Training Foundation of Yunnan Province, China (No. KKSY201702029).

References

[1] National Bureau of Statistics of China, *China Statistical Yearbook*, National Bureau of Statistics of China, Beijing, China, 2018.

[2] C. J. Bergstad, A. Gamble, O. Hagman, M. Polk, T. Gärling, and L. E. Olsson, "Affective-symbolic and instrumental-independence psychological motives mediating effects of socio-demographic variables on daily car use," *Journal of Transport Geography*, vol. 19, no. 1, pp. 33–38, 2011.

[3] S. Paul, K. Born, K. Mcelduff et al., "Exploring the characteristics of short trips: implications for walk mode choice," in *Proceedings of the Transportation Research Board 93rd Annual Meeting*, Transportation Research Board, Washington, DC, USA, 2014.

[4] T. Sugiyama, D. Merom, H. P. van Der Ploeg, G. Corpuz, A. Bauman, and N. Owen, "Prolonged sitting in cars: prevalence, socio-demographic variations, and trends," *Preventive Medicine*, vol. 55, no. 4, pp. 315–318, 2012.

[5] L. Ming, S. Guohua, C. Ying et al., "Research on excessive short distance car trips in urban area," *Journal of Beijing Jiaotong University*, vol. 38, no. 3, pp. 15–21, 2014.

[6] C. Beckx, S. Broekx, B. Degraeuwe, B. Beusen, and L. Int Panis, "Limits to active transport substitution of short car trips," *Transportation Research Part D: Transport and Environment*, vol. 22, pp. 10–13, 2013.

[7] J. Lee, S. Y. He, and D. W. Sohn, "Potential of converting short car trips to active trips: the role of the built environment in tour-based travel," *Journal of Transport & Health*, vol. 7, pp. 134–148, 2017.

[8] T. Jones, "Getting the British back on bicycles-the effects of urban traffic-free paths on everyday cycling," *Transport Policy*, vol. 20, pp. 138–149, 2012.

[9] T. Gehlert, C. Kramer, O. A. Nielsen, and B. Schlag, "Socioeconomic differences in public acceptability and car use adaptation towards urban road pricing," *Transport Policy*, vol. 18, no. 5, pp. 685–694, 2011.

[10] A. Carse, A. Goodman, R. L. Mackett, J. Panter, and D. Ogilvie, "The factors influencing car use in a cycle-friendly city: the case of Cambridge," *Journal of Transport Geography*, vol. 28, no. 100, pp. 67–74, 2013.

[11] L. Eriksson, J. Garvill, and A. M. Nordlund, "Interrupting habitual car use: the importance of car habit strength and moral motivation for personal car use reduction," *Transportation Research Part F: Traffic Psychology and Behaviour*, vol. 11, no. 1, pp. 10–23, 2008.

[12] H. T. Van, K. Choocharukul, and S. Fujii, "The effect of attitudes toward cars and public transportation on behavioral intention in commuting mode choice-A comparison across six Asian countries," *Transportation Research Part A: Policy and Practice*, vol. 69, pp. 36–44, 2014.

[13] A. Soltani, D. Pojani, S. Askari, and H. E. Masoumi, "Socio-demographic and built environment determinants of car use among older adults in Iran," *Journal of Transport Geography*, vol. 68, pp. 109–117, 2018.

[14] Y. Ding and H. Lu, "Activity participation as a mediating variable to analyze the effect of land use on travel behavior: a structural equation modeling approach," *Journal of Transport Geography*, vol. 52, pp. 23–28, 2016.

[15] G. Mattioli, J. Anable, and K. Vrotsou, "Car dependent practices: findings from a sequence pattern mining study of UK time use data," *Transportation Research Part A: Policy and Practice*, vol. 89, pp. 56–72, 2016.

[16] S. Cullinane and K. Cullinane, "Car dependence in a public transport dominated city: evidence from Hong Kong," *Transportation Research Part D: Transport and Environment*, vol. 8, no. 2, pp. 129–138, 2003.

[17] M. Verma, "Growing car ownership and dependence in India and its policy implications," *Case Studies on Transport Policy*, vol. 3, no. 3, pp. 304–310, 2015.

[18] D. Walton and S. Sunseri, "Factors influencing the decision to drive or walk short distances to public transport facilities," *International Journal of Sustainable Transportation*, vol. 4, no. 4, pp. 212–226, 2010.

[19] S. Kim and G. F. Ulfarsson, "Curbing automobile use for sustainable transportation: analysis of mode choice on short home-based trips," *Transportation*, vol. 35, no. 6, pp. 723–737, 2008.

[20] R. Cole, G. Turrell, M. J. Koohsari, N. Owen, and T. Sugiyama, "Prevalence and correlates of walkable short car trips: a cross-sectional multilevel analysis," *Journal of Transport & Health*, vol. 4, pp. 73–80, 2017.

[21] L. Steg and G. Tertoolen, "Affective motives for car use," in *European Transport Conference: Transport, Planning, Policy and Practice*, pp. 13–27, Cambridge, UK, 1999.

[22] L. Steg, C. Vlek, and G. Slotegraaf, "Instrumental-reasoned and symbolic-affective motives for using a motor car," *Transportation Research Part F: Traffic Psychology and Behaviour*, vol. 4, no. 3, pp. 151–169, 2001.

[23] L. Steg, "Car use: lust and must. Instrumental, symbolic and affective motives for car use," *Transportation Research Part A: Policy and Practice*, vol. 39, no. 2-3, pp. 147–162, 2005.

[24] D. Lois and M. López-Sáez, "The relationship between instrumental, symbolic and affective factors as predictors of car use: a structural equation modeling approach," *Transportation Research Part A: Policy and Practice*, vol. 43, no. 9-10, pp. 790–799, 2009.

[25] C. Bergstad, S. Fujii, and T. Gärling, "Effects of economic disincentives on private car use," *Transportation*, vol. 29, pp. 349–370, 2002.

[26] B. Gatersleben, *Affective and Symbolic Aspects of Car Use*, Elsevier, Amsterdam, Netherlands, 2007.

[27] A. De Nazelle, B. J. Morton, M. Jerrett, and D. Crawford-Brown, "Short trips: an opportunity for reducing mobile-source emissions?" *Transportation Research Part D: Transport and Environment*, vol. 15, no. 8, pp. 451–457, 2010.

[28] E. Maibach, L. Steg, and J. Anable, "Promoting physical activity and reducing climate change: opportunities to replace short car trips with active transportation," *Preventive Medicine*, vol. 49, no. 4, pp. 326-327, 2009.

[29] R. L. Mackett, "Why do people use their cars for short trips?" *Transportation*, vol. 30, no. 3, pp. 329–349, 2003.

[30] Kunming Traffic Transport Bureau, Data Report of Kunming Urban Residents Travel Survey, Kunming Traffic Transport Bureau, Kunming, China, 2016.

[31] A. M. El-Geneidy, P. R. Tétreault, and J. Surprenant-Legault, "Pedestrian access to transit: identifying redundancies and gaps using a variable service area analysis," in *Proceedings of the Transportation Research Board 89th Annual Meeting, Transportation Research Board*, Washington, DC, USA, 2009.

[32] Z. Fang, C. Lee-Fang, L. Min-Tang et al., "Forecasting transit walk accessibility: regression model alternative to buffer method," *Transportation Research Record*, vol. 1835, no. 1, pp. 34–41, 2003.

[33] M. C. Rojas López and Y. D. Wong, "Attitudes towards active mobility in Singapore: a qualitative study," *Case Studies on Transport Policy*, vol. 5, no. 4, pp. 662–670, 2017.

[34] B. Gardner and C. Abraham, "Going green? Modeling the impact of environmental concerns and perceptions of transportation alternatives on decisions to drive," *Journal of Applied Social Psychology*, vol. 40, no. 4, pp. 831–849, 2010.

[35] M. J. Roorda and T. Ruiz, "Long- and short-term dynamics in activity scheduling: a structural equations approach," *Transportation Research Part A: Policy and Practice*, vol. 42, no. 3, pp. 545–562, 2008.

[36] P. T. Aditjandra, X. Cao, and C. Mulley, "Understanding neighbourhood design impact on travel behaviour: an application of structural equations model to a British metropolitan data," *Transportation Research Part A: Policy and Practice*, vol. 46, no. 1, pp. 22–32, 2012.

[37] T. F. Golob, "Structural equation modeling for travel behavior research," *Transportation Research Part B: Methodological*, vol. 37, no. 1, pp. 1–25, 2003.

[38] C. A. Klöckner and T. Friedrichsmeier, "A multi-level approach to travel mode choice - how person characteristics and situation specific aspects determine car use in a student sample," *Transportation Research Part F: Traffic Psychology and Behaviour*, vol. 14, no. 4, pp. 261–277, 2011.

[39] V. Van Acker, P. L. Mokhtarian, and F. Witlox, "Car availability explained by the structural relationships between lifestyles, residential location, and underlying residential and travel attitudes," *Transport Policy*, vol. 35, pp. 88–99, 2014.

[40] L. Yu, B. Xie, and E. H. W. Chan, "Exploring impacts of the built environment on transit travel: distance, time and mode choice, for urban villages in Shenzhen, China," *Transportation Research Part E: Logistics and Transportation Review*, vol. 132, pp. 57–71, 2019.

[41] P. Næss, "Residential location, travel, and energy use in the Hangzhou metropolitan area," *The Journal of Transport and Land Use*, vol. 3, no. 3, pp. 27–59, 2010.

[42] S. Li, P. Zhao, H. Zhang, and J. Quan, "Walking behavior in the old downtown Beijing: the impact of perceptions and attitudes and social variations," *Transport Policy*, vol. 73, pp. 1–11, 2019.

Hindawi
Journal of Advanced Transportation
Volume 2020, Article ID 5847814, 16 pages
https://doi.org/10.1155/2020/5847814

Research Article

Safety Evaluation for Connected and Autonomous Vehicles' Exclusive Lanes considering Penetrate Ratios and Impact of Trucks Using Surrogate Safety Measures

Jian Zhang[1,2,3] **Kunrun Wu**,[4] **Min Cheng**,[4] **Min Yang**[4] **Yang Cheng**,[5] **and Shen Li**[6]

[1]*Jiangsu Key Laboratory of Urban ITS, Collaborative Innovation Center for Technology and Application of Internet of Things, School of Transportation, Southeast University, Nanjing, China*
[2]*Joint Research Institute on Internet of Mobility, Southeast University, #2 Southeast University Road, Nanjing 210096, China*
[3]*University of Wisconsin-Madison, Madison, USA*
[4]*School of Transportation, Southeast University, #2 Southeast University Road, Nanjing 210096, China*
[5]*Wisconsin Traffic Operations and Safety Laboratory, University of Wisconsin-Madison, Madison, USA*
[6]*Department of Civil & Environmental Engineering, University of Wisconsin-Madison, Madison, USA*

Correspondence should be addressed to Min Yang; yangmin@seu.edu.cn and Shen Li; sli299@wisc.edu

Received 6 November 2019; Accepted 31 December 2019; Published 22 January 2020

Guest Editor: Feng Chen

Plenty of studies on exclusive lanes for Connected and Autonomous Vehicle (CAV) have been conducted recently about traffic efficiency and safety. However, most of the previous research studies neglected comprehensive consideration of the safety impact on different market penetration rates (MPRs) of CAVs, traffic demands, and proportion of trucks in mixture CAVs with human's driven vehicle environment. On this basis, this study is to (1) identify the safety impact on exclusive lanes for CAVs under different MPRs with different traffic demands and (2) investigate the safety impact of trucks for CAV exclusive lanes on mixture environment. Based on the Intelligent Driver Model (IDM), a CAV platooning control algorithm is proposed for modeling the driving behaviors of CAVs. A calibrated 7-kilometer freeway section microscopic simulation environment is built by VISSIM. Four surrogate safety measures, including both longitudinal and lateral safety risk indexes, are employed to evaluate the overall safety impacts of setting exclusive lanes. Main results indicate that (1) setting one exclusive lane is capable to improve overall safety environment in low demand, and two exclusive lanes are more suitable for high-demand scenario; (2) existence of trucks worsens overall longitudinal safety environment, and improper setting of exclusive lanes in high trucks, low MPR scenario has adverse effect on longitudinal safety; and (3) setting exclusive lanes have better longitudinal and lateral safety improvement in high-truck proportion scenarios. Setting one or two exclusive lanes led to [+42.4% to −52.90%] and [+45.7% to −55.2%] of longitudinal risks while [−1.8% to −87.1%] and [−2.1% to −85.3%] of lateral conflicts compared with the base scenario, respectively. Results of this study provide useful insight for the setting of exclusive lanes for CAVs in a mixture environment.

1. Introduction

Recent research studies on Connected and Autonomous Vehicle (CAV) based on the Internet of Things (IoT), artificial intelligence, sensor technology, and other emerging technologies have made it ready for real-world applications in the near future [1]. It has been well recognized that CAV has the capability of enhancing traffic safety, efficiency, and reducing emission [2–4]. Early field experiments of this technology include California PATH [5] and SARTRE [6]. It seems perfect if all vehicles on roads are connected and autonomous. However, human-driven vehicles (HDVs) and CAVs will coexist in a long period, and some researchers argued that the safety impact is mainly decided by the market penetrate rates (MPRs) of CAVs [3]. On the contrary, CAV-HDV and HDV-CAV interactions still need more experimental data [7]. Hence, the early application of CAVs is making sense to build on exclusive lanes, which is a much simpler environment. Besides,

large quantities of optimization methods on autonomous driving have been conducted, such as multivehicle cooperative stability control of CAVs [8], platoon controllers for CAVs including the Proportional-Integral-Derivative controller ([9, 10]), car-following model-based controller [11] , interpolating controller [12], and so on. Cooperative vehicle and infrastructure for optimizing signal control on arterials or urban intersections and multivehicle platooning control have the possibility to be successfully applied on exclusive lanes for CAVs in the near future [13–15].

One primary consideration of this paper is to identify the safety impact on exclusive lanes for CAVs on different MPRs with different traffic demands. A considerable amount of previous studies agrees that exclusive lanes for CAVs enhance safety, capacity, and efficiency of freeway facilities compared with CAVs and HDVs sharing the same lanes (e.g., MPRs<100%) [16, 17]. However, none of them has discussed how to set one, two, or more exclusive lanes according to different traffic demands. It is irrational to place an exclusive lane with relatively low MPRs of CAVs on a congested freeway since compressing the headway to HDVs would induce higher traffic crash risk and worsen congestion. Hence, careful discussion on the impact of exclusive lanes for connected and autonomous vehicles is necessary.

Another equipollence consideration is the influence of trucks on safety impacts for CAV exclusive lanes on different traffic compositions [18]. Previous research studies often assumed that only a few trucks exist on traffic, which means that traffic mostly consists of cars. In fact, the existence of trucks is not only changing the speed distribution but also influences actual road capacity as it is longer, heavier, and clumsier than cars [19]. Traditionally, these differences between trucks and cars can be neglected in modeling the traffic system since the proportion of the truck is rare on most uncongested freeways. However, with the rapid development of China, road freight transportation, almost by trucks, takes up nearly three-quarters of the total freight volume in China [20], which produces large quantities of freight demands on the freeway. As the proportion of trucks increase, speed difference enlarged, and its safety impact is no longer negligible. Particularly in the situation that exclusive lanes have taken over one or two lanes for CAVs, the maintaining of overall safety impacts is questionable. Besides, experiments have conducted and pointed out that heavy-duty trucks' close-distance driving will result in a significant fuel reduction [21, 22]. Additional efforts need to be made to the influence of high-truck proportion toward the safety impact of freeway exclusive lanes for CAVs for the early application of CAVs.

The homogeneous CAV traffic is believed to be beneficial for the application and operation of autonomous vehicles, and the setting philosophy of CAV exclusive lanes still needs further investigation. Accordingly, in this paper, we try to make a supplement to previous research studies on investigating safety impacts of exclusive lanes for CAVs on different traffic demands and compositions to determine when it is better to set exclusive lanes.

The contribution of this paper is threefold. First, a platoon control algorithm is developed to incorporate the cooperation of autonomous vehicles in the traditional IDM model. Second, we deployed a simulation environment with surrogate safety measures technology to investigate the safety impact of the exclusive lane. Third, we conduct a comprehensive comparison analysis to analyse the safety impact on the impact of CAVs on the exclusive lane and pointed out useful perspectives for the operation of the CAV exclusive lane.

2. Literature Review

2.1. Evaluating Impacts of CAVs. Many research studies of realistically modeling CAV systems with platoon control in varied scenarios have been conducted in recent years; however, relatively few in the literature focus on exclusive lanes for CAVs. There are two major approaches for exclusive lane research studies: analytical modeling and computer simulation. One of the springboards is from the improvement of traffic flow, including increasing string stability, capacity, or preventing CAVs degraded to AVs (without cooperative) [23–26]. The above studies revealed the pros and cons of setting up exclusive lanes from the traffic flow theory perspective. On the contrary, Rahman and Abdel-Aty [27] applied surrogate safety measures to evaluate the safety impact of exclusive lanes for CAVs. Besides, other research studies on the safety impacts of CAVs applied surrogate safety measures [28, 29] presented the feasibility of this kind of evaluation. Details of aforementioned literatures are summarized in Table 1.

2.2. Simulation-Based Approaches. Simulation testbeds and approaches for research studies of CAVs or autonomous vehicles are still necessary since the proof that CAVs bring safety on roads is insufficiency. Microscopic simulation-based CAV studies have utilized different kinds of simulation platforms. Besides simulation platforms, CAV car-following algorithms are also necessary. The driving behavior for CAVs and human drivers are very different. To build car-following models for CAVs, earlier studies have applied Intelligent Driver Model (IDM) [21, 30, 31], Newell's car-following model [32, 33], full velocity difference (FVD) model [34], MICroscopic Model for Simulation of Intelligent Cruise Control (MIXIC) [35], and so on. Research [36] reviewed these car-following models and pointed out that the Intelligent Driver Model is one of the most used models, and it is considered to be more suitable to simulate behaviors of CAVs in the real world since it is able to model turbulence, oscillation, and other traffic flow characteristics.

2.3. Safety Impacts of Trucks. According to the Freeway Administration of Jiangsu Province (FAJ), China, the running speed of trucks in the Ninghu Freeway is at a range of 48 km/h to 78 km/h, far less than 65~119 km/h for human-driven cars. Such a speed difference is one of the main causes of crashes. Researchers have found the relationship between speed differences with accidents is given by the so-called Solomon curve or Crash Risk Curve [20, 37, 38]. The curve largely follows U-shape, which means that a larger

Table 1: Summary of previous research studies for connected and autonomous vehicles with mixture environment.

Study	Base model	Scenarios	Main results
[23]	A platooning model (similar with Wiedemann 99 for HDV)	1 exclusive lane	Exclusive lanes for CAV could provide up to 5.5 times the capacity of the conventional freeway when platoon size is 20, interplatoon spacing is 50 meters, and intraplatoon spacing is 1 meter
[24]	Cellular automata	1, 2 exclusive lanes and 3 exclusive rows for CAVs on 2 lanes. MPRs = 0, 10%, . . ., 90%	Exclusive lanes for CAV will greatly improve the traffic condition of the freeway on MPRs = 10%–80%
[25]	Cellular automata	0, 1, or 2 exclusive lanes. MPRs = 0, 10%, . . . , 90%	Setting CAV exclusive lanes at low MPRs deteriorates the performance of overall traffic flow throughput, particularly under a low-density level
[26]	Not available	1 exclusive lane with 3 strategies: forced-everywhere, forced-reserved, and optional-everywhere	Optional use of the exclusive lane without any limitation on the type of operation could improve congestion, increase 30% capacity for a four-lane freeway
[27]	IDM model for CAV, Wiedemann 99 for HDV	0 or 1 exclusive lane	Connected vehicles' platooning on the exclusive lane outperformed all lane scenarios
[28]	Wiedemann 99 for HDV, IDM model for CAV	MPRs = 0, 25%, 50%, 75%, and 100% on a freeway	CAVs bring about compelling benefit to road safety as traffic conflicts significantly reduce even at low penetration rates
[29]	Mixture (IDM, Wiedemann and modified Bando)	MPRs = 30%, 40%, 60%, 80%, and 100% on an arterial with 9 signalized intersections	CAVs reduce segment crash risk significantly in terms of five surrogate measures of safety

speed difference indicates more accidents. Due to the speed difference, conflicts between cars and trucks occurred. Hence, the Administration has tried to separate truck traffic by forbidding their running on the leftmost two lanes, but strong conflicts still exist on weaving areas, and safety impacts of trucks need investigation.

3. Methodologies

The evaluation of safety impacts of CAV exclusive lanes is implemented on a freeway designed in the PTV-VISSIM platform with the External Driver Model. Driving behaviors of CAVs, including car-following and lateral lane change decisions, are coded in C++ language as a Dynamic Link Library (DLL) plug-in, which allows users to override original VISSIM default driving behaviors. This section describes an overall simulation framework of evaluating safety impacts of CAV exclusive lanes, including model calibration, driving behaviors of CAVs and HDVs, and surrogate safety measure indexes. The overall architecture of this study is presented in Figure 1.

Three main assumptions of this study are as follows: (1) all CAVs would follow the proposed platooning control algorithm. (2) Communication technology of CAVs adopted Dedicated Short-Range Communications (DSRC) with a constant communication range of 300 meters. (3) The perception-reaction time for CAVs maintains a constant value.

3.1. CAVs with Platooning Control Algorithm

3.1.1. Longitudinal Car-Following Model. In this paper, the Intelligent Driver Model (IDM), proposed by [39], is chosen as a car-following model for CAVs, while human-driven vehicles (e.g., cars and trucks) follow Wiedemann 99 model, which originated from the default car-following model of VISSIM, and it has good performance on simulating human driver's driving behavior. The IDM model can be denoted as

$$a_{\mathrm{IDM}}(t+t_\alpha) = \max\left\{b_m, a_m\left[1-\left(\frac{v}{v_0}\right)^{\delta}-\left(\frac{s^*}{s}\right)^2\right]\right\},$$
$$s^* = s_0 + \max\left[0, vT + \frac{v\Delta v}{2\sqrt{a_m b}}\right], \tag{1}$$

where t_α = the perception-reaction time, a_m = the maximum acceleration, b_m = the maximum deceleration, v = the speed of the following vehicle, v_0 = the desired speed, δ = the acceleration exponent (with a constant value of 4), s = the gap distance between the leading vehicle and the following vehicle, s_0 = the minimum gap distance at standstill, T = the safe time headway, and b = the desired deceleration.

The parameters of the IDM model for calibrating driving behaviors of CAVs should be calibrated by field-tested data which are difficult to access in current automated technology level. Thankfully, previous research studies have built and calibrated this model for Adaptive Cruise Control (ACC), and later, researches extended their study based on similar values of the parameters. In this study, the parameters of the CAV behavior model are chosen from research studies [27–29], which are shown in Table 2.

3.1.2. Vehicular Interaction between CAV-CAV, CAV-HDV, and HDV-HDV/CAV. What needs to be pointed out is that the safe time headway T varies from interact types on Table 3. If the front vehicle is a CAV, then the follower will keep driver behavior with the leader by using an aggressive headway (0.85 s), while when the leading vehicle is an HDV, the follower will keep a conservative driving strategy with a safer time headway (2.0 s). Previous research studies have

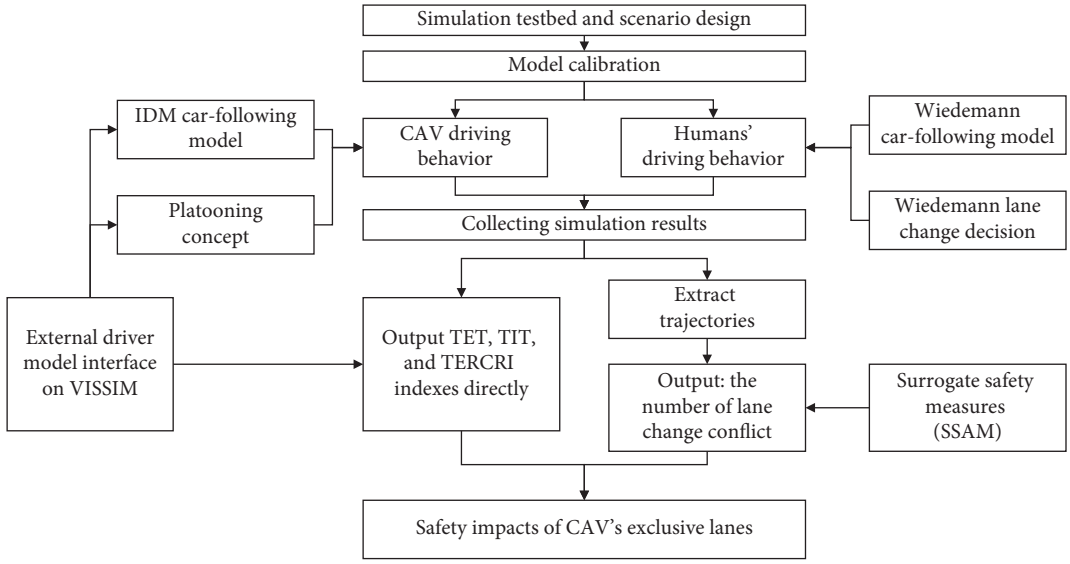

Figure 1: Architecture of the study on safety impacts of CAV's exclusive lanes.

Table 2: Parameter values of the IDM model.

Parameter	Value	Parameter	Value
a_m	1.0 m/s^2	T	0.85 s/2.0 s
b_m	−8.0 m/s^2	t_α	0.5 s
v_0	120 km/h	b	−2.8 m/s^2

Table 3: Value for the desired headway.

Interaction type (follower-leader)	Desired headway (sec)	Range (sec)	Literature
HDV-CAV HDV-HDV	1.52	1.0–1.8	[40], the value was calibrated from the FAJ
CAV-CAV	0.85	0.6–2.0	[41]
CAV-HDV	2.0	0.8–2.2	[42]

pointed out the proper range for desired headways of CAV-HDV, CAV-CAV, and HDV-HDV, which are also shown in Table 3.

Additionally, a headway examination is deployed. The reason for examination is derived from the point that the IDM model only considers the current speed difference between the leading vehicle and the following vehicle but ignores the acceleration of the leading vehicle. Since the communication delay and the perception-reaction time are unignorable, lacking of considering the acceleration of the leading vehicle might cause the following vehicle too late to act when the leading vehicle is in a sudden brake. In doing so, we propose a trimming method, which calculates the distance of the leading and the following vehicles in 2.0 seconds (Figure 2) by using the current acceleration calculated by the IDM model. If the gap between two vehicles after 2.0 s is smaller than the minimum gap at a standstill (2.0 m), the current vehicle's acceleration will decrease per 0.1 m/s^2, and repeat calculation until the gap is acceptable. The trimming method might increase safety, whereas reduce efficiency. However, how to achieve a balance between safety and efficiency still needs further investigation, which is not covered in this study. Some readers might also doubt the integrity of control logic shown in Figure 2 as it seems to be missing the logic of exiting the platoon when a CAV is ready to leave the freeway. Actually, as the CAV leaves the platoon, the CAV would try changing its lane close to the ramp under the premise of keeping safety. In this case, the CAV is no longer in the platoon control mode. The leaving freeway behavior of a single CAV makes no difference on the platoon control logic for remaining CAVs on the exclusive lane.

3.1.3. Lateral Lane Change Decision to Form or Join the Platoon. Derived from the IDM model, the platooning concept is implemented for regulating the driving behaviors from individual AVs to CAVs. To maintain the platoon, the CAVs on the searching mode will try to search the Nearest CAV (NCAV) in the DSRC communication range constantly. When an NCAV is found, the individual CAV will try to form a platoon from the rear, front, or middle cut-in by sending a join request. If the gap for lane change to form a platoon or join an existing platoon is not enough, the on platooning NCAV will slightly slow down to increase the

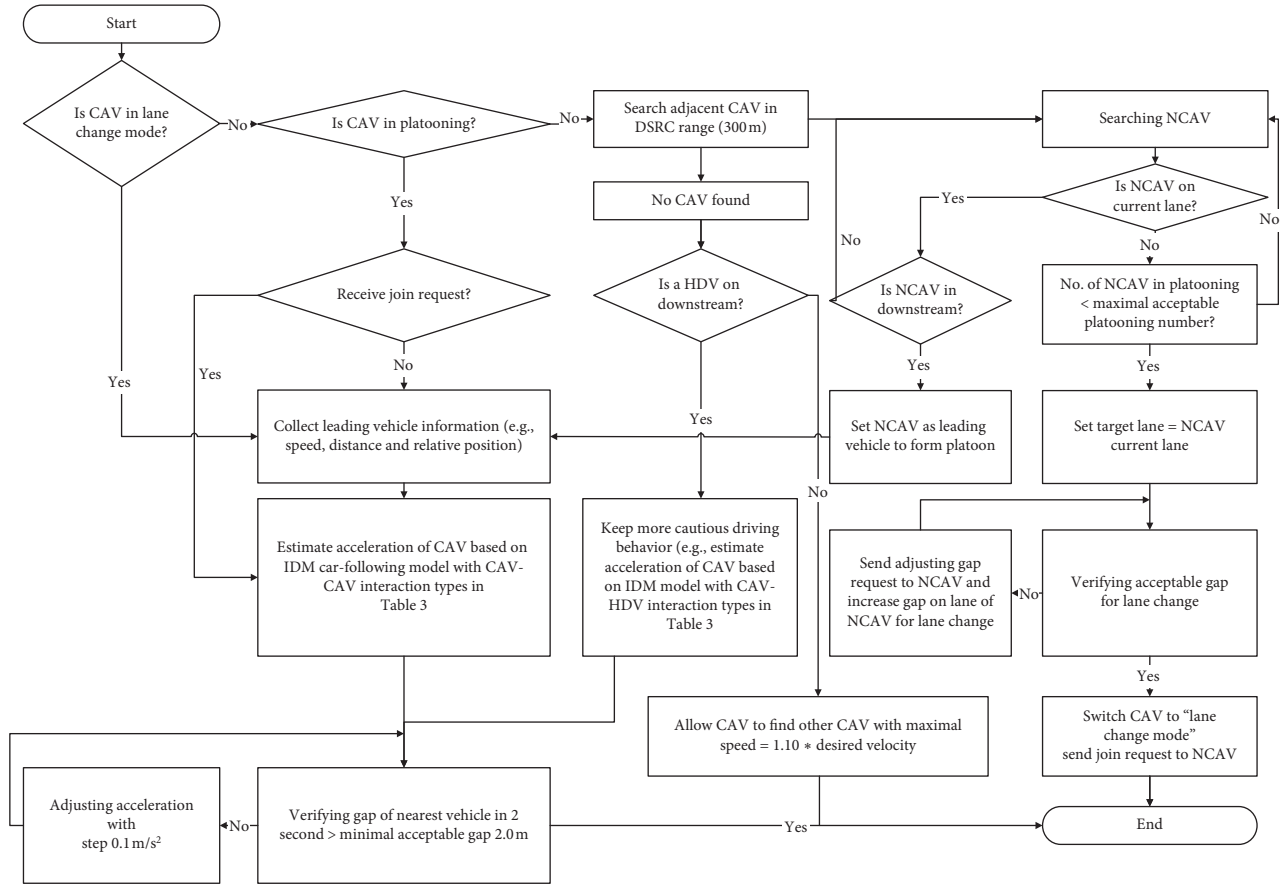

Figure 2: Platoon controlling algorithm for CAVs.

gap. If an HDV is found downstream on the current lane, the CAV will follow it with a cautious headway (e.g., change to CAV-HDV interaction types). If no vehicle is found downstream in the DSRC range, the individual CAV is allowed to cruise with an increasing 10% of the speed limit as the desired speed to search the NCAV. Note that if the current NCAV does not meet the platooning requirement, the CAV will set the second nearest CAV as NCAV.

3.2. Simulation Testbed Construction

3.2.1. Exclusive Lane Scenarios. The simulation testbed is an around 7 km segment of Ninghu Freeway, a four-lane freeway in Jiangsu province connecting Shanghai and Nanjing, China, with a speed limit of 120 km/h for cars and 80 km/h for trucks. The testbed section consists of three on-ramps and two off-ramps with approximately 30% trucks. In this study, we designed three scenarios of CAV's exclusive lanes, and Figure 3 formulates three deployment scenarios for testing. The base scenario serves as the base condition of the Ninghu segment for this study. The exclusive lane scenarios' access to one or two leftmost exclusive lanes for CAVs is studied. The left-lane deployment of exclusive lanes causes weaving activities around on-ramps and off-ramps. Therefore, the weaving length for CAVs toward or leaving the exclusive lane has to be considered. According to the experience on the existing bus managed lane, 300 meters of weaving length for the exclusive lane entry/exit is recommended by the FAJ.

3.2.2. Calibration and Validation. One of the most important parts of any simulation-based studies is calibration. In this study, humans' driving behavior data were collecting by the Administration of Ninghu Freeway from field detectors, and these data are applied for calibration and validation. Traffic volume and speed from field detectors on 16 : 30–19 : 30, September 30th, 2018, collected from 16 field detectors were aggregated into 10 minutes and used as vehicle inputs. The first 30 minutes of simulation time and the last 30 minutes cool-down time of the simulation are excluded for calibration and validation. The calibration target can be described as

$$\min \varepsilon = \sqrt{\frac{\sum_t \left(q^{\text{obs}}(t) - q^{\text{sim}}(t,\theta)\right)^2}{\sum_t \left(q^{\text{obs}}(t)\right)^2}} + \sqrt{\frac{\sum_t \left(v^{\text{obs}}(t) - v^{\text{sim}}(t,\theta)\right)^2}{\sum_t \left(v^{\text{obs}}(t)\right)^2}}, \tag{2}$$

where ε = calibrate error, $q^{\text{obs}}(t)$ = observed traffic volume on collecting interval t, $v^{\text{obs}}(t)$ = average observed travel speed on the interval t, θ = parameter vectors for simulation, $q^{\text{sim}}(t,\theta)$ = traffic volume on collecting the interval t in simulation, and $v^{\text{sim}}(t,\theta)$ = average travel speed on collecting interval t in simulation. Calibrate result shows that the average calibrate error is 4.66%, which meets the

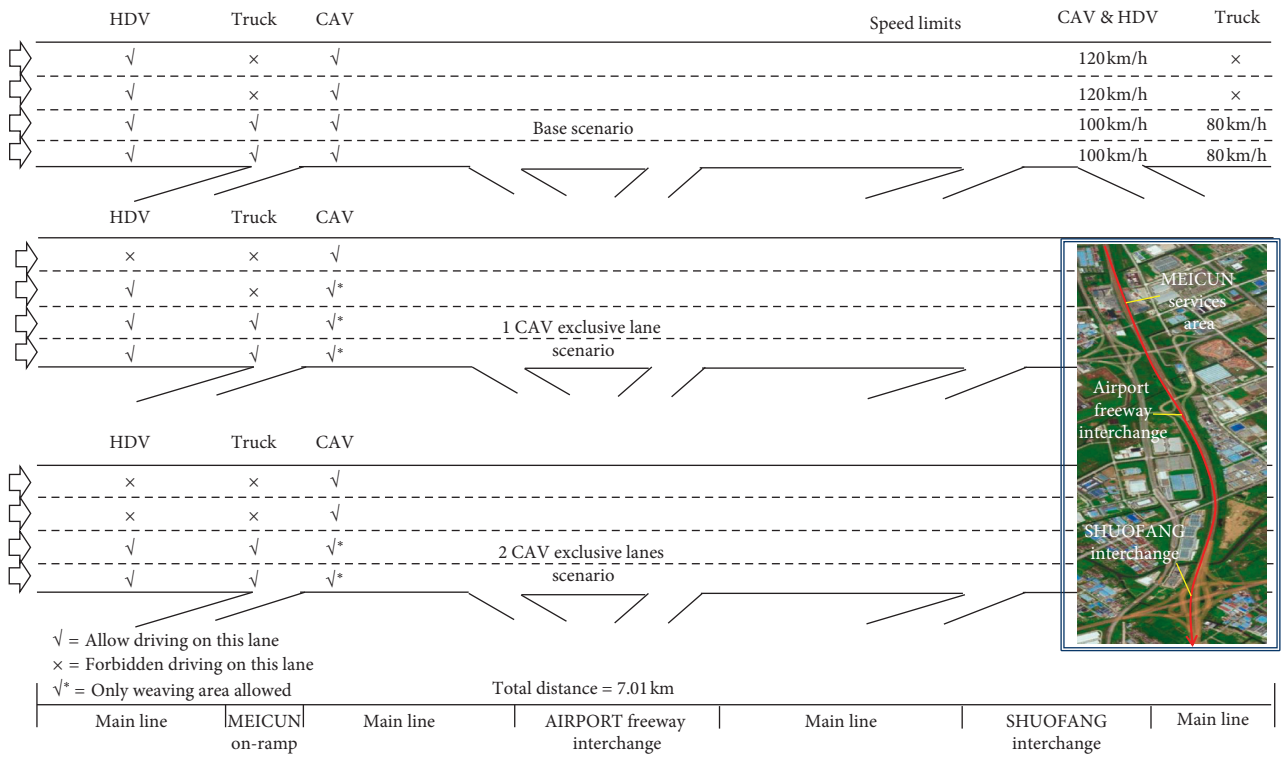

Figure 3: Description of three deployment scenarios.

requirement for further simulation. After calibration, CC0, CC1, and CC2 in Wiedemann 99 model are calibrated to 2.1 m, 1.52 s, and 0.60, respectively. Due to missing of statistic data, the lengths and weighs of cars and trucks are adopted to default normal distributions.

3.3. Surrogate Measures of Safety. Surrogate safety measures are a widely utilized technique to evaluate the risk of crashes on traffic facilities (e.g., freeway and urban road network); although crashes are rare, they may cause severe consequences. Machine learning and statistical-based approaches have been applied to analyze crashes attributes according to crash records [43], but records of crashes between CAVs and HDVs are insufficient yet. Therefore, many effective indexes have been proposed by former researchers for evaluating crash risks in mixture environment; among them, Time-to-Collision (TTC) is one of the most common indicators which can be used for calculating the safety between two individual vehicles for every simulation second or interval of subsecond. The TTC notion was firstly proposed by [44] which is referred to the time that remains until a collision between the leading and following vehicle if the speed of the following vehicle is over than the leading vehicle and the speed difference is maintained. The TTC notion can be described as

$$\mathrm{TTC}_i(k) = \begin{cases} \dfrac{x_{i-1}(k) - x_i(k) - l}{v_{i-1}(k) - v_i(k)}, & v_{i-1}(k) > v_i(k), \\ \infty, & \text{otherwise}, \end{cases} \tag{3}$$

where $\mathrm{TTC}_i(k)$ = the time-to-collision of the vehicle i at simulation instant k, x = the position of the vehicle i, v = the speed of the vehicle i, and l = the length of the preceding vehicle $i-1$.

3.3.1. Longitudinal Safety Measurement. It is intuitive that the smaller TTC value means higher crash risk. Although TTC reflects the rear-end collision risk closely, it needs to be aggregated to the more aggregated indicators for statistically compatible analysis. For this sake, two surrogate measures of safety, derived from TTC and denoted as Time Exposed Time-to-collision (TET) and Time Integrated Time-to-collision (TIT), proposed by [45], are used for building a relationship between simulation data and longitudinal safety of the CAV.

The TET represents the total time exposed in the risk of collision, characterized by TTC value lower than the threshold TTC^* value :

$$\begin{aligned} \mathrm{TET}(k) &= \sum_{i=1}^{N} \delta_t \times \Delta k, \\ \delta_t &= \begin{cases} 1, & \forall 0 < \mathrm{TTC}_i(k) \le \mathrm{TTC}^*, \\ 0, & \text{otherwise}, \end{cases} \\ \mathrm{TET} &= \sum_{k=0}^{T} \mathrm{TET}(k), \end{aligned} \tag{4}$$

where k = simulation time instant (warm-up time excluded), Δk = simulate time steps (=0.1 s), $\mathrm{TTC}_i(k)$ = the time-to-collision of the vehicle i at simulation instant k. N = the total

number of vehicles, T = the simulation period, and TTC^* = the threshold of TTC. TTC^* is applied to identify from considering ones driving is safe or unsafe, and its value varies from 1 s to 3 s.

The TIT notion is also an index that measures the entity of the TTC lower than TTC^*. The reciprocal transformation is put into consideration since lower TTC means higher collision risk, and it can be described as

$$\mathrm{TIT}(k) = \sum_{i=1}^{N}\left[\frac{1}{\mathrm{TTC}_i(k)} - \frac{1}{\mathrm{TTC}^*}\right] \times \Delta k, \quad \text{when } 0 < \mathrm{TTC}_i(k) \le \mathrm{TTC}^*,$$
$$\mathrm{TIT}(k) = \sum_{k=0}^{T} \mathrm{TIT}(k). \tag{5}$$

Additionally, the Rear-End Crash Risk Index (RCRI), proposed by [46], was designed on the background of rear-end crashes which are the most common type of crashes in traffic facilities and are used for evaluating longitudinal road safety. The index illustrates a rear-end crash may appear if a leading vehicle makes a sudden brake, and the following fails to react and decelerate to safe distance in time. In this case, the stopping distance of the following vehicle should be smaller than the leading vehicle for preventing collision, and this relationship can be expressed as

$$D_{\mathrm{stop},L} = v_L(k) \times h(k) + \frac{v_L^2(k)}{2 \times a_L(k)} + l,$$
$$D_{\mathrm{stop},F} = v_F(k) \times \mathrm{PRT} + \frac{v_F^2(k)}{2 \times a_F(k)}, \quad D_{\mathrm{stop},F} < D_{\mathrm{stop},L}, \tag{6}$$

where $D_{\mathrm{stop},L}$ and $D_{\mathrm{stop},F}$ are the stopping distance of the leading vehicle and the following vehicle, $v_L(k)$ and $v_F(k)$ are the speed of two vehicles at simulation instant k, $a_F(k)$ and $a_L(k)$ are the acceleration of two vehicles, $h(k)$ is the time headway, l is the length of the leading vehicle, and PRT is the perception-reaction time with a constant value of 1.5 s recommended by the American Association of State Highway and Transportation Officials (AASHTO). Similar to TTC, RCRI needs to be aggregate to an index for measuring surrogate safety, which is proposed by [27] and denoted as the Time Exposed Rear-End Crash Risk Index (TERCRI):

$$\mathrm{TERCRI}(k) = \sum_{i=1}^{N} \mathrm{RCRI}(k) \times \Delta k,$$
$$\mathrm{RCRI}(k) = \begin{cases} 1, & D_{\mathrm{stop},F} > D_{\mathrm{stop},L}, \\ 0, & \text{otherwise}, \end{cases} \tag{7}$$
$$\mathrm{TERCRI} = \sum_{k=0}^{T} \mathrm{TERCRI}(k).$$

3.3.2. Lateral Safety Measurement. The mentioned indexes above are all associated with longitudinal safety. However, angle and sideswipe crashes, which are highly associated with lateral safety, are also common at freeway mainline or weaving zones along with rear-end crashes. Thus, it is necessary to measure lateral safety for CAV environment. In order to evaluate the angle and sideswipe crash risk of CAVs, the Surrogate Safety Assessment Model (SSAM) is used in this study. SSAM is developed by the Federal Freeway Administration, which has several parameters to measure conflicts. SSAM utilizes trajectory files (∗.fzp) outputted from VISSIM and checks for traffic conflicts using predefined TTC and Post Encroachment Time (PET), Speed Difference (DeltaS), and some other thresholds. The default value of TTC and PET is 1.5 s and 5 s, respectively. Along with the investigation of conflicting vehicles, SSAM provides conflict results classified by the conflict type (i.e., rear-end, lane change, and crossing). In this study, the number of lane change conflicts (#LCC) of different scenarios is analyzed by SSAM.

Collection of surrogate safety measures is also implemented by the External Driver Model (EDM). The aggregated value of TET, TIT, TERCRI, and LCC is calculated directly by every simulation step for all vehicles. Note that although human-driven vehicles deployed the External Driver Model to collect SSAM data, their driving behavior maintaining is unchanged.

4. Results and Discussion

Traffic crashes are rare on freeways. Hence, surrogate safety measures are a widely used technology to evaluate the crash risk. In this paper, in order to evaluate the read-end collision risk and lane change conflict, four surrogate safety measures, including TET, TIT, TERCRI, and #LCC, are employed. The first three indexes were directly outputted by the modified External Driver Model, and the last index was transferred to SSAM to identify #LCC. It must be noted that although the threshold value of TTC was chosen as 2.0 s, a sensitivity analysis for TTC values of 1.0, 1.5, 2.0, 2.5, and 3.0 s was also conducted, and the result shows that the threshold has negligible effects on crash risks. We tested three scenarios (0, 1, or 2 exclusive lane (s)) with consideration of different traffic demands (2000, 4000, 6000, or 8000 veh/h) and compositions (truck proportion = 0, 10%, 20%, and 30%; CAV MPRs = 0, 10%, 20% and 30%). Note that the chosen ratios of truck and classifications of traffic demand were derived from the field data from the Ninghu Freeway.

4.1. Overall Analysis. Classified by traffic volume, original scatter values are converted to contour maps, and results are presented in Figures 4–7, which represent overall safety impacts of CAV exclusive lanes on different traffic demands and compositions. The input values of traffic demand cover all types of vehicles for this segment (e.g., not the single lane volume); therefore, the capacity constraint that the capacity of the freeway is around 2000 ver/h/ln can be met.

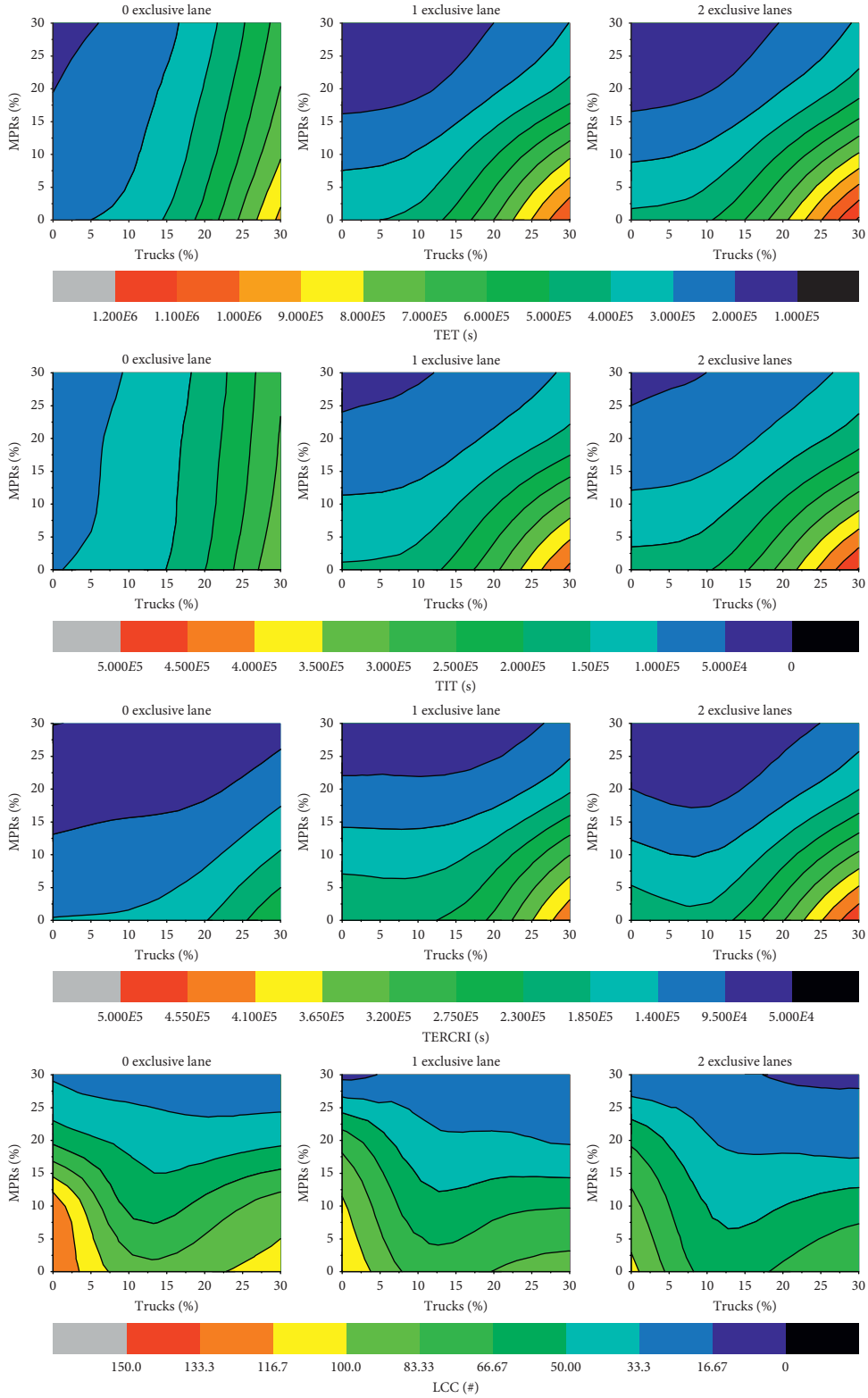

Figure 4: Safety evaluation results of CAV's exclusive lane on volume = 2000 veh/h.

Horizontal arrangement of figures has colored to the same color scales for comparison. The colors are generated by interpolation from blue to red, which stands for lower and higher values, respectively. It must be pointed out that although these figures seem to have little distinction among different colors, their absolute values are very different. Value of total TET in 2,000, 4,000, 6,000, and 8,000 veh/h with 0% truck, 0% MPRs, and 1 exclusive lane is 387553, 1131240, 1936829, and 2060508 seconds, respectively. On the contrary, for detailed analysis, a line chart analysis for

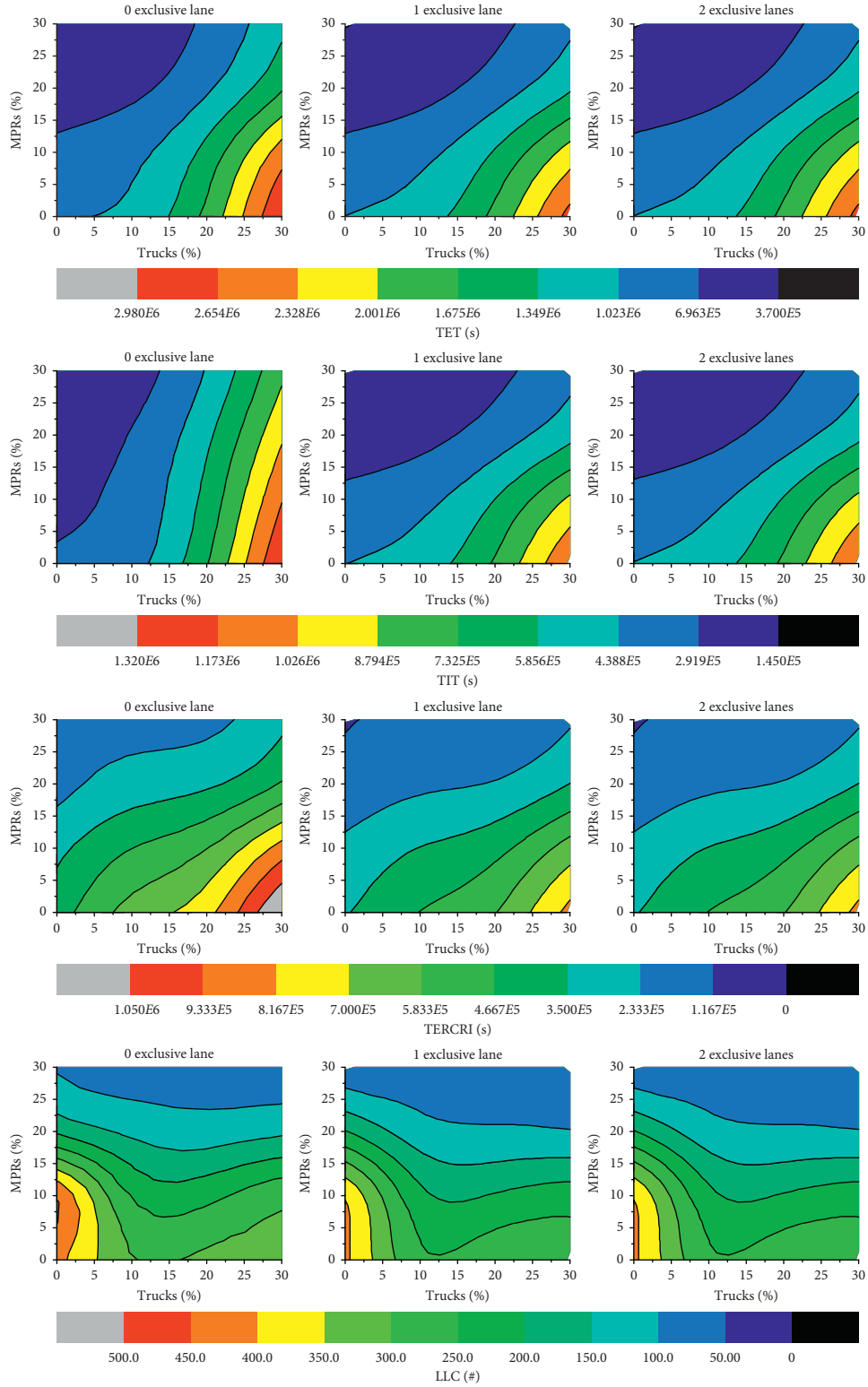

Figure 5: Safety evaluation results of CAV's exclusive lane on volume = 4000 veh/h.

TET and LCC on MPRs = 10% and 20% is presented in Figure 8. Finally, an overall longitudinal and lateral safety impact comparison of setting exclusive lane scenarios toward the base scenario is shown in Table 4.

For all situations, we found that, with the increase of truck proportion, longitudinal safety risk indexes (e.g., TET, TIT, and TERCRI) are at a rise in all scenarios, indicating that heterogeneity of traffic composition

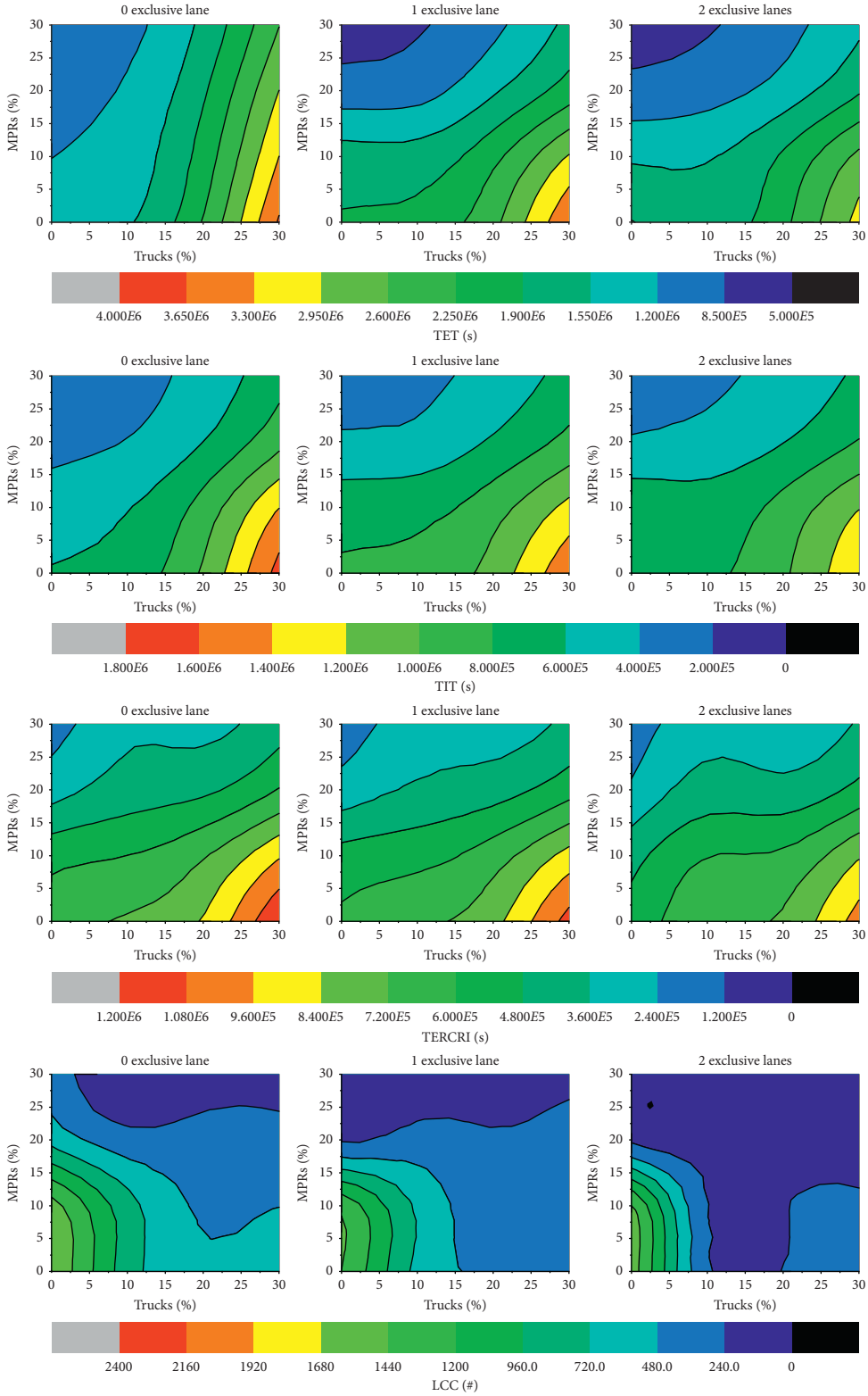

Figure 6: Safety evaluation results of CAV's exclusive lane on volume = 6000 veh/h.

contributes to rear-end crash risks. In general, the variations of three longitudinal safety risk indexes are largely similar, and since TET and TIT are different aggregate forms of TTC, their trend seem to be more similar. The similarity indicates that all three indexes are capable to be replaced by each other. In this regard, we choose TET to stand for longitudinal result in longitudinal safety impact analysis, while for #LCC, which represents lateral crash

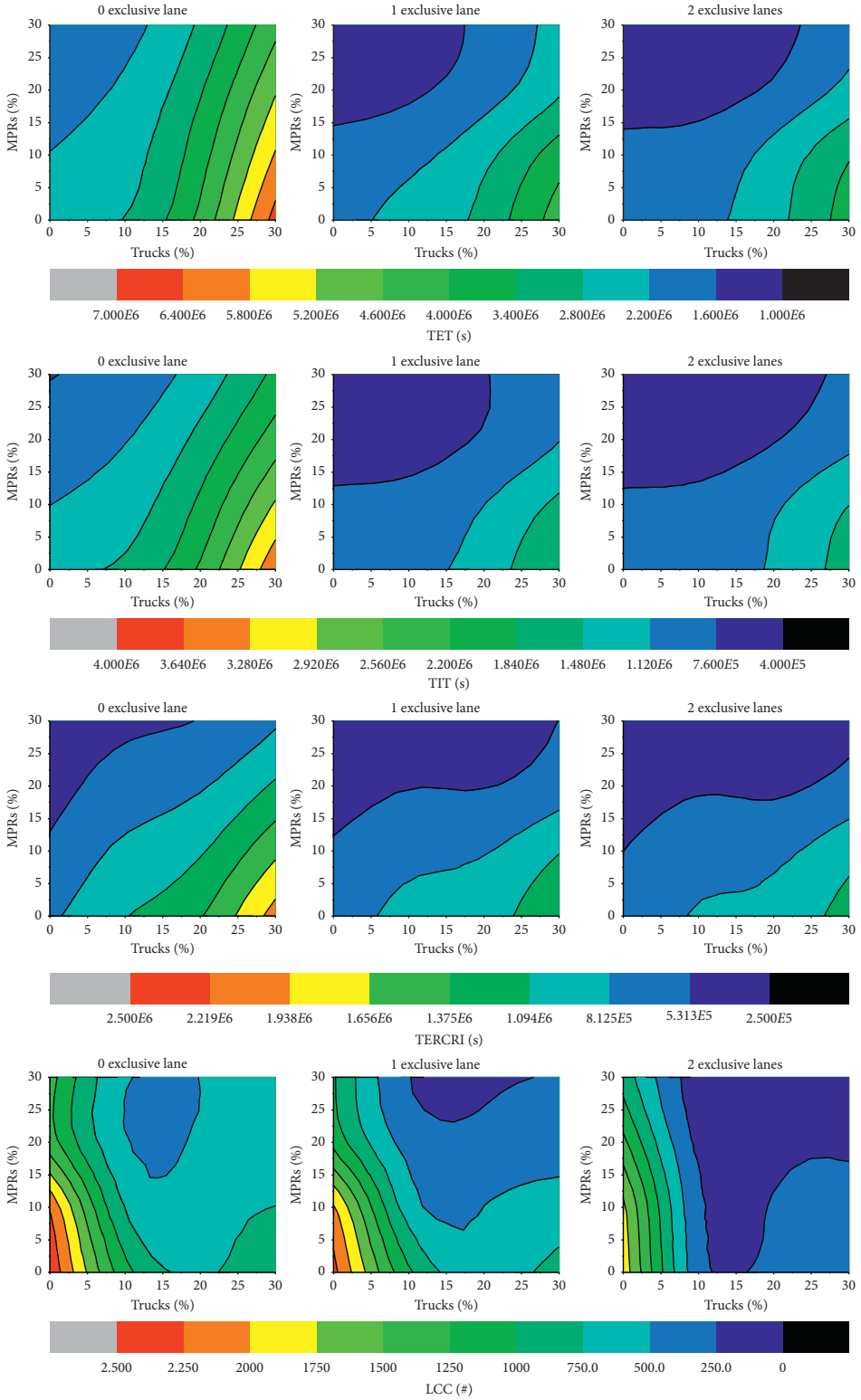

Figure 7: Safety evaluation results of CAV's exclusive lane on volume = 8000 veh/h.

risks, appeared to decrease with the increase of truck proportion firstly and then slowly rise in low MPRs of CAVs according to Figure 8 (1c-1d; 2c-2d; 3c-3d; 4c-4d). This difference reflects different driving behaviors between car and trucks. A possible explanation is that due to the limitation of available lanes, trucks' lane changes are less than cars, and with the increase of truck proportion, overall performance is deteriorating, and some radical

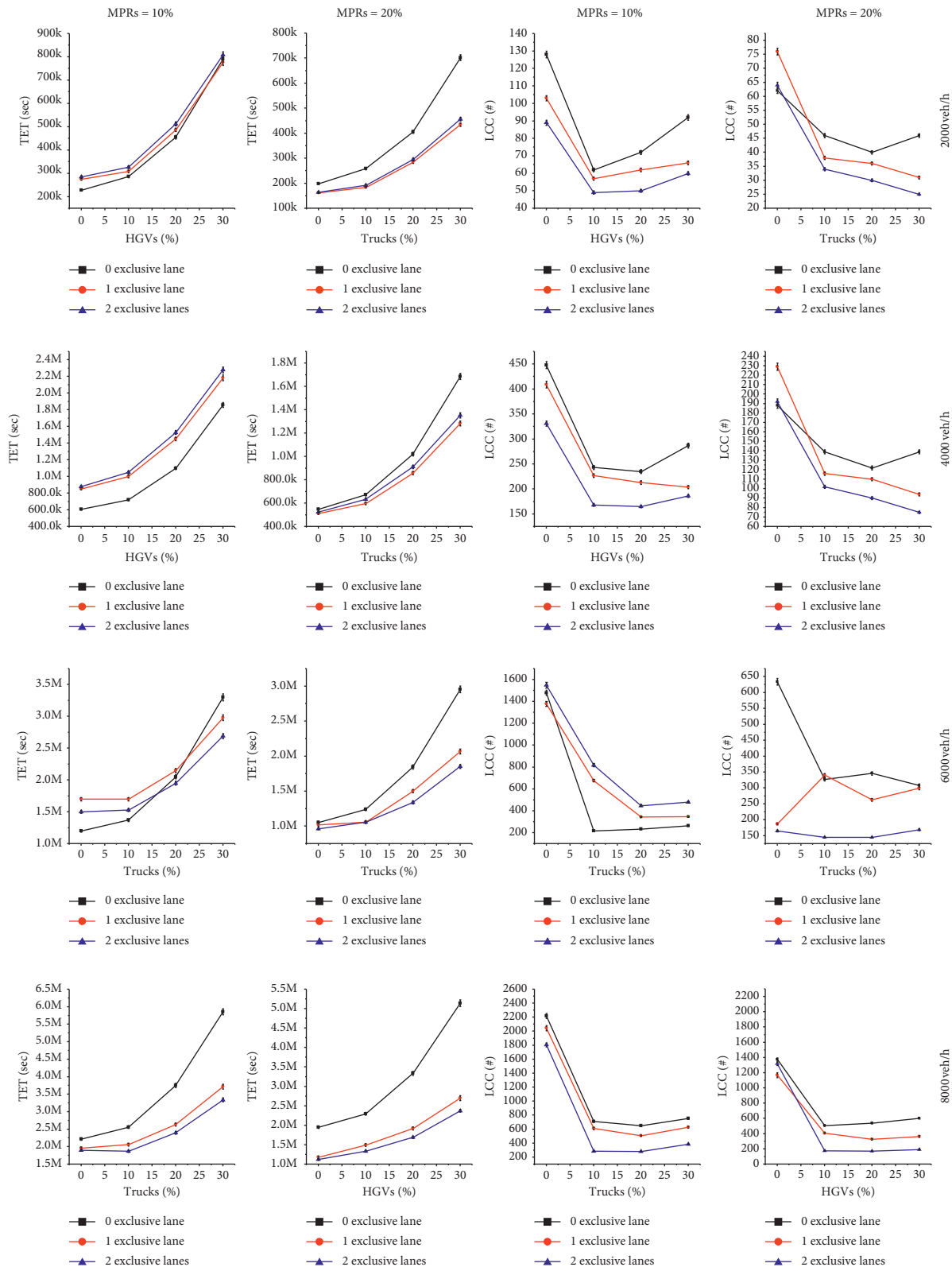

Figure 8: Comparison of safety impacts between MPRs = 10% and MPRs = 20%.

drivers would try to change the current lane for ensuring their efficiency. Since literature [47] has pointed out using simulation data for analyzing LCC has its limitation and it might not truly reflect the real-world situations, the impact of lane change still needs further examination from field test data [48].

Table 4: Safety impacts of setting exclusive lanes compared with the base scenario.

MPRs = 10%	Trucks (%)	2000 veh/h		4000 veh/h		6000 veh/h		8000 veh/h	
		TET (%)	LCC (%)	TET (%)	LCC (%)	TET (%)	LCC (%)	TET (%)	LCC (%)
1 exclusive lane	0	−20.5	19.5	−40.4	8.7	−42.4	11.0	11.6	7.9
	10	−7.6	8.1	−38.8	6.6	−24.4	17.1	19.7	13.8
	20	−7.0	13.9	−32.1	9.4	−5.2	23.0	29.6	21.8
	30	1.8	28.3	−17.5	28.9	9.6	27.6	36.5	16.6
2 exclusive lanes	0	−24.9	30.5	−44.7	26.1	−25.1	4.5	14.1	18.6
	10	−14.2	21.0	−45.7	30.9	−11.6	73.6	27.0	59.7
	20	−12.5	30.6	−39.0	29.8	4.9	47.8	35.9	56.9
	30	−2.3	34.8	−22.8	35.2	18.5	45.1	42.9	48.6
MPRs = 20%	Trucks (%)	2000 veh/h		4000 veh/h		6000 veh/h		8000 veh/h	
		TET (%)	LCC (%)	TET (%)	LCC (%)	TET (%)	LCC (%)	TET (%)	LCC (%)
1 exclusive lane	0	18.6	2.6	6.8	1.8	3.5	70.5	39.5	15.0
	10	28.9	17.4	11.2	16.5	14.8	39.8	35.0	19.7
	20	29.9	10.0	16.0	9.8	18.7	24.0	42.4	39.6
	30	38.1	32.6	23.9	32.4	30.0	2.9	47.5	39.7
2 exclusive lanes	0	17.1	3.2	4.4	2.1	8.6	74.0	42.4	4.1
	10	25.9	26.1	5.8	26.6	14.9	55.7	41.8	65.5
	20	27.1	25.0	10.8	26.2	27.4	58.1	49.3	68.3
	30	35.0	45.7	19.8	46.0	37.3	45.1	53.8	67.9
MPRs = 30%	Trucks (%)	2000 veh/h		4000 veh/h		6000 veh/h		8000 veh/h	
		TET (%)	LCC (%)	TET (%)	LCC (%)	TET (%)	LCC (%)	TET (%)	LCC (%)
1 exclusive lane	0	31.5	61.3	23.9	61.7	24.3	87.1	29.1	23.8
	10	40.7	4.0	27.8	3.9	25.9	60.4	32.9	52.8
	20	44.3	12.5	32.8	11.1	31.2	42.1	40.4	57.8
	30	52.9	14.3	40.1	13.8	36.5	50.8	45.1	54.3
2 exclusive lanes	0	31.7	38.7	24.4	38.3	25.6	85.3	35.2	33.1
	10	39.0	12.0	26.2	10.5	25.9	59.6	43.4	77.1
	20	43.0	37.5	30.9	36.1	33.4	47.4	50.5	77.6
	30	51.1	28.6	38.7	27.7	42.5	51.7	55.2	77.6

4.2. Safety Impacts of Exclusive Lanes. As the TIT, TET, and TERCRI indexes are shown in Figures 4–7 (1a–3c), we found that setting of exclusive lanes in MPRs < 10% led to slight increase of longitudinal safety risks on volume = 2000 veh/h (Figure 4 (1a–1c)) and continuing at a rise with the increasing of truck proportion (Figure 8 (1a–4a)). Compared with the base scenario, setting exclusive lanes in traffic demands > 4000 veh/h and MPRs < 10% inducing higher rear-end risks, which indicates only in situation that traffic demand is large enough could the CAV's exclusive lane have positive impact on safety. As the MPRs increased to 20% (Figure 8 (1b–4b)), the longitudinal and lateral safety improve proportionately compared with the base scenario.

As for the LCC index shown in Figures 4–7 (4a–4c), for all traffic demands, setting of exclusive lanes reduce overall LCCs, and the difference exists on the extent of decrease. Longitudinal comparison among demands shows that higher traffic demands have better improvement of LCC compared with low traffic demands.

Numerical comparison for exclusive lane scenarios is also conducted in Table 4 for further analyzing safety impact. As is depicted in Table 4, setting one or two exclusive lanes led to [+42.4% to −52.90%] and [+45.7% to −55.2%] for longitudinal crash risks (TET) while [−1.8% to −87.1%] and [−2.1% to −85.3%] for lateral crash risks compared with the base scenario, respectively. Only in MPRs = 10% and demands lower than 6000 veh/h scenarios, the setting of exclusive lanes has adverse effect on longitudinal, which indicates that in other scenarios, setting exclusive lanes for CAVs outweigh than the base scenario. It must be noted that the improvement of longitudinal crash risks arose with the increase of truck proportion. This is explainable as the driving behavior of trucks is largely homogenous. On the contrary, total longitudinal crash risks are at a sharp rise according to Figure 8 (1a–3b) with increasing of truck proportions, which indicates that setting exclusive lanes for CAVs have better safety improvement when truck's proportion is over 20%.

We also focused on the comparison of the number of exclusive lanes. As longitudinal indexes depicted on the low demand scenario, the distinction between one or two exclusive lanes is generally inconspicuous on low truck proportion, while in low traffic demand, high truck proportion, and low MPR condition, the setting of two exclusive lanes caused an increase of longitudinal rear-end risks compared with one exclusive lane scenario, indicating that setting two exclusive lanes for this situation is unwise. Only in demand = 8000 veh/h situation, two exclusive lane scenarios outweighs one exclusive lane scenario on both longitudinal and lateral safety improvement.

5. Conclusions and Future Study

In this work, safety evaluation of exclusive lanes for CAV on the freeway is conducted using a calibrated microscopic simulation model with surrogate safety measures. This paper firstly modelled the mixture environment [49, 50] of CAVs platooning with HDVs and then designed three exclusive lane scenarios and deployed surrogate safety measures to reveal pros and cons of exclusive lanes. In this paper, four surrogate safety measure indexes, including both longitudinal and lateral indexes, are developed. Results show that (1) setting one exclusive lane is capable of improving the overall safety in low demand, and setting two exclusive lanes is more suitable for the high-demand scenario; (2) the existence of trucks worsens the overall longitudinal safety, and improper settings of exclusive lanes in high truck's proportion and low MPRs situation could even worsen the longitudinal safety, which should be avoided; (3) setting exclusive lanes has better longitudinal and lateral safety improvement in high truck proportion scenarios; (4) when the MPRs are larger than 15%, setting exclusive lanes for CAVs can considerably reduce the overall crash risks, and the safety improves as the proportion of trucks increases; and (5) the variation among TET, TIT, and TERCRI is very similar, indicating that the three indexes can replace each other.

This paper highlights (1) the influence of trucks on the safety impact of setting exclusive lanes for CAVs on the freeway and (2) reveals the dynamic safety relationship among traffic demand, composition, MPRs, and the number of exclusive lanes. The authors hope these results can be helpful to determine when it is suitable to set the exclusive lane for CAVs. The proposed surrogated safety measures can be extended to other freeway scenarios (i.e., 2 or 3 lane freeway), and the application of exclusive lanes for CAVs has great potential in practice.

Due to inadequate data, this simulation-based research study still needs further examination and calibration with field-test data of autonomous vehicles. This paper also has some shortcomings as it only considered total safety impacts for freeway facility whereas neglecting detail investigation of its component. Merging speed and driving ability (e.g., lane change confidence, lane-keeping instability, and the merging location) on weaving areas can affect the crash risk ([51–53]), and these factors should be further analyzed. From authors view, more lateral safety risk indexes should be developed and examined to well-fit real-world situation for mixture CAV with HDV environment in future studies.

Data Availability

The data used to support the findings of this study are available from the corresponding author upon request.

Conflicts of Interest

The authors declare that there are no conflicts of interest regarding the publication of this paper.

Acknowledgments

This research was supported by the National Key R&D Program in China (Grant no. 2016YFB0100906) and the Fundamental Research Funds for the Central Universities (no. 2242019R40046). The work of the first author was supported in part by the Zhishan Young Scholar Support Program of Southeast University and the Science and Technology Major Project, Transportation of Jiangsu Province.

References

[1] J. Guanetti, Y. Kim, and F. Borrelli, "Control of connected and automated vehicles: state of the art and future challenges," *Annual Reviews in Control*, vol. 45, pp. 18–40, 2018.

[2] H. S. Mahmassani, "50th anniversary invited article-autonomous vehicles and connected vehicle systems: flow and operations considerations," *Transportation Science*, vol. 50, no. 4, pp. 1140–1162, 2016.

[3] A. Talebpour and H. S. Mahmassani, "Influence of connected and autonomous vehicles on traffic flow stability and throughput," *Transportation Research Part C: Emerging Technologies*, vol. 71, pp. 143–163, 2016.

[4] A. Alam, A. Gattami, and K. H. Johansson, "An experimental study on the fuel reduction potential of heavy duty vehicle platooning," in *Proceedings of the 13th International IEEE Conference on Intelligent Transportation Systems*, pp. 306–311, Funchal, Portugal, September 2010.

[5] J. K. Hedrick, D. H. Mcmahnon, and D. Swaroop, *Vehicle Modeling and Control for Automated Highway Systems*, University of California, Berkeley, CA, USA, 1993.

[6] W. Van Willigen, E. Haasdijk, and L. Kester, "A multi-objective approach to evolving platooning strategies in intelligent transportation systems," in *Proceeding of the Fifteenth Annual Conference on Genetic and Evolutionary Computation Conference-GECCO'13*, pp. 1397–1404, New York, NY, USA, 2013.

[7] T. Van Den Broek, J. Ploeg, and B. D. Netten, "Advisory and autonomous cooperative driving systems," in *Proceeding of the International Conference on Consumer Electronics*, pp. 279-280, Las Vegas, NV, USA, January 2011.

[8] S. Gong, A. Zhou, J. Wang, T. Li, and S. Peeta, "Cooperative adaptive cruise control for a platoon of connected and autonomous vehicles considering dynamic information flow topology," 2018, https://arxiv.org/abs/1807.02224.

[9] D. Swaroop and J. K. Hedrick, "String stability of interconnected systems," *IEEE Transactions on Automatic Control*, vol. 41, no. 3, pp. 349–357, 1996.

[10] G. J. L. Naus, R. P. A. Vugts, J. Ploeg, M. J. G. Van De Molengraft, and M. Steinbuch, "String-stable CACC design and experimental validation: a frequency-domain approach," *IEEE Transactions on Vehicular Technology*, vol. 59, no. 9, pp. 4268–4279, 2010.

[11] A. Kesting, M. Treiber, M. Schönhof, and D. Helbing, "Adaptive cruise control design for active congestion avoidance," *Transportation Research Part C: Emerging Technologies*, vol. 16, no. 6, pp. 668–683, 2008.

[12] A. Tuchner and J. Haddad, "Vehicle platoon formation using interpolating control: a laboratory experimental analysis," *Transportation Research Part C: Emerging Technologies*, vol. 84, pp. 21–47, 2017.

[13] A. Mirheli, L. Hajibabai, and A. Hajbabaie, "Development of a signal-head-free intersection control logic in a fully connected

and autonomous vehicle environment," *Transportation Research Part C: Emerging Technologies*, vol. 92, pp. 412–425, 2018.

[14] A. Ghiasi, O. Hussain, Z. (Sean) Qian, and X. Li, "A mixed traffic capacity analysis and lane management model for connected automated vehicles: a Markov chain method," *Transportation Research Part B: Methodological*, vol. 106, pp. 266–292, 2017.

[15] S. Gong, J. Shen, and L. Du, "Constrained optimization and distributed computation based car following control of a connected and autonomous vehicle platoon," *Transportation Research Part B: Methodological*, vol. 94, pp. 314–334, 2016.

[16] O. Hussain, A. Ghiasi, and X. Li, "Freeway lane management approach in mixed traffic environment with connected autonomous vehicles," 2016.

[17] S. Gong and L. Du, "Cooperative platoon control for a mixed traffic flow including human drive vehicles and connected and autonomous vehicles," *Transportation Research Part B: Methodological*, vol. 116, pp. 25–61, 2018.

[18] J. Wagner, M. Lukuc, and M. Moran, "Regulatory and legal review of automated and connected truck platooning technology," *Transportation Research Board*, 2017.

[19] D. Yang, X. Qiu, D. Yu, R. Sun, and Y. Pu, "A cellular automata model for car-truck heterogeneous traffic flow considering the car-truck following combination effect," *Physica A: Statistical Mechanics and its Applications*, vol. 424, pp. 62–72, 2015.

[20] Y. Zhang, Y. Jiang, W. Rui, and R. G. Thompson, "Analyzing truck fleets' acceptance of alternative fuel freight vehicles in China," *Renewable Energy*, vol. 134, pp. 1148–1155, 2019.

[21] F. Lattemann, K. Neiss, S. Terwen, and T. Connolly, "The predictive cruise control–a system to reduce fuel consumption of heavy duty trucks," *SAE Trans.*vol. 113, no. 2, pp. 139–146, 2004.

[22] M. R. I. Nieuwenhuijze, T. van Keulen, S. Oncu, B. Bonsen, and H. Nijmeijer, "Cooperative driving with a heavy-duty truck in mixed traffic: experimental results," *IEEE Transactions on Intelligent Transportation Systems*, vol. 13, no. 3, pp. 1026–1032, 2012.

[23] B. Ran and H.-S. Tsao, "Traffic flow analysis for an automated highway system," 1996.

[24] K. Ma and H. Wang, "Influence of exclusive lanes for connected and autonomous vehicles on freeway traffic flow," *IEEE Access*, vol. 7, pp. 50168–50178, 2019.

[25] L. Ye and T. Yamamoto, "Impact of dedicated lanes for connected and autonomous vehicle on traffic flow throughput," *Physica A: Statistical Mechanics and its Applications*, vol. 512, pp. 588–597, 2018.

[26] A. Talebpour, H. S. Mahmassani, and A. Elfar, "Investigating the effects of reserved lanes for autonomous vehicles on congestion and travel time reliability," *Transportation Research Record: Journal of the Transportation Research Board*, vol. 2622, no. 1, pp. 1–12, 2017.

[27] M. S. Rahman and M. Abdel-Aty, "Longitudinal safety evaluation of connected vehicles' platooning on expressways," *Accident Analysis & Prevention*, vol. 117, pp. 381–391, 2018.

[28] A. Papadoulis, M. Quddus, and M. Imprialou, "Evaluating the safety impact of connected and autonomous vehicles on motorways," *Accident Analysis & Prevention*, vol. 124, pp. 12–22, 2019.

[29] M. S. Rahman, M. Abdel-Aty, J. Lee, and M. H. Rahman, "Safety benefits of arterials' crash risk under connected and automated vehicles," *Transportation Research Part C: Emerging Technologies*, vol. 100, pp. 354–371, 2019.

[30] J. Wang, Y. Zheng, Q. Xu, J. Wang, and K. Li, "Controllability analysis and optimal controller synthesis of mixed traffic systems," in *Proceedings of the IEEE Intelligent Vehicles Symposium*, pp. 1041–1047, Paris, France, June 2019.

[31] A. Kesting, M. Treiber, and D. Helbing, "Enhanced intelligent driver model to access the impact of driving strategies on traffic capacity," *Philosophical Transactions of the Royal Society A: Mathematical, Physical and Engineering Sciences*, vol. 368, no. 1928, pp. 4585–4605, 2010.

[32] B. Xu, X. Jeff Ban, Y. Bian, J. Wang, and K. Li, "V2I based cooperation between traffic signal and approaching automated vehicles," in *Proceedings of the 2017 IEEE Intelligent Vehicles Symposium (IV)*, Los Angeles, CA, USA, June 2017.

[33] Z. Vander Laan and K. F. Sadabadi, "Operational performance of a congested corridor with lanes dedicated to autonomous vehicle traffic," *International Journal of Transportation Science and Technology*, vol. 6, no. 1, pp. 42–52, 2017.

[34] M. Zhou, X. Qu, and S. Jin, "On the impact of cooperative autonomous vehicles in improving freeway merging: a modified intelligent driver model-based approach," *IEEE Transactions on Intelligent Transportation Systems*, vol. 18, no. 6, pp. 1422–1428, 2017.

[35] B. van Arem, C. J. G. van Driel, and R. Visser, "The impact of cooperative adaptive cruise control on traffic-flow characteristics," *IEEE Transactions on Intelligent Transportation Systems*, vol. 7, no. 4, pp. 429–436, 2006.

[36] W. Do, O. M. Rouhani, and L. Miranda-Moreno, "Simulation-based connected and automated vehicle models on highway sections: a literature review," *Journal of Advanced Transportation*, vol. 2019, Article ID 9343705, 14 pages, 2019.

[37] D. Solomon, "Accidents on main rural highways related to speed, driver, and vehicle," 1964.

[38] F. Chen, M. Song, X. Ma, and X. Zhu, "Assess the impacts of different autonomous trucks' lateral control modes on asphalt pavement performance," *Transportation Research Part C: Emerging Technologies*, vol. 103, pp. 17–29, 2019.

[39] M. Treiber, A. Hennecke, and D. Helbing, "Congested traffic states in empirical observations and microscopic simulations," *Physical Review E*, vol. 62, no. 2, pp. 1805–1824, 2000.

[40] G. M. Arnaout and J.-P. Arnaout, "Exploring the effects of cooperative adaptive cruise control on highway traffic flow using microscopic traffic simulation," *Transportation Planning and Technology*, vol. 37, no. 2, pp. 186–199, 2014.

[41] İ. Altay, B. Aksun Güvenç, and L. Güvenç, "Lidar data analysis for time to headway determination in the drivesafe project field tests," *International Journal of Vehicular Technology*, vol. 2013, Article ID 749896, 9 pages, 2013.

[42] I. K. Nikolos, A. I. Delis, and M. Papageorgiou, "Macroscopic modeling and simulation of ACC and CACC traffic," in *Proceedings of the 2015 IEEE 18th International Conference on Intelligent Transportation Systems*, pp. 2129–2134, Las Palmas, Spain, September 2015.

[43] J. Zhang, Z. Li, Z. Pu, and C. Xu, "Comparing prediction performance for crash injury severity among various machine learning and statistical methods," *IEEE Access*, vol. 6, pp. 60079–60087, 2018.

[44] J. C. Hayward, *Near-Miss Determination through Use of a Scale of Danger*, vol. 384, Penn State University, State College, PA, USA, 1972.

[45] M. M. Minderhoud and P. H. L. Bovy, "Extended time-to-collision measures for road traffic safety assessment," *Accident Analysis & Prevention*, vol. 33, no. 1, pp. 89–97, 2001.

[46] C. Oh, S. Park, and S. G. Ritchie, "A method for identifying rear-end collision risks using inductive loop detectors," *Accident Analysis & Prevention*, vol. 38, no. 2, pp. 295–301, 2006.

[47] F. Huang, P. Liu, H. Yu, and W. Wang, "Identifying if VISSIM simulation model and SSAM provide reasonable estimates for field measured traffic conflicts at signalized intersections," *Accident Analysis & Prevention*, vol. 50, pp. 1014–1024, 2013.

[48] L. Li, J. Zhang, Y. Wang, and B. Ran, "Missing value imputation for traffic-related time series data based on a multi-view learning method," *IEEE Transactions on Intelligent Transportation Systems*, vol. 20, no. 8, pp. 2933–2943, 2019.

[49] L. Cheng, X. Chen, S. Yang, Z. Cao, J. De Vos, and F. Witlox, "Active travel for active ageing in China: the role of built environment," *Journal of Transport Geography*, vol. 76, pp. 142–152, 2019.

[50] Y. Pan, S. Chen, F. Qiao, S. V. Ukkusuri, and K. Tang, "Estimation of real-driving emissions for buses fueled with liquefied natural gas based on gradient boosted regression trees," *Science of the Total Environment*, vol. 660, pp. 741–750, 2019.

[51] F. Chen, M. Song, and X. Ma, "Investigation on the injury severity of drivers in rear-end collisions between cars using a random parameters bivariate ordered probit model," *International Journal of Environmental Research and Public Health*, vol. 16, no. 14, p. 2632, 2019.

[52] F. Chen and S. Chen, "Injury severities of truck drivers in single- and multi-vehicle accidents on rural highways," *Accident Analysis & Prevention*, vol. 43, no. 5, pp. 1677–1688, 2011.

[53] X. Gu, M. Abdel-Aty, Q. Xiang, Q. Cai, and J. Yuan, "Utilizing UAV video data for in-depth analysis of drivers' crash risk at interchange merging areas," *Accident Analysis & Prevention*, vol. 123, pp. 159–169, 2019.

Hindawi
Journal of Advanced Transportation
Volume 2020, Article ID 3594963, 14 pages
https://doi.org/10.1155/2020/3594963

Research Article

Analysis of Crossing Behavior and Violations of Electric Bikers at Signalized Intersections

Tianpei Tang,[1,2,3] Hua Wang ,[3,4] Jie Ma,[4,5] and Xizhao Zhou[1]

[1]*Business School, University of Shanghai for Science and Technology, Shanghai 200093, China*
[2]*School of Transportation and Civil Engineering, Nantong University, Nantong 226019, China*
[3]*School of Economics and Management, Tongji University, Shanghai 200092, China*
[4]*Department of Civil and Environmental Engineering, National University of Singapore, Singapore 117576*
[5]*School of Transportation, Southeast University, Nanjing 211189, China*

Correspondence should be addressed to Hua Wang; hwang191901@gmail.com

Received 26 August 2019; Accepted 30 September 2019; Published 20 January 2020

Guest Editor: Qiang Zeng

This paper focuses on investigating electric bikers' (e-bikers) crossing behavior and violations based on survey data of 3,126 e-bikers collected at signalized intersections in Nantong, China. We first explore e-bikers' characteristics of late crossing, incomplete crossing, and violating crossing behaviors by frequency analysis and duration distribution, and examine a few influential factors for e-bikers' red-light running (RLR) behavior, including site type, crossing length and traffic signal countdown timers (TSCTs). E-bikers' RLR behavior is further divided into three categories, namely GR near-violations, RR violations, and RG violations. Second, we use a binary logistic regression model to identify the relationship between e-bikers' RLR behavior and potential influential factors, including demographic attributes, movement information, and infrastructure conditions. We not only make regression analysis for respective violation type, but also carry out an integrated regression of a census of all three types of violations. Some insightful findings are revealed: (i) the green signal time and site type are the most significant factors to GR near-violations, but with little impact on the other two violation types; (ii) the waiting time, waiting position, passing cars and crossing length exert considerable impact on RR violations; (iii) for RG violations, TSCTs, leading violators and gender are the most significant factors; (iv) it is also unveiled that site type, green signal time and TSCTs have negligible impact on the whole violations regardless of the violation types. Thus, it is more meaningful to investigate the impacts of these variables on e-bikers' RLR behavior according to different violation types; otherwise, the potential relationship between some crucial factors and e-bikers' RLR behavior might be ignored. These findings would help to improve intersection crossing safety for traffic management.

1. Introduction

The ownership and usage of electric bikes (e-bikes), a type of electric powered two-wheeled vehicle, have skyrocketed over the past decade in China. In 2016, over 200 million e-bikes were ridden on China's roads and three million more were sold in the same year compared to just a few thousand in 1998 [1, 2]. Due to its advantages of labor-saving, flexibility, and compatibility with the urban scale, e-bike constitutes a substantial proportion of the travel modes in China, especially in small-to-medium-sized cities. For example, in 2017, over 40% of trips in the downtown area of Nantong, Jiangsu Province, were made using e-bikes [3]. Similarly, in Nanning, Guangxi Province, e-bikes were used for 34% of trips in 2015 [4].

The number of e-bikes in China has been rapidly increasing, causing significant traffic safety issues. The total number of accidents and fatalities involving e-bikers has increased drastically in the past decade. Between 2013 and 2017, in China, e-bikers contributed to 56,200 traffic accidents, resulting in 8,431 fatalities, 63,400 injuries, and direct property losses of 111 million Yuan [5]. In Jiangsu Province, more than 50% of the e-bike-related traffic accidents and over 40% of the subsequent fatalities in 2018 were caused by e-bikers' traffic rule violating behavior [6]. Moreover, previous studies found that this violating behavior, especially red-light running (RLR) behavior at signalized intersections, partially contributed to the accidents and fatalities associated with e-bikers [7–11].

Most of the studies have focused on cyclists' RLR behavior at signalized intersections. Investigations have been performed on the influence of individual characteristics and psychological factors on cyclists' RLR behavior. For instance, Johnson et al. [12, 13] discovered the significant risk factors influencing

cyclists' RLR behavior, such as gender, age, crash experience, and safety perception. Additionally, Wu et al. [14] revealed that gender, age, and conformity tendency significantly contributed to cyclists' red-light infringement. In another study, Pai and Jou [15] found that male or young cyclists were more prone to commit no-stopping RLR behavior. Similarly, Fraboni et al. [16] showed that male cyclists had a higher percentage of no-stopping crossings when the red light was on, whereas elderly cyclists (more than 50 years old) exhibited a stronger tendency to stop at a red light. A range of studies also discussed that the potential association of cyclists' RLR behavior was with other violations, such as unhelmeted riding [15], carrying passengers [15], using a phone [17], and listening to music [18, 19].

Among several studies related to e-bikers, the findings showed that e-bikers had a stronger intention to violate a red light than regular cyclists [14, 20–30]. Yang et al. [23], with a hazard-based duration model, established that the prominent contributors to red-light infringement of cyclists and e-bikers were rider type, gender, waiting position, conformity tendency, and traffic volume. A recent study conducted by Yang et al. [10] reported the psychological factors (e.g., attitude, perceived behavioral control, moral norm, and self-identity) that significantly influenced e-bikers' RLR intention by using the theory of planned behavior. Also, the influence of infrastructure conditions on red-light infringement has been discussed. Zhang and Wu [22] found that installing sunshades at intersections could reduce the RLR rates of cyclists and e-bikers on sunny/cloudy days. Schleinitz et al. [24] investigated the impacts of lane types and intersection types on red-light infringement and found that cyclists and e-bikers riding on the carriageway had the lowest RLR rate, and the intersection type had a substantial effect on red-light infringement.

However, the role of infrastructure conditions contributing to e-bikers' RLR behavior in China remains unclear. Although Schleinitz et al. [24] have discussed the impact of the lane types and intersection types on red-light infringement of cyclists and e-bikers, their findings are not necessarily applicable elsewhere due to the considerably different definitions of e-bikes between China and the Western countries. Also, Zhang and Wu [22] only investigated one specific infrastructure condition (sunshades) while other infrastructure conditions which might influence e-bikers' RLR behavior in China were ignored. Among the infrastructure conditions of signalized intersections, traffic signal countdown timers (TSCTs) are attention-worthy, which assist motorists/riders/pedestrians in decision-making at signalized intersections by providing them with real-time signal duration information. In general, TSCTs are equipped with two types of countdown timers: green signal countdown timers (GSCTs) and red signal countdown timers (RSCTs). GSCTs and RSCTs display the remaining time of the green signal and of the red signal, respectively. E-bikers can decide to wait or cross based on the time displayed on GSCTs/RSCTs. Previous studies conducted by Islam et al. [31, 32] suggested that the presence of GSCTs/RSCTs contributed to an improvement in the crossing safety and efficiency of drivers at signalized intersections. However, no unified and consistent conclusion exists concerning the impact of TSCTs on pedestrians' crossing behavior at signalized pedestrian crossings [33–41]. To the best of our knowledge, few previous studies have discussed the effect of TSCTs on e-bikers' RLR behavior at signalized intersections. Furthermore, there is hardly any understanding on the influence of other infrastructure conditions, such as red/green signal time, intersection (site) type, crossing length, and crossing width, on e-bikers' crossing behavior and violations at signalized intersections.

To address these shortages, the first aim of this work is to provide an unobtrusive observation method to observe and analyze e-bikers' crossing behavior and violations. The second aim is to investigate the impact of various contributing factors, especially infrastructure conditions, on e-bikers' red-light infringement at signalized intersections. The possible contributing factors (independent variables) were classified into three broad categories, demographic attributes, movement information, and infrastructure conditions (Table 1). The final outputs obtained from this work might provide solutions for reducing the occurrence of accidents and fatalities involving e-bikers at signalized intersections, especially in developing countries with high e-bike ownership.

The remainder of the paper is organized into three parts. The first part describes the site testing, video recording, and video coding method. The second part presents the observation and analysis of e-bikers' crossing behavior and violations at signalized intersections, including late crossing, incomplete crossing, and violating crossing. The final part details the modeling of the influence of various contributing factors on e-bikers' RLR behavior.

2. Data

2.1. Site Testing. The purpose of this work was to investigate the crossing behavior and violations of e-bikers at signalized intersections. The observational site testing was based on two criteria. First, the sites had to be selected based on the research objectives. The site type had to include X-intersections (four-armed intersections) and T-intersections (three-armed intersections) (Figure 1), as well as intersections with/without TSCTs. Second, a high volume of e-bikes had to be available during the period of video recording. Before the final observational sites were confirmed, we had carried out a pilot observation and tested fourteen sites. Finally, eight signalized intersections were selected for further investigation in this study (Table 2). The study sites were geographically well located across the road network of Nantong, China (Figure 2).

2.2. Video Recording. Video recording has been confirmed to be an effective field observation approach to studying traffic violation behavior at intersections [12, 22, 23, 33, 37]. In this study, video cameras (Sony HDR-CX680) were settled in the vantage and covert points to record footages of e-bikers' crossing behavior and violations. To obtain the required data, we had to ensure that the video recording covered the waiting area, the crossing process, the opposite lanes, and the light that was being displayed on at the traffic signals. The video data were recorded during the evening peak hours (5:00 p.m.–7:00 p.m.) on clear-weather weekdays (excluding Friday). As the

Table 1: Definitions of independent variables.

Categories	Variable	Variable type	Description
Demographic attributes	Gender	Categorical	0 = if female e-biker, 1 = if male e-biker
	Estimated age	Categorical	0 = if elderly e-biker (>50), 1 = if middle-aged e-biker (30–50), 2 = if young e-biker (<30)
	Waiting position[a]	Categorical	0 = if in designated area, 1 = if in nondesignated area (out of designated area, e.g., waiting beyond the stop line, occupying the motorized lanes or pavements)
Movement information	Waiting time	Continuous	Interval time between arrival time and begin-crossing time
	Leading violators	Continuous	Number of other violators in front of an e-biker who starts to cross
	Passing cars[b]	Continuous	Average number of motor vehicles passing path section per lane (flow) per min when an e-biker arrives
Infrastructure conditions	Site	Categorical	0 = if site 1, 1 = if site 2, 2 = if site 3, 3 = if site 4, 4 = if site 5, 5 = if site 6, 6 = if site 7, 7 = if site 8
	Site type	Categorical	0 = if X-intersection, 1 = if T-intersection
	Red signal time	Continuous	Interval time of red signal phase
	Green signal time	Continuous	Interval time of green signal phase
	Crossing length[c]	Continuous	Length of e-bikers crossing from stop line to opposite nonmotorized lanes
	Crossing width	Continuous	Width of straight crossing, represented by width of nonmotorized lane
	TSCTs	Categorical	0 = if TSCTs are uninstalled, 1 = if TSCTs are installed

[a]Refer to Figure 1 for illustration for waiting position. In video coding, if e-bikers perform a no-stopping crossing, waiting position is regarded as in designated area. [b]Refer to Figure 1 for illustration for passing car flows. [c]Refer to Figure 1 for illustration for crossing length.

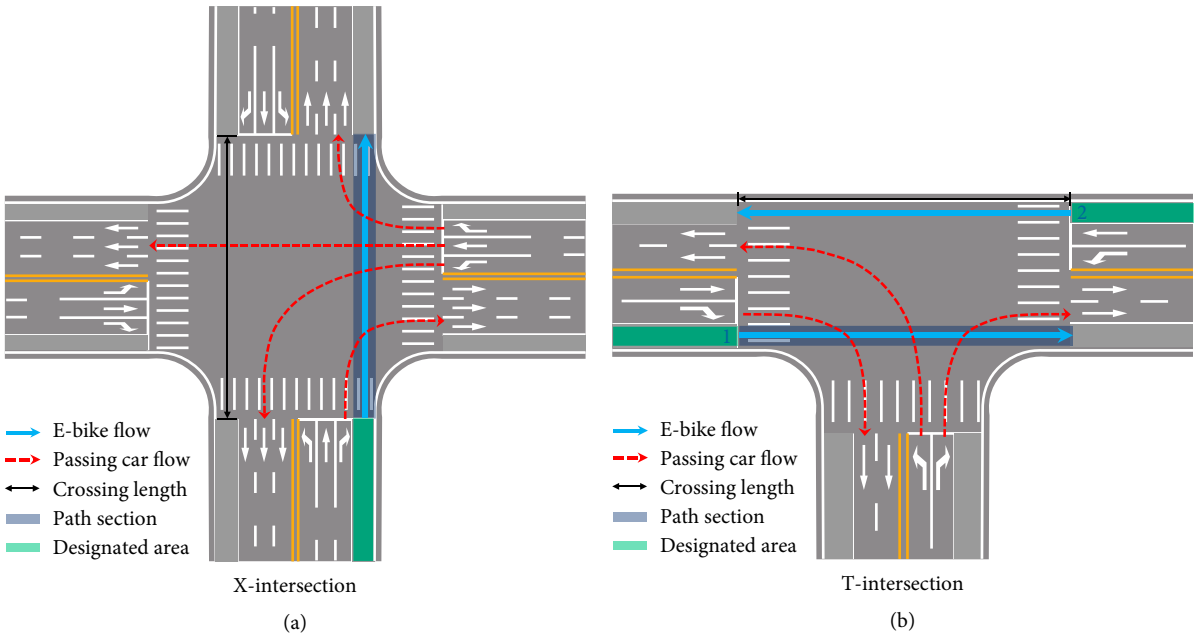

Figure 1: Illustrations of the intersections and variables.

approaching lanes had identical traits, we only recorded the data of one random direction of approaching lanes per one X-intersection (see the red arrows in Figure 2). According to the stipulation in the Chinese Road Traffic Safety Law, vehicles (motor and non-motor vehicles) are prohibited from passing when the red light is on. Hence, in the T-intersections (see in Figure 1(b)), the e-bike flows 1 and 2 were both subject to the red light, despite the e-bike flow 2 had no conflicts with passing car flows during the whole traffic signal cycle. Thus, considering the different traits of e-bike flows 1 and 2, we performed recording in two directions of approaching lanes which had straight-pass e-bikers (see yellow arrows in Figure 2). In addition, the recording time per site must reach at least one hour. To diminish the impacts of external factors on the crossing behavior, we had to ensure that no traffic police or wardens were regulating the traffic order during the observation.

Table 2: Descriptions of the selected signalized intersections.

Site	Site type	Width of nonmotorized lane (m)	Crossing length (m)	Green signal time (s)	Red signal time (s)	Yellow signal time (s)	All-red signal time (s)	TSCTs installation
1	X	3.0	54.8	27[a]	71	3	3	Uninstallation
2	X	4.5	63.8	52[a]	45	3	3	Uninstallation
3	X	4.5	51.4	34[a]	84	3	3	Installation
4	X	8.0	52.9	50[a]	47	3	3	Installation
5	T	3.5	25.1	22[b]	26	3	2	Installation
6	T	4.0	49.8	35[b]	44	3	3	Uninstallation
7	T	4.5	33.2	25[a]	34	3	2	Installation
8	T	3.5	37.5	20[a]	23	3	2	Uninstallation

[a]Straight green signal time; [b]Straight and left-turn green signal time.

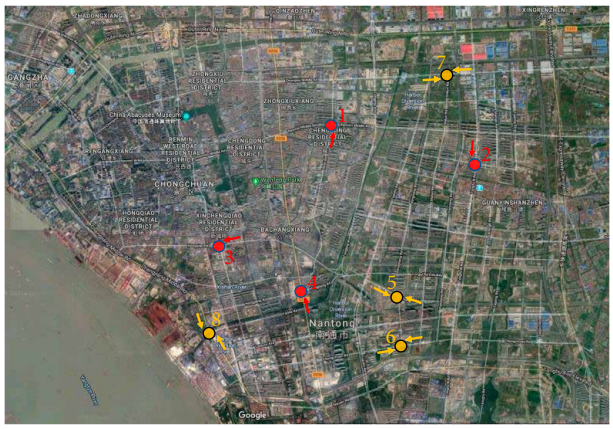

Figure 2: Field data collection sites.

2.3. Video Coding. In this work, only e-bikers who went right across the signalized intersection were coded. Right-turn e-bikers were not coded as they were not subject to the traffic light following the Chinese Road Traffic Safety Law; left-turn e-bikers were also excluded due to the limited field of view of the video cameras [22, 23]. To improve the efficiency of the video coding, all coders received extensive training on the coding scheme, and video data were coded simultaneously by two groups of coders. One group extracted the data related to e-bikers, and the other group extracted the data of motor vehicles which may conflict with e-bikers. The data of e-bikers include gender, estimated age, waiting position, waiting time, and leading violators. The data of motor vehicles include the number of passing cars when the e-biker arrived. The two groups of data were matched based on the arrival time of each e-biker and the signal cycle containing e-bikers' arrival time. To avoid potential bias in video coding, two independent coders performed the same coding task. One-way intraclass correlations (for continuous variables) and Cohen's kappa (for categorical variables) were used to validate the coding reliability. The calculated coefficients ranged from 0.85 to 0.97, indicating that the video coding was reliable.

3. Results and Discussion

To clarify the signal phase of e-bikers' arriving, waiting, starting crossing, and completing crossing, the traffic signal status was divided into four phases: steady green signal (SGS), last 10 s green signal (LGS), yellow signal (YS), and red signal (RS). SGS and LGS phases are referred to as the green signal (GS) phase (Figure 3). The reason for adding an LGS phase is that a high proportion (79%) of the e-bikers who arrived during the last 10 s of the GS phase were unable to complete the crossing before the initiation of the RS phase (Table 3). Thus, the application of four signal phases is beneficial for the discussion on the crossing behavior and violations.

3.1. General Observations. The data of the total number of 3,126 eligible subjects were obtained by video coding. Among the subjects, 59.4% ($n = 1,857$) were male and the proportions of young, middle-aged, and elderly e-bikers were 40.5% ($n = 1,266$), 49.2% ($n = 1,538$) and 10.3% ($n = 322$). The statistics showed that 26%, 17%, 5%, and 52% of e-bikers arrived at the study sites within the SGS, LGS, YS, and RS phases, respectively (Table 3).

3.1.1. Late Crossing. The late crossing is defined as a crossing behavior in which e-bikers start to cross after they have arrived during the LGS/YS phase. The time left to the RS onset that e-bikers started crossing is listed in Table 4, in which we summarized the minimum, maximum, mean, ratio, 15th percentile, and 85th percentile values by sites. The minimum values showed that e-bikers made a decision to cross even during the last seconds (from 0 to 2 s) to the RS onset. That is, some e-bikers chose to cross even when they arrived within the YS phase (generally 2-3 s in China). The maximum values indicated the total time before the RS onset, which was the sum of the SGS, LGS, and YS phases. The 15th percentile values showed the time (left to RS onset) that most of the observed e-bikers started to cross was more than that shown in Table 4. Considering the difference of the maximum time left to RS onset among the sites, the ratio of the mean time divided by the maximum time was used to compare the relative mean time when starting crossing on the same scale. The results showed that ratios of the mean time left to RS onset at Sites 5, 7, and 8 were lower than those of the other sites. Likewise, the

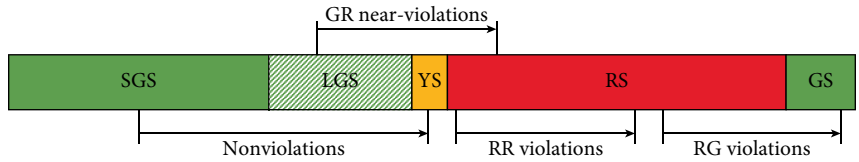

Figure 3: Signal phases and violation types.

Table 3: Statistics of signal phase upon arrival, crossing decision and incomplete crossing.

Signal phase	Arrival number		Decision			Incomplete crossing before RS/GS onset	
	Freq.	Per.	Wait	Cross	Cross Per.	Freq.	Per.
SGS	819	26%	3	816	100%	6[a]	1%[a]
LGS	547	17%	82	465	85%	369[a]	79%[a]
YS	141	5%	59	82	58%	82[a]	100%[a]
RS	1,619	52%	626	993	61%	569[b]	57%[b]
Total	3,126	100%	770	2,356	-	-	-

[a]Frequency and percent of e-bikers who started to cross during SGS/LGS/YS phases and unfinished it before RS onset. [b]Frequency and percent of e-bikers who started to cross during RS phase and unfinished it before GS onset.

Table 4: Time left to the RS onset.

Site	Min. (s)	Max. (s)	Mean (s)	Ratio	15th Percentile	85th Percentile
1	1	30	26	0.87	19	28
2	2	55	45	0.82	34	51
3	1	37	32	0.87	26	35
4	2	53	42	0.79	31	48
5	0	25	18	0.70	9	24
6	1	38	29	0.77	20	36
7	1	28	20	0.71	12	26
8	0	23	16	0.70	9	21

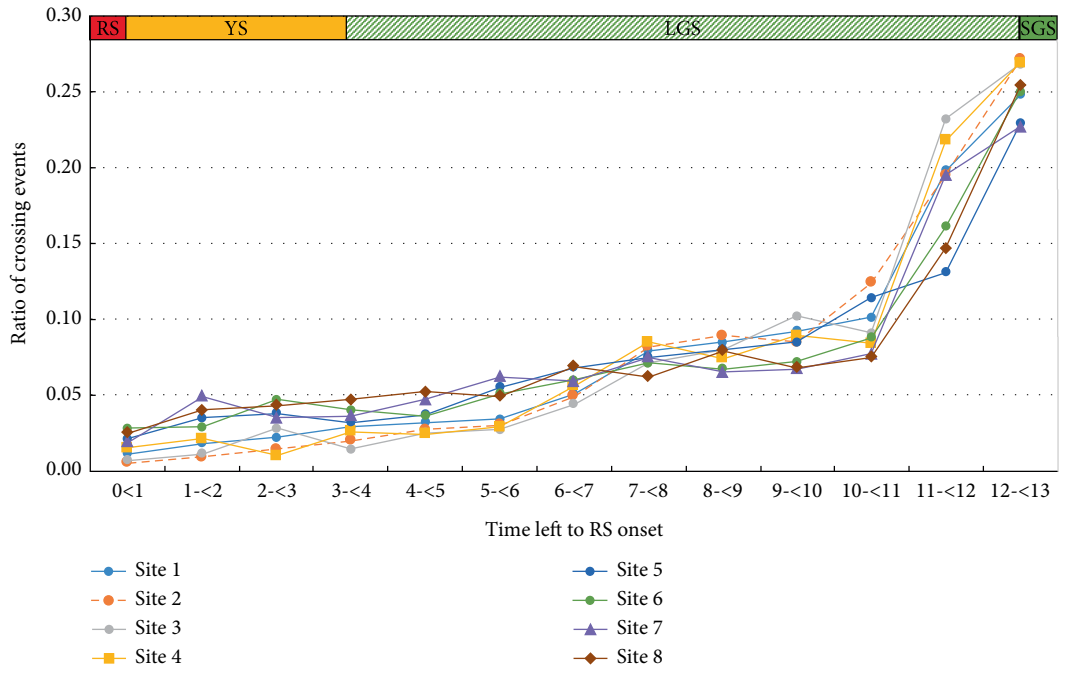

Figure 4: Ratio of crossing events during the time left to the RS onset (LGS and YS phases) in each site.

crossing lengths of Site 5, 7, and 8 were found to be shorter than the ones of the other sites. Inferentially, the shorter crossing length made e-bikers perceive that they might have the ability to complete the crossing safely even during the last few seconds. Therefore, we can consider crossing length as a possible contributing factor.

Next, we compared different sites using the same scale by a ratio of the crossing events. The ratio of the crossing events is defined as the number of the crossing events at each time left to RS onset divided by the total number of crossing events during LGS/YS phases. As shown in Figure 4, the ratios of the crossing events at Sites 5, 6, 7, and 8 were higher than those at Sites 1, 2, 3, and 4 during the last seconds to RS onset (time left to RS onset ranged from 0 to 6 s). Since the crossing length of Site 6 is longer than the average crossing length of all sites (49.8 m vs. 46.1 m), this result cannot be explained by the

Table 5: Descriptive statistics of violations in study sites.

Site	Site type	Violation type			Total violations	Total crossing	Violation ratio
		GR near-violations	RR violations	RG violations			
1	X	41	62	53	156	476	32.8%
2	X	33	41	40	114	317	36.0%
3	X	97	82	128	307	612	50.2%
4	X	79	51	99	229	544	42.1%
5	T	63	46	71	180	319	56.4%
6	T	42	47	53	142	277	51.3%
7	T	72	55	90	217	356	61.0%
8	T	30	40	35	105	225	46.7%
Total		457	424	569	1,450	3,126	46.4%

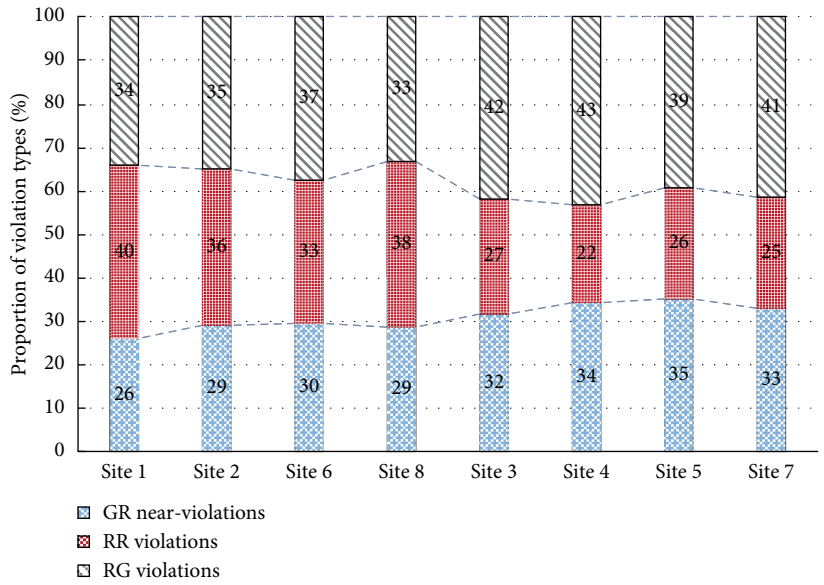

Figure 5: Proportion of violation types for each site.

influence of the crossing length and could have been caused by the specific site type. As seen in Figure 1(a), e-bikers experienced possible conflicts with right-turn vehicles (which are not generally subject to the traffic signal lights in China) in each approaching lane at X-intersections (Sites 1, 2, 3, and 4), which may deter the crossing events within the last few seconds to RS onset. Figure 1(b) showed that the e-bike flow 1 could experience the same conflicts with right-turn vehicles at the T-intersections as those at the X-intersections before the RS onset. However, since the e-bike flow 2 had no direct conflicts with the passing car flows during the whole traffic signal cycle, the e-bikers would perceive that completing the crossing was safe enough, and they made a faster decision to cross at Sites 5, 6, 7, and 8. Accordingly, the site type was also considered as a possible influencing factor in this study. Moreover, the ratios of crossing events dramatically increased after the interval from 10 to 11 s, subsequently reaching relatively high ratios of crossing events (from 0.227 to 0.271) within the interval of 12–13 s. On the whole, the curve trend in Figure 4 indicated that the ratios of crossing events were higher as the time left to RS onset was prolonged. This trend was due to the more time available to e-bikers to complete the crossing before the RS onset regardless of whether they had to wait for the next GS phase with the increased time left to the RS onset.

3.1.2. Incomplete Crossing. There are two types of the incomplete crossing. One incomplete crossing is defined as a crossing behavior in which e-bikers start crossing during the SGS/LGS/YS phases and cannot complete the crossing before the RS onset. Table 3 showed that the proportions of the incomplete crossing were 1%, 79%, and 100% during the SGS, LGS, and YS phases, correspondingly. The likelihood of e-bikers' crossing during the LGS phase was considerably higher than those during the YS phase (85% vs. 58%). Generally, the e-bikers who arrived during the SGS phase could complete the crossing before the RS onset, among which 1% incomplete crossing was due to faulty e-bikes or insufficient electricity supply. It was observed that about 79% of the e-bikers who started crossing during the LGS phase could not complete the crossing before the RS onset, while all of those who started crossing during the YS phase could not complete it. Accordingly, if the late-entry e-bikers

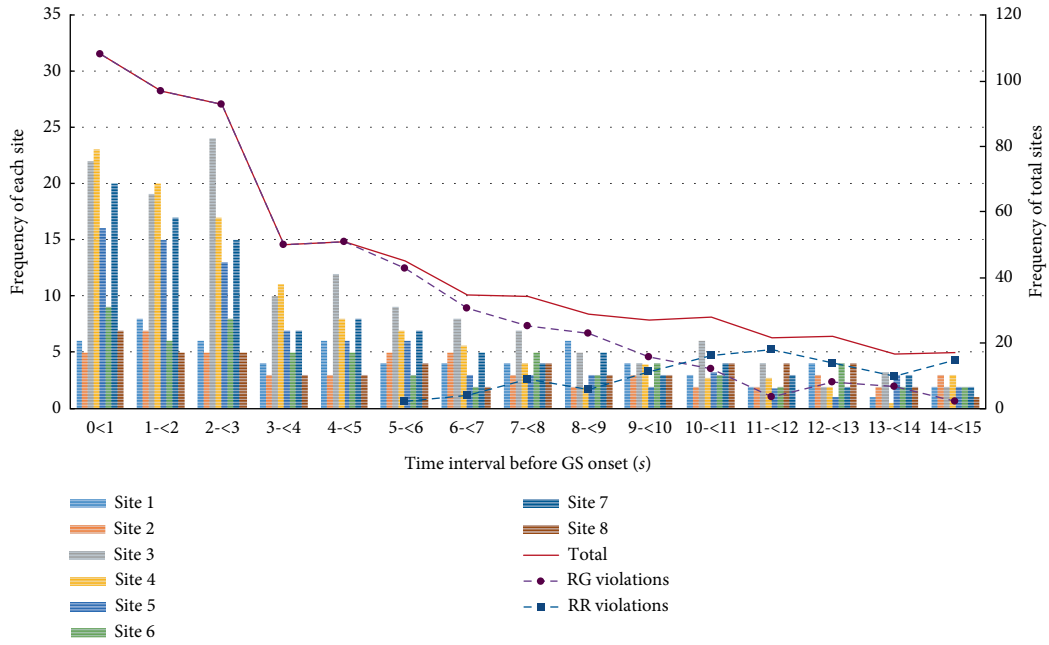

Figure 6: Crossing time distribution of RG/RR violations before GS onset.

Table 6: Results of the univariate analysis.

Variable	GR near-violations				RR violations				RG violations			
	−2log likelihood			$Pr > \chi^2$	−2log likelihood			$Pr > \chi^2$	−2log likelihood			$Pr > \chi^2$
	C_1	C_2	ΔC		C_1	C_2	ΔC		C_1	C_2	ΔC	
Gender	1,682.15	1,625.81	56.34	<0.0001	1,984.26	1,970.34	13.92	0.00	1,845.62	1,832.97	12.65	0.00
Estimated age	1,675.64	1,664.49	11.15	0.00	1,546.33	1,537.38	8.95	0.00	2,014.65	1,954.83	59.82	<0.0001
Waiting position	1,513.46	1,511.9	1.56	0.21	2,182.47	1,995.16	187.31	<0.0001	2,111.79	1,830.12	281.67	<0.0001
Waiting time	1,559.23	1,558.22	1.01	0.29	2,067.51	1,772.89	294.62	<0.0001	2,202.43	2,069.7	132.73	<0.0001
Leading violators	2,154.47	2,057.08	97.39	<0.0001	2,077.68	1,935.57	142.11	<0.0001	2,134.97	1,857.72	277.25	<0.0001
Passing cars	2,057.11	2,025.49	31.62	<0.0001	1,675.24	1,395.58	279.66	<0.0001	1,578.44	1,526.65	51.79	<0.0001
Site	2,071.39	2,069.36	2.03	0.15	2,095.61	2,094.52	1.09	0.28	2,007.11	2,005.26	1.85	0.17
Site type	1,578.33	1,390.76	187.57	<0.0001	2,117.23	2,050.41	66.82	<0.0001	2,064.39	2,002.86	61.53	<0.0001
Red signal time	1,607.82	1,606.58	1.24	0.26	1,509.11	1,500.09	9.02	0.00	1,553.40	1,545.29	8.11	0.00
Green signal time	2,194.35	2,066.93	127.42	<0.0001	1,693.72	1,692.23	1.49	0.21	1,509.17	1,507.02	2.15	0.14
Crossing length	1,588.46	1,490.85	97.61	<0.0001	2,134.53	1,907.14	227.39	<0.0001	1,864.35	1,781.98	82.37	<0.0001
Crossing width	1,524.16	1,521.89	2.27	0.13	2,022.49	2,020.7	1.79	0.18	1,802.47	1,800.87	1.60	0.19
TSCTs	2,074.25	1,771.58	302.67	<0.0001	1,517.60	1,502.84	14.76	0.00	1,564.34	1,234.62	329.72	<0.0001

who arrived during the LGS/YS phases maintain the average riding speed (less than 20 km/h), most of them might be unable to complete the crossing before the RS onset, which would lead to their exposure to conflicts with the passing cars (right-turn/left-turn/straight-pass vehicles) during the RS phase. Another incomplete crossing is defined as a crossing behavior in which the e-bikers start the crossing during the RS phase but cannot complete it before the GS onset. Approximately 61% of the e-bikers who arrived at the RS phase chose to cross, which is categorized as the most serious RLR behavior. Nearly 57% of these crossing e-bikers could not complete the crossing before the GS onset.

Table 7: Association of the predicted probabilities and the observed responses.

	GR near-violations	RR violations	RG violations
Percent concordant	85.7	86.3	83.9
Somers' D	0.701	0.745	0.698
Gamma	0.744	0.762	0.726
c	0.842	0.857	0.813

3.1.3. Violating Crossing. Based on the findings discussed above, e-bikers' crossing behaviors can be classified into four types: nonviolations, GR near-violations, RR violations, and RG violations (Figure 3). Nonviolations refer to the crossing behaviors in which e-bikers start to cross within the GS phases and complete it during the GS/YS phases. The Chinese Road Traffic Safety Law stipulates that vehicles (motor and nonmotor vehicles) which have crossed the stop line when the yellow light is on can continue the crossing; otherwise, they are prohibited from crossing. Thus, the e-bikers who start crossing during the YS phase are categorized as violators. In light of the stipulation, although the e-bikers who initiate the crossing within the GS phase and complete it during the RS phase are not categorized as violators, they would be exposed to the same level of danger as the e-bikers who start the crossing during the YS phase. Hence, the crossing behaviors, in which e-bikers start to cross within the GS/YS phase and complete it during the RS phase, are defined as GR near-violations. Additionally, the crossing behaviors in which e-bikers start to cross within the RS phase and complete it within the RS phase are classified as RR violations, while those that complete the crossing during the GS phase are denoted as RG violations. Since the e-bikers who started the crossing within the GS/YS phase and completed it by the GS/YS phases of the next cycle were extremely rare in our observations, this violation type is unconsidered. RR and RG violations are categorized as undisputed violations in compliance with the Chinese Road Traffic Safety Law, while GR near-violations are regarded as a special type of violations in this study.

The total number of violations among the observational subjects was 1,450. The descriptive statistics analysis of the violations at the study sites is presented in Table 5. The proportions of the GR near-violations, RR violations, and RG violations were 32%, 29%, and 39%, respectively. These findings revealed that the proportions of RG violations and GR near-violations were higher than that of RR violations; RG violations were the most prevalent of all types of violations. A plausible reason for the most prevalent RG violations is that most of passing cars were cleared at the end of the RS phase, and the e-bikers who arrived during the RS phase chose to cross during the last seconds to the GS onset for they could not endure a longer waiting time. For the second-prevalent GR near-violations, it could be due to that the light traffic volume (only right-turn vehicles) during the GS/YS phases led to e-bikers' weaker safety awareness and risk-ignorance of conflicting with passing cars from different directions in case of incomplete crossing before the RS phase. Furthermore, as shown in Figure 5, the proportions of RG violations and GR near-violations at Sites 3, 4, 5, and 7 with TSCTs were significantly more than those at Sites 1, 2, 6, and 8 without TSCTs, inferring that TSCTs installation might be associated with e-bikers' RLR behavior. Accordingly, our study considered TSCTs as a possible influencing factor. The violators corresponding to the three violation types are named GR near-violators, RR violators, and RG violators.

The time distributions before the GS onset when RG/RR violators started to cross were plotted at a 1 s interval, with a range from 0 to 15 s (Figure 6). We observed that most of the RG/RR violators started to cross within 0–3 s before the GS onset. This could be due to the installation of the 2-3 s All-Red clearance phase (which was used to clear all passing cars inside the intersection) in the traffic signals. Within the All-Red clearance phase, some e-bikers intended to cross through the traversable space-time gaps under light traffic volume. In the period earlier than 2-3 s before the GS onset, the number of RG/RR violations considerably declined. Moreover, we also found that only RG violations were in the interval from 0 to 5 s, indicating that the e-bikers who chose to cross during the last 5 s to the GS onset were unable to complete their crossing before the GS onset.

3.2. Effects of Independent Variables on RLR Behavior. As shown in Table 1, the independent variables were calibrated to compare the different impacts on the three violation types and explore the common influence on e-bikers' red-light infringement regardless of their violation types.

3.2.1. Different Violation Types. Based on the obtained data using the binary logistic model in SPSS, further analysis was conducted to determine the effects of the independent variables on the probability of e-bikers' RLR behavior. Previous studies have investigated the probability/rates of violation behaviors only for pedestrians who arrived and crossed during the red signal phase regardless of the differences in the violation types [9, 42–44]. The aforementioned three violation types were regarded as the subjects of the subsequent analysis. The 1,507 e-bikers who arrived at the GS/YS phases were included in the analysis of the GR near- violations, and 1,619 e-bikers who arrived at the RS phases were included in the analysis of the RR and RG violations.

Univariate analysis (variable added separately) was applied to choose the possible variables to be integrated into the binary logistic models for the three violation types. The analysis results of the deviances and the likelihood ratio test p-values are displayed in Table 6. The deviances $\Delta C = C_1 - C_2$represent the error associated with the model when only an intercept is entered into the model for the case of C_1 (without variable) and when the independent variable is entered into the model for the case of C_2 (with variable). The higher the value of ΔC is, the stronger the significance of the variable in the model is. Finally, the variables entered into the model for the GR near-violations were gender, estimated age, leading violators, passing cars, site type, green signal time, crossing length, and TSCTs. The variables entered into the models for the RR and RG violations were the following: gender, estimated age,

Table 8: Results of the final logistic regression models for three violation types.

Variables	GR near-violations			RR violations			RG violations		
	B	S.E.	Pr > χ^2	*B*	S.E.	Pr > χ^2	*B*	S.E.	Pr > χ^2
Gender									
Male vs. female	0.277	0.212	0.0042	0.224	0.182	0.0059	0.328	0.062	0.0037
Estimated age									
Young vs. elderly	0.331	0.083	0.0005	0.180	0.133	0.0036	0.303	0.261	0.0004
Middle-aged vs. elderly	0.382	0.171	0.0003	0.212	0.079	0.0003	0.346	0.047	0.0052
Waiting position									
In designated area vs. in nondesignated area	–	–	–	−0.226	0.072	<0.0001	−0.102	0.162	<0.0001
Waiting time	–	–	–	0.141	0.161	<0.0001	0.105	0.111	0.0043
Leading violators	0.072	0.233	0.0005	0.058	0.094	0.0031	0.084	0.032	<0.0001
Passing cars	−0.094	0.551	0.0073	−0.122	0.042	<0.0001	−0.078	0.319	0.0087
Site type									
T-intersection vs. X-intersection	0.274	0.092	<0.0001	0.111	0.620	0.6102	0.164	0.574	0.4531
Red signal time	–	–	–	0.130	0.355	0.3327	0.080	0.412	0.9165
Green signal time	−0.056	0.256	0.0002	–	–	–	–	–	–
Crossing length	−0.097	0.320	0.0056	−0.135	0.122	<0.0001	−0.065	0.061	0.0002
TSCTs									
Installing TSCTs vs. uninstalling TSCTs	0.313	0.162	<0.0001	0.060	0.526	0.7524	0.502	0.177	<0.0001
Intercept	3.892	1.328	0.0146	4.060	1.643	0.0223	3.310	2.011	0.0175

waiting position, waiting time, leading violators, passing cars, site type, red signal time, crossing length, and TSCTs.

The selected independent variables were added to the binary logistic models for the three violation types. The goodness-of-fit for these three models was estimated through the Hosmer–Lemeshow test. In essence, the Hosmer–Lemeshow test is a chi-square goodness of fit test for grouped data [45]. The test results showed that the three models had a relatively good fit for the obtained data as the chi-square (χ^2) statistics values were smaller than the critical value of the chi-square distribution (with a p-value for $Pr > \chi^2$ not less than 0.05). As shown in Table 7, the percentages of the concordant observations were close to 100, and the values of Somers' D, Gamma, and c were all close to 1, indicating that these three models provided adequate goodness-of-fit. The results of the logistic models for the three violation types are presented in Table 8.

A positive parameter estimate for a continuous variable suggests that the probability of RLR behavior increases with the rise in the value of the variable. For the categorical variable, it suggests that the maintenance at that particular level increases the probability of RLR behavior compared to the reference level. Based on the estimated results, we found that most of the independent variables in the final models were statistically significant at the 0.01 level, revealing that these variables contributed significantly to the likelihood of e-bikers' RLR behavior.

As shown in Table 8, for GR near-violations, installing TSCTs had 1.368 ($e^{0.313}$) times probability of RLR behavior than uninstalling TSCTs, revealing that the GSCTs installation would increase the proportion of the GR near-violations. This result is contrary to our expectations, because the e-bikers who know the real-time left to RS onset are more likely to accelerate their crossing using the e-bike's high-speed and accelerating performance. The next crucial variable was estimated age, which had the most pronounced positive effect on the GR near-violations than on the other violation types. Specifically, the likelihood that young and middle-aged e-bikers would decide to cross during the last few seconds were 1.392 ($e^{0.331}$)

Table 9: Results of univariate analysis for all violations.

Variable	−2log likelihood			Pr > χ^2
	C_1	C_2	ΔC	
Gender	2,067.56	2,020.64	46.92	<0.0001
Estimated age	1,695.37	1,687.21	8.16	0.00
Waiting position	1,605.32	1,590.20	15.12	0.00
Waiting time	2,169.72	1,994.08	175.64	<0.0001
Leading violators	2,067.24	1,820.87	246.37	<0.0001
Passing cars	1,569.80	1,258.04	311.76	<0.0001
Site	1,511.16	1,510.03	1.13	0.28
Site type	2,031.79	2,021.66	10.13	0.00
Red signal time	1,649.90	1,647.37	2.53	0.11
Green signal time	1,564.78	1,563.19	1.59	0.20
Crossing length	2,092.82	1,817.47	275.35	<0.0001
Crossing width	1,647.93	1,645.62	2.31	0.13
TSCTs	2,123.67	2,109.75	13.92	0.00

Table 10: Logistic regression model for all violations.

Variable	B	S.E.	Pr > χ^2
Gender			
Male vs. female	0.292	0.153	0.0003
Estimated age			
Young vs. elderly	0.241	0.415	0.0036
Middle-aged vs. elderly	0.325	0.076	0.0049
Waiting position			
In designated area vs. in nondesignated area	−0.183	0.133	0.0028
Waiting time	0.072	0.228	0.0002
Leading violators	0.081	0.052	<0.0001
Passing cars	−0.106	0.194	<0.0001
Site type			
T-intersection vs. X-intersection	0.113	0.523	0.5428
Crossing length	−0.082	0.097	<0.0001
TSCTs			
Installing TSCTs vs. uninstalling TSCTs	0.203	0.421	0.3262
Intercept	4.136	1.670	0.0288

and 1.465 ($e^{0.382}$) times than those of the elderly e-bikers. We also found that the green signal time influenced only the GR near-violations. To be specific, one unit increase in the green signal time decreased the likelihood of e-bikers' RLR behavior by 5.4%. Moreover, the site type was also a crucial contributor for GR near-violations, whereas it exerted no significant effect on the other types. The odds of e-bikers' RLR behavior at T-intersections was 1.315 ($e^{0.274}$) times than those at X-intersections. This result was due to the absence of conflicts of the e-bike flow 2 at T-intersections with passing cars during the whole traffic signal cycle (Figure 1). Thus, these e-bikers had a higher tendency to violate a red light. In addition to the above variables, gender, leading violators, passing cars, and crossing length also had significant effects on GR near-violations.

The findings for the RR violations showed that the waiting time influenced more considerably the RR violations than the RG violations ($e^{0.141}$ vs. $e^{0.105}$). The increase by one unit of waiting time augmented the likelihood of e-bikers' RLR behavior by 15.1%. The passing cars had the highest negative impact on the RR violations as compared to the influence of the other types ($e^{-0.122}$ vs. $e^{-0.094}$ vs. $e^{-0.078}$). Specifically, the rise in the number of passing cars by one unit decreased the probability of e-bikers' RLR behavior by 11.5%, indicating that e-bikers were less willing to undertake the risk of the crossing during the RS phase as the number of passing cars rose. The next crucial variable was the waiting position, which had a more significant negative impact on the RR violations than on the RG violations ($e^{-0.226}$ vs. $e^{-0.102}$). We found that the e-bikers waiting in the designated area were 0.798 less likely to commit red-light infringement than those waiting in the nondesignated area. The crossing length exerted the strongest effect on the RR violations than on the other types ($e^{-0.135}$ vs. $e^{-0.097}$ vs. $e^{-0.065}$). The elevation of the crossing length by one unit led to a decline in the probability of e-bikers' RLR behavior by 12.6%. Of the remaining variables, gender, estimated age, and leading violators were also significant variables, while the site type, red time, and TSCTs were insignificant. Interestingly, TSCTs had no significant effect on RR violations as compared with the other violation types. That is, the RR violations could not decide whether to cross or not in the remaining real-time of RSCTs.

TSCTs were the most significant contributor to the red-light infringement by the RG violations than to that by the other violation types. Due to the presence of RSCTs and the 2–3 s All-Red clearance phase, the e-bikers would be 1.652 ($e^{0.502}$) more likely to start crossing before the GS onset at the signalized intersections with RSCTs than those without RSCTs. The leading violators had the greatest influence on the RG violations of all violation types ($e^{0.084}$ vs. $e^{0.072}$ vs. $e^{0.058}$). The increase by one unit in the leading violators would augment the likelihood of red-light infringement during the few seconds left to the GS onset by 8.8%. Gender had the strongest effect on the RG violations as compared to that on the other violation types ($e^{0.328}$ vs. $e^{0.277}$ vs. $e^{0.224}$). Male e-bikers who arrived within the last few seconds of the RS phase were 1.388 more likely to violate a red light than female e-bikers. In addition to the above variables, the estimated age, waiting position, waiting time, passing cars, and crossing length were significant variables, while the site type, and red time were insignificant. It should note that passing cars had a lower effect on the RG violations than on the RR violations. The main reason was that the average number of passing cars was relatively lower when the RG violations began to cross against a red light within 0–3 s left to the GS onset.

Based on the analysis results above, we can conclude that the impact of the independent variables on the three violation types was different. However, there were still some commonalities. In the next part, the common impact of independent variables on e-bikers' red-light infringement, regardless of their violation types are discussed.

3.2.2. Red-Light Infringement. Three violation types were included for univariate analysis and binary logistic regression (Tables 9 and 10) to establish the common influence of the independent variables on the e-bikers' red-light infringement and compare our results with previous studies.

The site was excluded from the univariable analysis, while the site type remained, inferring that these two variables were inter-related as functions of each other, and the site type had a relatively stronger influence. The red signal and green signal times were also removed. This outcome could be due to the significant correlation between the red/green signal time and the waiting time, while the waiting time had a stronger effect on the RLR behavior than the red/green signal time. Additionally, the univariable analysis results rejected the crossing width. The possible reason is that the crossing width would widen as e-bike flow expands (which is not subject to the width of the nonmotorized lane) when e-bikers enter the intersection from the approaching lanes. The remaining variables were integrated into the binary logistic model for further estimate.

The results identified gender as a significant variable in influencing e-bikers' RLR behavior. More specifically, male e-bikers had 1.339 ($e^{0.292}$) times the probability of RLR

behavior than female e-bikers. In other words, male e-bikers were apt to suffer a higher risk than female e-bikers to obtain the benefits of violating a red light (e.g., saving time or reaching the opposite side expediently). Our results are in good agreement with those of Yang et al.'s [9]. The findings of a few investigations on cyclists' violating behavior showed that female cyclists were more likely to act in accordance with the traffic regulation [12–16]. Furthermore, using the social-psychological approach, Yang et al. [10] found that male e-bikers recognized the RLR behavior much easier compared to female e-bikers, which also supported the gender difference in red-light infringement.

The findings of this study revealed that age was a significant variable. Specifically, the young and middle-aged e-bikers had 1.273 ($e^{0.241}$) and 1.384 ($e^{0.325}$) times odds of RLR behavior compared to the elderly e-bikers. In previous studies, the effect of age on e-bikers' RLR behavior was still indefinite. Zhang and Wu [22] established that young cyclists and e-bikers that were younger than 30 years old had a stronger intention to commit RLR behavior. However, Yang et al. [23] discovered that young (<30) and middle-aged (30–50) e-bikers were more likely to violate a red light than elderly e-bikers, but the age was an insignificant variable. This discrepancy may be due to certain errors in the estimation of the e-bikers' age by video recording or other observational methods.

The waiting position was identified as a significant variable on the final logistic regression model. Specifically, e-bikers waiting in the designated area had 0.833 ($e^{-0.183}$) times the likelihood of RLR behavior than those waiting in the nondesignated area. To some extent, e-bikers' waiting position partially represented their risk-perception. The e-bikers waiting in the designated area had higher safety awareness and could perceive the high risk of e-biker-car crashes in the nondesignated area. Some studies indicated that risk-perception was insignificant for predicting pedestrians' or e-bikers' violating behaviors using the theory of planned behavior [10, 50]. However, they also underlined that although risk-perception was not a significant predictor, it did not necessarily mean that risk-perception had no impact on violating behaviors. Our findings indirectly verified that risk-perception had a strong influence on e-bikers' RLR behavior. The result was in line with a previous study on pedestrians' crossing behavior, in which Koh et al. [42] uncovered that pedestrians standing in the designated waiting area were less likely to violate than those standing in the nondesignated waiting area.

Waiting time significantly contributed to e-bikers' decision to violate a red light. The likelihood of RLR behavior increased with the prolongation of the waiting time. Specifically, an increase by one unit in the waiting time augmented the likelihood of RLR behavior by 7.5%. This result was consistent with the findings of previous studies on cyclists and e-bikers [23, 46, 47]. In the related studies on pedestrians' red-light infringement, the findings also indicated that the longer the waiting time was, the higher the odds of red-light infringement would be [42, 43, 48].

The effect of leading violators was evident from the analysis, given that the number of other violators in front of e-bikers who started to cross had a significantly positive effect on e-bikers' tendency to violate a red-light. Specifically, the increase in the number of leading violators by one unit resulted in the rise in the likelihood of e-bikers' RLR behavior by 8.4%, showing that e-bikers' RLR behavior was easily influenced by the crossing behavior of the surrounding e-bikers. This phenomenon was caused by a mentality pattern called conformity tendency. The result could be supported by the previous studies which revealed the significant effect of the conformity tendency on pedestrians' violating crossing behavior by the application of social-psychological methods [49, 50].

As expected, passing cars substantially contributed to e-bikers' RLR behavior. The odds of e-bikers' red-light infringement declined with the increase in the number of passing cars. This result was consistent with Yang et al.'s study [23]. They found that a decrease in the motor vehicle volume would increase the violation hazard of cyclists and e-bikers in a hazard-based duration model. In a study on pedestrians' crossing behavior, Zhou et al. [51] obtained similar results, that is, the number of the incoming cars influenced pedestrians' RLR behavior significantly at the signalized intersections. The main reason for this phenomenon was that the traversable space-time gap under the light traffic volume was larger than that under the heavy traffic volume, and e-bikers were able to cross through the gap under the light traffic volume more easily and safely. The likelihood of e-bikers' RLR behavior decreased by 10.1% with the increase by one unit in the number of passing cars.

The results confirmed that the site type was an insignificant variable in the model for the whole violations, which is supported by Koh et al. [42] who simultaneously considered that Site-type 1 (intersection type), Site-type 2 (number of crossing lanes), and the crossing length were the factors influencing pedestrian's crossing behavior at signalized intersections. Their results showed that Site-type 2 and the crossing length were the most significant factors, while Site type-1 was insignificant. These findings could be due to adding crossing length in our study, which exerted a stronger effect than the site type on the RLR behavior.

We found that the likelihood that e-bikers would violate a red light decreased with the increase in the crossing length. Specifically, the increase in the crossing length by one unit would diminish the odds of RLR behavior by 7.9%. This result is consistent with the findings of Koh et al. [42], who reported that the odds of pedestrian's red-light infringement decreased with the increase in the crossing length.

The signalized intersections with TSCTs had 1.225 times the probability of RLR behavior than those without TSCTs, whereas the results showed that the effect of TSCTs installation was not significant. However, from the above analysis of violation types, TSCTs installation had a significant effect on GR near-violations and RG violations. Moreover, RG violations were more sensitive to TSCTs installation compared to GR near-violations. Accordingly, it was more meaningful to understand the impact of TSCTs on e-bikers' RLR behavior based on the violation types. Previous studies have also supported this analytical approach. For example, Lipovac et al. [35] revealed that TSCTs had no statistically significant effect on the number of violations during the red light for pedestrians regardless of location and vehicle volume, while there was a statistically significant difference during the first and last

four seconds of the red light, at the crossing located in the city center with a heavy traffic volume. The results obtained by Fu and Zou [36] indicated that the RSCTs installation caused more children to choose a violating and running behavior during the RS phase, and the GSCTs installation had a significant effect by helping children to complete their crossing within the GS phase. Thus, the above results might have ignored the influence of TSCTs on pedestrians' violating behavior if the violation types or the signal phases had not been taken into account. Our findings depicted the effect of TSCTs on e-bikers' RLR behavior during the different traffic signal phases, which could provide suggestions for whether installing the TSCTs or not in the different signal phases at signalized intersections.

4. Limitations and Future Research

In this study, since the video recording could not provide complete coverage of the whole intersection, the left-turn e-bikers were excluded. Future studies are required to record a full coverage video information and code the left-turn e-bikers with advanced technologies (e.g., "Mega Eyes" of China Telecom) to investigate their crossing behavior and violations, and compare them with those of straight-pass e-bikers. In addition, the trip purposes of e-bikers during the morning peak, the evening peak and the nonpeak period are different, which would potentially influence the red-light running behavior. Thus, additional studies are needed to discuss the crossing behavior and violations of e-bikers during the morning peak and the nonpeak period in future works. Furthermore, the influence of unobserved factors such as trip purpose and psychological perspective on e-bikers' red-light infringement was not taken into account in this study. E-bikers' actual motivations for individual RLR behavior remain unclear. To address these problematic areas of our research, we consider using corresponding interviews and questionnaires as an effective method in future studies.

5. Conclusion

This paper investigated the e-bikers' crossing and violations, associated influencing factors, and their differences among the three violation types at signalized intersections using an observational study. Eight signalized intersections with different traffic conditions and characteristics were selected as the observational sites for this work. A total number of 3,126 e-bikers crossing the intersections were observed.

The late, incomplete, and violating crossing behaviors were discussed. It was observed that for late-entry e-bikers who arrived during the LGS/YS phases, some of them also chose to cross even during the YS phase. The analysis results revealed that the crossing length and site type were possibly associated with e-bikers' crossing behavior. Among the e-bikers who possibly could not complete the crossing before the RS onset, those who began to cross during the SGS phase generally could complete the crossing before the RS onset, whereas those who started to cross during the LGS/YS phases were likely unable to complete it. We classified the violations into three types: GR near-violations, RR violations, and RG violations. Our findings showed that the proportions of the RG violations and GR near-violations were higher than that of the RR violations, among which the RG violations were the most prevalent type. Moreover, the proportions of the RG violations and GR near-violations at the study sites with TSCTs were considerably more than those at the rest sites without TSCTs, inferring that TSCTs installation might influence e-bikers' RLR behavior. In addition, most RG violators intended to cross during the interval 0–3 s before the GS onset due to the presence of a 2-3 s All-Red clearance phase.

We used a binary logistic regression model to further elucidate the effect of the independent variables on e-bikers' red-light infringement. The findings indicated that the estimated age had the most pronounced positive effect on the GR near-violations as compared to its influence on the other violation types. Moreover, the green signal time and site type were the most significant contributors to the GR near-violations, whereas they exerted no significant effects on the other types. The waiting time, waiting position, passing cars, and crossing length most considerably contributed to the RR violations than to the other violation types. However, the effects of TSCTs, leading violators, and gender on RG violations were the most significant among the three violation types. Subsequently, in this study, we took into account a census of all three types of violations to summarize the common influence of the independent variables on e-bikers' red-light infringement. Our findings revealed that the gender, estimated age, waiting position, waiting time, leading violators, passing cars, and crossing length were the most significant variables, whereas the site, site type, red signal time, green signal time, crossing width, and TSCTs were insignificant. Nonetheless, the site type, green signal time, and TSCTs still had important impacts on the three violation types. In other words, it was more meaningful to investigate the effect of these independent variables on e-bikers' RLR behavior considering the specific violation types. Thus, the authors of previous studies [23, 42–44] might have ignored the effect of some crucial variables on riders/pedestrians' violations regardless of the differences in the violation types.

The findings of this study provided a better understanding of e-bikers' crossing behavior and violations at signalized intersections. Therefore, they could support the development and implementation of countermeasures to reduce e-bikers' red-light infringement and facilitate the design of proper signalized intersections for e-bikers by transport agencies, especially in countries with a high population of e-bikers.

Data Availability

The data used to support the findings of this study are available from the corresponding author upon request.

Conflicts of Interest

The authors declare that there are no conflicts of interest regarding the publication of this paper.

Authors' Contributions

The authors confirm contribution to the paper as follows: study conception and design: T. Tang, H. Wang, X. Zhou; data collection: J. Ma, H. Wang; analysis and interpretation of results: T. Tang, H. Wang, J. Ma; draft manuscript preparation: T. Tang, X. Zhou. All authors reviewed the results and approved the final version of the manuscript.

Acknowledgments

This research is supported by the Natural Science Foundation of the Jiangsu Higher Education Institutions of China (No. 19KJB580003), the Science and Technology Project of Nantong City (No. JC2019062), the National Natural Science Foundation Council of China (No. 71601142), the Humanities and Social Science Foundation of the Ministry of Education in China (No. 18YJCZH274), and the Applied Research Foundation of Social Science of Jiangsu Province (No. 19SYC-110). The data used to support the findings of this study are available from the corresponding author upon request.

References

[1] C. Cherry and R. Cervero, "Use characteristics and mode choice behavior of electric bike users in China," *Transport Policy*, vol. 14, no. 3, pp. 247–257, 2007.

[2] D. Zuev, D. Tyfield, and J. Urry, "Where is the politics? E-bike mobility in urban China and civilizational government," *Environmental Innovation and Societal Transitions*, vol. 30, pp. 19–32, 2019.

[3] Nantong Bureau of Natural Resources and Planning, *Nantong Urban Transport Development Annual Report*, Nantong Bureau of Natural Resources and Planning, Nantong, China, 2018.

[4] "Chinese e-bikes news, new management mode of e-bikes in Nanning, Chinese e-bikes news," http://news.ddc.net.cn/newsview_64066.html, 2015.

[5] Traffic Management Bureau of the Ministry of Public Security, "The people's Republic of China road traffic accident annual statistic report," Traffic Management Bureau of the Ministry of Public Security, Wuxi, China, 2018.

[6] "News in Jiangsu, Jiangsu Accelerates the Promotion of E-bike Legislation, News in Jiangsu," https://js.qq.com/a/20190713/000809.htm, 2019.

[7] L. Yao and C. Wu, "Traffic safety for electric bike riders in china: attitudes, risk perception, and aberrant riding behaviors," *Transportation Research Record*-, vol. 24, no. 2314, pp. 49–56, 2012.

[8] L. Bai, P. Liu, Y. Chen, X. Zhang, and W. Wang, "Comparative analysis of the safety effects of electric bikes at signalized intersections," *Transportation Research Part D: Transport and Environment*, vol. 20, pp. 48–54, 2013.

[9] X. Yang, M. Abdel-Aty, M. Huan, Y. Peng, and Z. Gao, "An accelerated failure time model for investigating pedestrian crossing behavior and waiting times at signalized intersections," *Accident Analysis and Prevention*, vol. 82, pp. 154–162, 2015.

[10] H. Yang, X. Liu, F. Su, C. Cherry, Y. Liu, and Y. Li, "Predicting e-bike users' intention to run the red light: an application and extension of the theory of planned behavior," *Transportation Research Part F: Traffic Psychology and Behaviour*, vol. 58, pp. 282–291, 2018.

[11] F. Chen, M. Song, and X. Ma, "Investigation on the injury severity of drivers in rear-end collisions between cars using a random parameters bivariate ordered probit model," *International Journal of Environmental Research and Public Health*, vol. 16, no. 14, p. 2632, 2019.

[12] M. Johnson, S. Newstead, J. Charlton, and J. Oxley, "Riding through red lights: the rate, characteristics and risk factors of noncompliant urban commuter cyclists," *Accident Analysis and Prevention*, vol. 43, no. 1, pp. 323–328, 2011.

[13] M. Johnson, J. Charlton, J. Oxley, and S. Newstead, "Why do cyclists infringe at red lights? An investigation of australian cyclists' reasons for red light infringement," *Accident Analysis and Prevention*, vol. 50, no. 1, pp. 840–847, 2013.

[14] C. Wu, L. Yao, and K. Zhang, "The red-light running behavior of electric bike riders and cyclists at urban intersections in china: an observational study," *Accident Analysis and Prevention*, vol. 49, no. 11, pp. 186–192, 2012.

[15] C. W. Pai and R. C. Jou, "Cyclists' red-light running behaviors: an examination of risk taking, opportunistic, and law-obeying behaviors," *Accident Analysis and Prevention*, vol. 62, pp. 191–198, 2014.

[16] F. Fraboni, V. Marín Puchades, M. De Angelis, L. Pietrantoni, and G. Prati, "Red-light running behavior of cyclists in Italy: an observational study," *Accident Analysis and Prevention*, vol. 120, pp. 219–232, 2018.

[17] D. De Waard, F. Westerhuis, and B. Lewis-Evans, "More screen operation than calling: the results of observing cyclists' behaviour while using mobile phones," *Accident Analysis and Prevention*, vol. 76, pp. 42–48, 2015.

[18] D. De Waard, P. Schepers, W. Ormel, and K. Brookhuis, "Mobile phone use while cycling: incidence and effects on behaviour and safety," *Ergonomics*, vol. 53, no. 1, pp. 30–42, 2010.

[19] K. Kircher, C. Ahlstrom, L. Palmqvist, and E. Adell, "Bicyclists' speed adaptation strategies when conducting self-paced vs. system-paced smartphone tasks in traffic," *Transportation Research Part F: Traffic Psychology and Behaviour*, vol. 28, pp. 55–64, 2015.

[20] X. Yang, M. Huan, B. Si, L. Gao, and H. Guo, "Crossing at a red light: behavior of cyclists at urban intersections," *Discrete Dynamics in Nature and Society*, vol. 2012, Article ID 490810, 12 pages, 2012.

[21] X. Yang, M. Abdel-Aty, M. Huan, B. Jia, and Y. Peng, "The effects of traffic wardens on the red-light infringement behavior of vulnerable road users," *Transportation Research Part F: Traffic Psychology and Behaviour*, vol. 37, pp. 52–63, 2016.

[22] Y. Zhang and C. Wu, "The effects of sunshields on red light running behavior of cyclists and electric bike riders," *Accident Analysis and Prevention*, vol. 52, pp. 210–218, 2013.

[23] X. Yang, M. Huan, M. Abdel-Aty, Y. Peng, and Z. Gao, "A hazard-based duration model for analyzing crossing behavior of cyclists and electric bike riders at signalized intersections," *Accident Analysis and Prevention*, vol. 74, pp. 33–41, 2015.

[24] K. Schleinitz, T. Petzoldt, S. Kröling, T. Gehlert, and S. Mach, "(E-)Cyclists running the red light – the influence of bicycle type and infrastructure characteristics on red light violations," *Accident Analysis and Prevention*, vol. 122, pp. 99–107, 2019.

[25] Q. Zeng, W. Gu, X. Zhang, H. Wen, J. Lee, and W. Hao, "Analyzing freeway crash severity using a bayesian spatial

generalized ordered logit model with conditional autoregressive priors," *Accident Analysis & Prevention*, vol. 127, pp. 87–95, 2019.

[26] Q. Zeng, H. Wen, H. Huang, X. Pei, and S. C. Wong, "Incorporating temporal correlation into a multivariate random parameters tobit model for modeling crash rate by injury severity," *Transportmetrica A: Transport Science*, vol. 14, no. 3, pp. 177–191, 2018.

[27] Q. Zeng, Q. Guo, S. C. Wong, H. Wen, H. Huang, and X. Pei, "Jointly modeling area-level crash rates by severity: a bayesian multivariate random-parameters spatio-temporal tobit regression," *Transportmetrica A: Transport Science*, vol. 15, no. 2, pp. 1867–1884, 2019.

[28] D. Zhao, W. Wang, C. Li, Z. Li, P. Fu, and X. Hu, "Modeling of passing events in mixed bicycle traffic with cellular automata," *Transportation Research Record*, vol. 2387, pp. 26–34, 2013.

[29] D. Zhao, W. Wang, G. P. Ong, and Y. Ji, "An association rule based method to integrate metro-public bicycle smart card data for trip chain analysis," *Journal of Advanced Transportation*, vol. 2018, Article ID 4047682, 11 pages, 2018.

[30] D. Zhao, G. P. Ong, W. Wang, and X. J. Hu, "Effect of built environment on shared bicycle reallocation: a case study on nanjing, china," *Transportation Research Part A*, vol. 128, pp. 73–88, 2019.

[31] M. R. Islam, D. S. Hurwitz, and K. L. Macuga, "Improved driver responses at intersections with red signal countdown timers," *Transportation Research Part C: Emerging Technologies*, vol. 63, pp. 207–221, 2016.

[32] M. R. Islam, A. A. Wyman, and D. S. Hurwitz, "Safer driver responses at intersections with green signal countdown timers," *Transportation Research Part F: Traffic Psychology and Behaviour*, vol. 51, pp. 1–13, 2017.

[33] T. Rosenbloom, A. Shahar, and A. Perlman, "Compliance of ultra-orthodox and secular pedestrians with traffic lights in ultra-orthodox and secular locations," *Accident Analysis and Prevention*, vol. 40, no. 6, pp. 1919–1924, 2008.

[34] P. Lambrianidou, S. Basbas, and I. Politis, "Can pedestrians' crossing countdown signal timers promote green and safe mobility?," *Sustainable Cities and Society*, vol. 6, pp. 33–39, 2013.

[35] K. Lipovac, M. Vujanic, B. Maric, and M. Nesic, "The influence of a pedestrian countdown display on pedestrian behavior at signalized pedestrian crossings," *Transportation Research Part F: Traffic Psychology and Behaviour*, vol. 20, pp. 121–134, 2013.

[36] L. Fu and N. Zou, "The influence of pedestrian countdown signals on children's crossing behavior at school intersections," *Accident Analysis and Prevention*, vol. 94, pp. 73–79, 2016.

[37] S. Biswas, I. Ghosh, and S. Chandra, "Effect of traffic signal countdown timers on pedestrian crossings at signalized intersection," *Transportation in Developing Economies*, vol. 3, no. 1, p. 2, 2017.

[38] G. Wu, F. Chen, X. D. Pan, M. Xu, and X. Y. Zhu, "Using the visual intervention influence of pavement markings for rutting mitigation – part I: preliminary experiments and field tests," *International Journal of Pavement Engineering*, vol. 20, no. 6, pp. 734–746, 2019.

[39] X. Y. Zhu, Z. W. Dai, F. Chen, X. D. Pan, and M. Xu, "Using the visual intervention influence of pavement marking for rutting mitigation – part II: visual intervention timing based on the finite element simulation," *International Journal of Pavement Engineering*, vol. 20, no. 5, pp. 573–584, 2019.

[40] D. Zhao, W. Wang, Y. Zheng, Y. Ji, W. Wang, and X. Hu, "Evaluation of interactions between buses and bicycles at stops," *Transportation Research Record*, vol. 2468, pp. 11–18, 2014.

[41] J. Jiang, D. Zhang, S. Li, and Y. Liu, "Multimodal green logistics network design of urban agglomeration with stochastic demand," *Journal of Advanced Transportation*, vol. 2019, Article ID 4165942, 19 pages, 2019.

[42] P. P. Koh, Y. D. Wong, and P. Chandrasekar, "Safety evaluation of pedestrian behaviour and violations at signalised pedestrian crossings," *Safety Science*, vol. 70, pp. 143–152, 2014.

[43] H. Guo, Z. Gao, X. Yang, and X. Jiang, "Modeling pedestrian violation behavior at signalized crosswalks in china: a hazards-based duration approach," *Traffic Injury Prevention*, vol. 12, no. 1, pp. 96–103, 2011.

[44] V. Cantillo, J. Arellana, and M. Rolong, "Modelling pedestrian crossing behaviour in urban roads: a latent variable approach," *Transportation Research Part F: Traffic Psychology and Behaviour*, vol. 32, pp. 56–67, 2015.

[45] D. W. Hosmer and S. Lemeshow, *Applied Logistic Regression*, John Wiley & Sons, New York, NY, USA, 2nd edition, 2000.

[46] J. Zhou, Q. Wang, and M. Zhang, "An empirical study on seven factors influencing waiting endurance time of e-Bike," *Journal of Transportation Systems Engineering and Information Technology*, vol. 17, no. 5, pp. 242–249, 2017.

[47] L. Huang and S. Ni, "Analysis on violation behavior of nonmotor vehicles at plane intersection," *Journal of Transportation Engineering and Information*, vol. 15, no. 2, pp. 64–70, 2017.

[48] G. Tiwari, S. Bangdiwala, A. Saraswat, and S. Gaurav, "Survival analysis: pedestrian risk exposure at signalized intersections," *Transportation Research Part F: Traffic Psychology and Behaviour*, vol. 10, no. 2, pp. 77–89, 2007.

[49] R. Zhou, W. J. Horrey, and R. Yu, "The effect of conformity tendency on pedestrians' road-crossing intentions in China: an application of the theory of planned behavior," *Accident Analysis and Prevention*, vol. 41, no. 3, pp. 491–497, 2009.

[50] H. Zhou, S. B. Romero, and X. Qin, "An extension of the theory of planned behavior to predict pedestrians' violating crossing behavior using structural equation modeling," *Accident Analysis and Prevention*, vol. 95, pp. 4717–424, 2016.

[51] Z. P. Zhou, Y. S. Liu, W. Wang, and Y. Zhang, "Multinomial logit model of pedestrian crossing behaviors at signalized intersections," *Discrete Dynamics in Nature and Society*, vol. 2013, Article ID 172726, 8 pages, 2013.

Hindawi
Journal of Advanced Transportation
Volume 2020, Article ID 2675197, 14 pages
https://doi.org/10.1155/2020/2675197

Research Article

Analysis on Illegal Crossing Behavior of Pedestrians at Signalized Intersections Based on Bayesian Network

Yingying Ma,[1] Siyuan Lu,[1] and Yuanyuan Zhang [2]

[1]*Department of Transportation Engineering, South China University of Technology, 381 Wushan Road, Guangzhou 510641, China*
[2]*School of Construction and Design, University of Southern Mississippi, 118 College Dr, Hattiesburg, MS 39406, USA*

Correspondence should be addressed to Yuanyuan Zhang; yuanyuan.zhang@usm.edu

Received 23 August 2019; Accepted 7 October 2019; Published 17 January 2020

Guest Editor: Feng Chen

Pedestrians do not always comply with the crossing rules of when and/or where to cross the road at signalized intersections. This risky behavior tends to undermine greatly the effectiveness of safety countermeasures at such locations. Thus, it is very important to understand illegal behavior to develop more effective and targeting measures. In order to address the problem, this paper aimed to analyze characteristics of illegal crossings and their impact on behavior choice. Firstly, illegal crossing behaviors at signalized intersections were classified into two categories, including "crossing at a red light" and "crossing outside of a crosswalk". Secondly, two sets of data were collected to understand the behaviors. One set of data was collected from video-based observation conducted at 3 signalized intersections in Guangzhou, China, capturing 3334 valid illegal crossing cases in total. Another set of data, from a questionnaire survey conducted online, resulted in 275 valid responses. Finally, presentational characteristics of illegal crossings at signalized intersection were analyzed and two Bayesian network-based behavior models were developed to investigate the characteristics and their impacts on the two types of illegal crossing behaviors, "crossing at a red light" and "crossing outside of a crosswalk," respectively. Findings reveal that, (i) illegal crossings occur at various types of signalized intersections, with a higher probability for "crossing outside of a crosswalk" compared to "crossing at a red light;" (ii) Arc routing crossing has the highest probability to occur at signalized intersections compared to other types of out-side-crosswalk crossings. (iii) The location of origin and destination of a pedestrian has a significant effect on crossing outside of a crosswalk, the location of origin and destination of "one is inside of a crosswalk and another is outside of a crosswalk" has a highest proportion. These findings provide better understanding of illegal crossings and their impact factors so that the effectiveness of management and control of pedestrians at signalized intersections can be improved.

1. Introduction

The National Highway Traffic Safety Administration (NHTSA) reports that during the 10-year period of 2008–2017, the number of pedestrian fatalities in the U.S. increased by 35 percent, from 4,414 deaths in 2008 to 5,977 deaths in 2017. While pedestrian deaths have been increasing, the number of all other traffic deaths combined decreased by six percent (ghsa.org/resources/Pedestrians19). In China, illegal crossing at signalized intersections is a serious problem. In 2014, there were 2242 pedestrian accidents in China, with 1247 deaths, averaging 3.42 deaths per day due to various illegal and risky pedestrian actions on the road. Illegal crossings mainly include pedestrians crossing at red lights or outside of marked crosswalks, with the latter usually being ignored. This hazardous behavior may cause incidents between them and drivers. Therefore, it is necessary to analyze pedestrian violation behaviors at signalized intersections to reduce them.

2. Literature Review

Existing studies on illegal crossing of pedestrians mainly focus on factors affecting crossing behavior of pedestrian, data collection, illegal crossing behavior and research methods, which are summarized in Table 1 and described afterwards.

2.1. Factors Affecting Crossing Behavior of Pedestrian. Most previous studies concerning crossing behavior impact factors mainly focus on pedestrian attributes, traffic conditions, road conditions and so on. Firstly, in terms of pedestrian attributes, age and gender are two main factors considered to describe

Table 1: Literature review on illegal crossings of pedestrians.

Study focus	Literature review		
	Pedestrian attributes	Traffic conditions	Road conditions
Factors	Age [1], gender [2], crowd size [3], clothing [3], luggage [4], cultural backgrounds [5], alcohol use [6, 7], social psychology [2, 8–10], etc.	Pedestrian flow [11], waiting time [12], left-turn ratio of vehicle [13], etc.	Distance of crosswalk [14], countdown displays [15], intersection type [16], etc.
Data collection	Data from video recording [1, 17–20], data from questionnaire survey [2, 8], virtual reality experimental data [21], reported data from police [22], database [6], etc.		
	Characteristics of illegal crossings	Influence mechanism of factors	Safety analysis of pedestrian
Illegal behaviors	Process of crossing in various states [3], crossing pattern [23], statistical analysis of violation [5], parameters of crossing [14], etc.	Analysis on relation between crossing at a red light and factors [5, 15, 24]	The gap acceptance of illegal crossing [1, 25] and risk of pedestrian-vehicle collisions [22, 26]
Research methods	Descriptive statistical method [27–30]; regression analysis methods: binary regression analysis [8], polynomial regression analysis [31], logical regression analysis [11] and hierarchical regression analysis [5]. Difference significance analysis: one-way ANOVA [32, 33] and T test [34]. Disaggregated method [35–37]; Structural equation model [38]; Petri Nets (PN) model [39] and traffic flow model [40]		

the pedestrians. It is shown that the male and middle-aged pedestrians have a high probability to cross the streets illegally [1, 2, 19]. Besides, crowd size [3, 23], clothing [3], and luggage [4] are also employed to explain the different crossing speeds and waiting time. In addition, culture is considered as another important factor impacting differences in crossing behaviors [5]. Psychological factors such as comfort perception, willingness to bypass, conformity, carelessness, anxiety, and personal preference are also analyzed in previous studies [2, 8–10]. A few studies take alcohol use into account to analyze risk of pedestrian-motor vehicle collisions [6, 7].

Secondly, as for traffic conditions, the relative studies mainly focus on vehicle flow, traffic density, pedestrian flow, phase time and so on. The results show that the proportion of crossing at a red light decreases with the increase of vehicle flow and pedestrian flow at signalized intersections [11], and the probability of crossing at a red light increases while the waiting time of pedestrian is too long to exceed their tolerance limit [12]. Besides, the left-turn ratio of vehicles is a key parameter usually used to analyze the probability of pedestrian-vehicle collisions [13].

Lastly, factors of road conditions, including crosswalk distance, countdown displays, type of intersection, illumination and so on, are also considered to analyze pedestrian crossings. Some results suggest that it has a negative correlation between the proportion of compliance with traffic rules and crosswalk distance; countdown displays significantly reduce pedestrian crossing behavior at a red light [15], and factors appear to have different influence on illegal crossings at different intersections [16]. Except for the factors above, weather [6], and social economics [35] are used to analyze the preference of crossings in a few studies.

The effect of pedestrian attributes, traffic conditions, and road conditions on pedestrian crossings, are usually considered. As for pedestrian attributes, apart from the factors mentioned, education, and income level are added in this paper to analyze illegal crossing behavior, from a more diversified perspective. More effective improvement measures or educational programs are developed to target different groups by learning their socioeconomic backgrounds. Besides, on road conditions, it is shown that safety island and location of traffic attractions are rarely involved in the previous studies, so this paper makes an exploratory analysis of these two factors because it can help to formulate design and restraint schemes of facilities in some important intersections after learning the influence of safety island and location of traffic attractions.

2.2. Data Collection. Data, on illegal crossings used for analysis, are usually obtained from video-based observation and questionnaire survey. Data from video-based observation is used to analyze characteristics of crossings, including crossing speed, crossing pattern, etc., and quantify some factors of pedestrian attributes, traffic conditions and road conditions [1, 17–20]. Data from questionnaire surveys are mainly used to obtain pedestrian psychological factors, behavioral reasons, preferences and so on [2, 8]. Applications of data are mainly divided into three categories: data of video recording used alone, data of questionnaire survey used alone, and the combination of them. The majority of studies use the two sources of data to analyze illegal crossings, however, they are usually used alone, only a few studies combine them into the model [24], while the subjects of the questionnaire are pedestrians who are recorded on the video. Also, a few studies on pedestrian crossings, applied virtual reality experimental data [21], reported data from police [22], and database [6] to their analysis.

Data from video-based observation and questionnaires are contained in some previous studies. However, these two sets of data are usually used separately, and only data from questionnaire survey are used for modeling, such as, regression analysis, while in a few papers, the subject of questionnaire survey was the pedestrians who were recorded in the video, but the contents of the questionnaire are mainly the reasons and psychology for illegal crossing, which was statistically analyzed without considering surrounding factors. It is said that in these papers it is difficult to model by combining data from video-based observation with questionnaire survey. In this paper, data from questionnaire survey in which the scenes of pedestrians crossing the streets were augmented by respondents recalling their recent crossing experiences were mainly used to model pedestrian illegal crossings considering factors of pedestrian attributes, traffic conditions and road conditions. Additional data from video recordings were only

used to analyze superficial characteristics of illegal crossings, it was not used in the illegal crossing model. Therefore, the subjects of the questionnaire survey are not necessarily the pedestrians, recorded on video in this paper, according to the objectives.

2.3. Illegal Crossing Behavior. According to the environment, illegal crossing behaviors can be divided into three categories of mid-block streets, signalized intersections, and unsignalized intersections. However, illegal crossing behavior at signalized intersections is important and difficult. Characteristics of illegal crossings, the influence mechanism of the factors and safety analysis of pedestrians are usually analyzed in the previous studies. Analyses on illegal crossing characteristics include process of crossing in various states [3], crossing pattern [23], statistical analysis of violation [5], parameters of crossing [14] and so on. Research of influence mechanisms mainly focuses on analysis on crossing behavior at a red light on which the effects of factors of pedestrian attributes, traffic conditions, and road conditions are analyzed [5, 15, 24]. As for pedestrian safety, the gap acceptance of illegal crossing [1, 25] and risk of pedestrian-vehicle collisions [22, 26], are analyzed.

In previous studies, research on illegal crossing behavior at signalized intersections mainly focuses on crossings at a red light, while behavior of crossing outside of a crosswalk in the spatial dimension is only statistically analyzed in a few studies, and it is especially lacking analysis on the relationship between behavior of crossing outside of a crosswalk and additional factors, however, it is a significant improvement to the design of pedestrian crossing facilities. This paper analyzes characteristics of illegal crossings and the influence mechanism of factors from temporal and spatial dimensions to fill in the gap of the research, by adding analysis on behaviors of crossing outside of a crosswalk.

2.4. Research Method of Illegal Behavior. The research methods used to analyze behaviors of illegal crossings mainly include descriptive statistical method, regression analysis method, significant difference analysis, disaggregated method, structural equation model, traffic flow model, and as utilized in previous studies. Descriptive statistical method is typically used to count the frequency of items of field observations and questionnaires [27–30]. Compared to descriptive statistical method, regression analysis, difference significance analysis and disaggregated method can reflect the relation between behaviors and factors. Binary regression analysis [8], polynomial regression analysis [31], sequence regression analysis [8], logical regression analysis [11] and hierarchical regression analysis [5] are the main regression analysis methods used to analyze relation between behaviors of illegal crossing and factors while correlation analysis is used to analyze the relation between the factors [21]. Difference significance analysis, including one-way ANOVA [32, 33] and T test [34] is used to analyze the differences between different dimensions of factors, and disaggregated method is mainly used to analyze the relationship between pedestrian crossing modes and influencing factors [35]. However, part of the research establishes structural equation models to study decision-making of pedestrians from the psychological perspective [38]. In terms of safety, part of the research establishes models based on the Petri Nets (PN) model [39] and traffic flow model [40], or applies GIS software [41] to analyze pedestrian-vehicle collisions.

The methodology of regression analysis, difference analysis, and nonaggregate method has become mature, which is helpful to understand pedestrian crossing behavior. In this paper, Bayesian network is proposed to analyze illegal crossings for its advantage in describing the relationship of illegal crossings and its influencing factors, forming a graphical network to intuitively reveal influencing mechanism of the factors, to make up for the shortcomings of relevant research methods.

In order to analyze illegal pedestrian crossings at signalized intersections, some work has been carried out in this paper: (i) The research data were collected from two sources of video recording and questionnaire surveys; (ii) Presentational characteristics of illegal crossings were analyzed from temporal and spatial dimensions based on data from video recording; (iii) Two models of crossing at a red light and crossing outside of a crosswalk are established based on Bayesian network to deeply reveal the causal relationship of illegal crossings and influencing factors based on data questionnaire surveys, by adding factors of education, income level, safety island, and location of traffic attractions.

3. Data Collection

This paper aimed to understand characteristics of illegal pedestrian crossings at signalized intersections and the influence mechanism of factors. To understand characteristics of illegal crossings, a video-based observation was conducted to record the whole crossing process at three signalized intersections in Guangzhou, China; and to further understand the relationship between illegal crossings and factors, an online questionnaire survey was conducted. The questionnaire survey and video-based observation were not conducted concurrently in this paper.

3.1. Video-Based Observation. In this observation, crossings at each of the selected signalized intersections were recorded for one hour, from 11:20 am to 12:20 pm on May 2, 2017 and on October 5, 2017 respectively. The observation time was chosen to cover the noon peak when pedestrian activities are more likely to be frequent. Characteristics of observed pedestrian crossings are shown in Table 2. After the videos were collected, data collectors reviewed the recordings to record information about the number of pedestrians, pedestrians crossing at a red light, pedestrians crossing outside of a crosswalk, and pedestrians occupying crosswalks during red lights, in each signal cycle. In total, there were 22-cycle recordings with 3334 pedestrian crossing cases that were processed and will be used to analyze characteristics of illegal crossings. Since panorama view was not available at signal intersections, this study only focuses on one-way pedestrian crossings.

3.2. Online Surveys. Another source was acquired from the online questionnaire survey on pedestrian crossings at signalized intersections. The online questionnaire aimed to

Table 2: Characteristics of observed pedestrian crossings.

Intersection	Direction	Length (m)	Width (m)	Number of lanes	Green ratio
Tianhe road-tiyudong road	South	15	6	8	0.21
	East	40	6	11	0.26
Tianrun road-longkou east road	South	7	3	2	0.34
	East	15	3	4	0.12
	North	10	3	2	0.34
	West	11	3	2	0.12
Huasui road-huacheng avenue	South	15	3	4	0.14
	East	27	3	6	0.40

collect data of personal attributes, traffic conditions and road facilities by acquiring pedestrian feedback. It was conducted in Guangzhou and distributed online between September 27, 2017 and October 3, 2017, resulting in 275 valid respondents. The respondents had to fill in the questionnaires by recalling their newest crossings. This could avoid inauthentic information caused by pedestrians in a hurry at intersections. Table 3 shows the statistics of the survey respondents. People aged 18–30 account for a high proportion, 43.27%, while that of other age groups are approximately 20% each. Education has an even distribution in each sub-group, with a proportion about 20–30%. However, respondents whose income is less than three thousand Chinese Yuan accounts for over 50%, with that of respondents earning three thousand to six thousand at approximately 21%. Regarding the conditions under which illegal crossing happened, about 60% of the respondents reported that they were "in a hurry" to their next destination. About 41% of the people were crossing alone, and 30% of the people cross the streets with one additional pedestrian.

Table 3: Statistics of questionnaire survey.

Variable	Item	Frequency	Percentage
Age	<18	58	21.09%
	18~30	119	43.27%
	31~45	46	16.72%
	>45	52	18.91%
Education	Middle school and below	52	18.91%
	High school	64	23.27%
	Bachelor's	92	33.5%
	Master's and above	69	25.09%
Monthly Income (Yuan)	<3 thousand	139	50.55%
	3–6 thousand	60	21.82%
	6–10 thousand	45	16.36%
	>10 thousand	31	11.27%
Being in a Hurry	Not hurried	74	26.91%
	Moderately hurried	163	59.27%
	Very hurried	38	13.82%
The Number of Companions	0	115	41.82%
	1	82	29.82%
	2	44	16%
	>2	34	12.36%

4. Analysis on Pedestrian Illegal Crossings at Signalized Intersections

Observations show that pedestrian crossings at a red light, pedestrians standing on crosswalks during red lights, and crossings outside of a crosswalk at signalized intersections are recorded. Illegal crossings are analyzed from temporal and spatial dimensions.

4.1. Temporal Dimension. Analysis on illegal crossings in the timing dimension included crossing at a red light and pedestrians intruding into the crosswalk while waiting at the red light which is shown in Figure 1(a). From the observation statistics in Table 4, it is shown that about 17 pedestrians on average cross at a red light every signal cycle, with a proportion of 11.5%, and pedestrian standing on crosswalks during red lights accounts for 3.5%. On long crosswalks pedestrians cross at a red light when the vehicle volume is getting fewer and they choose to cross at the end of green signals, when the signal light turns red rapidly before those pedestrians reach the opposite sides. On the other hand, on short crosswalks, pedestrians choose to cross immediately when they reach the intersection no matter what the signal light is, while a few people cross after stopping for a little time.

Table 4: Statistics on illegal crossings.

Illegal crossings	Mean (person)	SD	Proportion
Crossing at a red light	17	1.041	11.5%
Crossing out of crosswalks	40	5.368	27%
Standing on crosswalks during waiting time	5	4.110	3.5%

4.2. Spatial Dimension. The results show that pedestrian crossing outside of a crosswalk is a serious phenomenon among illegal crossings in Figure 1(b), with a proportion up to 27% in Table 4. If the trajectories of crossings are depicted for each pedestrian, it is easy to find that there are specific types of routes that are taken by pedestrians while crossing at the signalized intersections. Figure 2 displays three types of crossing routes, including "Arc-routing", "Broken line-routing", and "Straight line-routing". And it is also shown that pedestrian took different routes at different types of crosswalks.

(a) (b)

Figure 1: Pedestrian illegal crossings. (a) Standing on crosswalks during waiting time. (b) Crossing outside of crosswalk.

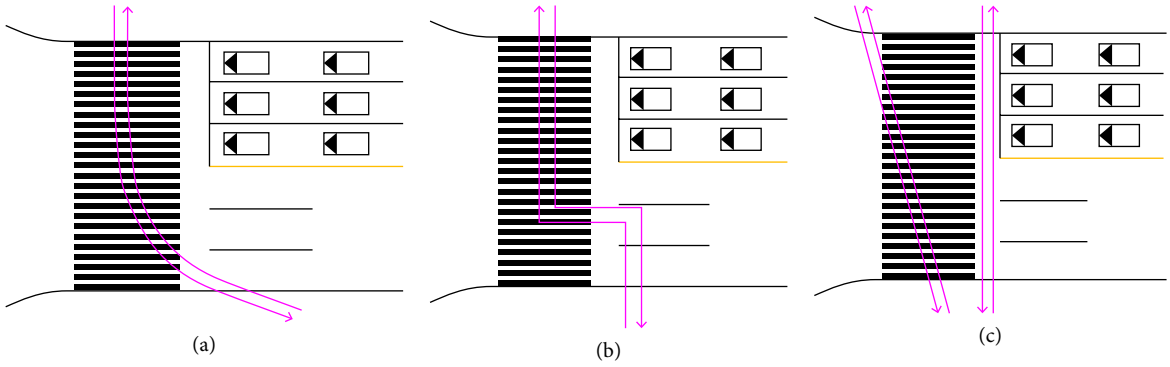

(a) (b) (c)

Figure 2: Classification of pedestrian crossing outside of a crosswalk. (a) Arc-routing. (b) Broken line-routing. (c) Straight line-routing.

Table 5: Proportion of three types of crossing outside of a crosswalk.

Classification	Mean (person)	SD	Proportion
Arc-routing crossing	23	8.65	58%
Broken line-routing crossing	3	1.602	8%
Straight line-routing crossing	14	4.272	34%

It is shown that some differences exist in the three illegal crossings of the location dimension in Table 5. Arc-routing crossing occupies the highest proportion of 58%, and straight line-routing crossing ranks the second, accounting for 34%. Broken line-routing crossing rarely occurs compared to other two illegal crossings. It can be concluded from statistical analysis that crossing outside of a crosswalk which is easily ignored by people has a higher probability than crossing at a red light, especially arc routing crossing.

The pairs of location of origin and destination of single pedestrians crossing the streets are classified into 4 categories, namely "both inside of the crosswalk", "both outside of a crosswalk and in the same side", "both outside of a crosswalk and in the different side", "one is inside of a crosswalk and another is outside of a crosswalk." Distribution of origin and destination of pedestrians crossing the streets is shown in Figure 3, where the lines with different colors denote different pairs of origin and destination. 640 samples of crossing outside of a crosswalk are statistically analyzed, the results are shown in Table 6. As it is shown that "one is inside of a crosswalk and another is outside of a crosswalk" has a highest proportion of 77.97% among the 4 categories. "Both outside of a crosswalk and in the same side" ranks second, with a proportion of 21.72%. "Both inside of the crosswalk" and "both outside of a crosswalk and in the different side" have a very small proportion.

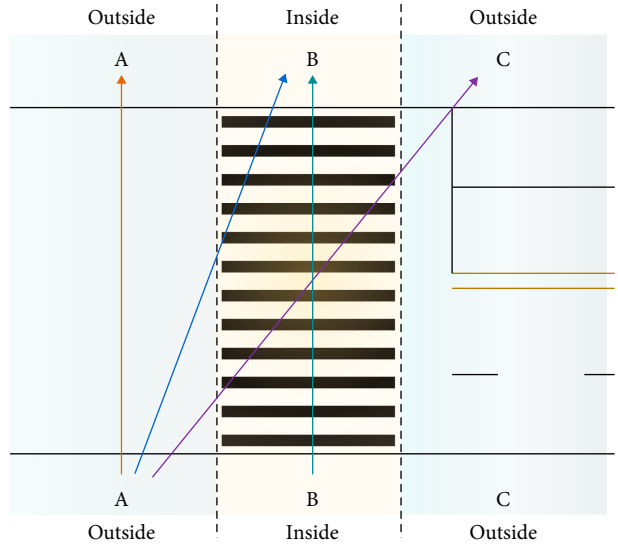

Figure 3: Distribution of origin and destination of pedestrian crossing the streets.

Table 6: Statistics on location of origin and destination of crossing outside of a crosswalk.

Classification	Origin	Destination	Frequency	Total
Both inside of the crosswalk	B	B	0.01%	0.01%
Both outside of a crosswalk and in the same side	A	A	5.47%	21.72%
	C	C	16.25%	
Both outside of a crosswalk and in the different side	A	C	0.15%	0.30%
	C	A	0.15%	
One is inside of a crosswalk and another is outside of a crosswalk	A	B	5.47%	77.97%
	C	B	60.78%	
	B	A	3.91%	
	B	C	7.81%	

Table 7: Variable definition of factors influencing illegal crossings.

Category	Variable	Definition and value
Personal attributes	Age (x_1)	1: <18 (state 4); 2: 18~30 (state 1); 3: 31~45 (state 2); 4: >45 (state 3)
	Education (x_2)	1: Middle school and below (state 4); 2: High school (state 1); 3: Bachelor's (state 2); 4: Master's and above (state 3)
	Income (x_3)	1: <3thousand Yuan (state 4); 2: 3~6 thousand Yuan (state 1); 3: 6~10 thousand Yuan (state 2); 4: >10 thousand Yuan (state 3)
	The number of companions (x_4)	1: 0 (state 4); 2: 1 (state 1); 3: 2 (state 2); 4: >2 (state3)
	Hurry (x_5)	1: not hurried (state 3); 2: moderately hurried (state 1); 3: very hurried (state 4)
Traffic conditions	Vehicle volume (x_6)	1: small (<300pcu/h∗lane) (state 3); 2: medium (250~550pcu/h∗lane) (state 1); 3: large (>500pcu/h∗lane) (state 2)
	Waiting time (x_7)	1: short (<30 s) (state 3); 2: medium (20~60 s) (state 1); 3: long (>50 s) (state 2)
	Pedestrian flow (x_8)	1: small (<40ped/circle) (state 3); 2: medium (35~60ped/circle) (state 1); 3: large (>55ped/circle) (state 2)
Road conditions	Crossing distance (x_9)	1: 1~2 lanes (state 3); 2: 3~4 lanes (state 1); 3: 5~6 lanes (state 2)
	Safety island presence (x_{10})	1: Yes (state 2); 2: No (state 1)
	Countdown device presence (x_{11})	1: Yes (state 2); 2: No (state 1)
	Location of traffic attractions (x_{12})	1: On anterolateral side of crosswalk (state 2); 2: On right ahead of crosswalk (state 1)
Crossing	Signal light color (x_{13})	1: Red (state 2); 2: Green (state 1)
	Crossing track (x_{14})	1: Part/not in the crosswalk (state 2); 2: Completely in the crosswalk (state 1)

5. Correlation Analysis on Factors Influencing Illegal Crossings

5.1. Variable Definition and Value. Personal attributes, traffic conditions, and road conditions are considered to have certain influence on illegal pedestrian crossings [1, 22, 42]. Personal attributes include age, education, income, and the number of companions, etc. Traffic conditions include vehicle volume, waiting time, and pedestrian volume. Road conditions include crossing distance, safety island presence and so on. The definition and value of each variable used in this study are shown in Table 7.

5.2. Correlation Analysis. Correlation analysis on factors influencing illegal crossings can help select the significant ones before modeling illegal crossings. GeNIe software is used to model behavior of illegal crossings, which internally get the optimal network after automatically finishing component analysis according to results of correlation analysis on the factors [43].

Correlation analysis is used to examine whether there is a significant relationship between two variables. And it indicates that two variables are significantly correlated when P value is less than 0.05, and they are correlated more significantly when P value is less than 0.03. In this part, crossing at a red light (x_{13}) and crossing outside of a crosswalk (x_{14}) are used to have correlation analysis with other variables (x_n, $n = 1, ..., 12$), the results are shown in Tables 8 and 9.

6. Modeling Illegal Crossings Based on Bayesian Network

Bayesian network has proven to be an effective method for representation and reasoning of uncertain knowledge [44], with the advantages of overcoming the difficulties in conceptual definition and computation based on rule relations and being able to learn causality. Bayesian uses graphical networks to reveal structures of one variable to another, so it can better describe the relationship of behavior and various factors, as well as one factor to another. Therefore, this paper tentatively proposes a new method to analyze pedestrian illegal crossings based on Bayesian network model, which can be used to analyze the mechanism between illegal crossings and related factors.

Table 8: Results of correlation analysis between variables (including crossing at a red light).

	x_1	x_2	x_3	x_4	x_5	x_6	x_7	x_8	x_9	x_{10}	x_{13}
x_1			**								**
x_2			*								
x_3	**	*			**						**
x_4								**			
x_5											**
x_6							**		*	*	**
x_7						**		**			*
x_8				**			**				
x_9						*					
x_{10}						*					
x_{13}	**		**		**	**	*				

Notes: **Significant at 0.01 level; *Significant at 0.05 level; x_n ($n = 1$–14) see Table 7.

Table 9: Results of correlation analysis between variables (including crossing outside of a crosswalk).

	x_1	x_2	x_3	x_4	x_5	x_9	x_{12}	x_{14}
x_1			**					*
x_2			*					
x_3	**	*			**			*
x_4								*
x_5			**					*
x_9								**
x_{12}								**
x_{14}	*		*	*	*	**	**	

Notes: **Significant at 0.01 level; *Significant at 0.05 level; x_n ($n = 1$–14) see Table 7.

6.1. Theories. A Bayesian network is a relationship network that uses statistical methods to represent probability relationships between different elements. Its theoretical foundation is the Bayes rule [45].

$$p(h|e) = \frac{p(e|h) \cdot p(h)}{p(e)}, \tag{1}$$

$p(h)$ is the prior probability of hypothesis h; $p(e)$ is the prior probability of evidence e; $p(h|e)$ is the probability of h given e; $p(e|h)$ is the probability of e given h.

Bayesian network is a graphical network based on probabilistic reasoning, which includes directed acyclic graph (DAG) and conditional probability table (CTP). DAG is the qualitative process to estimate the structure of illegal crossings and CTP is the quantitative process to get the probabilities of one variable to another.

6.1.1. Bayesian Network Structure. Based on a complete data set, three methods are usually used to build Bayesian network structure. That is, (i) modeling based on expert knowledge; (ii) obtaining from database learning. (iii) creating from a knowledge base. These methods are synthetically used to model Bayesian network, with expert knowledge as the dominant. However, in the absence of expert knowledge and knowledge base, it is an effective method to model Bayesian network structure from database learning.

6.1.2. Bayesian Network Parameter Learning. Maximum likelihood estimation, Bayesian estimation, and maximum expectation algorithm (EM algorithm) are usually used for probabilistic reasoning. In this paper, EM algorithm is used to estimate parameters because the data sample is incomplete.

Let X denote the set of observed variables, Z denote the set of the hidden variables, and Θ denote parameters of model, the maximum likelihood estimation is as follows,

$$LL(\Theta|X, Z) = \ln P(X, Z|\Theta). \tag{2}$$

Starting from the initial value Θ^0, the following steps can be iterated until convergence:

Step E: estimating the distribution of the hidden variable based on the current parameter of Θ^t, then calculating expectation of $LL(\Theta|X, Z)$, that is,

$$Q(\Theta|\Theta^t) = E_{Z|X,Q^t} LL(\Theta|X, Z). \tag{3}$$

Step M: search for maximized expectation likelihood of parameter, that is,

$$\Theta^{t+1} = \arg\max_{\Theta} Q(\Theta|\Theta^t). \tag{4}$$

$$LL(\Theta|X) = \ln P(\Theta|X) = \ln \sum_{Z} P(X, Z|\Theta). \tag{5}$$

6.2. Modeling. Two important steps were taken to establish Bayesian network models on influencing on illegal crossings of the factors, including structure learning and parameter learning.

GeNIe2.1 software is used to study Bayesian network structure of illegal crossings in this paper. In the absence of expert knowledge and knowledge base, database learning is used to model Bayesian network structure in this paper. Firstly, the database from questionnaires is imported into the software, and structure learning is completed by greedy search method (GTT) and K2 algorithm. Initial Bayesian network structures of crossing at a red light and crossing outside of a crosswalk are obtained. Secondly, the network structures are modified according to results of correlation analysis finished above. Finally, after many iterations, component analysis is finished in the software to obtain the optimal Bayesian network structures of illegal crossings shown in Figures 4 and 5.

Parameter learning is the second step to study Bayesian network to get the joint probability distribution. Firstly, an EM (Expectation Maximization) algorithm is used for parameter learning which is completed on the GeNIe2.1 software after obtaining the network structures. Secondly, marginal probabilities of father nodes of crossing at a red light and crossing outside of a crosswalk are calculated by using joint tree algorithm. The marginal probability is the summation of a set of probabilities of a factor which affects illegal crossings under several other factors. Finally, results of parameter estimation of crossing at a red light and crossing outside of a crosswalk are obtained in Tables 10 and 11.

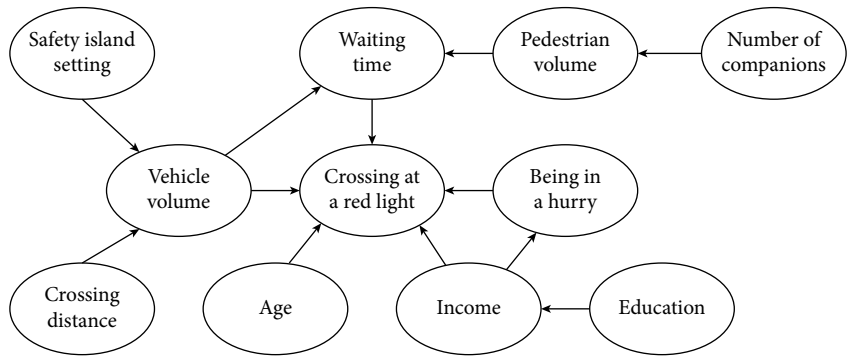

Figure 4: Bayesian network structure of pedestrian crossing at a red light.

6.3. Results

6.3.1. Bayesian Network Structure of Illegal Crossings. A father node is the starting node of an arrow in the graphical network. According to structure learning, age, monthly income, being in a hurry, vehicle volume, and waiting time have a direct influence on crossing at a red light. Crossing distance, safety island setting, education, number of companions, and pedestrian volume have an indirect influence on crossing at a red light shown in Figure 4.

Father nodes of crossing outside of a crosswalk include age, monthly income, education, being in a hurry, number of companions, crossing distance, and location of traffic attraction, which have a direct influence on crossing outside of a crosswalk, which is shown in Figure 5.

6.3.2. Parameter Estimation of Bayesian Network. The results of parameter estimation of Bayesian network of crossing at a red light and crossing outside of a crosswalk are obtained after parameter learning. The probabilities of different dimensions of the father nodes to cross at a red light and cross at a green light are listed in Table 10. Besides, the probabilities of different dimensions of the father nodes to cross inside of a crosswalk and cross outside of a crosswalk are listed in Table 11. Analysis on results of parameter estimation is analyzed in detail in the next section.

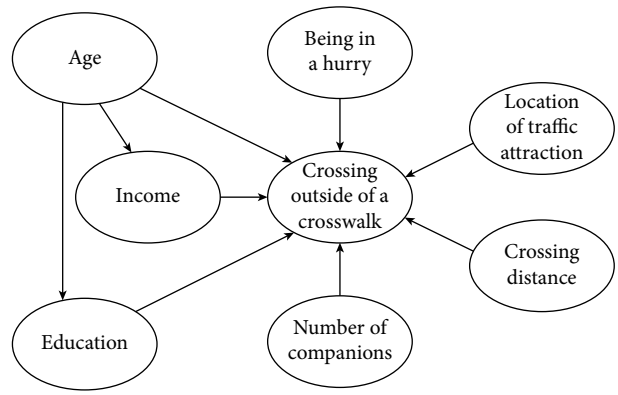

Figure 5: Bayesian network structure of crossing outside of a crosswalk.

7. Analysis on the Results

This paper establishes models of influence on illegal crossings of factors based on Bayesian network, and finishes parameter learning to understand how factors influence illegal crossings. Bayesian network can intuitively indicate the probability of illegal crossings under joined factors (father nodes), and probabilities of different states of father nodes can be obtained as well. Modeling illegal crossings based on Bayesian network can not only predict illegal crossings, but also reveal relationship between illegal crossings of factors.

7.1. Discussion Model of Crossing at a Red Light. From Bayesian network structure, it is indicated that a child node is influenced by its joint father nodes. Figure 6 shows that age, income, being in a hurry, vehicle volume, and waiting time have significant effect on crossing at a red light. And Figure 5 shows the probability distribution of different dimensions for each variable, in which the variables are influenced by their father nodes at the same time.

(i) *Age*. According to Figure 6(a), it has a highest probability of 14% to cross at a red light among people who are younger than 18 years old, and it shows that the younger the people are, the higher probability it is to cross at a red light.

(ii) *Income*. From Figure 6(b), pedestrians with different incomes have almost the same probability of crossing at a red light.

(iii) *Being in a hurry.* As it is shown in Figure 6(c) that the probability of crossing at a red light when people are in a hurry is 42%, which is much higher than that when people are not in a hurry or a little hurry.

(iv) *Vehicle volume.* It shows in Figure 6(d) that people have a 40% probability to cross at a red light when the vehicle volume is in the medium level at intersections, which is the result of vehicle volume and its father nodes influence on crossing at a red light.

(v) *Waiting time.* It is shown in Figure 6(e) that the longer people wait at intersections, the larger the probability of crossing at a red light is, and the probability can be up to 53% when people wait for a long time.

Table 10: Results of parameter estimation of Bayesian network of crossing at a red light.

State	Age				Income (thousand Yuan)			
	<18	18–30	0–45	>45	<3	3–6	6–10	>10
Green[1]	59%	66%	67%	69%	67%	63%	67%	66%
Red[2]	41%	34%	33%	31%	33%	37%	33%	34%
State	Being in a hurry			Vehicle volume			Waiting time		
	Not	Moderately	Very	Small	Medium	Large	Short	Medium	Long
Green	63%	70%	58%	66%	60%	70%	67%	63%	48%
Red	37%	30%	42%	34%	40%	30%	33%	37%	52%

[1]Means crossing at a green light. [2]Means crossing at a red light.

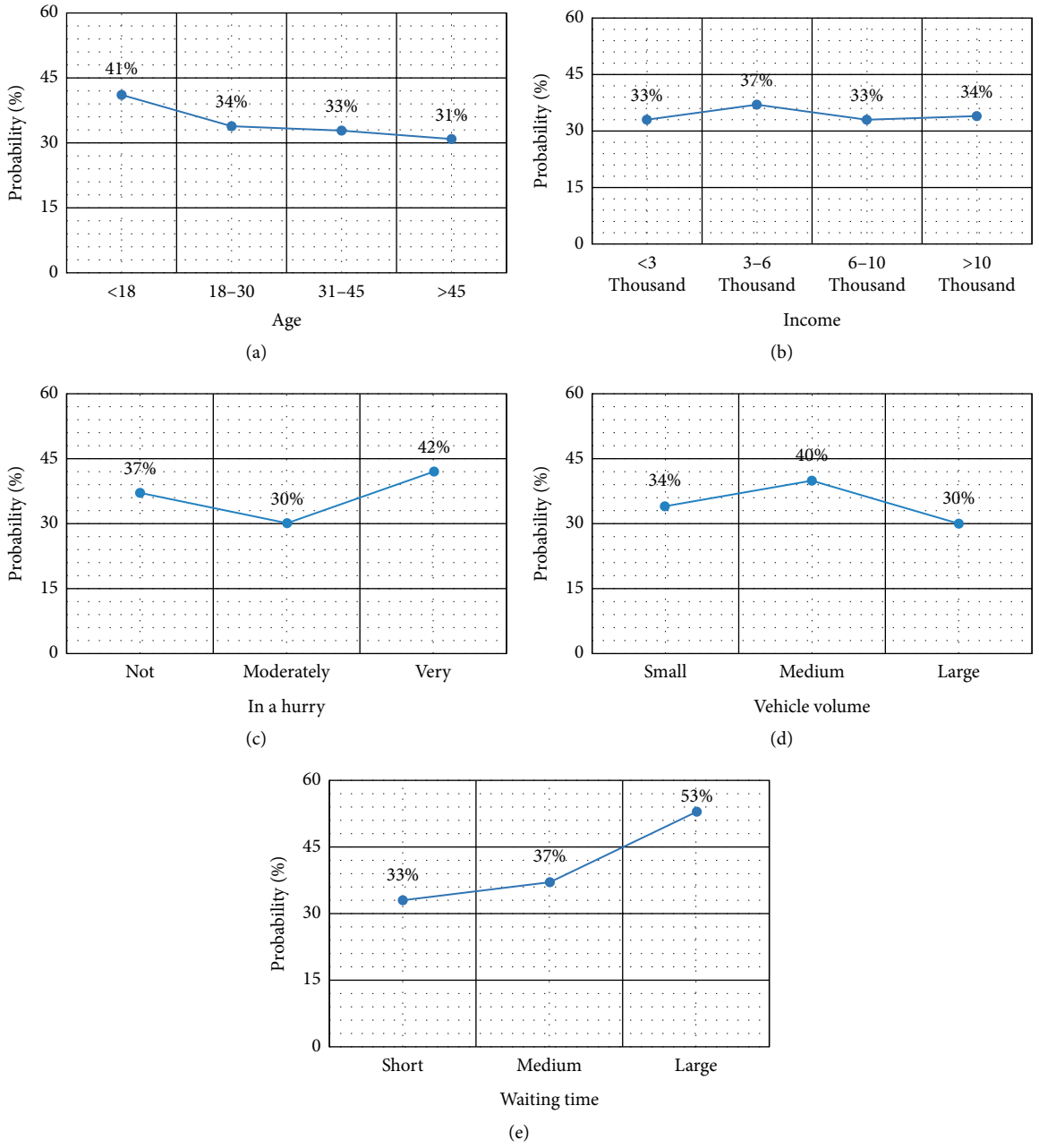

Figure 6: Probability distribution of father node to crossing at a red light. (a) Age, (b) Income, (c) Being in a hurry, (d) Vehicle volume and (e) Waiting time.

Table 11: Results of parameter estimation of Bayesian network of crossing outside of a crosswalk.

State	Age				Education			
	<18	18-30	30-45	>45	1	2	3	4
A	47%	49%	46%	48%	47%	49%	47%	46%
B	53%	51%	54%	52%	53%	51%	53%	54%
State	Income (thousand Yuan)				Number of companions			
	<3	3-6	6-10	>10	0	1	2	>2
A	46%	46%	48%	49%	48%	47%	47%	46%
B	54%	54%	52%	51%	52%	53%	53%	54%
State	Being in a hurry			Crossing distance (lanes)			Location of traffic attractions	
	Not	Moderately	Very	1-2	3-4	5-6	Front side	Right ahead
A	47%	46%	50%	48%	47%	47%	48%	46%
B	53%	54%	50%	52%	53%	53%	52%	54%

A means crossing outside of a crosswalk. B means crossing inside of a crosswalk.

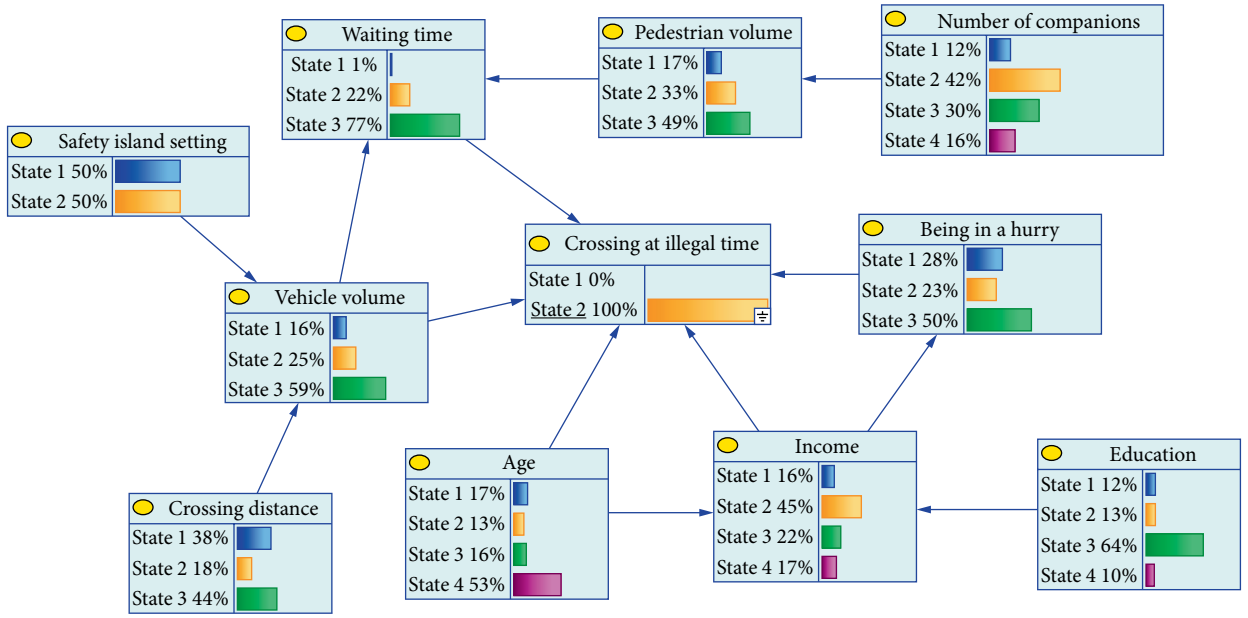

Figure 7: Probabilistic topology diagram when probability of crossing at a red light is 100%. Notes: state n ($n = 1 \sim 4$) sees Table 7. Notes: in the level of education, "1" means "Middle school and below"; "2" means "High school"; "3" means "Bachelor's"; "4" means "Master's and above."

The state of maximum probability of each father node is obtained when the probability of crossing at a red light is 100% in the Bayesian network structure in Figure 7 and Table 12. It is intuitive to see that the crossing at a red light has a higher probability to occur among people aged 31–45, with a high school education, with an income less than 3000, and with no companions, and in the medium traffic condition level of vehicle volume, pedestrian volume, and waiting time, and in a road condition of 3-4 lane-crossing distance as well.

7.2. Discussion Model of Crossing Outside of a Crosswalk. Figure 4 shows that age, education, income, number of companions, being in a hurry, and crossing distance have a significant effect on crossing outside of a crosswalk. And Figure 7 shows the probability distribution of different dimensions for each variable, as noted earlier, the variables are influenced by their father nodes at the same time.

(i) *Age*. From Figure 8(a), the probability of crossing outside of a crosswalk among people who aged 18–30 is 49%, which is higher than that of other age groups.

(ii) *Education*. It shows that people with high school education have the highest possibility to cross outside of a crosswalk. In general, people educated postgraduate and above have a lower probability to cross outside of a crosswalk.

(iii) *Income*. According to Figure 8(c), the people with an income of more than 10,000 yuan have the highest probability to cross outside of a crosswalk.

(iv) *The number of companions*. It is shown in Figure 8(d) that the more the number of companions, the lower the probability to cross outside of a crosswalk.

Table 12: The state of maximum probability of each father node when the probability of crossing at a red light is 100%.

Father node	Age	Education	Income	Number of companions	Hurry
State	31~45	High school	<3000	0	Moderately
Probability	53%	64%	47%	42%	50%
Father node	Vehicle volume	Waiting time	Crossing distance	Pedestrian volume	——
State	Medium	Medium	3~4 lanes	Medium	——
Probability	59%	77%	44%	49%	——

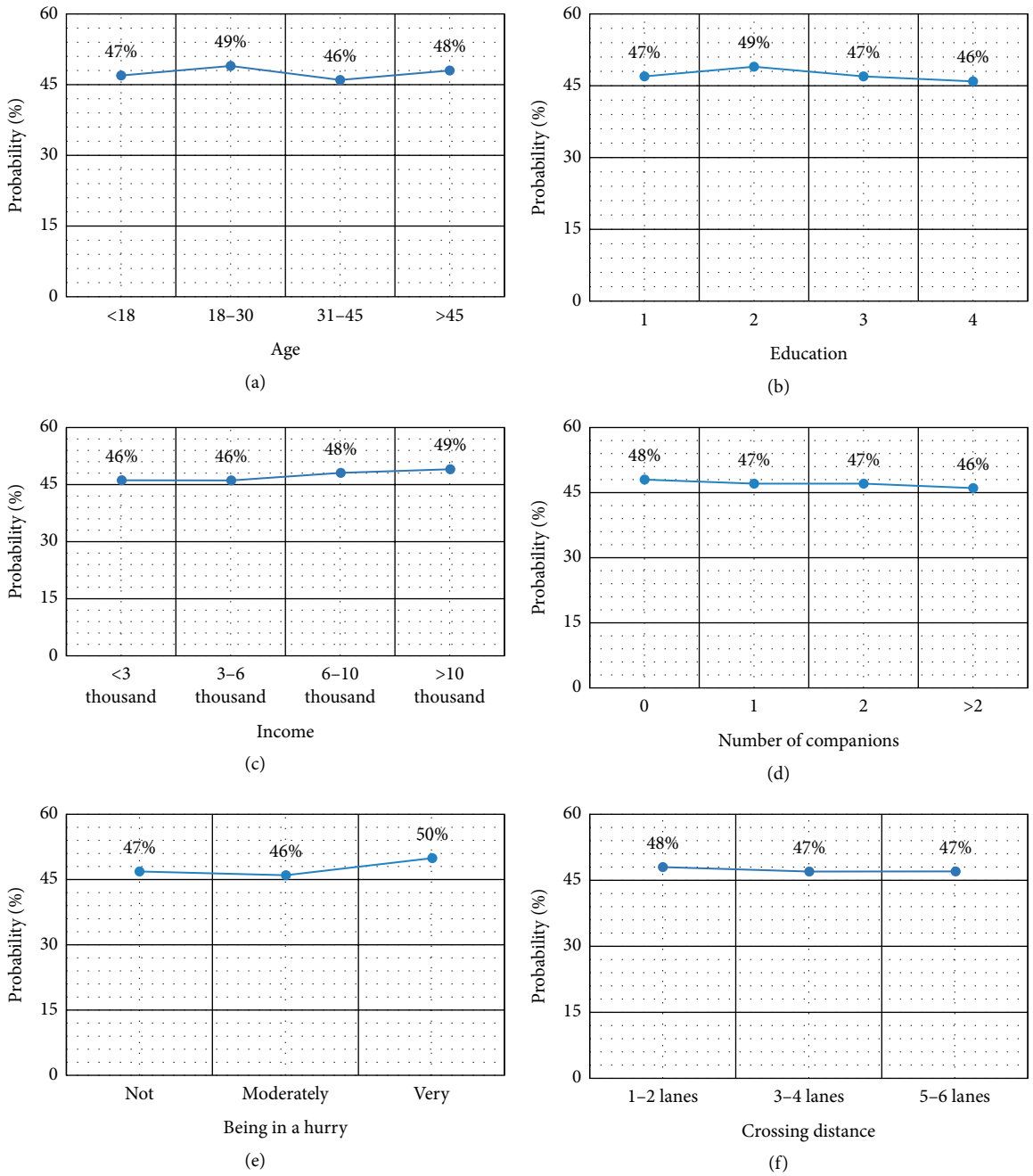

Figure 8: Probability distribution of father node to crossing outside of a crosswalk. (a) Age. (b) Education. (c) Income. (d) Number of companions. (e) Being in a Hurry. (f) Crossing distance.

(v) *Hurry.* It has a highest probability of 50% to cross outside of a crosswalk among the people who are in a hurry.

(vi) *Crossing distance.* The probability of crossing outside of a crosswalk is the largest at 48% in a road condition of 1~2 lanes-crossing distance. The smaller the

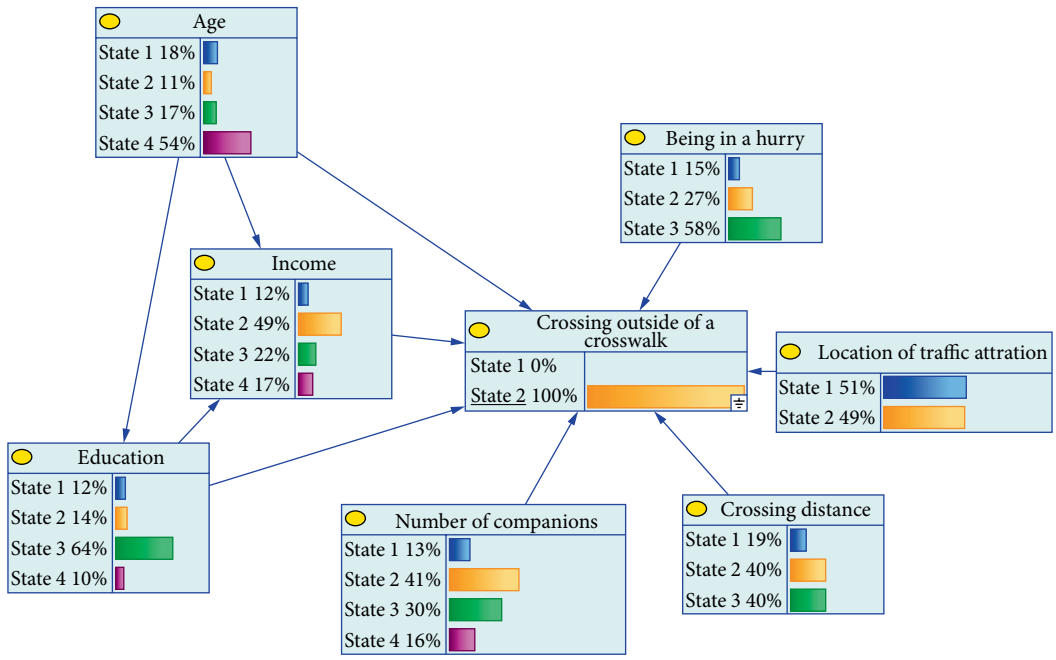

Figure 9: Probabilistic topology diagram when probability of crossing outside of a crosswalk is 100%. Notes: state n (n = 1–4) see Table 7.

Table 13: State of maximum probability of each father node when the probability of crossing outside of a crosswalk is 100%.

Father node	Age	Education	Income	Number of companions
State	18~30	High school	<3 thousand	0
Probability	54%	64%	49%	41%
Father node	Being in a hurry	Crossing distance	Location of traffic attraction	——
State	Moderately	1~2 lanes	Front side	——
Probability	58%	41%	51%	——

crossing distance, the higher the probability to cross outside of a crosswalk.

(vii) *Location of traffic attractions*. When the traffic attraction is on anterolateral side of crosswalk, people have a 60% possibility to cross outside of a crosswalk.

The state of maximum probability of each father node is obtained when the probability of crossing outside of a crosswalk is 100% in the Bayesian network structure in Figure 9 and Table 13. It is shown that the crossing at a red light has a higher probability to occur among people less than 30, with a high school education, and an income of less than 3,000 yuan, without any companions and in a hurry, and in a road condition of 1~2 lanes-crossing distance and in a traffic attraction on anterolateral side of crosswalk.

8. Conclusions

This paper analyzes characteristics of illegal crossings at signalized intersections and establishes models of influence on illegal crossings of factors based on data from video-based observations and a questionnaire survey. Bayesian network is used to develop models for crossing at a red light and crossing outside of a crosswalk. The results show that, (i) it has a proportion of 36.3% on average to cross outside of a crosswalk in every signal cycle at the intersections, and it occurred more frequently than crossing at a red light, of which the proportion is 27%. (ii) Arc routing crossing has a highest probability of 58% to occur at signalized intersections compared to other types of out-side-crosswalk crossings. (iii) The location of origin and destination of a pedestrian have a significant effect on crossing outside of a crosswalk, the proportions of "both outside of a crosswalk and on the same side" and "one is inside of a crosswalk and another is outside of a crosswalk" make up to about 99% among samples of crossing outside of a crosswalk. (iv) Among the five significant influencing factors, waiting time has the strongest influence on behavior of crossing at a red light. Some recommendations are provided based on the conclusions above.

(i) Waiting time is the most important factor of crossing at a red light and crossing outside of a crosswalk. Therefore, signal timing at intersections should be more considerate about pedestrians. Enough pedestrian signal time should be given to make sure that pedestrians can pass through, and each phase time should avoid an unreasonable waiting period.

(ii) Location of traffic attractions has a significant influence on crossing outside of a crosswalk. It is necessary to add some auxiliary facilities at intersections, such as

fencing, to prevent pedestrians from crossing outside of a crosswalk.

(iii) As it is shown that the probability of illegal crossings including crossing at a red light and crossing outside of a crosswalk is very high. Education is a powerful means to strengthen consciousness of traffic safety. Therefore, it is very important to provide more education on traffic safety to people, especially from childhood.

This paper analyzes illegal crossings from temporal and spatial dimensions, which provides better understanding of pedestrians' illegal crossing at signalized intersection. This paper, using Guangzhou as a case study, generates findings about characteristics of pedestrians' illegal crossing and influences mechanism of the impact factors in typical large Chinese cities. Besides, the method used in this paper, to analyze pedestrians' illegal crossing, can be transferred to solve similar problems for other countries and cities. The findings of the research in this paper could be considered as basic guidance for traffic design and management. However, there is room for improvement, including improving the questionnaire survey utilized in this paper, and combining expert knowledge with database and knowledge base to study Bayesian network by collecting diversified information.

Data Availability

The data used to support the findings of this study were supplied under license and so cannot be made freely available. Requests for access to these data should be made to [Yingying Ma, mayingying@scut.edu.cn].

Conflicts of Interest

The authors declare that they have no conflicts of interest.

Funding

The research and publication of this article was funded by Natural Science Foundation of Guangdong Province (2018A0313250) and Innovation Project of Department of Education of Guangdong Province (2017KTSCX005).

Acknowledgments

The authors want to thank William Kinkead for his help in refining the language and optimizing the structure of the paper. Thanks also should be given to student workers who helped spreading the surveys and those who took the survey.

References

[1] P. Onelcin and Y. Alver, "Illegal crossing behavior of pedestrians at signalized intersections: factors affecting the gap acceptance," *Transportation Research Part F: Traffic Psychology and Behaviour*, vol. 31, pp. 124–132, 2015.

[2] H. W. Guo, F. Zhao, W. Wang, Y. Zhou, Y. Zhang, and G. Wets, "Modeling the perceptions and preferences of pedestrians on crossing facilities," *Discrete Dynamics in Nature and Society*, vol. 2014, Article ID 949475, 8 pages, 2014.

[3] K. Shaaban, D. Muley, and A. Mohammed, "Analysis of illegal pedestrian crossing behavior on a major divided arterial road," *Transportation Research Part F: Traffic Psychology and Behaviour*, vol. 54, pp. 124–137, 2018.

[4] A. Jain, J. Ankit, and R. Rastogi, "Pedestrian crossing behaviour analysis at intersections," *International Journal for Traffic and Transport Engineering*, vol. 4, no. 1, pp. 103–116, 2014.

[5] N. Jiang, M. Shi, Y. Xiao, K. Shi, and B. Watson, "Factors affecting pedestrian crossing behaviors at signalized crosswalks in urban areas in Beijing and Singapore," in *International Conference on Transportation Information & Safety*, American Society of Civil Engineers, Reston, VA, USA, 2011.

[6] A. Khattak and L.-W. Tung, "Severity of pedestrian crashes at highway-rail grade crossings," *Journal of the Transportation Research Forum*, vol. 54, no. 2, pp. 1–11, 2015.

[7] G. S. Tulu, S. Washington, M. J. King, and M. Haque, "Why are pedestrian crashes so different in developing countries? A review of relevant factors in relation to their impact in Ethiopia," in *Australasian Transport Research Forum 2013 Proceedings*, Brisbane, Australia, 2013.

[8] E. Paschalidis, I. Politis, S. Basbas, and P. Lambrianidou, "Pedestrian compliance and cross walking speed adaptation due to countdown timer installations: a self report study," *Transportation Research Part F: Traffic Psychology and Behaviour*, vol. 42, pp. 456–467, 2016.

[9] J. Chen, J.-J. Shi, X.-L. Li, and Q. Zhao, "Pedestrian behavior and traffic violations at signalized intersections," in *International Conference of Chinese Transportation Professionals*, American Society of Civil EngineersReston, VA, USA, 2011.

[10] L. L. Thompson, F. P. Rivara, R. C. Ayyagari, and B. E. Ebel, "Impact of social and technological distraction on pedestrian crossing behaviour: an observational study," *Injury Prevention*, vol. 19, no. 4, pp. 232–237, 2013.

[11] A. Dommes, M.-A. Granié, M.-S. Cloutier, C. Coquelet, and F. Huguenin-Richard, "Red light violations by adult pedestrians and other safety-related behaviors at signalized crosswalks," *Accident Analysis & Prevention*, vol. 80, pp. 67–75, 2015.

[12] B. Tang, S. Jiang, and L. I. Yanmin, "Survival analysis on pedestrian"s maximum waiting time at signalized intersections," in *Transportation Research Board Meeting*, Washington, DC, USA, 2010.

[13] M. P. Pratt, J. A. Bonneson, and P. Songchitruksa, "Effect of left-turn operational mode on pedestrian safety," *Transportation Research Record: Journal of the Transportation Research Board*, vol. 2393, no. 1, pp. 95–103, 2013.

[14] Y. I. Demiroz, P. Onelcin, and Y. Alver, "Illegal road crossing behavior of pedestrians at overpass locations: factors affecting gap acceptance, crossing times and overpass use," *Accident Analysis & Prevention*, vol. 80, pp. 220–228, 2015.

[15] K. Lipovac, M. Vujanić, B. Maric, and M. Nešić, "The influence of a pedestrian countdown display on pedestrian behavior at signalized pedestrian crossings," *Transportation Research Part F: Traffic Psychology and Behaviour*, vol. 20, pp. 121–134, 2013.

[16] M. Khatoon, G. Tiwari, and N. Chatterjee, "Impact of grade separator on pedestrian risk taking behavior," *Accident Analysis & Prevention*, vol. 50, pp. 861–870, 2013.

[17] M. Iryo-Asano, W. K. M. Alhajyaseen, and H. Nakamura, "Analysis and modeling of pedestrian crossing behavior during the pedestrian flashing green interval," *IEEE Transactions on Intelligent Transportation Systems*, vol. 16, no. 2, pp. 958–969, 2015.

[18] Kadali B. Raghuram and N. Rathi, "Perumal V. Evaluation of pedestrian mid-block road crossing behaviour using artificial neural network," *Journal of Traffic and Transportation Engineering (English Edition)*, vol. 1, no. 2, pp. 111–119, 2014.

[19] P. P. Koh, Y. D. Wong, and P. Chandrasekar, "Safety evaluation of pedestrian behaviour and violations at signalised pedestrian crossings," *Safety Science*, vol. 70, pp. 143–152, 2014.

[20] B. R. Kadali and P. Vedagiri, "Effect of vehicular lanes on pedestrian gap acceptance behaviour," *Procedia – Social and Behavioral Sciences*, vol. 104, pp. 678–687, 2013.

[21] S. Jian, Y. Yan, and H. Wang, "Development and application of a simulation-enhanced platform for pedestrian crossing behaviors experiment," in *Transportation Research Board 90th Annual Meeting*, Washington DC, USA, 2011.

[22] M. J. King, D. Soole, and A. Ghafourian, "Illegal pedestrian crossing at signalised intersections: Incidence and relative risk," *Accident Analysis & Prevention*, vol. 41, no. 3, pp. 485–490, 2009.

[23] G. Ren, Z. Zhou, W. Wang, Y. Zhang, and W. Wang, "Crossing behaviors of pedestrians at signalized intersections observational study and survey in China," *Transportation Research Record: Journal of the Transportation Research Board*, vol. 2264, pp. 65–73, 2011.

[24] Y. Yan and S. Jian, "Study on pedestrian red-time crossing behavior," *Transportation Research Record: Journal of the Transportation Research Board*, vol. 2393, no. 1, pp. 117–124, 2013.

[25] P. P. Koh and Y. D. Wong, "Gap acceptance of violators at signalised pedestrian crossings," *Accident Analysis & Prevention*, vol. 62, pp. 178–185, 2014.

[26] M. King, D. W. Soole, and A. Ghafourian, "Relative risk of illegal pedestrian behaviours," in *2008 Australasian Road Safety Research, Policing and Education Conference*, Adelaide, South Australia, 2008.

[27] K. Lipovac, M. Vujanic, B. Maric, and M. Nesic, *Pedestrian Behavior at Signalized Pedestrian Crossings*, vol. 139, no. 2, pp. 165–172, 2013.

[28] F. Lange, "The dark side of stimulus control—associations between contradictory stimulus configurations and pedestrians" and cyclists" illegal street crossing behavior," *Accident Analysis & Prevention*, vol. 43, no. 6, pp. 2166–2172, 2011.

[29] J. Yang, W. Deng, J. Wang, Q. Li, and Z. Wang, "Modeling pedestrians" road crossing behavior in traffic system micro-simulation in China," *Transportation Research Part A: Policy and Practice*, vol. 40, no. 3, pp. 280–290, 2006.

[30] X. L. Zhuang and C. X. Wu, "Pedestrians" crossing behaviors and safety at unmarked roadway in China," *Accident Analysis and Prevention*, vol. 43, no. 6, pp. 1927–1936, 2011.

[31] R. Linda, A. Howard, W. A. Camden, and C. Macarthur, *Pedestrian crossing location influences injury severity in urban areas*, vol. 18, no. 6, pp. 365–370, 2012.

[32] J. Supernak, V. Verma, and I. Supernak, "Pedestrian countdown signals: what impact on safe crossing?," *Open Journal of Civil Engineering*, vol. 3, no. 3, pp. 39–45, 2013.

[33] F. Chen, H. Peng, X. Ma, J. Liang, W. Hao, and X. Pan, "Examining the safety of trucks under crosswind at bridge-tunnel section: a driving simulator study," *Tunnelling and Underground Space Technology*, vol. 92, p. 103034, 2019.

[34] O. Keegan and M. O"Mahony, "Modifying pedestrian behaviour," *Transportation Research Part A: Policy and Practice*, vol. 37, no. 10, pp. 889–901, 2003.

[35] Z. P. Zhou, Y.-S. Liu, W. Wang, and Y. Zhang, "Multinomial logit model of pedestrian crossing behaviors at signalized intersections," *Discrete Dynamics in Nature and Society*, Article ID 172726, 8 pages, 2013.

[36] F. Chen, S. Chen, and X. Ma, "Analysis of hourly crash likelihood using unbalanced panel data mixed logit model and real-time driving environmental big data," *Journal of Safety Research*, vol. 65, pp. 153–159, 2018.

[37] C. Feng, C. Suren, and J. A. A. Prevention, "Injury severities of truck drivers in single- and multi-vehicle accidents on rural highways," *Accident Analysis & Prevention*, vol. 43, no. 5, pp. 1677–1688, 2011.

[38] E. Moyano Díaz, "Theory of planned behavior and pedestrians" intentions to violate traffic regulations," *Transportation Research Part F: Traffic Psychology and Behaviour*, vol. 5, no. 3, pp. 169–175, 2002.

[39] R. Hamidun, N. E. Kordi, I. R. Endut, S. Z. Ishak, and M. F. M. Yusof, "Estimation of illegal crossing accident risk using stochastic petri nets," *Journal of Engineering Science and Technology*, vol. 10, pp. 81–93, 2015.

[40] C. Cherry, B. Donlon, X. Yan, S. E. Moore, and J. Xiong, "Illegal mid-block pedestrian crossings in China: gap acceptance, conflict and crossing path analysis," *International Journal of Injury Control and Safety Promotion*, vol. 19, no. 4, pp. 320–330, 2012.

[41] J. Cinnamon, N. Schuurman, and S. M. Hameed, "Pedestrian injury and human behaviour: observing road-rule violations at high-incident intersections," *PLoS One*, vol. 6, no. 6, p. e21063, 2011.

[42] U. Lachapelle and M.-S. Cloutier, "On the complexity of finishing a crossing on time: Elderly pedestrians, timing and cycling infrastructure," *Transportation Research Part A: Policy and Practice*, vol. 96, pp. 54–63, 2017.

[43] D. P. Yang and J. L. Li, "Research on personal credit evaluation model based on bayesian network and association rules," in *International Conference on Wireless Communications*, Honolulu, HI, USA, 2007.

[44] H. Kaur, R. Chauhan, and S. K. Wasan, "A Bayesian network model for probability estimation," in *Encyclopedia of Information Science and Technology*, M. Khosrow-Pour, Ed., pp. 1–8, Information Science Reference, Hershey, PA, USA, 3rd edition, 2015.

[45] W. Yao and J. Vassileva, "Bayesian network trust model in peer-to-peer networks," in *IEEE/WIC International Conference on Web Intelligence*, Halifax, Canada, 2003.

Hindawi
Journal of Advanced Transportation
Volume 2020, Article ID 9194028, 11 pages
https://doi.org/10.1155/2020/9194028

Research Article

A Vision-Based Video Crash Detection Framework for Mixed Traffic Flow Environment Considering Low-Visibility Condition

Chen Wang [1], **Yulu Dai** [1], **Wei Zhou** [1] **and Yifei Geng** [2]

[1] *Intelligent Transportation Research Center, Southeast University, Nanjing 211189, China*
[2] *School of Automation, Southeast University, Nanjing 211189, China*

Correspondence should be addressed to Chen Wang; wkobec@hotmail.com

Received 13 September 2019; Accepted 9 October 2019; Published 17 January 2020

Guest Editor: Feng Chen

In this paper, a vision-based crash detection framework was proposed to quickly detect various crash types in mixed traffic flow environment, considering low-visibility conditions. First, Retinex image enhancement algorithm was introduced to improve the quality of images, collected under low-visibility conditions (e.g., heavy rainy days, foggy days and dark night with poor lights). Then, a Yolo v3 model was trained to detect multiple objects from images, including fallen pedestrians/cyclists, vehicle rollover, moving/stopped vehicles, moving/stopped cyclists/pedestrians, and so on. Then, a set of features were developed from the Yolo outputs, based on which a decision model was trained for crash detection. An experiment was conducted to validate the model framework. The results showed that the proposed framework achieved a high detection rate of 92.5%, with relatively low false alarm rate of 7.5%. There are some useful findings: (1) the proposed model outperformed empirical rule-based detection models; (2) image enhancement method can largely improve crash detection performance under low-visibility conditions; (3) the accuracy of object detection (e.g., bounding box prediction) can impact crash detection performance, especially for minor motor-vehicle crashes. Overall, the proposed framework can be considered as a promising tool for quick crash detection in mixed traffic flow environment under various visibility conditions. Some limitations are also discussed in the paper.

1. Introduction

Emergency response to roadway crashes is very important for traffic management. On the one hand, people injured in a crash need to be sent to the nearest hospital in the first place to prevent their health condition from being worsened, on the other hand, serious crashes often cause nonrecurrent congestions, if emergency response or clearance is not carried out in time. In order to mitigate those negative impacts, roadway crashes need to be quickly detected.

Crash detection can be conducted by analyzing traffic flow data from roadway detectors, such as loops and microwaves. However, such method is often inaccurate due to systematic errors caused by both algorithms and data quality [1–5]. Thus, in practice, crashes were often detected by human observers through CCTV in Traffic Management Centers (TMC). The advantage of CCTV is that it can directly capture crash scenes within its range. With the development of intelligent transportation system (ITS), more and more CCTVs have been implemented in big cities and highways. Although human observations through CCTV can be reliable, it is sometime too labor-intensive and time-consuming. Thus, it is very meaningful to develop other reliable automatic crash detection methods based on CCTV [6, 7].

In recent years, computer vision technologies have undergone a fast development and largely utilized in transportation field [8, 9], thanks to the increasing power of computers and deep learning methods. The performance of vision-based object detection, based on deep learning methods, has been significantly improved. Thus, researchers have been focusing on developing crash detection models based on complex deep learning frameworks [10, 11]. Their results also showed the capability of computer vision in crash detection. However, sometimes a complex deep learning framework require high computational costs and difficult to be implemented in practice.

To note, previous literature mainly focused on detecting crashes in motorized traffic environment in developed

countries. In developing countries, a larger number of pedestrians and cyclists could share roadways with automobiles. Thus, crash detection in mixed traffic flow environment could be an even more important task for those countries. Moreover, in order to be used in practice, a vision-based crash detection model needs to be robust to various conditions, especially low-visibility ones such as heavy rain, fog, poor lights, and so on. Sometimes, even deep-learning based vision algorithms did not perform well in those low-visibility conditions [12–14], due to relatively low image quality. Thus, some additional efforts were often added to improve detection performance, such as image enhancement methods [15–19].

Considering these, a vision-based crash detection model framework was developed for mixed traffic flow environment in this study. Regarding low-visibility conditions, an image enhancement method was also introduced to improve image quality so that a deep learning algorithm can better identify moving objects. Regarding quick crash detection, a Yolo v3 model was employed to extract features from images, based on which a decision tree model was trained for detecting various crash types that could occur in mixed traffic flow environment. The paper is organized as follows: the second section discuss previous literature related to vision-based crash detection and image enhancement. Section 3 introduces the Retinex algorithm, Yolo v3, and decision tree-based framework of crash detection. Section 4 discusses the results of an experiment. Section 5 concludes the findings of this research.

2. Literature Review

In the past twenty years, researchers have conducted many studies on vision-based traffic crash detection, which can be classified into three categories: (1) modeling of traffic flow patterns; (2) modeling of vehicle interactions; and (3) analysis of vehicle activities [10].

The first method is to compare vehicle trajectories to typical vehicle motion patterns that can be learned from large data samples. In this framework, if a trajectory is not consistent with typical trajectory patterns, it can be considered as a traffic incident [20–22]. However, it is not easy to identify whether this incident is a crash due to limited crash trajectory data that can be collected in the real world. The second method determines crash occurrence based on speed change information, which applies social force model and intelligent driver model to model interactions among vehicles. This method requires a larger number of training samples. The third method largely depends on trackers because it needs to continuously calculate vehicle motion features (e.g., distance, acceleration, direction etc.) [23–27]. As such, aberrant behaviors [28, 29] related to traffic incidents could be detected. However, it is often difficult to be utilized in practice, limited by high computational costs and unsatisfactory tracking performance in congested traffic environment [30]. In general, fruitful results have been achieved for vision-based crash detection. However, most literature focused on motor vehicle crash instead of crashes involving nonmotorized modes, such as bicycle-rated and pedestrian-related crashes [7, 23, 31]. Moreover, many models are compute-intense, by constructing complicated deep learning structures.

Another practical issue for crash detection method is the ability to deal with low-visibility conditions (e.g., fog, heavy rain, dark night). Image enhancement methods were usually utilized to improve the robustness of video detection to low-visibility conditions. Image enhance methods can adjust digital images so that key features are more easily to be identified [32, 33]. Such technology was also used to provide better image quality to improve the performance of crash detection [34, 35]. There are two major types of image enhancement methods: physical model and tensile transformation. The first method usually develops a physical model considering fog formation. Sometimes, it is difficult to guarantee enough accuracy under various conditions. The second method normally uses histogram equalization [36], wavelet transform [37], homomorphic filtering [38] to enhance low-quality images (e.g., those with raindrops and fogs). The robustness of such a method could be limited in some conditions, for it requires large number of parameters and thresholds to be tuned.

3. Methods

In this study, a crash detection framework was proposed for mixed traffic flow environment. The framework has three major components. First, Retinex image enhancement algorithm was introduced to enhance image quality. Second, Yolo v3 was utilized to detect moving objects, such as vehicles, pedestrians, and bicyclists/motorcyclists. Third, a decision tree-based framework was proposed to determine various crash scenarios bin mixed traffic flow environment.

3.1. Retinex Image Enhancement Algorithms. Retinex is an image enhancement algorithm proposed by Edwin H. Land. The basic theory is that the color of an object is determined by the ability of the object to reflect light from long waves (red), medium waves (green), and short waves (blue), rather than the absolute value of the intensity of the reflected light. The color of an object is not affected by illumination nonuniformity, but possesses consistency. Unlike traditional linear and nonlinear algorithms that only enhance a certain type of image, Retinex algorithm can balance dynamic range compression, edge enhancement and color constancy. Thus, it can be used for the adaptive enhancements of various image types, which is a feasible choice in this research.

Figure 1 shows the theory of Retinex that a given image $S(x, y)$ can be decomposed into two different images: a reflected image $R(x, y)$ and a luminance image (also called as incident image) $L(x, y)$.

The image can be formulated as:

$$S(x, y) = R(x, y) \cdot L(x, y). \tag{1}$$

Convert it into logarithmic domain:

$$r(x, y) = \log R(x, y) = \log \frac{S(x, y)}{L(x, y)}. \tag{2}$$

And it can be written as:

$$r(x, y) = \log S(x, y) - \log[F(x, y) * S(x, y)]. \tag{3}$$

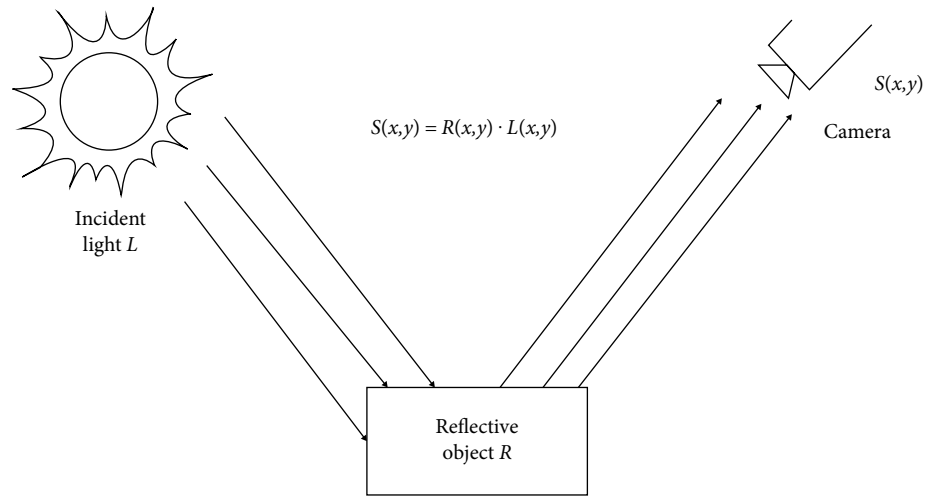

Figure 1: Schematic diagram of Retinex principle.

where $r(x, y)$ is the output image, $*$ is convolution operator, and $F(x, y)$ is surround function. The surround function, $F(x, y)$ is given as:

$$F(x, y) = \lambda e^{\left(-\left(x^2+y^2\right)\right)/c^2}, \tag{4}$$

where c is the scale that control the extent of the surround. Mathematically, solving $R(x, y)$ is a singular problem that can only be calculated by mathematically approximated estimates. The steps of Retinex are as follows:

Step 1. Read in the initial image $S(x, y)$, and separate R, G, and B channels of the image;
Step 2. Convert the pixel values of each channel from integers to floats and convert them to the logarithmic domain;
Step 3. Input the scale c, and calculate the value of λ which is equal to $1/\left(\iint F(x, y)dxdy\right)$;
Step 4. Calculate the value of $r(x, y)$ of each channel;
Step 5. Convert $r(x, y)$ from logarithmic domain to real domain;
Step 6. Stretch $R(x, y)$ linearly and output in the corresponding format.

3.2. Yolo v3. YOU ONLY LOOK ONCE (YOLO) is a state-of-the-art, real-time object detection system. The core idea of Yolo v3 is to use the picture as a network input, which is to return to the position of the bounding box and its subordinate categories (e.g., vehicles, trees, or pedestrians etc.) directly in the output layer. The overall stages of Yolo v3 which is consisted of four periods are illustrated below.

3.2.1. Bounding Box Prediction. Sum of squared error loss is used to predict the coordinate value, so the error can be calculated rapidly. Yolo v3 predicts the score of an object for each bounding box by logistic regression. Each bounding box needs four values to represent its position of the images: (x_i, y_i, w_i, h_i), which respect separately: (the x coordinate of center point, the y coordinate of center point, weight of bounding box, height of bounding box).

$$\begin{aligned} b_x &= \sigma\left(t_x\right) + c_x; \\ b_y &= \sigma\left(t_y\right) + c_y; \\ b_w &= p_w e^{t_w}; \\ b_h &= p_h e^{t_h}, \end{aligned} \tag{5}$$

where c_x, c_y are the coordinate offsets of the grid, p_w and p_h, are the side lengths of the preset anchor box, the resulting frame coordinates are b_x, b_y, b_w, b_h and the network learning goals are t_x, t_y, t_w, t_h.

If the bounding box prior overlaps a ground truth object by more than any other bounding box prior, then the value is 1. If the overlap does not reach a threshold (setting 0.5), the prediction of bounding box will be ignored, and it is displayed as no loss.

3.2.2. Class Prediction. To classify different kinds of objections, independent logistic classifiers are used instead of a SoftMax. When training, binary cross-entropy loss is used for the class predictions.

After learning by Logistic regression classifier, there are a set of weights: $w_0, w_1, \ldots, w_n$, and the n features of each sample can be written as $x_1, x_2, \ldots, x_n$, when the data of test samples are input, which can be combined with the weights linearly:

$$x = w_0 + w_1 x_1 + \ldots + w_n x_n. \tag{6}$$

The sigmoid function is:

$$f(x) = \frac{1}{1 + e^{-x}}. \tag{7}$$

The prediction probability in sigmoid function can be expressed as:

$$P(y = 1|x) = \pi(x) = \frac{1}{1 + e^{-g(x)}}. \tag{8}$$

$$P(y = 0|x) = 1 - P(y = 1|x), \tag{9}$$

where $g(x)$ is x.

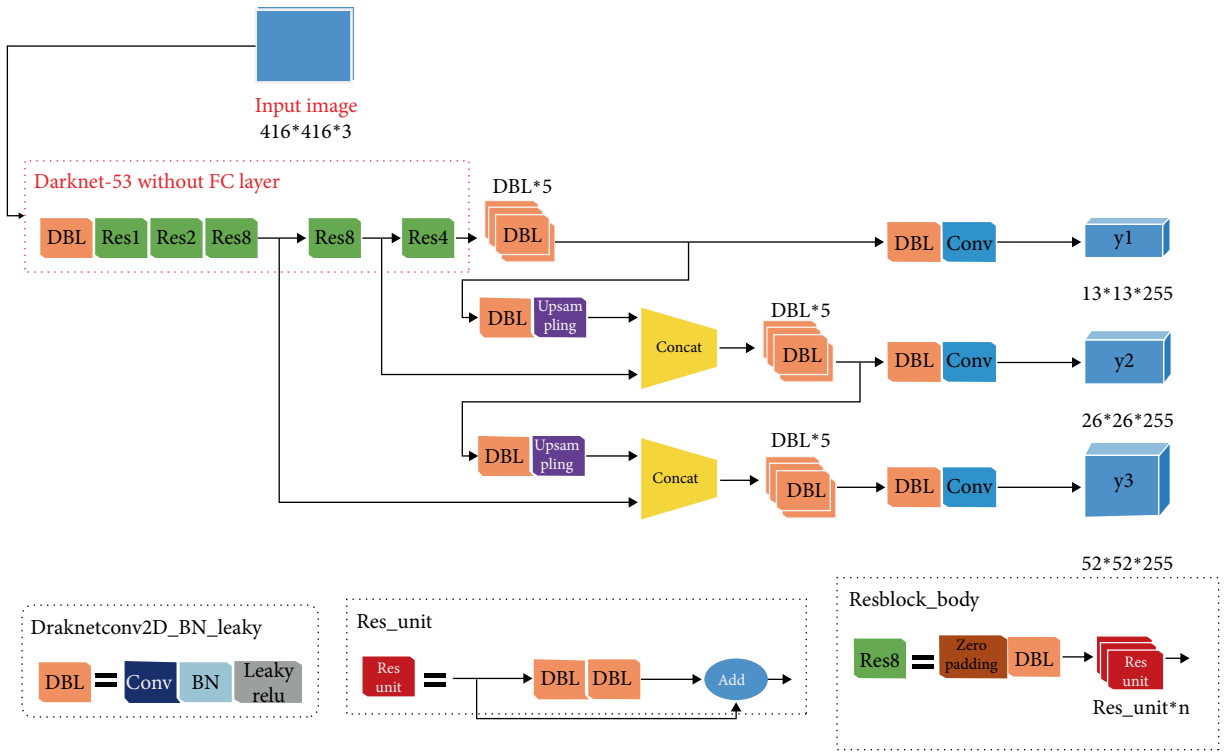

Figure 2: Yolo v3 flow chart.

3.2.3. Predictions Across Scales. Yolo v3 predicts different boxes at three different scales. Yolo v3 uses FPN (feature pyramid network) to extract feature from scales, and finally predicts a 3-D tensor, containing the bounding box information, object information, and class information.

3.2.4. Feature Extractor. Yolo v3 uses a complex network for performing feature extraction, which has 53 convolutional layers, called Darknert-53. This new network is much more powerful than Darknet-19 but still more efficient than ResNet-101 or ResNet-152.The loss function of YOLO is:

$$\begin{aligned}\text{Loss function} =& \lambda_{coord}\sum_{i=0}^{s^2}\sum_{j=0}^{B}\iota_{ij}^{obj}\left(x_i-\hat{x}_i\right)^2+\left(y_i-\hat{y}_i\right)^2\\&+\lambda_{coord}\sum_{i=0}^{s^2}\sum_{j=0}^{B}\iota_{ij}^{obj}\left(\sqrt{w_i}-\sqrt{\hat{w}_i}\right)^2+\left(\sqrt{h_i}-\sqrt{\hat{h}_i}\right)^2\\&+\sum_{i=0}^{s^2}\sum_{j=0}^{B}\iota_{ij}^{obj}\left(C_i-\hat{C}_i\right)^2+\lambda_{noobj}\sum_{i=0}^{s^2}\sum_{j=0}^{B}\iota_{ij}^{noobj}\left(C_i-\hat{C}_i\right)^2\\&+\sum_{i=0}^{s^2}\iota_{ij}^{obj}\sum_{c\in classes}\left(p_i(c)-\hat{p}_i(c)\right)^2.\end{aligned}\tag{10}$$

The flow chart of YOLO is shown in Figure 2.

3.3. Decision-Tree Based Crash Detection Framework. In mixed traffic flow environment, crashes could occur between motorists and nonmotorists. Thus, a motion-based method (e.g., modeling of vehicle interactions, analysis of vehicle activities, etc.) may not have full capability to detect such type of crashes. Moreover, since the computational cost of object detection and tracking has already been high, an even more complex framework by integrating other deep learning models (e.g., recursive neural network) would become too compute-intensive. Thus, in this paper, we consider a simplified framework for quick crash detection that can be implemented in practice.

Decision tree model was considered for crash classification, based on features obtained from Yolo v3. It has several advantages: (1) the cost of using the tree (i.e., predicting data) is logarithmic; (2) it requires little data preparation and can handle both numerical and categorical data; (3) it is simple to understand and to interpret.

Given training features X_i and label y, a decision tree recursively partitions the space:

$$\begin{aligned}Q_{left}(\theta)&=(x,y)\left|x_j<=t_m\right|,\\Q_{right}(\theta)&=\frac{Q}{Q_{left}(\theta)},\end{aligned}\tag{11}$$

where Q representing the data at node m, is a candidate split consisting of a feature j and threshold t_m, Q_{left}, and Q_{right} are subsets partitioned by the decision tree at node m.

The impurity at m can be calculated by an impurity function H (), the choice of which is based on the task being considered:

$$G(Q,\theta)=\frac{n_{left}}{N_m}H\left(Q_{left}(\theta)\right)+\frac{n_{right}}{N_m}H\left(Q_{right}(\theta)\right).\tag{12}$$

If it is a classification task with outcomes from 0 to k for node m, representing a region R_m with N_m observations, let

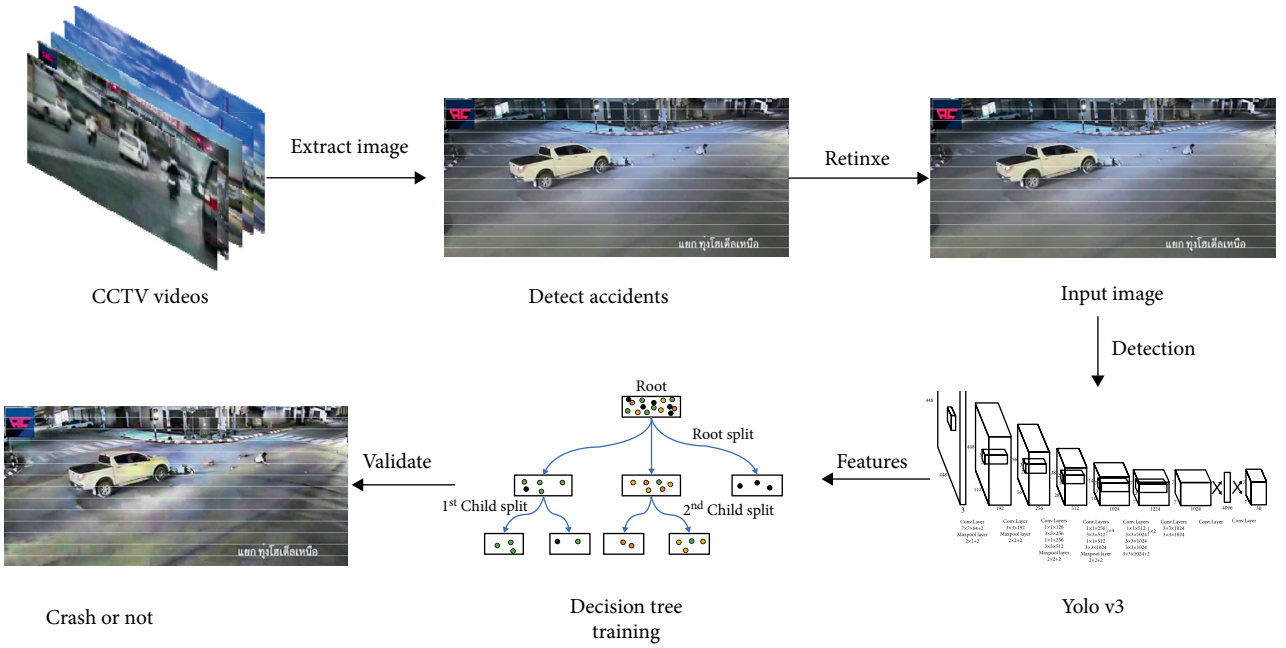

Figure 3: Crash detection framework for mixed traffic flow environment.

$$p_{mk} = \frac{1}{N_m} \sum_{x_i \in R_m} I(y_i = k), \tag{13}$$

be the proportion of class k observations in node m.

Gini Index is often used to measure impurity:

$$H(X_m) = \sum_k p_{mk}(1 - p_{mk}). \tag{14}$$

Entropy is another commonly used indicator of impurity:

$$H(X_m) = -\sum_k p_{mk} \log(1 - p_{mk}), \tag{15}$$

where X_m is the training data in node m.

Parameters are selected such that the impurity can be minimized:

$$\theta^* = \arg\min_\theta G(Q, \theta). \tag{16}$$

The framework is shown in Figure 3.

4. Experimental Evaluation

In order to validate the framework, an experiment was conducted on a computer with specification Intel(R) Core (TM) i5-4200 CPU @ 2.50 GHz (4 CPUs), ~2.5 GHz, 8 GB RAM with NVIDIA Corporation GeForce 840 M.

4.1. Dataset Used. We collected large number of CCTV videos from online since there is no public database for crash detection. Figure 4 shows the samples of the video data. In general, a video clip records 10–20 s before and after a crash. Our dataset has 127362 frames, in which 45214 contain crash scenes and 82148 are normal frames. There are various crash types observed, including multi-vehicle crashes, pedestrian-vehicle crashes, and cyclist-vehicle crashes. Moreover, many low-visibility conditions were included in the dataset, such as dark night with poor lights, heavy rains, and foggy days. In this study, 15000 crash frames and 40000 normal frames were used to create training samples, while the remaining frames were used for model testing.

4.2. Results and Discussion. First, Retinex was utilized to improved image quality. Figure 5 provides some examples of image enhancement. It can be found that more image details can be seen after the enhancement.

After image enhancement, Yolo v3 was used for detecting objects from images. In the training dataset, crash samples were extracted from videos including fallen people, fallen bicycle/motorcycle, and vehicle rollovers. Those samples were then distorted and scaled to further enlarge the crash sample size. Normal people, bicycle, motorcycle, and vehicles were also collected as normal samples. Figure 6 provides some examples in the training dataset.

After 5000 iterations, the model became convergent. Figure 7 provides the real-time detection performance based on Yolo v3. The training and testing accuracy of the Yolo model are shown in Figure 8. According to the graph, the training model has no overfitting issue.

Three crash types were observed in the current video dataset, including:

(1) Pedestrian/cyclist related crash: If this type occurs, fallen people, fallen cyclists, stopped vehicle, stopped people, and stopped cyclists could be detected in the scene.

(2) Minor motor-vehicle crash: If this type occurs, vehicle overlapping, stopped vehicles, and stopped people/cyclists could be detected in the scene.

(a) (b) (c)

Figure 4: Sample frames from the video dataset used to evaluate the accident. The dataset contains videos of accidents during the various environmental conditions such as (a) daytime (b) night (c) rain or fog, as well as from different cameras and view angles.

Figure 5: Images before and after Retinex.

(3) Serious motor-vehicle crash: If this type occurs, vehicle rollover, stopped vehicles, and stopped people/cyclists could be detected in the scene.

In order to detect those three crash types, a set of features were developed based on Yolo v3 outputs, including: number of moving vehicle (the number of moving vehicles), number of stopped vehicle (the number of stopped vehicles), number of stopped people (the number of moving pedestrians and cyclists), number of moving people (the number of stopped pedestrians and cyclists), fallen people (the number of fallen people), vehicle rollover (the number of vehicle rollover), intersection of union (IOU), and IOU duration. IOU is often used to measure the overlap between two bounding boxes (e.g., two vehicles). Note that in this study, IOU represents the maximum IOU values that remain unchanged over the observation period, while IOU duration indicates the longest time period that IOU remains changed. A decision tree was trained using these features as inputs, as shown in Figure 9. The average precision is 0.95. According to entropy and information gain of the tree model, some features were found as important including: fallen people, IOU duration, stopped people, stopped vehicle, and vehicle rollover.

Based on the findings, three empirical rule-based models were also developed as follows:

Rule 1: If fallen people or fallen nonmotorized vehicle is continuously detected during a period (e.g., 10 s), the condition can be determined as a crash.

Rule 2: If two vehicles are detected as overlapped during a period (e.g., 10 s), and other stopped people are detected around the vehicles, the condition can be determined as a crash.

Rule 3: If a car rollover is detected during a period (e.g., 2 s), the condition can be determined as a crash.

Rule 1 model could detect crash types related to pedestrians and cyclists (e.g., bicycles, motorcycles). A relative long period time detection may avoid miss-detection of those occasionally fallen off. Rule 2 model was designed for nonserious

(a)

(b)

Figure 6: Training samples of Yolo v3. (a) Crash samples and (b) normal samples.

Figure 7: Yolo v3 results.

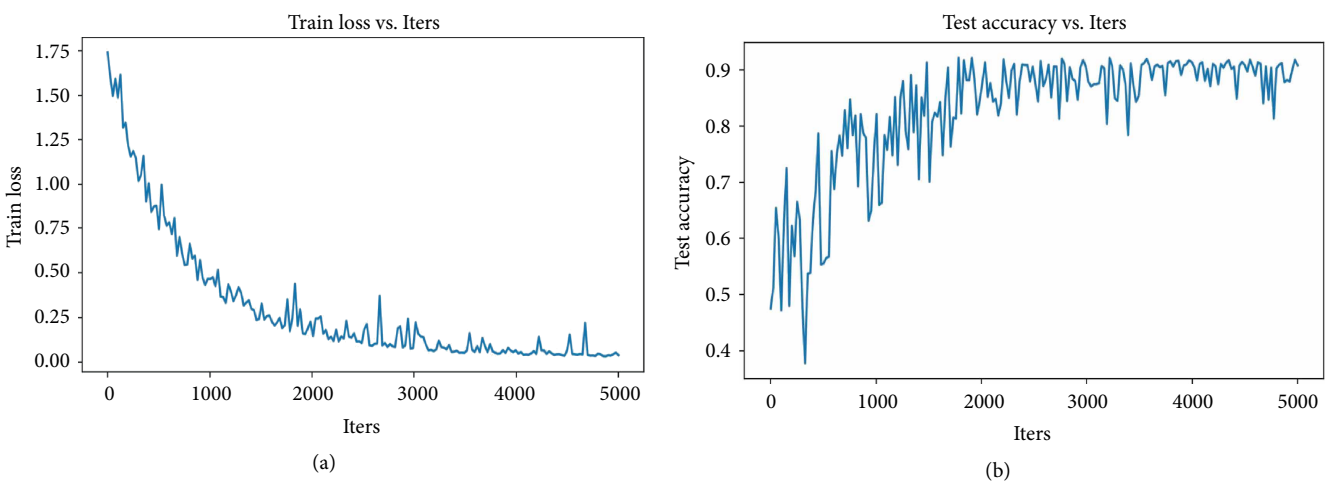

(a)

(b)

Figure 8: (a) Train loss within 5000 iterations; (b) test accuracy with 5000 iterations.

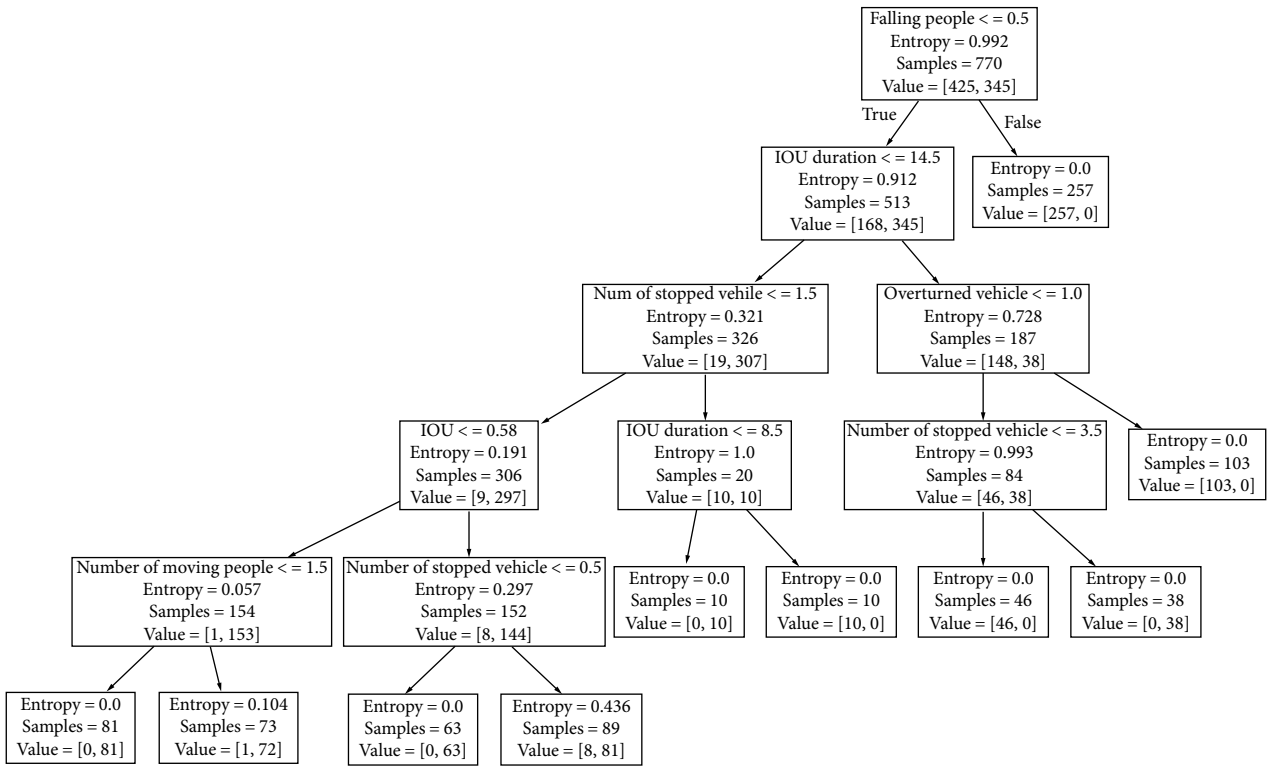

Figure 9: Trained decision tree model.

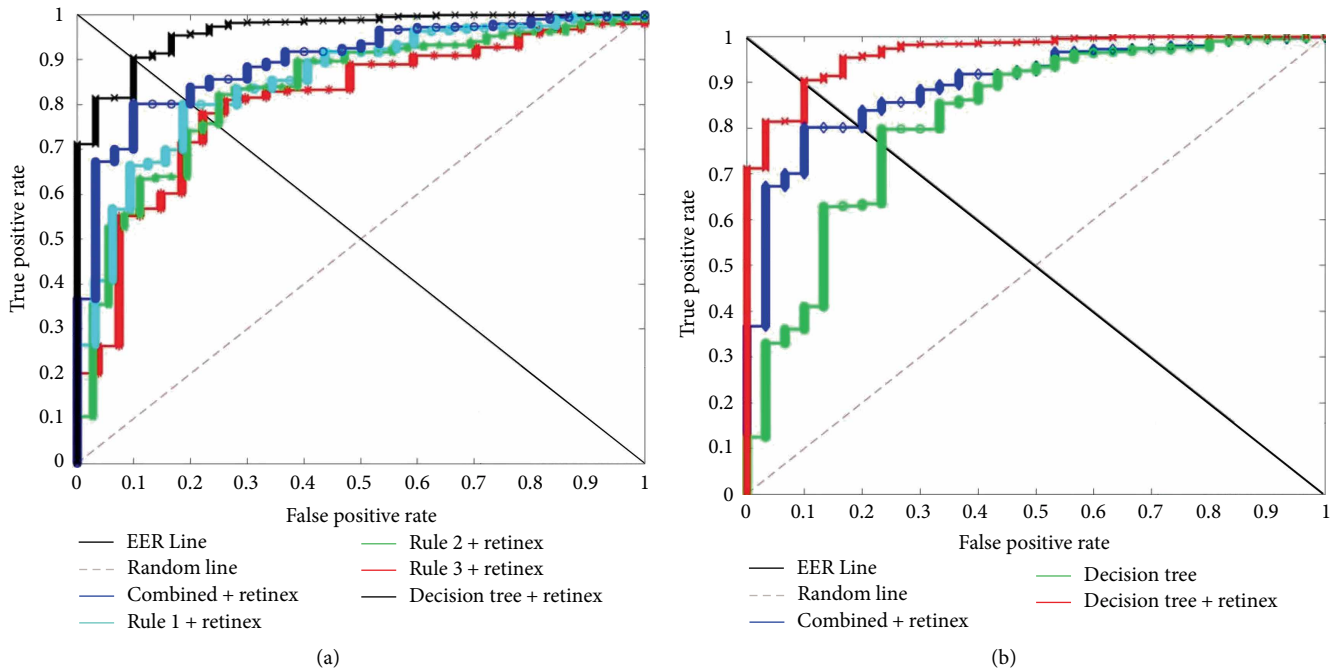

Figure 10: AUC comparison among multiple crash detection models. (a) AUC comparison among decision tree, combined-rule and single-rule detection models. (b) AUC comparison between crash detection models with/without Retinex enhancement.

crash types, including minor multivehicle and single-vehicle crashes. In those situations, vehicles may not be damaged seriously or no fallen objects could be detected. According to previous literature, such types could be detected by analyzing the intersection of vehicle motions. Rule 3 model can detect serious motor-vehicle crash types.

All model performances were compared, as shown in Figure 10. Figure 10(a) provides the ROC curves of all those

Table 1: Area under curve (AUC) for multiple crash detection models.

Models	Retinex + decision tree	Retinex + combined	Decision tree	Retinex + rule 1	Retinex + rule 2	Retinex + rule 3
AUC	0.9632	0.8744	0.8201	0.8519	0.8039	0.8295

models with Retinex enhancement in mixed traffic flow environment, which indicates the relationship between sensitivity (True Positive) and specificity (False Positive). It can be seen from Figure 10(a), the decision tree model had the best performance than other models, according to ROC curves. The combined rule model outperformed each single-ruled model. According to Figure 10(b), Retinex enhancement made a considerable improvement on crash detection performance for the decision tree model. Without Retinex, the overall performance of the decision tree model appeared to be lower than the combined rule-based model with Retinex.

Overall, the proposed framework can correctly detect 92.5 % of crashes in the testing dataset. The false alarm rate is 7.5 %. The AUC values for all crash detection models are listed in Table 1.

In general, decision tree-based model appeared to be better than empirical rule-based models. Although the proposed framework achieved relatively high detection accuracy, there are still some issues:

(1) Fallen pedestrians/cyclists can sometimes be blocked by other objects, increasing false alarm rate.

(2) In highly congested mixed traffic flow environment, crashes can also be falsely alarmed. This could be due to inaccurate detection of Yolo v3 model (e.g., bounding boxes prediction).

(3) Retinex can handle most low-visibility conditions in this study. However, when video quality is too low, crashes can still be missed or false alarmed. For example, fast-moving vehicle could be sometimes falsely detected as fallen vehicles, according to our observation.

4.3. Comparison with the Existing Methods. Due to the lack of public database, limited research has been identified on this topic. Since most studies were based on private datasets that cannot be accessed, their results are somewhat incomparable. However, we still listed the results here. Yun [39] achieved a detection rate of 0.8950 for crash detection. RTADS [20] reported a hit rate of 92% and false alarm rate of 0.77%. ARRS [21] presented a true positive rate of 0.63 with a false alarm rate of 0.06. Singh [27] reported a hit rate of 77.5% and a false alarm rate of 22.5%. Sadek [40] achieved 99.6% detection rate and 5.2% false alarm rate.

Although some literature has reported high detection rates, such could encounter over-fitting issues due to limited sample size. Second, some literature created complicated deep learning structures, requiring high computational capability. Third, limited literature has focused on crash detection in mixed traffic flow environment under low-visibility conditions.

5. Conclusions

The paper proposed a vision-based crash detection framework for mixed traffic flow environment considering low-visibility conditions. Retinex algorithm was introduced to enhance image quality of low-visibility conditions, such as night, foggy, and rainy days. A deep learning model (i.e., Yolo v3) was trained to detect objects in mixed traffic flow environment and a decision tree model was developed for crash detection, considering various crash scenarios between motorized and nonmotorized traffic. The proposed method achieved a hit rate of 92.5% and a false alarm rate of 7.5%. Interesting findings include: (1) the proposed model outperformed empirical rule-based detection models; (2) image enhancement method can largely improve crash detection performance under low-visibility conditions; (3) the accuracy of object detection (e.g., bounding boxes prediction) can impact crash detection performance, especially for minor motor-vehicle crashes.

Overall, the results are encouraging and the framework is promising. Admittedly, there are still some issues that can be further addressed. First, different image enhancement methods could be tried to improve the overall performance. Second, other deep learning method can be used and compared to original Yolo v3 model. Third, other more complex deep learning structure can be examined and compared to the current framework, in terms of accuracy and computational speed.

Data Availability

Data were large number of video clips.

Conflicts of Interest

The authors declare that they have no conflicts of interest.

Acknowledgments

This research has been supported by the National Key R&D Program of China (2018YFE0102700).

References

[1] G. Yuan, X. Zhang, Q. Yao, and K. Wang, "Hierarchical and modular surveillance systems in ITS," *IEEE Intelligent Systems*, vol. 26, no. 5, pp. 10–15, 2011.

[2] S. Xia, J. Xiong, Y. Liu, and G. Li, "Vision-based traffic accident detection using matrix approximation," in *2015 10th Asian Control Conference: Emerging Control Techniques for a Sustainable World, ASCC 2015*, IEEE, pp. 1–5, Kota Kinabalu, Malaysia, 2015.

[3] B. Li, Y. Liu, J. Ren, Y. Chen, L. Xin, and J. Shi, "Detecting and positioning of traffic incidents via video-based analysis of traffic states in a road segment," *IET Intelligent Transport Systems*, vol. 10, no. 6, pp. 428–437, 2016.

[4] C. Xu, Y. Wang, P. Liu, W. Wang, and J. Bao, "Quantitative risk assessment of freeway crash casualty using high-resolution traffic data," *Reliability Engineering and System Safety*, vol. 169, pp. 299–311, 2018.

[5] Y. Guo, Z. Li, Y. Wu, and C. Xu, "Evaluating factors affecting electric bike users' registration of license plate in china using bayesian approach," *Transportation Research Part F: Traffic Psychology and Behaviour*, vol. 59, pp. 212–221, 2018.

[6] X. Qu, J. Zhang, and S. Wang, "On the stochastic fundamental diagram for freeway traffic: model development, analytical properties, validation, and extensive applications," *Transportation Research Part B Methodology*, vol. 104, pp. 256–271, 2017.

[7] M. Zhou, X. Qu, and X. Li, "A recurrent neural network based microscopic car following model to predict traffic oscillation," *Transportation Research Part C: Emerging Technologies*, vol. 84, pp. 245–264, 2017.

[8] C. Wang, C. Xu, J. Xia, and Z. Qian, "Modeling faults among e-bike-related fatal crashes in China," *Traffic Injury Prevention*, vol. 18, no. 2, pp. 175–181, 2017.

[9] B. Dong, X. Ma, F. Chen, and S. Chen, "Investigating the differences of single- and multi-vehicle accident probability using mixed logit model," *Journal of Advanced Transportation*, vol. 2018, Article ID 2702360, 9 pages, 2018.

[10] C. S. Regazzoni, A. Cavallaro, Y. Wu, and J. Konrad, "Of video surveillance systems continues bound to take a approach to video," in *IEEE Signal Processing Magazine*, IEEE, pp. 16–17, 2010.

[11] X. Zhu, Z. Dai, F. Chen, X. Pan, and M. Xu, "Using the visual intervention influence of pavement marking for rutting mitigation II: visual intervention timing based on the finite element simulation," *International Journal of Pavement Engineering*, vol. 20, no. 5, pp. 573–584, 2019.

[12] G. Wu, F. Chen, X. Pan, D. M. Xu, and X. Y. Zhu, "Using the visual intervention influence of pavement markings for rutting mitigation-part I: preliminary experiments and field tests," *International Journal of Pavement Engineering*, vol. 20, no. 6, pp. 734–746, 2019.

[13] A. Yoneyama, C. H. Yeh, and C. C. JayKuo, "Robust vehicle and traffic information extraction for highway surveillance," *Eurasip Journal on Applied Signal Processing*, vol. 2005, no. 14, pp. 2305–2321, 2005.

[14] A. Dopfer and C. C. Wang, "What can we learn from accident videos?" in *2013 CACS International Automatic Control Conference (CACS)*, pp. 68–73, IEEE, Nantou, Taiwan, 2013.

[15] C. Wang, C. Xu, J. Xia, Z. Qian, and L. Lu, "A combined use of microscopic traffic simulation and extreme value methods for traffic safety evaluation," *Transportation Research Part C: Emerging Technologies*, vol. 90, pp. 281–291, 2018.

[16] C. Wang, C. Xu, and Y. Dai, "A crash prediction method based on bivariate extreme value theory and video-based vehicle trajectory data," *Accident Analysis and Prevention*, vol. 123, pp. 365–373, 2019.

[17] Y. Guo, Z. Li, Y. Wu, and C. Xu, "Exploring unobserved heterogeneity in bicyclists' red-light running behaviors at different crossing facilities," *Accident Analysis and Prevention*, vol. 115, pp. 118–127, 2018.

[18] C. Xu, H. Li, J. Zhao, J. Chen, and W. Wang, "Investigating the relationship between jobs-housing balance and traffic safety," *Accident Analysis and Prevention*, vol. 107, pp. 126–136, 2017.

[19] Z. Liu, S. Wang, B. Zhou, and Q. Cheng, "Robust optimization of distance-based tolls in a network considering stochastic day to day dynamics," *Transportation Research Part C: Emerging Technologies*, vol. 79, pp. 58–72, 2017.

[20] H. Tan, J. Zhang, J. Feng, and F. Li, "Vehicle speed measurement for accident scene investigation," in *2010 IEEE 7th International Conference on E-Business Engineering*, pp. 389–392, IEEE, Shanghai, China, 2010.

[21] W. Hu, X. Xiao, Z. Fu, D. Xie, T. Tan, and S. Maybank, "A system for learning statistical motion patterns," *IEEE Transactions on Pattern Analysis and Machine Intelligence*, vol. 28, no. 9, pp. 1450–1464, 2006.

[22] X. Li, A. Ghiasi, Z. Xu, and X. Qu, "A piecewise trajectory optimization model for connected automated vehicles: exact optimization algorithm and queue propagation analysis," *Transportation Research Part B: Methodology*, vol. 118, pp. 429–456, 2018.

[23] I. J. Lee, "An accident detection system on highway using vehicle tracking trace," in *2011 International Conference on ICT Convergence, ICTC 2011*, pp. 716–721, IEEE, Seoul, South Korea, 2011.

[24] Z. Hui, Y. Xie, M. Lu, and J. Fu, "Vision-based real-time traffic accident detection," in *Proceeding of the 11th World Congress on Intelligent Control and Automation*, pp. 1035–1038, IEEE, Shenyang, China, 2015.

[25] J. W. Hwang, Y. S. Lee, and S. B. Cho, "Hierarchical probabilistic network-based system for traffic accident detection at intersections," in *Proceedings – Symposia and Workshops on Ubiquitous, Autonomic and Trusted Computing in Conjunction with the UIC and ATC 2010 Conferences, UIC-ATC 2010*, pp. 211–216, IEEE, Xian, Shaanxi, China, 2010.

[26] Y. K. Ki and D. Y. Lee, "A traffic accident recording and reporting model at intersections," *IEEE Transactions on Intelligent Transportation Systems*, vol. 8, no. 2, pp. 188–194, 2007.

[27] D. Singh and C. K. Mohan, "Deep spatio-temporal representation for detection of road accidents using stacked autoencoder," *IEEE Transactions on Intelligent Transportation Systems*, vol. 20, no. 3, pp. 879–887, 2019.

[28] Z. Xu, W. Tao, S. Easa, X. Zhao, and X. Qu, "Modeling relationship between truck fuel consumption and driving behavior using data from internet of vehicles," *Computer-Aided Civil and Infrastructure Engineering*, vol. 33, no. 3, pp. 209–219, 2018.

[29] C. Ma, W. Hao, X. Wang, and W. Yan, "The impact of aggressive driving behavior on driver injury severity at highway-rail grade crossings accidents," *Journal of Advanced Transportation*, vol. 2018, Article ID 9841498, 10 pages, 2018.

[30] N. Wang, L. Qi, J. Dong, H. Fan, X. Chen, and H. Yu, "Two-stage underwater image restoration based on a physical model," in *Proceedings of SPIE 10225, Eighth International Conference on Graphic and Image Processing (ICGIP 2016)*, SPIE, Tokyo, Japan, 2017.

[31] Q. Wang, J. Gao, and Y. Yuan, "A joint convolutional neural networks and context transfer for street scenes labeling," *IEEE Transactions on Intelligent Transportation Systems*, vol. 19, no. 5, pp. 1457–1470, 2018.

[32] Q. Li, F. Xu, X. Zhao, Y. Yao, and Y. Li, "High resolution image restoration algorithm of wavefront coding system based on

wiener filter and wavelet de-noising," in *Optoelectronic Imaging and Multimedia Technology IV*, SPIE, Beijing, China, 2016.

[33] Y. S. Zhang, F. Zhang, and B. Z. Li, "Image restoration method based on fractional variable order differential," *Multidimensional Systems and Signal Processing*, vol. 29, no. 3, pp. 999–1024, 2018.

[34] Y. Zhang, L. Sun, C. Yan, X. Ji, and Q. Dai, "Adaptive residual networks for high-quality image restoration," *IEEE Transactions on Image Processing*, vol. 27, no. 7, pp. 3150–3163, 2018.

[35] S. Mei, J. Ji, J. Hou, X. Li, and Q. Du, "Learning sensor-specific spatial-spectral features of hyperspectral images via convolutional neural networks," *IEEE Transactions on Geoscience and Remote Sensing*, vol. 55, no. 8, pp. 4520–4533, 2017.

[36] Y. Wang and Z. Pan, "Image contrast enhancement using adjacent-blocks-based modification for local histogram equalization," *Infrared Physics and Technology*, vol. 86, pp. 59–65, 2017.

[37] W. He, Q. Wu, and S. Li, "Medical X-Ray image enhancement based on wavelet domain homomorphic filtering and CLAHE," in *2016 International Conference on Robots & Intelligent System (ICRIS)*, pp. 249–254, IEEE, Zhangjiajie, China, 2016.

[38] B. Shalchian, H. Rajabi, and H. Soltanian-Zadeh, "Assessment of the wavelet transform in reduction of noise from simulated PET images," *Journal of Nuclear Medicine Technology*, vol. 37, no. 4, pp. 223–228, 2009.

[39] K. Yun, H. Jeong, K. M. Yi, S. W. Kim, and J. Y. Choi, "Motion interaction field for accident detection in traffic surveillance video," in *2014 22nd International Conference on Pattern Recognition*, pp. 3062–3067, IEEE, Stockholm, Sweden, 2014.

[40] S. Sadek, A. Al-Hamadi, B. Michaelis, and U. Sayed, "Real-time automatic traffic accident recognition using HFG," in *2010 20th International Conference on Pattern Recognition*, pp. 3348–3351, IEEE, Istanbul, Turkey, 2010.

Hindawi
Journal of Advanced Transportation
Volume 2020, Article ID 1720949, 17 pages
https://doi.org/10.1155/2020/1720949

WILEY | Hindawi

Research Article

A Traffic Flow Evolution Process toward Mixed Equilibrium with Multicriteria of Route Choice Behaviour

Xiangjun Jiang, Zhongxiang Huang, and Zhenyu Zhao

School of Traffic & Transportation Engineering, Changsha University of Science & Technology, Changsha 410076, Hunan, China

Correspondence should be addressed to Xiangjun Jiang; 18874033439@163.com and Zhongxiang Huang; mehzx@126.com

Received 22 October 2019; Accepted 4 December 2019; Published 6 January 2020

Guest Editor: Qiang Zeng

Based on the price-quantity adjustment behaviour principle of disequilibrium theory, the route choices of travellers are also affected by a quantity signal known as traffic flow, while the route cost is considered as a price signal in economics. Considering the quantity signal's effect among travellers, a new route comfort choice behaviour criterion and its corresponding equilibrium condition are established. The network travellers are classified into three groups according to their route choice behaviour: travellers in the first group choose the shortest route following the route rapidity behaviour criterion with complete information forming the UE (user equilibrium) pattern, travellers in the second group choose the most comfortable route following the route comfort behaviour criterion with complete information forming the QUE (quantity adjustment user equilibrium) pattern, and travellers in the third group choose a route according to their perceived travel time with incomplete information forming the SUE (stochastic user equilibrium) pattern. The traffic flows of all three groups converge to a new UE-QUE-SUE mixed equilibrium flow pattern after interaction. To depict the traveller-diversified choice behaviour and the traffic flow interaction process, a mixed equilibrium traffic flow evolution model is formulated. After defining the route comfort indicator and the corresponding user equilibrium state, the equilibrium conditions of the three group flows are given under a mixed equilibrium pattern. In addition, an equivalent mathematical programming of the mixed equilibrium traffic flow evolution model is proposed to demonstrate that the developed model converges to the mixed equilibrium state. Finally, numerical examples are examined to evaluate the effect of route comfort proportions on the traffic network flow evolution and analyse the performance of the proposed model.

1. Introduction

The dynamic evolution process of traffic flow has been a hot issue in the transportation field, and various traffic flow dynamic models based on travellers' route adjustment behaviours have been examined. These models can depict the process of the traffic flow as it evolves from a disequilibrium state to an equilibrium state [1, 2]. Obviously, the network flow forms a Wardrop UE (user equilibrium) pattern if all travellers choose the actual shortest route in the route decision process and converges to a SUE (stochastic user equilibrium) pattern if all travellers adjust their routes according to the perceived route travel time. When a SO (system optimal) state is reached, all travellers select the route that can minimize the system travel time.

Although these classical traffic flow equilibrium conditions differ in the form of travel time, they share the same route rapidity choice criterion, which can embody the travellers' preference of route rapidity and reflect the price signal affection. It is apparent that all existing models in the literature were formulated based on a single-route rapidity choice preference, where the route travel time is the core indicator. This approach has been widely applied in various network traffic flow models, whereas with the rapid economic growth and social development, people-oriented considerations, such as traffic safety and travel satisfaction, have been the dominant research direction [3–8].

With the development of intelligent transportation systems and technologies, travellers can make their route choices according to the accurate information of the traffic

network [9, 10]. By relaxing the restrictions on the behavioural hypothesis conditions of the Smith model, Guo et al. established a discrete dynamic system to study the day-to-day evolution process of traffic flow from nonequilibrium to equilibrium. This assumed that travellers choose a travel route based on the self-estimated travel time, and the number of adjusted travellers is related to the route adjustment ratio [11, 12]. Zhao and Huang adopted the concept of satisfaction and established a parallel network traffic distribution model based on satisfaction criteria [13]. Tang et al. established a route-based traffic flow model based on road network disturbance factors and studied the influence of two typical factors, a bus station and an accident, on the traffic flow [14].

Ma et al. provided a methodology to derive the critical point from free flow to crowded flow and proposed a new capacity allocation strategy that can improve the capacity of a traffic network [15]. Cantarella and Watling formulated a discrete stochastic deterministic process model to study the impact of travellers' route selection behaviours on traffic flow evolution. The model considered travellers' travel habits and provided a general method to portray the traffic flow distribution [16]. Considering the social interaction of travellers, Wei et al. utilized a traffic flow evolution model in order to describe travellers' route choice behaviours and studied the impact of individual travellers' route choice decisions and their interactions on the traffic flow pattern of a road network [17].

Considering capacity constraints, Hoang et al. established the linear programming of a UE-DTA (user equilibrium dynamic traffic assignment), connected the UE solution to the SO solution, and proposed an incremental loading method that effectively reduced the difficulty in obtaining a UE solution [18]. Liu et al. analysed the interaction between travellers and traffic information providers through a network evolution model that considered the influence of user inertia on travellers' route decisions [19].

Different traveller route choice behaviour criteria lead to different network traffic flow distribution patterns [20, 21]. A network-mixed equilibrium is formed through the interaction of various traffic flows following different route choice behaviour criteria. At present, mixed equilibrium traffic flow studies have mainly examined the mixed equilibrium between UEs and other specific equilibrium traffic flows, including UE-SUE, UE-CN (Cournot–Nash), UE-SO, and UE-CN-SO. Zhou et al. established a discrete dynamic evolution model of mixed equilibrium traffic flow that describes travellers' route adjustment behaviours and simulates the evolution trajectory of traffic flow converging to a UE-SUE mixed equilibrium state with a given ATIS (advance traveller information system) market penetration [22].

Zhang et al. divided travellers into two categories according to travel behaviour principles: the UE principle and CN principle (CN is the intermediate state between perfect competition and perfect coordination, manifested as internal coordination and external competition). The interaction of traveller's route choice behaviours finally produces a result between the competition equilibrium and monopoly equilibrium: the UE-CN-mixed equilibrium [23]. Proble et al. classified travellers into two types (perfect cooperation and perfect competition) and proposed a UE-SO mixed equilibrium model in which perfectly cooperative travellers obey the SO criterion and perfectly competitive travellers obey the UE criterion [24]. Site et al. separated travellers into three categories: (a) travellers equipped with predictive ATIS, (b) travellers equipped with static ATIS and are subjected to it, and (c) travellers not equipped with ATIS or are not subjected to it. The researchers established a mixed equilibrium behaviour models with predictive ATIS and static ATIS [25].

After elaborating on the traffic behavioural implications of the price-quantity adjustment behaviour principle in economics, this paper summarizes a new route comfort behaviour, which has not been investigated so far, to simulate the route decision process of travellers' adjustment behaviours. Unlike the existing studies under a single-route rapidity choice behaviour criterion, a new route comfort choice behaviour criterion is proposed in this study to analyse the route adjustment process and to accurately model the traffic flow evolution from disequilibrium to mixed equilibrium. Specifically, given complete information, travellers in the first group, following the route rapidity choice behaviour criterion, are likely to choose the shortest route under current conditions, while travellers in the second group, following the route comfort choice behaviour criterion, are supposed to choose the most comfortable route with minimum traffic flow. Travellers in the third group with incomplete information follow the logit-based SUE principle based on the perceived travel time.

The resultant equilibrium of travellers under a predefined penetration of route decision behaviour criteria and complete information is referred to as a mixed equilibrium. A route flow adjustment model is proposed to analyse the mixed traffic flow of travellers with the multicriteria of route choice behaviours. The convergence of our day-to-day flow adjustment model to the mixed equilibrium state is demonstrated. In addition, we present a list of route flow evolution trajectories under different behaviour criteria percentages and show specific cases to refine the evolution process toward the mixed equilibrium state.

In previous studies that did not consider the existence of quantity signals in the traffic market, it was customary to assume that all travellers make route selection decisions based on the travel price signal, known as travel cost. This is difficult to achieve in a real traffic travel process because in addition to inaccuracies and partial network information, the behaviours of the travellers are heterogeneous. While some travellers choose a route according to the travel time and speed, some travellers may pay more attention to the comfort of travel or safety and other factors. Therefore, the mixed equilibrium traffic flow evolution model under the multicriteria of route choice behaviour not only takes into account the heterogeneity and bounded rationality of the traveller but also vividly explains the various traffic travel shift behaviours of the traveller. In addition, the model describes the dynamic evolution process of the actual network traffic flow more flexibly and objectively, which

provides the basis for the formulation of a network traffic flow control strategy and traffic construction plan.

2. Traffic Flow Equilibrium State and Route Choice Behaviour

2.1. Price-Quantity Adjustment Principle and Route Choice Behaviour. Based on the price-quantity adjustment behaviour principle of disequilibrium theory, individuals accept both commodity price signals and the trading quantity signals from the market in economics. This affects product decisions and furthermore influences the commodity demand and supply. As a specific travel market, residential travel route choice behaviour is influenced by the route travel time (price signal) and the route flow (quantity signal) as well. This makes a difference on traffic demand and supply in an origin-destination pair [26].

Since the shortest route choice reflects the travellers' pursuit of travel rapidity, the route rapidity choice criterion is widely used to depict the route choice behaviour that uses the route travel time as the only decision basis. This expresses the price signal effect in the traffic market, such as in the traditional Wardrop UE or SO assignment. Since a UE or SO assignment focuses on the route travel time decision behaviour, they are unable to describe the travel route choice behaviour that was influenced by the route flow.

As an important supplement to the traditional route rapidity choice criterion, this paper proposes a new route comfort choice criterion to portray the route adjustment behaviour that seeks a relatively comfortable route. The route comfort choice criterion assumes that the route flow is the decision basis of travellers, and travellers shift from a congested route to a low-flow route based on the experienced comfort. Hence, according to the price-quantity adjustment behaviour principle, the general pursuit of travellers in the travel route decision process is to choose a route that is both fast and comfortable. Applying the route rapidity and comfort adjustment criteria stimulatingly to individual travel route selection behaviour shows that individuals will comprehensively consider the route cost and the route surplus capacity to make a route decision. When applied to the traveller group, the aggregated effect performs as some travellers choose the shortest route and some travellers choose the most comfortable route, which is discussed in this study.

In the travel route decision process, travellers have some human properties that affect route decision behaviours and cause diversity in travellers' route choice behaviours. To provide variety, a navigation system in real life, such as Amap or Baidu Maps, provides three kinds of route choice in route planning: the shortest time, the shortest distance, and the minimum number of traffic lights. All these inform the different travel preference of travellers between travel rapidity and comfort. As the route choice behaviour affects the network traffic flow distribution pattern directly, it is more convincing to model the equilibrium traffic flow under the rapidity and comfort route decision criteria than the single rapidity or comfort preferences.

2.2. Route Rapidity Choice Criterion. Given a network $G = (N, A)$, where N is the set of nodes and A is the set of links, let the set of origin-destination pairs be W. The set of routes in OD pair $w \in W$ is denoted by R_w.

The traditional UE, SUE, and SO assignment models assume a perfect perception of travel cost and develop traffic flow adjustment processes over a single-route rapidity choice behaviour criterion. Based on this criterion, travellers select the fastest route that can minimize their travel time under the current alternative route information.

The flow of travellers on the route $r \in R_w$ is denoted by f_w^r. The traffic flow on the link $a \in A$, denoted by x_a, is given by

$$x_a = \sum_{w \in W} \sum_{r \in R_w} \delta_w^{ra} f_w^r, \quad a \in A, \tag{1}$$

where $\delta_w^{ra} = 1$ if route $r \in R_w$ contains link a and 0 otherwise. $t_a = t_a(x_a)$ is the travel time function on link $a \in A$, which is assumed positive, additive, and strictly increasing with respect to link flow x_a. Thus, the travel time function on the route is expressed by

$$c_w^r = \sum_{a \in A} \delta_w^{ra} t_a(x_a), \quad r \in R_w, r \in W. \tag{2}$$

Travellers in the first group equipped with complete network information will follow the UE route choice behaviour assumption, in which all travellers are supposed to shift to the alternative shorter route to reduce their actual travel time given the current information. The traffic flow evolution formed by this shift movement will converge toward a Wardrop UE equilibrium state where all routes of the OD pair share the same actual travel time. The equilibrium condition is

$$\begin{cases} f_w^r > 0, c_w^r = u_w, \\ f_w^r = 0, c_w^r \geq u_w, \quad r \in R_w, w \in W, \end{cases} \tag{3}$$

where u_w denotes the minimal travel time between OD pair w.

By contrast, travellers in the third group with incomplete network information will choose their routes in a logit-based SUE manner. All travellers in the third group will choose to shift their routes according to the perceived route travel time, which may result in multiple possible route adjustment trajectories in the same situation owing to differences in perception. The SUE equilibrium state is reached when the route perceived travel time of all alternative routes is equal, and the following condition holds

$$f_w^r = p_w^r \cdot d_w = \frac{\exp(-\theta c_w^r)}{\sum_{k \in R_w} \exp(-\theta c_w^r)} d_w, \quad r \in R_w, w \in W, \tag{4}$$

where p_w^r represents the probability that route r between OD pair w is chosen, θ is a perception parameter, and d_w is the traffic demand of OD pair w.

2.3. Route Comfort Choice Criterion. Travellers in the second group are assumed to choose the most comfortable route in the OD pair under the route comfort choice criterion. Comfort is a kind of physiological experience and is the comprehensive evaluation of the satisfaction degree of the objective reality environment in both physiology and psychology. This can be affected by various factors and differs between individuals owing to their disparate perceptions. There is no uniform definition of route comfort at present, so is the main measure indicators.

By applying the price-quantity adjustment principle in route choice behaviour research, the route surplus capacity is proposed as the indicator of the route comfort degree in this study. This is a general expression form of the traffic flow that reflects the impact of the quantity signal on the route decision process. The route surplus capacity is the difference between the route maximum capacity and the route flow, which concerns not only the physical capacity of the network route but also indicates the travel comfort degree. In addition, the route with a larger surplus capacity indicates a higher degree in the route service level, road infrastructure facilities, environmental satisfaction, travel fluency, and experience of comfort than a lower surplus capacity, and vice versa.

Let K_a denotes the maximum traffic capacity of link a. Then, the maximum traffic capacity of route $r \in R_w$ is expressed as

$$K_r = \min\left(\delta_w^{ra} K_a\right). \tag{5}$$

As the study subject of this research is the traffic evolution short-term behavior, the traffic capacity of route is assumed to be constant. The surplus capacity of route $r \in R_w$ is given by

$$s_w^r\left(f_w^r\right) = K_r - f_w^r. \tag{6}$$

The maximum surplus capacity in OD pair $w \in W$ is defined as

$$v_w = \max_{r \in R_w}\left\{s_w^r\left(f_w^r\right)\right\}. \tag{7}$$

When the traffic network travel demand is low, all of the route capacities are relatively high, so travellers in the second group select the maximum surplus capacity route, that is, the most comfortable travel route. With an increase in the network travel demand, the surplus capacities of all routes are reduced since the network gradually evolves to a congested state, as does the route comfort degree, apparently. Under this circumstance, travellers in the second group are supposed to shift to an alternative route whose surplus capacity is greater than that of the current route. In addition, the traffic flow will be stable in the equilibrium state where all route surplus capacities are the same and are equal to the maximum surplus capacity of the OD pair. This route shift behaviour is defined as route comfort choice behaviour, and the formed network equilibrium state is the quantity adjustment user equilibrium.

For the quantity adjustment use equilibrium, the route surplus capacities of all used routes between each OD pair are equal to the maximum surplus capacity and greater than (or equal to) the other routes with no flows. The corresponding equilibrium condition is given by

$$\begin{cases} f_w^r > 0, s_w^r\left(f_w^r\right) = v_w, \\ f_w^r = 0, s_w^r\left(f_w^r\right) \le v_w, \quad r \in R_w, w \in W. \end{cases} \tag{8}$$

3. Mixed Equilibrium Evolution

The traffic network travel information includes all alternative routes and their travel times, as well as the volume of traffic flow and degree of crowdedness. The route travel time is the rapidity indicator, while the route surplus capacity is used as the comfort indicator to represent the traffic volume and crowding degree of the network. Assuming that there are three groups of travellers in the network, the first group of travellers has complete travel information and obeys the route rapidity choice behaviour criterion, the second group has complete travel information and follows the route comfort choice behaviour criterion, and the third group chooses its routes in accordance with the logit-based route choice probability based on their incomplete travel information. The third group also behaves under the route rapidity decision criterion.

The multicriteria behaviour of the three groups of travellers affects the travel time and the distribution pattern of the traffic flow. The interaction between these traffic flows, caused by various travel decision behaviours, forms a new mixed equilibrium flow. To simulate the evolution trajectory of the mixed equilibrium flow toward the stable state, a day-to-day route flow adjustment process is presented as follows.

3.1. Route Adjustment Process Model. The proportion of travellers with complete information is denoted by α, in which travellers follow the route rapidity choice criterion represented by β, and the rest are assumed to choose the comfortable route rather than the shortest one. Hence, as the total traffic demand is denoted as D_w for the OD pair w, the travel demand of travellers in the first group is expressed as $d_w = \alpha\beta \cdot D_w$, the travel demand of travellers in the second group is denoted by $\overline{d}_w = \alpha(1-\beta) \cdot D_w$, and the travel demand of travellers in the third group is calculated by $\widehat{d}_w = (1-\alpha) \cdot D_w$.

The flows of travellers on route $r \in W$ in these groups are represented by f_w^r, $\overline{f}_w^r$, and $\widehat{f}_w^r$. These route flows are grouped into three vectors and can be expressed by

$$\begin{cases} \mathbf{f} = \left(f_w^r : w \in W, r \in R_w\right), \\ \overline{\mathbf{f}} = \left(\overline{f}_w^r : w \in W, r \in R_w\right), \\ \widehat{\mathbf{f}} = \left(\widehat{f}_w^r : w \in W, r \in R_w\right). \end{cases} \tag{9}$$

The traffic flow on link $a \in A$ is the aggregated link flow from both groups, which is

$$x_a = \sum_{w\in W}\sum_{r\in R_w} \delta_w^{ra}\left(f_w^r + \overline{f}_w^r + \widehat{f}_w^r\right), \quad a \in A. \tag{10}$$

Based on the general framework of the discrete day-to-day route flow dynamic model, the evolution process of the route flow from disequilibrium to the equilibrium state is presented as follows [27]:

$$\begin{pmatrix} \mathbf{f}^{(n+1)} \\ \overline{\mathbf{f}}^{(n+1)} \\ \widehat{\mathbf{f}}^{(n+1)} \end{pmatrix} = (1-\eta)\begin{pmatrix} \mathbf{f}^{(n)} \\ \overline{\mathbf{f}}^{(n)} \\ \widehat{\mathbf{f}}^{(n)} \end{pmatrix} + \eta\begin{pmatrix} \mathbf{y}^{(n)} \\ \overline{\mathbf{y}}^{(n)} \\ \widehat{\mathbf{y}}^{(n)} \end{pmatrix}, \tag{11}$$

where $(\mathbf{f}^{(n)}, \overline{\mathbf{f}}^{(n)}, \widehat{\mathbf{f}}^{(n)})$ is the route flow on day n, $(\mathbf{y}^{(n)}, \overline{\mathbf{y}}^{(n)}, \widehat{\mathbf{y}}^{(n)})^{\mathrm{T}}$ is the adjusted route flow on the next day $n+1$, and $\eta(0 \le \eta \le 1)$ is the route flow adjust ratio. Apparently, $(\mathbf{f}^{(n+1)}, \overline{\mathbf{f}}^{(n+1)}, \widehat{\mathbf{f}}^{(n+1)})^{\mathrm{T}}$, the route flow on day $n+1$, consists of two parts: the travellers who choose the current route, and the rest of the travellers, who shift to the alternative route. The existing models differ in their choices of target flows and adjustment ratios.

3.2. Excepted Route Flow. The adjusted route flow of first group $\mathbf{y}^{(n)}$ is given by the rational behavior adjustment process proposed (RBAP) by Yang and Zhang who assumed that a traveller's route adjustment mechanism urges the traveller to avoid shifts to a route whose travel cost is higher than the current cost. Thus, the aggregate travel cost of the system will decrease with the traveller's route adjustments. That is, with the dynamic evolution of traffic flow, the aggregate travel cost of the system will keep decreasing until it reaches an equilibrium state [2]. The mathematical expression of the rational behavior adjustment process is

$$\begin{cases} \Gamma \ne \phi, \dot{f}(t) \in \Gamma, \\ \Gamma \ne \phi, \dot{f}(t) = 0, \end{cases}$$
$$\Gamma = \left\{ z(t): \sum_{r\in R_w} z_w^r(t) = 0, c(t)^{\mathrm{T}} z(t) < 0 \right\}, \tag{12}$$

where $\dot{f}(t)$ denotes the derivative of the traffic flow with respect to time and Γ is the set of all feasible directions that can reduce the total travel time based on the current route travel time. $\mathbf{z}(t)$ is the vector of a slight change in the traffic flow. $\mathbf{c}(t)^{\mathrm{T}}\mathbf{z}(t) < 0$ indicates that in order to reduce their travel costs, travellers will make rational behavior decisions according to the traffic information of the route, which reduces the system travel time (see [2] for more details).

The travellers in the second group choose a travel route on the basis of the surplus capacity, and the route choice adjustment mechanism will encourage travellers to shift to the alternative route whose surplus capacity is higher than the current one. Travellers are assumed to make route choice decision in accordance with their current travel quantity information and their experienced expected travel comfort degree. To depict this quantity-oriented adjustment behavior, we assume that the expected route surplus capacity of travellers for w on day $n+1$, expressed as $\overline{\mathbf{v}}_w^{r,n+1}$, is the weighted sum of the expected route surplus capacity $\overline{\mathbf{v}}_w^r$ and the actual route surplus capacity $\mathbf{s}_w^{r,n}$ on day n. It is easy to see that travellers followed the route comfort choice behaviour criterion and adjusted their travel route based on the previous travel route surplus capacity in this study. Mathematically, this can be expressed as

$$\begin{aligned} \overline{\mathbf{v}}_w^{r,n+1} &= \rho \cdot \mathbf{s}_w^{r,n}(x) + (1-\rho).\overline{\mathbf{v}}_w^{r,n} \\ &= \rho \cdot \mathbf{s}_w^{r,n}(x) + (1-\rho)\cdot\left(\rho \cdot \mathbf{s}_w^{r,n-1}(x) + (1-\rho)\overline{\mathbf{v}}_w^{r,n-1}\right) \\ &= \rho \cdot \mathbf{s}_w^{r,n}(x) + (1-\rho)\cdot\left(\rho \cdot \mathbf{s}_w^{r,n-1}(x) + (1-\rho)^2\overline{\mathbf{v}}_w^{r,n-1}\right) \\ &= \cdots = \sum_{k=0}^{n} \rho\cdot(1-\rho)^k \cdot \mathbf{s}_w^{r,n-k}(x), \end{aligned} \tag{13}$$

where $\rho(0 < \rho \le 1)$ is the preference parameter that reflects the preference between actual route surplus capacity and expected route surplus capacity by travellers, and it is obvious that $s_w^r = \overline{v}_w$ holds if $\rho = 1$, which means that the equilibrium state is reached when all current route surplus capacities are equal to the expected surplus capacity, which is the maximum surplus capacity of the OD pair.

It is assumed that the travellers' behavior in the third group is a dynamic route adjustment behavior based on historical travel experience, where the predicted route travel cost of the travellers is a linear weight of the travellers' historical-experience travel costs, and the value of the weight decreases exponentially with time and distance. According to this assumption, the predicted travel time of route r on day $n+1$ of an OD pair can be expressed as the weighted sum of the predicted travel time and the actual travel time on day n [28].

$$\widetilde{\mathbf{c}}_w^{r,n+1} = (1-\kappa)\widetilde{\mathbf{c}}_w^{r,n} + \kappa\mathbf{c}_w^{r,n}(x^n). \tag{14}$$

It can be rewritten as

$$\widetilde{\mathbf{c}}_w^{r,n+1} = \sum_{l=0}^{n} \kappa(1-\kappa)^l \cdot \mathbf{c}_w^{r,n-l}, \tag{15}$$

where κ $(0 < \kappa \le 1)$ is the experience preference parameter, which reflects the memory decay characteristic of travellers with regard to historical travel experience information (see [28] for more details).

In conclusion, in order to depict the route adjustment behavior of the three groups of travellers, a rational-expected traffic flow assumption (REFA) is proposed based on the rational target flow assumption (RTFA) of Zhou et al. [22]. It is assumed that the expected traffic flow pattern of travellers in different groups is given by the optimal solution of the following minimization problem:

$$\min_{\mathbf{f}} \sum_{w\in W}\sum_{r\in R_w} \mathbf{c}_w^{r,n} \cdot f_w^r, \tag{16}$$

$$\min_{\overline{\mathbf{f}}} \sum_{w\in W}\sum_{r\in R_w} \left(\mathbf{v}_w^n\left(\overline{f}_w^r\right) - \mathbf{s}_w^{r,n}\left(\overline{f}_w^r\right)\right)\cdot \overline{f}_w^r, \tag{17}$$

$$\min_{\widehat{\mathbf{f}}} \sum_{w\in W}\sum_{r\in R_w} \widetilde{c}_w^{r,n}\cdot \widehat{f}_w^r + \frac{1}{\theta}\sum_{w\in W}\sum_{r\in R_w} \widehat{f}_w^r\cdot \ln \widehat{f}_w^r, \tag{18}$$

where equation (16) is the 0-1 assignment problem under a given route travel cost, indicating that travellers in the first group will choose the shortest route, which is subjected to the UE criterion. Equation (17) indicates that travellers from the second group will choose the route with the largest surplus capacity, and its optimal solution is attained in the quantity-adjusted user equilibrium state. Equation (18) is the classic logit-based stochastic assignment problem, where travellers will choose the route with the minimum perceived travel cost, and the expected traffic flow of the third group of travellers can be expressed as

$$\widehat{\mathbf{y}}_w^{r,n} = \widehat{\mathbf{d}}_w \cdot \widehat{\mathbf{p}}\left(\widetilde{c}_w^{r,n}, \theta\right). \tag{19}$$

It is easily seen from equation (18) that the REFA model is not characterized by a unique solution. Thus, multiple solutions may be obtained from the minimization problem (16)–(18), which inherits the multiple-evolution-trajectory problem (see [22] for more details).

4. Property Analysis

4.1. Equivalency. An equivalent linear programming model is demonstrated below to avoid the multiple-evolution-trajectory problem. The mixed equilibrium conditions $(\mathbf{f}^*, \overline{\mathbf{f}}^*, \widehat{\mathbf{f}}^*)^{\mathrm{T}}$ are the optimal solution of the following mixed-behaviour linear programming model:

$$\min_{\mathbf{f},\overline{\mathbf{f}},\widehat{\mathbf{f}}} Z(\mathbf{f},\overline{\mathbf{f}},\widehat{\mathbf{f}}) = \min_{(\mathbf{f},\overline{\mathbf{f}},\widehat{\mathbf{f}})} \begin{bmatrix} \mathbf{c}(\mathbf{f}) \\ -\mathbf{s}(\overline{\mathbf{f}}) \\ \widehat{\mathbf{c}}(\widehat{\mathbf{f}}) \end{bmatrix}^{\mathrm{T}} \begin{pmatrix} \mathbf{f} \\ \overline{\mathbf{f}} \\ \widehat{\mathbf{f}} \end{pmatrix}, \tag{20}$$

$$\Lambda\mathbf{f} - \mathbf{d} = 0, \tag{21}$$

$$\Lambda\overline{\mathbf{f}} - \overline{\mathbf{d}} = 0, \tag{22}$$

$$\Lambda\widehat{\mathbf{f}} - \widehat{\mathbf{d}} = 0, \tag{23}$$

$$\begin{aligned} \mathbf{f} &\geq 0, \\ \overline{\mathbf{f}} &\geq 0, \\ \widehat{\mathbf{f}} &\geq 0, \end{aligned} \tag{24}$$

where $Z(\mathbf{f},\overline{\mathbf{f}},\widehat{\mathbf{f}})$ is the comprehensive travel cost function, Λ is the OD-route incidence matrix, $\mathbf{c}(\mathbf{f})$ is the route travel time of the first group, $\mathbf{s}(\overline{\mathbf{f}})$ is the route surplus capacity of the second group, and $\widehat{\mathbf{c}}(\widehat{\mathbf{f}})$ denotes the modified route travel time concerned with individual memory recession and perception difference, which satisfies

$$\widehat{\mathbf{c}}(\widehat{\mathbf{f}}) = \mathbf{c}(\widehat{\mathbf{f}}) + \frac{1}{\theta}(\ln(\widehat{\mathbf{f}}) + I). \tag{25}$$

Proof. Clearly, the following necessary and sufficient optimality conditions for optimization problems (20)–(24) can be obtained according to the KKT (Karush–Kuhn–Tucker) optimality conditions:

$$\begin{bmatrix} \mathbf{c}(\mathbf{f}) - \Lambda\pi^* \\ \Lambda\overline{\pi}^* - \mathbf{s}(\overline{\mathbf{f}}) \\ \widehat{\mathbf{c}}(\widehat{\mathbf{f}}) - \Lambda\widehat{\pi}^* \end{bmatrix}^{\mathrm{T}} \begin{pmatrix} \mathbf{f} \\ \overline{\mathbf{f}} \\ \widehat{\mathbf{f}} \end{pmatrix} = 0, \tag{26}$$

$$\mathbf{c}(\mathbf{f}) - \Lambda\pi^* \geq 0, \tag{27}$$

$$\Lambda\overline{\pi}^* - \mathbf{s}(\overline{\mathbf{f}}) \geq 0, \tag{28}$$

$$\widehat{\mathbf{c}}(\widehat{\mathbf{f}}) - \Lambda\widehat{\pi}^* \geq 0, \tag{29}$$

$$\Lambda\mathbf{f} - \mathbf{d} = 0, \tag{30}$$

$$\Lambda\overline{\mathbf{f}} - \overline{\mathbf{d}} = 0, \tag{31}$$

$$\Lambda\widehat{\mathbf{f}} - \widehat{\mathbf{d}} = 0, \tag{32}$$

$$\begin{aligned} \mathbf{f} &\geq 0, \\ \overline{\mathbf{f}} &\geq 0, \\ \widehat{\mathbf{f}} &\geq 0, \end{aligned} \tag{33}$$

where π^*, $\overline{\pi}^*$, and $\widehat{\pi}^*$ are the optimal Lagrange multipliers corresponding to the flow conservation constraints shown in equations (21)–(23), respectively.

Since the route flow is strictly positive in the logit-based stochastic assignment model, which is $\widehat{f}_w^r > 0, r \in R_w$, then equation (26) becomes

$$\begin{bmatrix} \mathbf{c}(\mathbf{f}) - \Lambda\pi^* \\ \Lambda\overline{\pi}^* - \mathbf{s}(\overline{\mathbf{f}}) \end{bmatrix}^{\mathrm{T}} \begin{pmatrix} \mathbf{f} \\ \overline{\mathbf{f}} \end{pmatrix} = 0, \tag{34}$$

$$\widehat{\mathbf{c}}(\widehat{\mathbf{f}}) - \Lambda\widehat{\pi}^* = 0. \tag{35}$$

Combining equations (27), (28), and (34), we obtain

$$\begin{cases} \mathbf{f} > 0, & \mathbf{c}(\mathbf{f}) = \Lambda\pi^*, \\ \mathbf{f} = 0, & \mathbf{c}(\mathbf{f}) \geq \Lambda\pi^*, \end{cases} \tag{36}$$

$$\begin{cases} \overline{\mathbf{f}} > 0, & \mathbf{s}(\mathbf{f}) = \Lambda\overline{\pi}^*, \\ \overline{\mathbf{f}} = 0, & \mathbf{s}(\mathbf{f}) \leq \Lambda\overline{\pi}^*. \end{cases} \tag{37}$$

Therefore, the multipliers π^* and $\overline{\pi}^*$ signify the minimum route travel time and the maximum route surplus capacity, respectively.

Substituting equations (25) into (35), we have

$$\begin{aligned} \widehat{\mathbf{f}} &= \exp\left(-\theta\left(\mathbf{c} - \widehat{\pi}^*\right) - 1\right), \\ \widehat{f}_w^r &= \frac{\exp\left(-\theta c_w^r\right)}{\sum_{k\in R_w}\exp\left(-\theta c_w^r\right)}\widehat{d}_w, \quad r \in R_w. \end{aligned} \tag{38}$$

It can be seen that equations (36)–(38) are actually the equilibrium conditions of the travellers in the three groups. □

4.2. Uniqueness. Based on the variational inequality (VI) theory, it is clear that a route flow pattern $(\mathbf{f}^*, \overline{\mathbf{f}}^*, \widehat{\mathbf{f}}^*)^{\mathrm{T}}$ is a solution to the equivalent linear programming problem in (20)–(24) if and only if it solves the following VI problem:

$$\nabla Z\left(\mathbf{f}^*, \overline{\mathbf{f}}^*, \widehat{\mathbf{f}}^*\right)^{\mathrm{T}} \cdot \begin{pmatrix} \mathbf{f} - \mathbf{f}^* \\ \overline{\mathbf{f}} - \overline{\mathbf{f}}^* \\ \widehat{\mathbf{f}} - \widehat{\mathbf{f}}^* \end{pmatrix} = \begin{bmatrix} \mathbf{c}\left(\mathbf{f}^*, \overline{\mathbf{f}}^*, \widehat{\mathbf{f}}^*\right) \\ -\mathbf{s}\left(\mathbf{f}^*, \overline{\mathbf{f}}^*, \widehat{\mathbf{f}}^*\right) \\ \widehat{\mathbf{c}}\left(\mathbf{f}^*, \overline{\mathbf{f}}^*, \widehat{\mathbf{f}}^*\right) \end{bmatrix}^{\mathrm{T}} \begin{pmatrix} \mathbf{f} - \mathbf{f}^* \\ \overline{\mathbf{f}} - \overline{\mathbf{f}}^* \\ \widehat{\mathbf{f}} - \widehat{\mathbf{f}}^* \end{pmatrix} \geq 0. \tag{39}$$

This can be rewritten as follows:

$$\begin{aligned} &Z(\mathbf{f}(n), \overline{\mathbf{f}}(n), \widehat{\mathbf{f}}(n)) - Z\left(\mathbf{f}^*, \overline{\mathbf{f}}^*, \widehat{\mathbf{f}}^*\right) \\ &= \begin{bmatrix} \mathbf{c}\left(\mathbf{f}^*, \overline{\mathbf{f}}^*, \widehat{\mathbf{f}}^*\right) \\ -\mathbf{s}\left(\mathbf{f}^*, \overline{\mathbf{f}}^*, \widehat{\mathbf{f}}^*\right) \\ \widehat{\mathbf{c}}\left(\mathbf{f}^*, \overline{\mathbf{f}}^*, \widehat{\mathbf{f}}^*\right) \end{bmatrix}^{\mathrm{T}} \begin{pmatrix} \mathbf{f}(n) - \mathbf{f}^* \\ \overline{\mathbf{f}}(n) - \overline{\mathbf{f}}^* \\ \widehat{\mathbf{f}}(n) - \widehat{\mathbf{f}}^* \end{pmatrix} \geq 0. \end{aligned} \tag{40}$$

It can be readily seen that $(\mathbf{f}^*, \overline{\mathbf{f}}^*, \widehat{\mathbf{f}}^*)^{\mathrm{T}}$ is the extreme point of $Z(\mathbf{f}, \overline{\mathbf{f}}, \widehat{\mathbf{f}})$, which means that $(\mathbf{f}^*, \overline{\mathbf{f}}^*, \widehat{\mathbf{f}}^*)^{\mathrm{T}}$ is the mixed equilibrium route flow pattern. The comprehensive travel cost achieves its minimum $Z(\mathbf{f}^*, \overline{\mathbf{f}}^*, \widehat{\mathbf{f}}^*)$ and cannot be further reduced. Since $Z(\mathbf{f}, \overline{\mathbf{f}}, \widehat{\mathbf{f}})$ is a monotonically increasing function of route flow $(\mathbf{f}, \overline{\mathbf{f}}, \widehat{\mathbf{f}})$, it can be concluded that $(\mathbf{f}^*, \overline{\mathbf{f}}^*, \widehat{\mathbf{f}}^*)^{\mathrm{T}}$ is the optimal solution to the linear programming problem in equations (20)–(24).

4.3. Stability of Solution. Suppose that $(\mathbf{f}^*, \overline{\mathbf{f}}^*, \widehat{\mathbf{f}}^*)^{\mathrm{T}}$ and $(\mathbf{f}, \overline{\mathbf{f}}, \widehat{\mathbf{f}})^{\mathrm{T}}$ satisfy the VI problem (39). Then, we have

$$\begin{aligned} &\nabla Z^*\left(\mathbf{f}^*, \overline{\mathbf{f}}^*, \widehat{\mathbf{f}}^*\right)^{\mathrm{T}} \cdot \begin{pmatrix} \mathbf{f}' - \mathbf{f}^* \\ \overline{\mathbf{f}}' - \overline{\mathbf{f}}^* \\ \widehat{\mathbf{f}}' - \widehat{\mathbf{f}}^* \end{pmatrix} \\ &= \begin{bmatrix} \mathbf{c}\left(\mathbf{f}^*, \overline{\mathbf{f}}^*, \widehat{\mathbf{f}}^*\right) \\ -\mathbf{s}\left(\mathbf{f}^*, \overline{\mathbf{f}}^*, \widehat{\mathbf{f}}^*\right) \\ \widehat{\mathbf{c}}\left(\mathbf{f}^*, \overline{\mathbf{f}}^*, \widehat{\mathbf{f}}^*\right) \end{bmatrix}^{\mathrm{T}} \begin{pmatrix} \mathbf{f}' - \mathbf{f}^* \\ \overline{\mathbf{f}}' - \overline{\mathbf{f}}^* \\ \widehat{\mathbf{f}}' - \widehat{\mathbf{f}}^* \end{pmatrix} \geq 0, \end{aligned} \tag{41}$$

$$\nabla Z(\mathbf{f}, \overline{\mathbf{f}}, \widehat{\mathbf{f}})^{\mathrm{T}} \cdot \begin{pmatrix} \mathbf{f}' - \mathbf{f} \\ \overline{\mathbf{f}}' - \overline{\mathbf{f}} \\ \widehat{\mathbf{f}}' - \widehat{\mathbf{f}} \end{pmatrix} = \begin{bmatrix} \mathbf{c}(\mathbf{f}, \overline{\mathbf{f}}, \widehat{\mathbf{f}}) \\ -\mathbf{s}(\mathbf{f}, \overline{\mathbf{f}}, \widehat{\mathbf{f}}) \\ \widehat{\mathbf{c}}(\mathbf{f}, \overline{\mathbf{f}}, \widehat{\mathbf{f}}) \end{bmatrix}^{\mathrm{T}} \begin{pmatrix} \mathbf{f}' - \mathbf{f} \\ \overline{\mathbf{f}}' - \overline{\mathbf{f}} \\ \widehat{\mathbf{f}}' - \widehat{\mathbf{f}} \end{pmatrix} \geq 0. \tag{42}$$

Rewriting equation (41) for $(\mathbf{f}', \overline{\mathbf{f}}', \widehat{\mathbf{f}}')^T = (\mathbf{f}, \overline{\mathbf{f}}, \widehat{\mathbf{f}})^T$ and equation (42) for $(\mathbf{f}', \overline{\mathbf{f}}', \widehat{\mathbf{f}}')^T = (\mathbf{f}^*, \overline{\mathbf{f}}^*, \widehat{\mathbf{f}}^*)^T$ and adding the resulting inequalities, then

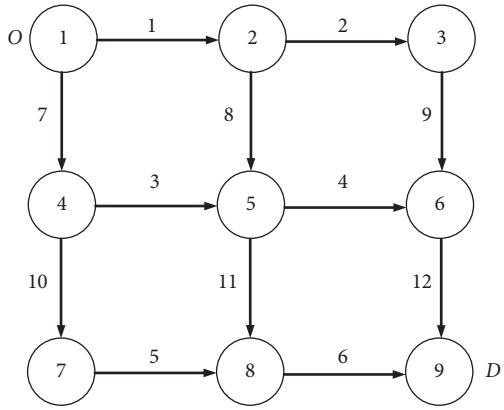

Figure 1: Test traffic network.

Table 1: Link-route incidence matrix.

$$\Delta^T = \begin{bmatrix} 1 & 1 & 0 & 0 & 0 & 0 & 0 & 0 & 1 & 0 & 0 & 1 \\ 1 & 0 & 0 & 1 & 0 & 0 & 0 & 1 & 0 & 0 & 0 & 1 \\ 1 & 0 & 0 & 0 & 0 & 1 & 0 & 1 & 0 & 0 & 1 & 0 \\ 0 & 0 & 1 & 1 & 0 & 0 & 1 & 0 & 0 & 0 & 0 & 1 \\ 0 & 0 & 1 & 0 & 0 & 1 & 1 & 0 & 0 & 0 & 1 & 0 \\ 0 & 0 & 0 & 0 & 1 & 1 & 1 & 0 & 0 & 1 & 0 & 0 \end{bmatrix}$$

Table 2: Parameters in link travel time functions.

Link	t_a^0	c_a
1	8	60
2	16	60
3	10	80
4	8	60
5	8	40
6	10	40
7	14	60
8	14	80
9	8	60
10	10	80
11	8	40
12	8	60

$$\begin{aligned} \Delta F(t) \cdot \Delta(t) &= \left[\nabla Z^*\left(\mathbf{f}^*, \overline{\mathbf{f}}^*, \widehat{\mathbf{f}}^*\right)^{\mathrm{T}} - \nabla Z(\mathbf{f}, \overline{\mathbf{f}}, \widehat{\mathbf{f}})^{\mathrm{T}}\right] \cdot \begin{pmatrix} \mathbf{f}^* - \mathbf{f} \\ \overline{\mathbf{f}}^* - \overline{\mathbf{f}} \\ \widehat{\mathbf{f}}^* - \widehat{\mathbf{f}} \end{pmatrix} \\ &= \begin{bmatrix} \mathbf{c}\left(\mathbf{f}^*, \overline{\mathbf{f}}^*, \widehat{\mathbf{f}}^*\right) - \mathbf{c}(\mathbf{f}, \overline{\mathbf{f}}, \widehat{\mathbf{f}}) \\ \mathbf{s}(\mathbf{f}, \overline{\mathbf{f}}, \widehat{\mathbf{f}}) - \mathbf{s}\left(\mathbf{f}^*, \overline{\mathbf{f}}^*, \widehat{\mathbf{f}}^*\right) \\ \widehat{\mathbf{c}}\left(\mathbf{f}^*, \overline{\mathbf{f}}^*, \widehat{\mathbf{f}}^*\right) - \widehat{\mathbf{c}}(\mathbf{f}, \overline{\mathbf{f}}, \widehat{\mathbf{f}}) \end{bmatrix}^{\mathrm{T}} \cdot \begin{pmatrix} \mathbf{f}^* - \mathbf{f} \\ \overline{\mathbf{f}}^* - \overline{\mathbf{f}} \\ \widehat{\mathbf{f}}^* - \widehat{\mathbf{f}} \end{pmatrix} \leq 0. \end{aligned} \tag{43}$$

4.4. Algorithm

Step 1 (initialization): let $n = 0$. Set the model parameters $\alpha, \beta, \eta, \rho, \kappa$, and θ and the convergence

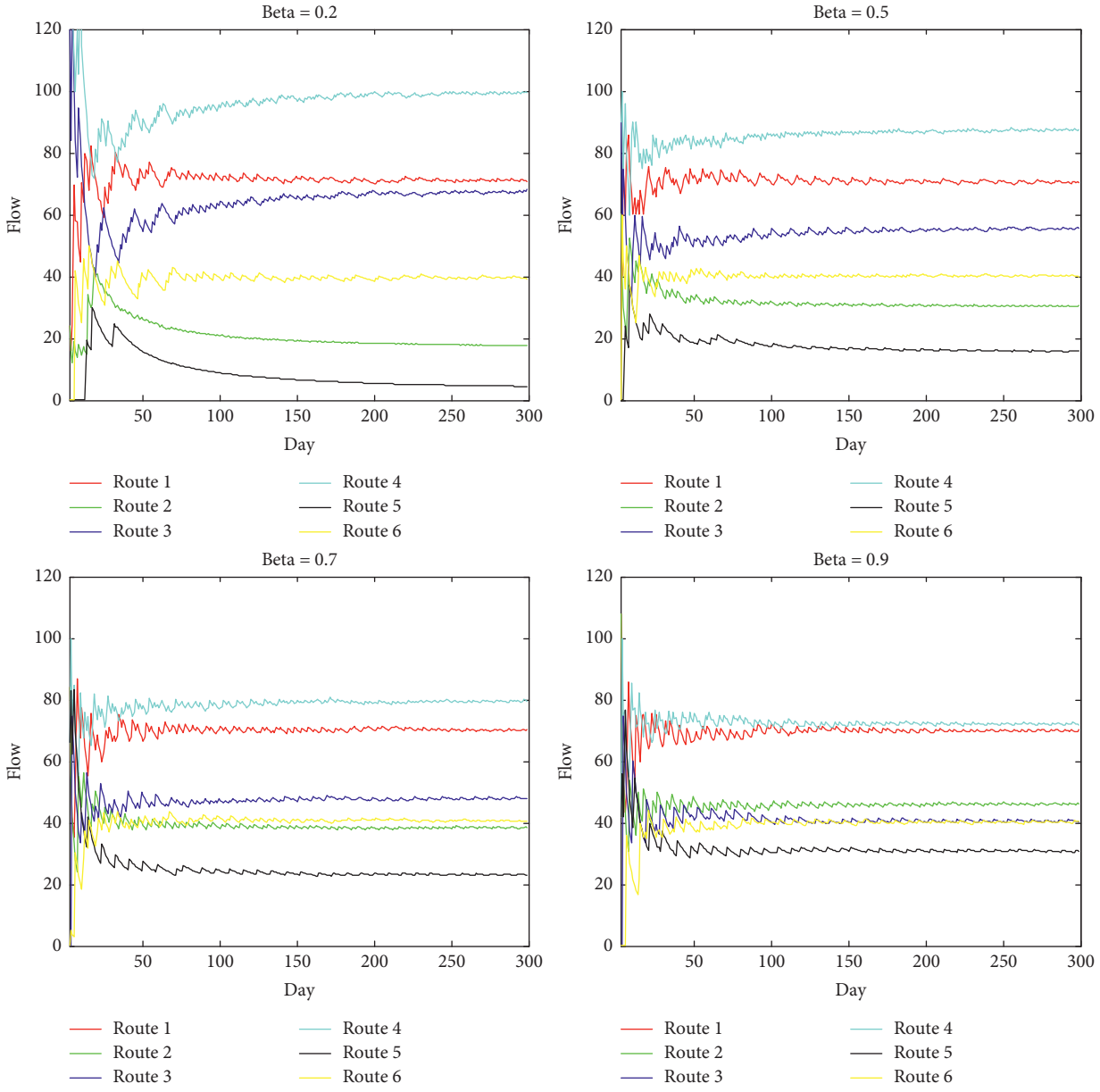

Figure 2: Flow evolution of test traffic network with different quantity adjustment ratios.

Table 3: Route flow and cost in equilibrium.

Route	Link	f	c
1	1, 2, 9, 12	78	218
2	1, 4, 8, 12	1	221
3	1, 6, 8, 11	79	218
4	3, 4, 7, 12	106	218
5	3, 6, 7, 11	1	226
6	5, 6, 7, 10	35	218

parameter ε. Input the link-route incidence matrix Δ, all-one matrix I, and the OD demand D.

Step 2: make an initial allocation. Solve the traffic flow assignment problem by using the shortest route loading method and 0-1 assignment based on the route surplus capacity and logit stochastic assignment method for the three groups of travellers. Hence, get the initial route flow pattern $f^{(0)}, \overline{f}^{(0)}$, and $\widehat{f}^{(0)}$.

Step 3: calculate the route flow $F^{(n)} = f^{(n)} + \overline{f}^{(n)} + \widehat{f}^{(n)}$, the link flow $x_a^{(n)} = \Delta' f^{(n)}$, and the link travel time by the BPR (Bureau of Public Roads) function. Update the route travel time, route surplus capacity, and perceived route travel time according to equations (1), (7), and (25).

Step 4: update the adjustment route flows $y^{(n)}, \overline{y}^{(n)}$, and $\widehat{y}^{(n)}$ in accordance with equations (16)–(18).

Step 5: Reassign the traffic route flow based on equation (11).

Step 6 (convergence examination): terminate the iteration and output the route flow pattern $f^{(n+1)}$,

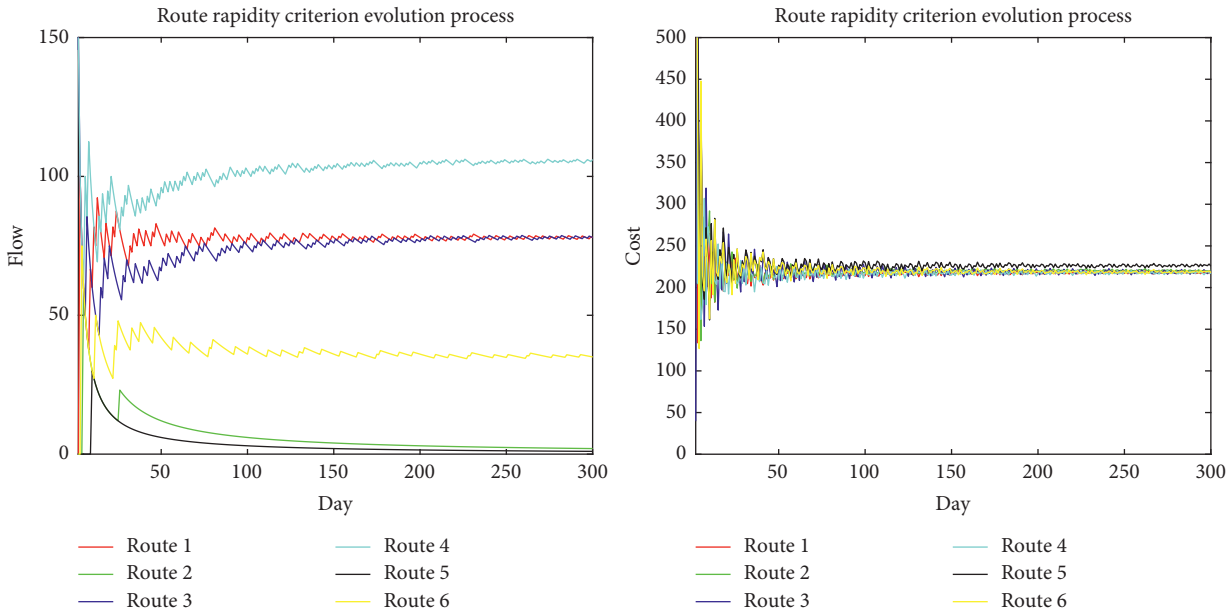

Figure 3: Evolutionary trajectories of route flows.

Table 4: Route flow and cost in equilibrium.

Route	Link	$\overline{f}$	s
1	1, 2, 9, 12	50	10
2	1, 4, 8, 12	50	10
3	1, 6, 8, 11	30	10
4	3, 4, 7, 12	50	10
5	3, 6, 7, 11	30	10
6	5, 6, 7, 10	30	10

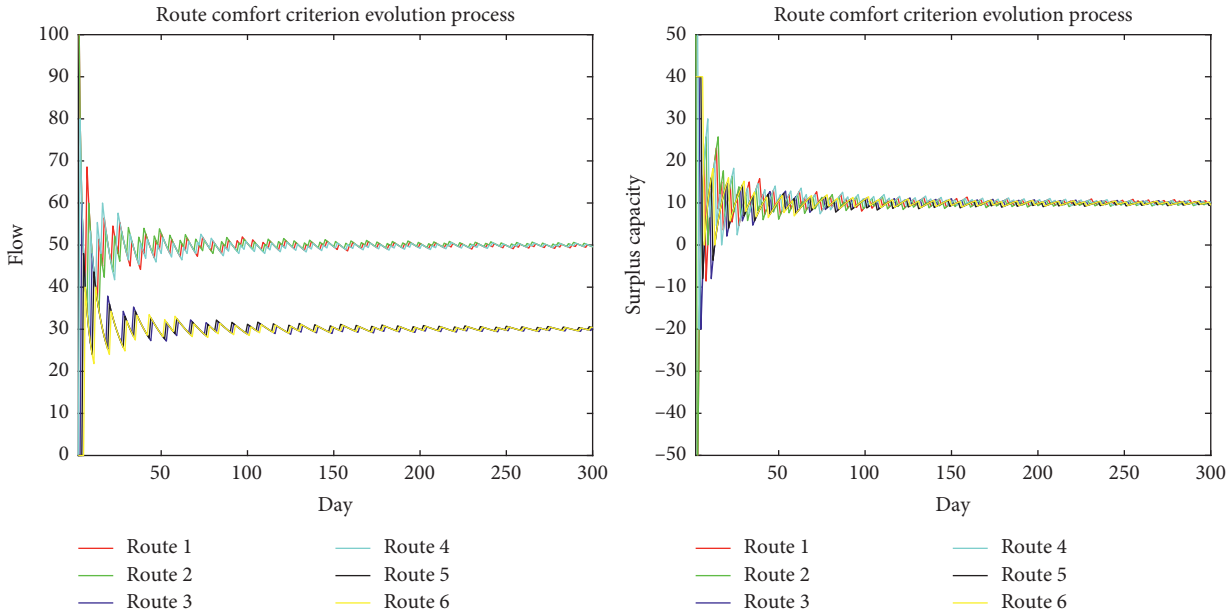

Figure 4: Evolutionary trajectories of route flows.

Table 5: Route flow and cost in mixed equilibrium for travellers in the first group.

Route	Link	f	c
1	1, 2, 9, 12	27	217
2	1, 4, 8, 12	0	226
3	1, 6, 8, 11	34	217
4	3, 4, 7, 12	38	217
5	3, 6, 7, 11	0	220
6	5, 6, 7, 10	21	217

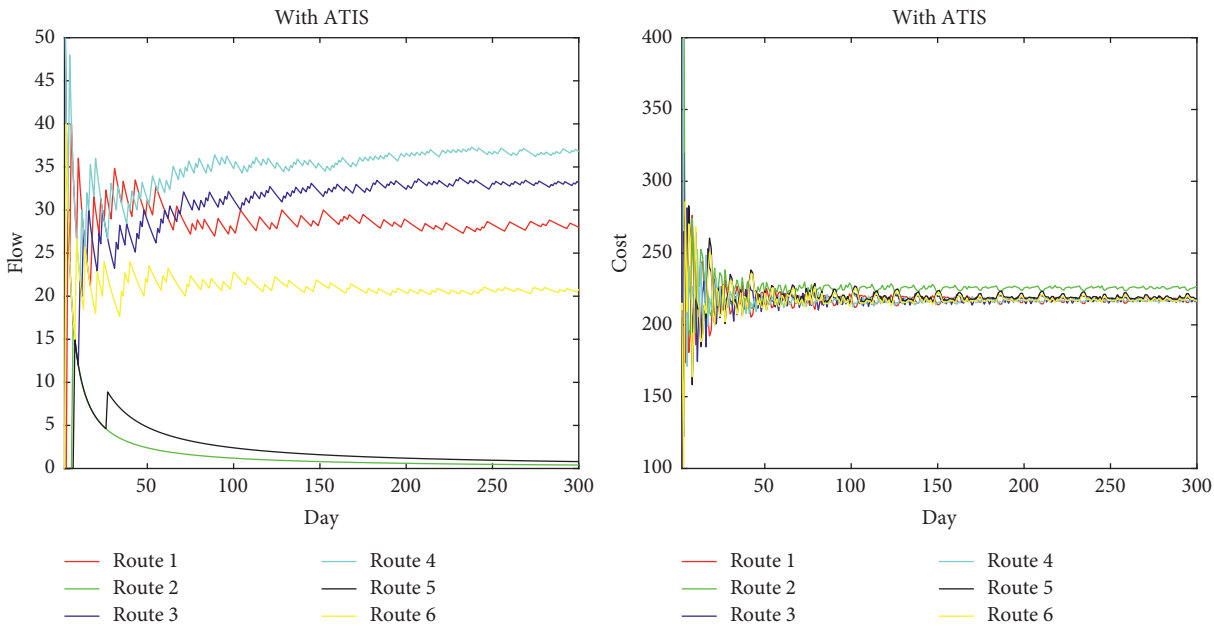

Figure 5: Evolutionary trajectories of route flows (a) and route travel costs (b) for travellers in the first group.

Table 6: Route flow and surplus capacity in mixed equilibrium for travellers in the second group.

Route	Link	$\overline{f}$	s
1	1, 2, 9, 12	30	30
2	1, 4, 8, 12	30	30
3	1, 6, 8, 11	10	30
4	3, 4, 7, 12	30	30
5	3, 6, 7, 11	10	30
6	5, 6, 7, 10	10	30

$\overline{f}^{(n+1)}$, and $\widehat{f}^{(n+1)}$. if $|(f^{(n+1)} - f^{(n)})/f^{(n+1)}| \le \varepsilon \cap |(\overline{f}^{(n+1)} - \overline{f}^{(n)})/\overline{f}^{(n+1)}| \le \varepsilon \cap |(\widehat{f}^{(n+1)} - \widehat{f}^{(n)})/\widehat{f}^{(n+1)}| \le \varepsilon$ holds. Otherwise, let $n = n + 1$, and go to Step 2.

5. Numerical Experiments

5.1. Proportion of Route Comfort Behaviour. In this subsection, we study the effects of the comfort criterion ratio on the traffic flow of each route in a network under the multicriteria behavior, where the tested network is shown in Figure 1. The incidence matrix of routes and links for the network is tabulated in Table 1, and a simplified link travel time function that is often used in practice is the equation developed by the U.S. BPR (Bureau of Public Roads), with free-flow travel time and link capacity given in Table 2.

$$t_a(x_a) = t_a^0\left[1 + 0.15\left(\frac{x_a}{c_a}\right)^4\right], \quad \forall a \in A. \tag{44}$$

The traffic demand pattern between the OD pairs is assumed to be $d = 300$. Assume that 80% of the travellers are equipped with complete information. The dispersion parameter θ is set to be 1, and the route adjustment flow ratio $\eta = 1/n$.

As we stated above, β represents the proportion of travellers who follow the route comfort behavior criterion. Keeping the other parameters constant, the route flow evolution trajectories in the test network are depicted in Figure 2 when β is set to 20%, 50%, 70%, and 90%. This shows that a larger β will make the corresponding trajectory smoother and steadier and the fluctuation smaller. This

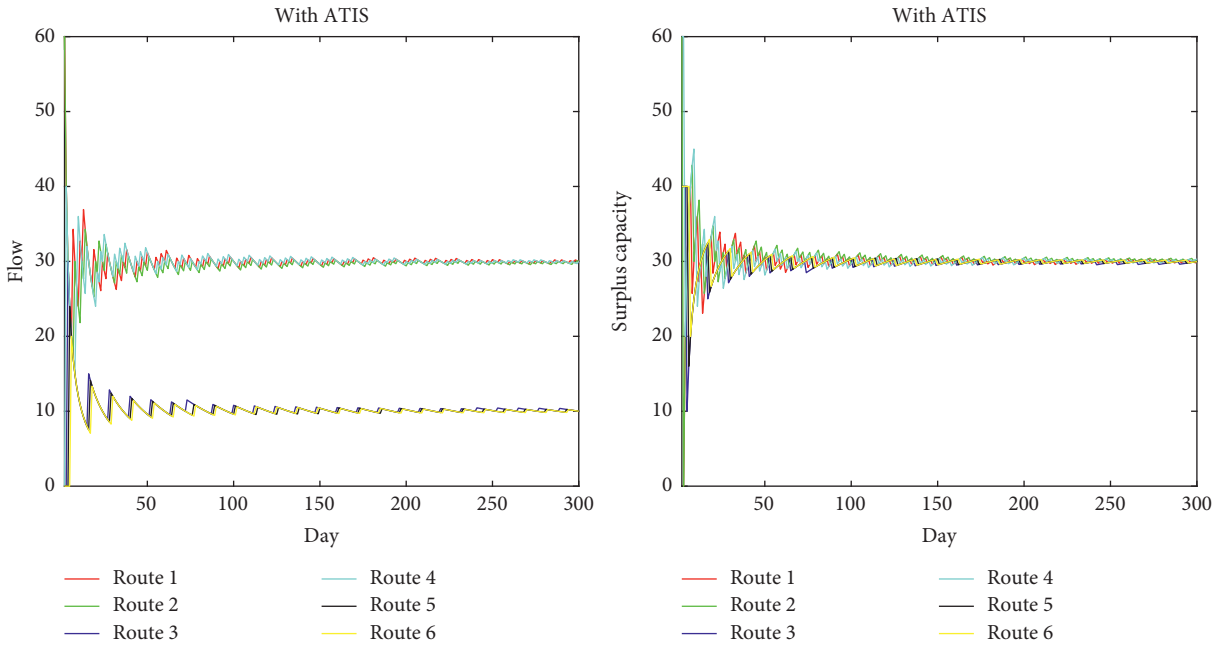

Figure 6: Evolutionary trajectories of route flows (a) and route surplus capacity (b) for travellers in the second group.

Table 7: Route flow and perceived cost in mixed equilibrium for travellers in the third group.

Route	Link	$\widehat{f}$	$\widehat{c}$
1	1, 2, 9, 12	14	224
2	1, 4, 8, 12	2	225
3	1, 6, 8, 11	13	225
4	3, 4, 7, 12	15	224
5	3, 6, 7, 11	5	226
6	5, 6, 7, 10	11	226

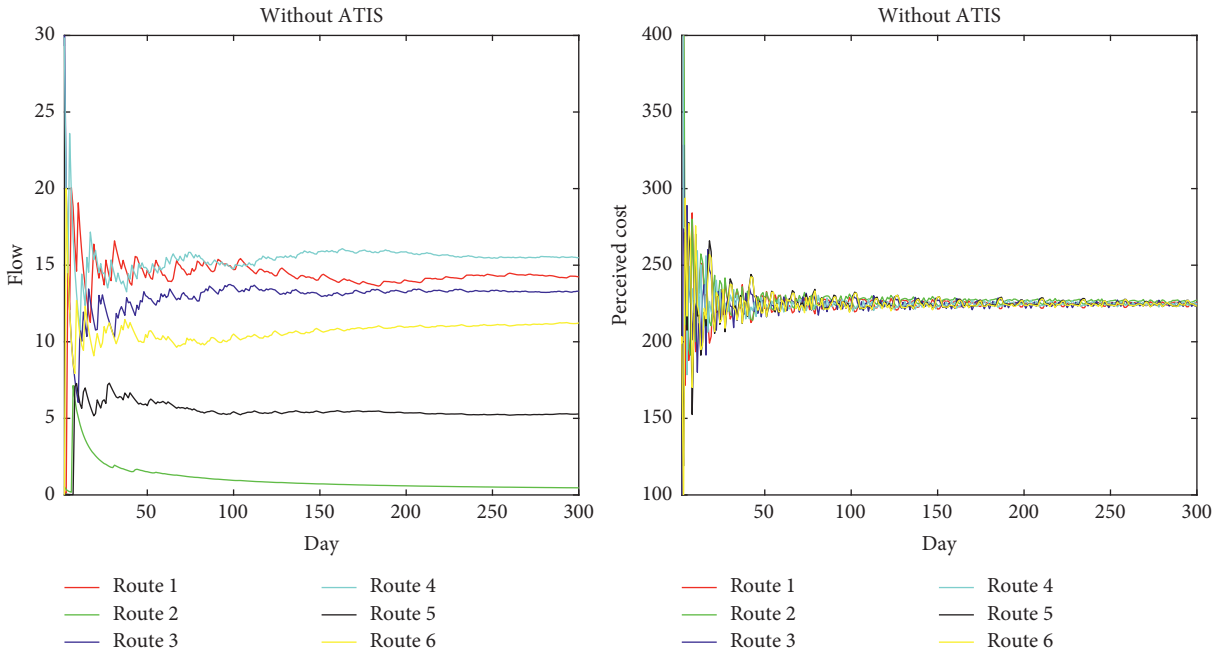

Figure 7: Evolutionary trajectories of route flows (a) and perceived travel costs (b) for travellers in the third group.

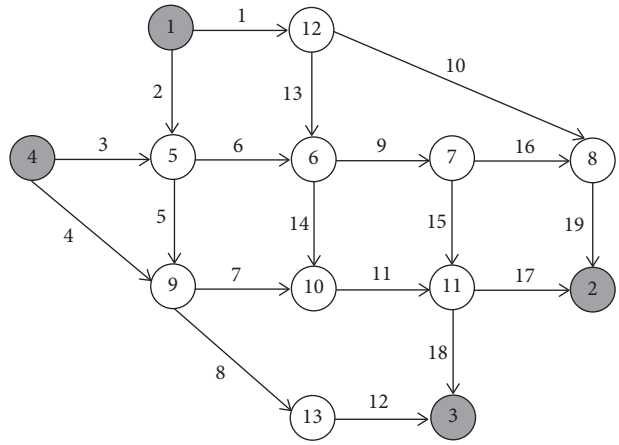

Figure 8: Test traffic network.

Table 8: Parameters in link travel time functions.

Link no.	1	2	3	4	5	6	7	8	9	10	11	12	13	14	15	16	17	18	19
t_a	6	5	6	7	6	8	5	10	11	16	12	8	6	7	5	9	10	8	5
c_a	200	200	150	200	100	100	150	150	200	100	200	150	150	100	250	200	150	200	100

Table 9: OD-route-link incidence matrix.

OD	Route	Link
(1, 2)	1	1, 10, 19
	2	2, 6, 9, 16, 19
	3	2, 6, 9, 15, 17
	4	2, 6, 14, 11, 17
	5	2, 5, 7, 11, 17
	6	1, 13, 9, 16, 19
	7	1, 13, 9, 15, 17
	8	1, 13, 14, 11, 17
(1, 3)	9	2, 5, 8, 12
	10	2, 6, 9, 15, 18
	11	2, 6, 14, 11, 18
	12	2, 5, 7, 11, 18
	13	1, 13, 9, 15, 18
	14	1, 13, 14, 11, 18
(4, 3)	15	4, 7, 11, 17
	16	3, 6, 9, 16, 19
	17	3, 6, 9, 15, 17
	18	3, 6, 14, 11, 17
	19	3, 5, 7, 11, 17
(4, 2)	20	4, 8, 12
	21	4, 7, 11, 18
	22	3, 5, 8, 12
	23	3, 6, 9, 15, 18
	24	3, 6, 14, 11, 18
	25	3, 5, 7, 11, 18

Table 10: Route flow and cost in mixed equilibrium for travellers in the first group.

OD	Route	f	c
(1, 2)	1	120	110
	2	0	114
	3	0	114
	4	0	116
	5	0	114
	6	0	114
	7	0	114
	8	0	116
(1, 3)	9	65	82
	10	3	82
	11	0	84
	12	0	83
	13	52	82
	14	0	84
(4, 3)	15	73	117
	16	37	117
	17	10	117
	18	0	119
	19	0	118
(4, 2)	20	109	85
	21	0	86
	22	11	85
	23	0	86
	24	0	87
	25	0	86

means that with an increase in the number of travellers who choose the travel route in accordance with the route comfort degree during the evolution process, which is reflected as a larger route surplus capacity in this study, the influence of the route travel cost decreases.

5.2. Single-Criterion Adjustment Evolution Process Research. The traffic demand pattern between the OD pairs is assumed to be $d = 300$. Assume that all travellers are equipped with complete information, and none of them follow the route

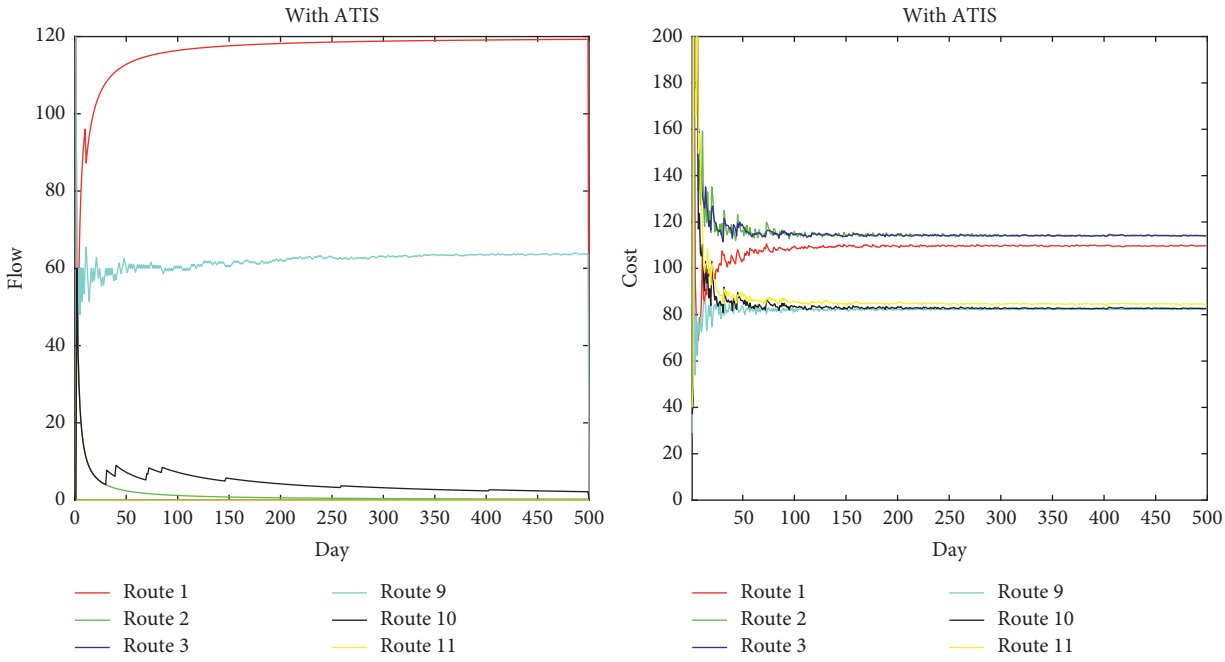

Figure 9: Evolutionary trajectories of route flows (a) and route travel costs (b) for travellers in the first group.

comfort decision behaviour criterion, the route adjustment flow ratio $\eta = 1/n$. Under this condition, all travellers with complete information choose the shortest route following the route rapidity behaviour criterion, forming a single UE equilibrium state. The route flow pattern and correspondent route travel time in the single UE equilibrium state are tabulated in Table 3, while Figure 3 shows the single rapidity criterion adjustment evolution process that converges to the UE equilibrium state after a fluctuant period.

The traffic demand pattern between the OD pairs is assumed to be $d = 240$. Assume that all travellers are equipped with complete information, and all of them follow the route comfort decision behaviour criterion, the route adjustment flow ratio $\eta = 1/n$. Under this condition, all travellers choose the most comfortable route following the route comfort behaviour criterion with complete information forms a single QUE equilibrium state. The route flow pattern and correspondent route travel time in the single QUE equilibrium state are tabulated in Table 4, while Figure 4 shows the single comfort criterion adjustment evolution process that converges to the QUE equilibrium state after a fluctuant period.

5.3. Mixed Equilibrium Evolution Process Research. In this section, numerical examples are presented to illustrate the application of the proposed route flow dynamic evolution model. The traffic demand pattern between the OD pairs is assumed to be $d = 300$. Assume that 80% of the travellers are equipped with complete information, and 50% of them follow the route comfort decision behaviour criterion. The dispersion parameter θ is set to be 0.5, and the route adjustment flow ratio is set to be $\eta = 1/n$.

Table 11: Route flow and surplus capacity in mixed equilibrium for travellers in the second group.

OD	Route	$\overline{f}$	s
(1, 2)	1	9	91
	2	9	91
	3	9	91
	4	9	91
	5	9	91
	6	9	91
	7	59	91
	8	9	91
(1, 3)	9	12	88
	10	12	88
	11	12	88
	12	12	88
	13	62	88
	14	12	88
(4, 3)	15	64	86
	16	14	86
	17	14	86
	18	14	86
	19	14	86
(4, 2)	20	53	97
	21	53	97
	22	3	97
	23	3	97
	24	3	97
	25	3	97

The route flow pattern and correspondent route travel time in the mixed equilibrium state for travellers in the first group are tabulated in Table 5, while Figure 5 shows the specific evolution process wherein the traffic flow gradually converges to the equilibrium state after a fluctuant period.

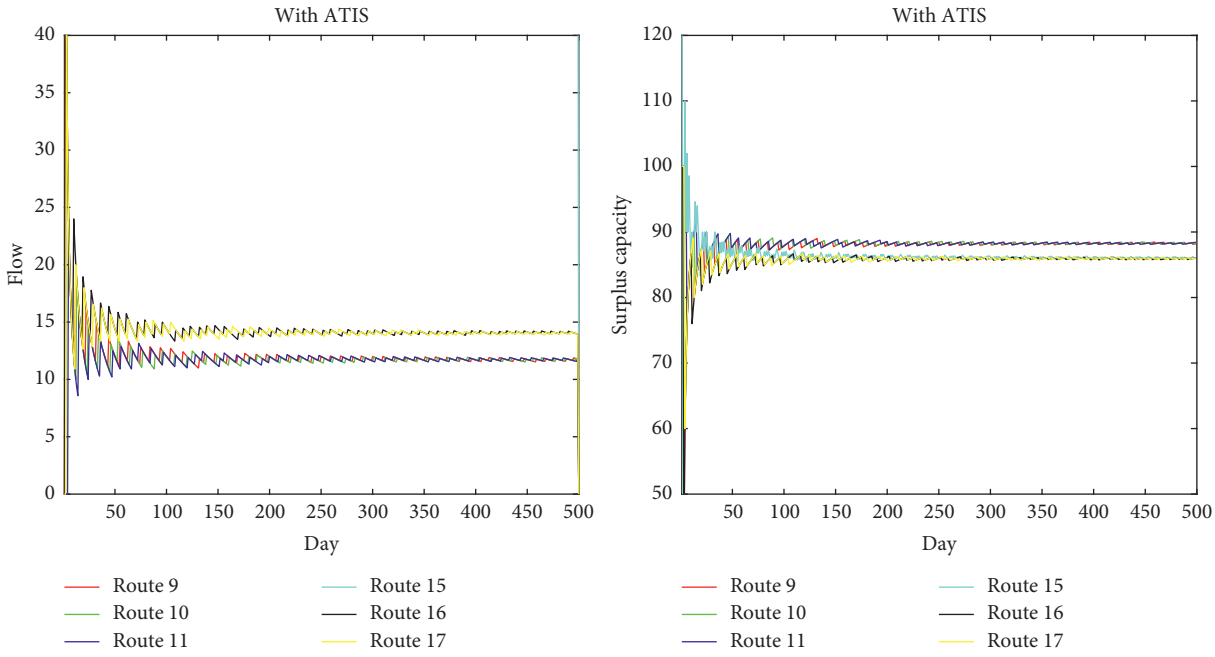

Figure 10: Evolutionary trajectories of route flows (a) and route surplus capacity (b) for travellers in the second group.

Table 12: Route flow and perceived cost in mixed equilibrium for travellers in the third group.

OD	Route	$\widehat{f}$	$\widehat{c}$
(1, 2)	1	50	114
	2	1	114
	3	2	114
	4	1	115
	5	1	114
	6	3	114
	7	1	115
	8	1	115
(1, 3)	9	20	86
	10	10	86
	11	1	86
	12	9	86
	13	18	86
	14	2	86
(4, 3)	15	19	120
	16	15	120
	17	12	120
	18	2	120
	19	12	120
(4, 2)	20	21	89
	21	10	89
	22	13	89
	23	8	89
	24	1	89
	25	7	89

The above observation indicates that travellers in first group will evolve to a UE state, in which the travel costs of all used routes between the same OD pairs are equal and minimal.

Meanwhile, the route flow pattern and correspondent route surplus capacity in the mixed equilibrium state for travellers in the second group are tabulated in Table 6, while Figure 6 shows the specific evolution process in which the traffic flow gradually converges to the equilibrium state after a fluctuant period. The above observation indicates that travellers in the second group will evolve to a quantity-adjusted user equilibrium state in which the route surplus capacities of all used routes between the same OD pairs are equal and maximum.

The route flow pattern and perceived route travel time in the mixed equilibrium state for travellers in the third group are tabulated in Table 7, while Figure 7 shows the specific evolution process wherein the traffic flow gradually converges to the equilibrium state after a fluctuant period. The above observation indicates that travellers in the third group will evolve to an SUE state where no travellers can unilaterally change routes to reduce his/her perceived travel costs.

To better analyse the performance of the proposed mixed equilibrium route flow dynamic model, a network is shown in Figure 8 [29]. The link travel time functions follow the BPR form, with the free-flow travel time and link capacity given in Table 8. The incidence matrix of routes and links for the network are tabulated in Table 9. The traffic demand pattern between the four OD pairs is assumed to be $(\overline{d}_{12}, \overline{d}_{13}, \overline{d}_{42}, \overline{d}_{42}) = (300, 300, 300, 300)$, the parameter θ is set to be 1, $\alpha = 80\%$, and $\beta = 50\%$. The route adjustment flow ratio is $\eta = 1/n$ to guarantee the convergence.

The route flow pattern and corresponding route travel time in mixed equilibrium state for travellers in the first group are tabulated in Table 10, while Figure 9 shows the specific evolution trajectories. The route flow pattern and correspondent route surplus capacity in the mixed equilibrium state for travellers in the second group are tabulated in Table 11, while Figure 10 shows the specific evolution process. The route flow pattern and perceived route travel

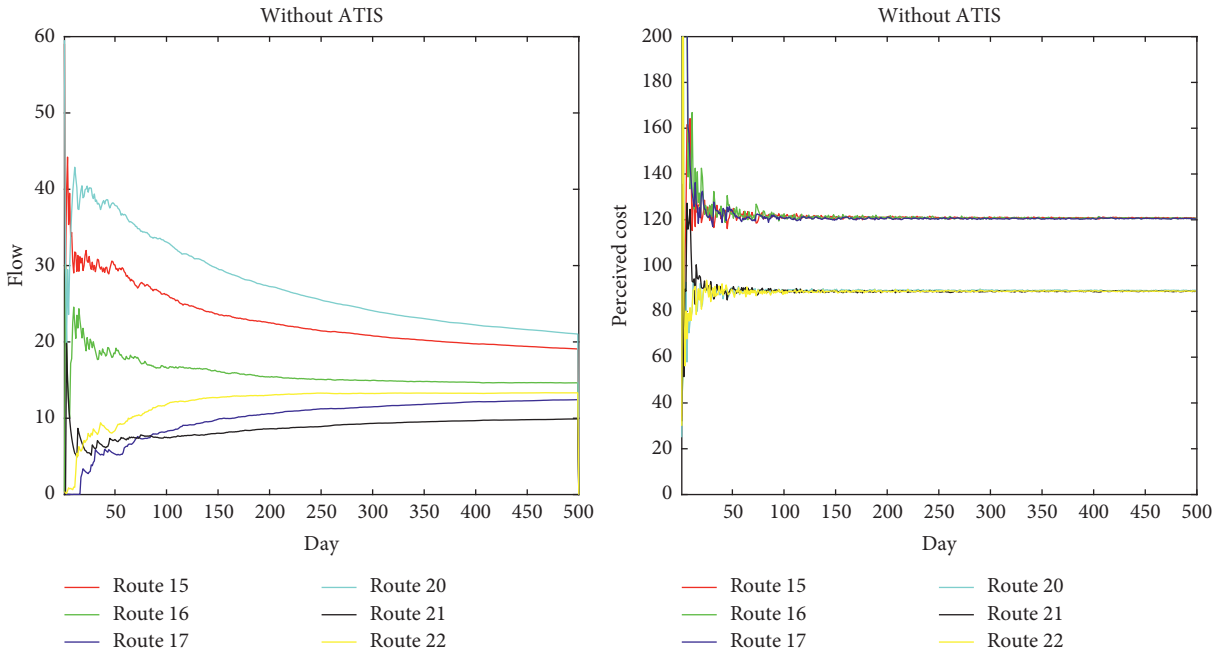

Figure 11: Evolutionary trajectories of route flows (a) and perceived travel costs (b) for travellers in the third group.

time in the mixed equilibrium state for travellers in the third group are tabulated in Table 12, while Figure 11 shows the specific evolution trajectories.

Clearly, from the above results, we can observe that traffic flows all converge to the stable state after a fluctuant period and that the proposed route adjustment process simulates the ideal traffic flow evolution of the three groups of travellers. Table 10 shows that for travellers in the first group, the demand is entirely loading in the routes with the minimum travel times in the stable state, and Table 11 shows the flows in the second group are stable because all of the surplus capacities of the routes are equal. Since different travellers have different perception errors, Table 12 proves that all the routes have the same minimum perceived travel cost and are eventually selected by the third group of travellers. Hence, the stable state is exactly the mixed equilibrium state formed by the different behaviours of these three groups of travellers.

6. Conclusions

Based on the non-Walrasian equilibrium theory proposed by R.W. Clower, a new route comfort choice behaviour criterion was proposed considering the quantity signal influence of a traffic network through the route surplus capacity indicator. A traveller who follows this travel route decision criterion is defined as a quantity adjustment traveller. This study divided the traffic network travellers into three categories: travellers in the first group receive complete travel information and choose the shortest route as assumed in the classical research, the second group of travellers follows the proposed travel route decision criterion and chooses the most comfortable route based on complete travel information, and the third group of travellers chooses its routes in accordance with the logit-based route choice probability owing to incomplete travel information.

This paper analysed the common route rapidity criterion and the proposed route comfort choice behaviour criterion with their corresponding equilibrium states and established a route flow adjustment process to depict the flow adjustment process of the interacting flows of the three groups of travellers that converge to a mixed equilibrium state. This mixed equilibrium not only considers the diversity of the route selection criteria of the travellers but also elaborates the interaction between the different travellers' groups. This means that all route choices made by the travellers from the three groups are determined on the basis of the comprehensive route cost generated by the sum of the flows of the three groups of travellers.

With the rapid development of science and technology and the urbanization process, new traffic patterns have emerged from large-scale urban infrastructure construction, road network expansion, and so on. To rationally characterize the traffic flow dynamic evolution process from disequilibrium to equilibrium, this paper classified the travellers and simulated the dynamic evolution of the network traffic flow by using the principles of economics. This deepens the understanding of network traffic flows and improves the level of urban traffic management.

Several issues have been left unsolved and are directions worthy of further study. First, it will be interesting to focus on a situation in which an information provider of an intelligent transportation system uses the optimal system as the decision-making principle. Another future research direction is choosing the most suitable quantity signal considering the effects of the road grade, functions, and service level of the traffic network. Moreover, the influence of the proportion of travellers who follow the quantity

adjustment path selection criteria in mixed equilibrium evolution is also a challenge for future research.

Data Availability

The data used to support the findings of this study are available from the corresponding author upon request.

Conflicts of Interest

The authors declare that there are no conflicts of interest regarding the publication of this paper.

Acknowledgments

This work was supported by the National Natural Science Foundation of China under grant numbers 51338002 and 51978082.

References

[1] F. Xiao, H. Yang, and H. Ye, "Physics of day-to-day network flow dynamics," *Transportation Research Part B: Methodological*, vol. 86, pp. 86–103, 2016.

[2] F. Yang and D. Zhang, "Day-to-day stationary link flow pattern," *Transportation Research Part B: Methodological*, vol. 43, no. 1, pp. 119–126, 2009.

[3] Q. Zeng, W. Gu, X. Zhang, H. Wen, J. Lee, and W. Hao, "Analyzing freeway crash severity using a Bayesian spatial generalized ordered logit model with conditional autoregressive priors," *Accident Analysis & Prevention*, vol. 127, pp. 87–95, 2019.

[4] Q. Zeng, H. Wen, H. Huang, and M. Abdel-Aty, "A Bayesian spatial random parameters Tobit model for analyzing crash rates on roadway segments," *Accident Analysis & Prevention*, vol. 100, pp. 37–43, 2017.

[5] F. Chen, H. R. Peng, X. X. Ma, J. Y. Liang, W. Hao, and X. D. Pan, "Examining the safety of trucks under crosswind at bridge-tunnel section: a driving simulator study," *Tunnelling and Underground Space Technology*, vol. 92, Article ID 103034, 2019.

[6] W. Hao, C. Kamga, and J. Daniel, "The effect of age and gender on motor vehicle driver injury severity at highway-rail grade crossings in the United States," *Journal of Safety Research*, vol. 55, pp. 105–113, 2015.

[7] W. Hao and J. Daniel, "Motor vehicle driver injury severity study under various traffic control at highway-rail grade crossings in the United States," *Journal of Safety Research*, vol. 51, pp. 41–48, 2014.

[8] W. Hao, C. Kamga, X. Yang, J. Q. Ma, and C. Wu, "Driver injury severity study for truck involved accidents at highway-rail grade crossings in the United States," *Transportation Research Part F*, vol. 43, pp. 379–386, 2016.

[9] L. Y. Xiang, G. Q. Guo, J. M. Yu, V. S. Sheng, and P. Yang, "A convolutional neural network-based linguistic steganalysis for synonym substitution steganography," *Mathematical Biosciences and Engineering*, vol. 17, no. 2, pp. 1041–1058, 2019.

[10] L. Xiang, X. Shen, J. Qin, and W. Hao, "Discrete multi-graph hashing for large-scale visual search," *Neural Processing Letters*, vol. 49, no. 3, pp. 1055–1069, 2019.

[11] R.-Y. Guo and H.-J. Huang, "A discrete dynamical system of formulating traffic assignment: revisiting Smith's model," *Transportation Research Part C: Emerging Technologies*, vol. 71, pp. 122–142, 2016.

[12] Y. Wenjuan, G. Renyong, and L. Qi, "A dynamic system model of formulating day-to-day traffic assignment based on stochastic user equilibrium," *Systems Engineering: Theory and Practice*, vol. 35, no. 12, pp. 3192–3200, 2015.

[13] C. L. Zhao and H. J. Huang, "Properties of boundedly rational user equilibrium under satisficting rule in traffic assignment problem," *Systems Engineering Practice*, vol. 34, no. 12, pp. 3073–3078, 2014.

[14] T.-Q. Tang, W.-F. Shi, H.-J. Huang, W.-X. Wu, and Z. Song, "A route-based traffic flow model accounting for interruption factors," *Physica A: Statistical Mechanics and Its Applications*, vol. 514, pp. 767–785, 2019.

[15] J. Ma, W. Han, Q. Guo, and Z. Wang, "Traffic dynamics on two-layer complex networks with limited delivering capacity," *Physica A: Statistical Mechanics and Its Applications*, vol. 456, pp. 281–287, 2016.

[16] G. E. Cantarella and D. P. Watling, "A general stochastic process for day-to-day dynamic traffic assignment: formulation, asymptotic behaviour, and stability analysis," *Transportation Research Part B: Methodological*, vol. 92, pp. 3–21, 2016.

[17] F. Wei, N. Jia, and S. Ma, "Day-to-day traffic dynamics considering social interaction: from individual route choice behavior to a network flow model," *Transportation Research Part B: Methodological*, vol. 94, pp. 335–354, 2016.

[18] N. H. Hoang, H. L. Vu, M. Panda, and H. K. Lo, "A linear framework for dynamic user equilibrium traffic assignment in a single origin-destination capacitated network," *Transportation Research Part B: Methodological*, vol. 126, pp. 329–352, 2017.

[19] W. Liu, X. Li, F. Zhang, and H. Yang, "Interactive travel choices and traffic forecast in a doubly dynamical system with user inertia and information provision," *Transportation Research Part C: Emerging Technologies*, vol. 85, no. 3, pp. 711–731, 2017.

[20] J. J. Tang, Y. W. Wang, W. Hao, F. Liu, H. L. Huang, and Yi. H. Wang, "A mixed path size logit-based taxi customer-search model considering spatio-temporal factors in route choice," *IEEE Transactions on Intelligent Transportation Systems*, pp. 1–12, 2019.

[21] W. Hao, Y. J. Lin, Y. Cheng, and X. F. Yang, "Signal progression model for long arterial: intersection grouping and coordination," *IEEE Access*, vol. 6, pp. 30128–30136, 2018.

[22] B. J. Zhou, M. Xu, Q. Meng, and Z. Huang, "A day-to-day route flow evolution process towards the mixed equilibria," *Transportation Research Part C: Emerging Technologies*, vol. 82, pp. 210–228, 2017.

[23] X. Zhang, H. Yang, and H.-J. Huang, "Multiclass multicriteria mixed equilibrium on networks and uniform link tolls for system optimum," *European Journal of Operational Research*, vol. 189, no. 1, pp. 146–158, 2008.

[24] C. Proble, M. Patriksson, S. A. Bagloee, M. Sarvi, and M. Patriksson, "A mixed user-equilibrium and system-optimal traffic flow for connected vehicles stated as a complementarity problem," *Comput. Civ. Inf. Eng.*, vol. 32, no. 7, pp. 562–580, 2017.

[25] P. D. Site, "A mixed-behaviour equilibrium model under predictive and static advanced traveller information systems (ATIS) and state-dependent route choice," *Transportation Research Part C: Emerging Technologies*, vol. 86, no. 12, pp. 549–562, 2018.

[26] Z. X. Huang, X. J. Jiang, and J. H. Wu, "An evolution model for network traffic flow based on price-quantity regulation,"

Journal of Management Sciences in China, vol. 20, no. 8, pp. 102–111, 2017.

[27] R.-Y. Guo, H. Yang, and H.-J. Huang, "A discrete rational adjustment process of link flows in traffic networks," *Transportation Research Part C: Emerging Technologies*, vol. 34, pp. 121–137, 2013.

[28] X. M. Lou, *Transport Network Flow Evolution Models with Bayesian Inference*, Southeast University, Shanghai, China, 2017.

[29] S. Nguyen and C. Dupuis, "An efficient method for computing traffic equilibria in networks with asymmetric transportation costs," *Transportation Science*, vol. 18, no. 2, pp. 185–202, 1984.

Hindawi
Journal of Advanced Transportation
Volume 2019, Article ID 7965479, 11 pages
https://doi.org/10.1155/2019/7965479

Research Article

Investigating the Affecting Factors of Speed Dispersion for Suburban Arterial Highways in Nanjing, China

Yongfeng Ma [1,2,3] **Xin Gu** [1,2,3] **Jaeyoung Lee** [4] **and Qiaojun Xiang** [1,2,3]

[1]*Jiangsu Key Laboratory of Urban ITS, Nanjing, China*
[2]*Jiangsu Collaborative Innovation Center of Modern Urban Traffic Technologies, Nanjing, China*
[3]*School of Transportation, Southeast University, Nanjing, China*
[4]*School of Traffic and Transportation Engineering, Central South University, Changsha, China*

Correspondence should be addressed to Yongfeng Ma; mayf@seu.edu.cn

Received 31 August 2019; Revised 29 October 2019; Accepted 7 November 2019; Published 31 December 2019

Academic Editor: Filomena Mauriello

Suburban arterial highways are usually characterized by mixed traffic environments, which is a major contributor to traffic crashes. It has been known that speed dispersion as a surrogate safety measure has a strong correlation with safety. The objective of this study is to identify the influencing factors of speed dispersion for suburban arterial highways. Two definitions of speed dispersion are proposed for comparison: (1) an individual vehicle speed variation along a highway segment and (2) a vehicle speed variation at a cross-section. Vehicle speeds, traffic composition, and driving interference data were obtained from high-resolution videos from 20 segments of the G205 highway in Nanjing, China. An exploratory factor analysis was used to detect initial relationships between latent influencing factors and 13 candidate variables selected based on traffic condition, road condition, and driving behavior. A multivariable regression model was applied to identify the impacts of latent influencing factors on speed dispersion. The results from the two models showed substantial differences. The road condition factor was not significant in the cross-sectional speed dispersion model, but was interpretive in the segmented speed dispersion model. Driving interferences and illegal driving behaviors had a greater effect on the segmented speed dispersion. Consequently, segmented speed dispersion showed a better performance for the analysis of suburban arterial highways. On the other hand, traffic disturbance caused by driving interferences and illegal driving behaviors is the greatest contributor to high speed dispersion on suburban arterial highways, which may be mitigated by effective traffic management measures. It is expected that this work will help traffic managers better understand speed dispersion in mixed traffic environments and to develop effective safety improvement strategies.

1. Introduction

Suburban arterial highways are located in the rural–urban fringe zone and they are often characterized by mixed traffic environment, resulting from a mix of user modes (e.g., pedestrians, motor vehicles, and nonmotor vehicles). Mixed traffic environment is one of the most important reasons that result in frequent traffic crashes of the suburban arterial highways. Consequently, the traffic safety issues of suburban arterial highways have been increasingly emphasized.

Crash-based safety analysis has been widely used to estimate safety situation of highways [1–5]. However, reliable crash data of suburban arterial highways in China are very rare. Surrogate safety measures based on roadway characteristics are often utilized in order to indirectly assess road safety management in case historical crash data are limited or unavailable [6]. Numerous studies have developed speed dispersion as a surrogate measure for traffic safety [6–14]. Chen et al. developed a speed-based model with appropriate speed measure to access roundabout safety performance [10]. Guo et al. proposed two new speed measures to estimate the safety level of freeway exits, in order to overcome the overestimation of safety level resulting from the conventional measure [11]. According to compare with historical crash data, the validation results affirmed the reasonability of the new speed measure to estimate the safety level. Quddus [13] found that speed variation is statistically and positively associated with accident rates. A 1% increase in speed variation is associated with a 0.3% increase in accident rates. On the other hand, some studies have also investigated the relationship between speed

dispersion and safety, and the speed dispersion is found to be statistically and positively associated with crash rates [15–19]. Garber and Gadiraju [16] concluded that crash rates have a positive relationship with the speed variance; however, have no significant correlation with the average speed. Similar to Garber and Gadiraju [16], Liu and Popoff [17] also found that the most prevalent source of human error contributing to collisions may be speed-related and will increase with travel speed. According to previous studies, speed dispersion is an acceptable surrogate measure to conduct safety analysis. A comprehensive study on identifying factors affecting speed dispersion is beneficial for helping authorities to develop relevant effective countermeasures to reduce speed dispersion, which could lead to a reduction in crash rates.

Although previous studies have explored the probability of crash occurrence by speed dispersion and developed speed dispersion models [20–24], they still have some limitations. Most of the models focused on rural or urban expressways; however, no study has focused on suburban arterial highways until now. Suburban arterial highways are common in developing countries, especially in China, and they have to meet the complex traffic demands of both highways and urban roads. The suburban arterial highways have three main characteristics: (1) typical mixed traffic environment owing to complex traffic composition, especially after the popularity of electric vehicles [25, 26]; (2) high-density accesses directly linked to the main road, owing to land commercialization; (3) numerous traffic interferences resulting from illegal traffic behaviors. Consequently, suburban arterial highways have a more complex traffic environment, and previous speed dispersion models, therefore, might not be appropriate.

More importantly, the definition of speed dispersion varies by data resource and research method. Speed dispersion can be expressed by the speed variation at a certain place in a certain time interval, or the speed variation along a road section. The proposed approaches to define speed dispersion in previous studies are briefly summarized in Table 1. Most conventional definitions are based on cross-sectional aggregated data, and thus may not be the most appropriate for suburban arterial highways, owing to a lack of consideration for all traffic compositions in the mixed traffic environment and the impacts of traffic interference along the segment, in addition to the probability of ecological fallacy [11]. Ecological fallacy describes the phenomenon in which what seems true for a group may not be true for the individual, because some information gets lost during the aggregation process [11].

Along with the definition of speed dispersion, some studies have also been conducted to explore the influencing factors of speed dispersion [12, 27–29]. Moreno and García [12] proposed two speed dispersions, average individual speed and accumulated speed uniformity. And it concluded that speed limit, and traffic calming density are two factors influencing the average individual speed, but the average operating speed is the only one influencing factor of accumulated speed uniformity. Park et al. [27] developed hierarchical linear regression models to predict the speed dispersion. The results indicated that the speed dispersion is positively related to tangent speed and curvature. Chung and Recker [28] investigated the relationship between speed dispersion and traffic flow parameters. However, the methodological approaches used in previous studies rarely considered the complex relationships between the influencing factors, and thus may not produce precise estimation of the effects of various candidate variables on speed dispersion. For example, Moreno and García [12] explored speed distribution based on continuous GPS-speed data on cross-town roads in the European areas, and developed a speed variation model. However, the data of zero-speed vehicles or parking cars are removed, which could result in a limitation of influencing factors.

Hence, the current study aims to contribute to the literature by identifying more influencing factors of speed dispersion for suburban arterial highways. To this end, exploratory factor analysis (EFA) was used to explore the relationship between candidate variables. Then, a multivariable regression model is developed to identify the correlation between speed dispersion and influencing factors. Note that, for comparison purpose, two different definitions of speed dispersion are proposed to develop regression models. These methods could help us attain a more precise and comprehensive understanding of the impacts of different variables on speed dispersion on suburban arterial highways. It is expected that this work will help traffic managers better understand speed dispersion in mixed traffic environments and to develop effective safety improvement strategies.

2. Methodology

2.1. Definition of Speed Dispersion. An individual vehicle speed is the result of the combined effects from road and traffic conditions, driving behaviors, vehicle performance, and weather, and thus, its variation may represent the characteristics of speed dispersion. Boonsiripant et al. [6] studied the relationship between speed distribution and safety, and his results showed that acceleration noise as a surrogate safety measure had better correlation with accidents than aggregated speed-based surrogate safety measures. This study could provide supporting evidence because acceleration has a strong relationship with individual vehicle speed variation. Therefore, speed dispersion is defined by the individual speed variation along a road segment, which not only provides a more comprehensive picture of the characteristics of a road segment during a particular period of time, but also avoids the ecological fallacy [11] owing to information loss during the aggregation process. The expression of speed dispersion is as follows:

$$SP_{segment} = \sqrt{\frac{\sum_{i=1}^{m}\left(v_{i,j} - \overline{v_j}\right)^2}{m-1}}, \tag{1}$$

$$v_{i,j} = \frac{\left((1/2)l_{i-1,j} + (1/2)l_{i,j}\right)}{t_{i,j}}, \tag{2}$$

$$\overline{v_j} = \frac{l_p}{t_j}, \tag{3}$$

Table 1: Summary of speed dispersion definitions in previous studies.

Author	Year	Method	Data
Solomon [18]	1964	Difference between individual vehicle speed and mean speed	Speed data along a segment
Garber & Gadiraju [16]	1989	Speed variance	Cross-sectional data
Aarts and Van Schagen [20]	1989	Difference between 85^{th} percentile speed and the average speed	Cross-sectional data
McFadden and Elefteriadou [22]	2000	The 85^{th} percentile maximum speed reduction	Cross-sectional data
Wang et al. [30]	2007	The standard deviation of the individual speed (SDIS); The average speed difference (ASD) of two neighbouring vehicles	Cross-sectional data
Guo et al. [11]	2011	The 85^{th} percentile individual speed difference; The 85^{th} percentile speed change rate	Cross-sectional data
Boonsiripant et al. [6]	2011	The variation of the 85^{th} percentile speed; Mean of 85^{th} percentile speed; Interquartile range of 85^{th} percentile speed; The difference between the 95^{th} percentile speed and the 5^{th} percentile speed (speed band); Mean of speed band; Variation of speed band	Cross-sectional data
Moreno and García [12]	2012	Ra-relative area measure of uniformity; Ea-relative area measure of speeding	Continuous speed data along a segment
Chung and Recker [28]	2014	The coefficient of variation of speed	Cross-sectional data
Wang et al. [31]	2016	Standard speed deviation (SD)	Cross-sectional data
Qiao et al. [32]	2017	The average of the speed deviation in the statistical time; The difference between the 85% speed and the 15% speed; The ratio of the SD to the average speed of the traffic flow	Continuous speed data in the statistical time
Gao et al. [43]	2019	The speed standard deviation, the coefficient of variation (CV)	Cross-sectional data

where, $SP_{segment}$ is the speed dispersion based on individual vehicle data along a highway segment p, $v_{i,j}$ is the speed of vehicle j at cross-section i, $l_{i-1,j}$ is the distance between cross-section $i-1$ and cross-section i; $(1/2)\,l_{i-1,j} = 5$ m, if $i = 0$; $l_{i,j}$ is the distance between cross-section i and cross-section $i+1$, $t_{i,j}$ is the travel time of vehicle from location $(1/2)\,l_{i-1,j}$ to location $(1/2)l_{i,j}$, $\overline{v_j}$ is the mean speed of vehicle j on the road segment p, l_p is the length of road segment p, and m is the number of cross-sections in the highway segment p.

For comparison, the conventional speed dispersion based on aggregated data at certain cross-sections was also considered. The expression is as follows:

$$SP_{cross\text{-}section} = \sqrt{\frac{\sum_{i=1}^{n}\left(v_i - \overline{v}\right)^2}{n-1}}, \tag{4}$$

where, $SP_{cross\text{-}section}$ is the speed dispersion based on cross-sectional data, v_i is the speed of vehicle i at the observed cross-section, $\overline{v}$ is the mean speed of vehicles through the observed cross-section in specific time interval, and n is the number of vehicles in the observed time interval.

2.2. Model Development. This study aims to propose a new analysis procedure for speed dispersion on suburban arterial highways. The overall modelling procedure that would achieve the objectives as follows:

(1) Factor analysis to identify latent influencing factors: EFA is utilized to detect initial relationships between the latent influencing factors and the selected candidate variables in the study. This process can help the model development, by extracting a small number of latent factors to represent the large number of selected candidate variables with minimal loss of information.

(2) Multivariable regression modelling to explore the impact of latent factors on speed dispersion: This step employs the multivariable regression method to develop a speed dispersion model. The latent factors are used as independent variables to estimate the relationships with speed dispersion. The effects of the selected candidate variables on speed dispersion can also be expressed.

(3) Model comparison between $SP_{segment}$ and $SP_{cross\text{-}section}$: This step is conducted to explore the effects of different definitions on the analysis results of speed dispersion.

3. A Case Study

3.1. Site Selection. Suburban arterial highways with characteristics of typical mixed traffic environments were selected. This paper focused on the influencing factors of speed dispersion under continuous conditions, in order to ensure the reliability of the study, all research road segments need to keep away from the signalized intersections to avoid interruption. In addition, the alignment should avoid the curve and the longitudinal slope. Finally, 20 segments on ten different sites of the G205 highway in Nanjing, which crosses a rural–urban fringe area, were selected (Figure 1). The average number of cross-sections is 10.7 for each segment. The cross-section was selected at intervals of 20 m from the beginning of each segment. Note that when the detection point falls on the crosswalk or the access to surroundings etc., it will extend forward to 5 m after the end of the above facilities. The suburban arterial highway characteristics are summarized in Table 2.

3.2. Data Collection. Many collection methods have been applied to research speed and safety; for instance, radar gun-based collection [11], loop detector-based collection [33, 34], GPS-based speed collection [9, 35], and video detection-based speed collection [36, 37]. To meet the research aims, a video-based collection method was adopted in this study, which can provide full and proper context for highway segments. High-resolution videos of suburban arterial highway segments were collected by unmanned aerial vehicle (UAV) (Figure 1). UAV photography allowed to shoot videos in the necessary surroundings, including the wind force below grade 4, sunny weather, good light, and no electromagnetic interference, which could output stable video pictures at a vertical angle. When processing the video data, the length of lane line was considered as a reference to calibrate the distance, so the error caused by the projection of the videos could be ignored. After the multiple tests, the final shooting location was determined to be at a height of approximately 200 m to ensure the ability to obtain high-resolution videos of highway segments with length of at least 350 m in good weather.

Video collection was conducted between 4 p.m. and 6 p.m. on weekdays except Friday, which also met UAV photography demands. The UAV could hover for 20 minutes at maximum and to obtain the stable data, a 15-minute useful highway segment video which takes out the periods of rise and fall are extracted each time. Finally, a total of ten-hour video data, 1 hour for a pair of highway segment, were collected in the survey.

As previously mentioned, earlier studies [38–41] have found that the speed dispersion was affected by the road conditions (e.g. median, roadside environment), traffic conditions (e.g. traffic volume, heavy vehicle mix rate), and road users' behavior (e.g. cross and turn around rate, familiar or not familiar road users). In order to explore the influencing factors of speed dispersion for suburban arterial highways, key variables including road condition, traffic condition, and driving interference variables were selected considering the difficulty of data acquisition (Table 3). The road condition variables, which described the road situation, were collected directly from the field site. The traffic condition variables describing the traffic flow state and driving interference showing the turbulence into the vehicles along the segment could be observed from the videos. Vehicle speeds were computed with the distance and the through time between adjacent cross-sections by video processing with VideoStudio. Instead of selecting cross-sections at a fixed interval distance, the selected cross-sections (Figure 1) are determined by the location of accesses, to avoid the overlap between the cross-section and the location of the access. In addition, the data from sections that are totally covered by trees or erroneous data are removed.

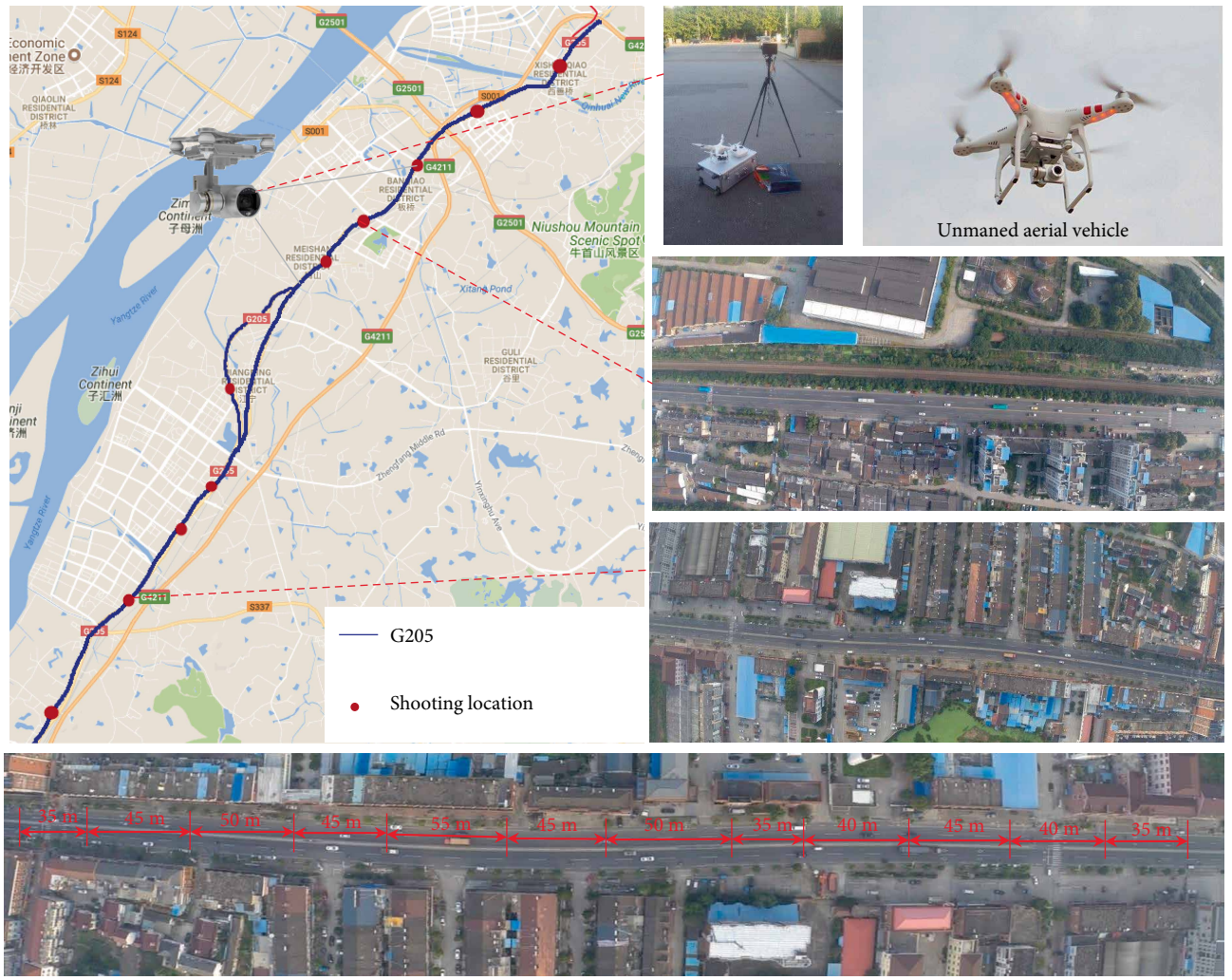

Figure 1: Scheme of shooting location and data collection.

Table 2: Segments characteristics.

Segments	Number of lanes	Median	Southbound/Northbound Land-use	Number of access
Xishan bridge—DiKan Xinyuan	4	No	Commercial, residential/agriculture	4/0
Dikan—Jianning	4	No	Commercial, residential/agriculture	4/0
Jianning—Daishan interchange	4	No	Industrial, commercial/agriculture	6/0
Daishan interchange—Tianbao	4	No	Industrial, office, commercial/agriculture	7/0
Meishan hospital—Yongan	4	Yes	Commercial, office, residential/commercial, residential	2/3
Meishan iron—Qiaogao road	4	Yes	Agriculture, residential/industrial, residential	0/3
Qiaogao road—Dingxin road	4	Yes	Agriculture, residential/agriculture, residential	1/1
S337—Yefu road	4	Yes	Commercial, residential/industrial, office, residential	5/4
Yefu road—Jingtong	4	Yes	Commercial, residential/agriculture, residential, office	5/2
Shuguang road—Xingfu road	6	Yes	Industrial, office, residential/industrial, office, residential	1/2

Table 3: Description of the candidate variables considered in this study.

Category	Variables	$SP_{segment}$			$SP_{cross-section}$		
		Max	Min	Mean	Max	Min	Mean
Road condition	Median (0 = if there is a median; 1 = otherwise)	1	0	0.4	1	0	0.5
	Roadside environment (1 = agriculture; 2 = industrial, residential, office; 3 = commercial)	Percentage	1	0.2	Percentage	1	0.2
			2	0.5		2	0.5
			3	0.3		3	0.3
Traffic condition	Heavy vehicle mix rate (%)	0.2	0.1	0.1	0.2	0.1	0.1
	Traffic volume (veh/h)	1336	432	614.9	1033	146	510
	Average speed (km/h)	58.3	33.4	46.2	63.6	21.9	47.3
	Headway (s)	30.1	4.1	10.2	35.3	3.5	9.6
Driving interference	Average lane changing rate (/veh)	1.4	0.2	0.7	0.4	0.0	0.1
	Right turn rate at access (/h)	982	0	166	530	0	16
	Left turn rate at access (/h)	582	0	222	442	0	21
	Cross and turn around rate (/h)	848	0	262	536	0	25
	Reverse driving (driving in the wrong direction) rate (/h)	230	0	49	176	0	16
	Illegal parking (parking on the road or road side illegally) rate (/h)	835	0	260	151	0	24
	Nonmotor vehicle volume driving on the motor road (veh/h)	1272	44	530	1272	0	462

4. Results and Analysis

4.1. Exploratory Factor Analysis (EFA). Correlation analysis was first conducted to explore the relationship between the 13 candidate variables. The results show that 75% of the correlation coefficients between variables are greater than 0.3. To avoid information loss due to clearing variables with multicollinearity and explore the interrelationship, the EFA was conducted to explore a small number of latent factors that could represent the observed candidate variables. The number of latent factors needed to describe the unique information in the observed candidate variables is classically determined based purely on the sufficiency of explanation of relationships among the candidate variables (i.e., the percentage of variance in the original variables accounted for by the set of factors selected).

EFA includes the following steps: (1) The Kaiser–Meyer–Olkin and Bartlett sphere test were conducted in SPSS to test if EFA was appropriate for the input data. The test result is between 0 and 1, and a high result indicates the EFA does well for the sample. In this paper, a sampling degree of 0.752 and 0.754 indicated the feasibility; (2) the number of the extracted latent factors was determined by Cattell's Scree Plot method, only factors that have the entire confidence interval greater than 1.0 were retained. Four latent influencing factors were retained in this paper and they were found to account for 72% of the variance in the candidate variables. An indicator, the communality of the variable, could show the variance percentage of each of the original 13 variables explained by the four factors together (the R^2 of the regression of each of the 13 variables on all four factors). For the retained four latent factors, ten original variables' communalities were in excess of 0.70, with the exception of "Illegal parking (parking on the road or roadside illegally) rate", "Roadside environment", "Cross and turn around rate", which were 0.631, 0.653, and 0.646. (3) then the varimax rotation (i.e., a rotation that maximizes the sum of the variances of the factors loadings) was conducted to facilitate interpreting the extracted latent traffic variables. The factor loadings which express the correlations between the 13 candidate variables and the latent influencing factors are shown in Table 4. Scores on each of the eight rotated factors were calculated for each combination (weighted average) of the 13 candidate variables. The factor loadings of the original variables on the rotated factors (i.e., the correlations between the variables and factors) form the basis for the interpretation of the factors. To aid in interpretation, the original candidate variables with large factor loadings were then selected to represent each latent influencing factor, which are shown in boldface in Table 4. The most indicative parameter for each factor is identified by a box around its loadings [42]. According to the bold variables, each of the three types of candidate parameters (i.e., road condition, traffic condition, and driving interference) provides some unique information for these four indicative parameters.

4.1.1. EFA of $SP_{segment}$. *Latent factor 1* is represented by the right and left turn rates at access, and the cross and turn around rate. This latent variable can be interpreted as the driving interference on the highway section, which can be denoted by the driving interference factor $F_{interference}$.

Latent factor 2 can be interpreted as the illegal driving behavior on the highway segment, which can be denoted by the illegal driving behavior factor $F_{i-drive}$. The selected three candidate variables with great factor loadings are the reverse driving rate, illegal parking rate, and nonmotor vehicle volume driving on the motor road.

Latent factor 3 is represented by the heavy vehicle mix rate, traffic volume, average speed, and the average lane changing rate. This latent variable can be interpreted as the traffic condition on the highway segment, for instance, traffic operation and traffic composition, which can be denoted by the traffic condition factor $F_{traffic}$.

Latent factor 4 can be interpreted as the road condition on the highway section, which can be denoted by the road condition factor F_{road}. The selected candidate variables with

Table 4: Rotated factor loadings for the EFA of candidate variables for $SP_{segment}$ and $SP_{cross\text{-}section}$.

Variable	Latent influencing factors							
	$SP_{segment}$				$SP_{cross\text{-}section}$			
	1	2	3	4	1	2	3	4
Median	−0.007	−0.191	−0.012	**0.92**	0.308	−0.082	−0.258	**0.787**
Roadside environment	0.206	0.173	0.178	**0.541**	0.057	0.194	−0.061	**0.775**
Heavy vehicle mix rate	−0.263	−0.054	**0.86**	0.127	**0.842**	−0.05	−0.182	0.153
Traffic volume	−0.142	0.244	**0.77**	0.017	**0.794**	−0.131	0.191	−0.062
Average speed	−0.075	0.032	**−0.72**	0.096	**−0.702**	−0.343	0.176	−0.331
Headway	−0.155	−0.098	**0.559**	−0.27	**0.875**	−0.043	−0.177	0.148
Average lane changing rate	−0.026	0.034	**0.858**	−0.055	0.127	−0.073	**0.856**	−0.07
Right turn rate at access	**0.88**	−0.1	0.08	0.025	0.007	**0.828**	−0.046	−0.061
Left turn rate at access	**0.78**	−0.258	0.126	0.025	0.052	**0.866**	−0.088	0.09
Cross and turn around rate	**0.675**	0.254	0.119	0.011	0.105	**0.794**	0.028	0.101
Reverse driving rate	−0.091	**0.794**	−0.173	−0.108	−0.228	0.185	**0.465**	−0.01
Illegal parking rate	−0.206	**0.873**	0.097	0.102	0.322	0.003	**0.648**	−0.089
Nonmotor vehicle volume driving on the motor road	−0.015	**0.737**	0.092	0.25	**−0.793**	−0.021	0.281	−0.155

large factor loadings are the median and roadside environment.

4.1.2. EFA of $SP_{cross\text{-}section}$. *Latent factor 1* is represented by the heavy vehicle mix rate, traffic volume, average speed, headway, and nonmotor vehicle volume driving on the motor road. This latent factor can be interpreted as the traffic condition at the highway cross-section, which is similar with $F_{traffic}$, and can be denoted by the traffic condition factor $F'_{traffic}$.

Latent factor 2 can be interpreted as the driving interference at the highway cross-section, which can be denoted by the driving interference factor $F'_{interference}$. The selected three candidate variables with great factor loadings are the right and left turn rates at access, and the cross and turn around rate.

Latent factor 3 is represented by the average lane changing rate, reverse driving rate, and illegal parking rate. This latent variable can be interpreted as the illegal driving behavior at the highway cross-section, which can be denoted by the illegal driving behavior factor $F'_{i\text{-}drive}$.

Latent factor 4 can be interpreted as the road condition at the highway cross-section, which can be denoted by the road condition factor F'_{road}. The selected candidate variables with large factor loadings are the median and roadside environment.

4.2. Speed Dispersion Modelling. To explore the impact of latent factors on different speed dispersions, two multivariable regression models were developed. Thus, the effects of the selected candidate variables on speed dispersion can be also identified.

4.2.1. Model 1-for Segment Data-Based Speed Dispersion $SP_{segment}$. A multivariable regression analysis was conducted to explore the effects of the latent factors on the speed dispersion on a suburban arterial highway segment. The regression result is as follows:

$$SP_{segment} = 0.292\,F_{interference} + 0.171\,F_{i\text{-}drive} + 0.157\,F_{traffic} + 0.123\,F_{road}, \quad (5)$$

where $SP_{segment}$ is the speed dispersion based on individual vehicle data along a highway segment, $F_{interference}$ is the driving interference factor, $F_{i\text{-}drive}$ is the illegal driving behavior factor, $F_{traffic}$ is the traffic condition factor, and F_{road} is the road condition factor, which could be calculated by candidate variables and EFA results.

$R^2 = 0.598$ indicates that the latent factors well explain the speed dispersion.

According to the model results, the most important latent factor is $F_{interference}$, which is positively related to the speed dispersion. $F_{interference}$ is determined by "the right and left turn rates at access" and "the cross and turn around rate" with a positive relationship. Therefore, the speed dispersion will rise along with the increasing driving interference rate. This reflects the adverse impact of traffic disorder on the speed dispersion. The more vehicles turn into the surrounding areas or taking U-turns, the speed of the straight-through vehicles will be affected. On the contrary, the speed dispersion may effectively decrease if traffic management measures are taken, for instance, implementing "no left turn" and "no U-turn" controls.

The second most important factor is the illegal driving behavior $F_{i\text{-}drive}$, which also has a positive relationship with the speed dispersion. The illegal driving behavior factor highly correlates with the rates of reverse driving, illegal parking, and nonmotor vehicle volume driving on the motor road. Reverse driving and illegal parking reduce the space that the vehicles can travel which have significant effects on the service level of the road. Moreover, these phenomena will also lead to the deceleration of the upstream fast-moving vehicles. Since the speed of nonmotor vehicle is small, higher volume of nonmotor vehicle tend to affect the speed of the vehicles. These candidate variables and $F_{i\text{-}drive}$ belong to the traffic management category, which indicates that the reasons contributing to large speed dispersion on suburban arterial highways are a lack of traffic and safety consciousness and ineffective traffic management measures.

The other two influencing factors are the traffic condition $F_{traffic}$ and the road condition F_{road}, which have a positive

correlation with the speed dispersion. $F_{traffic}$ is positively correlated with the average lane changing rate, heavy vehicle mix rate, and vehicle count, but negatively correlated with average speed. The reason for this is that a high average speed indicates good traffic conditions with less transverse interference, and in which the speed dispersion is low. This is consistent with the actual situation. F_{road} mainly includes whether to set the inner median and the roadside environment. Setting the inner median can effectively reduce the occurrence of illegal U-turn and crossing behavior, and reduce the interference to the traffic flow, thus reducing the speed dispersion. Moreover, with the development of land use and the increase in the number of accesses, the interference will increase, which will intensify the speed dispersion.

4.2.2. Model 2-for Cross-Section Data-Based Speed Dispersion $SP_{cross\text{-}section}$. For comparison, the influence analysis for cross-sectional speed dispersion definition $SP_{cross\text{-}section}$ was also conducted. The expression for $SP_{cross\text{-}section}$ is as follows:

$$SP_{cross\text{-}section} = 0.432\,F'_{traffic} + 0.185\,F'_{interference} + 0.114\,F'_{i\text{-}drive} + 0.029\,F'_{road}, \quad (6)$$

where $SP_{cross\text{-}section}$ is the speed dispersion based on i cross-sectional data, $F_{traffic}$ is the traffic condition factor, $F'_{interference}$ is the driving interference factor, $F'_{i\text{-}drive}$ is the illegal driving behavior factor, and F'_{road} is the road condition factor, which could be calculated by candidate variables and EFA results.

$R^2 = 0.526$ indicates that the latent factors interpret the speed dispersion well.

The latent factors can also be interpreted by the traffic condition, driving interference, illegal driving behavior, and road condition factors. As shown in Equation (4), the factor that have the greatest effect on $SP_{cross\text{-}section}$ is the traffic condition factor, which is positively correlated with $SP_{cross\text{-}section}$ and is mainly determined by the heavy vehicle mix rate, vehicle volume, average speed, headway, and nonmotor vehicle count driving on the motor road. Two other factors that affect $SP_{cross\text{-}section}$ are the driving interference and illegal driving behavior factors. However, the influence of the road condition factor on $SP_{cross\text{-}section}$ is insignificant.

4.2.3. Model Validation. A test dataset was used to calibrate the regression model. The observed speed dispersion was recorded as Field speed dispersion. The predicted value of speed dispersion was recorded as predicted speed dispersion. The numerical analysis between Field speed dispersion and predicted speed dispersion is shown in Table 5 and Figure 2. According to the results, the segment data-based speed dispersion model outperforms the model for cross-section data-based speed dispersion.

4.2.4. Model Comparison. The influences of the latent factors on the speed dispersion are different. For instance, the impact of the driving interference factor was the greatest in the $SP_{segment}$ model, but not in the $SP_{cross\text{-}section}$ model, in which the traffic condition factor had the greatest effect. The cross-sectional speed dispersion is affected by the vehicle speed distribution at a certain section through a certain time interval, which is determined by the number and types of vehicles through the cross-section. However, the segment-based speed dispersion analyzed the speed variation along a stretch of highway segment, which contains many factors, not only traffic condition, but also the road condition and driving interference. Therefore, the traffic condition factor plays a more important role in the $SP_{cross\text{-}section}$ model. Furthermore, the influence of the road condition factor in the $SP_{cross\text{-}section}$ model is not significant, in contrast to the $SP_{segment}$ model. This is because the segment-based data in the $SP_{segment}$ model can provide a comprehensive picture of the whole highway segment, which accumulates the effects of the road conditions.

Table 5: Model validation results.

Validation Dataset	Max	Min	Mean	RMSE	MAPE
Field $SP_{segment}$	7.206	4.183	5.541	0.998	15.6%
Predicted $SP_{segment}$	8.529	3.372	5.810		
Field $SP_{cross\text{-}section}$	24.021	5.999	11.638	5.125	19.8%
Predicted $SP_{cross\text{-}section}$	23.742	5.838	12.085		

Note: RMSE denotes root mean square error; MAPE denotes absolute percentage error.

Some of the candidate variables explained by the latent factors are different. For instance, nonmotor vehicle volume driving on the motor road, this variable is explained by the illegal driving behavior factor $F_{i\text{-}drive}$ in the segment-based factor analysis, but by the traffic condition factor F'_{road} in the cross-sectional factor analysis. This is because the variable has both traffic characteristics and driving characteristics. This behavior causes a decrease in the average speed at the observed cross-section in the cross-sectional analysis, which also contributes to a reduction in the speed dispersion. However, the same behaviors may disturb the adjacent motor vehicle and cause speed reduction and more lane changing behaviors, which are the main reasons for speed dispersion. Therefore, the variable nonmotor vehicle volume driving on the motor road shows more traffic characteristics in the $SP_{cross\text{-}section}$ model, but more driving characteristics in the $SP_{segment}$ model.

Similarly, the average lane changing rate has a high correlation with the traffic condition factor F_{road} in the segment-based analysis, but more explained by the illegal driving behavior factor $F'_{i\text{-}drive}$ in the cross-sectional analysis. Lane changing behaviors include free lane changing and compulsory lane changing. Lane changing behaviors observed at a certain cross-section are random, which cause a random characteristic in the cross-sectional analysis. However, free lane changing behaviors and compulsory lane changing behaviors are all observed and analyzed in the segment-based analysis, and thus the characteristics of the traffic condition factor are more obvious.

5. Conclusions

Suburban arterial highways are common in developing countries and have typical mixed traffic characteristics. For example, a mix of user modes, numerous direct-linking accesses to

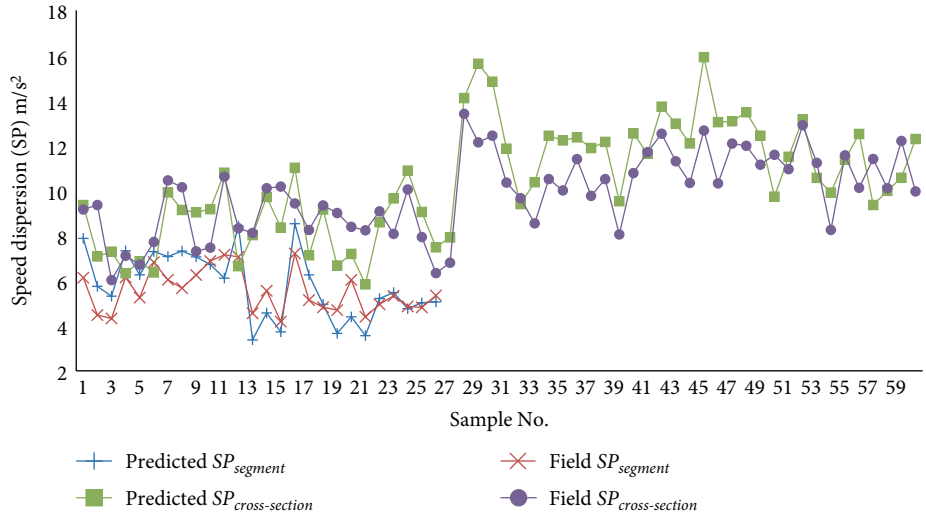

Figure 2: Comparison of field and predicted values of speed dispersion $SP_{segment}$ and $SP_{cross\text{-}section}$.

arterial highways, and disordered traffic resulting from illegal traffic behaviors, will cause an increased potential for traffic collisions. The safety issues of suburban arterial highways require more attention. This study sought to identify the influencing factors of speed dispersion for suburban arterial highways, which is a surrogate measure for safety risks. Two definitions of speed dispersion were presented and 20 different segments of the G205 highway in Nanjing were used for case study. In order to avoid the information loss, an exploratory factor analysis (EFA) was conducted to explore the relationship between the candidate variables. Finally, two multivariable regression models were developed to explore the impact of factors on different speed dispersions.

For exploring the influencing factors, thirteen variables which were selected from three different aspects, e.g. the traffic conditions, road conditions, and driving interference, were fully considered. The EFA results showed that the two different definitions of speed dispersion, which were calculated by individual vehicle data and aggregated data respectively would lead to the principal components results with different compositions and ranks. Another important finding is that the impacts of the same variable on $SP_{segment}$ and $SP_{cross\text{-}section}$ are different. For example, $SP_{cross\text{-}section}$ is significantly affected by the traffic condition factor; however, for $SP_{segment}$, the driving interference factor plays the most important role. One possible reason is that the cross-sectional vehicle data for the $SP_{cross\text{-}section}$ model are significantly affected by the traffic volume and traffic composition passing through the cross-section. However, the individual speed variation along a highway segment, which was used for modelling the $SP_{segment}$ model, shows comprehensive effects of all factors and reduces the impact of cross-sectional vehicle data on the $SP_{segment}$. This is also consistent with the actual situation.

In addition, the model results showed that the speed dispersion for suburban arterial highways will increase under one of the following conditions: (1) there are many accesses along the arterial highways; (2) there is no inner median; (3) nonmotor vehicle volume is high; (4) there are many traffic violations, for example, illegal parking. This indicates that the speed dispersion of the suburban arterial highway is mainly caused by the lack of safety consciousness of traffic participants and the neglect of road management. Therefore, it is essential that safety countermeasures aimed at reducing speed dispersion should be promoted, which is also beneficial to road safety. One of such countermeasures would be to set the inner median which could reduce the reverse driving behavior and the cross and turn around rate, thus reducing the interference on the traffic stream. Another way to reduce the speed dispersion is setting roadside parking lots or strengthen the management of parking on the road in order to decrease the impact of parking cars. Moreover, the management of accesses and U-turn would also reduce speed dispersion.

This work could enrich the knowledge of speed dispersion on suburban arterial highways and can be applied to transportation networks in other countries. Moreover, further development of video-based moving target detection technology will be beneficial to obtain more accurate speed trajectory of traffic participants and calculate the speed dispersion, thereby avoiding the influence of random error due to cross-section selection depending on the land use and the layout of accesses. In addition, we will collect crash data of suburban arterial highways, then explore the relationship between speed dispersion and crashes, and identify the significant influencing factors to traffic crashes.

Data Availability

The data used to support the findings of this study are available from the corresponding author upon request.

Conflicts of Interest

The authors declare that they have no conflicts of interest regarding the publication of this paper.

Funding

This study was funded by the National Natural Science Foundation of China (No. 51208100, No. 71871059).

Acknowledgments

The authors acknowledge the assistance provided by the graduate research assistants at the School of Transportation, Southeast University, in field data collection.

References

[1] F. Chen, S. Chen, and X. Ma, "Analysis of hourly crash likelihood using unbalanced panel data mixed logit model and real-time driving environmental big data," *Journal of Safety Research*, vol. 65, pp. 153–159, 2018.

[2] F. Chen, M. Song, X. Ma, and X. Zhu, "Assess the impacts of different autonomous trucks' lateral control modes on asphalt pavement performance," *Transportation Research Part C: Emerging Technologies*, vol. 103, pp. 17–29, 2019.

[3] F. Chen and S. Chen, "Injury severities of truck drivers in single-and multi-vehicle accidents on rural highways," *Accident Analysis & Prevention*, vol. 43, no. 5, pp. 1677–1688, 2011.

[4] F. Chen, M. Song, and X. Ma, "Investigation on the injury severity of drivers in rear-end collisions between cars using a random parameters bivariate ordered probit model," *International Journal of Environmental Research and Public Health*, vol. 16, no. 14, p. 2632, 2019.

[5] C. Xu, H. Li, J. Zhao, J. Chen, and W. Wang, "Investigating the relationship between jobs-housing balance and traffic safety," *Accident Analysis & Prevention*, vol. 107, pp. 126–136, 2017.

[6] S. Boonsiripant, M. O. Rodgers, and M. P. Hunter, "Speed profile variation as a road network screening tool," *Transportation Research Record*, vol. 2236, no. 1, pp. 83–91, 2011.

[7] C. Wang, C. Xu, J. Xia, Z. Qian, and L. Lu, "A combined use of microscopic traffic simulation and extreme value methods for traffic safety evaluation," *Transportation Research Part C: Emerging Technologies*, vol. 90, pp. 281–291, 2018.

[8] J. Chen, Z. Li, W. Wang, and H. Jiang, "Evaluating bicycle–vehicle conflicts and delays on urban streets with bike lane and on-street parking," *Transportation Letters*, vol. 10, no. 1, pp. 1–11, 2018.

[9] S. Boonsiripant, "Speed profile variation as a surrogate measure of road safety based on GPS-equipped vehicle data," *Georgia Institute of Technology*, 2009.

[10] Y. Chen, B. Persaud, and C. Lyon, "Effect of speed on roundabout safety performance: implications for use of speed as surrogate measure," in *Transportation Research Board 90th Annual Meeting*, TRID, Washington DC, United States, 2011.

[11] T. Guo, Y. Liu, and J. Lu, "Levels of safety at freeway exits: evaluations on the basis of individual speed difference," *Transportation Research Record*, vol. 2241, no. 1, pp. 10–18, 2011.

[12] A. T. Moreno and A. García, "Use of speed profile as surrogate measure: effect of traffic calming devices on crosstown road safety performance," *Accident Analysis & Prevention*, vol. 61, pp. 23–32, 2013.

[13] M. Quddus, "Exploring the relationship between average speed, speed variation, and accident rates using spatial statistical models and GIS," *Journal of Transportation Safety & Security*, vol. 5, no. 1, pp. 27–45, 2013.

[14] V. Gitelman, E. Doveh, and S. Bekhor, "The relationship between travel speeds, infrastructure characteristics, and crashes on two-lane highways," *Journal of Transportation Safety & Security*, vol. 10, no. 6, pp. 545–571, 2018.

[15] B. N. Fildes, G. Rumbold, and A. Leening, "Speed behaviour and drivers' attitude to speeding," vol. 16, Monash University Accident Research Centre, Report, p. 186, 1991.

[16] N. J. Garber and R. Gadiraju, "Factors affecting speed variance and its influence on accidents," *Transportation Research Record*, vol. 1213, pp. 64–71, 1989.

[17] G. X. Liu and A. Popoff, "Provincial-wide travel speed and traffic safety study in Saskatchewan," *Transportation Research Record*, vol. 1595, no. 1, pp. 8–13, 1997.

[18] D. Solomon, "Accidents on main rural highways related to speed, driver, and vehicle," GPO/Bureau of Public Roads (FHWA predessesor), 1964.

[19] H. D. Son, M. D. Fontaine, and B. Park, "Long-term speed compliance and safety impacts of rational speed limits," *Journal of Transportation Engineering*, vol. 135, no. 8, pp. 536–544, 2009.

[20] L. Aarts and I. Van Schagen, "Driving speed and the risk of road crashes: a review," *Accident Analysis & Prevention*, vol. 38, no. 2, pp. 215–224, 2006.

[21] D. Synder, "Speeding, coordination, and the 55-mph limit: comment," *The American Economic Review*, vol. 79, no. 4, pp. 922–925, 1989.

[22] J. McFadden and L. Elefteriadou, "Evaluating horizontal alignment design consistency of two-lane rural highways: development of new procedure," *Transportation Research Record*, vol. 1737, no. 1, pp. 9–17, 2000.

[23] Z. Feng, M. Yang, W. Kumfer, Y. Du, and H. Bai, "Effect of longitudinal slope of urban underpass tunnels on drivers' heart rate and speed: a study based on a real vehicle experiment," *Tunnelling and Underground Space Technology*, vol. 81, pp. 525–533, 2018.

[24] M. Yongfeng, Y. Li, and Z. Wenbo, "Analytical method of minimum spacing of signalized intersections on bidirectional two-lane highways," *Journal of Southeast University (English Edition)*, vol. 31, no. 4, pp. 547–552, 2015.

[25] C. Wang, C. Xu, J. Xia, and Z. Qian, "Modeling faults among e-bike-related fatal crashes in China," *Traffic Injury Prevention*, vol. 18, no. 2, pp. 175–181, 2017.

[26] M. Du and L. Cheng, "Better understanding the characteristics and influential factors of different travel patterns in free-floating bike sharing: evidence from Nanjing, China," *Sustainability*, vol. 10, no. 4, p. 1244, 2018.

[27] P. Y. Park, L. F. Miranda-Moreno, and F. Saccomanno, "Estimation of speed differentials on rural highways using hierarchical linear regression models," *Canadian Journal of Civil Engineering*, vol. 37, no. 4, pp. 624–637, 2010.

[28] C. L. Chung and W. W. Recker, "Characteristics of speed dispersion and its relationship to fundamental traffic flow parameters," *Transportation planning and technology*, vol. 37, no. 7, pp. 581–597, 2014.

[29] J. Li, W. H. K. Lam, and X. Li, "Modeling the effects of rainfall intensity on the heteroscedastic traffic speed dispersion on

urban roads," *Journal of Transportation Engineering*, vol. 142, no. 6, p. 05016002, 2016.

[30] H. Wang, W. Wang, X. Chen, J. Chen, and J. Li, "Experimental features and characteristics of speed dispersion in urban freeway traffic," *Transportation Research Record*, vol. 1999, no. 1, pp. 150–160, 2007.

[31] F. Wang, S. Ruan, and M. Dai, "Characteristics of speed dispersion in urban expressway," *World Academy of Science, Engineering and Technology, International Journal of Civil, Environmental, Structural, Construction and Architectural Engineering*, vol. 10, no. 3, pp. 288–292, 2016.

[32] J. Qiao, L. Sun, X. Liu, and J. Rong, "Reducing the impact of speed dispersion on subway corridor flow," *Applied Ergonomics*, vol. 65, pp. 362–368, 2017.

[33] C. Xu, W. Wang, P. Liu, R. Guo, Z. Li, and F. Zhang, "Real-time freeway crash risk assessment using structural equation modeling and segmentation analysis approach," in *Transportation Research Board 93rd Annual Meeting*, TRID, Washington DC, 2014.

[34] C. Xu, Y. Wang, P. Liu, W. Wang, and J. Bao, "Quantitative risk assessment of freeway crash casualty using high-resolution traffic data," *Reliability Engineering & System Safety*, vol. 169, pp. 299–311, 2018.

[35] J. Bao, P. Liu, X. Qin, and H. Zhou, "Understanding the effects of trip patterns on spatially aggregated crashes with large-scale taxi GPS data," *Accident Analysis & Prevention*, vol. 120, pp. 281–294, 2018.

[36] X. Gu, M. Abdel-Aty, Q. Xiang, Q. Cai, and J. Yuan, "Utilizing UAV video data for in-depth analysis of drivers' crash risk at interchange merging areas," *Accident Analysis & Prevention*, vol. 123, pp. 159–169, 2019.

[37] S. Li, Q. Xiang, Y. Ma, X. Gu, and H. Li, "Crash risk prediction modeling based on the traffic conflict technique and a microscopic simulation for freeway interchange merging areas," *International Journal of Environmental Research and Public Health*, vol. 13, no. 11, p. 1157, 2016.

[38] A. Montella, V. Punzo, S. Chiaradonna, F. Mauriello, and M. Montanino, "Point-to-point speed enforcement systems: Speed limits design criteria and analysis of drivers' compliance," *Transportation Research Part C: Emerging Technologies*, vol. 53, pp. 1–18, 2015.

[39] Q. Hussain, W. K. Alhajyaseen, K. Brijs, A. Pirdavani, N. Reinolsmann, and T. Brijs, "Drivers' estimation of their travelling speed: a study on an expressway and a local road," *International Journal of Injury Control and Safety Promotion*, vol. 26, no. 3, pp. 216–224, 2019.

[40] P. Colonna, P. Intini, N. Berloco, and V. Ranieri, "The influence of memory on driving behavior: how route familiarity is related to speed choice. An on-road study," *Safety Science*, vol. 82, pp. 456–468, 2016.

[41] P. Intini, N. Berloco, P. Colonna, S. Ottersland Granås, and E. Olaussen Ryeng, "Influence of road geometric design consistency on familiar and unfamiliar drivers' performances: crash-based analysis," *Transportation Research Record*, 2019.

[42] T. F. Golob, W. Recker, and Y. Pavlis, "Probabilistic models of freeway safety performance using traffic flow data as predictors," *Safety Science*, vol. 46, no. 9, pp. 1306–1333, 2008.

[43] C. Gao, J. Xu, Q. Li, and J. Yang, "The effect of posted speed limit on the dispersion of traffic flow speed," *Sustainability*, vol. 11, no. 13, p. 3594, 2019.

Hindawi
Journal of Advanced Transportation
Volume 2019, Article ID 2061532, 11 pages
https://doi.org/10.1155/2019/2061532

Research Article

Physiological Characteristics and Nonparametric Test for Master-Slave Driving Task's Mental Workload Evaluation in Mountain Area Highway at Night

Haiwei Wang,[1] Jianrong Liu,[2] and Feng You [2]

[1]*School of Transportation and Economic Management, Guangdong Communication Polytechnic, Guangzhou 510650, China*
[2]*School of Civil Engineering and Transportation, South China University of Technology, Guangzhou 510640, China*

Correspondence should be addressed to Feng You; youfeng77@126.com

Received 25 August 2019; Accepted 15 October 2019; Published 3 December 2019

Guest Editor: Feng Chen

With the rapid development of advanced mobile intelligent terminals, driving tasks are diverse, and new traffic safety problems occur. We propose a new research on physiological characteristics and nonparametric tests for the master-slave driving task, especially for evaluation of drivers' mental workload in mountain area highway in nighttime scenario. First, we establish the experimental platform based driving simulator and design the master-slave driving task. Second, based on the physiological data and subjective evaluation for mental workload, we use statistical methods to composite the physical changes evolution analysis in a driving simulator. Finally, we finished nonparametric test of the drivers' psychological load and road test. The results show that in compassion with the daytime scenario, drivers should pay much effort to driving skills and risk identification in the nighttime scenario. Thus, in the same driving condition, drivers should bear the higher level of mental workload, and it has been subjected to even greater pressures and intensity of emotions.

1. Introduction

1.1. Problem and Motivation. Driving safety is one of the eternal themes in road traffic engineering. When the advanced driver assistance system (ADAS) and on-board intelligent terminals have been used increasingly, the drivers' mental workload changed from the single task to multiple tasks. The drivers cannot obtain road-related information due to excessive mental stress, which will influence decision-making for driving. And the drivers are exposed to the frequent traffic accidents.

In the field of cognitive psychology, human cognitive resources are limited. They have to allocate the resources to spatiotemporal scenarios and activities when engaged in a psychological activity, namely, the drivers will expend more cognitive resources if they are involved in multiple driving tasks. Accordingly, for the driving behavior, drivers cannot quickly collect and process environmental and driving information. The risk of road traffic accidents increases.

1.2. Related Works. In traffic accident research, the driver's own reasons cause cognitive errors in the road traffic environment, the traffic state is judged incorrectly. And the proportion on traffic accidents is caused by slow brain response accounting for more than half. Especially, relevant traffic safety research shows that the number on traffic accidents caused by the driver's own responsibility, especially for traffic fatal accidents, is increasing year by year. In response to this problem, researchers have carried out research working on the mental load on the driver during driving. Some researchers used FMRI and FNIRS to collect data on the driver's brain physiological activity. Through driving experiments, the researchers selected significant physiological indicators for evaluating brain mental load [1–4]. Based on the physiological indicators and Human Factors Engineering, studies have considered changes in heart rate variability power spectral density. In the driving task, the driver's mental load increases as driving tasks increase, but the heart rate variability power spectral density decreases [5–7].

With the application and the promotion of physiological sensors, researchers have applied physiological instruments to collect the driver's electrocardiogram and EEG data [8, 9]. Based on the above data, a driving mental load prediction model is established [10, 11] and the rationality of human-computer interaction analyzed [12].

Some researchers use driving simulators to analyze the relationship between the driver's mental load and driver's vision [13]. In addition, based on real driving scenarios, the research has focused on the impact of using mobile phones on driving behavior [14, 15] and road safety [16].

As the research progressed, the researchers designed driving experiments on simulators to analyze the gaze point variation for the driver's view field under different mental loads [17]. There is a significant difference in the distribution of the gaze points under mental load levels. Specifically, as the mental load increases, the concentrated area of the gaze points will shrink [18].

In references [19–21], the driver's psychological load also has a greater impact on travel time, especially at intersections [22–24]. For semiautonomous vehicles [25], the human-machine sharing technology allows the driver and the OBU to share control of the vehicle, reducing the driver's psychological load [26–28]. In addition, intelligence, networking, and electrification have become the trend of the current automotive industry. In response to the demand for new energy vehicles bench testing [29], part of the research is devoted to the relationship between human-machine interface design and driver's psychological load [30–32].

In summary, mental load significantly affects the driver's environmental perception and driving concentration. In China, more research is needed on the driver's psychological load. For example, the team of Harbin Institute of Technology studied the relationship between the drivers physiological characteristics and driving behavior [33]. The team of Jilin University [34, 35], Sun Yat-sen University [36] and Tongji University [37] analyzed the relationship between fatigue and driving risk based on the drivers' physiological features.

From the above literature review, researchers have carried out research on the mental load characteristics of drivers. However, for research convenience, the scenario is limited to the daytime. Some studies have proposed the driver's adaptation ability in nighttime, but the driver's physiological characteristics lack intensive study in the nighttime scenario. In addition, traffic accidents in China occur frequently in the nighttime, currently. Thereby, how to combine the driver's task (primary and secondary driver's task) and improve safety in the nighttime has become an urgent issue to be addressed.

1.3. Contributions. The main contribution of this article is to study driving behavior in the nighttime scenario. It is based on 4 types of driving experiments on a driving simulator: a single driving task experiment and a master-slave driving task experiment, respectively, in nighttime and daytime. By analyzing the physiological data such as EEG, ECG, respiration, and skin electricity, and evaluating the mental load of drivers, this article reveals the variation law of drivers' physiological parameters based on statistics in the nighttime and the daytime scenario. The results can be used for road safety evaluation in the night scenario.

The remainder of the paper is organized as follows. Section 2 briefs surveys influencing factors of driver cognitive status and physiological indicators of mental workload. Section 3 presents driving simulator experiment method. The Section 4 provides driving simulator experiment results and analysis. Section 5 is nonparametric test of driver's psychological load and actual road test. Section 6 has conclusions and related future work. The framework of this paper is illustrated in Figure 1.

2. Influencing Factors of Driver Cognitive Status and Physiological Indicators of Mental Workload

2.1. Factors Affecting Driver's Mental Load. The cognitive process of drivers is divided into 3 stages—the perception stage, the decision-making stage, and the operational stage.

The driver obtains outside driving environment information through sensory organs such as sight, hearing, smell, and touch during driving. Then, through the brain nerve to judge and process the information related to it, the driving behavior decision is made. Finally, the behavioral decision making for driving is performed. The mental workload refers to an additional work task that the driver needs to handle when the driver operates the vehicle, the traffic environment around it for the road restriction conditions, and the information processing capabilities on the brain that occur with frequency. This ability produces different effects and different mental stresses.

Currently when various types of ADAS continue to develop, drivers will generate higher mental workloads, especially information mental loads, and their mental load directly affects driving behavior and vehicle driving conditions. Besides, continuous driving under higher mental load is likely to cause driver judgment, decision or manipulation error, and affect road traffic safety. The main factors affecting the driver's mental load are summarized as follows.

(1) Individual characteristics affect the driver's mental load, including age, gender, education, income, travel experience, and so on. Besides, stable individual characteristics include these effects, which are about the emotional load on the driver's mental load, such as cognitive ability and cognitive style. Research result shows that different individual characteristics respond differently to the same type on outside driving or in-car driving information. However, the influence about this individual characteristic on the driver's mental load is relatively fixed. In different driving tasks, the driver's cognitive ability and cognitive style are influenced by themselves, the environment and the interaction between the two. Therefore, cognitive ability and cognitive style are in a changing state for the individual driver. And both will directly affect the driver's judgment and decision [38].

(2) The driving information search, processing and decision-making task characteristics affect the driver's mental load in three aspects: information presentation, release method, and driving environment. Based on published way information, such as color, text, symbols, and different driving environments such as weather, traffic conditions, and the outside environment, research scholars have conducted research on

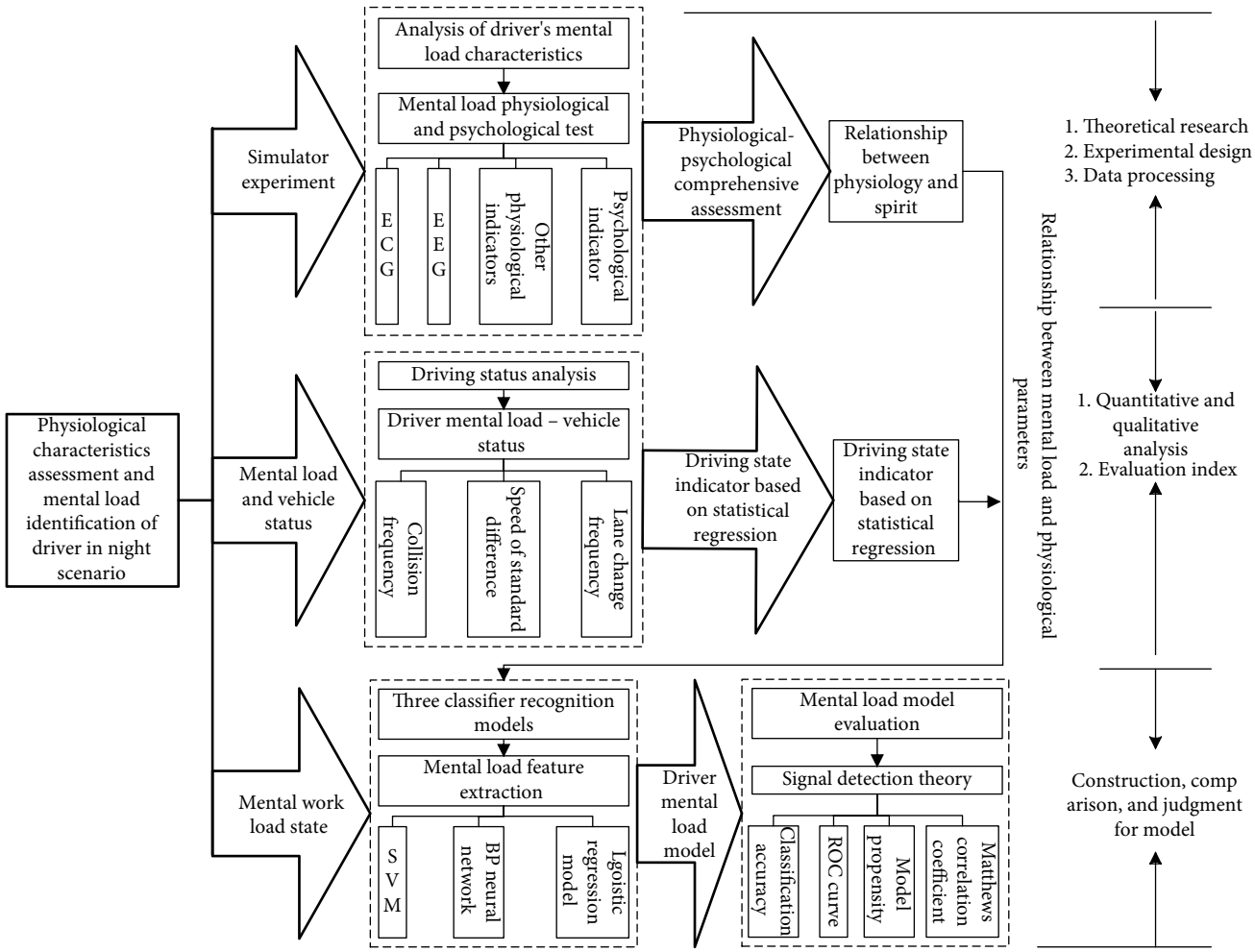

Figure 1: The framework of the paper.

driver's mental load in various aspects [39]. Because different information sources have differences in information release features and driver information schemas, the task complexity about information search and processing is different. Besides, different information sources will have influence on different degrees on mental workload. In addition, the road driving environment is the main influencing factor on the driver's visual and psychological load. The environmental complexity determines the intensity on the driver's mental load. Vehicle speed is an important feature in road driving environment. Many scholars have carried out research on the driver's mental load based on the relationship between vehicle speed, the driver's reaction time and operation time. Some studies have shown that higher vehicle speeds will place higher demands on the driver's response time and operating time. In the process of information search and decision, the driver will bear greater mental load [40].

2.2. Physiological Index on Driver's Mental Load. Yi-Ching Lee proposed multiple resource-related theories in his research. They proposed that the interference generated by the two mission resources occupying two channels is much smaller than the interference generated by the same one channel [41]. According to this theory, research scholars believe that driving operations, information search, reaction decision-making, and other information processing activities in driving tasks are processes in which multiple resources share the same neural channel. With the increase in various information processing tasks, the driver's information processing ability is weakened. And the perception and driving ability in the driving environment and the surrounding area will also be weakened. Besides, this weakening is also reflected in changes in the driver's physiological indexes. Therefore, in the driving activities, human physiological parameters can reflect the psychological and physiological state objectively and accurately.

The physiological measurement sensors can record the changes of drivers various physiological data in real time and continuously. They can be utilized to evaluate the mental load of the drivers in various driving scenarios. According to generation mechanisms, the parameters are divided into 2 categories: one related to the central nervous system and the anther one is related to the peripheral nervous system. The

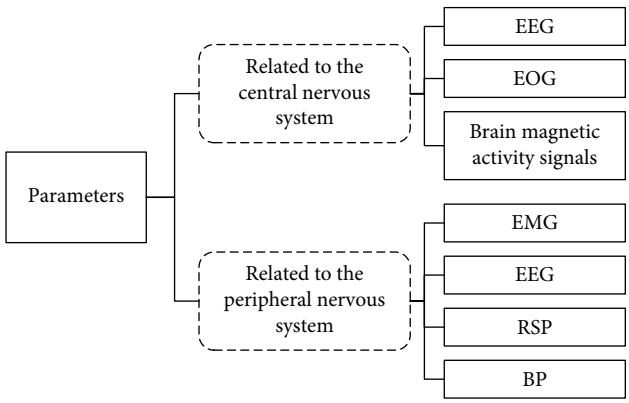

Figure 2: Evaluation parameters of mental load of drivers.

former covers EEG, EOG, and brain magnetic activity signals. And the latter includes EMG, ECG, RSP, BP, etc. (shown in Figure 2). To specifically evaluate the driving mental workload in daytime and nighttime scenarios, the article is based on ECG and EEG signals. This paper will select the following physiological index parameters for testing and research determination.

2.2.1. ECG Index. ECG index mainly reflects the activity on the heart. By the common dominance between the sympathetic and vagal nerves, the brain processes and judges the external information resources. The sympathetic nerve is mainly to raise the level of awakening of the organism. The vague nerve is mainly to cause the excited state organism to return to its lower arousal level. So the awakening biological level is closely related to the strength of the driver's mental load. Therefore, this paper extracts BPM, HRV, LF/HF, and other indicators in the ECG test as the test physiological indicators on the mental load intensity in the driver's multiple tasks.

2.2.2. EEG Index. During the driving task, the driver's psychological changes and subtle action decisions will be reflected in the brain waves. By monitoring changes in EEG indicators, the driver's psychological changes can be obtained objectively and accurately. The multi-information task in the driving process will stimulate the driver's visual and psychological, and then reflect in the brain waves.

2.2.3. EDA Index. The body's activity is enhanced by the stimulating effects on the sympathetic nerves. Then, the formed electrophysiological indicators can objectively reflect the changes in the activity on the sympathetic nervous system. It also directly reflects the stress changes that the brain produces when dealing with unexpected information. Drivers may experience different psychological reactions due to increased information load in the process of driving the vehicle.

2.2.4. RES Index. Increased respiratory rate as the intensity of mental load increases, the level of driver's wake-up brain, and mood swings during driving. If the driver's mental stress is too high, there will be an increase in respiratory rate.

Figure 3: Driving simulator experiment.

3. Driving Simulator Experiment Method

3.1. Driving Simulator Experiment Design. Many pilot traffic behavior experiments are carried out in the driving simulator. The driving simulator can simulate different driving environments. And compared with the external road environment, the interference to the test driver's physiological instruments is smaller, and the measured human physiological data relatively more accurate. The testing experimental time is mainly based on the experimental research method on mental load in human factors engineering. Then, human subjective evaluation test method and physiological parameter acquisition method are adopted [42]. At the same time, in order to avoid the impact on physiological fatigue caused by long-time driving experiments about the experimental results, the design time for each experiment is 30 minutes.

As shown in Figure 3, for driving simulator experiment, the experiment requires the experimenter to complete the daytime and night driving experiment under the mountain highway traffic environment on the driving simulator. Each group was tested for 30 minutes. In order to reduce fatigue driving impact on various test indexes, the driver was required to rest for about 3 hours after each experiment. After the experiment, driving operation impact in single-task or master-slave task experiment is statistically analyzed when using subjective evaluation method on questionnaire and objective indicators on the physiological tester. The master-slave driving task is used to illustrate multi-task driving behavior. Here we add the conception of "multi-task driving behavior". When the driver is running a vehicle, he performs other activities simultaneously, such as talking to the passenger, turning on the air conditioner, or listening to music. At this time, driving a vehicle is a master driving task, and the others are the slave driving tasks.

The specific experimental operation steps are shown in Table 1. Before formal experiment, the experimental subject is required to perform a single driving task exercise for a temporal period to familiarize with the driving environment. The subjects were prepared for physiological patches and data acquisition, and then entered the formal driving simulator

Table 1: Driving simulator experiment and master-slave driving task design.

Experiment flow	Experimental content/Experimental time
Basic driving tasks	Familiar with driving environment of mountain roads, Data Acquisition of Driver's Benchmark Physiology/30 min
Master-slave driving task one	Collection of physiological data from master-slave tasks/8 min
Master-slave driving task two	Collection of physiological data from master-slave tasks/8 min
Task of test recovery	Collection of baseline physiological data/5 min

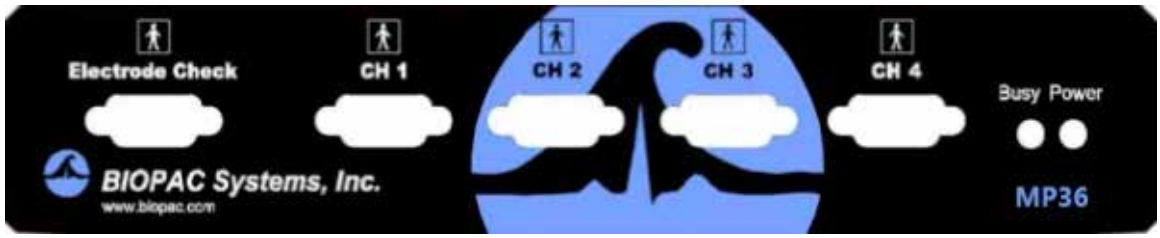

Figure 4: BIOPAC physiological instrument panel.

experiment stage. First, a 30 minute single driving experiment was conducted. The data in this stage are used as the benchmark data for data analysis to compare and analyze driver's changes on physiological parameters in other driving experiment tasks. Subsequently, according to the experimental content, the following experiments are carried out, respectively. The first is the master-slave driving task experiment one, which is speech memory class task. And the experiment time is 8 min. The second is the master-slave driving task experiment two, which is simple calculation class task. And the experiment time is 8 min. After a 5 minute recovery period, the tester parked and sat down and collected baseline physiological data indicators. Finally, the tester conducts a subjective scoring assessment on his or her own tasks. During the whole experimental process, the tester maintains uninterrupted and safe driving, and the speed is maintained at 60–70 km/h. In order to eliminate the mutual interference between the daytime or nighttime experiments, the daytime driving experiment and the night driving experiment are performed independently, and the same tester can only perform one set of experimental contents per day.

3.2. Experimental Sample. The experimental sample consists of 18 drivers with legal driving licenses aged 20–35 years old. They are healthy, have no heart disease or nervous system diseases, and they have adequate sleep and no alcohol or other drugs before the experiment.

3.3. Experiment Apparatus. For driving simulator, we set mountain highway scene in daytime and night for experiment, driving speed is 60–70 km/h, traffic flow is set as general mountain highway traffic, one-way lane, circular closed route, typical landform characteristics about mountain highway such as long longitudinal slope, bend, continuous bend, etc.

For BIOPAC MP36 named as multi-channel physiological recorder, as shown in Figure 4, it is used to monitor physiological indicators such as ECG, PEG, EEG and RES, which is as a basis for quantitative testing and evaluation on driver's mental load. Among them, the accuracy on ECG, EEG, and PEG is in the range of 10-6 mv. The breathing and heartbeat frequencies are measured in units as times percent minute. Because human physiological changes are very subtle, the selected sampling frequencies are 1000 Hz, such as 1000 times per second while collecting experimental data. The electrocardiogram test electrode patch is located at the upper and lower body slanting sternum across the heart. EDA test electrodes stick to the left finger position, as far as possible do not interfere with driving. The breath test strap needs to be wrapped around the chest undulation, and the brain electrode patch is attached to brain forehead close to the hairline. Figure 5 shows the details of testing position to physiologic instrument.

For stopwatch, it is used to record test time. And it specifies the time of each voice task.

3.4. Experimental Content Design. When performing the experiment, the tested driver needs to continue uninterrupted driving at a speed from 60 km/h to 70 km/h on the set mountain highway. In the driving environment during the day and night, the driver's physiological characteristics are different, which is the key research experiment in this paper. In order to avoid the influence between different driving scenarios on the driver's physiological characteristics and mental load, the same driving scene is set in the experiment.

At the same time, when performing experiments on master-slave tasks, two voice tasks are designed as cognitive tasks in the experiment, and auditory stimulation add the speech feedback is adopted. Two voice tasks are short-term memory tasks and simple computing tasks. For short-term memory tasks, such tasks will consume drivers' short-term memory resources and occupy their cognitive channels. For example, a speech content that is repeatedly heard but each content is not repeated, subjects are required to repeat what they hear immediately, and try to maintain the correct rate of repeating content. For simple computational tasks, in order to avoid the interference on mental load caused by the problem itself, it is

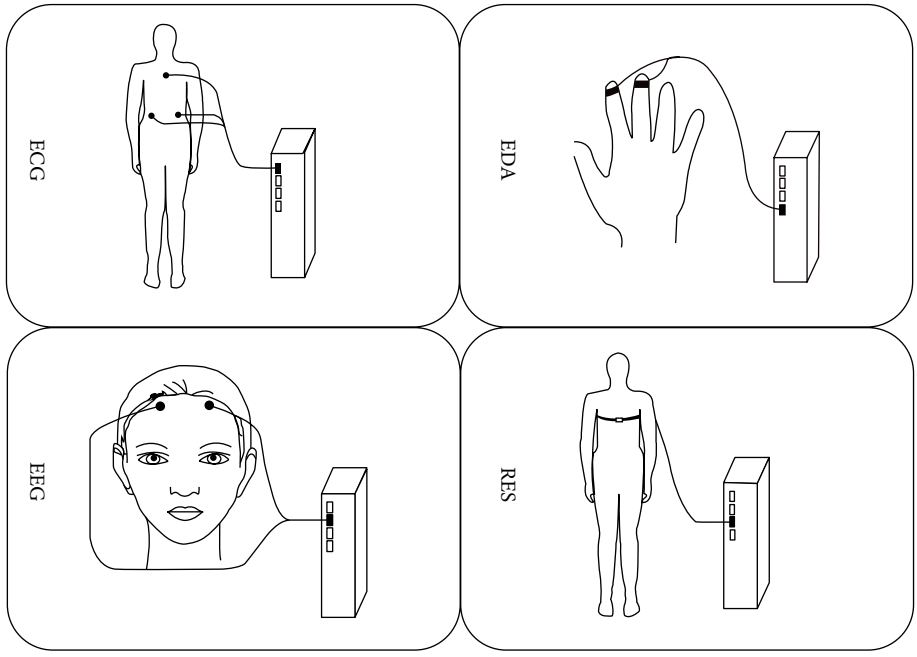

Figure 5: Testing position of physiologic instrument.

necessary to ensure that the difficulty coefficients are consistent and not repetitive. Besides, the subjects are asked to answer the computational questions they hear immediately, and to respond and answer in 1-2 seconds as much as possible. They are asked to answer as accurately as possible.

3.5. Measurement Methods. There are many ways to measure the driver's mental load. It can be classified into three categories: subjective evaluation measurement, behavioral performance measurement, and physiological indicator measurement [43]. The subjective evaluation measurement is a method that we measure the mental load perceived by the driver in the form of questionnaire evaluation. This method has very high effectiveness and it is easy to operate. The subjective evaluation content is based on the driver's overall experience in the completed driving task. It consists of six factors: mental load, physical demand, time demand, effort level, performance level, and frustration. The driver scores in turn from six factors from 1 to 10 points to assess the workload in the task. The behavioral performance measurement is a method that we use the driver's task performance as mental load evaluation index to derive the driver's mental load in the task. Physiological indicator measurement refers to assessing mental load by observing driver's physiological response during the task process. It can reflect the driver's mental load changes objectively and in real time.

When measuring driver's mental load, the subjective evaluation measurement method is the most main direct method to describe its subjective feelings, but it cannot describe the change process on mental load. In the evaluation process, there may be the risk of insensitivity or judgment error in its own change state judgment. And there is no standard discrimination system for the indexes. Physiological parameters are mainly ECG, EEG, EDA, RES, and so on. The evaluation method using physiological parameter index has objectivity, accuracy and dynamics, high time precision and good continuity, which can effectively correct the judgment errors on the other two evaluation methods. In order to test and verify mental load change during driving more reasonably, this paper combines physiological index test with subjective evaluation test to analyze and verify the effect between master-slave task on driver's mental load during daytime and night driving, and then we analyze and verify the effectiveness on evaluation method.

4. Driving Simulator Experiment Results Analyzing

The original data on ECG, EEG, RA, RF, and EDA are denoised and filtered by physiological instrument. And then physiological signals in different task stages are extracted and processed. Heart rate BPM, ECG, RR interval standard deviation, heart rate variability power spectral density, EEG four different frequency spectral density, EEG power spectral density integral value, respiratory frequency and amplitude, EDA activity level, and so on are obtained. They are used as a basis for assessing the physiological indexes at the driver's mental stress level. As shown in Figure 6, the test path starts from South China University of Technology, passing through Guangyuan Expressway, South China Expressway, Guanghe Expressway, Guangzhou-Shenzhen Expressway, etc.

When the driver performs single and master tasks in day and night, the average value about physiological indexes is extracted separately. The subjective score on the driver's mental load is based on the questionnaire evaluation method on work load methods in NASA-TLX. The subjective evaluation average scores for day and night are obtained, as shown in Tables 2 and 3.

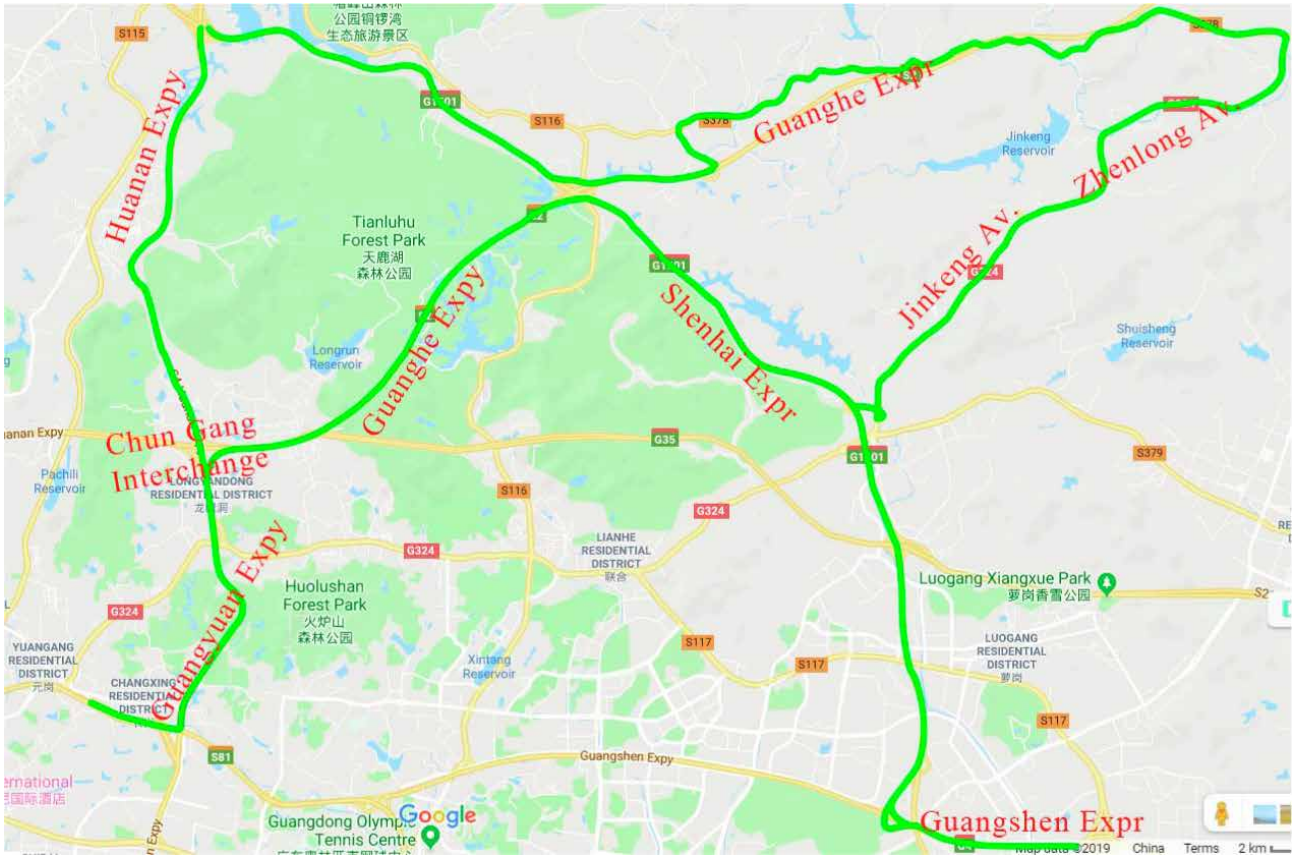

Figure 6: The test path for this research.

Table 2: Average of ECG index (day).

Physiological index	Single driving	Master-slave task one	Master-slave task two
MHR (mean heart rate)	75.34	83.17	84.22
RR (interval standard deviation)	0.057	0.049	0.046
LF (NU) (low frequency)	0.769	0.711	0.558
HF (NU) (high frequency)	0.153	0.22	0.249
LF/HF	4.02	2.62	1.76

Table 3: Average of ECG index (night).

Physiological index	Single driving	Master-slave task one	Master-slave task two
MHR (mean heart rate)	74.41	76.58	77.79
RR (interval standard deviation)	0.061	0.046	0.057
LF (NU) (low frequency)	0.678	0.617	0.449
HF (NU) (high frequency)	0.197	0.330	0.425
LF/HF	2.27	1.68	1.12

From the data obtained, the heart rate mean and heart rate variability indexes are similar at daytime and nighttime. The heart rate mean increases with the difficulty of the master-slave task, and the low-frequency normalized index LF (NU) in the power spectral density. The increase in task difficulty is significantly reduced. Among them, in the heart rate variability power spectral density, LF (low frequency) indicates activity intensity about sympathetic nerve, and HF (high frequency) indicates activity intensity about the vague nerve. LF/HF characterizes tension degree between two different nerves, so LF continued lowering indicates that the sympathetic excitation is reduced and the vague nerve occupies the main frequency band. Analysis on variance shows significant differences. The LF/HF value at night is significantly lower than the daytime value, which indicates that the nondriving mission at night has more serious interference with the driver's driving process as the difficulty value increases.

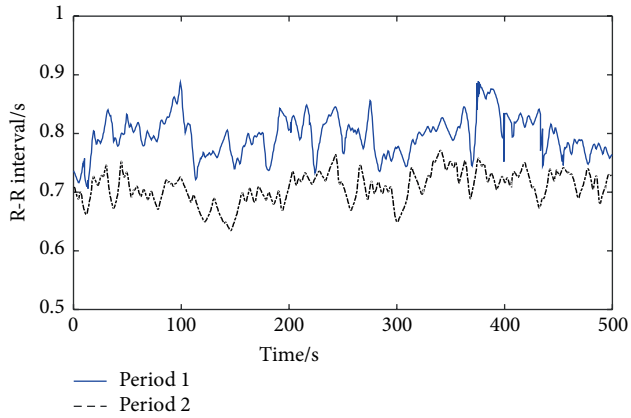

Figure 7: Comparison of RR interval series (single driving vs. master-slave task).

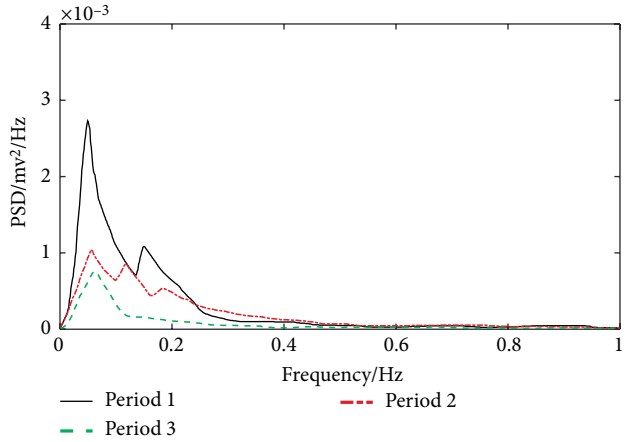

Figure 8: Comparison of HRV-PSD (single driving vs. master-slave task).

Table 4: Difference of psychological with load subjective evaluation under different driving tasks (day).

Driving a—Driving b	Inspection statistics	Standard error	Statistics of standard inspection	Sig.	Significance
Per. 1-Per. 2	−9.448	5.522	−1.713	0.086	Not significant
Per. 1-Per. 3	−26.247	5.522	−4.751	0.000049	Very prominent
Per. 2-Per. 3	−16.788	5.522	−3.044	0.0019	Significant

Table 5: Difference of psychological with load subjective evaluation under different driving tasks (night).

Driving a—Driving b	Inspection statistics	Standard error	Statistics of standard Inspection	Sig.	Significance
Per. 1-Per. 2	−16.896	5.522	−3.058	0.0019	Not significant
Per. 1-Per. 3	−30.946	5.522	−5.601	0.000067	Very prominent
Per. 2-Per. 3	−14.049	5.522	−2.539	0.0109	Significant

Figures 7 and 8 are the driver's R-R interval contrast and heart rate spectral density comparison chart, respectively, on single task and master-slave task in night environment. In Figure 7, Period 1 represents the R-R interval value at the single task phase in the nighttime environment. Period 2 represents the R-R interval value at the master-slave task 2. Since the R-R interval value at the master-slave task 1 phase and the single task phase does not change much during the test, Figure 7 only shows the comparison between the R-R interval values at the single task and the master-slave task 2. In Figure 8, Period 1 represents the heart rate variability power spectral density for a single task in a nighttime environment. Period 2 represents the heart rate variability power spectral density for the master-slave task 1. Period 3 represents the heart rate variability power for the master-slave task 2. From overall process, it is obvious that the influence at master-slave task on the heart rate during driver's driving process varies greatly with influence on the mental load.

5. Nonparametric Test of Driver's Psychological Load and Actual Road Test

5.1. Nonparametric Test for Driver's Psychological Load. From the above calculation results, under the complex master-slave task conditions, the driver's subjective score has a significant increase compared to the single-task driving condition and the simple master-slave task driving situation. This difference is more significant at night. In order to determine whether these judgments are in line with statistical principles, nonparametric tests are performed on driver's subjective evaluation.

According to the characteristics for subjective evaluation data distribution, this paper chooses independent sample Kruskal-wallis test for processing. Per. 1 represents single-going driving conditions. Per. 2 represents simple master-slave mission driving conditions. Per. 3 represents complex master-slave mission driving. Under different task driving conditions, the subjective evaluation results on psychological load are shown in Tables 4 and 5.

Through the statistical numerical calculation results, there are significant differences in the psychological evaluation on mental load under three different mission driving conditions. In particular, the difficulty level at the master-slave task has a significant impact on its outcome. Among them, under the same master-slave task difficulty, the night driving stage has a more obvious impact on the driver's mental load level. This scoring result indicates that during driver's driving process, other non-driving tasks have a certain degree of adverse effect on the driver's mental load. This adverse effect is more obvious at night.

Figure 9: Specific experimental situation and device placement.

Table 6: Mean heart rate comparison of parameter results (actual road vs. driving simulator, night).

Mean heart rate	Single driving	Simple master-slave task	Complex master-slave task
Driving simulator	74.39	76.60	77.82
Actual road	75.27	77.37	79.99

Table 7: Comparison of night power spectral density LF/HF parameter results (actual road vs. driving simulator).

Power spectral density LF/HF	Single driving	Simple master-slave task	Complex master-slave task
Driving simulator	2.28	1.69	1.13
Actual road	2.13	1.55	1.04

5.2. Actual Road Comparison Experiment. In order to verify the authenticity on the relevant data changes in a simulated pilot experiment, the experiment designing the actual road was added on the basis of the simulated driving experiment. The experiment uses vehicles running on actual roads. At the same time, in order to make the experimental results more contrast, the participants in the actual road experiment are the drivers who have conducted simulated driving experiments. Figure 9 shows the specific experimental situation and device placement. The experiment not only selects typical mountain road sections similar to the driving simulator experiment, but also tries to balance the various road types and micro hills, hills and heavy hills on the mountain roads.

According to the experimental data analysis about the driving simulator, MHR, LF/HF, β, β/α, and NASA-TLX in actual experiment are compared and analyzed. In order to obtain a more intuitive comparison result, the data used are normalized before the comparative analysis and then compared. This paper focuses on result comparison between simulated driver's driving data in the actual driving and driver's nighttime environment in the night environment.

The result comparison on MHR parameters is shown in Table 6. In the simulation experiment, for three driving conditions, the variation amplitudes are 2.21 and 1.22, respectively, while in the actual vehicle, the variation amplitudes are 2.1 and 2.62. It shows that driver is subjected to a higher level at mental stress when handling complex nondriving tasks for a real vehicle. For simulated driving, because it is indoor environment, the driver is relaxed, the load it bears is slightly lower. But the heart rate trend is increasing when trying to increase the interference at nondriving tasks.

The comparison about LF/HF parameter results is shown in Table 7. In the simulation experiment, the driving range in the three driving conditions is 0.59 and 0.56. In actual driving, the decreasing ranges are 0.58 and 0.51, respectively. The driving trends in the two driving environments are the same, and the amplitude changes are similar. Besides, it shows that driver is in a similar state to handle nondriving tasks in experimental environments.

6. Discussion and Conclusions

In this paper, based on the driving simulation experiment, the influence on the master-slave mission on the driver's mental load and information cognition ability during daytime and nighttime driving is analyzed. The main conclusions are as follows.

(1) Whether it is day or night, the master-slave mission has a greater impact on the driver's mental load than on a single mission. It reduces the driver's information processing ability and increases driving risk. As the difficulty on the task which is nondriving related tasks increases and the time continues, the driver obviously feels that the subjective pressure increases, and the driving activity has an adverse effect on traffic safety.

(2) The subjective scores on the driver's mental workload questionnaire are basically consistent with the results about multi-index physiological characteristics test. The transient characteristics on physiological indexes can not only measure driver's subtle physiological changes in the subtle, but also measure the trend on mental load. This point indicates that the physiological index test is an effective test method for evaluating the driver's mental load. In the following study, an eye movement physiology index closer to the information receiving channel will be introduced as an effective evaluation method for judging mental load. It provides a more objective and feasible evaluation method for studying driver behavior.

(3) Compared to daytime, the night road environment requires a higher visual and information reception capability for the driver. Therefore, the driver's heart rate and brain electrophysiological indexes are more obvious during the day, especially in the final stage on the master-slave driving task. Drivers are more annoyed and uneasy, which can affect driving safety at night, while requiring drivers to have higher driving skills and driving risk control.

Based on research results in this paper, for drivers driving at night, it is suggested that relevant departments should consider further strengthening scientific management and adjustment of relevant regulations, which aims to minimize the risk of road traffic accidents. In the future work, we will consider increase the number on experimental samples and the difference in driver's driving experience for comparative experiments, which can verify the rationality and universality about research conclusions. Besides, we will consider the experiment under Cooperative Vehicle-Infrastructure Systems [44–47].

Data Availability

The data used to support the findings of this study are available from the corresponding author upon request.

Conflicts of Interest

The authors declare that there are no conflicts of interests regarding the publication of this article.

Acknowledgments

This work was partially supported by National Natural Science Foundation of China (51808151), and the Fundamental Research Funds for Guangdong Communication Polytechnic (20181014).

References

[1] H.-W. Wang, H.-Y. Wen, and L. I. U. Min, "Experimental evaluation of nighttime driver's physiological characteristics in driving simulator," *Journal of Jilin University (Engineering and Technology Edition)*, vol. 47, no. 2, pp. 420–428, 2017.

[2] J. A. Veltman, "A comparative study of psychophysiological reactions during simulator and real flight," *International Journal of Aviation Psychology*, vol. 12, no. 1, pp. 33–48, 2002.

[3] F. Nocera, A. Couyoumdjian, and F. Ferlazzo, "Crossing the pillars of hercules: the role of spatial frames of reference in error making," *The Quarterly Joural of Experimental Psychology*, vol. 59, no. 1, pp. 204–221, 2006.

[4] F. Chen, H. Peng, X. Ma, J. Liang, W. Hao, and X. Pan, "Examining the safety of trucks under crosswind at bridge-tunnel section A driving simulator study," *Tunnelling and Underground Space Technology*, vol. 92, p. 103034, 2019.

[5] A. J. Tattersall and G. R. J. Hockey, "Level of operator control and changes in heart rate variability during simulated flight maintenance," *Human Factors: The Journal of the Human Factors and Ergonomics Society*, vol. 37, no. 4, pp. 682–698, 1995.

[6] W. Jian, Y. Lin-lin, Z. Bing, and D. Wei-wen, "Identification of driver individualities using Gaussian mixture model," *Journal of Jilin University (Engineering and Technology Edition)*, vol. 1, pp. 38–43, 2015.

[7] X. Zhi, G. Hong-zhi, and Y. Hai, "Driver eye movement features on text message from traffic signs," *Journal of Beijing University of Technology*, vol. 37, no. 12, pp. 1830–1835, 2011.

[8] Y. Man-juan, W. Ling-tao, and T. Cheng-cheng, "Study of influence of foreign characters in guide signs on legibility," *Journal of Highway and Transportation Research and Development*, vol. 6, no. 2, pp. 91–95, 2012.

[9] G. Zhen-hai, D. Li-fei, Y. Zhao Hui, and Huili, "Assessment of driver's cognitive workload under multitask based on physiological signals," *Automotive Engineering*, vol. 1, pp. 33–37, 2015.

[10] Y. M. Li-li, "Influential factors analysis of drivers' mental workload with the use of vehicle navigation system," *Journal of Safety and Environment*, vol. 11, no. 6, pp. 202–204, 2011.

[11] S. Rubio, E. Diaz, J. Matin, and J. M. Puente, "Evaluation of subjective mental workload: a comparison of SWAT, NASA-TLX, and workload profile methods," *Applied Psychology*, vol. 53, no. 1, pp. 61–86, 2004.

[12] S. Pala, T. Schnell, N. L. Becklinger et al., "Adaptation of the cognitive avionic tool set (CATS) into automotive human machine interface design process," *SAE Paper*, vol. 1, p. 0594, 2011.

[13] M. A. Recarte and L. M. Nunes, "Mental workload while driving: effects on visual search, discrimination, and decision making," *Journal of Experimental Psychology*, vol. 9, no. 2, pp. 119–137, 2003.

[14] C. Bi, Y. Yuan, R. Zhang, Y. Xiang, Y. Wang, and J. Zhang, "A dynamic mode decomposition based edge detection method for art images," *IEEE Photonics Journal*, vol. 9, no. 6, pp. 1–13, 2017.

[15] N. Arbabzadeh and M. Jafari, "A data-driven approach for driving safety risk prediction using driver behavior and roadway information data," *IEEE Transactions on Intelligent Transportation Systems*, pp. 1–15, 2017.

[16] C. Bi, B. Fu, J. Chen et al., "Machine learning based fast multi-layer liquefaction disaster assessment," *World Wide WebInternet and Web Information Systems*, pp. 1–16, 2019.

[17] C. Bi, Y. Yuan, J. Zhang, Y. Shi, Y. Wang, and R. Zhang, "Dynamic mode decomposition based video shot detection," *IEEE Access*, vol. 6, pp. 21397–21407, 2018.

[18] F. Chen, M. Song, and X. Ma, "Investigation on the injury severity of drivers in rear-end collisions between cars using a random parameters bivariate ordered probit model," *International Journal of Environmental Research and Public Health*, vol. 16, no. 14, p. 2632, 2019.

[19] B. Yu, Z. Z. Yang, and B. Yao, "An improved ant colony optimization for vehicle routing problem," *European Journal of Operational Research*, vol. 196, no. 1, pp. 171–176, 2009.

[20] B. Yu, W. H. K. Lam, and M. L. Tam, "Bus arrival time prediction at bus stop with multiple routes," *Transportation Research Part C*, vol. 19, no. 6, pp. 1157–1170, 2011.

[21] D. Ma, X. Luo, S. Jin, W. Guo, and D. Wang, "Estimating maximum queue length for traffic lane groups using travel times from video-imaging data," *IEEE Intelligent Transportation Systems Magazine*, vol. 10, no. 3, pp. 123–134, 2018.

[22] D. Ma, X. Luo, S. Jin, D. Wang, and W. Guo, "Lane-based saturation degree estimation for signalized intersections using travel time data," *IEEE Intelligent Transportation Systems Magazine*, vol. 9, no. 3, pp. 136–148, 2017.

[23] B. Yao, P. Hu, X. Lu, J. Gao, and M. Zhang, "Transit network design based on travel time reliability," *Transportation Research Part C*, vol. 43, pp. 233–248, 2014.

[24] D. Ma, X. Luo, W. Li, S. Jin, W. Guo, and D. Wang, "Traffic demand estimation for lane groups at signal-controlled intersections using travel times from video-imaging etectors," *IET Intelligent Transport Systems*, vol. 11, no. 4, pp. 222–229, 2017.

[25] F. Chen, M. Song, X. Ma, and X. Zhu, "Assess the impacts of different autonomous trucks' lateral control modes on asphalt pavement performance," *Transportation Research C: Emerging Technologies*, vol. 103, pp. 17–29, 2019.

[26] R. H. Zhang, Z. C. He, H. W. Wang, F. You, and K. N. Li, "Study on self-tuning tyre friction control for developing main-servo loop integrated chassis control system," *IEEE Access*, vol. 5, pp. 6649–6660, 2017.

[27] X. J. Sun, H. Zhang, W. J. Meng, R. H. Zhang, K. L. Li, and T. Peng, "Primary resonance analysis and vibration suppression for the harmonically excited nonlinear suspension system using a pair of symmetric viscoelastic buffers," *Nonlinear Dynamics*, vol. 94, no. 2, pp. 1243–1265, 2018.

[28] F. You, R. Zhang, L. Guo, H. Wang, H. Wen, and J. Xu, "Trajectory planning and tracking control for autonomous lane change maneuver based on the cooperative vehicle infrastructure system," *Expert Systems with Application*, vol. 42, no. 14, pp. 5932–5946, 2015.

[29] F. Jie, Q. Liu, K. Liufu, Y. Deng, J. Fang, and Q. Li, "Design of bionic-bamboo thin-walled structures for energy absorption," *Thin-Walled Structures*, vol. 135, pp. 400–413, 2019.

[30] H. Xiong, X. Zhu, and R. Zhang, "Energy recovery strategy numerical simulation for dual axle drive pure electric vehicle based on motor loss model and big data calculation," *Complexity*, vol. 2018, pp. 1–14, 2018.

[31] H. Xiong, Z. Tan, R. Zhang, Z. Zong, and Z. Luo, "Numerical calculation model performance analysis for aluminum alloy mortise-and-tenon structural joints used in electric vehicles," *Composites Part B: Engineering*, vol. 161, pp. 77–86, 2019.

[32] Y. Zhang, Q. Liu, Z. He, Z. Zong, and J. Fang, "Dynamic impact response of aluminum honeycombs filled with expanded polypropylene foam," *Composites Part B*, vol. 156, pp. 17–27, 2019.

[33] W. Qi, Z. Wang, R. Tang, and L. Wang, "Driving risk detection model of deceleration zone in expressway based on generalized regression neural network," *Journal of Advanced Transportation*, vol. 2018, Article ID 8014385, p. 8, 2018.

[34] W. Lin-hong, L. Shi-wu, Z. Ru-bo, Y. Zhi-fa, J. Bin-kui, and Z. Xue-ping, "Impact of roadside landscape color on driver mean heart rate," *Journal of Jilin University (Engineering and Technology Edition)*, vol. 1, pp. 74–80, 2013.

[35] L. Yang, B. Wang, R. Zhang, H. Zhou, and R. Wang, "Analysis on location accuracy for the binocular stereo vision system," *IEEE Photonics Journal*, vol. 10, no. 1, pp. 1–16, 2018.

[36] H. Xiong, M. Zhang, R. Zhang et al., "A new synchronous control method for dual motor electric vehicle based on cognitive-inspired and intelligent interaction," *Future Generation Computer Systems*, vol. 94, pp. 536–548, 2019.

[37] G. Wu, F. Chen, X. D. Pan, M. Xu, and X. Y. Zhu, "Using the visual intervention influence of pavement markings for rutting mitigation-part I: preliminary experiments and field tests," *International Journal of Pavement Engineering*, vol. 20, no. 6, pp. 734–746, 2019.

[38] L. Wang, Y. Wang, and Y. Bie, "Automatic estimation method for intersection saturation flow rate based on video detector data," *Journal of Advanced Transportation*, vol. 2018, Article ID 8353084, p. 9, 2018.

[39] L. Wang, L. Zhang, H. Li, Y. Ma, and R. Zhang, "High selective production of 5-hydroxymethylfurfural from fructose by sulfonic acid functionalized SBA-15 catalyst," *Composites Part B: Engineering*, vol. 156, pp. 88–94, 2019.

[40] S. Larue Grégoire, W. Christian, S. Michelle, and A. Rakotonirainy, "Validation of a driving simulator study on driver behavior at passive rail level crossings," *Human Factors: The Journal of the Human Factors and Ergonomics Society*, vol. 60, no. 6, pp. 743–754, 2018.

[41] Y.-C. Lee, J. D. Lee, and L. Ng Boyle, "Visual attention in driving: the effects of cognitive Load and visual disruption," *Human Factor*, vol. 49, no. 4, pp. 721–733, 2007.

[42] A. Nguyen, M. M. Borghese, and I. Janssen, "Pedestrian traffic safety and outdoor active play among 10–13 year olds living in a mid-sized city," *Preventive Medicine Reports*, vol. 10, pp. 304–309, 2018.

[43] C. Ma, W. Hao, W. Xiang, and W. Yan, "The impact of aggressive driving behavior on driver-injury severity at highway-rail grade crossings accidents," *Journal of Advanced Transportation*, vol. 2018, pp. 1–10, 2018.

[44] R. Oliveira, C. Montez, A. Boukerche, and M. S. Wangham, "Reliable data dissemination protocol for VANET traffic safety applications," *Ad Hoc Networks*, vol. 63, pp. 30–44, 2017.

[45] J. Casselgren and U. Bodin, "Reusable road condition information system for traffic safety and targeted maintenance," *IET Intelligent Transport Systems*, vol. 11, no. 4, pp. 230–238, 2017.

[46] L. Xin, L. Wu, and X. Yang, "Exploring the impact of social economic variables on traffic safety performance in Hong Kong: a time series analysis," *Safety Science*, vol. 109, pp. 67–75, 2018.

[47] P. Najaf, M. T. Isaai, M. Lavasani, and J.-C. Thill, "Evaluating traffic safety policies for developing countries based on equity considerations," *Journal of Transportation Safety & Security*, vol. 9, no. sup1, pp. 178–203, 2017.